Phononics 2011

1st International Conference on Phononic Crystals, Metamaterials & Optomechanics

May 29-June 2 2011, Santa Fe, New Mexico, USA

Welcome from the Chairs of *Phononics 2011*

Ihab El-Kady
Sandia National Laboratories

Mahmoud I. Hussein
University of Colorado at Boulder

Dear Colleagues and Conference Participants,

We would like to thank you all for your participation in Phononics 2011: The First International Conference on Phononic Crystals, Metamaterials and Optomechanics – which is being held in Santa Fe, New Mexico, USA, from May 29 – June 2, 2011.

For decades there has been a strong passion within the physics and engineering communities for the study of the propagation of elastic and acoustic waves in periodic and nonperiodic media across different length scales. In recent years this interest has lead to the emergence of phononic crystals and acoustic metamaterials as new types of material systems with a potential to revolutionize many technological applications. In parallel, the conventional discipline of heat transfer has witnessed a strategic shift towards the nanoscale in pursuit of a more fundamental understanding of the underlying thermal phenomena. This transformation has been guided by the conviction that for best results a rigorous mechanistic description of phonon transport ought to be adopted. Optomechanics is another key area of research which studies coupled phenomena involving phonons. The coherent intersection between optical and mechanical waves lies at the micro/nanoscale. This area of research holds promise to solve important issues in the general field of optics and more specifically for photonic devices.

The rapid and simultaneous growth of these closely-related disciplines has provided a converging point of historical significance for the science of phonons. Two years ago, in June

2009, an International Workshop on Phononic Crystals was co-organized by Professors Ali Adibi and Abdelkrim Khelif. This workshop took place in Nice, France and was attended by around thirty experts in the field from around the world. Building on this effort, we along with our colleagues in the organizing committees felt it is timely to establish a larger international forum that unifies all the phonon-related areas by creating a conference where experts could interact and cross-fertilize. *Phononics 2011* - the first international conference of its kind - aims to fulfill this mission.

Phononics 2011 aims to bring together researchers with emphasis in both theory and experiments. As such, sessions cover theoretical studies, numerical simulations, fabrication, and characterization of appropriate structures. Furthermore, these areas can be broken down by their frequency ranges which entail different modeling approaches. More specifically, this conference covers seven themes: (1) Phononic crystals, (2) Phononic metamaterials, (3) Wave propagation in periodic structures, (4) Nanoscale phonon transport, (5) Phononic MEMS and RF applications, (6) Optomechanics, and (7) Fabrication and characterization for phononics. For more information on the conference and its themes, please visit the conference website at: *www.phononics2011.org*.

We hope that *Phononics 2011*, and the subsequent *Phononics 20xx* conferences which will take place on a biannual basis, will provide a unique avenue for dissemination and exchange of knowledge in all the themes related to phonons, across the different length scales and disciplines. It is our aspiration that this forum's participants will together lay the foundation for the emerging field of *phononics*.

Yours sincerely,

Ihab El-Kady
Sandia National Laboratories

Mahmoud I. Hussein
University of Colorado at Boulder

Albuquerque and Boulder, April 2011

Table of Contents

Extended Abstracts

Phononics

2011

1st International Conference on Phononic Crystals, Metamaterials & Optomechanics

Information About the Conference

The study of phonons - although a core discipline in the conventional condensed matter physics literature - is currently being viewed in a new light. Whether examined at the nanoscale, microscale or larger scales, the analysis and manipulation of phonons (aka *phononics*) is opening up a new technological frontier with a potential impact that could match that of electronics almost half a century ago. Indeed a rival field, photonics, is gathering similar momentum. Looking closely, phononics encompass a range of interconnected disciplines, usually labeled in terms of the type of host "material" that provides the medium for phononic wave propagation. These include *phononic crystals*, *phononic metamaterials*, *crystalline materials* and *periodic structures*. The application domains that these phononic materials are impacting, with increasing promise, range from vibration isolation in MEMS components, through frequency sensing in RF communications, to nano-scale thermal transport control in semiconductors. With the recent advent of metamaterials, exotic applications are now added to the list such as acoustic cloaking and superlensing. The interaction of mechanical waves with their optical counterpart in a lattice, i.e., optomechanics, is opening up yet another barrage of opportunities especially in telecommunications.

Phononics 2011 provides a unique avenue for dissemination and exchange of knowledge in all the themes mentioned previously. In particular, the conference is divided into the following topical themes:

(1) Phononic crystals,

(2) Phononic metamaterials,

(3) Wave propagation in periodic structures,

(4) Nanoscale phonon transport,

(5) Phononic MEMS and RF applications,

(6) Optomechanics,

(7) Fabrication and characterization for phononics

The number of abstracts submitted to the conference exceeded 180, including over 60 distinguished invited speakers, and represent a large number of nations from across the globe. The figure below captures the geographical distribution of the most recent visitors to the conference website (in April 2011). Furthermore, the *Felix Bloch Lecture* is being inaugurated at *Phononics 2011* as a named lecture to honor researchers who have made outstanding contributions to the field. More information on the Felix Bloch lecture and this year's lecturer is available in a separate brochure. For more information on the conference and the participants, please visit the conference website at: *www.phononics2011.org*.

Courtesy: Web-Stat.com

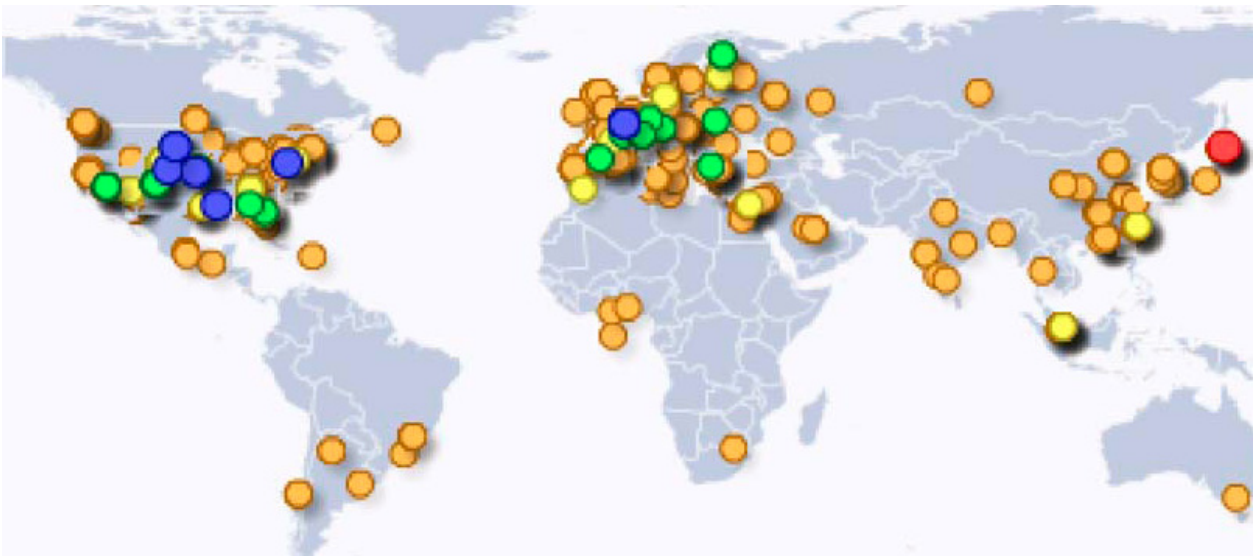

Visits to *www.phononics.org* from across the globe

Conference Organizers and Committees

Conference Chairs:

Ihab El-Kady
Sandia National Laboratories / University of New Mexico (USA)

Mahmoud I. Hussein
University of Colorado at Boulder (USA)

International Organizing Committee (IOC):

Chiara Daraio
California Institute of Technology (USA)
Abdelkrim Khelif
Georgia Institute of Technology / CNRS (USA/France)
Roy H. Olsson III
Sandia National Laboratories (USA)
Peter Rakich
Sandia National Laboratories (USA)
Massimo Ruzzene
Georgia Institute of Technology (USA)
Jose Sanchez-Dehesa
Univ. Politecnica de Valencia (Spain)
Tsung-Tsong Wu
National Taiwan University (Taiwan)

Technical Program Committee (TPC):

Mehmet F. Su
University of New Mexico (USA)
Osama R. Bilal
University of Colorado at Boulder (USA)
Ryan M. Camacho
Sandia National Laboratories (USA)
Bruce L. Davis
University of Colorado at Boulder (USA)
Bernardo G. Farfan
University of New Mexico (USA)
Zayd C. Leseman
University of New Mexico (USA)
Charles M. Reinke
Sandia National Laboratories (USA)

Local Organizing Committee (LOC) (Prior to Venue Change):

Tamer Elnady
Ain Shams University (Egypt)
Sherif Sedky
American University in Cairo (Egypt)
Ehab Abdel Rahman
American University in Cairo (Egypt)
Mohammed El-Beltagy
Cairo University (Egypt)
Amal Esawi
American University in Cairo (Egypt)
Hany Hamdy
Beni-Suef University (Egypt)
Hanadi Salem
American University in Cairo (Egypt)

Scientific Advisory Board (SAB):

A. Adibi (USA)
A. Balandin (USA)
A. El-Sabbagh (Egypt)
A. Esawi (Egypt)
A. J. H. McGaughey (USA)
A. Khelif (France/USA)
A. N. Norris (USA)
A. S. Phani (USA)
B. Bonello (France)
B. Djafari-Rouhani (France)
B. Li (Singapore)
C. Daraio (USA)
C. Hladky-Hennion (France)
C. Reinke (USA)
C.T. Chan (USA)
D. Donadio (Germany)
E. Abdel Rahman (Egypt)
E. N. Economou (Greece)
E. Shaner (USA)
F. McCormick (USA)
G. Bogart (USA)
G. Cole (Austria)
G. Fytas (Germany/Greece)
G.- K. Hu (China)
G. M. Hulbert (USA)
G. Orris (USA)
G. Piazza (USA)
H. Hamdy (Egypt)
H. Salem (Egypt)
H. Tang (USA)
I. El-Kady (USA)
I. Maasilta (Finland)
I. Psarobas (Greece)
J. Christensen (Spain)
J. H. Page (Canada)
J. Li (Hong Kong)
J. S. Jensen (Denmark)
J. Sanchez-Dehesa (Spain)
J. Vasseur (France)
J. Wen (China)
K. Maute (USA)
K. P. Pipe (USA)
L-. W. Cai (USA)
M. Aspelmeyer (Austria)
M. Descour (USA)
M. El-Beltagy (Egypt)
M. I. Hussein (USA)
M. J. Leamy (USA)
M. L. Dunn (USA)
M. Lipson (USA)
M. M. Farag (Egypt)
M. Ruzzene (USA)
M. Sigalas (Greece)
M. Spector (USA)
M. Su (USA)
O. Painter (USA)
O. Sigmund (Denmark)
P. Deymier (USA)
P. E. Hopkins (USA)
P. Rakich (USA)
R. Camacho (USA)
R. H. Olsson (USA)
S. A. Cummer (USA)
S. Benchabane (France)
S. Nemat-Nasser (USA)
S. Sedky (Egypt)
S. Thorne (USA)
T. Carmon (USA)
T. Elnady (Egypt)
T. Huang (USA)
T. Kippenberg (Switzerland)
T. T. Wu (Taiwan)
U. Jonas (Greece)
V. Laude (France)
V. Romero-Garcia (Spain)
W. Akl (Egypt)
X. Zhang (USA)
Y. Pennec (France)
Z. C. Leseman (USA)

Sponsors

The conference chairs and organizing committee members wish to acknowledge and express their deepest gratitude towards the following institutions for their financial support:

- **Sandia National Laboratories, USA**
- **Office of Naval Research, USA**
- **National Science foundation, USA**
- **FEI Electron Microscopes, USA**

The conference organizers also wish to express their appreciation to the following institutions for their direct support to the efforts of the conference chairs:

- **Sandia National Laboratories, USA**
- **University of Colorado at Boulder, USA**
- **University of New Mexico, USA**

Furthermore, the conference organizers are grateful to the following institutions for their honorary and technical sponsorship in support of the conference efforts:

- **Sandia National Laboratories, USA**
- **University of Colorado at Boulder, USA**
- **University of New Mexico, USA**
- **National Taiwan University, Taiwan**
- **Universidad Politecnica de Valencia, Spain**
- **Centre National de la Recherche Scientifique, France**
- **Georgia Institute of Technology, USA**
- **California Institute of Technology, USA**
- **American University in Cairo, Egypt**
- **Ain Shams University, Egypt**
- **Cairo University, Egypt**
- **Beni Suef University, Egypt**
- **Acoustical Society of Egypt, Egypt**

Acknowledgments

The conference chairs would like to express their deepest gratitude to the members of the International Organizing Committee for their efforts in inviting speakers and their invaluable feedback on the organization of the conference and its structuring.

We would also like to acknowledge the tremendous effort and support of the Technical Program Committee members in the organization of the technical program.

We further wish to express our sincerest gratitude to members of Local Organizing Committee for their efforts especially at the early stages prior to the change of venue from Sharm El-Sheikh, Egypt to Santa Fe, New Mexico, USA.

In addition, we wish to voice our deepest appreciation to our sponsoring organizations for the financial and technical support of the conference efforts.

We would like to extend our warmest thanks to all the conference participants. The enthusiasm they showed and their early confirmation to attend was very important for the successful launch of this new conference.

Moreover, we wish to acknowledge the efforts of those individuals who went out of their way to ensure the success of the conference well beyond the call of duty. As such we would like to voice our gratitude to Dr. Mehmet F. Su, Chair of the Technical Program Committee for his tremendous efforts pertaining to the conference website and electronic abstract submissions. Prof. Zayd C. Leseman, Co-Chair of the Technical Program Committee for his efforts in pursuing prospective sponsors and his tremendous help in the review of the final conference program. Last but certainly not least we wish to thank Ms. Linda Wood, Department of Program and Business Development, Sandia National Laboratories for her pivotal efforts in securing the conference venue and facilities, and her dedication to ensuring that the finest details are addressed and well taken care of.

Finally, we would like to thank our respective spouses Inas El-Shazly and Alaa Ahmed for their continuous emotional support and their patience during long hours that have been spent on ensuring a successful conference especially after the unforeseen venue change and the tremendous effort that went in relocating the conference.

Yours sincerely,

Ihab El-Kady & Mahmoud I. Hussein
Albuquerque and Boulder, April 2011

Santa Fe, New Mexico

History of Santa Fe

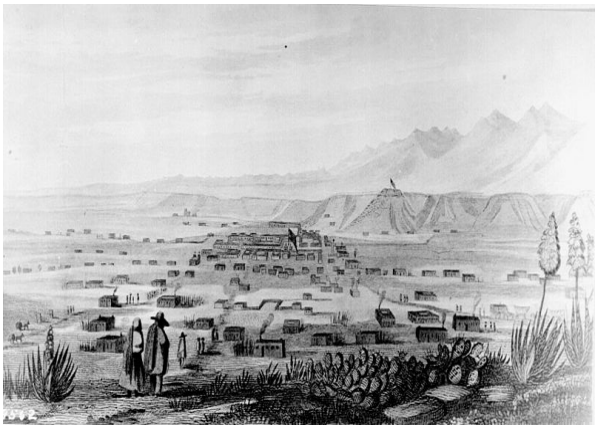

Santa Fe, New Mexico is the third oldest surviving American city founded by European colonists and has a very rich and exciting history. This region was originally settled by a number of Pueblo Indian villages that were founded between 1050 and 1150 AD. In the year 1540, Spanish colonists under Francisco Vásquez de Coronado claimed "The Kingdom of New Mexico" under the Spanish Crown, and the capital of Santa Fe was established in 1598. Shortly after this, in the year 1610, the famous San Miguel Chapel was constructed, making it the oldest standing church in the United States. Turbulent times followed, with a number of Pueblo revolts and attempts to drive out the Spanish. This region remained under Spanish control until the Mexican War or Independence in 1810, when Mexico gained control of the city. In 1846, the United States declared war on Mexico and gained New Mexico through the treaty of Guadalupe Hidalgo. In the year 1912, New Mexico, with Santa Fe as its capital, became the 47th state to join the union.

Santa Fe, the capital of New Mexico, is located approximately 300 miles south of the Colorado boarder. With an elevation of 7,199 ft, Santa Fe is the highest state capital in the United States, as well as the oldest. The local population of about 72,000 makes Santa Fe the fourth largest city in New Mexico, and it continues to grow. With Santa Fe Institute, Sandia National Laboratories, Los Alamos National Laboratories in close proximity, Santa Fe routinely hosts a number of well-renowned technical conferences. Its rich history and emphasis on artistic culture also make it a very popular tourist destination (Source Wikipidia.com).

Santa Fe's Art

Santa Fe has been home to many famous artists, including painter Georgia O'Keeffe and photographer Eliot Porter. Much of the art showcased in the city's hundreds of galleries focuses on Santa Fe's breathtaking landscapes, Spanish influence, and southwestern style. Santa Fe is also home to the Santa Fe opera, a major performing arts venue that has hosted a myriad of plays, festivals, and concerts.

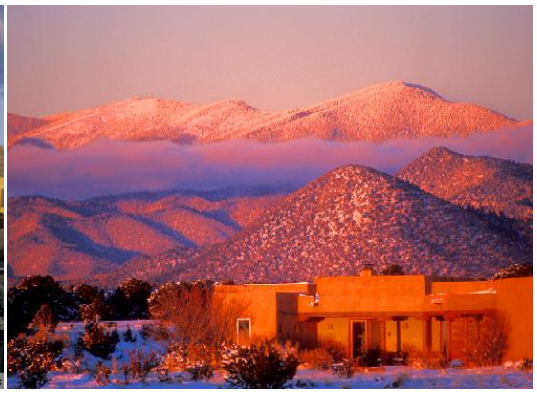

Economy and Tourism

Tourism accounts for the second largest percentage of Santa Fe's economy. With its gorgeous mountains and breathtaking views, much of the tourism in Santa Fe revolves around nature and outdoor activities such as skiing, hiking, camping, and rafting. Host to thousands of galleries, Santa Fe is also famous for its emphasis on the arts, being named the second largest art center in the United States after New York City.

Transportation

Air: The closest international airport to Santa Fe is the Albuquerque Sunport (ABQ) and is approximately two hours away by shuttle. Santa Fe is home to a smaller airport (SAF), so connecting flights may be available.

Bullet Train: The Rail Runner Express runs between downtown Albuquerque and Santa Fe, and a cab can then be taken from the depot in Santa Fe to the conference hotel. Please visit http://www.nmrailrunner.com for the Rail Runner website.

Shuttle: There are several reliable shuttles that run between the Albuquerque Sunport and Santa Fe, and the cost is approximately $25/person each way. Please visit http://www.sandiashuttle.com for the Sandia Express shuttle service website.

Day 0: May 29th Sunday

17:00	**Registration**
19:30	**Reception**
21:00	**Adjourn**

Day 1: May 30th Monday

7:30	**Registration**	
8:00	**Opening Ceremony**	
Serial Sessions	**Phononic Crystals**	
8:30	**J.H. Page (Plenary)**	
9:00	**M. Sigalas (Plenary)**	
9:30	**B. Bonello (Keynote)**	
9:55	**B. Djafari-Rouhani (Keynote)**	
10:20	**Coffee**	
10:45	**V. Laude (Keynote)**	
11:10	**C. Hladky-Hennion (Keynote)**	
11:35	**T.T. Wu (Org. Colloquium)**	
12:00	**M.I. Hussein (Org. Colloquium)**	
12:25	**Lunch**	
Serial Sessions	**Phononic Metamaterials**	
14:00	**A.N. Norris (Plenary)**	
14:30	**S.A. Cummer (Plenary)**	
15:00	**J. Christensen (Keynote)**	
15:25	**J. Li (Keynote)**	
15:50	**G. Orris (Keynote)**	
16:15	**S. Sanchez-Dehesa (Org. Colloquium)**	
16:40	**A. Khelif (Org. Colloquium)**	
17:05	**Coffee**	
Parallel Sessions:	**Phononic Crystals**	**Phononic Metamaterials**
17:30	**O. Wright (Invited Oral)**	**A. Krokhin (Invited Oral)**
17:50	**G.A. Gazonas (Invited Oral)**	**D. Torrent (Invited Oral)**
18:10	**Y. Achaoui (Contrib. Oral)**	**A. Spadoni (Contrib. Oral)**
18:25	**P.H. Otsuka (Contrib. Oral)**	**R. Pourabolghasem (Contrib. Oral)**
18:40	**N.-K. Kuo (Contrib. Oral)**	**B. Assouar (Contrib. Oral)**
18:55	**R. Lucklum (Contrib. Oral)**	**Y. Wang (Contrib. Oral)**
19:10	**Adjourn**	

Day 2: May 31st Tuesday

8:00	**Announcements**	
Serial Sessions	**Periodic Structures**	
8:30	**P. Deymier** (Plenary)	
9:00	**G.M. Hulbert** (Plenary)	
9:30	**J.S. Jensen** (Keynote)	
9:55	**J. Wen** (Keynote)	
10:20	**Coffee**	
10:45	**M.J. Leamy** (Keynote)	
11:10	**A.S. Phani** (Keynote)	
11:35	**V. Romero-Garcia** (Keynote)	
12:00	**C. Daraio** (Org. Colloquium)	
12:25	**Lunch**	
Serial Sessions	**Phonon Transport**	
14:00	**B. Li** (Plenary)	
14:30	**A. Balandin** (Plenary)	
15:00	**A.J.H. McGaughey** (Keynote)	
15:25	**K.P. Pipe** (Keynote)	
15:50	**P.E. Hopkins** (Keynote)	
16:15	**I. Maasilta** (Keynote)	
16:40	**I. El-Kady** (Org. Colloquium)	
17:05	**Coffee**	
Parallel Sessions:	**Periodic Structures**	**Phonon Transport**
17:30	**M.M. Neves** (Invited Oral)	**M. Maldovan** (Invited Oral)
17:50	**O. Umnova** (Invited Oral)	**H. Elsayed-Ali** (Invited Oral)
18:10	**N. Swinteck** (Contrib. Oral)	**K. Muralidharan** (Contrib. Oral)
18:25	**V. Tournat** (Contrib. Oral)	**B.L. Davis** (Contrib. Oral)
18:40	**H. Estrada** (Contrib. Oral)	**E. Chavez** (Contrib. Oral)
18:55	**M. Zubtsov** (Contrib. Oral)	**M.C. George** (Contrib. Oral)
19:10	**Adjourn**	

Day 3: June 1st Wednesday

8:00	**Announcements**	
Serial Sessions	**Optomechanics**	
8:30	**O. Painter (Plenary)**	
9:00	**H. Tang (Plenary)**	
9:30	**T. Carmon (Keynote)**	
9:55	**T. Kippenberg (Keynote)**	
10:20	**Coffee**	
10:45	**S. Benchabane (Keynote)**	
11:10	**G. Cole (Keynote)**	
11:35	**P. Rakich (Org. Colloquium)**	
12:00	**R. Camacho (Org. Colloquium)**	
12:25	**Lunch**	
Parallel Sessions	**Optomechanics**	**Fab Characterization & Applications**
14:00	**C.W. Wong (Invited Oral)**	**B. Kim (Invited Oral)**
14:20	**M.S. Kang (Invited Oral)**	**M. Ziaei-Moayyed (Invited Oral)**
14:40	**C.M. Reinke (Invited Oral)**	**M.F. Su (Invited Oral)**
15:00	**Poster Session***	
17:05	**Coffee**	
17:30	**Sia Nemat-Nasser (Felix Bloch Lecture)**	
18:30	Free Time	
19:00	**Banquet (Phononics 2013 Announcement)**	
22:00	**Adjourn**	

*Poster Session:

1- S. Alaie
2- G. Bastian
3- O.R. Bilal
4- S. Bringuier
5- C.-T. Bui
6- A.L. Chen
7- W.S. Chang
8- M. Frazier
9- D.F. Goettler
10- M.V. Golub
11- Q. Guo
12- T.J. Isotalo
13- H. Ketata
14-G. Kevin L. Manktelow
15- Y. Pennec
16- O. Poncelet
17 & 18- V. Romero-Garcia (2)
19- M. Senesi
20- A. Tomchek
21- V. Tournat
22- Y.-S. Wang
23- A. Young
24- X.-Z. Zhou
25- G. Zhu

Day 4: June 2nd Thursday

8:00	**Announcements**	
Serial Sessions	**Fabrication and Characterization for Phononics**	
8:30	**G. Bogart (Plenary)**	
9:00	**G. Piazza (Keynote)**	
9:25	**G. Fytas (Keynote)**	
9:50	**Z.C. Leseman (Org. Colloquium)**	
10:15	**Coffee**	
Serial Sessions	**Phononic MEMS and RF Applications**	
10:40	**A. Adibi (Plenary)**	
11:10	**Y. Pennec (Keynote)**	
11:35	**J. Vasseur (Keynote)**	
12:00	**I. Psarobas (Keynote)**	
12:25	**R.H. Olsson (Org. Colloquium)**	
12:50	**Lunch**	
Parallel Sessions:	**Phon. Crystals & Phon. Transport**	**Periodic Structures**
14:00	**S. Alaie (Contrib. Oral)**	**A. Leonard (Contrib. Oral)**
14:15	**R.A. Wildman (Contrib. Oral)**	**G. Theocharis (Contrib. Oral)**
14:30	**M.V. Golub (Contrib. Oral)**	**V.J. Sánchez-Morcillo (Contrib. Oral)**
14:45	**F. Scarpa (Contrib. Oral)**	**G. Wang (Contrib. Oral)**
15:00	**R.J. Magyar (Contrib. Oral)**	**Y. Xiao (Contrib. Oral)**
15:15	**M. Blair (Contrib. Oral)**	**S. Chen (Contrib. Oral)**
15:30	**Coffee**	
Parallel Sessions:	**Phonon Transport**	**Fabrication and Characterization**
15:55	**P.-O. Chapuis (Contrib. Oral)**	**T.J. Isotalo (Contrib. Oral)**
16:10	**M. C. George (Contrib. Oral)**	**D.F. Goettler (Contrib. Oral)**
16:25	**M. Prunnila (Contrib. Oral)**	**D. Lanzillotti-Kimura (Contrib. Oral)**
16:40	**Adjourn**	

1st International Conference on Phononic Crystals, Metamaterials & Optomechanics

Sunday: May 29	Detailed Program Information
Registration (Promenade)	**5:00pm - 7:30 pm**
Reception (Pool)	**7:30 pm - 9:00 pm**
Adjourn	**9:00 PM**

Monday: May 30 Detailed Program Information

Registration (Promenade)	**7:30 am - 12:00 pm**
Opening Ceremony (Mesa BR)	**8:00 am - 8:30 am**
Track 1: Phononic Crystals	
Session: 1 (Mesa Ballroom)	**8:30 am - 10:20 pm**
Session Chair: T. T. Wu	
Author: J.H. Page	**Category: Plenary Talk**
Paper #: 0109	**Time:** 8:30 am -9:00 am
Title: Ultrasonic Wave Transport in Phononic Crystals	
Abstract: *Ultrasonic experiments on phononic crystals provide a powerful method for investigating the profound effects of periodic structure on wave propagation. We summarize recent progress that has been achieved by combining experiments with multiple scattering theory and FDTD calculations to study bandgap, negative refraction and focusing phenomena.*	
Author: M. Sigalas	**Category: Plenary Talk**
Paper #: 0061	**Time:** 9:00 am -9:30 am
Title: Phononic Crystal Sensors	
Abstract: *Numerical studies of phononic crystals for sensors applications are presented. The sensitivities of the structures on their parameters are studied. Particular attention was given in structures that can be probed with both electromagnetic and elastic waves.*	
Author: B. Bonello	**Category: Keynote Talk**
Paper #: 0024	**Time:** 9:30 am -9:55 am
Title: Phononic Crystals to Control the Propagation of Elastic Waves: Recent Advances	
Abstract: *In this paper, we briefly review the recent advances made worldwide to control the propagation of elastic waves using phononic crystals (PCs). We show how new effects, including the opening of band gaps in silicon PC plates and the negative refraction of elastic waves, could be at the origin of new Micro ElectroMechanical Systems compatible with CMOS processes.*	

Author: B. Djafari-Rouhani	**Category: Keynote Talk**
Paper #: 0059	**Time:** 9:55 am -10:20 am
Title: Engineering of the Band gaps and transmissions in Phononic and phoxonic Crystal Slabs and Waveguides	
Abstract: *We report on our theoretical works about the engineering of band structures in phononic as well as dual phononic-photonic slabs and strips waveguides. Besides the conventional structure made of a periodic array of holes in a plate, we discuss the more recent geometry of pillars on a membrane or on a substrate. We discuss the best phoxonic structures displaying dual phononic-photonic band gaps and slow modes.*	
Coffee Break (Promenade)	**10:20 am - 10:45 am**
Track 1: Phononic Crystals	
Session: 2 (Mesa Ballroom)	**10:45 am - 12:25 pm**
Session Chair: J. H. Page	
Author: V. Laude	**Category: Keynote Talk**
Paper #: 0087	**Time:** 10:45 am -11:10 am
Title: Evanescent Bloch Waves in Phononic Crystals: Complex Band Structure, Losses, and Guidance	
Abstract: *The complex band structure of evanescent Bloch waves in phononic crystals is elucidated by formulating an eigenvalue problem for the wavevector versus the frequency. It is used to explore the effects of material losses and the phononic crystal guidance mechanism. The method, originally formulated for plane waves, is extended to finite element models.*	
Author: C. Hladky-Hennion	**Category: Keynote Talk**
Paper #: 0056	**Time:** 10:10 am -11:35 am
Title: Negative refraction of elastic waves in 2D phononic crystals	
Abstract: *Negative refraction of elastic waves is evidenced in a two-dimensional phononic crystal (PC), made of a triangular lattice of steel rods embedded in epoxy. Experiments are carried out on a prism shaped PC inserted inside an epoxy block. The influence of different parameters is discussed in terms of image reconstruction.*	

Author: T. T. Wu	**Category: Org. Colloquium**
Paper #: 0127	**Time:** 11:35 am -12:00 pm
Title: Focusing and Waveguiding of Lamb Waves in Phononic Plates	
Abstract: *In this talk, focusing of Lamb waves using the GRIN PC will be introduced first, and then followed by a concept demonstration of utilizing the focusing feature to compress Lamb waves into a phononic plate waveguide. Results of the study showed that beam width of the lowest anti-symmetric Lamb wave in a silicon PC thin plate can be compressed efficiently and fitted into the tungsten/silicon PC plate waveguide over a wide range of frequency.*	

Author: M. I. Hussein	**Category: Org. Colloquium**
Paper #: 0182	**Time:** 12:00 am -12:25 pm
Title: Multiscale Dispersive Design: A Building Blocks Approach to Phononics	
Abstract: *When infinite in extent, spatial periodicity constitutes a periodic "material". When truncated to finite dimensions, a periodic "structure" is formed. Between the two entities there is an abundance of opportunities for shaping a desired dynamical response. In this work we will re-visit the concept of Multiscale Dispersive Design and use it towards the exploration of new avenues in phononics.*	

Lunch Break (Chamisa)	**12:25 pm - 2:00 pm**
Track 2: Phononic Metamaterials	
Session: 3 (Mesa Ballroom)	**2:00 pm - 5:05 pm**
Session Chair: M. Spector	
Author: A. N. Norris	**Category: Plenary Talk**
Paper #: 0037	**Time:** 2:00 pm -2:30 pm
Title: Metal Water: A Metamaterial for Acoustic Cloaking	
Abstract: *A generic metamaterial is described that is suitable for making acoustic cloaking devices. The fundamental property is that it mimics the acoustic properties of water, yet can be modified to display anisotropic elastic properties suitable for cloaking. It has the important property that the amount of void space is conserved: a "conservation of cloaked space".*	

Author: S. A. Cummer	**Category: Plenary Talk**
Paper #: 0068	**Time:** 2:30 pm -3:00 pm
Title: Phononic Metamaterials for Transformation Acoustics Applications	
Abstract: *We review the detailed development and derivation of the concept of transformation acoustics and demonstrate several approaches for engineering materials with the acoustic properties needed to realize transformation acoustics devices.*	

Author: J. Christensen	**Category: Keynote Talk**
Paper #: 0144	**Time:** 3:00 pm -3:25 pm
Title: Perforated acoustic metamaterials	
Abstract: *In this presentation we focus on perforated plates, which is governing the study of enhanced acoustic transmission through subwavelength apertures and in addition supports metamaterial typical phenomena like perfect imaging, negative refraction such as full attenuation of sound . We will discuss both theoretical and experimental results related to these items.*	

Author: J. Li	**Category: Keynote Talk**
Paper #: 0132	**Time:** 3:25 pm -3:50 pm
Title: Transformation Acoustics Media with Periodically Layered Structures	
Abstract: *Periodically layered structures have been used to construct acoustic superlenses and hyperlenses as precursors for transformation acoustics. With the transformation approach, we can now investigate the bandwidth and relationship between an acoustic hyperlens and superlens and construct transformation media through bending periodically layered structure.*	

Author: G. Orris	**Category: Keynote Talk**
Paper #: 0135	**Time:** 3:50 pm -4:15 pm
Title: Impedance Matching for Aqueous Inertial Metafluid Devices	
Abstract: *Several interesting metafluid devices have been investigated for use at frequencies in the low tens of kilohertz, including gradient index lenses, directional antennas and tuneable scattering elements. For 3D or orthotropic devices whose operating frequencies are less than a few 10's of kHz additional and significant practical issues can arise for inertial metafluids: dynamic impedance matching, mass and volume.*	

Author: J. Sanchez-Dehesa	**Category: Org. Colloquium**
Paper #: 0140	**Time:** 4:15 Pm -4:40 Pm
Title: Applications of Metafluids based on Phononic Crystals	
Abstract: *Acoustic metamaterials or metafluids based on the homogenizat ion of periodic distributions of sound scatterers (phononic crystals) are reviewed. It will be shown that periodically microstructured solids effectively behave like fluidlike materials with dynamical mass anisotropy. Also, it will be shown that the acoustic refractive index can be locally tailored in order to get molding of the sound waves. Applications of these types of metafluids as acoustic cloaks, gradient index refractive lenses, perfect absorbers and radial sonic crystal will be reported.*	
Author: A. Khelif	**Category: Org. Colloquium**
Paper #: 0139	**Time:** 4:40 pm -5:05 pm
Title: Locally resonant structures for low frequency surface acoustic band gaps	
Abstract: *We present in this paper a theoretically and experimentally study of the propagation of surface acoustic waves in a two-dimensional array of cylindrical pillars on the surface of a semi-infinite substrate. Low-frequency, markedly lower than those expected from the Bragg mechanism, band gaps were demonstrated.*	
Coffee Break (Promenade)	**5:05 pm - 5:30 pm**
Parallel Sessions	
Track 1: Phononic Crystals	
Session: 4 (Mesa Ballroom A)	**5:30 pm - 7:10 pm**
Session Chair: M. Sigalas	
Author: O. Wright	**Category: Invited Oral**
Paper #: 0084	**Time:** 5:30 pm -5:50 pm
Title: Dynamic Imaging of Gigahertz Phonons on Phononic Crystal Slabs	
Abstract: *Surface phonon propagation on microscopic phononic crystal slabs of Si is dynamically imaged in two dimensions at frequencies up to 1 GHz by an ultrafast optical technique. The acoustic dispersion relations obtained by spatial and temporal Fourier transforms reveal stop bands and the eigenmode patterns. Phonon guiding and confinement in phononic crystal waveguides and cavities are also presented.*	

Author: G. A. Gazonas	**Category: Invited Oral**
Paper #: 0149	**Time:** 5:50 pm -6:10 pm
Title: Resonance in m-layered Goupillaud-type Elastic Media	
Abstract: *Explicit analytical and recursive stress solutions and corresponding natural frequencies are derived for an m-layered Goupillaud-type elastic medium from a coupled firstorder system of difference equations using z-transform methods. The exact solutions can serve to verify computational methods for modeling wave propagation phenomena such as resonance and bandgap formation in periodic media.*	

Author: Y. Achaoui	**Category: Contrib. Oral**
Paper #: 0116	**Time:** 6:10 pm -6:25 pm
Title: Locally resonant and Bragg band gaps for surface acoustic waves	
Abstract: *We investigate the propagation of surface acoustic waves in a square lattice phononic crystal of cylindrical pillars on an anisotropic substrate. It is shown that the propagation of surface acoustic phonons is prohibited in two distinct frequency ranges. We identify two mechanisms responsible for band gaps, i.e. local resonances and Bragg diffraction, and point out the difference between them.*	

Author: P. H. Otsuka	**Category: Contrib. Oral**
Paper #: 0085	**Time:** 6:25 pm -6:40 pm
Title: Observation and Simulation of Surface Acoustic Waves in Phononic Crystals	
Abstract: *We present an analysis of surface acoustic waves propagating in a microscopic phononic crystal waveguide consisting of a silicon crystal containing a square array of holes. Experiments are performed using an ultrafast optical method and the results are compared with an FEM simulation.*	

Author: N. -K. Kuo	**Category: Contrib. Oral**
Paper #: 0106	**Time:** 6:40 pm -6:55 pm
Title: Demonstration of Ultra High Frequency Fractal Air/Aluminum Phononic Crystalsl	
Abstract: *This work presents, for the first time, the design and the experimental demonstration of an air/aluminum nitride (AlN) phononic band gap (PBG) structure patterned in a fractal fashion which exhibits two frequency stop bands for symmetric lamb waves respectively at 900 MHz (bandwidth of 11%) and 1.075 GHz (bandwidth of 13.5%) with a maximum acoustic attenuation of 45 dB.*	

Author: R. Lucklum	**Category: Contrib. Oral**
Paper #: 0065	**Time:** 6:55 pm -7:10 pm
Title: Liquid Sensor Utilizing Phononic Crystals	
Abstract: *A phononic crystal device is investigated as a sensor platform combining bandgap engineering with resonant transmission. We compare several approaches: a one-dimensional arrangement with a thin liquid analyte layer, two-dimensional phononic crystals with and without symmetry reduction and incidence directions normal and perpendicular to the plate.*	

Track 2: Phononic Metamaterials

Session: 5 (Mesa Ballroom C)	**5:30 pm - 7:10 pm**
Session Chair: J. Sanchez-Dehesa	
Author: A. Krokhin	**Category: Invited Oral**
Paper #: 0021	**Time:** 5:30 pm -5:50 pm
Title: Narrow Fluid Channel as a Metamaterial Sound Absorber	
Abstract: *Abnormally high level of absorption has been observed for sound waves propagating through a narrow water channel clad between two metal plates. Absorption is due to resonant excitation of Rayleigh waves on the both metal surfaces. These waves may either produce strong turbulent motion in a viscous fluid or radiate its energy into the metal, giving rise to deep minima in the transmission spectrum.*	

Author: D. Torrent	**Category: Invited Oral**
Paper #: 0026	**Time:** 5:50 pm -6:10 pm
Title: Fabrication and Experimental Characterization of Anisotropic Fluid-Like Materials	
Abstract: *We report a method to obtain acoustic metamaterials or metafluids with cylindrically anisotropic mass density. The method uses a periodically corrugated structure embedded in a two dimensional waveguide. This structure represents a periodic multilayered fluid-fluid composite that, in the low frequency limit, behaves as a fluid-like metamaterial with mass anisotropy. Also, an experimental method to characterize these structures is presented, showing that the resonances in these closed structures can be used to derive the acoustic parameters of these metafluids.*	

Author: A. Spadoni	**Category: Contrib. Oral**
Paper #: 0091	**Time:** 6:10 pm -6:25 pm
Title: Phononic Transport in Structural Networks with Internal Resonances and Dissipation	
Abstract: *The transport of mechanical energy can be controlled with phononic crystals and acoustic meta-materials. The latter can designed to control wave fields with wavelengths much larger than the meta-material's inner structure. This presentation proposes the employ-ment of structural lattices and dissipation to improve the performance of meta-materials.*	
Author: R. Pourabolghasem	**Category: Contrib. Oral**
Paper #: 0150	**Time:** 6:25 pm -6:40 pm
Title: Phononic Band Structure of a Silicon Plate with Periodic Array of Cylindrical Metallic Pillars	
Abstract: *We investigate theoretically the phononic band structure in a 2D array of cylindrical pillars on the surface of a slab. Simulations are based on the finite element method (FEM) using tungsten pillars on silicon as the structure of interest. We show that the phononic structure supports band gaps and study the behavior of band structure with respect to lattice symmetry and geometrical parameters.*	
Author: B. Assouar	**Category: Contrib. Oral**
Paper #: 0063	**Time:** 6:40 pm -6:55 pm
Title: Elastic Waves Propagation in a Locally Resonant Phononic Stubbed Plates	
Abstract: *We report in this study on the phonon transport in a locally resonant (LR) phononic stubbed plate. First, we will discuss the opening of LR band gap (BG) as function as the nature of the stubs and geometrical parameters to figure out the evolution of the BG. Second, we will discuss the waveguiding in such structures based on the calculation of the band structures and the transmission coefficient.*	
Author: Y. Wang	**Category: Contrib. Oral**
Paper #: 0115	**Time:** 6:55 pm -7:10 pm
Title: A wide band underwater strong acoustic absorbing material	
Abstract: *To meet the demand of underwater acoustic absorbing material for wide band strong acoustic absorption, we introduced network structure into locally resonant phononic crystal and fabricated a new kind of metal-polymer composites. Experimental and theoretical results showed that excellent underwater acoustic absorption capability and strong mechanical strength could be obtained simultaneously.*	
Adjourn	**7:10 PM**

Tuesday: May 30 Detailed Program Information

Registration (Promenade)	**7:30 am - 12:00 pm**
Announcements (Mesa BR)	**8:15 am - 8:30 am**
Track 3: Periodic Structures	
Session: 6 (Mesa Ballroom)	**8:30 am - 10:20 pm**
Session Chair: A. Norris	
Author: P. Deymier	**Category: Plenary Talk**
Paper #: 0073	**Time:** 8:30 am -9:00 am
Title: Phononic crystals with complete phase space properties	
Abstract: *We review and demonstrate properties of phononic crystals over their complete phase space, namely, spectral (ω-space), wave vector (k-space) and phase (φ-space) properties. The later two properties are applied to acoustic imaging with a phononic crystal flat lens and to inter-ference-driven acoustic Boolean logic.*	
Author: G.M. Hulbert	**Category: Plenary Talk**
Paper #: 0137	**Time:** 9:00 am -9:30 am
Title: Structurally-Inspired Phononic Metamaterials	
Abstract: *The distinction between materials and structures has blurred. The development of phononic metamaterials based upon novel structural systems is considered in this work. In particular, a Negative-Poisson Ratio (NPR) structure is used as the foundation for developing phononic metamaterials comprising a 'structural' framework of stiff material and a more compliant material that can dissipate energy.*	
Author: J. S. Jensen	**Category: Keynote Talk**
Paper #: 0055	**Time:** 9:30 am -9:55 am
Title: Optimal Design of Nonlinear Wave Devices	
Abstract: *The method of topology optimization is applied to wave propagation problems with nonlinearities. In the general case the iterative design procedure should be based on transient simulation of the wave propagation, but in the special case of non-instantaneous nonlinearities a steady-state optimization formulation can be applied. The latter case is exemplified by the design of a 1D optical diode.*	

Author: J. Wen	**Category: Keynote Talk**
Paper #: 0117	**Time:** 9:55 am -10:20 am

Title: Phononic Crystals with Applications to Sound and Vibration Control

Abstract: *A two dimensional binary locally resonant phononic crystal (PCs) has been fabricated and thoroughly analyzed. A lumped-mass method has been proposed as an efficient tool to calculate the band structure of PCs. The concept of PCs is introduced into the design of beam and plate structures, and the acoustic materials to improve their vibration and sound performance.*

Coffee Break (Promenade)	**10:20 am - 10:45 am**

Track 3: Periodic Structures

Session: 7 (Mesa Ballroom)	**10:45 am - 12:25 pm**
Session Chair: G. Hulbert	
Author: M.J. Leamy	**Category: Keynote Talk**
Paper #: 0071	**Time:** 10:45 am -11:10 am

Title: New Directions in the Analysis of Nano-Scale Phononic and Nonlinear Metamaterial Systems

Abstract: *This talk will focus on two directions being pursued by the author and his coworkers in the areas of (i) multi-scale modeling of phonon spectra and dispersion in reduced dimensional nano-scale systems (e.g., carbon nanotubes), and (ii) analysis of phononic wave propagation in nonlinear metamaterials using asymptotic techniques.*

Author: A. S. Phani	**Category: Keynote Talk**
Paper #: 0107	**Time:** 10:10 am -11:35 am

Title: Lattice Materials: A Unified Structural Mechanics Perspective

Abstract: *Lattice materials with a periodic microstructure are suitable for multifunctional structures with high specific stiffness, favourable acoustic and thermal properties. Their mechanical response under static and dynamic loads is considered from a unified structural mechanics perspective combining Bloch wave theory with Finite Element Method.*

Author: V. Romero-Garcia	**Category: Keynote Talk**
Paper #: 0101	**Time:** 11:35 am -12:00 pm
Title: Theoretical and Experimental Evidence of Evanescent Modes in Finite Sonic Crystals	
Abstract: *Evanescent modes in complete sonic crystals (SC) and SC with point defects are both theoretically and experimentally reported in this paper. Finite element method and an extension of the plane wave expansion with supercell approximation to solve the invers problem k(ω) is used to predict the evanescent modes. Experimental data and numerical results are in good agreement with the predictions.*	

Author: C. Daraio	**Category: Org. Colloquium**
Paper #: 0155	**Time:** 12:00 am -12:25 pm
Title: From Newton's Cradle to New Acoustic Crystals	
Abstract: *The bouncing beads of Newton's cradle fascinate children and executives alike, but their symmetric dance hides a complex dynamic behavior. By assembling grains in crystals we are developing new materials and devices with unique properties. We have constructed twodimensional systems that can redirect mechanical waves, and have developed new materials for absorbing vibrations and explosive blasts.*	

Lunch Break (Chamisa)	**12:25 pm - 2:00 pm**
Track 4: Phonon Transport	
Session: 8 (Mesa Ballroom)	**2:00 pm - 5:05 pm**
Session Chair: P. Deymier	
Author: Baowen Li	**Category: Plenary Talk**
Paper #: 0042	**Time:** 2:00 pm -2:30 pm
Title: Phononics: a new science and technology in processing information and controlling heat flow by phonons	
Abstract: *Heat due to lattice vibration is usually regarded as harmful for information processing. However, studies in recent years have changed this mindset. I will demonstrate via numerical simulation, theoretical analysis and experiments that, phonons, can be manipulated like electrons. They can be used to carry and process information. Basic phononic devices such as thermal diode, thermal transistor, thermal logic gate and thermal memory can be worked via nonlinear lattice and/or low dimensional nanostructures such as nanowire, nanotube, graphen nanoribbon etc. .*	
Author: A. Balandin	**Category: Plenary Talk**
Paper #: 0133	**Time:** 2:30 pm -3:00 pm
Title: Nanoscale Phonon Engineering: From Quantum Dots and Nanowires to Graphene and Topological Insulators	
Abstract: *I describe the nanoscale phonon engineering concept and its possible applications. Nanostructures offer new ways for controlling phonon transport via tuning phonon dispersion. Engineering the phonon spectrum can become as powerful a technique as the electron bandgap engineering, which revolutionized electronics. I outline recent examples of phonon engineering in quantum dot superlattices, nanowires, graphene ribbons and topological insulators. Particular attention is given to the phonon thermal transport in graphene and graphene's applications in thermal management.*	
Author: A. J. H. McGaughey	**Category: Keynote Talk**
Paper #: 0047	**Time:** 3:00 pm -3:25 pm
Title: Predicting Phonon Properties Using the Spectral Energy Density	
Abstract: *The spectral energy density technique for predicting phonon dispersion relations and relaxation times is presented. This technique, which uses atomic velocities obtained from a molecular dynamics simulation, incorporates the full anharmonicity of the atomic interactions. Results for a Lennard-Jones face centered cubic crystal are provided.*	

Author: K. P. Pipe	**Category: Keynote Talk**
Paper #: 0108	**Time:** 3:25 pm -3:50 pm
Title: Effect of Interface Roughness on Phonon Transport in Superlattices	
Abstract: *We present a boundary perturbation method to analyze phonon reflection, transmission, and mode conversion at a rough interface, and extend these calculations using a transfer matrix approach to examine the effects of interface roughness on phonon transport in multilayer thin films.*	

Author: P. E. Hopkins	**Category: Keynote Talk**
Paper #: 0080	**Time:** 3:50 pm -4:15 pm
Title: Phonon scattering at structurally variant boundaries	
Abstract: *Phonon scattering at boundaries drives the thermal transport in nanosystems. In this work, I will discuss various projects in which solid boundaries and interfaces are used to reduce the thermal conductance in nanosystems. These studies include cross plane thermal conductivity in periodic, porous silicon films and thermal boundary conductance across ran-dom and quantum dot roughened Si interfaces.*	

Author: I. Maasilta	**Category: Keynote Talk**
Paper #: 051	**Time:** 4:15 Pm -4:40 Pm
Title: Phononic Thermal Transport in Thin Nanoscale Membranes	
Abstract: *We have studied experimentally the thermal conductance of thin free-standing sili-con nitride membranes at sub-Kelvin temperatures as a function of membrane thickness be-tween 40 nm and 750 nm, using normal metal-insulator-superconductor (NIS) thermometry. Effects of dimensionality cross-over from 3D to 2D phonons are seen, however not all obser-vations follow the simplest theory.*	

Author: I. El-Kady	**Category: Org. Colloquium**
Paper #: 0183	**Time:** 4:40 pm -5:05 pm
Title: Thermal Conductivity Reduction in Phononic Crystals: Interplay of Coherent versus Incoherent Scattering	
Abstract: *In this talk we pose the question: Can the coherent scattering events brought by the periodicity of the Phononic Crystal (PnC) lattice affect the high frequency THz phonons that dominate heat transfer process? In other words, can PnC patterning be used to manipulate the thermal conductivity of a material? We report both theoretically and experimentally on the role of coherent versus incoherent scattering of phonons by a 2D PnC structure and the efficacy of each process in both the cross plane and in plane directions of the PnC lattice.*	

Coffee Break (Promenade)	**5:05 pm - 5:30 pm**

Parallel Sessions	
Track 3: Periodic Structures	
Session: 9 (Mesa Ballroom A)	**5:30 pm - 7:10 pm**
Session Chair: C. Daraio	
Author: M. M. Neves	**Category: Invited Oral**
Paper #: 0121	**Time:** 5:30 pm -5:50 pm
Title: Using classical FEM to predict the dynamical response of periodic devices in acoustic and vibration applications	
Abstract: *The task of predicting the dynamical response and tailoring wave propagation filters for practical frequency ranges is here presented. Finite element steady-state analysis is performed on periodic devices of finite length considering periodic distribution of materials, addition of masses to a tube and periodic curvatures. Validation obtained with prototypes, one for attenuation of axial vibration and other for sound propagation, is also mentioned.*	
Author: O. Umnova	**Category: Invited Oral**
Paper #: 0076	**Time:** 5:50 pm -6:10 pm
Title: An Effective Medium Model for Sonic Crystals with Composite Resonant Elements	
Abstract: *Using a self-consistent method, analytical expressions are derived for the parameters of an effective medium of composite scattering elements in air. The scatterers consist of concentrically arranged thin elastic shells and 4-slit cylinders. Predictions and data confirm that the use of coupled resonators results in a substantial insertion loss peak related to the modified resonance of the shell.*	

Author: N. Swinteck	**Category: Contrib. Oral**
Paper #: 0069	**Time:** 6:10 pm -6:25 pm
Title: Phase-controlling properties in phononic crystals	
Abstract: *We deliver a complete phase-space analysis of two well-studied PC systems to reveal the mechanisms behind phase-manipulation of propagating elastic waves in these composite structures. A triangular-array of steel cylinders embedded in a host matrix of methanol and a square-array of Polyvinylchloride cylinders embedded in a host matrix of air show band structures and equi-frequency contours (EFCs) with very different features, yet phase-control is possible in both systems. We find that phase-control depends on (1) whether or not the wave and group velocity vectors in the PC are collinear and (2) whether or not the excited Bloch waves in the PC have the same phase velocity. The results gathered in this study can be used to draw general conclusions about the reality of phase-control in many other types*	
Author: V. Tournat	**Category: Contrib. Oral**
Paper #: 0009	**Time:** 6:25 pm -6:40 pm
Title: Elastic waves in a three-dimensional hexagonal close-packed granular crystal: observation of rotational modes and nonlinear effects	
Abstract: *Noncohesive granular phononic crystals show peculiar features related to the elastic nonlinearities at the contacts and the rotational degrees of freedom of the grains. Evidence of rotational mode propagation and non reciprocity for nonlinear acoustic effects is found in a hexagonal close-packed crystal layer with a gravityinduced elasticity gradient.*	
Author: H. Estrada	**Category: Contrib. Oral**
Paper #: 0041	**Time:** 6:40 pm -6:55 pm
Title: The Role of Array Symmetry in the Transmission of Ultrasound through Periodically Perforated Plates	
Abstract: *We present angle-resolved experimental results on the role of array symmetry in the transmission features of periodically perforated plates. A very rich interplay between Fabry-Perot single-hole resonances, coherent scattering and plate vibration is found. By comparing several spatial hole arrangements, the effects of the geometry are disentangled from the contribution of plate vibrations.B.*	
Author: M. Zubtsov	**Category: Contrib. Oral**
Paper #: 0057	**Time:** 6:55 pm -7:10 pm
Title: EFIT Simulation of Ultrasonic Wave Propagation in Complex Microfluidic Structures	
Abstract: *The Elastodynamic Finite Integration Technique (EFIT) is used to simulate ultrasonic wave propagation in complex microfluidic structures comprising fluidic channels, phononic crystal structures and piezoelectric transducers. An EFIT computational math is combined with MATLAB coding. The viability of the approach is demonstrated.*	

Track 4: Phonon Transport	
Session: 10 (Mesa Ballroom C)	**5:30 pm - 7:10 pm**
Session Chair: B. Li	
Author: M. Maldovan	**Category: Invited Oral**
Paper #: 0156	**Time:** 5:30 pm -5:50 pm
Title: Understanding and Controlling High-Frequency Phonon Thermal Energy Transport in Nanostructures	
Abstract: *We present a novel theoretical approach based on the kinetic theory of transport processes to understand and accurately describe the transport of high-frequency phonon thermal energy in nanostructures over a broad range of temperatures and across multiple length scales, i.e. from nano to micro. Good agreement with experiments is obtained.*	
Author: H. Elsayed-Ali	**Category: Invited Oral**
Paper #: 0078	**Time:** 5:50 pm -6:10 pm
Title: Coherent phonons in polycrystalline bismuth film monitored by ultrafast electron diffraction	
Abstract: *The generation of coherent phonons in polycrystalline bismuth film is observed by ultrafast time-resolved electron diffraction. The dynamics of the diffracted intensities from the (110), (202), and (024) lattice planes show pronounced oscillations at 130□150 GHz. The anisotropy in the energy transfer rate of coherent optical phonons is discussed.*	

Author: K. Muralidharan	**Category: Contrib. Oral**
Paper #: 0104	**Time:** 6:10 pm -6:25 pm

Title: Nanostructured two-dimensional phononic materials

Abstract: *Phononic properties of nanostructured two-dimensional materials such as graphene and boron nitride (BN) sheets are calculated using the method of molecular dynamics. Nanophononic crystals composed of periodic array of holes in graphene exhibit Bragg scattering at non-cryogenic temperatures leading to reduction in thermal conductivity. The transport of phonons across non-periodic arrays of asymmetric holes in BN sheets is discussed in the context of scattering and non-linear effects that may lead to thermal rectification.*

Author: B. L. Davis	**Category: Contrib. Oral**
Paper #: 0174	**Time:** 6:25 pm -6:40 pm

Title: Reduction of Thermal Conductivity in Silicon Slabs by Unit Cell Nanostructuring

Abstract: *Just like unit cell structuring has seen much interest in phononic crystals for the control of sound and vibration, the same can be done at the nanoscale for the control of thermal properties. Here we present ideas for unit cell nanostructuring within thin silicon slabs for the purpose of reducing the thermal conductivity.*

Author: E. Chavez	**Category: Contrib. Oral**
Paper #: 0111	**Time:** 6:40 pm -6:55 pm

Title: Acoustic phonon relaxation rates in nanometer-scale membranes

Abstract: *The elastic continuum model is applied to analyse the acoustic phonon modes for single and threelayer membranes. The dispersion relations are computed using a numerical approach and are compared with experimental and theoretical results. These values are used to compute the rate of relaxation, considering a three-phonon Umklapp process.*

Author: M. C. George	**Category: Contrib. Oral**
Paper #: 0081	**Time:** 6:55 pm -7:10 pm

Title: Thermal conductance behavior of self-assembled lamellar block copolymer thin films

Abstract: *We measure the thermal conductance of both disordered and self-assembled lamellar polystyrene-block-poly(methyl methacrylate) copolymer films and compare the results to literature reports on thin homopolymer films and polymer brushes. We see a 150% increase in thermal conductivity for a single self-assembled PS-b-PMMA layer.*

Adjourn **7:10 PM**

Wednesday: June 1 Detailed Program Information

Registration (Promenade)	**7:30 am - 12:00 pm**
Announcements (Mesa BR)	**8:15 am - 8:30 am**
Track 5: Optomechanics	
Session: 11 (Mesa Ballroom)	**8:30 am - 10:20 pm**
Session Chair: S. Cummer	
Author: O. Painter	**Category: Plenary Talk**
Paper #: 0180	**Time:** 8:30 am -9:00 am
Title: Optomechanical Crystals	
Abstract: *Rapid advances have been made in the field of cavity optomechanics, in which the usually feeble radiation pressure force of light is used to manipulate (and precisely monitor) mechanical motion. These advances have moved the field from the multi-km interferometer of a gravitational wave observatory, to the optical table top, and now all the way down to a silicon microchip. In this talk I will describe these advances, and discuss our own work to realize radiation pressure within nanoscale structures in the form of photonic-phononic crystals (optomechanical crystals).*	
Author: H. Tang	**Category: Plenary Talk**
Paper #: 0138	**Time:** 9:00 am -9:30 am
Title: Integrated Transduction and Active Manipulation Methods for Nanoelectromechanical Systems	
Abstract: *This talk will discuss integrated NEMS transduction schemes that have been devel-oped by my research group. Methods for achieving active control and manipulation of nano-mechanical motion will be also presented.*	
Author: T. Carmon	**Category: Keynote Talk**
Paper #: 0181	**Time:** 9:30 am -9:55 am
Title: Mechanical Whispering-Gallery Modes	
Abstract: *We experimentally excite mechanical Whispering-Gallery resonances that are vibrating from 50 MHz to 12 GHz rates.*	

Author: T. Kippenberg	**Category: Keynote Talk**
Paper #: 0178	**Time:** 9:55 am -10:20 am
Title: Cooling of a Micromechanical Oscillator into the Quantum Regime	
Abstract: *Using optical sideband cooling, a micromechanical oscillator is cooled to a phonon occupancy below 10 phonons, corresponding to a probability of finding it in its quantum ground state more than 10% of the time.*	

Coffee Break (Promenade)	**10:20 am - 10:45 am**

Track 5: Optomechanics

Session: 12 (Mesa Ballroom)	**10:45 am - 12:25 pm**
Session Chair: O. Painter	
Author: S. Benchebane	**Category: Keynote Talk**
Paper #: 0086	**Time:** 10:45 am -11:10 am
Title: Phoxonic Crystals: a Review	
Abstract: *Periodically structured materials exhibiting simultaneous photonic and phononic band gaps offer unprecedented ways to tailor photon–phonon interactions. A review of the works reported on these materials, sometimes termed "phoxonic crystals", is presented before highlighting theoretical and experimental results demonstrating phoxonic band gaps in structures relying on guided elastic waves.*	
Author: G. D. Cole	**Category: Keynote Talk**
Paper #: 0157	**Time:** 10:10 am -11:35 am
Title: Cavity Quantum Optomechanics	
Abstract: *The overarching research objective of cavity quantum optomechanics is to investigate quantum effects of micro- and nanoscale systems and their implications for the foundations and applications of quantum physics. Our ultimate goal is to gain access to a completely new parameter regime for experimental physics with respect to both size and complexit.*	
Author: P. Rakich	**Category: Org. Colloquium**
Paper #: 0128	**Time:** 11:35 am -12:00 pm
Title: Fundamental Limits of Transduction Efficiency and Bandwidth in Nano-Optomechanics	
Abstract: *Through systematic examination of material and topological degrees of freedom in nano-optomechanical systems, we identify the fundamental barriers and opportunities for the creation of large photon-phonon coupling.*	

Author: R. Camacho	**Category: Org. Colloquium**
Paper #: 0130	**Time:** 12:00 pm -12:25 pm
Title: Mechanical Transduction in Periodic Media	
Abstract: *The possibility of increasing mechanical transduction efficiencies via periodic patterning of the material density is investigated. A 2D simulation suggesting low mechanical impedance over a relatively large bandwidths is presented.*	
Lunch Break (Chamisa)	**12:25 pm - 2:00 pm**
Parallel Sessions	
Track 5: Optomechanics	
Session: 13 (Mesa Ballroom A)	**2:00 pm - 3:00 pm**
Session Chair: P. Rakich	
Author: C. W. Wong	**Category: Invited Oral**
Paper #: 0146	**Time:** 2:00 pm -2:20 pm
Title: Strong Optomechanical Coupling in Slot-type Photonic Crystal Cavities	
Abstract: *Strong dispersive optomechanical coupling of an air-slot mode-gap photonic crystal cavity is demonstrated. The zero-point motion coupling rate can be as high as 2.56MHz. Optical and 10s of MHz mechanical frequency spectra are shown experimentally, supported by theory and numerical models.*	
Author: M. S. Kang	**Category: Invited Oral**
Paper #: 0093	**Time:** 2:20 pm -2:40 pm
Title: Forward Stimulated Light Scattering by Acoustic Resonances in Photonic Crystal Fiber	
Abstract: *Forward stimulated light scattering by transverse acoustic resonances tightly trapped in a photonic crystal fiber core is a recently reported nonlinear-optical optoacoustic phenomenon. The principles and characteristics of the scattering are described. Some potential applications are also discussed*	
Author: C. M. Reinke	**Category: Invited Oral**
Paper #: 0170	**Time:** 2:40 pm -3:00 pm
Title: Analysis of Optomechanical Forces in Nano-Photonic Waveguides	
Abstract: *We present a theoretical analysis of optomechanical forces in nano-scale photonic waveguides. In particular, we show that significant forces due to radiation pressure can be generated in dielectric slab and photonic crystal waveguides having sub-micron dimensions. We also investigate how such forces can be optimized for optomechanical transduction.*	

Track 6&7: Fabrication Characterization & Applications	
Session: 14 (Mesa Ballroom C)	**2:00 pm - 3:00 pm**
Session Chair: G. R. Bogart	
Author: B. Kim	**Category: Invited Oral**
Paper #: 0113	**Time:** 2:00 pm -2:20 pm
Title: Thermal Conductivity Reduction in Lithographically Patterned Single Crystal Silicon Phononic Crystal Structures	
Abstract: *In-plane thermal conductivity of lithography-based phononic crystals has been investigated. Sub-micron holes were lithographically patterned in a 500nm-thick single crystal silicon thin-film and the thermal conductivity was measured as low as 30 W/mK (at and slightly above room temperature, 20~80^{o}C), which is a 50% reduction even after accounting for the effect of volume reduction of the holes.*	
Author: M. Ziaei-Moayyed	**Category: Invited Oral**
Paper #: 0126	**Time:** 2:20 pm -2:40 pm
Title: Silicon Carbide Phononic Crystals for Communication, Sensing, and Energy Management	
Abstract: *We demonstrate design, fabrication, and characterization of silicon carbide phononic crystals used to confine energy in lateral overtone cavities in 2-3GHz range with high f.Q products in air. The SiC cavities are fabricated in a CMOS-compatible process with applications in communication systems, sensing, and thermal energy management*	
Author: M. Su	**Category: Invited Oral**
Paper #: 0169	**Time:** 2:40 pm -3:00 pm
Title: Designing High-Q Compact Phononic Crystal Resonators	
Abstract: *Phononic crystals provide a promising method of producing resonators with very high quality factors up to the theoretical limit possible in the host material. In this study we consider Silicon based solid-solid phononic crystal resonator designs with different lattices (simple cubic, hexagonal/triangular and honeycomb), number of inclusions and cavity shapes.*	

Poster Session (Chapel)	**3:00 pm - 5:05 pm**
Session Chair: I. El-Kady & M. I. Hussein	
Author: S. Alaie	**Category: Poster 1**
Paper #: 165	**Time:** 3:00 pm -5:05 pm
Title: Device Level Harmonic Finite Element Analysis of Phononic Crystals Operating at GHz Frequencies	
Author: G. Bastian	**Category: Poster 2**
Paper #: 0185	**Time:** 3:00 pm -5:05 pm
Title: Isotopically Enriched Semiconductor Superlattices for Thermoelectric Applications	
Author: O. R. Bilal	**Category: Poster 3**
Paper #: 0173	**Time:** 3:00 pm -5:05 pm
Title: Phononic Band Gap Optimization for Combined In-Plane and Out-of-Plane Waves	
Author: S. Bringuier	**Category: Poster 4**
Paper #: 0163	**Time:** 3:00 pm -5:05 pm
Title: Acoustic Logic Gates Implemented using a Phase Controlling Phononic Crystal	
Author: C.-T. Bui	**Category: Poster 5**
Paper #: 0050	**Time:** 3:00 pm -5:05 pm
Title: Temperature and Size Dependence of Thermal Conductivity in Single Crystal ZnO Nanowires	
Author: A.L. Chen	**Category: Poster 6**
Paper #: 0082	**Time:** 3:00 pm -5:05 pm
Title: Propagation of the Elastic Wave in One-dimensional Randomly Disordered Solid-liquid Phononic Crystals	
Author: W.S. Chang	**Category: Poster 7**
Paper #: 0038	**Time:** 3:00 pm -5:05 pm
Title: Nanoscale Tip Fabrication for Plasmon Induced Field- Enhancement	
Author: M. Frazier	**Category: Poster 8**
Paper #: 172	**Time:** 3:00 pm -5:05 pm
Title: Dissipative Effects in Acoustic Metamaterials	
Author: D.F. Goettler	**Category: Poster 9**
Paper #: 164	**Time:** 3:00 pm -5:05 pm
Title: nanoFIBrication of Phononic Crystals in Freestanding Membranes	
Author: M.V. Golub	**Category: Poster 10**
Paper #: 0018	**Time:** 3:00 pm -5:05 pm
Title: 2D Wave Propagation in Periodically Layered Composite Structures with Damages	
Author: Q. Guo	**Category: Poster 11**
Paper #: 0176	**Time:** 3:00 pm -5:05 pm
Title: Convergence of the Reduced Bloch Mode Expansion Method for Electronic Band Structure Calculations	
Author: T.J. Isotalo	**Category: Poster 12**
Paper #: 0088	**Time:** 3:00 pm -5:05 pm
Title: Low-Temperature Thermal Conductance of Periodically Perforated Silicon Nitride Membranes	

Author: H. Ketata	**Category: Poster 13**
Paper #: 0099	**Time:** 3:00 pm -5:05 pm
Title: Influence of Filling Fraction and Constituent Materials on Acoustic Waves in Phononic Lattice	
Author: Kevin L. Manktelow	**Category: Poster 14**
Paper #: 166	**Time:** 3:00 pm -5:05 pm
Title: Intensity-Dependent Dispersion in Nonlinear Phononic and Photonic Layered Systems	
Author: Y. Pennec	**Category: Poster 15**
Paper #: 0090	**Time:** 3:00 pm -5:05 pm
Title: Band-gap operating in the gigahertz frequencies for a bi-layer phononic crystal slab	
Author: O. Poncelet	**Category: Poster 16**
Paper #: 123	**Time:** 3:00 pm -5:05 pm
Title: Dynamical effective properties of elastic multilayers	
Author: V. Romero-Garcia	**Category: Poster 17**
Paper #: 0102	**Time:** 3:00 pm -5:05 pm
Title: Interaction between Periodic Arrays and Finite Impedance Surface: Analytical Results and Experimental Data	
Author: V. Romero-Garcia	**Category: Poster 18**
Paper #: 0058	**Time:** 3:00 pm -5:05 pm
Title: Acoustic Beams in Finite Sonic Crystals	
Author: Matteo Senesi	**Category: Poster 19**
Paper #: 0184	**Time:** 3:00 pm -5:05 pm
Title: Multi-field Internally Resonating Metamaterials	
Author: A. Tomchek	**Category: Poster 20**
Paper #: 177	**Time:** 3:00 pm -5:05 pm
Title: Characterization of Band Gap Resonances in Finite Periodic Structures	

Author: V. Tournat	**Category: Poster 21**
Paper #: 0011	**Time:** 3:00 pm -5:05 pm
Title: Out-of-plane acoustic modes in monolayer phononic granular membranes	
Author: Y.-S. Wang	**Category: Poster 22**
Paper #: 0060	**Time:** 3:00 pm -5:05 pm
Title: Surface/Interface Effects on Band Structures of Nanosized Phononic Crystals	
Author: A. Young	**Category: Poster 23**
Paper #: 0167	**Time:** 3:00 pm -5:05 pm
Title: Strain Based Tuning of Ring Resonators Via Hydrostatic Pressure Actuation of Membranes	
Author: X.-Z. Zhou	**Category: Poster 24**
Paper #: 0040	**Time:** 3:00 pm -5:05 pm
Title: Band Gap Calculation for 2D Solid-Fluid Phononic Crystals by the Method Based on Dirichlet-to-Neumann Map	
Author: G. Zhu	**Category: Poster 25**
Paper #: 0044	**Time:** 3:00 pm -5:05 pm
Title: Phonons on Complex Networks	
Coffee Break (Promenade)	**5:05 pm - 5:25 pm**
Felix Bloch Lecture (Mesa Ballroom)	**5:30 pm - 6:30 pm**
Free Time	6:30 pm - 7:00 pm
Banquet (Ortiz Ballroom) & Phononics 2013 Announcement	**7:00 pm - 10:00 pm**

Thursday: June 2 Detailed Program Information

Registration (Chamisa)	**7:30 am - 12:00 pm**
Announcements (Mesa BR)	**8:15 am - 8:30 am**
Track 6: Fabrication and Characterization for Phononics	
Session: 14 (Ortez Ballroom)	**8:30 am - 10:15 am**
Session Chair: F. McCormick	
Author: G. Bogart	**Category: Plenary Talk**
Paper #: 0075	**Time:** 8:30 am -9:00 am
Title: Larger Scale Fabrication of Nanometer to Micron Sized Periodic Structures in 2D and 3D: Approaches and Trends	
Abstract: *Fabrication of periodic structures for photonic or phononic wavelength interaction and manipulation at the small scale (<100um x 100 um) in planar dimensions using a variety of materials and techniques has been documented in the literature. Often structures are conceived and built with only a single device needing to be made. Some applications require that structures be fabricated in three dimensions or with multiple layers placing additional constraints on the fabricator.*	
Author: G. Piazza	**Category: Keynote Talk**
Paper #: 0105	**Time:** 9:00 am -9:25 am
Title: Microfabricated GHz Phononic Band Gap Structures	
Abstract: *This paper reports the latest development on the synthesis of phononic band gaps (PBG) in AlN/Air and SiC/Air structures operating in the GHz range by means of inverted cylindrical geometries or fractal-based designs. Finite element methods used to design and confirm the PBG dispersion curve and amplitude-frequency response are also presented.*	
Author: D. Schneider	**Category: Keynote Talk**
Paper #: 0131	**Time:** 9:25 am -9:50 am
Title: High Frequency Soft Phononics	
Abstract: *Propagation of hypersonic elastic/acoustic waves in polymer- and colloid-based nanostructures emerges as a powerful characterization tool of thermo- mechanical properties and reveals new structure related collective phenomena .Particle vibration spectroscopy and engineering of the phonon dispersion band diagram are highlighted in this presentation.*	

Author: Z. C. Leseman	**Category: Org. Colloquium**
Paper #: 0125	**Time:** 9:50 am -10:15 am

Title: Fabrication of 2-D Phononic Crystals via Focused Ion Beam

Abstract: *A technique for the fabrication of 2-D Phononic Crystals (PnCs) is described that utilizes a focused ion beam (FIB) instrument. In particular, the details of the microfabrication procedure are discussed which creates the main structure from which the PnC is created. Following the microfabrication is the nanoFIBrication of the microstructure to create a PnC with nanoscale features. Results will be presented for the fabrication of a 33 GHz PnC.*

Coffee Break (Chamisa)	**10:15 am - 10:40 am**

Track 7: Phononic MEMS and RF Applications

Session: 15 (Ortez Ballroom)	**10:40 am - 12:50 pm**
Session Chair: A. Khelif	
Author: A. Adibi	**Category: Plenary Talk**
Paper #: 0179	**Time:** 10:40 am -11:10 am

Title: A Waveguide-based Phononic Crystal Micro/Nano-mechanical High-Q Resonator

Abstract: *In this paper, we report the design, analysis, fabrication, and characterization of a very high frequency (VHF) phononic crystal (PnC) micro/nano mechanical resonator architecture based on silicon (Si) PnC slab waveguides. The PnC structure completely surrounds the resonant area and the resonator is excited by a thin aluminum nitride-based piezoelectric transducer stack directly fabricated on top of the resonator. This architecture highly suppresses the support loss of the resonator to the surroundings while providing mechanical support and electrical signal delivery to the resonator.*

Author: Y. Pennec	**Category: Keynote Talk**
Paper #: 0054	**Time:** 11:10 am -11:35 am

Title: Band Gaps and Defect Modes in Phononic Strip Waveguides

Abstract: *We study the elastic wave propagation in different geometries of strip waveguides obtained by extracting a row out of a phononic crystal slab made up of a square array of air holes in a silicon plate. We show that the existence of band gaps is strongly dependent on the cutting direction. We also study the existence of localized modes in cavities inserted inside the perfect strip waveguides.*

Author: J. Vasseur	**Category: Keynote Talk**
Paper #: 0053	**Time:** 11:35 am -12:00 pm
Title: Tunable magnetoelastic phononic crystals	
Abstract: *The feasibility of contactless tunability of the band structure of two dimensional phononic crystals is demonstrated by employing magnetostrictive materials and applying an external magnetic field. The influence of the amplitude and of the orientation with respect to the inclusion axis of the applied magnetic field are studied in details. Applications to tunable selective frequency filters are discussed.*	

Author: I. E. Psarobas	**Category: Keynote Talk**
Paper #: 0070	**Time:** 12:00 pm -12:25 pm
Title: Multi-phonon Processes in PhoXonic Cavities	
Abstract: *Long lifetime photons and phonons, confined in the same region of space, inside a phoXonic cavity, can interface with each other via strong nonlinear acousto-optic interactions. We unveil physics of distinct importance as the hypersonic modulation of light is substantially enhanced through multi-phonon exchange mechanisms.*	

Author: R. H. Olsson	**Category: Org. Colloquium**
Paper #: 0122	**Time:** 12:25 pm -12:50 pm
Title: Micromachined Phononic Band-Gap Crystals and Devices	
Abstract: *Micromachined phononic crystals are an emerging technology with applications in radio frequency communications, sensors and thermal energy harvesting. This paper presents work at Sandia National Laboratories in the realization of micromachined phononic crystal devices across a broad frequency range and in a number of material systems.*	

Lunch Break (Chamisa)	**12:50 pm - 2:00 pm**

Parallel Sessions	
Track 1 & 4: Phononic Crystals & Phonon Transport	
Session: 17 (Ortez Ballroom A)	**2:00 pm - 3:30 pm**
Session Chair: A. Adibi	
Author: S. Alaie	**Category: Contrib. Oral**
Paper #: 0152	**Time:** 2:00 pm -2:15 pm
Title: On the Validity of 2D Numerical Simulation of Bandgap for Slab of Phononic Crystals	
Abstract: *This work suggests a criterion for verification of Phononic bandpaps simulated by two dimensional elastodynamic models. The bandgap of a phononic crystals (PnCs) was studied using both 2D and 3D finite element analyses. Comparing the numerical results with experiment, this study indicates that validity of 2D models depends on the ratio of the thickness to the excitation wavelength.*	
Author: R. A. Wildman	**Category: Contrib. Oral**
Paper #: 0147	**Time:** 2:15 pm -2:30 pm
Title: Multi-Objective Optimization of Phononic Bandgap Materials for Wide Band, Low Frequency Operation	
Abstract: *Phononic bandgap materials are optimized for maximization of bandgap size and minimization of center frequency using a genetic programming method for inclusion shape design and material choice. Maximizing the bandgap size allows for a material design that can block a wide range of frequencies. Minimizing the center frequency will give designs that are small compared to the effective wavelength.*	
Author: M. V. Golub	**Category: Contrib. Oral**
Paper #: 0072	**Time:** 2:30 pm -2:45 pm
Title: Propagation and Transmission of Elastic SH-Waves in Functionally Graded Phononic Crystals	
Abstract: *The boundary value problem of elastic SH-wave propagation in one-dimensional phononic crystals composed of functionally graded interlayers arisen from the solid diffusion of homogeneous isotropic material of the crystal is considered. The localization phenomena, transmission and band gaps due to the material gradation are investigated.*	

Author: F. Scarpa	**Category: Contrib. Oral**
Paper #: 0022	**Time:** 2:45 pm -3:00 pm
Title: Band-gap Acoustic States in 1D and 2D Single Layer Graphene Sheet Systems	
Abstract: *We evaluate the pass-stop band characteristics of mechanical wave propagating in periodic nanostructures made with nanoribbons or graphene sheets with non-reconstructed defects..*	

Author: R. J. Magyar	**Category: Contrib. Oral**
Paper #: 0046	**Time:** 3:00 pm -3:15 pm
Title: Divide and Conquer Quantum Mechanical Methods for Phononic Applications	
Abstract: *Density functional theory is a highly efficient computational framework that describes structural properties of materials such as phonon frequencies and densities of states. In this talk, we suggest how the divide and conquer scheme may be well suited to determine phononic response in materials with supermolecular scale features.*	

Author: M. W. Blair	**Category: Contrib. Oral**
Paper #: 0145	**Time:** 3:15 pm -3:30 pm
Title: Improved Lattice-Bath Phonon Relaxation in Nanoscale Oxides	
Abstract: *Electron paramagnetic resonance (EPR) spectroscopy has been used to study energy transport properties of bulk and nanophosphor oxyorthosilicate samples. The bulk samples displayed a slight phonon bottleneck while energy relaxation in the nanophosphor samples was not influenced by the lattice-bath relaxation time and was more rapid.*	

Coffee Break (Chamisa)	**3:30 pm - 3:55 pm**

Track 4: Phonon Transport

Session: 18 (Ortez Ballroom A)	3:55 pm - 4:40 pm
Session Chair: Z. C. Leseman	
Author: P.-O. Chapuis	**Category: Contrib. Oral**
Paper #: 0049	**Time:** 3:55 pm -4:10 pm

Title: Heat dissipation in silicon and quartz nanoridges

Abstract: *We have investigated experimentally the effect of confinement of thermal acoustic phonons in 100 nm large ridges of silicon and quartz. We quantify the deviation to Fourier and ballistic predictions as a function of two characteristic numbers, the constriction Knudsen number describing the transmission of the phonons and a dimensionless number based on the nanoridges volume/surface ratio.*

Author: F. Alzina	**Category: Contrib. Oral**
Paper #: 0094	**Time:** 4:10 pm -4:25 pm

Title: Dispersion of Confined Acoustic Phonons in Ultra-Thin Si Membranes

Abstract: *The dispersion curves of confined acoustic phonons in ~10 and ~30 nm Si membranes were measured using Brillouin Light Scattering (BLS) spectroscopy. The dispersion relations of the confined phonons were calculated from a semi-analytical model based on continuum elasticity theory. Green's function simulations were used to simulate the Brillouin spectra.*

Author: M. Prunnila	**Category: Contrib. Oral**
Paper #: 0103	**Time:** 4:25 pm -4:40 pm

Title: Acoustic Phonon Transmission and Heat Conduction Through Vacuum

Abstract: *We describe theoretically how acoustic phonons can directly transmit energy and conduct heat between bodies that are separated by a vacuum gap. This effect is enabled by introducing a coupling mechanism, such as piezoelectricity, that strongly couples electric field and lattice deformation.*

Track 2: Periodic Structures	
Session: 19 (Ortez Ballroom B)	**2:00 pm - 3:30 pm**
Session Chair: R. H. Olsson III	
Author: A. Leonard	**Category: Contrib. Oral**
Paper #: 0030	**Time:** 2:00 pm -2:15 pm
Title: Tailoring Stress Waves in 2-D Highly Nonlinear Granular Crystals: Simulations and Experiments	
Abstract: *We study the propagation of elastic stress waves in two-dimensional highly nonlinear granular crystals composed of square packings of spheres with and without cylindrical intruders, via experiments and numerical simulations. By varying the intruder material, we show the ability to alter the propagating wave front characteristics. Experiments agree well with discrete particle simulations.*	
Author: G. Theocharis	**Category: Contrib. Oral**
Paper #: 0079	**Time:** 2:15 pm -2:30 pm
Title: Control of Vibrational Energy in Nonlinear Granular Crystals	
Abstract: *We describe recent work on nonlinear granular crystals. We explore phenomena related to vibrational energy localization, re-distribution, and rectification enabled by the spatial discreteness, disorder, and nonlinearity of granular crystals. In addition, we note how an understanding of dynamic phenomena in granular crystals can enable the design of novel engineering devices.*	
Author: V. J. Sánchez-Morcillo	**Category: Contrib. Oral**
Paper #: 0098	**Time:** 2:30 pm -2:45 pm
Title: Second harmonics, instabilities and hole solitons in 1D phononic granular chains	
Abstract: *The propagation of nonlinear compressional waves in a 1D compressed granular chain driven at one end by a harmonic excitation is theoretically studied. The chain is described by a FPU lattice model with quadratic nonlinearity. We predict and describe different nonlinear phenomena, as the generation of second harmonics, modulational instabilities and the existence of hole (or dark) solitons.*	

Author: G. Wang	**Category: Contrib. Oral**
Paper #: 0067	**Time:** 2:45 pm -3:00 pm
Title: Broadband Vibration Attenuation Induced by Periodic Arrays of Feedback Shunted Piezoelectric Patches on Beams	
Abstract: *The effect of periodic arrays of feedback shunted piezoelectric patches in vibration attenuation of flexible beams is analyzed theoretically and experimentally. Broadband vibration attenuations are observed no mater in or out of the band gaps. The proposed concept is validated experimentally on a suspended epoxy beam.*	
Author: Y. Xiao	**Category: Contrib. Oral**
Paper #: 0148	**Time:** 3:00 pm -3:15 pm
Title: Longitudinal Vibration Band Gaps in Rods with Periodically Attached Multi-Degree-of-Freedom Vibration Absorbers	
Abstract: *Band gap behavior in rods with periodically mounted multi-degree-of-freedom resonators (vibration absorbers) is concerned. Explicit expressions are derived for the calculation of complex band structures. The effects of absorber parameters on the band gap properties are studied. The band gap formation mechanisms of the system are explained by analytical models with explicit formulations.*	
Author: S. Chen	**Category: Contrib. Oral**
Paper #: 0031	**Time:** 3:15 pm -3:30 pm
Title: Active Control of Band Gaps by Periodically Distributed Piezo-shunts	
Abstract: *Periodic arrays of inductive or negative capacitive shunted piezoelectric patches are employed to control the band gaps of phononic beams. An epoxy beam with periodically surface- bonded piezoelectric patches is designed. The band gaps, when each piezo-patch is connected to a single inductive or negative capacitive circuit, are investigated in detail.*	
Coffee Break (Chamisa)	**3:30 pm - 3:55 pm**

Track 6: Fabrication and Characterization for Phononics	
Session: 20 (Ortez Ballroom B)	**3:55 pm - 4:40 pm**
Session Chair: M. F. Su	
Author: T. J. Isotalo	**Category: Contrib. Oral**
Paper #: 0143	**Time:** 3:55 pm -4:10 pm
Title: Techniques for Self-Assembled Phononic Crystals	
Abstract: *In this project, we study the assembly of periodic arrays of nanospheres and their crystalline properties. The vertical deposition technique is investigated along with the effects of substrate surface modifications for improvement of order and directed self-assembly. Dipping speed and PS sphere concentration are taken as the primary parameters affecting crystalline quality.*	
Author: D. F. Goettler	**Category: Contrib. Oral**
Paper #: 0151	**Time:** 4:10 pm -4:25 pm
Title: The Effect of Phononic Crystal Lattice Type and Lattice Spacing on the Reduction of Bulk Thermal Conductivity in Silicon and Silicon Nitride	
Abstract: *Phononic crystals are a promising method of reducing a material's bulk thermal conductivity. Changing a phononic crystal's lattice type or its lattice spacing are two ways of reducing a material's thermal conductivity. Results of different lattice types and lattice spacings on the reduction of bulk thermal conductivity in silicon and silicon nitride at room temperature will be presented.*	
Author: D. Lanzillotti-Kimura	**Category: Contrib. Oral**
Paper #: 0158	**Time:** 4:25 pm -4:40 pm
Title: Nanophononics using Acoustic and Optical Cavities	
Abstract: *We report pump-probe time experiments in acoustic and optical cavities. We demonstrate that the generated coherent acoustic phonon spectra can be inhibited or enhanced in the cavity. Simulations highlight the role of the phonon density of states in the coherent phonon generation, extending concepts at the base of the Purcell effect to the field of phononics.*	
Adjourn	**4:40 PM**

1ST INTERNATIONAL CONFERENCE ON PHONONIC CRYSTALS, METAMATERIALS & OPTOMECHANICS

Extended Abstracts

Track 1: Phononic Crystals

Phononics 2011: First International Conference on Phononic Crystals, Metamaterials and Optomechanics
Santa Fe, New Mexico, USA, May 29-June 2, 2011
PHONONICS-2011-0024

Phononic Crystals to Control the Propagation of Elastic Waves: Recent Advances

Bernard Bonello, Laurent Belliard, Juliette Pierre, Mathieu Rénier, Olga Boyko

Institut des NanoSciences de Paris (INSP) UMR CNRS 7588,
Université Pierre et Marie Curie, boîte 840
4 place Jussieu, 75252 Paris cedex 05, France
bernard.bonello@insp.jussieu.fr, laurent.belliard@upmc.fr, juliette.pierre@insp.jussieu.fr,
mathieu.renier@insp.jussieu.fr, olga.boyko@insp.jussieu.fr

Abstract: In this paper, we briefly review the recent advances made worldwide to control the propagation of elastic waves using phononic crystals (PCs). We show how new effects, including the opening of band gaps in silicon PC plates and the negative refraction of elastic waves, could be at the origin of new Micro ElectroMechanical Systems compatible with CMOS processes.

The most attractive property that can be achieved in a phononic crystal (PC) is the existence of frequency bands in which no acoustic waves are allowed to propagate. It is thus not surprising that, since more than twenty years, a great deal of work has been devoted to the computation of the band structures of a large variety of PCs, including solid/fluid and solid/solid heterostructures. The research in this field has now reached maturity and several devices based upon the intrinsic properties of PCs have been proposed already, some of which being of primary interest for communication technologies (filters, waveguides, resonators, (de)multiplexers, signal processing devices…) or more generally, for manipulating the propagation or the focusing of elastic waves (gradient index PCs, acoustical super-lenses…). This paper presents an overview of recent works on the topics. We mostly, but not exclusively, stress on recent advances made with PCs inserted within slabs or membranes which have the important advantage of confining the elastic energy in the thickness of the device, yielding therefore to low loss structures.

The first experimental demonstration[1,2] of stop bands in 2D PC goes back to the early 70's but it is only recently that PCs in silicon plates, compatible with CMOS process, have been achieved at high frequencies. For instance, a decreasing in the transmission by almost 40 dB was measured in a PC designed to stop all plate modes in the band 120-150 MHz and elaborated[3] from a silicon-on-insulator substrate. Rejection of bulk acoustic waves by 25 dB was also measured in the MHz regime with PCs made of tungsten rods embedded into a silica matrix.[4] In both cases these stop bands resulted from the Bragg reflection on the inclusions. Actually, other processes can be exploited as well to achieve a large decrease in the transmission through the heterostructure, at specific frequencies. Indeed, it has been shown[5] that a very selective filter is obtained when a resonant cavity is attached to a waveguide arranged within a 2D PC. In that case, the dip in the transmission spectrum does not result from the coherent scattering of the waves but rather from the trapping of elastic energy in the cavity. However, up to now the experimental demonstrations have been limited to structures with fluid background, not really useable for RF applications.

Almost the same idea is at work in the case of PCs made of periodic array of dots on a membrane. These structures have at least two features being of primary usefulness for MEMS devices: first, not surprisingly, they exhibit band gaps due to Bragg reflection on the dots but also, more unexpectedly, they feature flat bands at frequencies that could be well below the Bragg gap. These low frequency gaps originate from the confinement of elastic energy on the dots and are therefore very sensitive to their geometrical and physical parameters. Secondly, the elaboration of this new type of phononic plates is compatible with CMOS processes, making these heterostructures very promising in a large field of applications (sensing, wireless communication, thermal transport…) and consequently, widely investigated worldwide.[6-10]

Phononics 2011: First International Conference on Phononic Crystals, Metamaterials and Optomechanics

Santa Fe, New Mexico, USA, May 29-June 2, 2011

PHONONICS-2011-0024

With the rapid growing of information and communication technologies there is an urgent need in frequency selective devices working in the GHz range. Various micromechanical 2D resonators showing Q-factor as high as $6x10^3$ have been proposed to this end.[11] In particular, a silicon-chip-based cavity, allowing for the simultaneous confinement of mechanical and optical modes, has recently been used[12] to successfully couple 2 GHz phonons and light at telecom wavelength (1.5 μm).

The optical approach has inspired a lot of works devoted to the bending, focusing, or collimation of elastic waves at both micro- (MHz) and nano-scales (GHz). Particularly interesting is a flat gradient-index PC lens[13] that has been designed to focus bulk elastic waves at wavelengths much larger than the lattice parameter. This could be achieved by modulating either the radii or the physical nature of the cylindrical inclusions, along the direction normal to the wave vector. It has also been shown by our group that, as a consequence of the folding of some branches in the dispersion curves, both SAW[14] and Lamb waves[15] can undergo negative refraction when going across the interface between a PC and a homogeneous medium. Identical properties could be achieved with locally resonant materials[16] as well, but in this latter case, the phenomenon results from mass density and compressibility both negative rather than from dispersion. Note that most of the investigations in that field are still prospective but they could eventually lead to very interesting devices, as super-lenses, suitable to overcome the diffraction limit when focusing an ultrasonic beam.

In summary, an abundant literature covers now many aspects of PCs as a basis to micromechanical, or microelectronic devices. In this talk, we will try to identify which of them are the most promising.

References

[1] H. J. Shutherland and R. Lingle, *J. Composite Materials* **6**, 490 (1972).
[2] T. R. Trauchert and A. N. Guzetsu, *J. Appl. Mech.* **39**, 98 (1972).
[3] S. Mohammadi, A. A. Eftekhar, A. Khelif, W. D. Hunt, and A. Adibi, *Appl. Phys. Lett.* **92**, 221905 (2008).
[4] I. El-Kady, R. H. Olsson III, and J. G. Fleming, *Appl. Phys. Lett.* **92**, 233504 (2008).
[5] J. O. Vasseur, M. Beaugeois, B. Djafari-Rouhani, Y. Pennec, and P. A. Deymier, *Phys. Stat. Sol. (c)* **1**, 2720 (2004).
[6] Y. Pennec, B. Djafari-Rouhani, H. Larabi, A. Akjouj, J. N. Gillet, J. O. Vasseur, and G. Thabet, *Phys. Rev. B* **80**, 144302 (2009).
[7] A. Khelif, Y. Achaoui, S. Benchabane, and V. Laude, *Phys. Rev. B* **81**, 214303 (2010).
[8] M. Oudich, Y. Li, B. Assouar, Z. Hou, *New Journal of Physics* **12**, 083049 (2010).
[9] T.-T. Wu, Z.-G. Huang, T.-C. Tsai, and T.-C. Wu, *Appl. Phys. Lett.* **93**, 111902 (2008).
[10] J.-C. Hsu and T. T. Wu, *Appl. Phys. Lett.* **90**, 201904 (2007).
[11] S. Mohammadi, A. A. Eftekhar, W. D. Hunt, and A. Adibi, *Appl. Phys. Lett.* **94**, 051906 (2009).
[12] M. Eichenfield, J. Chan, R. M. Camacho, K. J. Vahala, and O. Painter, *Nature* **462**, 78 (2009).
[13] Sz-C. S. Lin, T. J. Huang, J.-H. Sun, and T. T. Wu, *Phys. Rev. B* **79**, 094302 (2009).
[14] B. Bonello, L. Belliard, J. Pierre, O. Boyko, B. Perrin, J. O. Vasseur, *Phys. Rev. B* **82**, 104109 (2010).
[15] J. Pierre, O. Boyko, L. Belliard, J. O. Vasseur, B. Bonello, *Appl. Phys. Lett*. **97**, 121919 (2010).
[16] Z. Liu, X. Zhang, Y. Mao, Y. Y. Zhu, Z. Yang, C. T. Chan, and P. Sheng, *Science* **289**, 1734 (2000).

Phononics 2011: First International Conference on Phononic Crystals, Metamaterials and Optomechanics
Santa Fe, New Mexico, USA, May 29-June 2, 2011
PHONONICS-2011-0040

Band Gap Calculation for 2D Solid-Fluid Phononic Crystals by the Method Based on Dirichlet-to-Neumann Map

Xiao-Zhou Zhou[1], Ni Zhen[1], Yue-Sheng Wang[1], Chuanzeng Zhang[2]

[1] *Institute of Engineering Mechanics, Beijing Jiaotong University, Beijing 100044, China*
zhouzhou_buaa@163.com
[2] *Department of Civil Engineering, University of Siegen, D-57068 Siegen, Germany*
c.zhang@uni-siegen.de

Abstract: A method based on the Dirichlet-to-Neumann map which relates the potential function to its derivatives on the boundary of the unit cell is presented for the phononic band gap calculation with solids stuffing in a fluid. The transverse mode existing in the solid stuffing is considered. The band structures along the irreducible Brillouin zone are calculated. The results show that the method can yield accurate results with fast convergence.

Since the pioneer work of Kushwaha [1], a great deal of attention has been focused on special properties of the so-called phononic crystals [1-11] which are the artificial periodic elastic materials with the structures analogy to traditional natural crystals and photonic crystals. A physical character of these materials is the existence of phononic band gaps in which the sound or elastic waves are forbidden.

To calculate the band gaps for phononic crystals, several numerical methods have been developed, such as the plane wave expansion (PWE) method [1-6], the multiple scattering theory (MST) method [7, 8], and the finite difference time domain (FDTD) method [9, 10]. Among them, the PWE method is the most popular one because of its simplicity. For the systems with solid stuffing in a fluid, PWE method has to neglect the transverse mode existing in solid stuffing and simply treat the solid as an artificial "fluid". This approximation can yield accurate results only when the solid component is so stiff that the wave propagating in the surrounding fluid can hardly be transmitted into the solid. Up to now, there are few efficient numerical methods for calculating the band structures of the mixed system with solid and fluid components [11].

In this paper, a method based on the Dirichlet-to-Neumann (DtN) map [12] which relates the potential function to its derivatives on the boundary of the unit cell is presented for the band gap calculation of the phononic crystals with solid stuffing in a fluid. The boundary conditions between the solid stuffing and the fluid host as well as the transverse mode existing in the solid stuffing are considered. This method expresses the scattered fields as the cylindrical wave expansions and imposes the Bloch condition on the boundary of the unit cell. A linear eigenvalue equation is obtained. For a given frequency, the Bloch wave vectors along the irreducible Brillouin zone are calculated. This method is applied to analyze the band gaps of two-dimensional solid-fluid phononic crystals with a square lattice. The results show that the method can yield accurate results with fast convergence for various material combinations, including the case with soft stuffing.

As an example, a square lattice of aluminium (Al) cylinders in a mercury host with filling fraction $f = 0.4$ is considered. The material properties are $\rho_1 = 2700 kg/m^3$ and $c_{L1} = 6410 m/s$ for Al, and $\rho_2 = 13600 kg/m^3$ and $c_{L2} = 1451 m/s$ for mercury. The normalized frequencies $\bar{\omega}$ are calculated by both PWE and DtN-based methods, see Fig. 1 For the PWE method the solid stuffing is considered as a fluid but with the material parameters of actual Al. In the figure, the black circular dots represent the band structures obtained from the DtN-based method, and the gray triangular dots from the PWE method. Obviously, no matter which method we use to calculate, there is no complete band gap for Al cylinders in a mercury host with the filling fraction $f = 0.4$. The frequency bands calculated by two methods are similar, but those from DtN-based method are lower than those from PWE method. That is to say, neglecting the transverse mode in solid sactterers will induce an higher estimate of the eigenfrequencies.

Phononics 2011: First International Conference on Phononic Crystals, Metamaterials and Optomechanics

Santa Fe, New Mexico, USA, May 29-June 2, 2011

PHONONICS-2011-0040

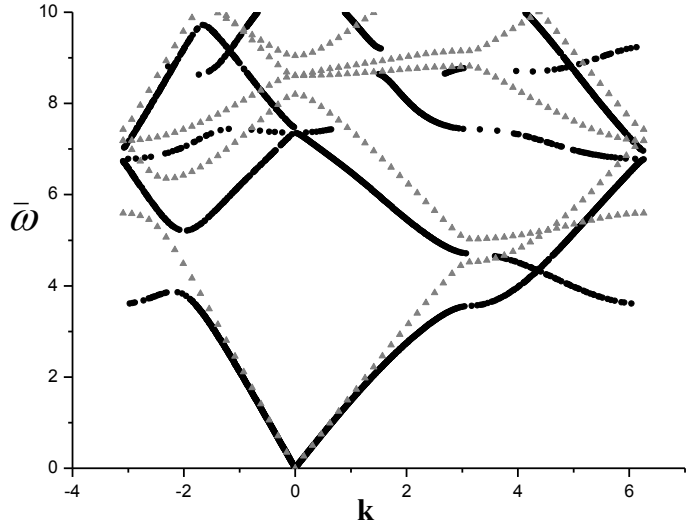

Figure 1 The dispersion curves of Al cylinders in mercury in a square lattice with $f = 0.4$. The black circular dots represent the band gaps from the DtN-based method, and the gray triangular dots from the PWE method.

References

[1] M. S. Kushwaha, P. Halevi, L. Dobrzynsi, and B. Diafari-Rouhani, Phys. Rev. Lett. **71**, 2022 (1993).
[2] M. S. Kushwaha, P. Halevi, G. Martinez, Phys. Rev. B. **49**, 2313 (1994).
[3] M. S. Kushwaha, P. Halevi, Appl. Phys. Lett. **64**, 1085 (1994).
[4] J. O. Vasseur, B. Djafari-Rouhani, L. Dobrzynsi, M. S. Kushwaha, and P. Halevi, J. Phys.: Condens. Matter **6**, 8759 (1994).
[5] M. S. Kushwaha, B. Djafari-Rouhani, J. Appl. Phys. **80**, 3191 (1996).
[6] M. S. Kushwaha, P. Halevi, J. Acoust. Soc. Am. **101**, 619 (1997).
[7] M. Kafesaki, and E. N. Economou. Phys. Rev. B, **60**, 11993 (1999).
[8] Z. Liu, C. T. Chan, and Ping Sheng, Phys. Rev. B. **62**, 2446 (2000).
[9] Y. Tanaka, Y. Tomoyasu, and S. Tamura. Phys. Rev. B, **62**, 7387 (2000).
[10] D. Garcia-Pablos, M. Sigalas, F. R. Montero de Espinosa, M. Torres, M. Kafesaki, and N. Garcia, Phys. Rev. Lett. **84**, 4349 (2000).
[11] D. Caballero, J. Sanchez-Dehesa, C. Rubio, R. Martinez-Sala, J. V. Sanchez-Perez, F. Meseguer, and J. Llinares, Phys. Rev. E. **60**, 6316 (1999).
[12] J. H. Yuan, and Y. Y. Lu. Opt. Soc. Am., **23**, 3217 (2006).

Phononics 2011: First International Conference on Phononic Crystals, Metamaterials and Optomechanics
Santa Fe, New Mexico, USA, May 29-June 2, 2011
PHONONICS-2011-0056

Negative refraction of elastic waves in 2D phononic crystals

Anne-Christine Hladky-Hennion[1], Charles Croënne[1], Bertrand Dubus[1], Jérôme Vasseur[1], Nichlas Swinteck[1, 2], Pierre A. Deymier[2] and Bruno Morvan[3]

[1] *Institut d'Électronique, de Microélectronique et de Nanotechnologie, UMR CNRS 8520, Cité Scientifique, 59652 Villeneuve d'Ascq Cedex, France,*
anne-christine.hladky@isen.fr, charles.croenne@isen.fr, bertrand.dubus@isen.fr, jerome.vasseur@univ-lille1.fr
[2] *Department of Materials Science and Engineering, University of Arizona, Tucson, Arizona 85721, USA*
swinteck@email.arizona.edu, deymier@email.arizona.edu,
[3] *Laboratoire Ondes et Milieux Complexes, FRE-3102 CNRS, Place Robert Schuman, 76610 Le Havre, France*
bruno.morvan@univ-lehavre.fr

Abstract: Negative refraction of elastic waves is evidenced in a two-dimensional phononic crystal (PC), made of a triangular lattice of steel rods embedded in epoxy. Experiments are carried out on a prism shaped PC inserted inside an epoxy block. The influence of different parameters is discussed in terms of image reconstruction.

Phononic crystals (PC's) may exhibit dispersion curves with a negative slope i.e. the wave vector and the group velocity vector associated with an acoustic wave point in opposite directions. This property is typical of a left handed material and implies a negative index of refraction in the Snell-Descartes law. Negative index PC's have the advantage of allowing the realization of flat super-lenses able to focus elastic waves with a resolution lower than the diffraction limit [1]. It has been shown that super-resolution can be achieved using a PC lens made of a triangular array of steel cylinders immersed in methanol and surrounded with water [2]. To go further for practical applications, it is more appropriate to consider a PC slab made with a solid matrix. In that case, longitudinal and transverse waves are coupled together in the PC, which makes the problem more complex.

In a recent paper, C. Croënne *et al* [3] have shown theoretically and experimentally the negative refraction of an elastic wave in a triangular array of steel rods in an epoxy block. The dispersion curves are presented in the first Brillouin zone and show that in the upper part, a branch with a negative slope is observed (Fig. 1). It corresponds to a mode with a predominantly longitudinal behavior. Moreover, the Equi-Frequency Contours (EFC), i.e. the intersection of the 3D dispersion curves with a horizontal plane, are circular: it means that the wavevector of the elastic wave and the group velocity are antiparallel, for any propagation direction (Fig. 2). As expected, the radius of the EFC clearly decreases as the frequency increases. Experiments have confirmed the theoretical simulations obtained using the finite element method. They are carried out on a prism shaped PC inserted inside an epoxy block. Measurement of the refraction angle at the output side of the PC shows the negative refraction of transverse or longitudinal waves through a solid PC. In the present paper, we analyze in details the elastic waves inducing a negative refraction. However, in the studied device, the refraction index of the PC is not matched with the refraction index of water, for immersed applications. Therefore, solutions are presented to match the refractive index of the PC with respect to the surrounding fluid. Finally, the occurrence of the focal spot is discussed (Fig. 3 and 4) and it is shown that many parameters are of interest in the construction of the focal spot: negative slope in the dispersion curve, the Equi Frequency Contours, index matching as well as impedance matching.

This work is supported by the Agence Nationale de la Recherche : ANR-08-BLAN-0101-01, SUPREME project.

Phononics 2011: First International Conference on Phononic Crystals, Metamaterials and Optomechanics
Santa Fe, New Mexico, USA, May 29-June 2, 2011
PHONONICS-2011-0056

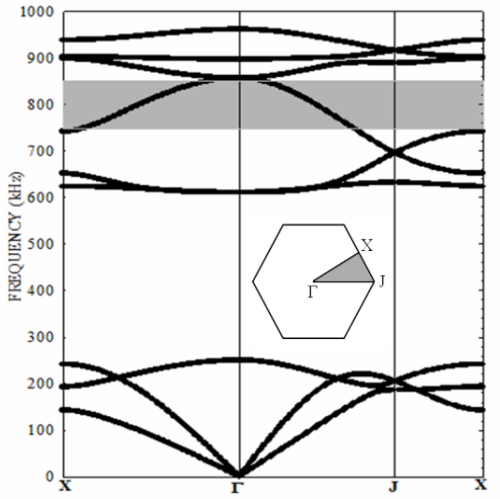

Figure 1: (a) Elastic band structure for the 2D PC made of a triangular array of steel rods in an epoxy matrix. The radius of the rods is 1 mm, the lattice parameter is 2.84 mm. In the frequency range [750 kHz, 860 kHz] (grey part) a negative branch is observed, corresponding to a mode with a predominantly longitudinal behaviour.

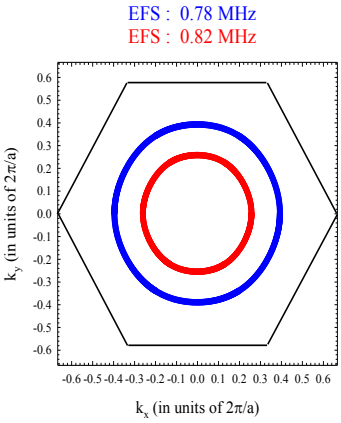

Figure 2: Equi Frequency Contours of the PC at 780 kHz (thick line) and 820 kHz (thin line).

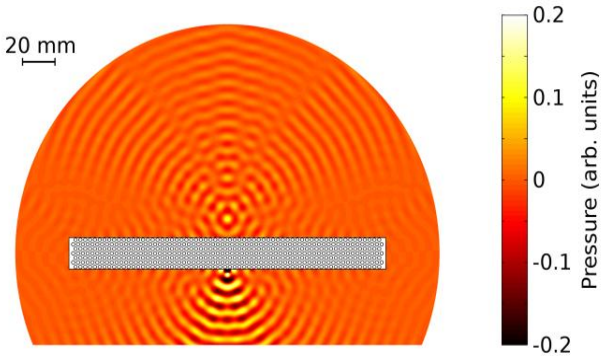

Figure 3: Simulated pressure field (normalized to a source amplitude of 1) for a PC-made flat lens immersed in a fluid, at 786 kHz. Fluid refractive index is matched to PC index. A point source is located below the lens, 3-mm away from the bottom interface. For clarity, the colorscale is cut to ±0.2 and thus some parts of the field map below the lens are out of colorscale (black/white regions). Losses are not taken into account.

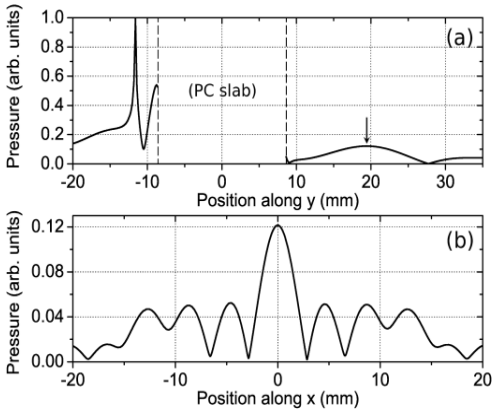

Figure 4: Plot of the pressure field amplitude (a) along the line perpendicular to the slab which includes the source point and (b) along the line parallel to the slab which includes the focal point, for the simulation of Fig. 3. Here the focal point is defined as the point of maximum amplitude on plot (a) (indicated by an arrow). On graph (a), the PC slab is situated between the two dashed lines

References

[1] A. Sukhovich, L.J. Jing, J.H. Page, Phys. Rev. B **77**, 014301 (2008).
[2] A. Sukhovich, B. Merheb, K. Muralidharan, J. O. Vasseur, Y. Pennec, P. A. Deymier and J. H. Page, Phys. Rev. Lett. **102**, 154301 (2009).
[3] C . Croënne, D. Manga, B. Morvan, A. Tinel, B. Dubus, J. Vasseur and A.-C. Hladky-Hennion, to be published in Phys. Rev. B, (2011).

Phononics 2011: First International Conference on Phononic Crystals, Metamaterials and Optomechanics
Santa Fe, New Mexico, USA, May 29-June 2, 2011
PHONONICS-2011-0059

Engineering of the Band gaps and transmissions in Phononic and phoxonic Crystal Slabs and Waveguides

B. Djafari Rouhani, C. Li, H. Larabi, Y. El Hassouani, Y. Pennec

Institut d'Electronique, de Microélectronique et de Nanotechnologies, UMR CNRS 8520, Université de Lille1, Avenue Poincaré, Cité Scientifique, 59652 Villeneuve d'Ascq, France
bahram.djafari-rouhani@univ-lille1.fr

Abstract: We report on our theoretical works about the engineering of band structures in phononic as well as dual phononic-photonic slabs and strips waveguides. Besides the conventional structure made of a periodic array of holes in a plate, we discuss the more recent geometry of pillars on a membrane or on a substrate. We discuss the best phoxonic structures displaying dual phononic-photonic band gaps and slow modes.

Following a great deal of works devoted to 2D phononic crystals [1] and their point and linear defects [2], the study of slabs of phononic crystals has become a topic of major interest during the last few years. Indeed, with an appropriate choice of their geometrical and physical parameters, these finite thickness structures can also exhibit absolute band gaps, similarly to the case of 2D structures. This makes them suitable to support the same confinement, guiding and filtering functionalities as in 2D phononic crystals, with the additional property of confinement in the vertical direction.

We have studied two types of phononic crystal slabs, namely the conventional case of a periodic array of holes in a plate such as silicon [3], and the new case of a periodic array of pillars on a membrane [4-7] (such as Si/SiO_2). We introduced the latter structure in 2008 especially because it can exhibit a low frequency gap, where the acoustic wavelength in any constituent material is several times larger than the period [4]. This gap is associated with a bending of the first three acoustic branches; its existence requires appropriate geometrical parameters, especially as concerns the thickness of the membrane and the height of the pillars whereas it remains robust against the choice of the constituting materials. One or more higher gaps can also appear in the band structure depending on the height of the pillars [4,5]. In particular, associated with the local resonances of the pillars, there are opening of gaps due to the bending of the acoustic branches (when they cut a local resonance) instead of their folding. Among different considered lattices, the triangular lattice provides better flexibility than the square and honeycomb lattices as concerns the choice of the geometrical parameters [5]. This is in contrast to the case of holes in a membrane where the honeycomb lattice provides the largest band gaps. When the thickness of the membrane increases, the absolute gap closes and one progressively recovers the case of pillars deposited on a semi-infinite substrate. Then, the band structure displays one or several surface localized branches below the bulk bands of the substrate.

We have studied the waveguiding phenomena in the above phononic crystals, especially in the case of pillars on a membrane [6]. Different types of linear defects are considered either by removing a row of pillars or by replacing in a row the materials or geometrical parameters of the pillars. In each case, we have made a detailed analysis of the confined modes, the transmitting or non-transmitting character of the corresponding bands, and the possibility of polarization conversion which could frequently occur.

Phonon transmission between two substrates connected by a periodic array of pillars has also been studied [7]. In particular, we have evidenced the existence of Fano resonances when a Perot-Fabry resonance inside a pillar falls in the vicinity of a zero of transmission; the latter results from the excitation by the normally incident wave of surface waves at the boundaries between the substrates and the pillars [7]. This and other features in the transmission spectrum, such as the regular oscillations associated with Fabry-Perot resonances inside the pillars or the existence of transmission gaps associated to the periodicity, are also discussed as a function of the geometrical and material parameters.

In a second part, we discuss the simultaneous existence of phononic and photonic band gaps in the above crystal slabs [5, 8], considering different lattices such as square triangular and honeycomb, as

Phononics 2011: First International Conference on Phononic Crystals, Metamaterials and Optomechanics
Santa Fe, New Mexico, USA, May 29-June 2, 2011
PHONONICS-2011-0059

well as the more general case of boron nitride (BN) lattices. With a periodic array of holes in a Si membrane [8], complete phoxonic band gaps can be obtained with the honeycomb lattice as well as with BN lattices close to honeycomb. Otherwise, all investigated structures present the possibility of a complete phononic gap together with a photonic gap of a given symmetry, either odd or even, depending on the geometrical parameters. With a periodic array of Si dots on a SiO_2 membrane [5], an appropriate choice of the geometrical parameters allows the existence of an absolute phoxonic gap. In contrast to the case of holes in a membrane, the more flexible lattice to keep the phononic gap open is now the triangular one, especially as concerns the thickness of the membrane. Moreover, this geometry allows the existence of the complete photonic gap over a wide range of parameters.
Let us mention a new idea [9] to create a complete photonic band gap by taking advantage of the anisotropy of the dielectric tensor (different refraction indices for the propagation of TE and TM modes).

Confined modes associated with defects such as waveguides and cavities in these structures will be useful for novel acousto-optic and sensing devices. In this work, we study the design of different waveguides that allow phononic and photonic dual guidance and confinement, especially with the possibility of single mode slow light and/or sound. Several structures are considered, among them one is obtained in a honeycomb lattice by cutting the crystal along the ΓK direction and by pushing the two half-crystals far from each other. In this way, the width of the waveguide can be taken as a parameter. Moreover, additional holes of different sizes are introduced on the sides of the waveguide.

As an alternative to the waveguides in a crystal slab, we also study 1D periodic waveguides constituted by making a nano-structuration in a suspended silicon strip waveguide One example is constituted by a 1D waveguide in which the sides are periodically rough. A similar case is obtained when periodical stubs are attached on both sides of the waveguide. We demonstrate the possibility of phononic and photonic dual band gaps in these structures and are investigating the designs of cavities that insure the confinement of both waves.

Finally, we would like to mention a calculation about the thermal transport in the frame of the above geometries. Namely, by using a lattice dynamic model, we have studied the directional thermal conductivity κ of a thin Si membrane covered by a 1D array of stretched Ge dots and discussed κ as a function of the angle of the heat flux with respect to the stretching direction [10].

Acknowledgments: This work was supported in part by the European Commission Seventh Framework Programs (FP7) under the FET-Open project TAILPHOX N° 233883 and IP project NANOPACK N° 216716.

References

[1] M.S. Kushwaha, P. Halevi, L. Dobrzynski and B. Djafari-Rouhani, *Phys. Rev. Lett.* **71,** 2022(1993); M.M. Sigalas and E.N. Economou, *Solid State Commun*. **86,** 141 (1993). For a recent review, see Y. Pennec, J.O. Vasseur, B. Djafari-Rouhani, L. Dobrzynski and P.A. Deymier, *Surf. Sci. Rep*.**65**, 229-291 (2010).
[2] A. Khelif, B. Djafari Rouhani, J.O. Vasseur and P.A. Deymier, *Phys. Rev.* B **68**, 024302 (2003); Y. Pennec, B. Djafari-Rouhani, J.O. Vasseur, H. Larabi, A. Khelif, A. Choujaa, S. Benchabane, and V. Laude, *Appl. Phys. Lett.* **87,** 261912 (2005).
[3] J.O. Vasseur, P.A. Deymier, B. Djafari-Rouhani, Y. Pennec and A.C. Hladky-Hennion, *Phys. Rev. B* **77,** 085415 (2008).
[4] Y. Pennec, B. Djafari-Rouhani, H. Larabi, J.O. Vasseur and A.C. Hladky-Hennion, *Phys. Rev. B* **78,** 104105 (2008).
[5] Y. El Hassouani, C. Li, Y. Pennec, E.H. El Boudouti, H. Larabi, A. Akjouj, O. Bou Matar, N. Papanikolaou, S. Benchabane, V. Laude, A. Martinez and B. Djafari-Rouhani, *Phys. Rev. B* **82,** 155405 (2010).
[6] Y. Pennec, B. Djafari-Rouhani, H. Larabi, A. Akjouj, J.N. Gillet, J. Vasseur and G. Thabet *Phys. Rev. B* **80,** 144302 (2009).
[7] Y. Pennec, B. Djafari-Rouhani and H. Larabi, Proc. SPIE, Vol. 7223 (Photonic and Phononic Crystal Materials and Devices IX), 72230F (2009). Ibidem *IUTAM Symposium on Recent Advances of Acoustic Waves in Solids*, Taipei, May 2009; Springer IUTAM Book Series, Volume 26, 2010, Edited by Tsung-Tsong Wu and Chien-Ching Ma, pages 127-138.
[8] Y. Pennec, B. Djafari Rouhani, E.H. El Boudouti, C. Li, Y. El Hassouani, J.O. Vasseur, N. Papanikolaou, S. Benchabane, V. Laude and A. Martinez, *Opt. Express*, **18**, 14301 (2010).
[9] D. Bria, M.B. Assouar, M. Oudich, Y. Pennec, J. Vasseur and B. Djafari Rouhani, *J. Appl. Phys*. (2011, under press).
[10] J.N. Gillet, B. Djafari Rouhani and Y. Pennec, Proceedings of Therminic 2009, Leuven, Belgium, October 2009, p. 203.

Phononics 2011: First International Conference on Phononic Crystals, Metamaterials and Optomechanics
Santa Fe, New Mexico, USA, May 29-June 2, 2011
PHONONICS-2011-0060

Surface/Interface Effects on Band Structures of Nano-sized Phononic Crystals

Ni Zhen[1], Yue-Sheng Wang[1], Ch. Zhang[2]

[1] *Institute of Engineering Mechanics ,Beijing Jiaotong University, Beijing 100044, China*
yswang@bjtu.edu.cn
[2] *Department of Civil Engineering, University of Siegen, D-57068 Siegen, Germany*
c.zhang@uni-siegen.de

Abstract: In this paper, the band structure of transverse waves propagating in a 2D phononic crystal composed of nanosized holes or elastic inclusions embedded in an elastic solid is calculated by using the method based on the Dirichlet-to-Neumann map. The Young-Laplace equation is applied to take into account of the surface/interface effects of the nanosized holes/inclusions. Detailed calculations are presented for the systems with or without the surface/interface effects. The results show that all bands descend with the first bandgap becoming lower and wider due to the existence of the surface/interface effects.

Introduction

Phononic crystals, due to their unique feature of band gap, exhibit potential applications in sound shielding, vibration isolation, design of new acoustic devices, etc., and therefore received considerable attention in the last decade.[1] With the rapid development of the communication technique, the size of acoustic devices is required to be smaller and smaller. For instance, the gigahertz communication generally requires the nanosized devices. In this case the influence of surface/interface energy and stress becomes significant.[2,3] It is expected that a phononic crystal should also exhibit unique physical properties when its lattice scale and scatterers' size are in the nanoscale.[4] Such nano phononic crystals will have potential application in design of nanostructure devices, nano electric-mechanical systems (NEMS), etc. In this paper, the wave propagation behaviors in nanosized phononic crystals will be studied by considering the surface/interface effects.

The method based on the Dirichlet-to-Neumann map[5] will be used to calculate the band structures. The method not only has advantages in accuracy, fast convergence and memory-saving but also can deal with the particular boundary conditions. This allows us to consider the surface/interface effects using the Young-Laplace equation.[6]

Problem statement and numerical method

The considered system is a 2D phononic crystal composed of circular holes or elastic inclusions in an elastic solid in a square lattice. The lattice constant, a, and the scatterers' radius, r_0, are all in nanoscales. Set the *z*-axis along and the *xy*-plane perpendicular to the axis of the scatterer. Then we consider a harmonic transverse wave polarized in the *z*-direction and propagating in the *xy*-plane. The governing equation of this purely transverse harmonic wave is $\nabla^2 w + k^2 w = 0$ where w is the displacement component in *z*-direction with the time harmonic factor $e^{-i\omega t}$ suppressed; and $k = c_t / \omega$ are the wave number with c_t being the transverse wave velocity and ω the angular frequency.

To taking into account of the surface/interface effects, we impose the following famous Young-Laplace equation[6] on the surface/ionterface of the hole/inclusion:

$$[\sigma_{rz}] = -\frac{1}{r_0}\frac{\partial \sigma^s_{\theta z}}{\partial \theta},\ \sigma^s_{\theta z} = 2\left(\mu^s - \tau_0\right)\varepsilon^s_{\theta z}, \tag{1}$$

where $\sigma^s_{\theta z}$, $\varepsilon^s_{\theta z}$, μ^s are the surface stress, strain and modulus; τ_0 is the residual stress (generally we take $\tau_0 = 0$); and $[\sigma_{rz}]$ represents the difference between the bulk stresses of the matrix and scatterer.

The method based on the Dirichlet-to-Neumann map (DtN map) will be used to calculate the band structures of the nanosized phononic crystals with consideration of surface/interface effects. The

Phononics 2011: First International Conference on Phononic Crystals, Metamaterials and Optomechanics
Santa Fe, New Mexico, USA, May 29-June 2, 2011
PHONONICS-2011-0060

method was first developed by Yuan and Lu[5] for calculating the band structures of photonic crystals. It can be extended to the phononic crystals in a straight forward manner when the purely transverse wave is considered. The key steps of the method are: (*i*) represent the general solution of the wave equations by the cylindrical wave expansions with coefficients being determined by using the Young-Laplace equation at the surface/interface; (*ii*) obtain the DtN map, which relates the displacement component with its normal derivation on the boundary of the square unit cell based on the general solution (For the purpose of numerical computation, the discrete form of the DtN map should be given. To this end, we select N points on each edge of the square unit cell and write the DtN map in a $4N\times4N$ matrix); (*iii*) then apply the Bloch theorem and the periodicity conditions to the boundaries of the unit cell, and formulate the problem in an eigenvalue equation; (*iv*) finally solve the eigenvalue equation to obtain the dispersion relation, i.e. the band structures.

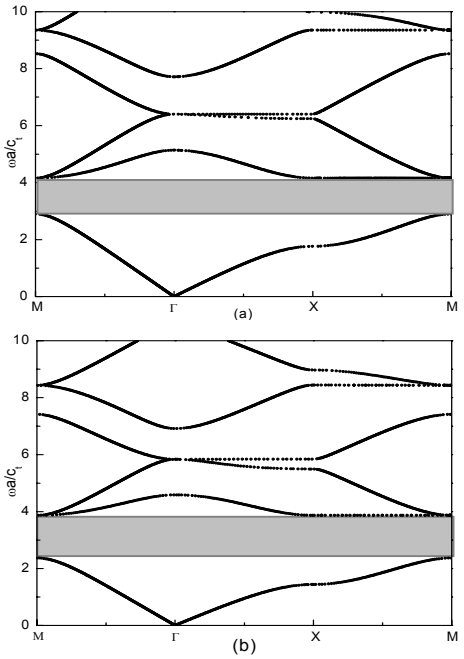

Figure 1 The band structures of the phononic crystal with a square lattice of vacuum cylindrical holes in an aluminum host with the filling fraction of 0.55: (a) neglecting the surface effect; (b) taking into account of the surface effect, $(\mu^s-\tau_0)/\mu_{\text{matrix}}r_0$=–0.06.

Results and Discussion

Two systems are computed by using the DtN-based method. One is a square lattice of vacuum cylindrical holes in an aluminum host; another is a square lattice of aluminum cylinders in a tungsten host. The band structures for these two systems with and without the surface/interface effects are presented in Figs. 1 and 2.

The results show that, due to the existence of the surface/interface effects, all bands descend and the first band gap becomes lower and a little wider. Further calculations show that the position of the band gap decreases with a very slight increase of the width as the absolute value of the parameter $(\mu^s-\tau_0)/\mu_{\text{matrix}}r_0$ increases.

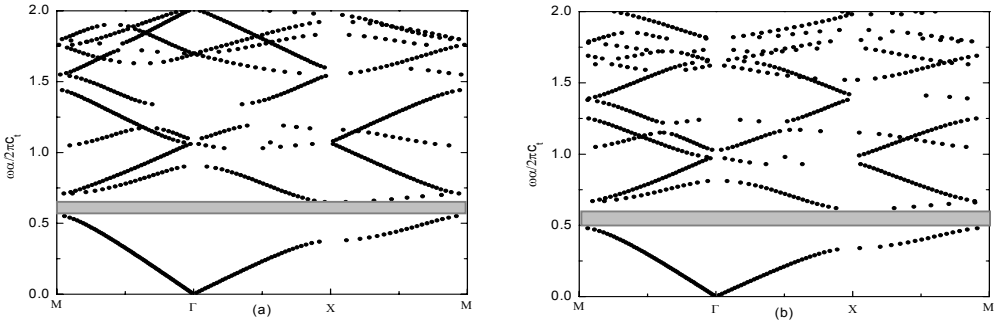

Figure 2 The band structures of the phononic crystal with a square lattice of aluminum cylinders in a tungsten host with the filling fraction of 0.55: (a) neglecting the interface effect; (b) taking into account of the interface effect, $(\mu^s-\tau_0)/\mu_{\text{matrix}}r_0$=–0.06.

References

[1] Y. Pennec, B. Djafari-Rouhani, H. Larabi, J. Vasseur, and A. –C. Hladky-Hennion, *Phys. Status Solidi C* **6**, 2080-2085 (2009).
[2] R. E. Miller, and V. B. Shenoy, *Nanotechnology* **11**, 139-147(2000).
[3] S. M. Hasheminejad, and R. Avazmohammadi. *Comp. Sci. Tech*. **69**, 2538-2546(2009).
[4] N. Gomopoulos, D. Maschke, C. Y. Koh, E. L. Thomas, W. Tremel, H. -J. Butt, and G. Fytas, *Nano Lett.* **10**, 980-984(2010).
[5] J. H. Yuan, and Y. Y. Lu, *Opt. Soc. Am*. **23**, 3217-3222(2006).
[6] M. E. Gurtin, and A. I. Murdoch, *Arch. Ration. Mech. Anal.*, **57**, 291-323(1975).

Phononics 2011: First International Conference on Phononic Crystals, Metamaterials and Optomechanics
Santa Fe, New Mexico, USA, May 29-June 2, 2011
PHONONICS-2011-0061

Phononic Crystal Sensors

M. M. Sigalas, N. Aravantinos-Zafiris

Department of Materials Science, University of Patras, 26504 Patras, Greece,
sigalas@upatras.gr, naravadinos@upatras.gr

Abstract: Numerical studies of phononic crystals for sensors applications are presented. The sensitivities of the structures on their parameters are studied. Particular attention was given in structures that can be probed with both electromagnetic and elastic waves.

Phononic materials are computationally studied using the finite difference time domain (FDTD) method for possible applications as sensors. The structures studied where similar with the ones used in photonic crystal sensors applications.[1] They are structures with air holes and that allows the detectable materials to be more accessible in the structure. Consequently, the changes in the frequency response of elastic waves propagating in those structures are higher.

The first structure studied was an epoxy slab with a square lattice of air holes. The lattice constant is 333nm, the radius of the air holes is 100nm and the thickness of the slab is 333nm. The transmission of elastic waves propagating through this structure shows a gap at around 6 GHz (solid line in Fig. 1). Covering the surface of this structure with a 16.6nm thick layer of water (see dash line in Fig. 1) changes the upper and lower band gap edges. Therefore it can be used a sensor for detecting different materials such as moisture and liquids or even proteins and other biological molecules.

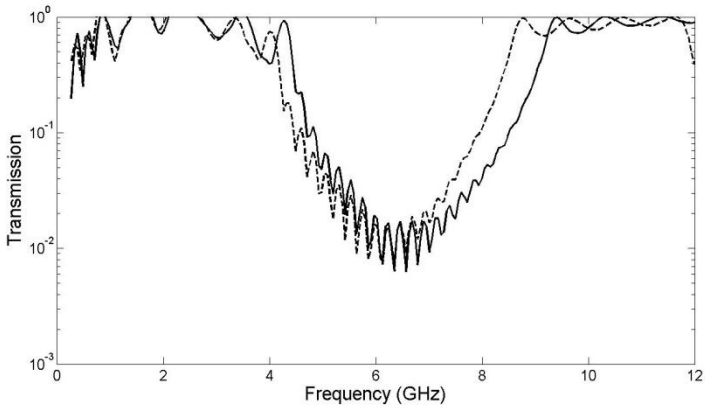

Figure 1 The transmission spectrum of elastic waves in an epoxy slab with a square lattice of air holes.

The second structure studied is a three dimensional structure consisting of alternate layers of air rods perpendicular to each other. This is the so called layer by layer structure.[2] The background material is silicon. The separation of the rods in each layer is 1000nm, the width of the rods 500nm and the thickness of each layer is 333.3nm. A band gap appears at around 1.2 GHz (see solid line in Fig. 2). Covering the surface of the air rods with a 33.3nm layer of water, the response of elastic waves propagating through the structure changes (see dash line in Fig. 2).

Phononics 2011: First International Conference on Phononic Crystals, Metamaterials and Optomechanics

Santa Fe, New Mexico, USA, May 29-June 2, 2011

PHONONICS-2011-0061

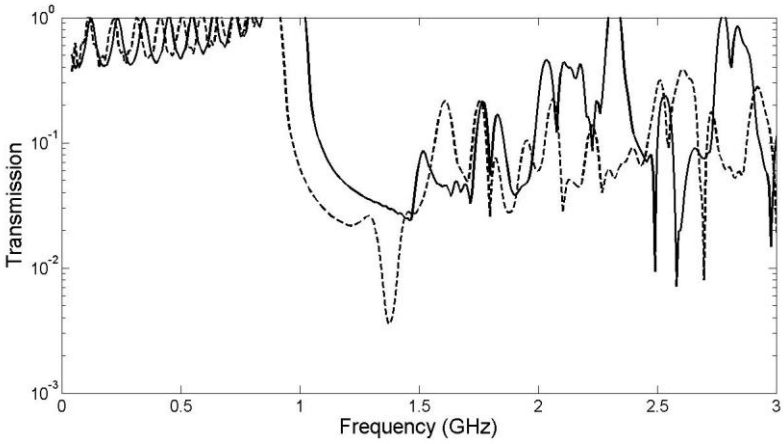

Figure 2 The transmission spectrum of elastic waves in a layer by layer structure made of air holes in silicon.

The different parameters affecting the sensitivity of these structures will be presented, such as the size of the holes and the thickness of the slab. Results for defect structures will be presented. Also, the possibility of using those structures as hybrid sensors that can be probed with both electromagnetic and elastic waves will be discussed.

References

1. E. Chow, et. al., Opt. Lett. 29, 1093 (2004); S. Zlatanovic, et. al., Sensors Actuators B 141, 13 (2009).
2. K. M. Ho, et. al, Solid State Commun. 89, 413 (1994).

Phononics 2011: First International Conference on Phononic Crystals, Metamaterials and Optomechanics
Santa Fe, New Mexico, USA, May 29-June 2, 2011
PHONONICS-2011-0065

Liquid Sensor Utilizing Phononic Crystals

Ralf Lucklum[1] , Mikhail Zubtsov[1], Manzhu Ke[1,2]

[1] *Institute of Micro and Sensor Systems, Otto-von-Guericke-University, Magdeburg, Germany*
ralf.lucklum@ovgu.de, mikhail.zubtsov@ovgu.de
[2] *Department of Physics, Wuhan University, China*
mzke@whu.edu.cn

Abstract: A phononic crystal device is investigated as a sensor platform combining bandgap engineering with resonant transmission. We compare several approaches: a one-dimensional arrangement with a thin liquid analyte layer, two-dimensional phononic crystals with and without symmetry reduction and incidence directions normal and perpendicular to the plate.

Motivation:

Ultrasonic sensors and acoustic microsensors have been successfully exploited as chemical sensors for liquids. Ultrasonic sensors first of all use the dependence of speed of sound on the composition of a liquid mixture whereas acoustic microsensors achieve chemical sensitivity with a specific coating. Time-of-flight and resonance frequency, respectively, are the most utilized measurement parameters. Both principles cannot be combined with microfluidic systems without severe limitations. The demand on sensors is permanently increasing which provide data related to material properties like concentration of an analyte in a fluid, conversion rate in a microreactor or adsorption of biomolecules. Phononic crystals have the capability to closing this gap since characteristic dimensions can be scaled in an appropriate range without losing its most pronounced feature, the acoustic band gap.

Sensor Scheme:

Phononic crystals are periodic composite materials with spatial modulation of acoustically relevant parameters like elasticity, mass density and longitudinal and transverse velocities of elastic waves. When applied as sensor, the material of interest constitutes one component of the phononic crystal, e.g., a fluid in the holes of a phononic crystal with a solid matrix. If the value of interest, let's say the concentration of a contaminant in a liquid mixture, changes acoustic properties of this mixture, the acoustic properties of the phononic crystal will also change. Transmission or reflection coefficients are appropriate parameters for measurement and used to localize a characteristic feature of the phononic crystal. For a sensor application, a transmission peak within the band gap or a transmission dip outside the band gap is the most favorable feature since the respective frequency of maximum/minimum transmission is easy to determine. The sensor scheme therefore relies on the determination of the frequency dependence of maximum/minimum transmission on the physical or chemical value of interest.

Sensitivity:

The sensitivity of the sensor, S_f can be defined as the ratio of frequency shift, Δf, and change of the input parameter, Δx:

$$S_f = \frac{\Delta f}{\Delta x} \tag{1}$$

The sensitivity has been found to be dependent on the probing frequency, f_0. Furthermore, in terms of the detection limit the peak half band width, f_{HBW}, must be considered, hence the reduced sensitivity, S_{fr}, gives much better insights to the sensor capabilities:

$$S_f = \frac{\Delta f}{\Delta x f_0 \Delta f_{HBW}} \tag{2}$$

Phononics 2011: First International Conference on Phononic Crystals, Metamaterials and Optomechanics
Santa Fe, New Mexico, USA, May 29-June 2, 2011
PHONONICS-2011-0065

Sensor Realizations:

The simplest realization of a sensor is the parallel arrangement of several layers of metal plates and a liquid in between. The transmission properties can by analytically calculated; the results can serve as proof-of-principle. Furthermore, relations relevant for a sensor application could be revealed. It is possible to realize geometries with well-defined transmission peaks in the band gap. The number of peaks increases with the number of layers, whereas breaking symmetry reduces the number of peaks. The sensitivity related to those peaks is different and in the order of macroscopic sensors. Peaks could be found which are independent of liquid properties; they may act as reference. The peak half band width decreases with the number of layers. Experiments have been performed at frequencies around 1 MHz, requiring mm dimensions.

Sensors utilizing 2D phononic crystal have been studied in two basic arrangements, with in-plane excitation and detection of waves and an incidence direction perpendicular to the plate. For comparison reasons, the design has been optimized for similar probing frequencies. In both realizations a liquid fills all holes of the phononic crystal plate; in the latter case it also covers both surfaces. In the 'classical' arrangement a design with a band gap between 1.2 MHz and 1.9 MHz could be found which moves when a liquid with different properties is applied. More importantly, a specific peak could be identified which represents changes in liquid properties. However, an unfavorable large number of peaks appears in the band gap when the phononic crystal holes are liquid filled. To reduce the number of peaks and improve the separation the symmetry of the lattice has been reduced by stretching and distorting. The reduced sensitivity achieved so far is similar to the one-dimensional case and indicates similar physical background for the appearance of these narrow transmission windows. They are basically supported by resonance-like phenomena. From the sensor point of view the respective vibration modes are of superior importance since it allows distinguishing between volume and surface/interfacial effects. Detail about simulation tools are given in [1].

When applying normal incidence of waves, also a characteristic transmission peak, see Fig. 1, could be found which strongly depends on liquid sound velocity. Again, this extraordinary transmission feature is supported by resonance phenomena in the phononic crystal structure. The half band width of this peak is larger; hence the reduced sensitivity is lower than in the other realizations. On the other hand, the effect is more robust and the insertion loss of the device is much lower, an important issue from a practical point of view. Since the peak frequency position is completely defined by material properties of the participating materials and geometry (hole radius and lattice constant) no calibration is needed. We therefore could also analyze sytematic error propagation. This analysis could, for example, clarify systematic differences between theory and experiment. Details will be given in [2].

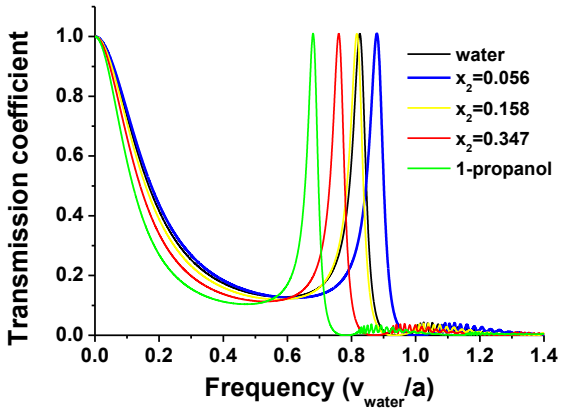

Figure 1 Results of FDTD calculations of the transmission spectrum of ultrasonic waves through a 2D phononic crystal at normal incidence. The phononic crystal consists of a steel plate with square lattice of holes. The composition of the liquid gradually changes from pure water (black) to pure propanol (green). The shift of the maximum transmission peak frequency reflects the extreme in speed of sound having the highest resonance frequency at molar ratio $x_2 = 0.056$.

References

[1] M. Zubtsov, R. Grundmann, R. Lucklum, subm. to Phononics 2011.
[2] M. Ke, M. Zubtsov, R. Lucklum, subm. to Phononics 2011.

Phononics 2011: First International Conference on Phononic Crystals, Metamaterials and Optomechanics
Santa Fe, New Mexico, USA, May 29-June 2, 2011
PHONONICS-2011-0072

Propagation and Transmission of Elastic SH-Waves in Functionally Graded Phononic Crystals

Mikhail V. Golub[1], Sergey I. Fomenko[1], Tinh Quoc Bui[2], Chuanzeng Zhang[2]

[1] *Institute for Mathematics, Mechanics and Informatics, Kuban State University, Stavropolskaya Str. 149, 350040 Krasnodar, Russian Federation*
m_golub@inbox.ru; sfom@yandex.ru;
[2] *Department of Civil Engineering, University of Siegen, D-57068 Siegen, Germany*
tinh.buiquoc@gmail.com; c.zhang@uni-siegen.de;

Abstract: The boundary value problem of elastic SH-wave propagation in one-dimensional phononic crystals composed of functionally graded interlayers arisen from the solid diffusion of homogeneous isotropic material of the crystal is considered. The localization phenomena, transmission and band gaps due to the material gradation are investigated.

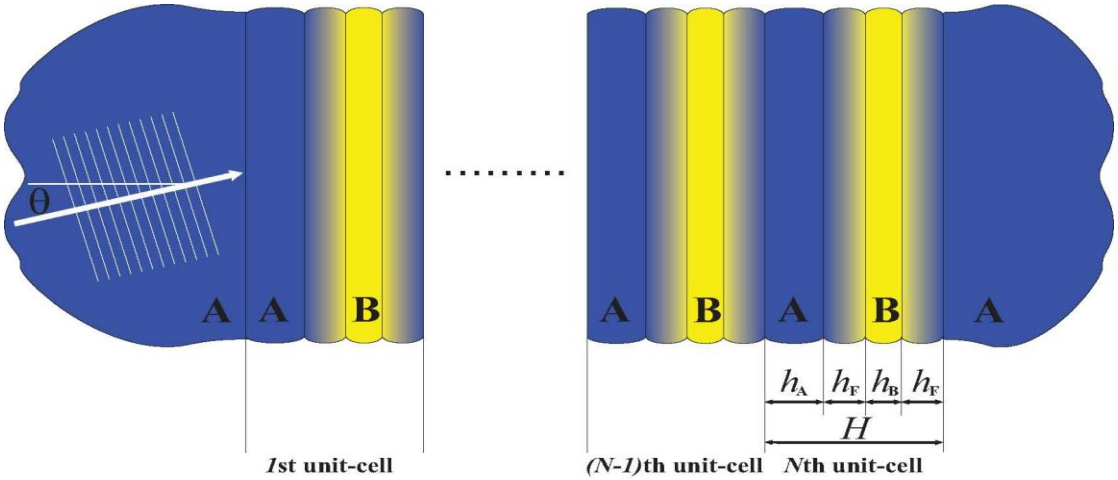

Figure 1 Geometry of the problem: periodic composite of functionally graded unit-cells.

The present work aims to propose a detailed study to band-structure analysis and elastic wave propagation in one-dimensional phononic crystals of functionally graded materials (FGM) by using the boundary integral equation method and an extended transfer matrix method. The structure of the phononic crystals is composed of finite periodically spaced unit-cells in one-dimension made of both functionally graded and isotropic materials (Figure 1). The power and exponential laws representing the material properties of the FGM are used. In both cases two approaches are used, namely, approximate modeling of the FGM structure by a certain number of isotropic layers and exact solution of the boundary value problem (Figure 2).

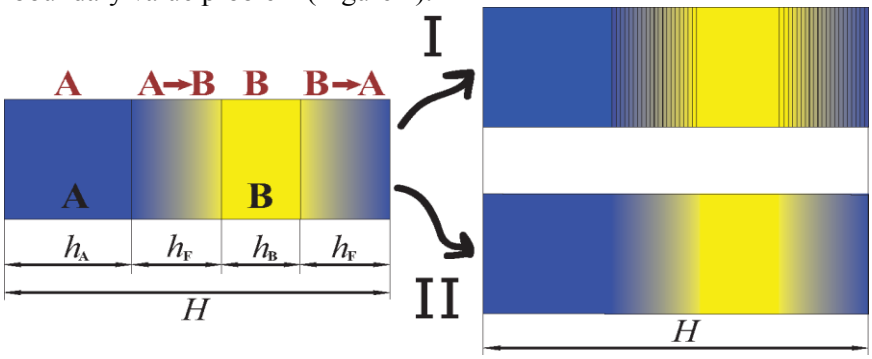

Figure 2 Models used for the simulation of functionally graded unit-cells (isotropic layers or exact solution).

Typical phenomena involving wave localization and transmission are analyzed, and the possibility of the damaged layers introduced following reference[1] is discussed. The comparison of the band gaps calculated using the present approaches as a special case of one-dimensional (1D) phononic crystal for SH propagation with that of FGM rod[2] is successfully carried out. This illustrates the applicability and the accuracy of the pro-

Phononics 2011: First International Conference on Phononic Crystals, Metamaterials and Optomechanics
Santa Fe, New Mexico, USA, May 29-June 2, 2011
PHONONICS-2011-0072

posed methods compared with the existing reference solutions. The model can be extended to other types of waves (P-SV waves) and cases with different types of internal inhomogeneities (cracks, imperfect bonding etc.).

The plane SH-wave in an elastic media is governed by the following equation

$$\frac{\partial}{\partial z}\left(\mu(z)\frac{\partial u(x,z,t)}{\partial z}\right)+\mu(z)\frac{\partial^2 u(x,z,t)}{\partial x^2}=\rho(z)\frac{\partial^2 u(x,z,t)}{\partial t^2} \tag{1}$$

Here $\rho(z)$ and $\mu(z)$ are the mass density and the shear modulus of the periodic layered structure. The material constants in the homogenous layers A and B of the unit-cell are continuously varied through a diffusion layer between A and B (Figure 1). The displacement $u(z)$ and stress $\tau(z)=\mu\,\partial u/\partial z$ fields are continuous at the interfaces of the layered structure.

The transfer matrix method for phononic crystals with FGM sublayers can be modified in the following way. Let us consider the j-th layer of the unit-cell bounded by the $z=z_j^{(1)}$ and $z=z_j^{(2)}$ planes. From the governing equation (1) the generalized displacement and stress state vector $\mathbf{v}=\{u,\tau\}$ is expressed in terms of the T-matrix [3,4]

$$\mathbf{v}(z)=\mathbf{T}_j(z-z_j^{(1)})\mathbf{v}_j^{(1)},\qquad z\in[z_j^{(1)},z_j^{(2)}],$$

where $\mathbf{v}_j^{(1)}$ is the incoming wave field, $\mathbf{T}_j$ is the T-matrix (transfer matrix) that is expressed in term of the fundamental solutions $\mathbf{v}_{j1}=\{u_{j1},\tau_{j1}\}$ and $\mathbf{v}_{j2}=\{u_{j2},\tau_{j2}\}$

$$\mathbf{T}_j(z)=\begin{pmatrix}u_{j1} & u_{j2}\\ \tau_{j1} & \tau_{j2}\end{pmatrix}$$

Here $\mathbf{v}_{j1}$ and $\mathbf{v}_{j2}$ are solutions of the following boundary value problems

$$\frac{d\mathbf{v}_{jk}}{dz}=\mathbf{B}(z+z_j^{(1)})\mathbf{v}_{jk},\quad \mathbf{v}_{j1}\big|_{z=0}=\{1,0\},\ \mathbf{v}_{j2}\big|_{z=0}=\{0,1\};\ \mathbf{B}(z)=\begin{pmatrix}0 & 1/\mu\\ -\mu q^2 & 0\end{pmatrix} \tag{2}$$

The T-matrix of a homogenous layer (A or B) is represented by an explicit formula (see e.g. reference[5]). Except the particular cases (e.g., exponential law) the T-matrix of the FGM layer is evaluated numerically. The numerical solution of the boundary value problem (2) is an explicit approach to be developed following reference[6]. Both models (see Figure 2) for the problem are compared with respect to their efficiency and accuracy. The convergence of both approaches, the band gaps and the transmission coefficients for different material gradation laws are investigated by numerical examples.

The work is supported by the Ministry of Education and Science of Russian Federation (Project 1.1.2/10463), the German Research Foundation (DFG, Project No. ZH 15/11-1) and the German Academic Exchange Service DAAD, which are gratefully acknowledged.

References

[1] J. Baik, R. Thompson, *Journal of Nondestructive Evaluation*, **4**, 177-196 (1984).
[2] M.-L. Wu, L.-Y. Wu, W.-P. Yang, L.-W. Chen, *Smart Materials and Structures* **18**, 115013 (2009).
[3] M. Born, E. Wolf, *Principles of Optics: Electromagnetic Theory of Propagation, Interference and Diffraction of Light*. Oxford, Pergamon Press (1964).
[4] O. Matsudaa, Ch. Glorieux, *Journal of Acoustical Society of America* **121 (6)**, 3437-3445 (2007).
[5] F.-M. Li, Y.-S. Wang, *International Journal of Solids and Structures* **42**, 6457-6474 (2005).
[6] E.V. Glushkov, N.V. Glushkova, *Journal of Computational Acoustics*, **9(3)**, 889-898 (2001).

Phononics 2011: First International Conference on Phononic Crystals, Metamaterials and Optomechanics
Santa Fe, New Mexico, USA, May 29-June 2, 2011
PHONONICS-2011-0073

Phononic crystals with complete phase space properties

P.A. Deymier[1], N. Swinteck[1], S. Bringuier[1], K. Muralidharan[1], J.O. Vasseur[2], J-F. Robillard[2], A.-C. Hladky-Hennion[2], A. Sukhovich[3] and J.H. Page[3]

[1] *Department of Materials Science and Engineering, University of Arizona, Tucson, Arizona 85721, USA,* deymier@email.arizona.edu, swinteck@email.arizona.edu, stefanb@email.arizona.edu, Krishna@email.arizona.edu

[2] *Institut d'Électronique, de Microélectronique et de Nanotechnologie, UMR CNRS 8520, Cité Scientifique, 59652 Villeneuve d'Ascq Cedex, France,* jerome.vasseur@univ-lille1.fr, jean-francois.robillard@isen.fr, anne-christine.hladky@isen.fr,

[3] *Department of Physics and Astronomy, University of Manitoba, Winnipeg, Manitoba, R37 2N2, Canada* jhpage@cc.umanitoba.ca, alexey.sukhovich@geoazur.obs-vlfr.fr

Abstract: We review and demonstrate properties of phononic crystals over their complete phase space, namely, spectral (ω-space), wave vector (*k*-space) and phase (*φ*-space) properties. The later two properties are applied to acoustic imaging with a phononic crystal flat lens and to interference-driven acoustic Boolean logic.

Phononic crystals (PC) are composite materials which derive their spectral (ω-space) and wave vector (*k*-space) properties from the scattering of elastic waves by periodic arrays of elastic inclusions embedded in an elastic matrix. Perfect PCs and ones with defects have been shown to exhibit numerous useful spectral capabilities including transmission band gaps, local modes for guiding, filtering and multiplexing [1]. *k*-space properties result from features in the band structure that impact refraction. Phase (*φ*-space) properties can result from non-collinear wave and group velocity vectors in the PC as well as the degree of refraction [2]. PC may show negative refraction leading to the possibility of developing flat lenses for focusing acoustic waves. To illustrate *k*-space functionalities, we discuss acoustic wave focusing (resulting from negative refraction) and subwavelength imaging capabilities of a PC flat lens consisting of a triangular array of steel cylinders in methanol, all surrounded by water (Fig. 1). The image resolution of the PC flat lens beats the Rayleigh diffraction limit because bound modes in the lens can be excited by evanescent waves emitted by the source. These are modes that only propagate in the direction parallel to the water/lens interface. These modes resonantly amplify evanescent waves that contribute to the reconstruction of an image. By employing a combination of experimental and computational (Finite Difference Time Domain (FDTD)) methods, we explore the effect on the image resolution and focal point on various structural and operational parameters such as source frequency, geometry of the lens, source position and time. The mechanisms by which these factors affect resolution are discussed in terms of the competition between the contribution of propagative modes to focusing and the ability of the source to excite bound modes of the PC lens.

We also demonstrate that the band structure of a two-dimensional PC constituted of a square array of cylindrical Polyvinylchloride (PVC) inclusions in an air matrix can be used to control the relative phase of acoustic waves. Phase control is due to the propagation of acoustic waves in the PC with wave vectors that are not collinear with their group velocity vectors. This condition implies that excited Bloch waves travel at different phase velocities in the direction of their group velocity. By modulating the phase between waves in the PC, destructive or constructive interference can occur and through this information can be encoded. In addition to phase control between pairs of acoustic beams, the band structure of this PC allows for superposition of wave vectors via the excitation of the same Bloch modes. This unique feature once again permits the possibility of destructive or constructive interferences within the PC; therefore it is another mechanism in which information can be encoded through relative phase. These two schemes of encoding information in phase establish the Boolean logic necessary for gating functions. The realization of the NAND and XOR gates (fig. 1) was demonstrated through FDTD technique. There are also operating frequencies for which the circular equi-frequency contour (EFC) in air is larger than the first Bril-

Phononics 2011: First International Conference on Phononic Crystals, Metamaterials and Optomechanics
Santa Fe, New Mexico, USA, May 29-June 2, 2011
PHONONICS-2011-0073

louin zone of the PC, allowing several Bloch modes to exit the crystal, leading to the phenomenon of beam splitting. This PC illustrates the possibility of extending the range of functionalities from spectral and wave vector properties to phase (φ-space) properties.

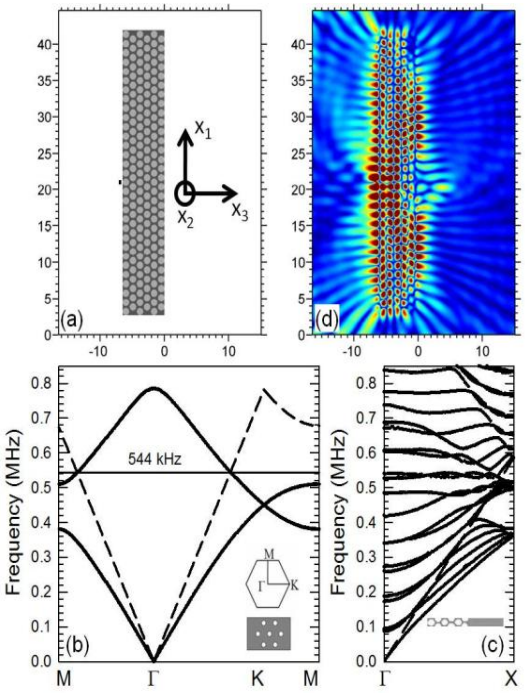

Figure 1: (a) Phononic Crystal system consisting of a triangular lattice of steel cylinders (light grey) in a methanol matrix (dark grey), all surrounded by water (white). The short thick line located close to the center of the left side of the crystal represents the sound source. (b) FDTD dispersion curves of the infinite crystal (solid lines). The dashed line represents the dispersion curve in water. The intersection of the water cone with a negative group velocity band determines the frequency that results in a negative effective index of -1 for the PC. The inset shows the triangular crystal lattice of the PC with the corresponding unit cell and the contour of the first Brillouin zone. (c) FDTD band structure in the ΓX direction (parallel to the surface) for a finite 6-layer crystal. Modes above water line correspond to propagating modes, while those which fall below are modes bound to the PC slab, which exhibit evanescent character. The inset depicts the supercell used in the calculation. (d) FDTD calculation of the average of the absolute value of the pressure over one period. On the exiting (right) side of the PC, an image is formed in the center accompanied by pressure lobes that decrease in magnitude as the distance from the surface of the crystal increases.

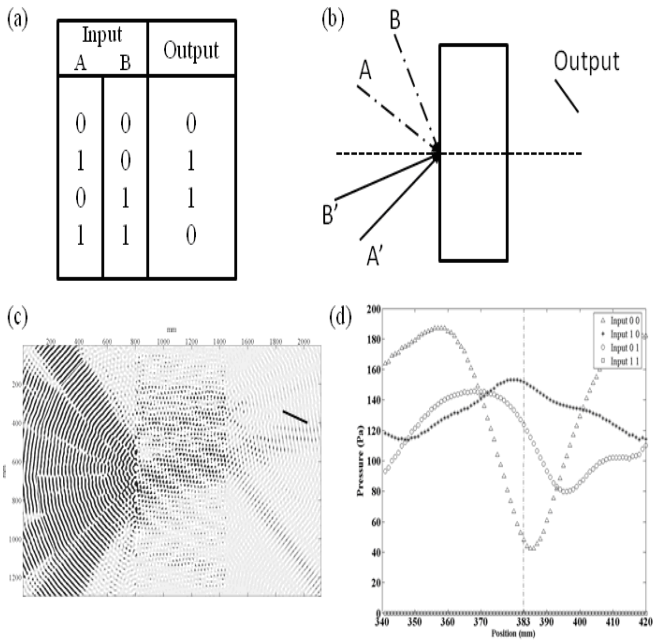

Figure 2: (a) Truth table for XOR logic gate. (b) schematic of PC logic gate, A' and B' are constant amplitude sources which are in phase. A and B are amplitude modulated sources which are out of phase with respect to A' and B'. (c) FDTD results for input (1 1) with output (0), black line represents where pressure detector is placed. (d) Average pressure cuts of all input cases. Pressure value for input (0 0) at 383mm is taken to be the pressure threshold.

References

[1] Yan Pennec, Jérôme O. Vasseur, Bahram Djafari-Rouhani, Léonard Dobrzynski, Pierre A. Deymier, Surf. Sci. Reports **65**, 229 (2010).
[2] A. Sukhovich, B. Merheb, K. Muralidharan, J.O. Vasseur, Y. Pennec, P.A. Deymier, J.H. Page, Physical Review Letters **102**, 154301 (2009)

Phononics 2011: First International Conference on Phononic Crystals, Metamaterials and Optomechanics
Santa Fe, New Mexico, USA, May 29-June 2, 2011
PHONONICS-2011-0082

Propagation of the Elastic Wave in One-dimensional Randomly Disordered Solid-liquid Phononic Crystals

A L Chen[1] , Y S Wang[2], C Zhang[3]

[12] Institute of Engineering Mechanics, Beijing Jiaotong University, Beijing 100044, China, alchen@bjtu.edu.cn, yswang@bjtu.edu.cn
[3] Department of Civil Engineering, University of Siegen, D-57068 Siegen, Germany c.zhang@uni-siegen.de

Abstract: The wave propagation and localization in one-dimensional (1D) randomly disordered solid-liquid phononic crystals are studied in this paper. The transfer matrix method is used to calculate the localization factor which is introduced to describe the band structures for the disordered phononic crystals. The fluid-structure interaction is considered and the oblique incidence is studied.

Introduction

Since Kushwaha[1] proposed the concept of the phononic crystal (PNC) in 1993, an artificial periodic elastic/acoustic structure that exhibits so-called "phononic band gaps", a lot of results on the mechanism and the tuning of band gaps for various systems as well as the defect states of the systems with point or line defects have been reported, cf. the website http://www.phys.uoa.gr/phononics/. When a point, line or surface defect is introduced into an ordered PNC, waves will be localized near the defects[2]. This property can be used to design new acoustic wave devices such as wave filters, waveguides, resonators, et al. PNCs mentioned above are strictly periodic in which all waves are extended states or have little defects in which some waves are localized states but most waves are extended states, so the Bloch theorem can be used[3]. Random disorder, caused by randomly distributed material defaults or manufacture errors during production process, is a different case. It is well known that the presence of the disorders may lead to localization phenomenon like the well-known Anderson localization of electron waves in disordered lattices[4]. Researches on randomly disordered PNCs are limited. In this paper we will study the acoustic waves propagating in the one-dimensional (1D) randomly disordered solid-liquid PNC. The general case of wave propagation in an arbitrary direction will be considered. The transfer matrix method[5] will be employed by considering the coupling conditions of the solid and liquid media at the interface. Instead of calculating the transmitted waves, we will use a well-defined localization factor to characterize the band structures and localization phenomenon of the system.

The Method

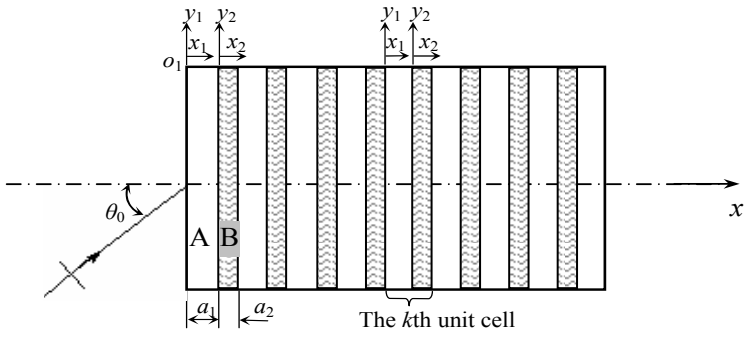

Figure 1 Schematic diagram of a 1D phononic crystal

Consider a 1D PNC shown in Fig.1. The PNC consists of n unit cells. Each unit cell includes two subcells made by two different materials (the solid material A and the liquid material B) and denoted by subscript j =1,2. In this paper the transfer matrix method is used. As we know, the transfer matrix is 2×2 and 4×4 for the liquid and solid layer, respectively. Considering the fluid-structure interaction condition the 4×4 transfer matrix for the solid layer can be deduced to the 2×2 matrix.

The solutions to the equations of wave motion are obtained by introducing potential functions to those equations. The transfer matrix between two consecutive sub-layers is obtained according to conditions

Phononics 2011: First International Conference on Phononic Crystals, Metamaterials and Optomechanics
Santa Fe, New Mexico, USA, May 29-June 2, 2011
PHONONICS-2011-0082

at the interface between the solid and fluid. The localization factor γ of the 1D PNCs is calculated by the transfer matrix method. The formulate of the localization factor is given as[6]

$$\gamma_m = \lim_{n\to\infty} \frac{1}{n} \sum_{k=1}^{n} \ln \left\| \hat{\boldsymbol{\nu}}_{2R,m}^{(k+1)} \right\| \tag{1}$$

When the localization factors in the figures are equal to zero then the according frequency intervals are known as pass bands. When the localization factors are bigger than zero then the intervals are known as band gaps.

Numerical Examples and Discussions

We consider the PNC composed of Al (material A) and Water (material B). The disordered parameter is the thinkness of the liquid layer (a_2) which can be expressed as $a_2 = \overline{a}_2[1+\sqrt{3}\delta(2t-1)]$ where $t \in (0,1)$ is a random variable; and δ is the disordered degree. It is understood that $\delta = 0$ is the case of a perfect periodic structure. For clarity of discussion, we introduce dimensionless frequency $\Omega_{L1} = \omega\overline{a}_1 / c_{L1}$ where c_{L1} is the longitudinal wave speed in the solid material.

The influences of the disordered degree on the band structures of the 1D ordered (the black solid line) and disordered (the blue dashed line and the red dotted line) PNCs for the wave incidence at an angle of 30° are described in Fig. 2. It can be seen from the figure that for 1D ordered solid-liquid PNCs the pass bands are narrower than the band gaps. For instance, consider the frequency intervals (0.725, 0.824) and (1.451, 1.495) (the zones marked by circles). It is observed that the location factor becomes positive in the pass bands (excluding the lowest pass bands) when δ is nonzero and increases in its value as δ increases. This behavior is the so-called localization of elastic waves. It should be noticed that there are two peaks at the frequencies 1.660 and 3.167 which means that the localization are stronger at these frequencies.

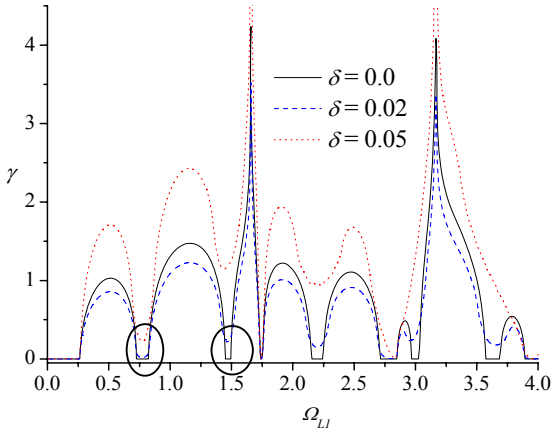

Figure 2 The influences of the disordered degree for the incident at an angle of 30°

Conclusions

The concept of the localization factor is introduced to describe the band structures and localization behaviors of 1D perfect and randomly disordered phononic crystals. The results show that the localization factor is an accepted and effective parameter in characterizing localization behavior of disordered phononic crystals. As the disorder of the system increase, the value of the localization factor increases in the bands. This localization behavior is more pronounced at higher frequencies.

Acknowledgements

The authors are grateful to the support by the National Science Foundation under Grant No.10902012 and 10632020.

References

[1] M. S. Kushwaha, P. Halevi, G. Martinez, L. Dobrzynski and B. Djafarirouhani, *Phys. Rev. Lett.* 71: 2022-2025(1993).
[2] A. Khelif, Y. Achaoui, S. Benchabane, V. Laude and B. Aoubiza, *Phys. Rev. B*, 81: 214303(2010).
[3] K. Huang and R. Q. Han, *Solid Physics*, Higher Education Press, Beijing (1988).
[4] P. W. Anderson, *Phys. Rev.* 109: 1492-1505(1958).
[5] E. L. Tan, *Ultrasonics*, 50: 91-98(2010).
[6] A. Wolf, J. B. Swift, H. L. Swinney and J. A. Vastano, *Phys. D*, 16: 285-317(1985).

Phononics 2011: First International Conference on Phononic Crystals, Metamaterials and Optomechanics
Santa Fe, New Mexico, USA, May 29-June 2, 2011
PHONONICS-2011-0084

Dynamic Imaging of Gigahertz Phonons on Phononic Crystal Slabs

Oliver B. Wright[1], Ryota Chinbe[1], Paul H. Otsuka[1], Motonobu Tomoda[1], Osamu Matsuda[1], Yukihiro Tanaka[1], Istvan A. Veres[2], Sihan Kim[3], Heonsu Jeon[3]

[1] Division of Applied Physics, Graduate School of Engineering, Hokkaido University, Sapporo 060-8628 Japan, assp@kino-ap.eng.hokudai.ac.jp
[2]Recendt, Research Center for Non Destructive Testing, Linz 4020, Austria
[3] Department of Physics and Astronomy and Inter-university Semiconductor Research Center, Seoul National University, Seoul 151-747, South Korea

Abstract: Surface phonon propagation on microscopic phononic crystal slabs of Si is dynamically imaged in two dimensions at frequencies up to 1 GHz by an ultrafast optical technique. The acoustic dispersion relations obtained by spatial and temporal Fourier transforms reveal stop bands and the eigenmode patterns. Phonon guiding and confinement in phononic crystal waveguides and cavities are also presented.

Surface acoustic wave devices based on one-dimensional (1D) periodic structures have found extensive application in high-frequency signal processing. 2D phononic crystals exhibit interesting physical properties, such as omnidirectional stop bands, that allow potential improvements to these devices. Here we present results of real-time imaging of optically-induced surface phonons at frequencies up to ~1 GHz in phononic crystal slab structures based on honeycomb lattices[1]. These structures exhibit complete stop bands for Lamb wave propagation.

We use optical pulses of duration ~200 fs, wavelength 830 nm and repetition rate 80 MHz from a Ti:sapphire femtosecond laser. A 415 nm pump beam derived from this laser excites phonon wave packets at a point on the sample surface by thermoelastic expansion. The 830 nm beam, after being delayed relative to the pump beam, is used to probe the sample with an interferometer. The beams are focused to spots of about 1 μm in diameter. The probe spot is scanned across the sample relative to the pump to generate images at various delay times over an area ~ 200×200 μm^2, allowing movies of the out-of-plane velocity of the surface motion to be obtained at acoustic frequencies up to ~ 1 GHz[2,3].

The samples are based on microscopic honeycomb lattices of circular holes patterned in (111) silicon-on-insulator wafers by a dry etching process. The silicon oxide (insulator) is then removed by wet

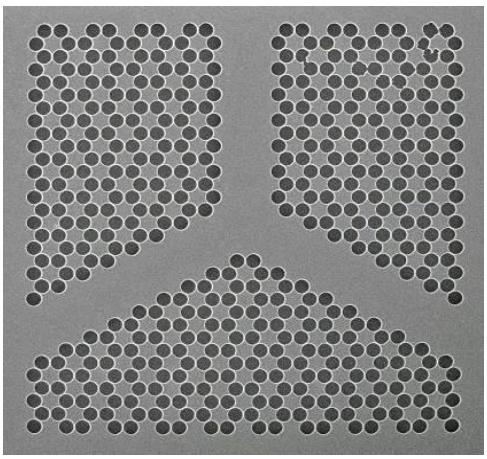

Figure 1 Electron microscope image of a (111) Si slab sample consisting of a Y-shaped waveguide formed by holes of diameter 5.8 μm arranged in a honeycomb lattice with center-to-center spacing 6.6 μm. The thickness of the slab is 6.5 μm.

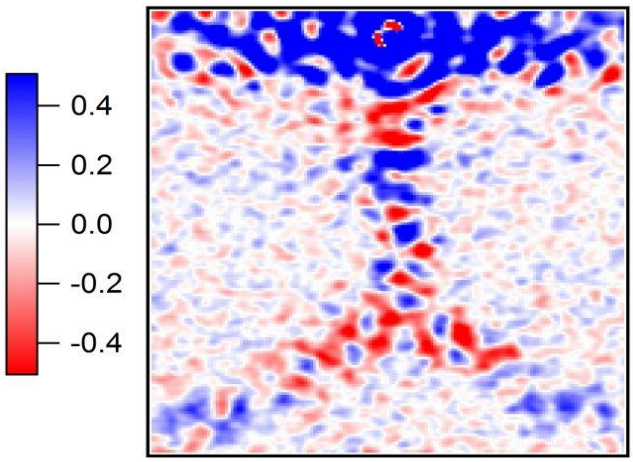

Figure 2 Corresponding image of the surface motion in the Y-shaped waveguide. The frequency is 322 MHz, lying at the top of the first stop band. A 200 × 200 μm^2 region is shown.

Phononics 2011: First International Conference on Phononic Crystals, Metamaterials and Optomechanics

Santa Fe, New Mexico, USA, May 29-June 2, 2011

PHONONICS-2011-0084

etching to leave free standing crystalline Si slabs of thickness 6.5 μm. A typical sample pattern, with the *x* axis corresponding in the [-2, 1, 1] direction of the crystal, is shown in Fig. 1; a Y-shaped region with no holes forms a phononic crystal waveguide. The center-to-center spacing of the holes is a=6.6 μm, whereas the diameter is $2r$=5.8 μm. The ratio r/a=0.44. The expected first complete phononic stop band lies between ~ 230 and 320 MHz for this phononic slab, as verified by simulations based on the orthogonal plane wave method.

Figure 2 shows a snapshot of a 200 μm square region of this sample at a frequency of 322 MHz. The excitation point is just outside the top end of the waveguide. This image was obtained from the temporal Fourier transform of time-domain data. Because this frequency corresponds to the top of the first stop band, the phononic waveguide transmits relatively efficiently.

We have in this way visualized the propagation of surface phonons in microscopic two-dimensional phononic crystals, phononic crystal waveguides and phononic crystal cavities based on this slab geometry. The dispersion relations, including stop bands, and the eigenmode patterns in two dimensions at individual frequencies are extracted by spatial and temporal Fourier transforms.

In addition we have conducted finite element time domain numerical simulations of phonon propagation in these phononic crystal structures that agree substantially with the experimental results. This work should lead to new diagnostic techniques for the propagation of surface acoustic waves in phononic structures, including surface acoustic wave devices[4].

References

[1] S. Mohammadi, A. A. Eftekhar, W. D. Hunt, and A. Adibi, *Appl. Phys. Lett* **94**, 051906 (2009).
[2] D. Profunser, E. Muramoto, O. Matsuda, O. B. Wright and U. Lang, *Phys. Rev. B* **80**, 014301 (2009).
[3] D. Profunser, O. B. Wright and O. Matsuda, *Phys. Rev. Lett.* **97**, 055502 (2006).
[4] T. Fujikura, O. Matsuda, D. M. Profunser, O. B. Wright, J. Masson, and S. Ballandras, *Appl. Phys. Lett.* **93**, 261101 (2008).

Phononics 2011: First International Conference on Phononic Crystals, Metamaterials and Optomechanics

Santa Fe, New Mexico, USA, May 29-June 2, 2011

PHONONICS-2011-0085

Observation and Simulation of Surface Acoustic Waves in Phononic Crystal

Paul H. Otsuka[1], István A. Veres[2], Keisuke Nanri[1], Sorasak Danworaphong[3], Motonobu Tomoda[1], Oliver B. Wright[1], Osamu Matsuda[1], Dieter Profunser[1], Abdelkrim Khelif[4], Vincent Laude[4], Sarah Benchabane[4]

[1]Graduate School of Engineering, Hokkaido University, Japan
paul@eng.hokudai.ac.jp
[2]Recendt, Research Center for Non Destructive Testing, Linz 4020, Austria
[3]School of Science, Walailak University, Thailand
[4]FEMTO-ST, Besancon, France

Abstract: We present an analysis of surface acoustic waves propagating in a microscopic phononic crystal waveguide consisting of a silicon crystal containing a square array of holes. Experiments are performed using an ultrafast optical method and the results are compared with an FEM simulation.

By modifying the structure inside a phononic crystal, waveguide devices that control the path of propagation of surface acoustic waves can be created[1,2]. Such devices are useful in signal processing and filtering applications. Optical generation and detection of surface waves has proved effective in visualising their propagation in real time[3,4]. We present results of real-time imaging and simulation of laser-induced surface acoustic waves at frequencies up to ~1 GHz in phononic crystals with a waveguide structure.

We generate and detect surface acoustic waves in phononic crystal waveguides using an optical pump-and-probe method[3,4]. The phononic crystals, made by deep reactive ion etching, contain microscopic circular holes 100 μm deep in (100) silicon arranged in a square array, with the waveguide channel formed by the absence of selected holes. The optical pulses used for excitation and detection are generated by a mode-locked Ti:sapphire laser. A 415 nm pump beam derived from this laser thermo-elastically excites the acoustic waves and an 830 nm probe beam delayed relative to the pump beam is used for detection with an interferometer. The optical pulse duration is ~200 fs and the repeti-

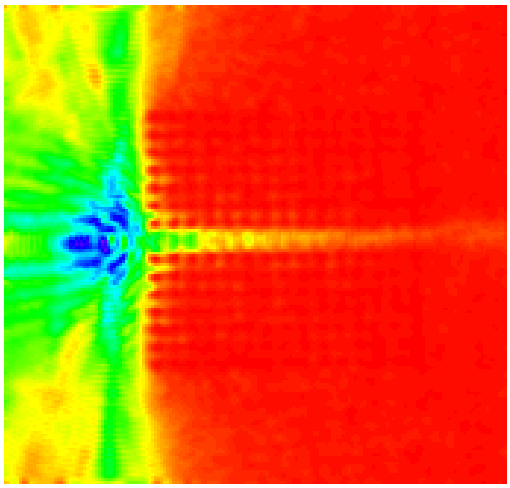

Figure 1 Experimental image of surface acoustic waves at 656 MHz propagating in a linear phononic crystal waveguide. Image size is 160×160 μm^2. The horizontal direction corresponds to the [011] crystalline direction.

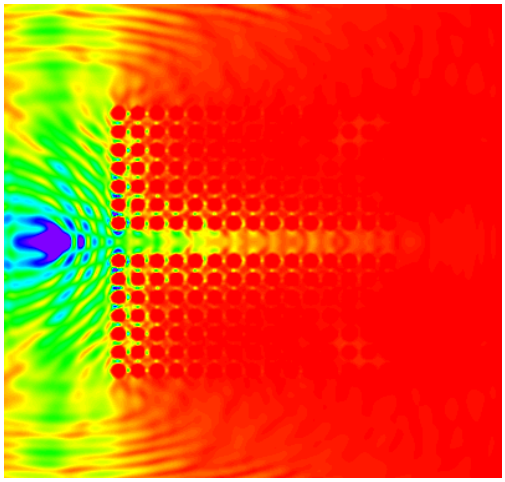

Figure 2 Simulation image of surface acoustic waves at 656 MHz propagating in a linear phononic crystal waveguide. Image size is 160×160 μm^2. The horizontal direction corresponds to the [011] crystalline direction.

Phononics 2011: First International Conference on Phononic Crystals, Metamaterials and Optomechanics
Santa Fe, New Mexico, USA, May 29-June 2, 2011
PHONONICS-2011-0085

tion rate is 80 MHz. The beams are focused to a spot of about 1 μm in diameter. The probe beam is scanned across the sample to generate images of regions of about 160×160 μm^2 in area. By varying the probe delay time, we build up animations of the surface waves propagating through the waveguides.

The experimental results are compared with a numerical simulation based on the Finite Element Method (FEM). The three-dimensional (3D) model consists of approximately 150 million nodes, and the resulting out-of-plane surface displacements are taken as the numerical counterpart of the experimental images. Movies of the surface wave propagation in the time domain are first obtained.

For both experiment and simulation results, we then use a dual Fourier transform method consisting of 1D temporal and 2D spatial Fourier transforms to extract the acoustic fields and slowness surfaces in 2D at individual frequencies. Time-resolved images reveal effects such as diffraction, refraction, reflection, resonance and waveguiding. The results show significant dependence of the wave propagation on frequency. In particular, the transmission through the waveguide channel shows peaks at particular frequencies. At other frequencies, there is strong attenuation due to the waves leaking into the phononic crystal region. Figure 1 shows the modulus of the experimentally measured field amplitude in a linear phononic crystal waveguide sample at 656 MHz. This frequency lies well above the first phononic stop band. The phononic crystal in this case is made up of a square lattice of circular holes with radius 6.5 μm, corresponding to a filling fraction of 70%. The pump pulses are focused at about 20 μm to the left of the opening of the waveguide, and the excited surface acoustic waves (SAW) propagate outwards from this point. Figure 2 shows the corresponding simulation results at the same frequency, exhibiting good agreement with the experiment. In both cases, there is significant attenuation of the excited waves in the waveguide channel. At other frequencies, for example at 328 MHz corresponding to the first phononic stop band, we observe much less attenuation in the waveguide.

This research allows the identification of the mechanisms responsible for the interaction of surface waves with phononic crystal devices, as well as being useful for the design and analysis of novel SAW waveguide devices.

References

[1] A. Khelif, A. Choujaa, S. Benchabane, B. Djafari-Rouhani, V. Laude, *Appl. Phys. Lett.* **84**, 4400 (2004).
[2] R. H. Olsson III, I. El-Kady, and J. G Fleming, *Sensors Actuators A*, **145–146**, 87 (2008).
[3] D. Profunser, E. Muramoto, O. Matsuda, O. B. Wright and U. Lang, *Phys. Rev. B* **80**, 014301 (2009).
[4] D. Profunser, O. B. Wright and O. Matsuda, *Phys. Rev. Lett.* **97**, 055502 (2006).

Phononics 2011: First International Conference on Phononic Crystals, Metamaterials and Optomechanics
Santa Fe, New Mexico, USA, May 29-June 2, 2011
PHONONICS-2011-0087

Evanescent Bloch Waves in Phononic Crystals: Complex Band Structure, Losses, and Guidance

Vincent Laude[1], Rayisa P. Moiseyenko[1,2]. Younes Achaoui[1], Sarah Benchabane[1], and Abdelkrim Khelif[1,2]

[1] *Institut FEMTO-ST, Université de Franche-Comté and CNRS, Besançon, France,*
vincent.laude@femto-st.fr, rayisa.moiseyenko@femto-st.fr, younes.achaoui@femto-st.fr, sarah.benchabane@femto-st.fr
[2] *Georgia Institute of Technology, GT-CNRS UMI 2958, Georgia Tech Lorraine, Metz, France*
akhelif3@mail.gatech.edu

Abstract: The complex band structure of evanescent Bloch waves in phononic crystals is elucidated by formulating an eigenvalue problem for the wavevector versus the frequency. It is used to explore the effects of material losses and the phononic crystal guidance mechanism. The method, originally formulated for plane waves, is extended to finite element models.

Phononic crystals are two- or three-dimensional periodic structures that consist of two materials with different elastic constants. They possibly give rise to absolute stop bands for a right choice of geometrical conditions and combination of materials. In addition, their unique dispersion properties can be used to design efficient waveguides, cavities or to obtain unusual refraction properties. Band structures are usually employed to describe infinite phononic crystals, as they provide information regarding any wave propagating in the periodic medium (Bloch waves). However, it is well-known that evanescent waves must be considered in propagation problems whenever scattering, diffusion, or diffraction by an object of finite size are investigated. In the context of phononic crystals, evanescent waves appear very naturally within frequency band gaps: since no waves can propagate within a band gap, only evanescent waves are left to explain the exponentially-decreasing transmission of acoustic waves. Furthermore, the mechanisms behind the creation of phononic crystal cavities and waveguides based on defects involve that only evanescent waves are present outside the defect, so that energy confinement can be guaranteed. A description of the effect of material losses on the propagation of elastic or acoustic waves can also be obtained – at least for incident monochromatic waves – by considering complex wavevectors.

In a recent paper[1], we extended the classical plane wave expansion (PWE) method so that it includes complex wave vectors in the direction of propagation. To do so, it is necessary to consider a fixed frequency and to solve for the wave vector $k(\omega)$, in contrast to the traditional way of obtaining band structures by considering any Bloch wave vector within the first Brillouin zone and solving for the frequency of allowed modes $\omega(k)$. The extended PWE method was used to generate band structures for two-dimensional solid-solid or solid-void phononic crystals. With the method, both propagative and evanescent solutions are found at once. The decay constants within band gaps are thus found and shown to depend on the wave polarization. Complex band structures also allow us to identify clearly the different branch systems in the band structure as these become continuous functions of the frequency. They also connect propagating bands below and above band gaps through evanescent bands, so that band folding can be unambiguously followed. Furthermore, the distribution of the acoustic fields of evanescent modes can be computed. Their transformation from below to above a band gap and within was shown to be perfectly continuous along the corresponding complex branch of the band structure.

As suggested above, complex band structures can be obtained for lossy phononic crystals. We have specifically considered the case of viscoelastic media. In order to include material damping, the rank-4 viscosity tensor η_{ijkl} is introduced. This tensor has the same symmetry as the elastic tensor c_{ijkl}. Attenuation can be assumed to increase linearly with frequency, as it proper to polymers but also to crystalline solids such as silicon, quartz or lithium niobate. For monochromatic waves, a complex-valued elastic tensor can then be written as $c_{ijkl} + i\omega\eta_{ijkl}$. More generally, any frequency dependent complex elastic tensor could be considered to model loss, without any further modification of the method. We have computed complex band structures via the extended PWE method for various phononic crystals, e.g. composed of steel rods in lossy epoxy[2] or of hollow holes in a silicon matrix, as depicted in Figure 1. Significantly, we have found that in contrast to homogeneous materials, the real part of the wavevector is more affected by losses than its imaginary part is. This effect is especially pronounced whenever the group velocity is small, for instance at the edges of a band gap. It also causes flat bands to acquire en-

Phononics 2011: First International Conference on Phononic Crystals, Metamaterials and Optomechanics

Santa Fe, New Mexico, USA, May 29-June 2, 2011

PHONONICS-2011-0087

hanced losses. Furthermore, the group velocity is limited by losses to finite values larger than zero, the value of the limit increasing with the level of viscosity.

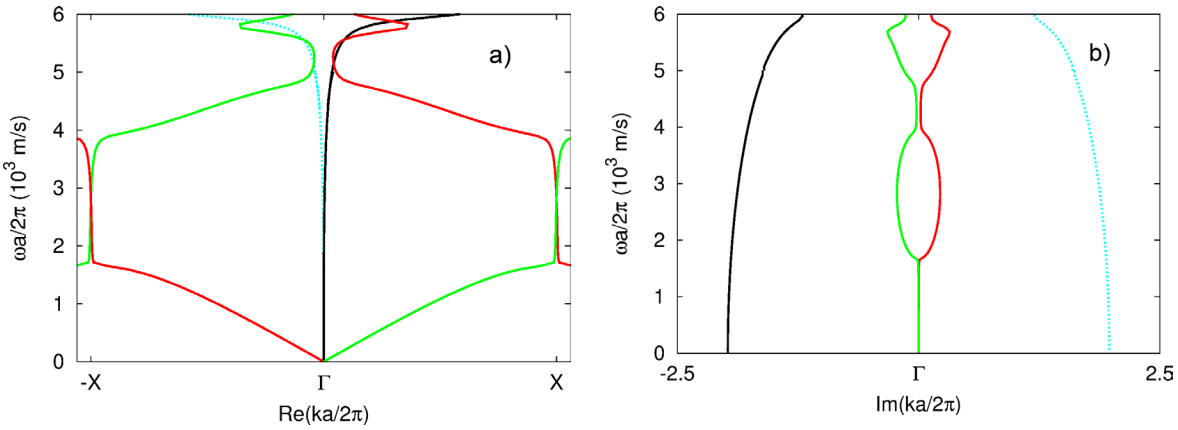

Figure 1 Complex dispersion relation computed with the EPWE method for a lossy square-lattice phononic crystal of silicon with cylindrical holes, with filling fraction 57%, and η44 = 0.08 Pa.s. In the complex band structure, the reduced frequency is presented as a function of (a) the real part and (b) the imaginary part of the wave vector. Only pure shear waves are shown for simplicity.

It is well known that the PWE method, though it is able to represent an almost arbitrary distribution of material constants within the unit-cell, can suffer in certain cases from some convergence problems or computational inefficiency. The finite element method (FEM) is also well suited to the representation of arbitrary material distributions, but is in contrast immune from the above detrimental effects. FEM is generally used to compute classical $k(\omega)$ band structures, but there is a strong interest to extend it to complex band structures. We introduce a general variational framework to obtain extended FEM algorithms. For definiteness, the popular example of two-dimensional phononic crystals of steel rods in water is considered. Complex band structures limited to purely longitudinal waves are obtained in this case.

After analyzing the perfectly periodic phononic crystal, we turn to the defect-based guidance mechanism. As argued above, guidance relies on the fact that all Bloch waves are evanescent in the phononic crystal surrounding the defect, providing the frequency falls within a complete band gap. A usual procedure is the super-cell technique, whereby a pseudo-periodic unit-cell is created by surrounding the defect with a few rows of phononic crystal. Computing the complex band structure for the super-cell gives a very precise understanding of the strength of the guidance (*via* the absolute value of the imaginary part of the wavevector for evanescent Bloch waves). Furthermore, the dispersion and the interaction of the different guided modes can be identified. We especially observe band gaps for guided modes that appear along the direction of the defect for frequencies within the two-dimensional phononic crystal complete band gap.

Financial support by the Agence Nationale de la Recherche under grant ANR-09-BLAN-0167-01 is gratefully acknowledged.

References

[1] V. Laude, Y. Achaoui, S. Benchabane, and A. Khelif, Phys. Rev. B **80**, 092301 (2009).
[2] R. P. Moiseyenko and V. Laude, to be published in Phys. Rev. B.

Phononics 2011: First International Conference on Phononic Crystals, Metamaterials and Optomechanics
Santa Fe, New Mexico, USA, May 29-June 2, 2011
PHONONICS-2011-0106

Demonstration of Ultra High Frequency Fractal Air/Aluminum Phononic Crystals

Nai-Kuei Kuo, Gianluca Piazza

University of Pennsylvania, Philadelphia, Pennsylvania 19103 , USA,
kuo1@seas.upenn.edu, piazza@seas.upenn.edu

Abstract: This work presents, for the first time, the design and the experimental demonstration of an air/aluminum nitride (AlN) phononic band gap (PBG) structure patterned in a fractal fashion which exhibits two frequency stop bands for symmetric lamb waves respectively at 900 MHz (bandwidth of 11%) and 1.075 GHz (bandwidth of 13.5%) with a maximum acoustic attenuation of 45 dB.

Thanks to the advancements introduced by microfabrication techniques, the research activities in phononic band gap (PBG) structures have recently matured from a theoretical exercise or the fabrication of hand-assembled components to the physical demonstration of large scale manufacturable structures operating in the high frequency range [1,2,3]. More intriguingly, recent experimental demonstrations have evolved to the point that realizing PBG-based devices, such as resonators [4,5] and waveguides [2], operating in the very high frequency (VHF) range is possible. However, in order to employ the PBG structures for commercial applications (*i.e.* wireless communications), it is necessary to expand the operation of these structures to a higher frequency range, which requires the miniaturization of the PBG unit cell. In this work, a novel fractal PBG structure design is introduced in order to operate in the ultra high frequency (UHF) range using a lithographically-defined minimum feature size of 0.7 μm. The unit cell consists of a center square with four smaller squares repeating at its four corners (Figure 1). Due to its unique geometry, the fractal PBG design prohibits the acoustic wave propagation of higher order modes of vibration (Figure 2) instead of the fundamental ones, which are generally blocked by the conventional circular scatterers distanced by the same pitch. Therefore, the fractal PBG enables operation at higher frequency for the same lithographically defined geometrical dimensions. To demonstrate a PBG structure in the range of 1 GHz, its key dimensions are designed to be: 5 μm for the lattice constant, *a*; 2 μm for the center square length, *c*; and 1.5 μm for the side square length (Figure 1), *s*. Lastly, the unit cell thickness is set to 1 μm in order to obtain sufficient electro-mechanical coupling for in-plane integration with the lamb wave transducers.

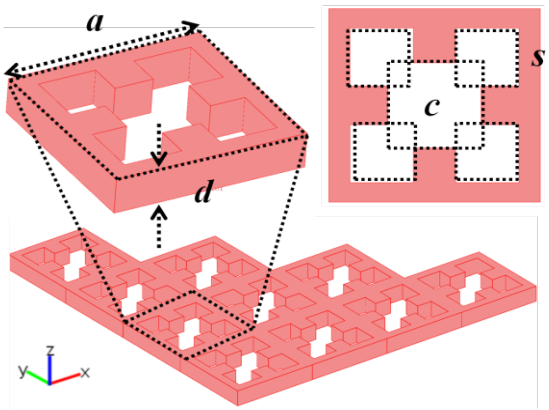

Figure 1 The array and unit cell of the fractal PBG structure with its physical key parameters: lattice constant, *a*, center square length, c, side square length, s, and thickness, *d*.

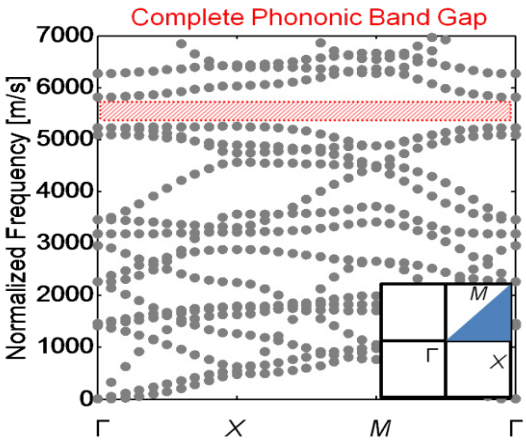

Figure 2 The dispersion relationship between the normalized frequency and the wave vectors in the reciprocal space of the first symmetric Brillouin zone. The red-shaded area is the complete frequency band gap displayed by the fractal structure with key parameter ratios $c/a = 0.44$, $s/c = 0.68$, and $d/a = 0.2$.

Experimental Results

In this experiment, AlN lamb wave transducers are integrated in the same plane of the PBG structure to efficiently launch longitudinal acoustic waves in the PBG (Figure 3a). 14 transducers were used to cover

Phononics 2011: First International Conference on Phononic Crystals, Metamaterials and Optomechanics
Santa Fe, New Mexico, USA, May 29-June 2, 2011
PHONONICS-2011-0106

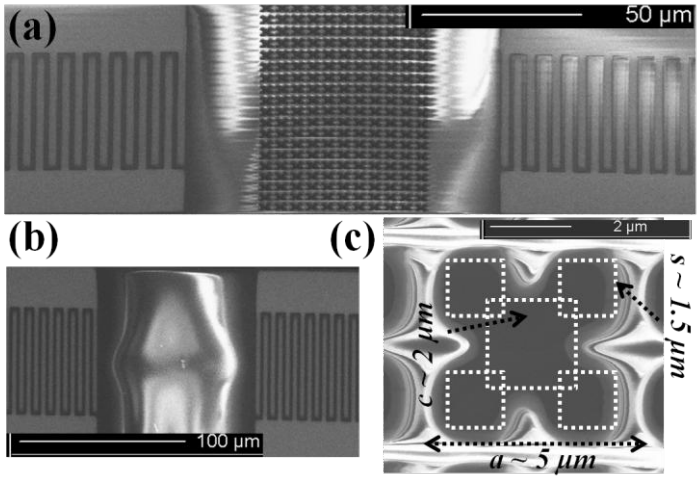

Figure 3 SEM images of : **(a)** the AlN lamb wave transducers and the fractal PBG array; **(b)** the AlN bulk acoustic delay-line used as reference device; **(c)** the zoomed-in view of the unit cell of the fractal PBG structure and its physical key parameters: a = 5 µm, c = 2 µm, s = 1.5 µm.

the frequency range of interest and extract the PBG response. The entire set of devices, the reference plate and the PBG were all simultaneously micro-fabricated in a post-CMOS compatible process (Figure 3). The AlN delay-line transducers were designed to serve as the reference of the acoustic responses (Figure 3b). The PBG response was measured via an Agilent N5230 PNA-L network analyzer after a standard short-open-load-through (SOLT) calibration. Approximately 4-5% bandwidth of each transducer was taken and summed to cover the entire frequency range of interest. Then, the PBG response was normalized with respect to the delay-line reference response. Figure 4 shows the existence of two frequency stop bands centered at 900 MHz and 1.075 GHz with bandwidths of 11% and 13.5%, respectively. The designed PBG structure exhibits a maximum acoustic attenuation of 45 dB. The experimental data were confirmed by means of COMSOL finite element methods (FEM). The eigenfrequency analysis in the FEM approach offers an efficient way to estimate the frequency of operation of the band gaps and the associated bandwidths.

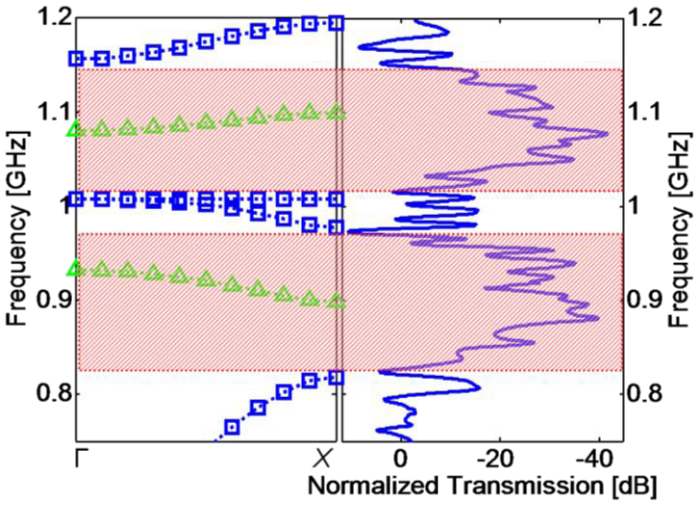

Figure 4 The COMSOL FEM dispersion curve versus the experimental normalized acoustic transmission of the PBG structure. Note: the blue square dotted lines represent the longitudinal modes; the green triangular dotted lines represent non-longitudinal ones (shear and transverse modes).

Conclusion

The operation of the fractal PBG design in air/aluminum nitride at 1 GHz has been experimentally demonstrated and confirmed by COMSOL FEM. Having reached the GHz range, it now becomes feasible to start considering the demonstrations of PBG-based RF devices for practical applications. Simultaneously, exotic PBG designs will be explored to further simply manufacturing processes in the UHF and SHF range.

References

[1] S. Mohammadi, et al., *Appl. Phys. Lett.*, **95**, 093501 (2008).
[2] R. H. Olsson III, et al., *Meas. Sci. Technol.*, **20**, 012002 (2008).
[3] N. Kuo, et al., *Appl. Phys. Lett.*, **95**, 093501 (2009).
[4] S. Mohammadi, et al., *Appl. Phys. Lett.*, **94**, 051906 (2009).
[5] C.-Y. Huang, et al., *Appl. Phys. Lett.*, **97**, 031913 (2009).

Phononics 2011: First International Conference on Phononic Crystals, Metamaterials and Optomechanics
Santa Fe, New Mexico, USA, May 29-June 2, 2011
PHONONICS-2011-0109

Ultrasonic Wave Transport in Phononic Crystals

J.H. Page[1], E.J.S. Lee[1], A. Sukovich[1], Hefei Hu[1], C. Qiu[2], Zhengyou Liu[2], Y. Tanaka[3], T. Okada[3], S. Tamura[3], B. Merheb[4], J-F. Robillard[5], J.O. Vaseur[5] and P.A. Deymier[4]

[1] Department of Physics and Astronomy, University of Manitoba, Winnipeg, MB Canada R2T 2N2
[2] Department of Physics, Wuhan University, Wuhan 430072, People's Republic of China
[3] Department of Applied Physics, Hokkaido University, Sapporo 060-8628, Japan
[4] Department of Materials Science and Engineering, University of Arizona, Tuscon AZ 85721 USA
[5] Institut d'Electronique, de Micro-électronique et de Nanotechnologie, UMR CNRS 8520, Cité Scientifique, 59652 Villeneuve d'Ascq Cedex, France
jhpage@cc.umanitoba.ca

Abstract: Ultrasonic experiments on phononic crystals provide a powerful method for investigating the profound effects of periodic structure on wave propagation. We summarize recent progress that has been achieved by combining experiments with multiple scattering theory and FDTD calculations to study bandgap, negative refraction and focusing phenomena.

Phononic crystals - periodic composite materials with lattice spacings comparable to the wavelength of acoustic or elastic waves – may be considered ideal systems for studying wave phenomena in periodic media. Ultrasonic techniques are well suited for investigating the properties of these materials since the wave field can be measured directly; thus, a rather complete picture of wave propagation is accessible, allowing the transmission coefficient, the dispersion relations, unusual refraction and focusing effects, and the dynamics of the wave fields to be investigated. We study high quality three- and two-dimensional crystals (Fig. 1), which are most often constructed by embedding mm-size monodisperse spheres or rods in a liquid or solid matrix. Such structures produce band gaps, at frequencies around 1 MHz, where wave propagation is inhibited, with transmission through crystals of finite thickness proceeding by tunneling[1]. While band gaps are most commonly produced by Bragg scattering, they can also occur by a hybridization mechanism, involving the coupling of a strong scattering resonance with the propagating modes of the embedding medium. We investigate these two types of band gaps in 2D crystals made from nylon rods immersed in water, where the lattice constant *a* can be tuned by changing the separation between the scatterers. Since the bandgap frequencies for these two types of gap depend differently on *a*, their different physical origins can be identified experimentally. We observe both types of gap separately, and also the competition between the hybridization and Bragg mechanisms when they occur at similar frequencies in the same crystals. Further confirmation of the different character of the hybridization gaps in our crystals is revealed by comparison with random samples, where the hybridization gaps persist but the Bragg gaps are destroyed. These data for the crystals and random systems are interpreted using Multiple Scattering Theory[2] and a Spectral Function Approach[3], yielding additional insight into the observed behaviour. We show that, typically, the group velocity is negative in a hybridization gap, but positive and large in a Bragg gap, providing a signature for distinguishing between hybridization and Bragg gaps in pulse propagation experiments.

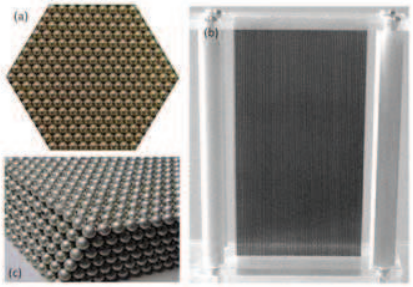

Figure 1 Some phononic crystals used in our ultrasonic experiments. (a) Top view of a fcc crystal of 1-mm-diameter tungsten carbide beads in water. (b) Front view of a triangular crystal of 1-mm-diameter steel rods, also immersed in water. (c) A mesoscopic opal made by brazing 4-mm-diameter aluminium beads in a fcc structure.

We also study mesoscopic opals – single-component phononic crystals made by brazing aluminum beads to form a solid face-centred-cubic structure that is more analogous to atomic crystals. In these crystals, the origin of the band gaps is different to the two cases considered above, being similar to the tight-binding model for electronic materials. The data are compared with predictions of Finite Difference Time Domain (FDTD) calculations, with good agreement being found for the frequencies at

Phononics 2011: First International Conference on Phononic Crystals, Metamaterials and Optomechanics
Santa Fe, New Mexico, USA, May 29-June 2, 2011
PHONONICS-2011-0109

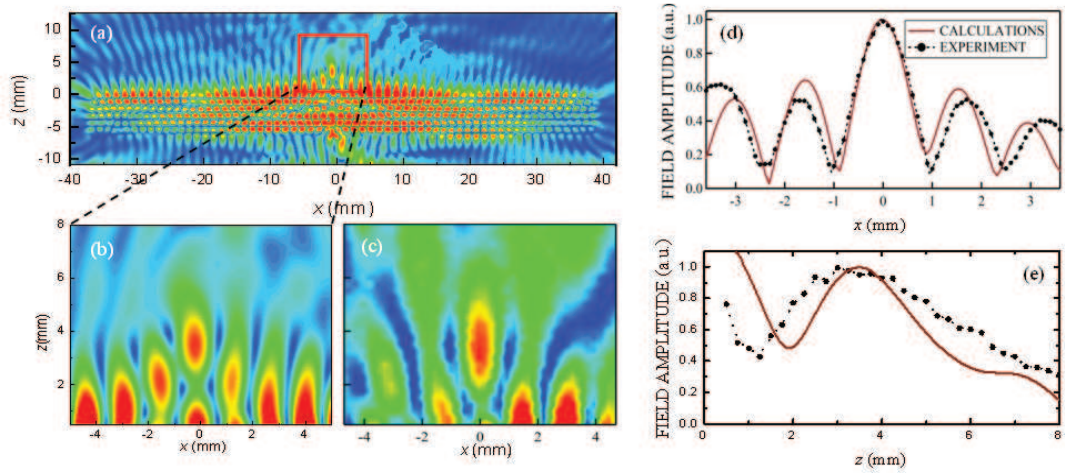

Figure 2 Super-resolution focusing of ultrasound at 530 kHz by a flat 2D phononic crystal consisting 1-mm-diameter steel rods arranged in a triangular lattice and immersed in methanol. The medium outside the crystal is water. (a) FDTD calculations of the average pressure amplitude when a 0.55 mm wide source is placed 0.1 mm below the surface of the crystal, at x = 0 mm and z = -6.35 mm. The crystal contains 6 layers of rods, with the output side of the crystal at z = 0. An image of the source is seen near x = 0 and z = 3.5 mm, as shown (b) and (c) for FTDT simulations and experiments, respectively. (d) and (e) Comparison of experiment and theory for the field amplitude through the peak of the focal spot along directions parallel and perpendicular to the lens surface. The experimental results and theoretical predictions for the half width of the focal spot parallel to the surface, $\Delta/2$, are found to be 0.37λ and 0.35λ.

which the band gaps occur. The bandgap properties of this crystal are contrasted with those of a disordered mesoglass, in which the most striking effect of disorder is three dimensional Anderson localization of ultrasound[4].

Since focusing of acoustic waves by negative refraction in flat phononic crystals was first demonstrated several years ago[5], there has been increasing interest in the possibility that focusing with resolution better than the diffraction limit of $\lambda/2$ may be achievable. In addition to demonstrating negative refraction directly, we show how super-resolution can be realized with two-dimensional phononic crystals in which the equifrequency contours are circular and well matched in size to the contours of the medium outside the crystal [6,7]. The phononic crystals are made of stainless steel rods assembled in a triangular crystal lattice and immersed in a liquid. To achieve matching of the equifrequency contours inside and outside the crystal, the liquid surrounding the rods in the crystal was chosen to be methanol, which has a lower sound velocity than the water outside. At a frequency close to that at which equifrequency contour matching occurs (0.55 MHz for this crystal), an image of a subwavelength source was obtained with a resolution of 0.37λ. Our experimental results are compared with theoretical predictions by the Finite Difference Time Domain (FDTD) method, which predicts an optimum resolution of 0.35λ – in good agreement to that observed experimentally (Fig. 2). Super-resolution imaging in these crystals is shown to be related to the coupling between the incident evanescent waves from the source and a bound slab mode of the phononic crystal lens, leading to amplification of evanescent waves by the slab mode. This phenomenon is only observed when the source is located very close to the lens and is very sensitive to the location of the source parallel to the lens surface, as well as to site disorder in the phononic crystal lattice. A simple model to predict the resolution limit is in good agreement with the experiments and FDTD simulations.

References

[1] Suxia Yang, J.H. Page, Zhengyou Liu, M.L. Cowan, C.T. Chan and Ping Sheng, *Phys. Rev. Lett.* **88**, 104301 (2002).
[2] J. Mei, Z. Liu, J. Shi, and D. Tian, *Phys. Rev. B* **67**, 245107 (2003).
[3] Xin Zhang, Zhengyou Liu, Fugen Wu, and Youyan Liu, *Physical Review E* **73**, 066604 (2006).
[4] H. Hu, A. Strybulevych, J.H. Page, S.E. Skipetrov and B.A. van Tiggelen, *Nature Physics* **4**, 945 (2008).
[5] Suxia Yang, J.H. Page, Zhengyou Liu, M.L. Cowan, C.T. Chan and Ping Sheng, *Phys. Rev. Lett.* **93**, 024301 (2004).
[6] A. Sukhovich, Li Jing and J.H. Page, *Phys. Rev. B* **77**, 014301 (2008).
[7] A. Sukhovich, B. Merheb, K. Muralidharan, J.O. Vasseur, Y. Pennec, P.A. Deymier and J.H. Page, *Phys. Rev. Lett.* **102**, 154301 (2009).

Phononics 2011: First International Conference on Phononic Crystals, Metamaterials and Optomechanics
Santa Fe, New Mexico, USA, May 29-June 2, 2011
PHONONICS-2011-0116

Locally resonant and Bragg band gaps for surface acoustic waves

Younes Achaoui[1], Abdelkrim Khelif [1,2], Sarah Benchabane[1], Laurent Robert[1], and Vincent Laude[1]

[1] *Institut FEMTO-ST, Université de Franche-Comté and CNRS, Besançon France*
younes.achaoui@femto-st.fr, sarah.benchabane@femto-st.fr, vincent.laude@femto-st.fr
[2] *International Joint Laboratory GeorgiaTech-CNRS UMI 2958; 2-3 Rue Marconi 57070 Metz, France*
akhelif3@mail.gatech.edu

Abstract: We investigate the propagation of surface acoustic waves in a square lattice phononic crystal of cylindrical pillars on an anisotropic substrate. It is shown that the propagation of surface acoustic phonons is prohibited in two distinct frequency ranges. We identify two mechanisms responsible for band gaps, i.e. local resonances and Bragg diffraction, and point out the difference between them.

The last years have seen a significant rise in the number of studies of band gap materials for acoustic waves. Basically, these artificial materials can be classified into two distinct families: phononic crystals[1] and acoustic metamaterials[2]. Indeed, they can both prohibit the propagation of acoustic waves in certain frequency ranges for all directions of incidence, but the physical phenomena behind are markedly different. The key parameter to obtain band gaps in the case of phononic crystals is periodicity, while the local frequency resonance of each basic cell dominates in the case of acoustic metamaterial. Furthermore, the position of band gaps in acoustic metamaterials can be significantly lower in frequency than the Bragg band gaps of phononic crystals. These sub-wavelength composites are good alternatives to overcome cumbersome devices in the sonic regime for instance.

Many works have been reported in the case of bulk waves for both phononic crystals and metamaterials. In the case of guided waves, drilling holes in a semi-infinite media as well as in thin plates was shown to prohibit the propagation of acoustic waves for wavelengths of the order of the lattice pitch[3,4]. More recently, low-frequency gaps and waveguiding in phononic crystals of pillars (or dots) on a plate have been demonstrated[5,6]. Here, we investigate experimentally the omnidirectional locally resonant and Bragg band gaps for surface acoustic waves on a semi-infinite substrate supporting a periodic array of pillars.

In our experiment, a square lattice array of cylindrical nickel pillars grown on a lithium niobate substrate has been considered. Surface acoustic waves are generated and detected using chirped interdigital transducers (CIDTs). These transducers are broadband sources placed on both sides of the periodic structure, as depicted in Figure 1. Several different samples have been fabricated in order to vary the direction of propagation and the investigated frequency range. Figure 2 shows examples of the ectrical transmission measured for propagation in the X-crystallographic direction using a network analyzer and radio-frequency probes. Figure 2-a and 2-b show the results obtained in two distinct frequency ranges. The red line shows the electrical response when no phononic crystal is present and is used as a reference. The green line shows the measurement in the presence of the phononic crystal.

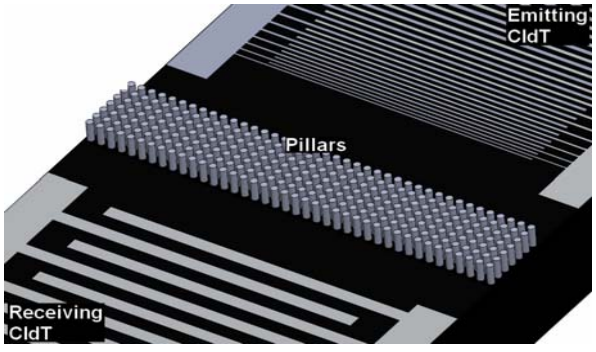

Figure 1 Schematics of the experimental setup used for investigating the interaction between the phononic crystal and surface acoustic waves. The periodic structure is a square lattice of nickel pillars grown on the surface of a lithium niobate substrate. Chirped interdigital transducers are placed on both sides for the emission and the detection of broadband surface acoustic waves using the piezoelectricity of lithium niobate.

Phononics 2011: First International Conference on Phononic Crystals, Metamaterials and Optomechanics
Santa Fe, New Mexico, USA, May 29-June 2, 2011
PHONONICS-2011-0116

With the periodic structure in between the two chirped transducers, we observe the appearance of a low frequency attenuation dip in the vicinity of 80 MHz (figure 2-a) and a second high frequency attenuation range in the vicinity of 140 MHz (figure 2-b). Transmission close to unity, i.e. with no noticeable loss, is observed between the two band gaps. Attenuation above 210 MHz is attributed to the conversion of guided modes to bulk waves propagating inside the substrate. The physical origin of the two gaps has been further investigated using optical interferometry. It is observed that the energy of surface waves is stored inside the pillars in the case of the low frequency gap, while the same waves are scattered on the surface in the case of the second band gap, leading to destructive interferences characteristic of the Bragg mechanism. We also obtained the group delay and the phase shift that is induced by the periodic structure on the propagation of surface waves.

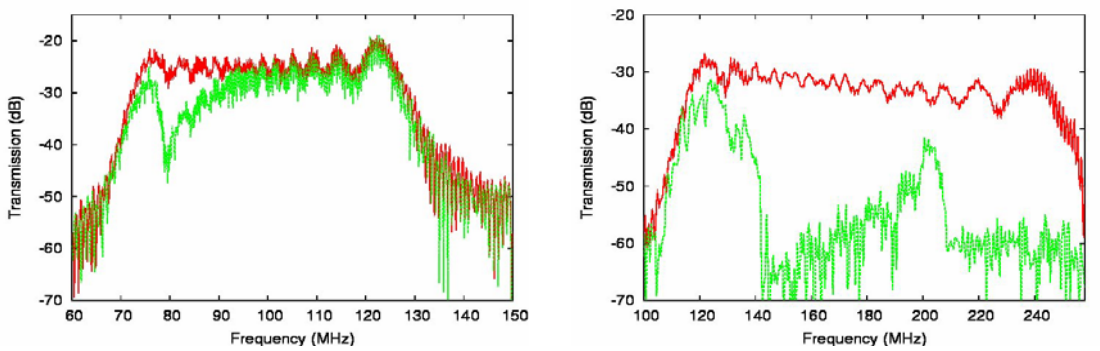

Figure 2 Measured electrical transmission using chirped interdigital transducers with (green line) and without (red line) the periodic structure in between. Case of (a) the locally resonant band gap (around 80 MHz) and (b) the Bragg band gap (around 140 MHz).

In order to account for the above results, we have computed dispersion curves and displacement field maps using a finite element method. We find that the pillars on the surface support locally resonant modes that extend inside the sound cone, and that band gaps for guided surface acoustic waves can be clearly defined.

According to our previous theoretical work[7], the main parameter that can shift in frequency the locally resonant band gap is the height of the pillars. Indeed, the locally resonant band gap is a consequence of the interaction of a resonance of the pillar with surface waves propagating on the substrate supporting the periodic structure. This resonance is also a function of the elastic constants of the pillars, of their mass density and of the geometrical details. For the same material choice, we have varied experimentally the height of the pillars and have monitored the corresponding change in the lower band gap frequency position. Increasing the height of the pillars results in a clear down-shift of the lower band gap, leading us to the conclusion that the latter results from a local resonance of the pillars.

Financial support by the Agence Nationale de la recherche under grant ANR-09-BLAN-0167-01 is gratefully acknowledged.

References :

[1] M.S. Kushwaha, P.Halevi, L. Dobrzynski, and B Djafari-Rouhani, Phys. Rev. Lett. **71**, 2022 (1993).
[2] Z. Liu, X. Zhang, Y. Mao,Y. Y. Zhu, Z. Yang, C. T. Chan, and P. Sheng, Science **289**, 1734 (2000).
[3] S. Benchabane, L. Robert, J.-Y. Rauch, A. Khelif, and V. Laude, Phys. Rev. E **73**, 065601 (R) (2006).
[4] S. Mohammadi, A. Eftekhar, W. Hunt, and A. Adibi, Appl. Phys. Lett. **94**, 104301 (2009).
[5] T.-T Wu, Z.-G Huang, T.C Tsai, and T.-C. Wu, Appl. Phys. Lett. **93**. 111902 (2008).
[6] Y. Pennec, B. Djafari-Rouhani, H. Larabi, J. O. Vasseur, and A. C. Hladky-Hennion, Phys. Rev. B **78**, 104105 (2008).
[7] A. Khelif, Y. Achaoui, S. Benchabane, V. Laude, and B. Aoubiza, Phys. Rev. B **81**, 214303 (2010).

Phononics 2011: First International Conference on Phononic Crystals, Metamaterials and Optomechanics
Santa Fe, New Mexico, USA, May 29-June 2, 2011
PHONONICS-2011-0127

Focusing and Waveguiding of Lamb Waves in Phononic Plates

Tsung-Tsong Wu, Jia-Hong Sun, Yan-Ting Chen
Institute of Applied Mechanics, National Taiwan University, Taipei, Taiwan
wutt@ntu.edu.tw

Abstract: In this talk, focusing of Lamb waves using the GRIN PC will be introduced first, and then followed by a concept demonstration of utilizing the focusing feature to compress Lamb waves into a phononic plate waveguide. Results of the study showed that beam width of the lowest anti-symmetric Lamb wave in a silicon PC thin plate can be compressed efficiently and fitted into the tungsten/silicon PC plate waveguide over a wide range of frequency.

Propagation of Lamb waves in thin plates with phononic crystal (PC) structures has attracted much interest due to the existence of absolute band gap (ABG) and the potential applications in filters, resonators, and waveguides in the past couple of years.[1-3] In comparison to the ABG, researches on the negative refraction and focusing of waves in phononic thin plates have just been started recently. Preliminary results showed that focusing of Lamb waves in thin plate can be achieved either by the negative refraction or using the gradient-index (GRIN) PC structure.[4,5]

In this talk, focusing of Lamb waves due to the features of GRIN PC will be introduced first, and then a concept demonstration of utilizing the focusing features to compress Lamb waves into a phononic plate waveguide. The band structure of an air/silicon PC plate (thickness:50 μm, lattice constant a =100μm and, radius r =40μm) with square lattice was studied and the equal frequency contours (EFCs) of the lowest anti-symmetric mode (A_0), the symmetric mode (S_0) and shear horizontal mode (SH_0) are shown in Figure 1. The results revealed that the A_0 mode is close to a circle (i.e., behave like an isotropic medium), while the S_0 and SH_0 modes are rather anisotropic. Figure 1 is the equal frequency contours (EFCs) evaluated at 3 MHz.

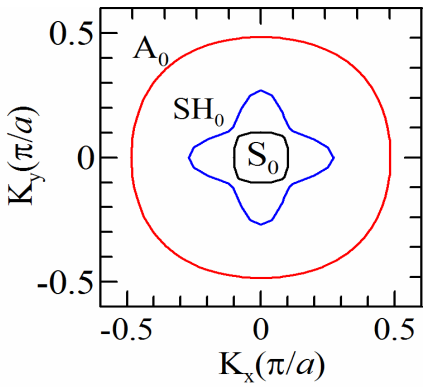

Figure 1 The equal frequency contours of the lowest anti-symmetric mode (A_0), symmetric mode (S_0) and shear horizontal mode (SH_0).

To design a GRIN PC plate for focusing the A_0 mode, we chose a refractive index profile in the form of a hyperbolic secant as[6]

$$n(y) = n_0 \operatorname{sech}(\alpha y) \tag{1}$$

where n_0 is the refractive index along the center axis (x-axis) and α is the gradient coefficient. For small anisotropic ratio and the overall waves propagating along the x-direciton, the refractive index of the A_0 mode was approximated by the refractive index along the ΓX direction as

$$n = \frac{v}{v_{\Gamma X}} = \frac{v}{d\omega / dk_{\Gamma X}}. \tag{2}$$

where $v_{\Gamma X}$ is the group velocity along the ΓX direction and v is the referenced group velocity of the A_0 mode of a homogeneous silicon plate with the same thickness (evaluated at 3 MHz). Consider a GRIN PC contained 15 rows of air holes (y= [−7 a, +7 a]) arranged in square lattice with graded filling fractions and operated at 3 MHz. By setting the radii of the holes at the center row (y = 0) and the boundary rows (y= ±7 a), the gradient coefficient can be determined accordingly.

Phononics 2011: First International Conference on Phononic Crystals, Metamaterials and Optomechanics
Santa Fe, New Mexico, USA, May 29-June 2, 2011
PHONONICS-2011-0127

To demonstrate the focusing of Lamb wave in the designed GRIN PC plate, numerical simulations were conducted with a line source placed at x= -2a. The result showed focusing of the wave beam along the propagation direction and reach maximum amplitude at x=28a approximately, and then, diverging out again. The simulation results also showed that the neck of the focus region extends for a long distance, which started from around 22a to 34a in this case.

To test the feasibility of compressing the wave beam of a plate wave into a wave guide with small aperture, the GRIN PC plate was terminated at x=22a and utilized as a beam width compressor. A phononic plate waveguide formed by removing one layer of cylinders from a silicon PC plate with periodic stubbed tungsten cylinders[7,8] (square lattice) on one of the plate surfaces was employed. By choosing the lattice constant of the PC waveguide as 150 μm and the radius and height of the tungsten cylinders as 36 μm and 273 μm, respectively, a complete band gap can be found in the range of 2.6-3.4 MHz. Figure 2 shows a combination of the GRIN PC beam width compressor and the aforementioned PC waveguide. The simulation result for operating frequency at 3 MHz demonstrates that the compressing and guiding of the wave beam into the designed waveguide can be achieved successfully. By taking the amplitude of the line source as unit, the result shows that the amplitude at the entrance of the waveguide is amplified to about 3.2. In addition, after propagating for a distance of 15 a in the waveguide, the wave amplitude still preserve a value of 2.8. Since the aperture of the line source is $15a$, the results showed that the FWHM of the compressing is about 17.3%. To demonstrate that the proposed GRIN PC plate focusing device is suitable for compressing wave with a range of frequency, numerical simulations with operating frequencies at 2.7 and 3.4 MHz were also conducted and the results showed that the focusing and compressing of Lamb waves are still valid with the amplitudes at the entrance of the waveguide equal to 2.5 and 2.6, respectively.

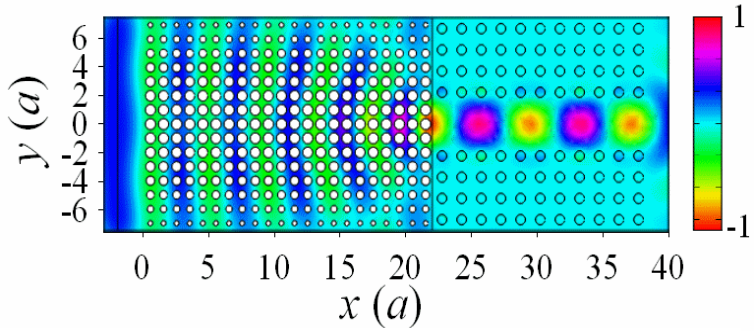

Figure 2 Simulation of the wave propagation along the x-direction in a GRIN PC plate adjoined with a PC plate waveguide at 3 MHz.

In summary, focusing of Lamb wave can be achieved by using a GRIN air/silicon PC thin plate. The refractive index profile in the form of a hyperbolic secant can be utilized approximately to design the GRIN PC plate. The results showed that the beam width of the lowest anti-symmetric Lamb mode can be compressed efficiently over a range of frequency and can potentially be utilized as a beam width compressor for compressing Lamb waves into a PC plate waveguide in the MEMS area.

References

[1] R. H. Olsson III, I. F. El-Kady, M. F. Su, M. R. Tuck, and J. G. Fleming, *Sensors and Actuators A* **145**, 87-93 (2008).
[2] S. Mohammadi, A. A. Eftekhar, W. D. Hunt, and A. Adibi, *Appl. Phys. Lett.* **94**, 051906 (2009).
[3] C.-Y. Huang, J.-H. Sun, and T.-T. Wu, *Appl. Phys. Lett.* **97**, 031913 (2010).
[4] M. Farhat, S. Guenneau, S. Enoch, A. B. Movchan, and G. G. Petursson, *Appl. Phys. Lett.* **96**, 081909 (2010).
[5] T.-T. Wu, Y. T. Chen, J. H. Sun, S.-C. S. Lin, T. J. Huang, submitted to *Appl. Phys. Lett.*
[6] S.-C. S. Lin, T. J. Huang, J.-H. Sun, and T.-T. Wu, *Phys. Rev. B* **79**, 094302 (2009).
[7] T.-C. Wu, T.-T. Wu, and J.-C. Hsu, Phys. Rev. B **79**, 104306 (2009).
[8] Y. Pennec, B. Djafari Rouhani, H. Larabi, A. Akjouj, J. N. Gillet, J. O. Vasseur, and G. Thabet, *Phys. Rev. B* **80**, 144302 (2009).

Phononics 2011: First International Conference on Phononic Crystals, Metamaterials and Optomechanics
Santa Fe, New Mexico, USA, May 29-June 2, 2011
PHONONICS-2011-0147

Multi-Objective Optimization of Phononic Bandgap Materials for Wide Band, Low Frequency Operation

Raymond A. Wildman and George A. Gazonas

Weapons and Materials Research Directorate, U.S. Army Research Laboratory,
Aberdeen Proving Ground, MD, USA
raymond.a.wildman@us.army.mil, george.aristotle.gazonas@us.army.mil

Abstract: Phononic bandgap materials are optimized for maximization of bandgap size and minimization of center frequency using a genetic programming method for inclusion shape design and material choice. Maximizing the bandgap size allows for a material design that can block a wide range of frequencies. Minimizing the center frequency will give designs that are small compared to the effective wavelength.

Phononic crystals have received much attention for their interesting properties, in fact, material choice and geometry can be engineered to obtain band stop filters[1], negative bulk properties[2], and cloaking[3]. Here, we wish to optimize two goals simultaneously: bandgap size and center frequency. Maximizing the bandgap size allows for structures that can block a wide range of frequencies. In many instances, a narrowband filter is of little use. The second goal is to minimize the center frequency of the bandgap. The center frequency determines the absolute range of frequencies that will be blocked. Seeking a low center frequency will yield a material that blocks propagating waves that have long wavelengths compared to the unit cell size, ultimately leading to smaller structures.

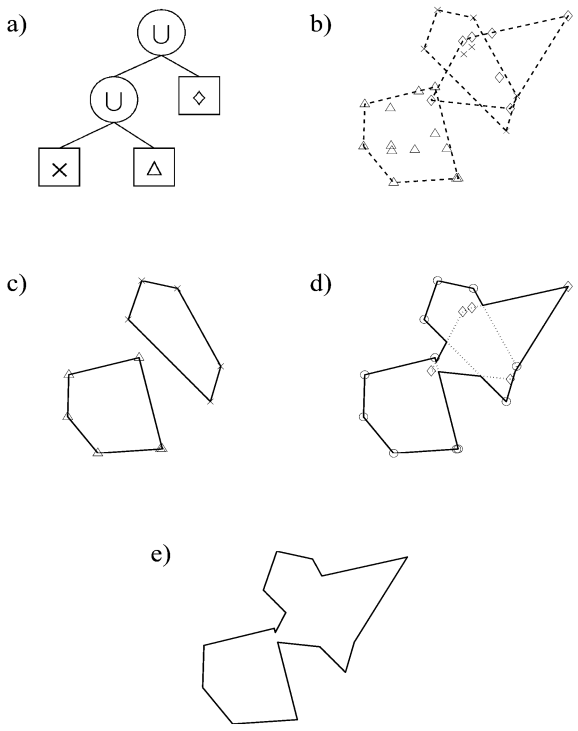

Figure 1 Decoding process. **(a)** Tree representation of a Boolean expression. **(b)** Point lists with their convex hulls, corresponding to leaf nodes in the tree. **(c)** Union of the left-most subtree. **(d)** Union of the result of **(c)** with remaining leaf node. **(e)** Final result.

Multi-objective optimization of phononic crystals has been discussed previously[4], where those authors optimized one dimensional structures for optimal pass-band and stop-band operation. Here, we optimize two dimensional, elastic structures using a genetic programming approach[5] and allow the optimizer to choose among several materials. The materials chosen are based on those that have been shown to lead to low frequency operation[6]. Results show that a set of Pareto optimal designs can be achieved for wide band and low frequency operation.

Optimization Method

Genetic programming (GP) is an optimization method derived from genetic algorithms (GAs), but uses a tree shaped chromosome to represent computer programs or general mathematical expressions. It has also been adapted to optimize geometry and topology in a general way[5]: As shown in Figure 1, Boolean expressions can be used to combine convex polygons, generating complex geometries from a few simple building blocks. In this approach, the convex polygon operands are represented as the convex hull of a list of points. A few advantages include: representation of large homogeneous regions with a small number of parameters, representation of both sharp corners and smooth regions, and

Phononics 2011: First International Conference on Phononic Crystals, Metamaterials and Optomechanics
Santa Fe, New Mexico, USA, May 29-June 2, 2011
PHONONICS-2011-0147

adaptability to inhomogeneous geometries.

Genetic algorithms (and by extension genetic programming) are well-suited to multi-objective problems because they already use a population of potential solutions. There have been many examples of multi-objective GAs, of which Ref. 4 is an example. Implementing Pareto optimization in a GA only involves changes to the selection operator, so any GP implementation is identical.

In contrast to Ref. 5, this application benefits from inhomogeneous structures[7]. Optimizing inhomogeneous structures using genetic programming requires a few modifications to the chromosome of Ref. 5. First, Boolean operations are no longer applicable because we require the operands to have some material properties. Instead, we apply an overlapping scheme based on a priority value (real valued and rounded to the nearest integer before use) stored in each operand. Given a sub-tree with two convex polygon operands, the operand with the higher priority is placed on top of the other. If two operands have identical priority values, then the union is used, taking the material properties from the left operand. The priority values, as well as the material values, are involved in crossover and mutation. In this application, a database of materials will be used rather than allowing the optimization scheme to vary the actual bulk material properties as in Ref. 7.

Forward Problem

The forward problem is based on formulating the elastic wave equation as an eigenvalue problem, so that a band diagram can be computed[1]. Essentially, Floquet boundary conditions are applied to two edges of a square unit cell and the elastic wave equation is discretized using linear finite elements. After testing and basis function substitution, a matrix equation is formed

$$\boldsymbol{Ax} = \omega \boldsymbol{Bx}, \tag{1}$$

which is a generalized eigenvalue problem in ω and $\boldsymbol{x}$. A local search algorithm is applied to find the lower band maximum ω_1 and upper band minimum ω_2, which gives the relative bandgap size

$$\frac{\omega_2 - \omega_1}{\sqrt{\omega_1 \omega_2}}, \tag{2}$$

and center frequency

$$\frac{\omega_1 + \omega_2}{2}. \tag{3}$$

Results

Pareto optimization was applied for the simultaneous optimization of bandgap size and center frequency using three materials: epoxy, lead, and silicone rubber[6]. The epoxy is fixed as the matrix material, and the algorithm is free to choose among it and the lead and rubber to form the inclusions.

Initial generations show two distinct clusters of (Pareto optimal) designs based on material: designs using lead show high center frequency and bandgaps, and designs using the rubber show the opposite. As the algorithm combines materials, the Pareto front (shown in Figure 2 as the "o" after 95 generations) begins to fill. Full results will be given at the conference.

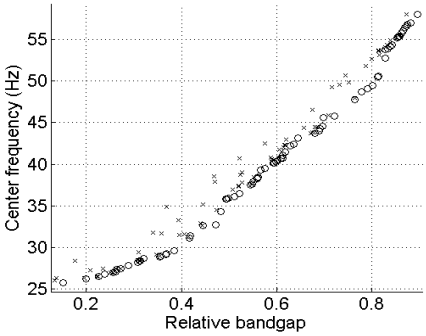

Figure 2 Pareto curve (o) after 95 generations

References

[1] G.A. Gazonas, D.S. Weile, R.A. Wildman, and A. Mohan, *Int. J. Solids Struct.* **43**, 5852-5866 (2006).
[2] J. Li and C.T. Chan, *Phys. Rev. E* **70**, 055602 (2004).
[3] Y. Cheng, F Yang, and J.Y. Xu, *Appl. Phys. Lett.*. **92**, 151913 (2008).
[4] M.I. Hussein, K. Hamza, G.M. Hulbert, R.A. Scott, and K. Saitou, *Struct. Multidisc. Optim.* **31**, 60-75 (2006).
[5] R.A. Wildman and D.S. Weile, *IEEE Trans. Antennas Propag*. **55**, 629-636 (2007).
[6] Z. Liu, X. Zhang, Y. Mao, Y.Y. Zhu, Z. Yang, C.T. Chan, and P. Sheng, *Science* **289**, 1734-1736 (2008).
[7] R.A. Wildman and D.S. Weile, *Electromagnetics* **30**, 222-236 (2010).

Phononics 2011: First International Conference on Phononic Crystals, Metamaterials and Optomechanics
Santa Fe, New Mexico, USA, May 29-June 2, 2011
PHONONICS-2011-0149

Resonance in *m*-layered Goupillaud-type Elastic Media

George A. Gazonas[1] and Ani P. Velo[2]

[1] *Weapons and Materials Research Directorate, U.S. Army Research Laboratory, Aberdeen Proving Ground, MD, USA, george.aristotle.gazonas@us.army.mil*
[2] *Department of Mathematics and Computer Science, University of San Diego, San Diego, CA 92110, USA, avelo@sandiego.edu*

Abstract: Explicit analytical and recursive stress solutions and corresponding natural frequencies are derived for an *m*-layered Goupillaud-type elastic medium from a coupled first-order system of difference equations using *z*-transform methods. The exact solutions can serve to verify computational methods for modeling wave propagation phenomena such as resonance and bandgap formation in periodic media.

The study of natural vibrations in elastic media include the study of resonance, as resonance can enhance the performance of many sensors and devices, yet can devastate structures subjected to sustained temporally-periodic loading. Despite the long history of developments in the field, exact solutions for the natural modes of vibration and the resonance response of multilayered (*m*-layered) elastic media have been primarily limited to the analysis involving only a few layers. Laplace transform methods are used in Ref. 1 to derive the transient resonance response of a free-fixed elastic bar; the analytical solution consists of a product of a temporal term and time-harmonic function in the solution, which becomes unbounded at large times. Ref. 2 provides closed-form, time-domain expressions for transient waves in an *m*-layered elastic medium, with an illustration of the transient resonance response of a single isotropic elastic layer sandwiched between two half-spaces that is subjected to a temporally periodic sawtooth function. Ref. 3 studies the natural frequencies of anisotropic *m*-layers, and illustrates beat phenomena in two and three layer systems using an efficient numerical eigensolution scheme that is based on semi-analytical methods. Exact expressions for the reflection coefficients for a two-dimensional elastic layer overlying an elastic half-space are obtained in Ref. 4, but the transient response of the system at resonance is not analyzed. A general method to determine the natural frequencies of composite rods for power ultrasonic applications with a specific solution for a two-rod system is presented in Ref. 5. The method can be extended to *m*-layered systems, but the general problem of determining the natural frequencies of arbitrary layer-thickness and material properties can only be solved using numerical methods. Exact analytical expressions are derivable, however, for the transient resonance response of an *m*-layered medium if we specialize the medium to be of Goupillaud-type[6]. Both recursive relations and explicit analytical expressions are derived that are exact for discretely layered and periodic media of Goupillaud-type (Figure 1); such solutions are invaluable for verification of computational methods involving transient of wave phenomena in such media. A related inverse problem in reflection seismology for finding the coefficients of a first order 2 *x* 2 hyperbolic system is treated in Ref. 7. In order to numerically solve the continuous initial-boundary-value problem, several difference schemes (stencils) are applied as discretizations to the corresponding differential equations. The difference scheme IVp, given in equation (3.1.11), pg. 517 of Ref. 7 is similar to our recursive relations (1) derived using the method-of-characteristics.

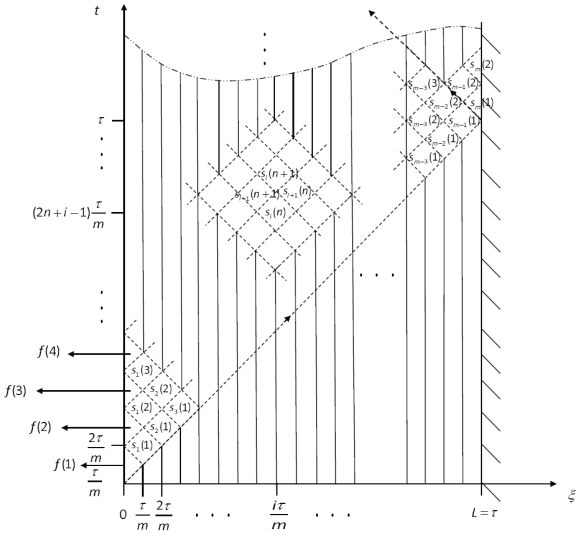

Figure 1 Lagrangian diagram for an elastic *m*-layered medium of equal wave travel time (Goupillaud-type medium) subjected to an arbitrary, discrete input *f(n)* on the left boundary and fixed on the right boundary.

Phononics 2011: First International Conference on Phononic Crystals, Metamaterials and Optomechanics
Santa Fe, New Mexico, USA, May 29-June 2, 2011
PHONONICS-2011-0149

Resonance in *m*-layers

Explicit analytical stress solutions are derived from a coupled first-order system of difference equations (1) using z-transform methods, and the determinant of the global system matrix $|A_m|$ in the z-space is a palindromic polynomial with real coefficients; the zeros are distinct and proven to lie on the unit circle for $1 \le m \le 5$ layers (Ref. 8), and for certain classes of m-layered designs of tridiagonal Toeplitz variety, i.e., continuants (Ref. 9). Stresses $s_i(n)$ in the layers with impedance contrast $\alpha_i = c_i\rho_i / c_{i+1}\rho_{i+1}$ due to loading $f(n), n \ge 1$ are given with reference to Figure 1 as,

$$
\begin{aligned}
s_1(n+1) &= -s_1(n) + \frac{2\alpha_1}{1+\alpha_1} s_2(n) + \frac{2}{1+\alpha_1} f(n+1), \\
s_2(n+1) &= -s_2(n) + \frac{2\alpha_2}{1+\alpha_2} s_3(n) + \frac{2}{1+\alpha_2} s_1(n+1), \\
&\cdots \\
s_{m-1}(n+1) &= -s_{m-1}(n) + \frac{2\alpha_{m-1}}{1+\alpha_{m-1}} s_m(n) + \frac{2}{1+\alpha_{m-1}} s_{m-2}(n+1), \\
s_m(n+1) &= -s_m(n) + 2s_{m-1}(n)\,.
\end{aligned}
\tag{1}
$$

Resonance frequencies $\omega_k = \arg z_k$, $1 \le k \le \left\lfloor \frac{m}{2} \right\rfloor$ are identified as the zeros of the determinant of m-layered tridiagonal Toeplitz systems found from z-transform of (1) above as,

$$
z_k = 2\varsigma\Theta - 1 \pm 2i\sqrt{\varsigma\Theta(1-\varsigma\Theta)}, \qquad \Theta = \cos^2\frac{\pi k}{m+1}\,, \qquad 0 < \varsigma < 1\ . \tag{2}
$$

A particular resonance response generated through sinusoidal loading of the boundary is shown in Figure 2; current efforts are focused on determining the limitations in using finite system (1) to generate acoustic bandgaps for infinite periodic media such as those investigated in Ref. 10, Figure 3.

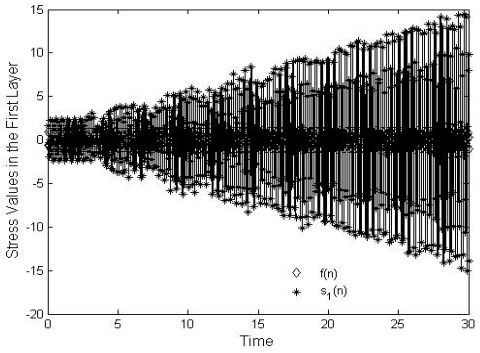

Figure 2 Resonance response of Layer 1 in a *47*-layered medium; stress values formed from interlacing sequences: $f(n) = \sin(n\omega_k)$, and $s_1(n)$, $k = 9, \varsigma = 1/2$.

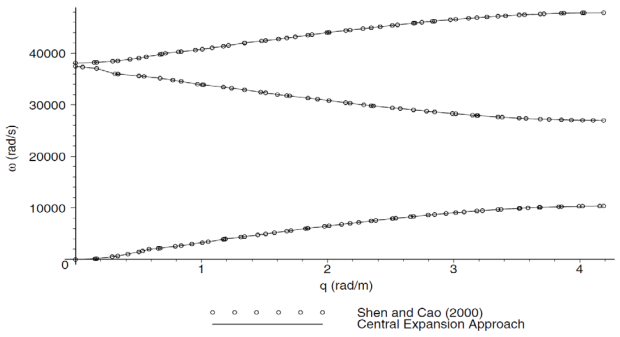

Figure 3 Dispersion graphs showing acoustic bandgap formation in a three-material unit cell (after Ref. 10).

References

[1] R.R. Churchill, *Operational Mathematics,* McGraw-Hill, NY (1972).
[2] G. Caviglia, and A. *J.* Morro, *Acous. Soc. Am.* **116(2)**, 643–654 (2004).
[3] J. Kaplunov, and A. Krynkin, *J. Sound Vibrat.* **294**, 663–677 (2006).
[4] M.S. Fokina, and V.N. Fokin, *J. Comput. Acoust.* **9(3)**, 1079–1093 (2001).
[5] K.F. Graff, *Wave Motion in Elastic Solids,* Dover Publications, NY (1975).
[6] P. Goupillaud, *Geophysics,* **36** 754–760 (1961).
[7] K. Bube, and R. Burridge, *Siam Rev.* **25(4)**, 497–559 (1983).
[8] G.A. Gazonas, and A.P. Velo, *(in review),* (2011).
[9] T. Muir, *A Treatise on the Theory of Determinants*, Dover Publications, NY (1960).
[10] A.P. Velo, G.A. Gazonas, E. Bruder, and N. Rodriguez, *Siam J. Appl. Math.* **69(3)**, 670–689 (2008).

Phononics 2011: First International Conference on Phononic Crystals, Metamaterials and Optomechanics
Santa Fe, New Mexico, USA, May 29-June 2, 2011
PHONONICS-2011-0152

On the Validity of 2D Numerical Simulation of Bandgap for Slab of Phononic Crystals

S. Alaie[1] , I. El-Kady[2], Z.C. Leseman[1]

[1] *Mechanical Engineering, University of New Mexico, Albuquerque, NM USA 87131*
alaie@unm.edu, zleseman@unm.edu
[2] *Sandia National Laboratories, , Albuquerque, NM US 87105*
ielkady@sandia.gov

Abstract: This work suggests a criterion for verification of Phononic bandpaps simulated by two dimensional elastodynamic models. The bandgap of a phononic crystals (PnCs) was studied using both 2D and 3D finite element analyses. Comparing the numerical results with experiment, this study indicates that validity of 2D models depends on the ratio of the thickness to the excitation wavelength.

In order to attain a fast estimation of bandgaps in PnCs, simulation of an infinitely thick model is an alternative to finite thickness models[1]. In order to reduce the three-dimensional equations to those for a two-dimensional model, plane stress condition is a common assumption employed in elastic media[2]. Since in the two dimensional analysis the degrees of freedom (DOFs) for each node is 2, and the model is limited to an area instead of a volume, this model is computationally cheaper than 3D models. In this model the medium is assumed so thin such that the out-of-plane components of stress vanishes[2]. However this assumption leads to neglecting out-of-plane modes in vibration of PnCs. In this paper a PnC, consisting a silicon dioxide and tungsten inclusions, is studied using 3D and 2D harmonic finite element analyses (HFEAs). Results of the current analyses are verified by comparing them to experimental results[3]. This study evaluates the efficiency and inefficiencies of these methods for prediction of phononic bandgap.

In harmonic analysis the governing equations are solved in the frequency domain and the steady state solution is attained without time discretization[4,5]. In order to apply the boundary conditions, a set of nodes are harmonically excited at a discretized range of frequencies. Consequently, the transmission spectrum of a PnC is achieved using the steady state solutions to the PnC model under line excitation in 2D model or surface excitation in 3D model (See Fig. 1). In Fig. 1 the current three dimensional numerical space is illustrated. The phononic crystal consists of one row of 19 tungsten inclusions inside a silicon dioxide matrix. The lattice constant *a* is 2.5 μm in the x and y directions and the tungsten rods have radii of 0.6 μm. The thickness of the PnCs is 1.85 μm. To model an infinite periodic structure along y direction, periodic boundary conditions are employed on the bottom and top nodes. The exterior domains, shown in Fig 1 , comprises perfectly matched layers (PMLs). The PMLs serve to attenuate the outgoing waves, and reflect little to no energy back into the PnC[6]. Longitudinal waves are launched into the PnC by harmonic excitation of the nodes on the left surface of the leftmost exterior domain (See Fig. 1). In the 2D, model all the dimensions are similar to the shown 3D model but the numerical space is a 2D rectangle due to plane stress assumptions.

Material	Tungsten	Silicon dioxide
Density (kg/m^3)	19250	2200
Young's Modulus (GPa)	409	75
Poisson's Ratio	0.25	0.17

Table 1 Materials that constitute the PnC.

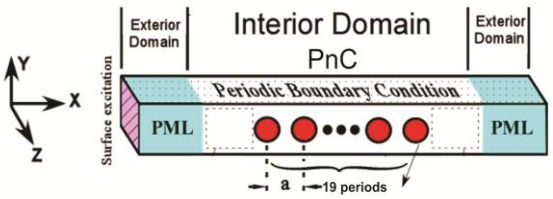

Figure 1 Numerical space of the 3D model for the PnC.

In Table 1 the density, elastic modulii, and Poisson's ratios of silicon dioxide and tungsten are shown. In the 3D simulation, only extensional elastic waves are taken into account, in order to make more accurate comparison to the

Phononics 2011: First International Conference on Phononic Crystals, Metamaterials and Optomechanics
Santa Fe, New Mexico, USA, May 29-June 2, 2011
PHONONICS-2011-0152

2D case in which no flexural modes are allowed. For this reason only symmetric forces are applied on the boundary condition of the left exterior domain (see Fig 1).

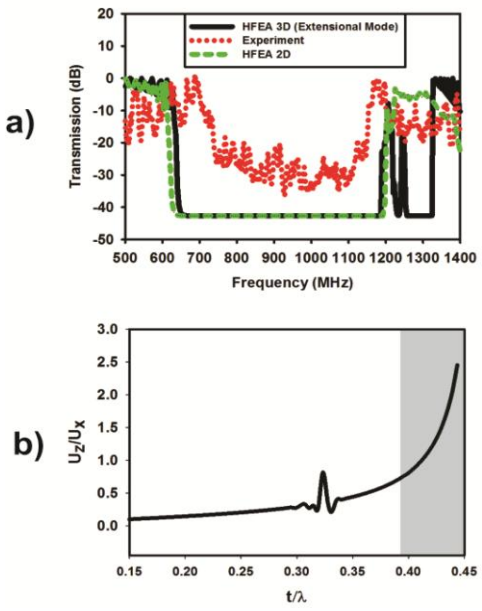

Figure 1 (a) Transmission spectrum based on the 2D HFEA (red dotted line), 3D HFEA (green dashed line), and the experiment (red dotted line). **(b)** Ratio of out-of-plane to in-plane displacements versus dimensionless excitation frequency. The shaded gray region indicates the frequencies at which the 2D and 3D finite elements analyses do not agtree.

The scaled transmission of the PnC predicted by the FEA using 2D and 3D approaches are presented in Fig. 2a. In this plot HFEA 2D stands for the prediction of a 2D elastodynamic model for the transmission through the PnC. The 3D simulation is compared with the 2D model along with the actual experimental results previously reported by Su et al.[3]. Here, the borders of bandgp are defined by transmission of -10 (dB). The comparison shows that both finite element models predict a similar primary bandgap. The predicted beginning frequency is about 80 MHz smaller than the experimental prediction. Moreover, the actual end frequency of the band gap is only 20 MHz smaller than the numerical results, which shows a good agreement between the theoretical 2D, theoretical 3D, and experimental piramary bandgaps. However, Fig. 2a also demonstrates that the 2D model fails to predict the experimental secondary bandgap ranging from 1180 MHz to 1400 MHz. In contrast to the 2D model, the 3D model clearly shows this band gap.

The discrepancy between the 2D and 3D analyses at the higher frequencies raises the question of validity of the 2D analysis. This question is addressed in Fig. 2b. Here, the ratio of out-of-plane displacement (U_z) to the in-plane displacement (U_x) on the right side of the PnC (See Fig 1) is depicted for different dimensionless frequencies defined as the ratio of the PnC thickness t to the wavelength λ. Additionally, this dimensionless frequency in the abscissa of Fig. 2b corresponds to the frequency in abscissa of Fig 2a. The shaded region in Fig. 2b shows the dimensionless frequencies corresponding to the secondary band gap where the two dimensional FEA is not in agreement with the experiment and 3D model. One can notice that in the shaded box the three dimensional FEA shows a range from 0.7 and 2.5 for the ratio of out-of-plane to in-plane displacements. This high ratio indicates that the out-of-plane displacements are not insignificant in the problem while the 2D analysis inherently does not take these displacements into account. It also indicates that the nature of the problem is not 2D at the frequencies associated with the secondary bandgap. The trend of dimensionless lateral displacements shown in Fig. 2b suggests that the 2D analysis is not applicable when the ratio of the thickness to wavelength approaches to 0.5. Another physical explanation is that when the wavelength approaches to half of the thickness, the out-of-plane mode of vibration is greatly excited because the excitation frequency is close to the natural frequency of this mode. However at lower frequencies the 2D and 3D analyses do not show a significant difference. In essence, Fig 1 suggests that at the dimensionless excitation frequencies much smaller than 0.37 the 2D HFEA is an accurate alternative to 3D the model. Since a 2D model requires a smaller numerical space, one might consider attaining a fast approximation of a phononic bandgap, when the wavelength is much greater than half of the thickness.

References

[1] I. Olsson III, R. H., and El-Kady, I. F., *Measurement Science and Technology* **20**, 012002 (2008).
[2] Saad, M., H., *Elasticity, Theory, Applications, and Numerics*, Academic Press, USA (2004).
[3] Su, M. F., Olsson III, R. H., Leseman, Z. C., El-Kady, I. F., *App. Phys. Lett.* **96**, 053111 (2010).
[4] Hussein, M. I., Hulbert, G. M., Scott, R. A., *Journal of Sound and Vibration* **307**, 865-893 (2007).
[5] Jensen, J. S., *Journal of Sound and Vibration* **301**, 319-340 (2007).
[6] Basu, U., Chopra, A. K., *Comput. Methods Appl. Mech. Eng*. **192**, 1337–1375 (2003).

Phononics 2011: First International Conference on Phononic Crystals, Metamaterials and Optomechanics
Santa Fe, New Mexico, USA, May 29-June 2, 2011
PHONONICS-2011-0155

From Newton's Cradle to New Acoustic Crystals

Chiara Daraio

Engineering and Applied Sciences, California Institute of Technology, 1200 E California Blvd. Pasadena CA 91125, USA. Daraio@caltech.edu

Abstract: The bouncing beads of Newton's cradle fascinate children and executives alike, but their symmetric dance hides a complex dynamic behavior. By assembling grains in crystals we are developing new materials and devices with unique properties. We have constructed two-dimensional systems that can redirect mechanical waves, and have developed new materials for absorbing vibrations and explosive blasts.

In this paper, I will discuss recent progress obtained in the study of nonlinear acoustic crystals. In particular, I will discuss the response of granular crystals excited by impulsive loading and continuous vibrations. Granular crystals are here defined as highly ordered aggregates of particles in elastic contact with each other, preferably in linear or network shaped arrangements. In our work, the assemblage of the novel acoustic materials is achieved by aligning granular components inside a selected matrix (Fig. 1) or in a self-standing crystal, designing contact interactions for the control of stress transfer between particles. The design of these materials starts from a well-understood local phenomenon (i.e. the elastic Hertzian contact interactions between particles) and creates global structures with unique properties (the granular crystals). This work leverages theoretical understanding of the highly nonlinear dynamic response of the fundamental components[1] for the design of experiments, and it is informed by discrete numerical simulations. The potential applications targeted by our work are: i) mechanical systems with tunable acoustic/elastic properties; ii) devices with controllable acoustic bandgaps within the audible range, noise mitigation and vibration absorbing layers; iii) novel shock-energy-trapping and pulse-disintegrating devices and micro- or macro-impact shielding; iv) new acoustic lenses with a tunable focal point and v) new methods of Non Destructive Evaluation, Structural Health Monitoring (NDE/SHM) and modal testing. In this paper, I will focus on recent results obtained with two-dimensional granular systems excited by impulsive loading and continuous vibrations. I will present how granular crystals can control the propagation of acoustic waves by varying the static compression applied to the system, the particles' geometry and material properties.

Figure 1 (Left) Example of a three-dimensional acoustic crystal realized aligning 2mm φ beads in vertical lodgings in a soft polymer matrix[2]; (right) zoomed in view from top.

Background

A chain of spherical particles (i.e. a longer version of the well known "Newton's cradle" toy) hides an intriguing elegant complexity, and a myriad of tunable mechanical phenomena that have been attracting increasing attention in the scientific community[1-6]. Some of the earliest findings in this discrete system[1-4] reported the formation of new, highly nonlinear solitary waves, with a finite wavelength, when the system is impacted at one end by a striker. The presence of defects and impurities has been shown to cause scattering and energy trapping[5]. When the system is highly precompressed its response can be varied to become weakly nonlinear or linear, depending on the ratio between the dynamic excitations' amplitude and the amplitude of the static compressive force[3]. When these systems are driven in the linear or weakly nonlinear regime, they present tunable band gaps in their dispersion relation[6]. In our current work, we have extended these findings to two-dimensional systems[7] (Fig. 2) composed of uniform and heterogeneous materials.

Phononics 2011: First International Conference on Phononic Crystals, Metamaterials and Optomechanics
Santa Fe, New Mexico, USA, May 29-June 2, 2011
PHONONICS-2011-0155

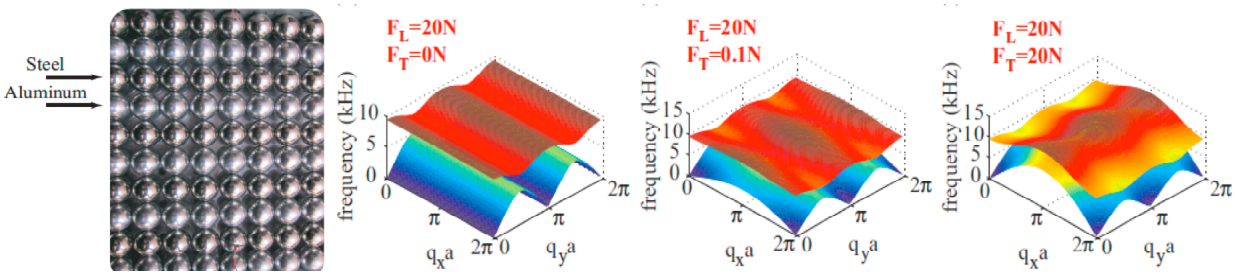

Figure 2 (Left) Two-dimensional acoustic crystal realized aligning steel and aluminium particles in alternating layers. (right) Dispersion relations calculated for a constant longitudinal static force (F_L = 20N) and a transversal force (F_T) taking the values 0, 0.1 and 20N.

studied periodic arrays of particles with variable precompression using theory, discrete numerical models and experiments. We consider different configurations of the lattices, using spheres made of different materials. Experimental measurements of the transmitted power spectral density are performed highlighting the presence of band gaps in two-dimensional diatomic (two-particle periodicity, Fig. 2) or triatomic crystals. Depending on the static force applied, the edge frequency of the acoustic and optical bands can be tuned. In the layered diatomic square packing studied, when the static transversal force is equal to 0, a quasi one-dimensional response is observed. When the static transversal force is increased, the propagation of waves can be tuned from 1-D to 2-D, enabling transversal energy propagation. These systems could be used as tunable, load-bearing vibration absorbers or acoustic filters for frequencies belonging to the audible range.

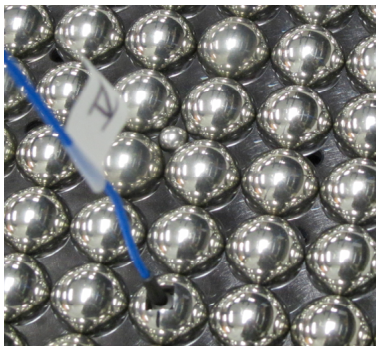

Figure 3 Digital image of the experimental setup used to study the effect of a defect in a 2-D squared array of stainless steel particles. The image shows the interstitial defect and one of the triaxial accelerometers embedded in a particle to detect the waves.

We also study the effects of defects in a squared packing of uniform particles, when the system in non-precompressed and excited by transient pulses. The defect corresponds to an interstitial impurity of different materials (Fig. 3). We analyze the response of the traveling signal as a function of the materials properties for the defect particles and study the resulting energy trapping, redirection and particles oscillations. The defects behave as energy scatterers and, depending on their materials properties, can trap variable amount of energy and momentum. The interaction of multiple defects on the same lattice will also be discussed. The work includes experiments and numerical simulations based on a discrete particle model.

Future developments will include the use of numerical optimization to control wave propagation and energy transmission selecting optimal particles' geometry, materials and arrangements.

Acknowledgements
The work described in this extended abstract has been performed in collaboration with Dr. Stephane Griffiths and Mr. Ivan Szelengowicz at Caltech. The work was supported by Office of Naval Research - YIP, by the United Technologies Research Center, and by an ARO/MURI.

References

[1] Nesterenko, V.F., *Dynamics of Heterogeneous Materials*., NY, Springer−Verlag (2001).
[2] Daraio, C.; Nesterenko, V.F.; Jin, S.; APS - Shock Compression of Condensed Matter, 197-200, American Institute of Physics, Conference Proceedings, Portland (OR), (2003).
[3] Daraio, C.; Nesterenko, V.F.; Herbold, E.; Jin, S. *Physical Review E*, 73, 026610, (2006).
[4] Sen, S. et al. *Physics Reports* 462, 21–66, (2008).
[5] S. Job, et al. *Phys. Rev. E* 80, 025602(R), (2009).
[6] Herbold, E.B. et al. *Acta Mechanica* 205, 1-4, 85-103, (2009).
[7] Gilles, B., Coste, C. Powders and Grains, 4th International Conference on Micromechanics of Granular Media, (2001).

Phononics 2011: First International Conference on Phononic Crystals, Metamaterials and Optomechanics

Santa Fe, New Mexico, USA, May 29-June 2, 2011

PHONONICS-2011-0163

Acoustic Logic Gates Implemented Using A Phase Controlling Phononic Crystal

Stefan Bringuier[1] , Nichlas Z. Swinteck[1], Jerome O. Vasseur[2], Jean-Francois Robillard[2], Keith Runge, Krishna Muralidharan[1], Pierre Deymier[1]

[1] University of Arizona, AZ, USA
stefanb@email.arizona.edu, swinteck@email.arizona.edu, krishna@email.arizona.edu, deymier@email.arizona.edu
[2] Institut d'Electronique, de Micro-electronique et de Nanotechnologie, France
jerome.vasseur@univ-lille1.fr, Jean-Francois.Robillard@isen.fr
krunge@bellsouth.net

Abstract: A Phononic crystal (PC) consisting of a square array of cylindrical Polyvinylchloride inclusions in air, is used to construct a variety of acoustic logic gates. This PC has a unique band structure that allows for the control of the relative phase between incident acoustic waves. The realization of the gates is demonstrated through simulations employing the finite-difference-time-domain method.

Phononics 2011: First International Conference on Phononic Crystals, Metamaterials and Optomechanics

Santa Fe, New Mexico, USA, May 29-June 2, 2011

PHONONICS-2011-0163

Phononics 2011: First International Conference on Phononic Crystals, Metamaterials and Optomechanics
Santa Fe, New Mexico, USA, May 29-June 2, 2011
PHONONICS-2011-0165

Device Level Harmonic Finite Element Analysis of Phononic Crystals Operating at GHz Frequencies

S. Alaie[1], I. El-Kady[2], and Z. C. Leseman[1*]

[1] *Mechanical Engineering, University of New Mexico, Albuquerque, NM USA 87131*
alaie@unm.edu, and zleseman@unm.edu
[2] *Sandia National Laboratories, Albuquerque, NM USA 87105*
ielkady@sandia.gov

Abstract: The vibrational behavior of a phononic crystal is studied at gigahertz frequencies. The phononic crystal is comprised of a silicon slab with tungsten inclusions filtering out waves within the frequency range of 0.7 GHz to 1.1 GHz. Comparisons show that the harmonic finite element analysis is capable of more accurately explaining the experimental results than FDTD when compared to experiments.

For this poster, the vibrational behavior of a phononic crystal is studied at gigahertz frequencies. The phononic crystal is comprised of a silicon slab with tungsten inclusions filtering out waves within the frequency range of 0.7 GHz to 1.1 GHz. Two-dimensional harmonic finite element analysis (FEA) is employed to model the transmission of stresswaves launched from a transmitter and passing through the crystal. The numerical results are compared with another prevalent numerical method, finite difference time domain (FDTD), as well as with experimental results. These comparisons show that the harmonic finite element analysis is capable of more accurately explaining the experimental results than FDTD. This more favorable comparison is attributed to a resonance that course between the transmitter and the phononic crystal.

Phononics 2011: First International Conference on Phononic Crystals, Metamaterials and Optomechanics

Santa Fe, New Mexico, USA, May 29-June 2, 2011

PHONONICS-2011-0165

Phononics 2011: First International Conference on Phononic Crystals, Metamaterials and Optomechanics
Santa Fe, New Mexico, USA, May 29-June 2, 2011
PHONONICS-2011-0173

Phononic Band Gap Optimization for Combined In-Plane and Out-of-Plane Waves

Osama R. Bilal, Mahmoud I. Hussein

Department of Aerospace Engineering Sciences, University of Colorado at Boulder, CO 80309, USA
osama.bilal@colorado.edu, mih@colorado.edu

Abstract: Utilizing the reduced Bloch mode expansion method for fast band structure calculations and specialized genetic algorithms for a search among numerous topologies, optimal phononic crystal unit cell designs are generated for (1) in-plane, (2) out-of-plane and (3) combined in-plane and out-of-plane elastic wave propagation in a 2D geometrically periodic *single material* media. This process of natural evolution yields elegant designs with exceptionally large, and low, frequency band gaps.

Phononic crystals are material systems with the distinct feature of unit cell repetition. The unit cell is composed of at least two types of material phases with different properties or a single material with a non-uniform geometric structure. An important dispersion-related characteristic of wave propagation through phononic crystals is the existence of frequency band gaps, where waves do not propagate. The widths of these bands, and their locations in the frequency domain, depend on the topology of the unit cell, material-wise or geometry-wise. Through topology optimization, the configuration of the unit cell can be designed to exhibit a maximum value of band gap width divided by band gap central frequency, i.e., *large and low band gap*. This problem has been investigated earlier for bi-material media with a focus on either in-plane (P/SV) wave propagation or out-of-plane (SH) wave propagation[1-3]. In this paper we consider geometrically periodic square lattices formed from only one material (silicon), and investigate three band-gap optimization problems: (1) in-plane waves only, (2) out-of-plane waves only and (3) combined in-plane and out-of-plane waves.

We build our elastodynamic model based on the wave equation for a two-dimensional media under plain strain conditions[1,4]. In this model, incident in-plane waves travel at the speed of the material's longitudinal velocity c_l and incident out-of-plane waves travel at the speed of the material's transverse velocity c_t. The phononic band structure is calculated by employing Bloch theory and using the finite element method to expand the equation of motion in real space. Furthermore, the reduced Bloch mode expansion (RBME) method[3] is used to substantially reduce the size of the computational model and hence make it feasible to search, using genetic algorithms (GA), among an exceedingly large design space representing a multitude of different possible material distributions within the unit cell domain.

Unit Cell Representation and Design Objective

The square unit cell Y is composed of $n \times n$ pixels forming a matrix G, which we reduce in size following the underlying lattice symmetry. Each of the pixels can be assigned to either a *no material* or a *material* (silicon), i.e., $g_{ij} \in \{0,1\}$. We formulate our objective function in terms of the size of a particular band gap normalized with respect to its central frequency:

$$f(g) = \frac{max\,(min_{j=1}^{n_k}(\omega_{i+1}^2(k_j,g)) - max_{j=1}^{n_k}(\omega_i^2(k_j,g)),0)}{(min_{j=1}^{n_k}(\omega_{i+1}^2(k_j,g)) + max_{j=1}^{n_k}(\omega_i^2(k_j,g)))/2}, \quad (1)$$

where $min_{j=1}^{n_k}(\omega_i^2(k_j,g))$ and $max_{j=1}^{n_k}(\omega_i^2(k_j,g))$ denote the minimum and maximum, respectively, of the i^{th} frequency ω_i over the entire discrete wave vector set, k_j, $j=1,\ldots,n_k$, tracing the border of the irreducible Brillouin zone.

Genetic Algorithm

For the initialization step in the GA, we observed that almost any randomly generated design at high unit cell resolution (i.e. $n \geq 24$ pixels) exhibits no band gap. To address this problem, we use the area

Phononics 2011: First International Conference on Phononic Crystals, Metamaterials and Optomechanics
Santa Fe, New Mexico, USA, May 29-June 2, 2011
PHONONICS-2011-0173

between the two dispersion branches of interest as an indicator for the fitness of the unit cell designs used in the GA selection operation:

$$Fitness = \phi f(g) + F \tag{2}$$

$$F = \begin{cases} 0 & \text{if } f(g) > 0 \text{ (band gap exists)} \\ Area & \text{if } f(g) = 0 \text{ (no band gap)} \end{cases}, \tag{3}$$

$$Area = \sum_{j=1}^{n_k} [(\omega_{i+1}^2(k_j, g)) - (\omega_i^2(k_j, g))]. \tag{4}$$

In Eq. (2), ϕ is chosen to be a large number $(\phi = 10^4)$ in order to guarantee that any design that has a band gap is selected over a design that has no band gap. Furthermore, the GA initialization procedure is set to ensure that each two adjacent pixels in a row have the same material type. At each evolutionary step, a simple single point crossover is carried out between the two selected designs with a tournament selection operator. Finally the GA is programmed to terminate when the generation counter reaches the max number of generations. Following termination, the best surviving design passes through a simple one-point flip local search for fine-tuning.

Results and Conclusion

Upon implementing our GA- and RBME-based search methodology, we obtained the following optimal unit cell designs. Fig. (1): first band gap for out-of-plane waves, band gap size f = 0.7884; Fig. (2): second band gap for out-of-plane waves, band gap size f = 0.8945; Not shown: first band gap for in-plane waves, band gap size f = 0; Fig. (3): second band gap for in-plane waves, band gap size f = 0.8705; Fig. (4): lowest possible band gap for combined out-of plane and in-plane waves; band gap size f^* = 0.6938, where the superscript "*" denotes a modified objective function that describes maximization of a combined band gap among the band structures of the two types of waves. We note that the out-of-plane designs show a continuous solid media approaching the limiting case of separate square inclusions in air. The in-plane designs on the other hand show a mostly solid material with delicately shaped air holes. The optimal design for the combined case appears to be a blend among the out-of-plane and in-plane design traits. All designs are amenable to fabrication upon post-optimization smoothening.

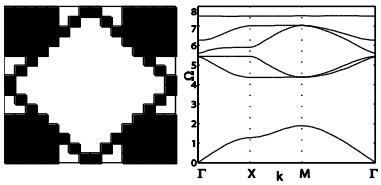

Figure 1. Optimal design for 1st band gap for out-of-plane waves

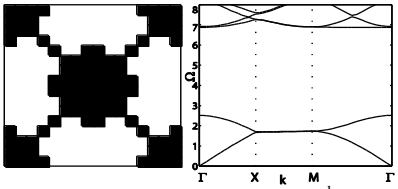

Figure 2. Optimal design for 2nd band gap for out-of-plane waves

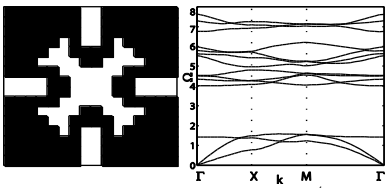

Figure 3. Optimal design for 1st band gap for out-of-plane waves

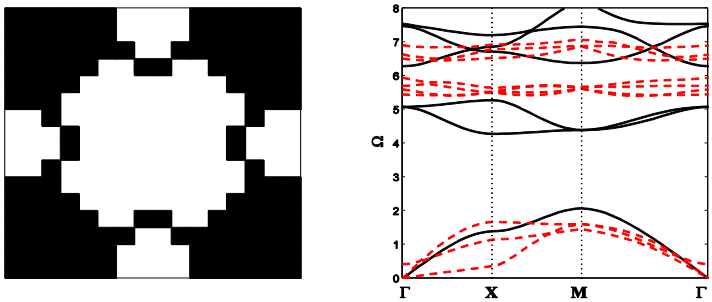

Figure 4. Optimal design for combined in-plane (red-dashed) and out-of-plane (black) waves

References

[1] O. Sigmund and J.S. Jensen, *Philosophical Transactions of the Royal Society A*. **361**, 1001-1019 (2003).
[2] M. I. Hussein, K. Hamza, G. M. Hulbert, and K. Saitou, *Waves in Random and Complex Media*, **17**, 491-510 (2007).
[3] M. J. Rupp, A Evgrafov, K. Maute and M. L. Dunn, *Structural and Multidisciplinary Optimization*, **34**, 111-122 (2007).
[4] M. I. Hussein, *Proceedings of the Royal Society A*. **465**, 2825-2848 (2009).

Phononics 2011: First International Conference on Phononic Crystals, Metamaterials and Optomechanics
Santa Fe, New Mexico, USA, May 29-June 2, 2011
PHONONICS-2011-0182

Multiscale Dispersive Design: A Building Blocks Approach to Phononics

Mahmoud I. Hussein

Department of Aerospace Engineering Sciences, University of Colorado at Boulder, CO 80309, USA
mih@colorado.edu

Abstract: A key feature in most applications in phononics is an underlying spatial periodicity. When infinite in extent, this spatial symmetry constitutes a periodic "material". When truncated to finite dimensions, a periodic "structure" is formed. Between the two entities there is an abundance of opportunities for shaping a desired wave propagation or vibration response. In this work we will revisit the concept of Multiscale Dispersive Design and use it towards the exploration of new avenues in phononic crystals and metamaterials applications.

Within phononic crystals and metamaterials, various wave phenomena occur across the underlying spatial periodicity inducing mechanisms of wave interference and/or local resonance that lead to a banded frequency response. Similar physical behavior is possible within finite structures composed of periodic materials although the periodicity truncation in itself alters the dynamical characteristics (see, e.g., Ref. 1). In some cases these alterations are mild (for example, the frequency range of the band gaps are practically retained), but in other cases significant changes to the dynamical response are realized, such as the possible appearance of resonances in the band gap. It has been shown in several studies that if a substantially large number of unit cells is retained in the truncated structure, or the finite periodic material portion of a structure, then the frequency response of the underlying unit cell will still dominate[1].

In this paper, we will revisit the concept of Multiscale Dispersive Design (MDD) previously proposed by the author and collaborators[2,3]. This is essentially a design methodology whereby periodic unit cells are designed for desired frequency band properties, and with appropriate scaling, these cells are used as *building blocks* for forming fully periodic or partially periodic structures with related dynamical characteristics. Through this approach, which is hierarchical and integrated, structures can be devised for a wide range of wave propagation and vibration response tailored to specification.

As an example we consider the problem of designing a passive demultiplexer using phononic crystals, a problem previously studied in the literature[4]. From Ref. 3, Fig. 1 shows a two-dimensional plate-like structure formed from three types of phononic crystal building blocks each based on a unit cell with a unique band gap: the group of cells with a black inclusion function as "walls" for all waves in the frequency range of $3 \le \Omega \le 4$ (Ω denotes non-dimensional frequency), and the group of cells with an orange or a blue inclusion functions as a "gate" that allow passage of waves in the range of $3.4 \le \Omega \le 4$ or $3 \le \Omega \le 3.8$, respectively. By employing a portion of each type of periodic material (i.e., with at least 3-4 unit cells in each direction), the underlying band gap properties will still take effect in the truncated configuration. In this manner a passive demultiplexer is formed by the macroscale layout shown in Fig. 1.

The building blocks approach demonstrated by this demultiplexer example is being extended to a variety of new applications in phononics. A description and analysis of these applications and their potential impact to the engineering of novel devices, or coupled material/structure systems, will be discussed.

Phononics 2011: First International Conference on Phononic Crystals, Metamaterials and Optomechanics
Santa Fe, New Mexico, USA, May 29-June 2, 2011
PHONONICS-2011-0182

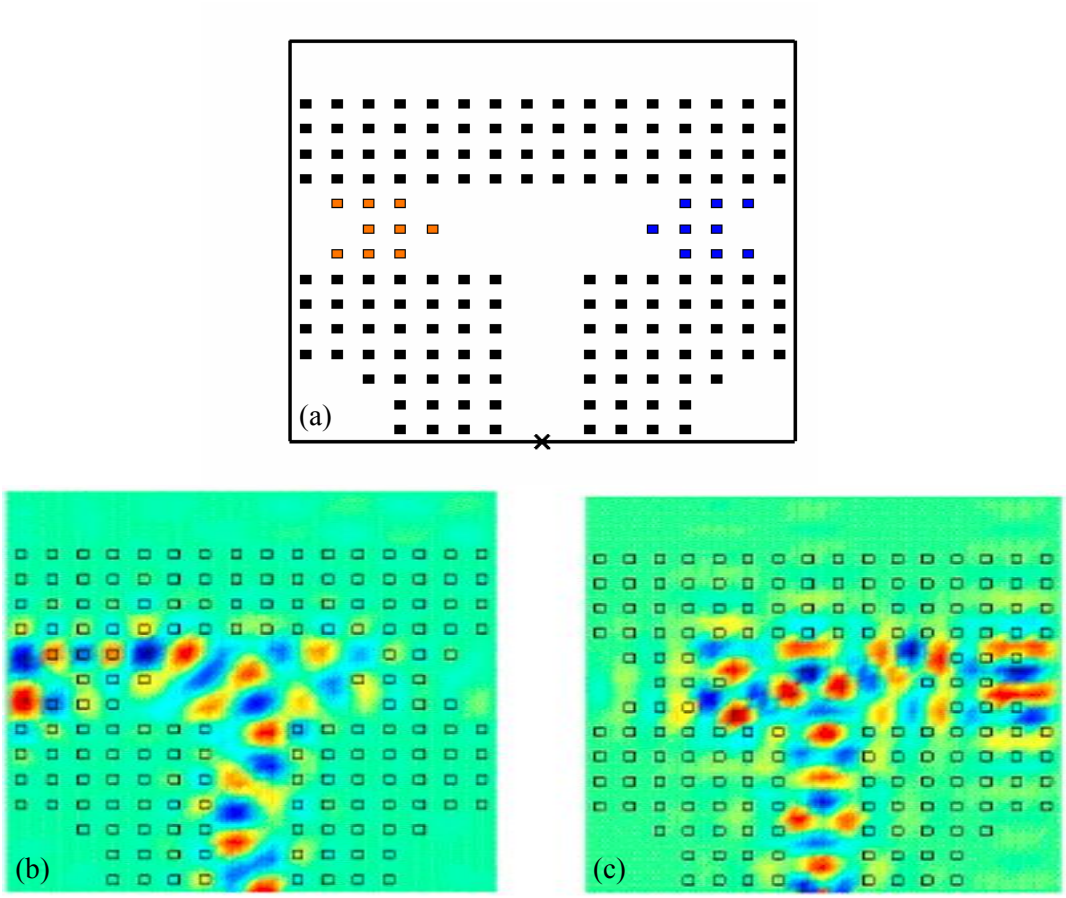

Figure 1. (a) Frequency demultiplexer formed from a combination of phononic crystal building blocks. In this passive structure, low frequency waves are turned to the left (b), and high frequency waves are turned to the right (c).

References

[1] M. I. Hussein, G. M. Hulbert and R. A. Scott, *Journal of Sound and Vibration*, **289**, pp. 779-806 (2006).
[2] M. I. Hussein, G. M. Hulbert and R. A. Scott, *Journal of Sound and Vibration*, **307**, pp. 865-893 (2007).
[3] M. I. Hussein, G. M. Hulbert and R. A. Scott, ASME IMECE 2005, Paper IMECE2005-81325, pp. 1-10 (2005).
[4] Y. Pennec, B. Djafari-Rouhani, J. O. Vasseur, A. Khelif, P. A. Deymier, *Physical Review E*, **69**, 046608 (2004).

1ST INTERNATIONAL CONFERENCE ON PHONONIC CRYSTALS, METAMATERIALS & OPTOMECHANICS

Extended Abstracts

Track 2: Phononic Metamaterials

Phononics 2011: First International Conference on Phononic Crystals, Metamaterials and Optomechanics
Santa Fe, New Mexico, USA, May 29-June 2, 2011
PHONONICS-2011-0021

Narrow Fluid Channel as a Metamaterial Sound Absorber

Arkadii Krokhin[1,2], Victor Garcia-Chocano[2], José Sánchez-Dehesa[2], Tomás López-Rios[3]

[1] *University of North Texas, 1155 Union Circle 311427, Denton, TX 76203, USA,*
arkady@unt.edu
[2] *Wave Phenomena Group, Universidad Politécnica de Valencia, C/Camino de Vera s.n., E-46022 Valencia, Spain,*
jsdehesa@upvnet.upv.es,
[3] *Institut Néel, CNRS and University Joseph Fourier, BP166, 38042 Grenoble Cedex 9, France*
Tomas.Lopez-Rios@grenoble.cnrs.fr

Abstract: Abnormally high level of absorption has been observed for sound waves propagating through a narrow water channel clad between two metal plates. Absorption is due to resonant excitation of Rayleigh waves on the both metal surfaces. These waves may either produce strong turbulent motion in a viscous fluid or radiate its energy into the metal, giving rise to deep minima in the transmission spectrum.

Sound waves can propagate over a long distance in water. In bulk medium attenuation caused by viscosity of water grows quadratically with the wave frequency f. For many practical applications of noise control it is necessary to design materials with high level of absorption. "Perfectly" absorbing metamaterials are of great interest in optics since they may modify thermal emission and increase the efficiency of photovoltaic devices[1,2]. A standard method to increase sound absorption is to perforate a sample with micropores. High porosity strongly increases the area of acoustic impedance mismatch and also increases the effects of internal friction. Here we propose tailored, highly absorptive acoustic metamaterial based on a narrow, but still macroscopic, water channel formed by two massive brass plates. Our motivation is based on the ability of surface plasmons to strongly absorb light incidenting on metal grating (so-called Wood anomaly), as well as to support extraordinary transmission of light through subwavelength holes in thin metallic films. Acoustic counterpart of extraordinary transmission due to excitation of a surface mode has been recently observed[3], while anomalous absorption of sound caused by Rayleigh waves is still missing.

The experimental setup is shown in Fig. 1. We used a couple of 1.5´´ immersion transducers that were placed face to face at a distance of 16 cm. A slit of width d is obtained between two adjacent 12× 12cm^2 brass plates of equal thickness h immersed in water. The slit forms a narrow water channel with high aspect ratio $h/d \gg 1$. Transmission through the water channel has been measured within frequencies from 0.2 to 1.5MHz that corresponds to the wavelengths in water from 0.7 to 0.1cm. Due to mismatch of acoustic impedances between water and brass only ~10% of acoustic energy passes through the metal plates. However, at the Fabry-Perot (FP) resonances, when $2h = n\lambda_l$ the plates become practically transparent, giving rise to sharp peaks in the transmission spectra. Here $\lambda_l = c_l/f$ is the wavelength of a longitudinal wave propagating in metal with speed c_l. Away from the FP resonances sound propagates mostly through the water channel. Typical transmission spectra obtained for different plate thicknesses h and apertures d are shown in Fig. 2. The frequency interval between two FP peaks scales as $1/h$, therefore only one peak is displaced for $h = 2$mm, two for $h = 3$mm and three for $h = 5$mm. Each measured spectrum exhibits a deep minimum (marked by an arrow above it) at frequency lower than the first FP peak. The amplitude of this peak strongly depends on the aperture, unlike its position, which is almost independent on d. The latter means that this minimum is irrelevant to resonant reflection of the wave from a finite aperture. The only reason for such low transmission is dissipation of acoustic energy in the water channel. We argue that resonant increase of dissipation is due to excitation of Rayleigh waves.

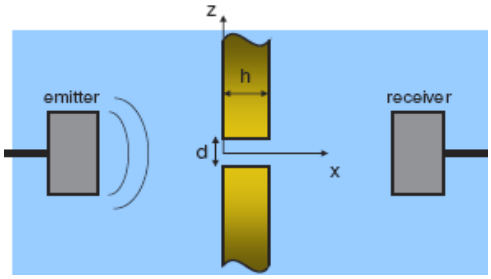

Figure 1 Experimental set up. The plates, the emitter and receiver are immersed in water.

Phononics 2011: First International Conference on Phononic Crystals, Metamaterials and Optomechanics
Santa Fe, New Mexico, USA, May 29-June 2, 2011
PHONONICS-2011-0021

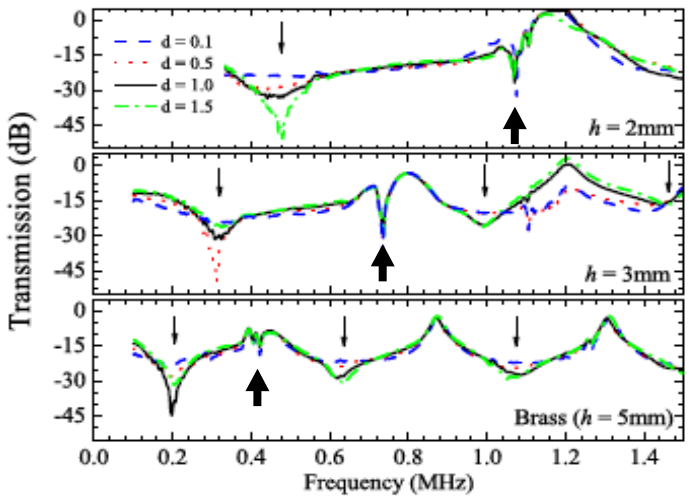

Figure 2 The measured transmission spectra of the water channel with different aspect ratios. The position of each resonance corresponding to a real (complex) solution of Eq. (1) is marked by thin (bold) arrow.t. Note the missing first resonance ($n = 1$) for $\boldsymbol{d = 0.1}$ mm.

In a fluid channel with hard walls the dissipation of acoustic energy is weak since propagating sound wave induces laminar Poiseuille flow where dissipation is due to perpendicular to the walls gradient of fluid velocity, $\frac{\partial V_x}{\partial z}$. If the walls are elastic, the Rayleigh wave can be excited at discrete frequencies in a finite-length channel. Vibrating walls induce turbulent flow where all the derivatives $\frac{\partial V_i}{\partial x_k}$ with $i,k = x,z$ are different from zero. Since the energy dissipated due to viscosity is proportional to $\left(\frac{\partial V_i}{\partial x_k}\right)^2$, it is clear that excitation of Rayleigh wave leads to strong reduction of acoustic transmission.

In a narrow channel the Rayleigh waves propagating along the both surfaces are coupled. Our analysis shows that resonant excitation of coupled Rayleigh waves occurs at the frequencies $f_n = \left(\frac{\pi n}{h}\right) c_t x_n$. Here c_t is the speed of shear wave in metal, $n = 1,3,5$ ..., and x_n is a solution of the following dispersion equation

$$(2-x^2)^2 - 4\sqrt{1-x^2}\sqrt{1-\left(\frac{c_t x}{c_l}\right)^2} = \frac{\rho_f}{\rho_m} x^4 \sqrt{\frac{1-(c_t x/c_l)^2}{(c_t x/c_f)^2 - 1}} \cot\left(\frac{\pi n d}{2h}\sqrt{\left(\frac{c_t x}{c_f}\right)^2 - 1}\right). \quad (1)$$

Here $\rho_f(\rho_m)$ is the density of the fluid (metal) and c_f is the speed of sound in fluid. Eq. (1) describes the eigenmode with symmetric vibrations of the plates. The real solutions of this equation for $n = 1,3,$ and 5 fit well the resonant minima marked by solid arrows in Fig. 2. For small aperture $d = 0.1$ mm the first minima is missing. Accordingly, there is no real solution for $n = 1$ for such narrow aperture. However, for $n = 3$ and 5 there are real solutions and the corresponding resonances are well observed. Apart from real solutions, Eq. (1) has a complex root for each n. This root gives rise to leaky Rayleigh wave which has been predicted[4] but has never been observed in acoustic experiment. The leaky wave radiates energy into metal plates that leads to the deep minima marked by bold arrows. For the plates with $h = 2$ and 5mm these minima overlap with the FP peaks, therefore for these cases the minima are not very deep. However, for $h = 3$mm this minimum is well resolved. Absorption of sound at each of the minima in Fig. 2 exceeds by orders of magnitude absorption in bulk water, thus demonstrating metamaterial behavior of water in narrow channels with elastic boundaries.

This work is supported by the US Office of Naval Research (grant No. N000140910554), by the US Department of Energy (grant No. DEFG02-06ER46312), and by the Spanish Ministerio de Ciencia e Innovación (TEC2007-67239 and CSD2008-66). AK acknowledges support by the Spanish Ministerio de Educación (No. SAB2009-0006).

References

[1] S. Han, A. Stein, D. Norris, *Phys. Rev. Lett.* **99,** 053906 (2007); N.I. Landy, *et al*., *Phys. Rev. Lett.* **100**, 207402 (2008).
[2] E. E. Narimanov and A. V. Kildishev, *Appl. Phys. Lett.* **95,** 041106 (2009).
[3] H. Estrada, *et al*., Phys. Rev. Lett. **102**, 144301 (2009).
[4] N.E. Glass and A.A. Maradudin, J. Appl. Phys. **54,** 796 (1983).

Phononics 2011: First International Conference on Phononic Crystals, Metamaterials and Optomechanics
Santa Fe, New Mexico, USA, May 29-June 2, 2011
PHONONICS-2011-0026

Fabrication and Experimental Characterization of Anisotropic Fluid-Like Materials

Daniel Torrent[1] , José Sánchez-Dehesa[1]

[1] Departamento de Ingeniería Electrónica, Universidad Politécnica de Valencia, Valencia, Spain

datorma1@upvnet.upv.es, jsdehesa@upvnet.upv.es

Abstract: We report a method to obtain acoustic metamaterials or metafluids with cylindrically anisotropic mass density. The method uses a periodically corrugated structure embedded in a two dimensional waveguide. This structure represents a periodic multilayered fluid-fluid composite that, in the low frequency limit, behaves as a fluid-like metamaterial with mass anisotropy. Also, an experimental method to characterize these structures is presented, showing that the resonances in these closed structures can be used to derive the acoustic parameters of these metafluids. An excellent agreement between theory and experiment is obtained.

Radial Wave Crystals [1,2] are a new type of periodic media that present band-gaps and wave localization but in the radial direction, that is, they are crystals in polar or spherical coordinate systems. Fluid-like materials with anisotropic mass density are the basis of radial wave crystals, as well as of cloaking shells [3] and a wide variety of devices based on the field of transformation acoustics. This anisotropy is not a natural property of common materials; therefore it is worth to include these systems in the field of metafluids, despite being parameters with positive values.

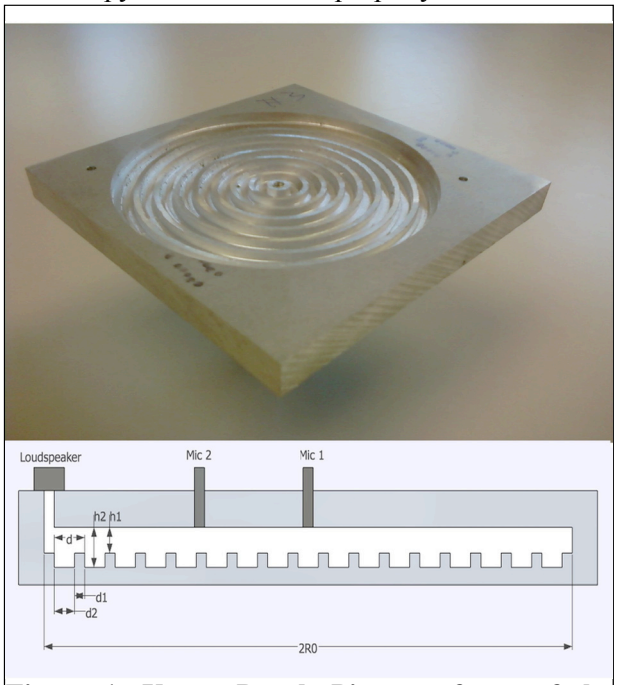

Figure 1: Upper Panel: Picture of one of the samples analyzed in the present work. Lower Panel: Schematic view of the experimental set up.

It has been shown that sonic crystals (periodic arrangement of sound scatterers) in the low frequency limit behave as effective fluid-like materials with anisotropic properties [4], where the anisotropy appears in the dynamical mass density. Even when the scatterers have elastic properties the effective medium behaves as a fluid-like material. These results suggest that mass anisotropy must be based on the periodicity of sub wavelength units placed in non-symmetric lattices.

However the mentioned anisotropy appears in rectangular coordinates, thus anisotropic devices having cylindrical or spherical symmetry cannot be designed with this approach. Such is the case of acoustic cloaking shells and radial wave crystals, in which the mass density tensor has constant components when expressed in a polar or spherical coordinate system, depending on the dimensionality of the problem.

It has been found that one way to obtain cylindrical or spherical anisotropy is by multilayered cylinders or spheres [5], which are special cases of one-dimensional periodic systems. It has been shown that the anisotropic properties obtained from the one-dimensional wave equation can be transformed to polar or spherical coordinates.

However this method need that all the layers are made of fluid-like materials, what implies that the multilayered structure has to be done by a set of alternating fluid materials with different physical properties. It is obvious that such a structure will not be, in principle, stable.

Phononics 2011: First International Conference on Phononic Crystals, Metamaterials and Optomechanics
Santa Fe, New Mexico, USA, May 29-June 2, 2011
PHONONICS-2011-0026

One solution was reported in [5], where all the layers were made of sonic crystals. However the large amount of cylinder required for realizing such a structure makes that approach difficult to achieve. Another approach could be make every layer of porous materials, but still some elastic effects should be taken into account that could decrease the functionality of the device, apart of having to add strong viscoelastic effects.
In this work the approach reported in [6] is explained, where a corrugated structure embedded into a waveguide was used to produce the multilayered system (see Figure 1). It was shown that the mentioned structure behaves as a fluid-fluid periodic medium, where each groove can be described as a fluid-like material in which the speed of sound is that of air and the density is given by the ratio of the height of the groove and the "background" height [7].
Once assumed that each groove acts as a fluid material, it can be shown that, in the low frequency limit, the structure shown in Figure 1 behaves as an anisotropic fluid-like cylinder where the mass anisotropy ratio is given by

$$\gamma^2 = \frac{1}{2}\left(d_1 + d_2\frac{h_1}{h_2}\right)\left(d_1 + d_2\frac{h_2}{h_1}\right)$$

Therefore the resonances of the structure can be used to characterize the effective medium. These resonances where measured by the set up shown in the lower part of Figure 1. In brief, an external sound field is excited and the response of the structure is measured by the two microphones. The peaks of the taken spectra are analyzed and the experimental values of the anisotropy rations for three different samples are obtained, showing an excellent agreement between theory and experiment.
It will be shown also how to realize metamaterials with the same acoustic parameters but with the tensor rotated 90 degrees, that is, replacing the radial component by the angular one and vice versa. In this case, the corrugated structure is made of angular sections off different height in place of concentric grooves, but the behavior can be shown to be equivalent.
This method allows designing anisotropic fluid-like metafluids with any orientation of the tensorial mass density, being a promising method to fabricate more complex structures requiring such anisotropy, specially radial wave crystals, which are not only anisotropic but also inhomogeneous metafluids.

Work partially supported by the Spanish MICINN under contracts TEC 2007-67239 and Consolider CSD2008-00066, and by the U.S. Office of Naval Research through the Grant N000140910554. Daniel Torrent also acknowledges the contract provided by the program Campus de Excelencia Internacional 2010 UPV.

References

1. D. Torrent and J. Sánchez-Dehesa, Phys. Rev. Lett. 103, 064301 (2009).
2. D. Torrent and J. Sánchez-Dehesa, New J. Phys. 12, 073034 (2010).
3. S.A. Cummer and D. Schurig, New J. Phys. 9, 45 (2007).
4. D. Torrent and J. Sánchez-Dehesa, New J. Phys. 10, 023004 (2008).
5. D. Torrent and J. Sánchez-Dehesa, New J. Phys. 10, 063015 (2008).
6. D. Torrent and J. Sánchez-Dehesa, Phys. Rev. Lett. 105, 174301 (2010).
7. P.M. Morse and K.U. Ingard, Theoretical Acoustics (Princeton University Press, New Jersey, 1986).

Phononics 2011: First International Conference on Phononic Crystals, Metamaterials and Optomechanics
Santa Fe, New Mexico, USA, May 29-June 2, 2011
PHONONICS-2011-0037

Metal Water: A Metamaterial for Acoustic Cloaking

Andrew N. Norris[1], Adam J. Nagy[2]

Mechanical & Aerospace Engineering, Rutgers University, Piscataway NJ, USA
[1]norris@rutgers.edu, [2]adnagy@eden.rutgers.edu

Abstract: A generic metamaterial is described that is suitable for making acoustic cloaking devices. The fundamental property is that it mimics the acoustic properties of water, yet can be modified to display anisotropic elastic properties suitable for cloaking. It has the important property that the amount of void space is conserved: a "conservation of cloaked space".

Acoustic cloaking can, in theory, be achieved using widely different material properties. The reason is that for a given mapping function the transformed version of the original scalar wave equation can be interpreted in terms of different material constitutive theories[1]. In this sense acoustic cloaking is distinct from its counterpart for electromagnetic waves, for which the material corresponding to the transformed Maxwell equations is uniquely defined by the transformation function. The first mechanism proposed for acoustic cloaking[2,3] was based on the concept of *anisotropic density*, and a single bulk modulus. Compressible fluids with anisotropic density are physically permissible[4], by layering homogeneous fluids, for instance. The range of inertial properties required for achieving cloaking is great, however, and could be very difficult to achieve by layering. Significant cloaking of a cylinder was shown to be possible[5] using hundreds of homogeneous fluids to reproduce the smoothly varying properties of the transformed fluids. The number of independent fluids can be reduced to three[6] but only if the three fluids have vastly different properties, e.g. one fluid must have extremely large density, another must have very large compressibility, etc..

An alternative route to acoustic cloaking is possible using *pentamode materials*[7] (PM). These can be considered as generalizations of compressible fluids that have anisotropic compressibility but isotropic density. As such, they are limiting cases of anisotropic elastic materials in which five of the six Kelvin moduli vanish. The Kelvin moduli are the eigenvalues of the 6x6 matrix of elastic moduli in Voigt notation (suitably represented in tensor form). Anisotropic inertia and pentamode materials are in fact limiting cases of a spectrum of material properties that yield the acoustic equation in the original untransformed coordinates. This material non-uniqueness may be ascribed to a "gauge" freedom in how the transformed particle displacement vector is defined; the full range of acoustically transformed material is described in[8]. The transformed elasticity equations display a similar nonuniqueness[9,10] which can also be associated with the choice of the displacement gauge relation[11]. Pentamode materials with anisotropic elastic behavior, like fluids with anisotropic density, are not found in nature. Zero elastic moduli implies structural instability, exemplified by the ability of water to flow. But in the case of water, the PM flows from one isotropic state to an identical one. PMs for cloaking cannot flow without change of state, and must have non-zero but small shear rigidity for stability.

Metal Water: Pentamode Material with Small Shear Rigidity

Water is the quintessential PM, however it is isotropic and therefore of no use in cloaking. Yet, any structural material for an acoustic cloak should be able to replicate homogeneous water in an acoustic sense. It must have the same *effective* compressibility and density as water, and display very small shear rigidity. We describe here a class of metamaterial with these properties, and more importantly, which can be modified to reproduce the PM properties of a cloak. The effective properties hold for wavelengths longer than the microstructure, so that the model is broadband. A metal microstructure in the form of a regular foam is chosen because it has relatively small shear rigidity, while exhibiting the bulk modulus and density of water simultaneously, see Figure 1. The large relative density of metal means that the structure is mostly void space.

An important property of PM cloaking is that the total mass of the cloak must equal the mass of the water in the space occupied by the cloak and the cloaked region[1,8]. Hence the amount of void space present in MW is preserved under the transformation from homogeneous "water" to the inhomogeneous PM. This "Archimedes principle" amounts to a Principle of Conservation of Cloaking Space, as

Phononics 2011: First International Conference on Phononic Crystals, Metamaterials and Optomechanics
Santa Fe, New Mexico, USA, May 29-June 2, 2011
PHONONICS-2011-0037

shown in Figure 1c. One can think of the original void space in the isotropic MW as micro-cloaked regions. The coordinate transformation has the effect of blowing up one of these while simultaneously shrinking the others.

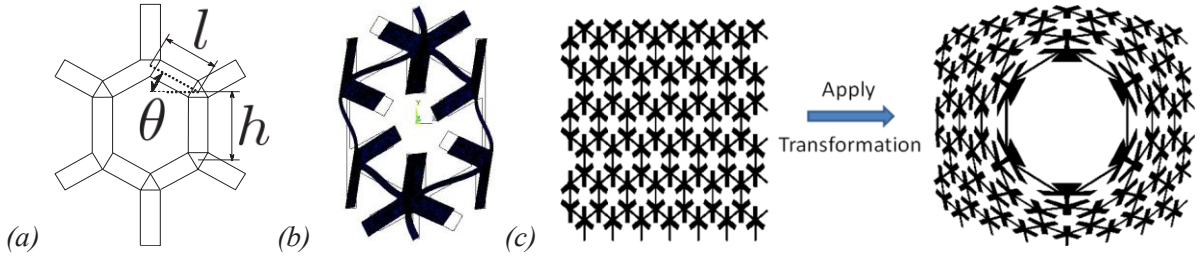

Figure 1 (a) A schematic of a unit cell. (b) Static deformation under a load used to calculate the effective elastic moduli of the periodic system. (c) The isotropic MW is transformed via the coordinate mapping into a functionally graded cylindrically anisotropic MW structure. The total amount of void in both pictures is preserved: Conservation of Cloaking Space.

The MW design begins with a hexagonal unit cell, depicted in Figure 1a. For the 2D structures considered here, the unit cell comprises thin load bearing struts, with islands of mass at the vertices, Figure 1b. The periodic structure is shown in Figure 1c, both in the original isotropic state on the left, and after transformation to the locally orthotropic structure on the right. The effective elasticity of the macroscopic foam can be calculated asymptotically to leading order in the thickness/length small parameter ε as

$$C=\begin{pmatrix} c_{11} & c_{12} & c_{16} \\ c_{12} & c_{22} & c_{26} \\ c_{16} & c_{26} & c_{66} \end{pmatrix} = C_0 \begin{pmatrix} \alpha & 1 & 0 \\ 1 & \dfrac{1}{\alpha} & 0 \\ 0 & 0 & O(\varepsilon) \end{pmatrix}, \quad \alpha = \frac{l\cos^2\theta}{(h+l\sin\theta)\sin\theta}, \quad \begin{pmatrix} 2.20 & 2.10 & 0 \\ 2.10 & 2.20 & 0 \\ 0 & 0 & 0.016 \end{pmatrix}. \qquad (1)$$

By way of comparison, water (or any compressible liquid) is described by stiffness matrix with $\alpha = 1$, $c_{66} = 0$. The matrix of numbers in equation (1) shows the FEM derived effective moduli (in GPa) for the isotropic MW. Note the small value of c_{66}. Numeric results above were obtained using the ANSYS FEM package with MATLAB for data manipulation, utilizing the homogenization theory outlined in[12]. Numerical experiments show that this value of shear modulus produces very small mode coupling and hence scattering of acoustic waves. The parameter α introduces the necessary anisotropy, which is determined by the unit cell parameters θ and l / h via equation (1). The connection with the cloaking transformation is that it defines C_0 and α (and the density) as functions of r. The microstructure is thus directly related to the coordinate mapping.

The presentation will develop these ideas through specific examples of cloak designs. Simulations of acoustic wave scattering will be shown that demonstrate the effectiveness of MW as a candidate metamaterial for not only 2D but 3 dimensional cloaking structures. Results from experiments that are anticipated will be reported if available.

References

[1] A. N. Norris, *Proc. R. Soc.A*, **464**, 2411-2434 (2008).
[2] S. A. Cummer and D. Schurig, *New J. Phys*. **9**, 1367-2630 (2007).
[3] H. Chen and C. T. Chan, *Appl. Phys. Lett*. **91**, 131518 (2007).
[4] M. Schoenberg and P. N. Sen, *J. Acoust. Soc.Am*. **73**, 61-67 (1983).
[5] D. Torrent and J. Sanchez-Dehesa *New J. Phys*. **10**, 023004 (2008).
[6] A. N. Norris and A. J. Nagy, *J. Acoust. Soc. Am*. **128**, 1606-1616 (2010).
[7] G. W. Milton and A. V. Cherkaev, *J. Eng. Mater. Technol*. **117**, 483-493 (1995).
[8] A. N. Norris, *J. Acoust. Soc. Am*. **125**, 839-49 (2009).
[9] G. W. Milton, M. Briane and J. R. Willis, *New J. Phys*. **8**, 248-267 (2006).
[10] M. Brun, S. Guenneau and B. Movchan, *Appl. Phys. Lett*. **94**, 061903 (2009).
[11] A. N. Norris, *Wave Motion* (accepted) (2011).
[12] B. Hassani, E. Hinton, *Computers & Structures*. **69**, 719-738 (1998).

Phononics 2011: First International Conference on Phononic Crystals, Metamaterials and Optomechanics

Santa Fe, New Mexico, USA, May 29-June 2, 2011

PHONONICS-2011-0063

Elastic Waves Propagation in a Locally Resonant Phononic Stubbed Plates

Mourad Oudich[1], Badreddine Assouar[1,2], Zhilin Hou[3]

[1] *Institut Jean Lamour, Nancy University – CNRS, Boulevard des Aiguillettes, BP 70239, 54506 Vandoeuvre, France*

[2] *International Joint Unit, CNRS – Georgia Institute of Technology, School of Electrical and Computer Engineering, 777 Atlantic Dr. NW, Atlanta, GA 30332-0250, USA*

[3] *Department of Physics, South China University of Technology, Wushan Shan 510640 Guangzhou, China*

Badreddine.Assouar@gatech.edu

Abstract: We report in this study on the phonon transport in a locally resonant (LR) phononic stubbed plate. First, we will discuss the opening of LR band gap (BG) as function as the nature of the stubs and geometrical parameters to figure out the evolution of the BG. Second, we will discuss the waveguiding in such structures based on the calculation of the band structures and the transmission coefficient.

The propagation of an elastic wave in periodic composite material, called phononic crystal (PC), has received much attention over the past decade. The main mechanisms responsible for the opening of acoustic band gap (BG) are based on the Bragg scattering and local resonance (LR) which can be occurs almost two orders lower than the usual Bragg gap in the frequency region. Since the pioneer work of Liu *et al*[1], most works dealt with the bulk waves. In this communication, we will present the acoustic property of a novel PC structure constructed by periodically depositing a single-layer or two-layer stubs on the surface of thin homogenous plate.

A locally resonant stubbed plate was studied using the finite element (FE) method. We have developed a numerical model capable to cope with a structure having a large elastic constant mismatch. Two structures were investigated: i. simple periodic silicone rubber stubs on epoxy homogenous plate; ii. composite stubs (Pb/silicone rubber) on epoxy plate. The BG and dispersion relation of LR structure were analysed as function of the filling fraction and the thickness of the stubs. The waveguiding of Lamb waves in such structure was also studied using FE method combined to supercell technique.

Numerical results showed that extremely low frequency BG of Lamb waves can be opened by the local resonance mechanism (an example is given in fig. 1.a). We found that the width of such a BG depends strongly on the thickness and the area of the cross section of the stubs. The physics behind the opening of the LRBG in our phononic structures can be understood by a simple "spring-mass" model.

The concept of the proposed structure is simple and easy to perform. The displacement field of the oscillating modes was analyzed to explain how the coupling of the modes induced the opening of the BG. The basis explanation is related to the coupling between the Lamb waves and the localized modes in the stubs (fig. 1.b) when both kinds of modes have the same symmetry and polarization.

Concerning the waveguiding of Lamb modes in the LRPC, we have obtained a very original property compared to the waveguiding in the traditional PC. Indeed, the possibility of guiding only one mode in the waveguide, which is very useful and suitable for filtering and demultiplixing applications, was pointed out.

[1]Z. Liu, X. Zhang, Y. Mao, Y. Y. Zhu, Z. Yang, C. T. Chan, and P. Sheng, *Science* **289**, 1734 (2000)

Phononics 2011: First International Conference on Phononic Crystals, Metamaterials and Optomechanics

Santa Fe, New Mexico, USA, May 29-June 2, 2011

PHONONICS-2011-0063

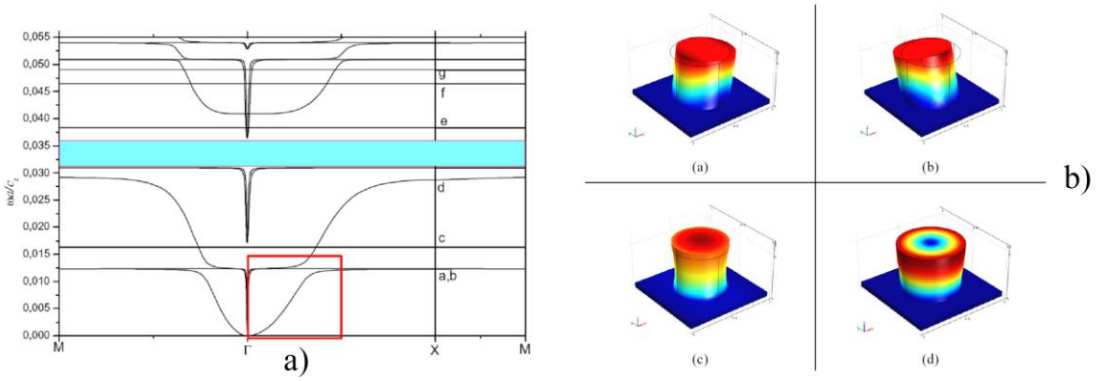

Figure 1. a. Band structures of the plate with the simple stub (only one rubber layer). b. The displacement distribution of the modes labeled as (a), (b), (c) and (d) in Fig. 1.a

Phononics 2011: First International Conference on Phononic Crystals, Metamaterials and Optomechanics
Santa Fe, New Mexico, USA, May 29-June 2, 2011
PHONONICS-2011-0068

Phononic Metamaterials for Transformation Acoustics Applications

Steven A. Cummer[1]

[1] *Department of Electrical and Computer Engineering, Duke University, PO Box 90291, Durham, NC 27708, USA, cummer@ee.duke.edu*

Abstract: We review the detailed development and derivation of the concept of transformation acoustics and demonstrate several approaches for engineering materials with the acoustic properties needed to realize transformation acoustics devices.

Transformation acoustics[1–4] is a paradigm for the creation of sound-manipulating materials and devices that are either difficult or impossible to derive through other theoretical approaches. It is based on the idea of a coordinate transformation of an arbitrary initial sound field. If the device you imagine can be defined in terms of a coordinate transformation, by squeezing, stretching, and/or displacing the sound field in a finite region, then transformation acoustics provides the mathematics for taking this coordinate transformation and deriving the properties of a material in that same finite region that will have exactly the same effect on the sound field as the coordinate transformation. The technique is very general and can be used to create many different kinds of devices, the most remarkable of which is perhaps the so called "cloak of silence", in which a coating surrounds an objects in order to reduce or eliminate the acoustic scattering from the composite object.[1–3]

Figure 1 shows simulated acoustic wave interaction with and scattering from a rigid cylinder and from a composite object made of the same rigid cylinder surrounded by an anisotropic and inhomogeneous cloaking shell with properties derived through transformation acoustics[1]. With the shell surrounding the cylinder, the net scattering is essentially zero.

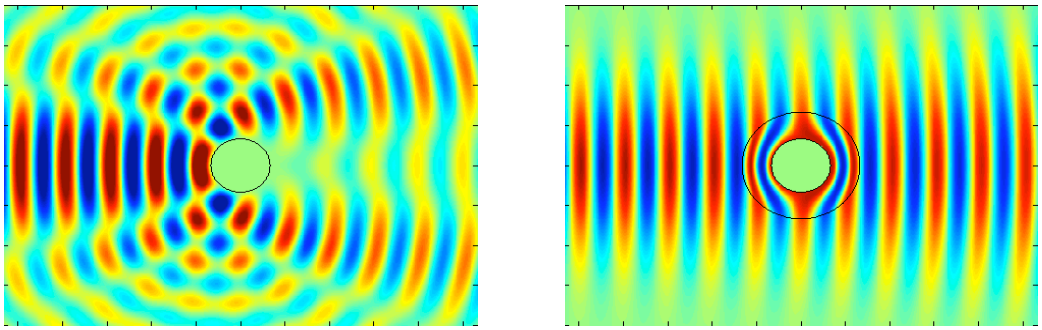

Figure 1 Left: A snapshot of simulated pressure field from an acoustic beam interacting with a rigid scatterer. Right: The same pressure field but one in which the rigid scatterer is surrounded by a shell with material properties defined by transformation acoustics theory. COMSOL Multiphysics was used for the simulations.

Transformation acoustics theory has lead to renewed interest in obtaining a new class of acoustic composites, also known as metamaterials, capable to achieve the large range of material parameters needed by these applications. Metamaterials are typically obtained from periodic arrangements of highly subwavelength unit cells composed of different types of basic materials. For example, alternating layers of very thin materials[5,6], arrays of perforated thin plates[7], and also arrays of inclusions embedded in a background fluid[8,9] have been shown to approximate the inhomogeneous and anisotropic profiles required in cloaking or hyperlens designs. Experimental work has just shown that arrays of rotationally asymmetric inclusions create effective mass anisotropy in close agreement with simulations[10].

Phononics 2011: First International Conference on Phononic Crystals, Metamaterials and Optomechanics

Santa Fe, New Mexico, USA, May 29-June 2, 2011

PHONONICS-2011-0068

Most metamaterials reported so far are designed through analytical methods and thus are applicable to a relatively small pool of unit cell geometries that can be handled by these analytical techniques. Numerical techniques[11,9], on the other hand, expand the range of available unit cell geometries and, consequently, the range of obtainable material parameters. In this presentation we illustrate this point in two applications.

The first application involves the design of a compact and broadband acoustic ground cloak in air, i.e. a cloak capable of hiding objects positioned on rigid flat surfaces. The good performance of the cloak is assessed experimentally by measuring the acoustic field around the cloak and comparing this field with the target field measured in the absence of the cloak. Furthermore, comparisons of these measurements with simulations of the theoretical device having the target ideal material parameters show the effectiveness of the employed numerical method to design metamaterials with prescribed material properties.

The second application illustrates the extended range of material parameters available in metamaterials obtained through numerical methods. We design and measure a flat graded-index lens similar to that described by Torrent and Sanchez-Dehesa[12]. We show how our design technique allows us to better match the lens impedance to that of the surrounding environment, and in the same time achieve higher contrast between the refractive index of different parts of the device, thus resulting in a thinner lens for a given focal length. As before, measurements of the acoustic fields around the lens agree very well with theoretical predictions, further validating our design method.

References

[1] Cummer, S. A. and D. Schurig, "One path to acoustic cloaking", *New Journal of Physics* **9**, 45 (2007).

[2] Chen, H. and C. T. Chan, "Acoustic cloaking in three dimensions using acoustic metamaterials", *Applied Physics Letters* **91**, 183518 (2007).

[3] Cummer, S. A., B.-I. Popa, D. Schurig, D. R. Smith, J. Pendry, M. Rahm, and A. Starr, "Scattering theory derivation of a 3D acoustic cloaking shell", *Phys. Rev. Lett.*. **100**, 024301 (2008).

[4] Cummer, S. A., M. Rahm, and D. Schurig, "Material parameters and vector scaling in transformation acoustics", *New Journal of Physics* **10**, 115025 (2008).

[5] Torrent, D., and J. Sanchez-Dehesa, "Acoustic cloaking in two dimensions: a feasible approach", *New Journal of Physics* **10**, 063015 (2008).

[6] Cheng, Y., F. Yang, J. Y. Xu, and X. J. Liu, "A multilayer structured acoustic cloak with homogeneous isotropic materials", *Appl. Phys. Lett*. **92**, 151913 (2008).

[7] Pendry, J. B., and J. Li, "An acoustic metafluid: realizing a broadband acoustic cloak", *New. J. Phys*., **10**, 115032 (2008).

[8] Torrent, D. and J. Sanchez-Dehesa, "Anisotropic mass density by two-dimensional acoustic metamaterials", *New Journal of Physic*s **10**, 023004 (2008).

[9] Popa, B. I., and S. A. Cummer, "Design and characterization of broadband acoustic composite metamaterials", *Phys. Rev. B* **80**, 174303 (2009).

[10] Zigoneanu, L., B.-I. Popa, A. F. Starr, and S. A. Cummer, "Design and measurement of a broadband 2D acoustic metamaterial with anisotropic effective mass density", J. Appl. Phys., in press (2011).

[11] Fokin, V., M. Ambati, C. Sun, and X. Zhang, "Method for retrieving effective properties of locally resonant acoustic metamaterials", *Phys. Rev. B*, **76**, 144302 (2007)

[12] Climente, A., D. Torrent, and J. Sanchez-Dehesa, "Sound focusing by gradient index sonic lenses", *Appl. Phys. Lett*., **97**, 104103 (2010)

Phononics 2011: First International Conference on Phononic Crystals, Metamaterials and Optomechanics
Santa Fe, New Mexico, USA, May 29-June 2, 2011
PHONONICS-2011-0091

Phononic Transport in Structural Networks with Internal Resonances and Dissipation

Alessandro Spadoni

Institute of Mechanical Engineering
École Polytechnique Fédérale de Lausanne (EPFL)
1015-CH Lausanne
alex.spadoni@epfl.ch

Abstract: The transport of mechanical energy can be controlled with phononic crystals and acoustic meta-materials. The latter can designed to control wave fields with wavelengths much larger than the meta-material's inner structure. This presentation proposes the employment of structural lattices and dissipation to improve the performance of meta-materials.

Phononic crystals (PCs) and acoustic meta-materials (AMs) are composed of periodic, multiple-phase domains, one of which is usually a solid. These systems are designed to control the propagation of elastic or acoustic waves[1,2]. The periodic modulation of material phases results in acoustic impedance mismatch, which in turn produces an effective medium with stop[1] and pass bands. These are frequency regions where wave propagation is allowed and forbidden respectively. Each of these regimes induces a response that can be exploited to control acoustic fields.

Band gaps encourage the employment of PCs and AMs for sound attenuation[3]; disorder and nonlinearity produce wave modes that allow energy propagation even within band gaps[4,5]. Nonlinearity can also be exploited to shift wave frequencies into a band gap to obtain acoustic rectifiers or acoustic diodes[6]. Pass bands also provide significant acoustic-field control and can be engineered to yield negative refraction[7], which has been used in the past to focus sound[8]. Such disparate response characteristics all arise as a result of nonlinear dispersion.

The geometric and material properties of each phase determine the frequency response of PCs. Phenomena like band gaps and negative refraction occur subsequently at fixed frequencies, which depend upon the design of the crystal. The fixed operational range of PCs restricts their deployment in practical applications. Accordingly, tunable PCs that can be controlled by external fields have been proposed. Some noteworthy examples include: temperature-sensitive[9], magneto-sensitive[10], and electric-sensitive electrorheological materials[10]. Strain-induced geometric transformations of voids in elastomeric domains permit the suppression of certain band gaps and the promotion of new ones[11].

AMs are capable of all these unusual characteristics, but are not restricted to having a lattice constant of the order of the acoustic wavelength[2]. In essence, this allows one to dramatically shrink metamaterials and structures designed to control acoustic fields. In the case of AMs, nonlinear dispersion is attributed to internal resonances[2]. AMs based on split-ring[12] and Helmholtz[13] resonators have been devised to obtain negative refraction and negative phase velocity[12] as well as negative group velocity[13]. While these simple AMs are designed with a lattice constant much larger than the acoustic wavelength, they have a fixed operational regime as they only have a single characteristic internal degree of freedom. Structural lattices (SLs) can be made to be periodic and their internal members can be designed to respond at desired frequencies[14]. Given the continuous nature of internal beam or plate-like members, the operational frequency range of SLs is virtually infinite. The same rich dynamic behavior may even preclude the need for external tuning to match any specific frequency regime.

SLs have been shown to induce band gaps[14,15] and a highly anisotropic response, dependent on frequency, even if the underlying structural network is statically isotropic[14]. The strong dynamic anisotropy, in turn, produces caustics in the wave field. This phenomenon allows the channeling of mechanical energy in preferential directions which depends on the SLs underlying symmetries.

Simple arrangements of SLs have been shown to induce limited band gaps[15] but little effort has been invested to study the repercussions of complexity in SLs. A structural network known as the chiral honeycomb[16] has been shown[14] to have a very complex dynamic behavior, apparent in the band struc-

Phononics 2011: First International Conference on Phononic Crystals, Metamaterials and Optomechanics
Santa Fe, New Mexico, USA, May 29-June 2, 2011
PHONONICS-2011-0091

ture illustrated in Fig. 1. Significant band gaps are present even at low frequencies. Their appearance at different frequency regimes derives from the complexity of the medium, which is composed of rings connected by slender ligaments. Within the first 10 wavemodes, the first band gap results from dispersion induced by ligament resonance (indicated by dashed red lines in Figure 1) while a second, larger gap coincides with the resonance of rings (indicated by dashed blue lines in Figure 1), which can also yield negative group velocity.

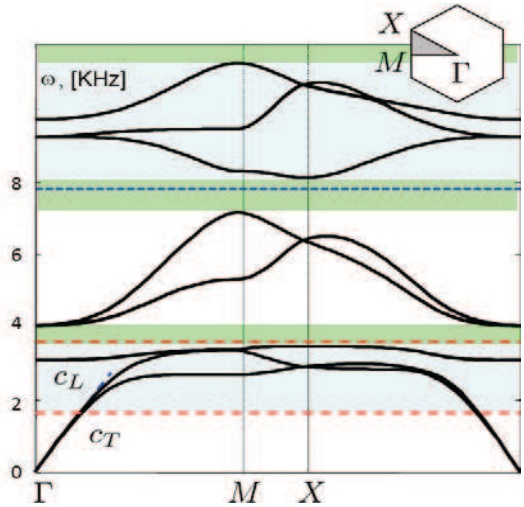

Figure 1 Band structure for a plane chiral lattice with coinciding longitudinal and shear-wave velocities. Red lines indicate resonance of beam-like members while blue lines indicate resonance of rings.

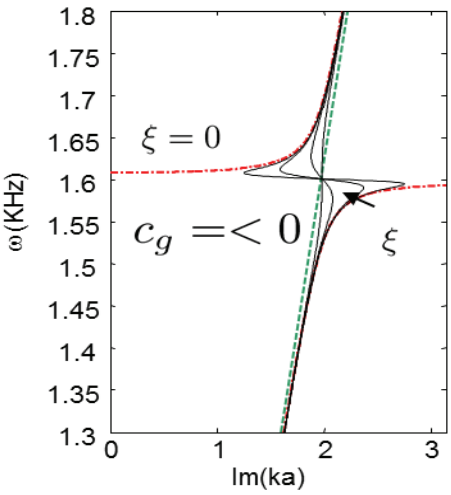

Figure 2 Dispersion relation for a 1D acoustic meta-material with a single characteristic internal resonance with damping. Absence of dissipation leads to localized wavemodes while its presence induces negative and supersonic group velocity.

The presence of dissipation (indicated by ξ in Figure 2) in AMs can induce negative as well as supersonic group velocities. As a result, the unexplored effect of dissipation is a promising research avenue. A lack of dissipation, or its neglect in mathematical models, leads to a system's response with a marked, albeit very narrow, band gap at a frequency corresponding to resonance conditions of the characteristic internal degrees of freedom (indicated by dashed red lines in Figure 2). At this frequency, the group velocity c_g is undefined and strong localization occurs. The phase of internal resonators is responsible for negative group velocity[13]. A simple analogy with a linear oscillator leads to the conclusion that dissipation alters the oscillator's phase and by extension the group velocity in AMs. A simple model shows that weak dissipation up to a critical value induces $c_g < 0$. As this critical value is breached, supersonic velocity can be obtained as the local slope of the dispersion relation becomes positive (Figure 2).

References

[1] M. S. Kushwaha, P. Halevi, L. Dobrzynski, and B. Djafari-Rouhani, *Phys. Rev. Lett* **71**, 2022 (1993).
[2] Z. Liu, X. Zhang, Y. Mao, Y. Y. Zhu, Z. Yang, C. T. Chan, P. Sheng, *Science* **289**(5485), 1734-1736, (2000).
[3] R. Martinez-Sala, J. Sancho, J. V. Sanchez, V. Gomez, J. Llinares, F. Meseguer, *Nature* **378**, 241 (1995).
[4] K. Aydin, K. Guven, N. Katsarakis, C. M. Soukoulis, and E. Ozbay, *Optics Express* **12**, 5896 (2004).
[5] F. Geniet, and J. Leon, *Phys. Rev. Lett.* **89**, 134102 (2002).
[6] B. Liang, X. S. Guo, J. Tu, D. Zhang, and J. C. Cheng, *Nature Materials* **9**(12), 989 (2010).
[7] X. Zhang, and Z. Liu, *Appl. Phys. Lett.* **85**, 341 (2004).
[8] S. Yang, J. H. Page, Z. Y. Liu, M. L. Cowan, C. T. Chan, and P. Sheng, *Phys. Rev. Lett.* **93**, 024301 (2004).
[9] K. L. Jim, C. W. Leung, S. T. Lau, S. H. Choy, and H. L. W. Chan, *Appl. Phys. Lett.* **94**, 193501 (2009).
[10] J. F. Robillard, O. Bou Matar, J. O. Vasseur, P. A. Deymier, M. Stippinger, A. C. Hladky Hennion, Y. Pennec, and B. Djafari-Rouhani, *Appl. Phys. Lett.* **95**, 124104 (2009).
[11] K. Bertoldi, and M. Boyce, *Phys. Rev. B* **77**, 052105 (2008).
[12] S. Guenneau, A. Movchan, G. Pétursson, and S. A. Ramakrishna, *New Journal of Physics* **9**(399), 1367 (2007).
[13] N. Fang, D. Xi, J. Xu, M. Ambati, W. Srituravanich, C. Sun, and X. Zhang, *Nature Materials* **5**, 452 (2006).
[14] A. Spadoni, M. Ruzzene, S. Gonella, and F. Scarpa, *Wave Motion* **46**(7), 435 (2009).
[15] A. S. Phani, J. Woodhouse, and N. A. Flecka, *J. Acoust. Soc. Am.* **119**(4) (2006).
[16] D. Prall, and R. S. Lakes, *Int. J. Mech. Sci.* **39**(3), 305 (1997).

Phononics 2011: First International Conference on Phononic Crystals, Metamaterials and Optomechanics
Santa Fe, New Mexico, USA, May 29-June 2, 2011
PHONONICS-2011-0099

Influence of Filling Fraction and Constituent Materials on Acoustic Waves in Phononic Lattice

H.Ketata[1] , M.H.Ben Ghozlen[2]

[1]*Sfax university, Sfax Preparatory Engineering Institute, Route Menzel Chaker km 1.5-3018 Sfax, Tunisia,*

hassiba.ketata@yahoo.fr

[2] *Sfax university, Faculty of Sciences of Sfax, Route de la Soukra km 4-3038 Sfax, Tunisia*

mohhghozlen@gmail.com

Abstract: The purpose of the present numerical study is to elucidate the change of characteristics, of bulk and surface acoustic waves propagating, on the free surface of the half-infinite system when we introduce two-dimensional (2D) periodic elastic implantation.

Introduction

The propagation of elastic/acoustic waves phononic crystal (PC) has received much attentions in the last twenty years. The existence of full band gaps, which have been demonstrated by a lot of theoretical[2] and experimental[3] works, should have many potential applications. In the previous studies, most of works are concentrated on the bulk waves propagation, only few papers are devote to the surface wave propagating on the surface of the half-infinite system[4] or Lamb waves[5] propagating in finite-thickness plate. In fact, surface acoustic wave and Lamb wave device are widely used as detectors and sensors in practice. So it is worthwhile to give more studies on this subject. Several numerical analytical methods, such as plane-wave-expansion method (PWE), the multi-scattering theory(MST), and the finite different time-domain method (FDTD), have been developed to investigate the physical properties of the phononic crystal material.

In the present study PWE procedure is used to obtain the general wave solution in the infinite system firstly, and then the stress-free boundary condition on the surface is used, which lead to a stress-free-boundary-condition determinant. For such determinant, a root searching procedure is usually required to find its zeroes. The shortcoming of the numerical root searching procedure is that the desirable roots usually cannot be selected out easily when the order of the determinant is relatively large

Plane-wave expansion method

In the composite material, in absence of external force, the equations of motions are:

$$\rho(\mathrm{r})\frac{\partial^2 \mathrm{u_i}(\mathrm{r},\mathrm{t})}{\partial t^2} = \frac{\partial}{\partial \mathrm{x_j}}\left[\mathrm{c_{ijkl}}(\mathrm{r})\frac{\partial \mathrm{u_k}(\mathrm{r},\mathrm{t})}{\partial \mathrm{x_l}}\right] \qquad (1)$$

where $u(r,t)=u(r)e^{i\omega t}$ is the position and harmonic time dependent displacement vector of components u_i *(i=1,2,3)* in the Cartesian coordinate system ($Ox_1x_2x_3$). If we limit the wave propagation to the *(x_1Ox_2)* transverse plane, a 2D Bloch wave vector $\boldsymbol{k_0}$ *(*$\boldsymbol{k}_1$*;*k_2*,0)* is considered. The Bloch theorem is used for the displacement vector $u(r) = \sum_G U_{k_0}^G e^{i(G+k_o)r}$. Where G=($G_1$,$G_2$) is a reciprocal-lattice vector. The physical characteristics (c_{ijkl}, ρ) in the composite system denoted α in a general way are developed in 2D Fourier series in the reciprocal space $\alpha(r) = \alpha_A$ in the cylinder A and $\alpha(r) = \alpha_B$ in the matrix B then $\alpha(r) = \sum_G \alpha_G e^{iGr}$. Then equation (1) can be separated into the following three equations:

$$\omega^2 \sum_{G'} \mathrm{R}^{\mathrm{G-G'}} \mathrm{U_i^{(k_0+G')}} = \sum_{G'} \sum_{\mathrm{j,k,l}} \mathrm{C_{ijkl}^{G-G'}} (\mathrm{k_0+G})_\mathrm{j} (\mathrm{k_0+G'})_\ell \, \mathrm{U_k^{(k_0+G')}} \quad (\mathrm{i}=1,2,3) \qquad (2)$$

In order to obtain the surface wave solution a wave vector $\boldsymbol{k}$ *(*$\boldsymbol{k}_1$*,* k_2*,* λ*)* is considered then the problem is reduced to a generalized eigenvalue equation with respect to λ^2, which determines the spatial

Phononics 2011: First International Conference on Phononic Crystals, Metamaterials and Optomechanics

Santa Fe, New Mexico, USA, May 29-June 2, 2011

PHONONICS-2011-0099

variation of the wave with the distance z from the surface. If we truncate the expansions of equation(2) by choosing n reciprocal lattice vectors, and we put $u(r) = \sum_G A_G e^{i\lambda z} e^{i(G+k_o)r}$ we have

$$(\lambda^2 \delta_{G,G'} - Q_{G,G'})A_{G'} = 0 \quad (3)$$

where $Q_{G,G'}$ is a 3nx3n matrix. Equation (3) gives 3n eigenvalue λ_l^2, then we put $A_G^l = X_l \varepsilon_G^l$; ε is a unit polarization vector.

We search the surface wave solutions for which the lattice displacement may decay exponentially into the medium (z >0). Hence, all λ_l s must have positive imaginary part. The surface wave should satisfy the stress-free boundary conditions at the surface z=0:

$$c_{i3mn}\partial_n u_m|_{z=0} = 0 \quad \text{(i=1,2,3)} \quad (4)$$

They lead to 3n homogeneous linear equations for the relative weights X_l of 3n wave amplitudes.

Numerical examples

An example of the numerical calculation, for the propagation of bulk acoustic waves, we consider epoxy (elastically isotropic) is assumed for the background material(B) and two kinds of 2D lattices with the cylinders(A) filled with (i) Si, (ii) Cu. A big difference between mass density quotients ($\frac{\rho(A)}{\rho(B)}$) drags a change in acoustic stop bands extension (Figure 1).

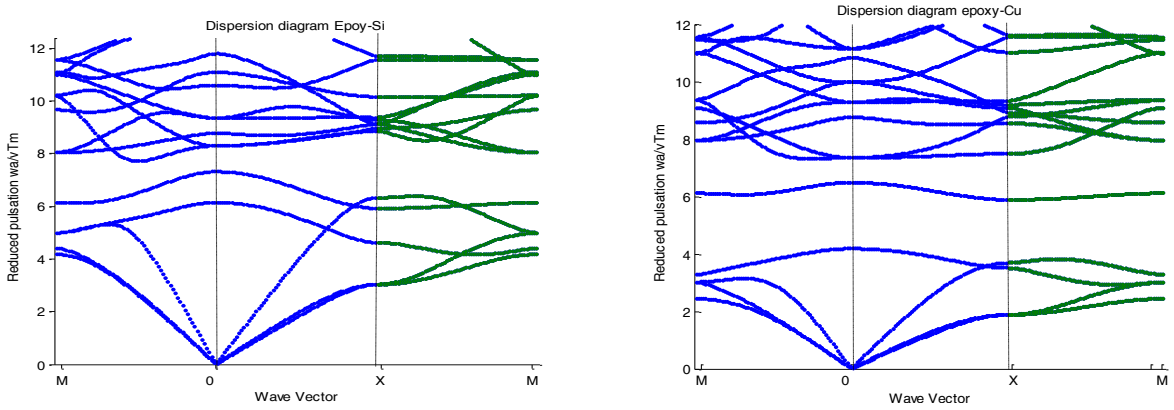

Figure 1 Dispersion relations of bulk acoustic waves in tow-dimensional square lattice consisting of (i) Si, (ii) Cu in a epoxy substrate(vTm= is the transverse sound velocity in epoxy, and a is the lattice spacing)

n=9, f=0.567, $\frac{\rho(Si)}{\rho(epo)} = 1.97$, $\frac{\rho(Cu)}{\rho(epo)} = 7.568$.

Other examples are treated and significant plots relative to stress and displacement distributions are achieved to recognised diverse bulk and surface wave mode.

References

[1].Y.Tanaka, S.I.Tamura, Physical Review B. 58.7958(1998).

[2]J.O.Vasseur, B. Djafari-Rouhani, L. Dobrzynski, M.S. Kushwaha, and P. Halevi, J. Phys . Condens. Matter 6? 8759 (1994)

[3] R. E. Vines, J. P. Wolfe, and A. G. Every, Phys. Rev. B 60, 11871 (1999).

[4]X. Zhang. T. Jackson, E. Lafond, P. Deymier, J. Vasseur, Appl. Phys. Lett. 88 - 041911 (2006)

[5]A. Khelif, B.Aoubiza, S. Mohammadi, A. Adibi, V. Laude, Phys ; Rev. E 74 – 046610 (2006).

Phononics 2011: First International Conference on Phononic Crystals, Metamaterials and Optomechanics
Santa Fe, New Mexico, USA, May 29-June 2, 2011
PHONONICS-2011-0115

A wide band underwater strong acoustic absorbing material

Yuren Wang , Heng Jiang, Meng Chen

Key Laboratory of Microgravity, Institute of Mechanics, Chinese Academy of Sciences, 100190 Beijing, China, yurenwang@imech.ac.cn, hiheu@hotmail.com, yemao007@163.com

Abstract: To meet the demand of underwater acoustic absorbing material for wide band strong acoustic absorption, we introduced network structure into locally resonant phononic crystal and fabricated a new kind of metal-polymer composites. Experimental and theoretical results showed that excellent underwater acoustic absorption capability and strong mechanical strength could be obtained simultaneously.

Excellent underwater acoustic absorbing materials are urgently needed for their important applications in both military and commercial uses, such as sonar evasion by stealthy coating, underwater acoustic communication system[1-3]. In the past decade, locally resonant phononic crystal (LRPC) has inspired great interest because it can exhibit an obvious phononic band-gap in the acoustic spectrum with crystal lattice constants two orders of magnitude smaller than the relevant sonic wavelength[4-7]. Recent theoretical calculation has indicated that the maximum viscoelastic energy dissipation is generated at locally resonant frequency when considering viscoelastic deformation in LRPC[8-10]. It means that the LRPC can also be employed to expand the content of acoustic absorbing materials study. However, contrary to the aim of producing a strong absorption just at ertain narrow frequency in LRPC, acoustic absorbing material is usually need to be designed to have a strong absorbance in a wide range of frequencies. To solve this conflict, some anomalous structures need to be introduced into LRPC. It should be noticed that composite materials with interpenetrating network structures are usually found to exhibit unexpected merit due to the cooperative interaction among their component materials, such as bones and muscle in mammals and the trunks and limbs in plants[11]. We introduced interpenetrating network structure into LRPC unit, developed a modern underwater acoustic absorbing material[12,13].

The most striking difference between the LRPC and the new material is different resonant unit structures. Resonant units in the LRPC have the same size and distribute discretely in the polymer matrix. Those resonant units in the new material have different sizes and physically connected by the porous metal and the filled polymers. It is reasonable to deduce that a broad size distribution and multiple morphologies of resonant units are helpful for the realization of the wide band acoustic absorption. In this paper, we report the strong underwater acoustic absorption of a new composite material[12,13]. The study is focused on the sound attenuation mechanism in this new material. It should be noticed that these resonant units and interpenetrating network structure are different from the traditional structure of anechoic materials.

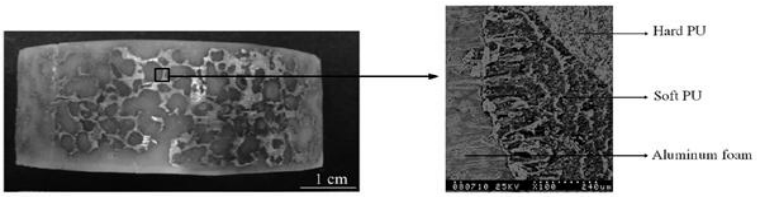

Figure 1 Optical and SEM images of a typical sample.

Figure 1 shows the interpenetrating network structure and hard-soft-hard multilayer morphology in the new material. The interpenetrating network structure is constructed in relatively large scale of millimeter-sized building blocks in the new material to work effectively for sound wave absorption.

Figure 2 illustrates the changes of underwater sound absorption coefficients for the new material and other materials as a function of frequency. Fig. 3 exhibits the engineering stress-engineering strain curves of the new material and its component materials. The comparison of underwater acoustic

Phononics 2011: First International Conference on Phononic Crystals, Metamaterials and Optomechanics
Santa Fe, New Mexico, USA, May 29-June 2, 2011
PHONONICS-2011-0115

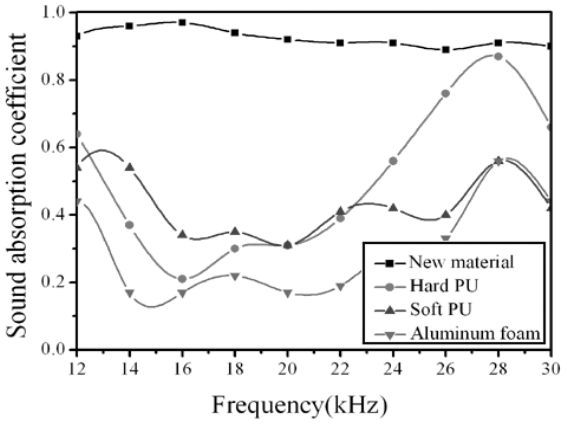

Figure 2 Underwater absorption coefficients for different materials.

absorption and compression resistance tal result between the new material and its separate components shows that the new material possesses both better sound absorption property and higher mechanical strength than its components. Figure 2 is that strong underwater acoustic absorbance with the absorbing coefficient over 0.9 can be achieved in a wide frequency range for the new material, while sound absorbing coefficients for any component materials have the values not higher than 0.9. The underwater acoustic absorption capability of the new material is much better than that of traditional acoustic absorbing materials from the measured spectrum. The strong acoustic absorption characteristic of the new material is not originated from its component or simple linear superposition of the component materials. It is reasonable to deduce that the combination of LRPC structure units and cooperative effect from the interpenetrating network plays an important role in achieving strong wide band acoustic absorbing material.

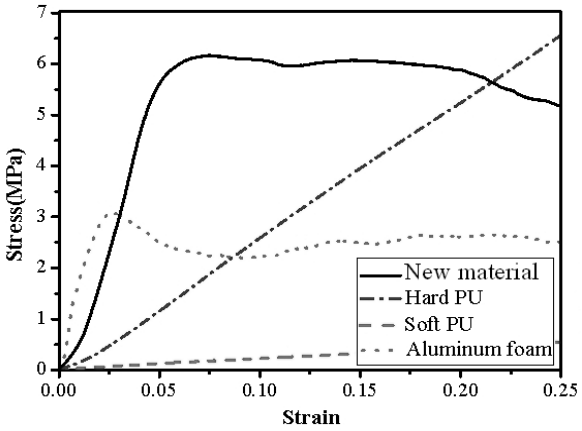

Figure 3 Compressive stress-strain curves of the new material and its component materials.

Figure 3 exhibits the comparison of compression resistance experimental result between the new material and its separate components. The new material shows compressive strength over 6MPa, while that could not be achieved by PU and aluminum foam. It means that the new material can keep a good mechanical behavior even in 500 meters water depth. Compression resistance capacity of this composite material is originated from whole effects achieved by structural design. The interpenetrating network structure unified strong wide band sound absorption capability and high mechanical strength in the new material, while it appears to be conflicting in normal circumstances.

References

[1] M. K. Hinders, B. A. Rhodes, and T. M. Fang, *J. Sound Vib.* **185**, 219-246 (1995).
[2] D. Odell, K. Hertel, and C. Nelson, Oceans'02 MTS/IEEE **1**, 266-271 (2002).
[3] M. Heinemann, A. Larraza, and K. B. Smith, *J. Acoust. Soc. Am.* **113**, 3111-3116 (2003).
[4] Z. Liu, X. Zhang, Y. Mao, Y.Y. Zhu, Z. Yang, C.T. Chan, and P. Sheng, *Science* **289**, 1734-1736 (2000).
[5] G. Wang, X. Wen, J. Wen, L. Shao, and Y. Liu, *Phys. Rev. Lett.* **93**, 154302 (2004).
[6] M. Hirsekorn, *Appl. Phys. Lett.* **84**, 3364-3366 (2004).
[7] C. Goffaux, J. Sánchez-Dehesa, A. Levy Yeyati, Ph. Lambin, A. Khelif, J. O. Vasseur, *Phys. Rev. Lett.* **88**, 225502 (2002).
[8] H. Zhao, Y. Liu, J. Wen, D. Yu, and X. Wen, *Phys. Rev. A* **367**, 224-232 (2007).
[9] H. G. Zhao, Y. Z. Liu, J. H. Wen, D. L. Yu, G. Wang, and X. S. Wen, *Chin. Phys. Lett.* **23**, 2132-2134 (2006).
[10] H. Zhao, Y. Liu, D. Yu, G. Wang, J. Wen, and X. Wen, *J. Sound Vib.* **303**, 185-194 (2007).
[11] X. Jia, *Natural Biomaterials and Bionic Engineering Materials*, Chemical Industry Press, China (2007).
[12] H. Jiang, Y. Wang, M. Zhang, Y. Hu, D. Lan, Q. Wu, and H. Lu, *Chin. Phys. B* **19**, 026202 (2010).
[13] H. Jiang, M. Zhang, Y. Wang, Y. Hu, D. Lan, and B. Wei, *Chin. Phys. Lett.* **26**, 106202 (2009).

Phononics 2011: First International Conference on Phononic Crystals, Metamaterials and Optomechanics
Santa Fe, New Mexico, USA, May 29-June 2, 2011
PHONONICS-2011-0132

Transformation Acoustics Media with Periodically Layered Structures

Zixian Liang, Jensen Li

Department of Physics and Materials Science, City University of Hong Kong, Tat Chee Avenue, Kowloon Tong, Hong Kong
jensen.li@cityu.edu.hk

Abstract: Periodically layered structures have been used to construct acoustic superlenses and hyperlenses as precursors for transformation acoustics. With the transformation approach, we can now investigate the bandwidth and relationship between an acoustic hyperlens and superlens and construct transformation media through bending periodically layered structures.

By drawing analogies between electromagnetic and acoustic waves, many recent developments in acoustic metamaterials and transformation acoustics have their roots in the corresponding electromagnetic waves theory. For example, an acoustic cylindrical cloak and an electromagnetic cylindrical cloak share the same coordinate transform in arriving their designs [1,2]. However, similar to the situation in making metamaterials with negative refractive indices, quite different strategies for making the acoustic metamaterials are actually needed due to the different materials properties in the two contexts.

Here, we discuss the usage of periodically layered materials with the transformation approach. Such a scheme has the advantage that acoustic anisotropy can be generated easily and the anisotropy guides sound energy in a well controlled manner. For an acoustic hyperlens, solid plates are stacked in the angular direction to form a cylindrical shell, Figure 1(a), while for an acoustic superlens, planar solid plates are stacked along the horizontal direction [3-5]. By using the transformation approach, we are then able to investigate the acoustic hyperlens using the transfer matrix method. Figure 1 shows the coordinate mapping which transforms the hyperlens with angularly stacked brass plates into its rectangular (Cartesian) equivalence. The transformed rectangular hyperlens still has periodic stacking along the horizontal direction but the material parameters now change along the y-coordinate as well. In fact, the transformed rectangular hyperlens becomes a 2D superlens if we drop the y-dependence of the materials parameter by just employing the material parameters at the bottom boundary. Now, we can calculate the transfer function across the transformed hyperlens and it is shown in Figure 2. The two "light" lines (white dashed lines) now represent the one for air ($k_x = \omega / c_{air}$, with higher slope) and the one at the exit of the lens $k_x = R_2 / R_1 (\omega / c_{air})$. The large transfer amplitudes between the two light lines indicate the hyperlens transports the near field information efficiently and also converts them into far field at the exit of the hyperlens. At the same time, there are several bands beyond the second light line, indicating the guiding modes circulating around the hyperlens. While the superlens relies on these guiding modes at Fabry-Perot resoannces to transport the near-field information for deep subwavelength resolution, the hyperlens have these guiding modes at the

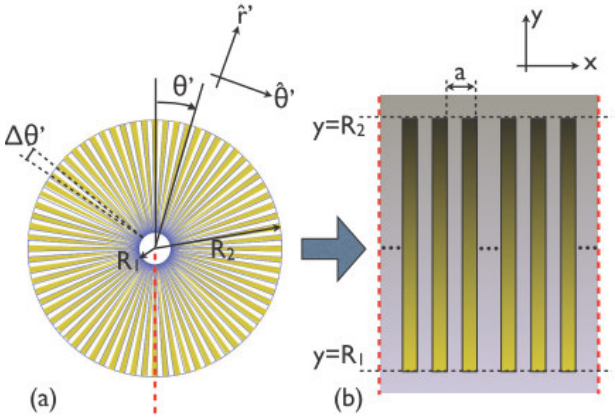

Figure 1 Transforming (a) the cylindrical hyperlens into (b) the transformed rectangular hyperlens through mapping $x = R_1 \theta'$ and $y = r'$. R_1 = 2.7cm, and R_2 = 21.8cm are set for calculations.

Phononics 2011: First International Conference on Phononic Crystals, Metamaterials and Optomechanics
Santa Fe, New Mexico, USA, May 29-June 2, 2011
PHONONICS-2011-0132

few particular frequencies indeed stay in near fields after exit of lens and they will quickly decay instead of propagating. The transfer function calculation thus shows the working principle of both hyperlens and superlens and explains how the hyperlens can work in broad frequency bandwidth with sub-wavelength resolution.

Apart from guiding the sound waves along a fixed direction of fluid perforation using the periodically layered material, the same periodic material, after a simple geometrical transformation, can be used to construct transformation acoustical devices. In particular, we bend the metamaterial using a certain mathematical function. The resultant curved metamaterial can be used to construct transformation acoustical devices by cutting the metamaterial into particular shapes. As an example, we demonstrate a design of acoustic carpet cloak using the mentioned strategy. We bend planar solid brass plates which are periodically stacked vertically within water using a squared cosine function. Now, all the brass plates are having the same shape of squared cosine function and the material is still periodic in the vertical direction. The material is then cut into a shape of the carpet cloak which is shown as thin black lines for the curved brass plates in Figure 3. The carpet cloak is working in a background fluid of water and the background fluid can percolate freely between the curved brass plates. Now, instead of guiding the sound waves only along the fluid perforations, the periodically layered structure can guide the sound energy in a two dimensional manner so that the carpet cloak cancels the scattering of the curved bump below the cloak if it is situated on a hard surface. We have simulated a particular situation where a Gausian beam is impinging on the cloak at approximately 60 degrees. Although there is a small impedance mismatch between the cloak and the background water to have a little spurious reflection at the microstructured cloak boundary, the scattering of the bump is largely reduced and there is a reflected beam at the same angle as if it is just a flat hard surface.

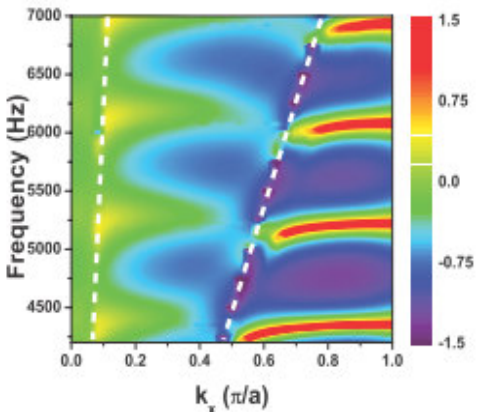

Figure 2 Transfer amplitude (in log10 scale) of the hyperlens against different tangential wave number. The wave number is normalized to π/a where a is the periodicity of the hyperlens at inner boundary.

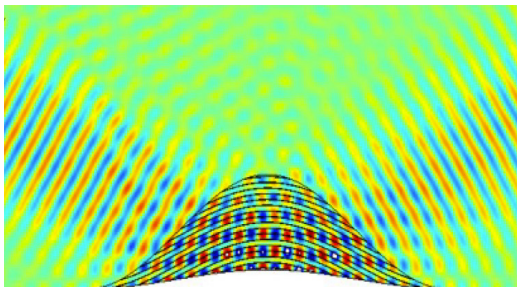

Figure 3 Curved periodically layered metamaterials employing brass plates and background water to guide sound waves in water as a carpet cloak

Therefore, we have investigated how to use periodically layered structure to generate anisotropy and such anisotropy can be well designed and explained with the transformation approach to guide sound waves, either at a single direction for subwavelength imaging or in a two dimensional manner for transformation acoustical devices.

References

[1] S. A. Cummer, and D. Schurig, *New J. Phys.* **9**, 45 (2007).
[2] H. Chen, and C. T. Chan, *Appl. Phys. Lett.* **91**, 183518 (2007).
[3] J. Li, L. Fok, X. Yin, G. Bartal, and X. Zhang, *Nature Mater.* **8**, 931 (2009).
[4] J. Zhu, J. Christensen, J. Jung, L. Martin-Moreno, X. Yin, L. Fok, X. Zhang, and F. J. Garcia-Vidal, *Nature Phys.* **7**, 52 (2011).
[5] H. Jia, M. Ke, R. Hao, Y. Ye, F. Liu, and Z. Liu, *Appl. Phys. Lett.* **97**, 173507 (2010).

Phononics 2011: First International Conference on Phononic Crystals, Metamaterials and Optomechanics
Santa Fe, New Mexico, USA, May 29-June 2, 2011
PHONONICS-2011-0135

Impedance Matching for Aqueous Inertial Metafluid Devices

Gregory J. Orris, Theodore P. Martin, Christopher N. Layman and Michael Nicholas

Acoustics Division
Naval Research Laboratory
Washington, DC 20375

Abstract: Several interesting metafluid devices have been investigated for use at frequencies in the low tens of kilohertz, including gradient index lenses, directional antennas and tuneable scattering elements. For 3D or orthotropic devices whose operating frequencies are less than a few 10's of kHz additional and significant practical issues can arise for inertial metafluids: dynamic impedance matching, mass and volume.

The application of transformational optics to acoustic metamaterials offers promising new acoustic devices, ranging from tunable sound blocking with superior efficiency, to acoustical diodes. Metamaterial designs typically require high anisotropy in either mass density or elastic moduli (or both), which can be achieved through inertial variation of material properties or by using resonant scatterers, though the latter is usually only functional within a narrow bandwidth. Many inertial approaches obtain this anisotropy through the use of rigid scatterers and boundaries, which are easily achievable in air. However, high relative mass densities are restricted to about an order of magnitude in aqueous environments, resulting in poorly approximated rigidity. Similarly, few options exist for scattering constituents with high bulk modulus/low mass density (both relative to water), as in Figure 1. Nevertheless, we have investigated several interesting devices that are functional in water at frequencies of around a few tens of kilohertz, including gradient index lenses, directional antennas and resonance-based vector sensors.[1-3]

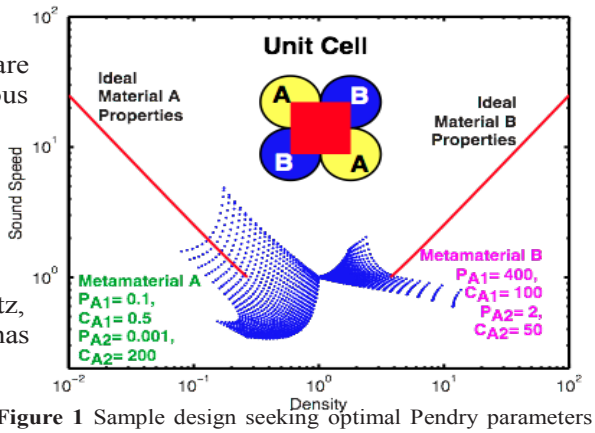

Figure 1 Sample design seeking optimal Pendry parameters using a "diatomic" lattice of cylindrical scattering elements. The filled regions represent effective parameters achievable using already extreme material parameters 2 orders of magnitude larger than the background – they fail to cover the necessary phase space.

One can design and implement a gradient index lens, for example, without impedance matching at the front interface by relying on internal subwavelength scattering from high impedance contrast elements.[1,4] This has the unfortunate effect of seriously degrading the ultimate performance of the device by reflecting much of the incident signal back away from the device. To address this shortcoming, we have investigated a new class of phononic crystal consisting of an interleaved set of two distinct types of scattering centers: One with a mass and bulk modulus much higher than the surrounding medium, the other lower. Through a judicious choice of media and size, a perfect impedance matching can be made at the front interface that has the net effect of substantially increasing the device efficiency.

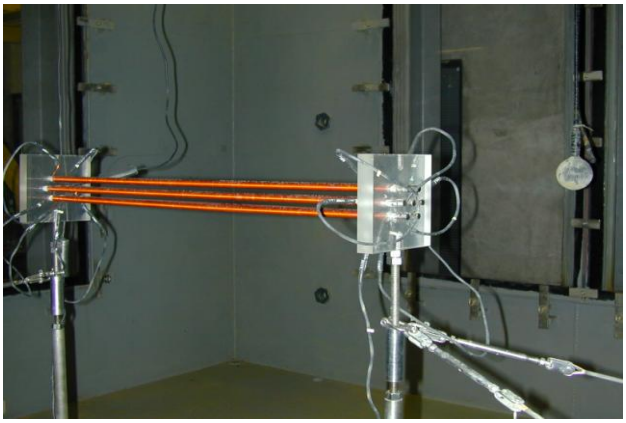

Figure 2 Design of sample apparatus and placement in NRLs Salt Water Tank Facility at the midway point in the tank. The 10cm acoustic transducer used to ensonify the phononic crystal is seen as the white sphere to the right of the apparatus.

We explore metamaterial applications where device functionality can be obtained without

Phononics 2011: First International Conference on Phononic Crystals, Metamaterials and Optomechanics

Santa Fe, New Mexico, USA, May 29-June 2, 2011

PHONONICS-2011-0135

extreme material parameters, such as with directional antennas.[2] We also investigate devices with tunable impedance matching; our initial design consists of cylindrical scatterers each consisting of a stainless steel tube wrapped with a single layer of copper wire (i.e., a solenoid) with a standard magneto-rheological fluid consisting of Fe micro-particles suspended in a mineral oil base. Using the "magic number" results of Torrent, *et al.*[4] to achieve effective parameters of an equivalently larger cylinder of equal circumference, seven of these tubes were then arranged in a hexagonal unit cell, as seen in Figure 2.

References

[1] T. P. Martin, M. Nicholas, G. J. Orris, L.-W. Cai, D. Torrent, and J. Sanchez-Dehesa. Sonic gradient index lens for aqueous applications. *Applied Physics Letters*, **97**(11):113503, 2010.

[2] C. N. Layman, T. P. Martin, G.J. Orris, "An Acoustic Directional Antenna with Isotropic Materials", MRS 2011, 1015988, W14.2.

[3] D. Torrent and J. Sanchez-Dehesa. Anisotropic mass density by radially periodic fluid structures. *Phys. Rev. Lett.*, **105**(17):174301, Oct 2010.

[4] D. Torrent, A. Hakansson, F. Cervera, and J. S´anchez-Dehesa. Homogenization of two-dimensional clusters of rigid rods in air. *Phys. Rev. Lett.*, **96**(20):204302, May 2006.

Phononics 2011: First International Conference on Phononic Crystals, Metamaterials and Optomechanics
Santa Fe, New Mexico, USA, May 29-June 2, 2011
PHONONICS-2011-0139

Locally resonant structures for low frequency surface acoustic band gaps

Abdelkrim Khelif [1] , Younes Achaoui[2], Boujamaa Aoubiza[3]

[1] *International Joint Laboratory GeorgiaTech-CNRS UMI 2958; 2-3 Rue Marconi 57070 Metz, France*
abdelkrim.khelif@gatech.edu
[2] *Institut FEMTO-ST, Université de Franche-Comté, CNRS; 32-avenue de l'Observatoire 25044 Besançon, France younes.achaoui@femto-st.fr*
[3] *Laboratoire de Mathématiques,, Université de Franche-Comté, CNRS; 32-avenue de l'Observatoire 25044 Besançon, France*

Abstract: We present in this paper a theoretically and experimentally study of the propagation of surface acoustic waves in a two-dimensional array of cylindrical pillars on the surface of a semi-infinite substrate. Low-frequency, markedly lower than those expected from the Bragg mechanism, band gaps were demonstrated.

We investigate theoretically and experimentally the propagation of acoustic waves in a two-dimensional array of cylindrical pillars on the surface of a semi-infinite substrate.

Through the computation of the band structure of the periodic array and of the transmission of waves through a finite length array, we show that the phononic structure can support a number of surface propagating modes in the non-radiative region of the substrate, or sound cone, as limited by the slowest bulk acoustic wave. The modal shape and the polarization of these guided modes are more complex than those of classical surface waves propagating on a homogeneous surface. Significantly, an in-plane polarized wave and a transverse wave with sagittal polarization appear that are not supported by the free surface (ref:1).

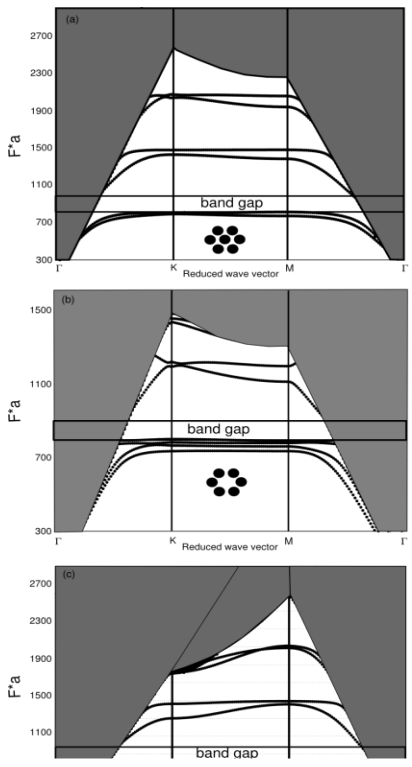

In the band structure, guided modes define band gaps that appear at frequencies markedly lower than those expected from the Bragg mechanism. We identify them as originating from local resonances of the individual cylindrical pillars and show their dependence with the geometrical parameters, in particular with the height of the pillars. The frequency positions of these band gaps are invariant with the symmetry and thereby the period of the lattices, which is unexpected in band gap based on Bragg mechanism.

The role of the period remains important for defining the non-radiative region limited by the slowest bulk modes and influencing the existence of new surface mode of the structures. The transmission of surface acoustic waves across a finite array of pillars shows the signature of the locally resonant band gaps for surface modes and their dependence with the symmetry of the source and its polarization. Numerical simulations are based on the efficient finite element method and considering pillars on a Lithium Niobate substrate.

Figure 1: Band structure of a phononic crystal composed of cylindrical silicon pillars on a silicon substrate, calculated along high symmetry directions of the first irreducible Brillouin zone for: **(a)** square; **(b)** triangular; **(c)** honeycomb. The lattice parameter is a for triangular and square lattice and $\sqrt(3) a)$

Phononics 2011: First International Conference on Phononic Crystals, Metamaterials and Optomechanics

Santa Fe, New Mexico, USA, May 29-June 2, 2011

PHONONICS-2011-0139

for the honeycomb lattice. The radius is $r/a=0.32$ and the relative height of the cylinders h/a equals 0.6. The gray region represents the sound cone of the substrate. The sound line limiting the sound cone is given by the smallest phase velocity in the substrate for every propagation direction.

References

[1] Locally resonant surface acoustic wave band gaps in a two-dimensional phononic crystal of pillars on a surface», Khelif, A. and Achaoui, Y. and Benchabane, S. and Laude, V. and Aoubiza, B. , *Physical Review B*, Vol.81, 214303, 2010.

Phononics 2011: First International Conference on Phononic Crystals, Metamaterials and Optomechanics
Santa Fe, New Mexico, USA, May 29-June 2, 2011
PHONONICS-2011-0140

Applications of Metafluids based on Phononic Crystals

José Sánchez-Dehesa, A. Climente, V. García-Chocano, E. Reyes-Ayona and D. Torrent

[1] Wave Phenomena Group, Universidad Politécnica de Valencia, Valencia, Spain.

jsdehesa@upvnet.upv.es

Abstract: Acoustic metamaterials or metafluids based on the homogenization of periodic distributions of sound scatterers (phononic crystals) are reviewed. It will be shown that periodically microstructured solids effectively behave like fluidlike materials with dynamical mass anisotropy. Also, it will be shown that the acoustic refractive index can be locally tailored in order to get molding of the sound waves. Applications of these types of metafluids as acoustic cloaks, gradient index refractive lenses, perfect absorbers and radial sonic crystal will be reported.

It was demonstrated that a periodic distribution of solids rods in air behaves in the homogenization limit like effective fluids in which the dynamical mass density follows a simple analytical expression mainly dependent of the lattice filling ratio [1, 2]. It was shown later that mixing solids of different material in the lattice increases the tailoring possibilities of the mass density and that the acoustic refractive index can be locally adjusted to design, for example, gradient index sonic lenses [3]. Moreover, for the case of non-isotropic distribution of scatterers (i.e., for lattices other than the square or hexagonal) the sound propagation inside the homogeneous structure depends on the direction and the effective mass density becomes a tensor [4], a non-exiting property in fluids or gases found in nature. So, these micro structured solids define a class of acoustic metamaterials or metafluids whose acoustic parameters, mass density and bulk modulus, are both positive and can be easily obtained by using effective medium theories (homogenization). Metafluids with anisotropic mass density are the ingredients that might be possible acoustic cloaks [5, 6] or radial wave crystals [7, 8].

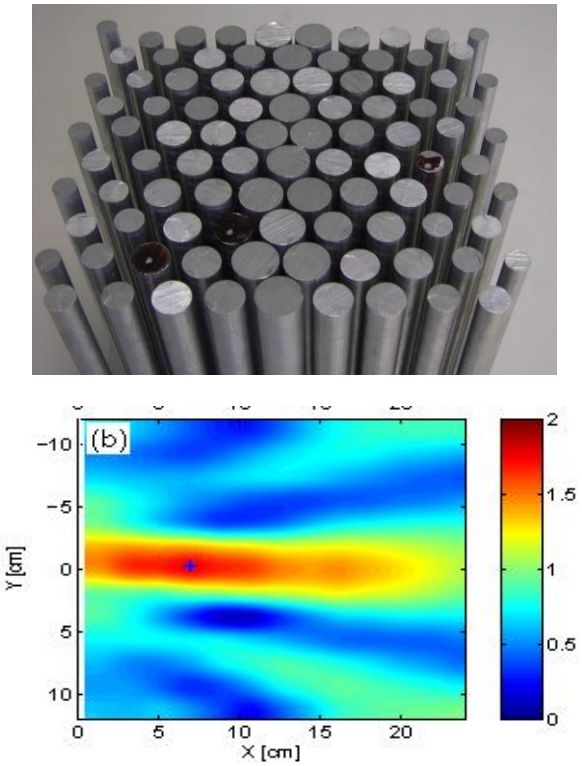

Figure 1: Upper Panel: Picture of a GRIN lens. Lower Panel: Sound amplification obtained.

Gradient index (GRIN) sonic lenses have been fabricated by using the tailoring possibilities of metafluids described above and their focusing performance has been demonstrated for airborne sound [9] and underwater [10]. Figure 1 shows a photograph of GRIN lens together with the sound amplification obtained. A sound amplification of two was obtained by this lens in which the building units are aluminum rods. It has been demonstrated that the position of the focal spot, x_f, follows the analytical formula obtained from ray theory:

$$x_f = d - \frac{y(d)}{y'(d)}\sqrt{\frac{1-(y'(d))^2\,[n^2(y(d))-1]}{n^2(y(d))}}$$

Phononics 2011: First International Conference on Phononic Crystals, Metamaterials and Optomechanics

Santa Fe, New Mexico, USA, May 29-June 2, 2011

PHONONICS-2011-0140

GRIN lenses with larger sound amplification can be achieved by using scattering units having a mismatch of impedance with the background substantially reduced. An approach to achieve this goal will be here introduced.

The feasibility of tailoring the index gradient can be also employed to design perfect absorbers in which the sound energy impinging to some area is guided to a region where its energy is totally dissipated.

Finally, it will be reported how the homogenization theory is applied to obtain the effective parameters of metafluids embedded in viscous media. The viscosity produces two main contributions to the resulting metafluids. Firstly, the homogenization condition is achieved for larger wavelengths. An secondly, the waves propagating inside the metafluid have longitudinal and transversal components that basically depends on the lattice filling ratio. As an example, figure 2 represents a case studied by our effective medium theory.

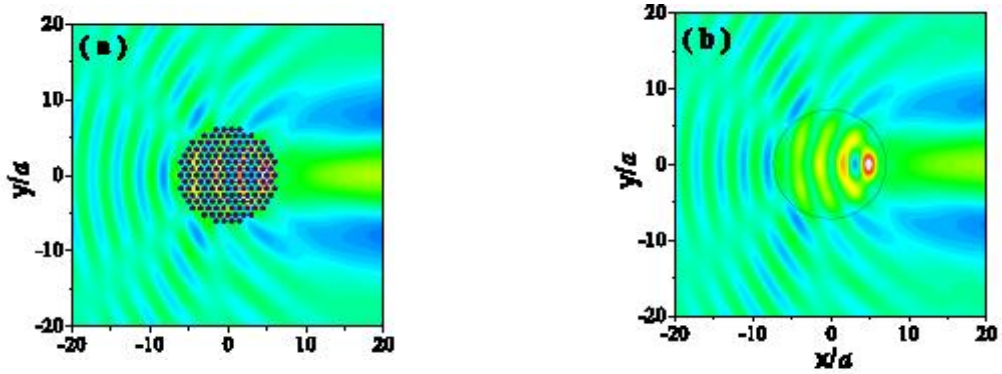

Figure 2. (a) Pressure map (amplitude) representing the scattering of a sound wave impinging a cluster of rigid cylinder embedded in glycerin. (b) The corresponding map obtained for a cylinder made of a metafluid whose parameters are obtained by a homogenization theory that takes into account the viscosity of glycerin.

Work partially supported by the Office of Naval Research (Award N000140910554), and by the Spanish MICINN under contracts TEC 2010-19751 and CSD2008-00066 (CONSOLIDER program).

References

1. D. Torrent, A. Hakansson, F. Cervera and J. Sánchez-Dehesa, Phys. Rev. Lett. 96, 204302 (2006).
2. D. Torrent and J. Sánchez-Dehesa, Phys. Rev. B 74, 224305 (2006).
3. D. Torrent and J. Sánchez-Dehesa, New J. Phys. 9, 323 (2007).
4. D. Torrent and J. Sánchez-Dehesa, New J. Phys. 10, 023004 (2008).
5. S.A. Cummer and D. Schurig, New J. Phys. 9, 45 (2007).
6. L.W. Cai and J. Sánchez-Dehesa, New J. Phys. 9, 450 (2007).
7. D. Torrent and J. Sánchez-Dehesa, New J. Phys. 10, 063015 (2008).
8. D. Torrent and J. Sánchez-Dehesa, Phys. Rev. Lett. 103, 064301 (2009).
9. D. Torrent and J. Sánchez-Dehesa, New J. Phys. 12, 073034 (2010).
10. A. Climente, D. Torrent and J. Sánchez-Dehesa, Appl. Phys. Lett. 97, 104103 (2010).
11. T. Martin, G. Orris, L.W. Cai, D. Torrent and J. Sánchez-Dehesa, Appl. Phys. Lett. (2010).

Phononics 2011: First International Conference on Phononic Crystals, Metamaterials and Optomechanics
Santa Fe, New Mexico, USA, May 29-June 2, 2011
PHONONICS-2011-0144

Perforated acoustic metamaterials

Johan Christensen and F.J. Garcia de Abajo
Instituto de Optica - CSIC Serrano 121, 28006 Madrid, Spain
Johan.christensen@gmail.com

The discovery of the phenomenon of extraordinary optical transmission (EOT) through subwavelength holes by Ebbesen and co-workers has become a milestone theme within the field of nanophotonics and has sparked considerable fundamental but also technological interests [1]. Alongside the discovery of EOT, metamaterials for EM radiation have also become a topic of intense research that has lead to negative refraction, perfect lenses and perfect absorbers [2].
Acoustic metamaterials on the other hand have been introduced in 2000 by locally resonating spheres [3] and has since then given rise to a vast amount of innovative metamaterial structures, e.g., see [4]. In this presentation we focus on perforated plates, which is governing the study of enhanced acoustic transmission through subwavelength apertures [5] and in addition supports metamaterial typical phenomena like perfect imaging [6], negative refraction [7] such as full attenuation of sound [8]. We will discuss both theoretical and experimental results related to these items, e.g., such as the possibility of sub-diffraction-limited imaging by means of a slow fluid slab as shown in Fig. 1, [6].

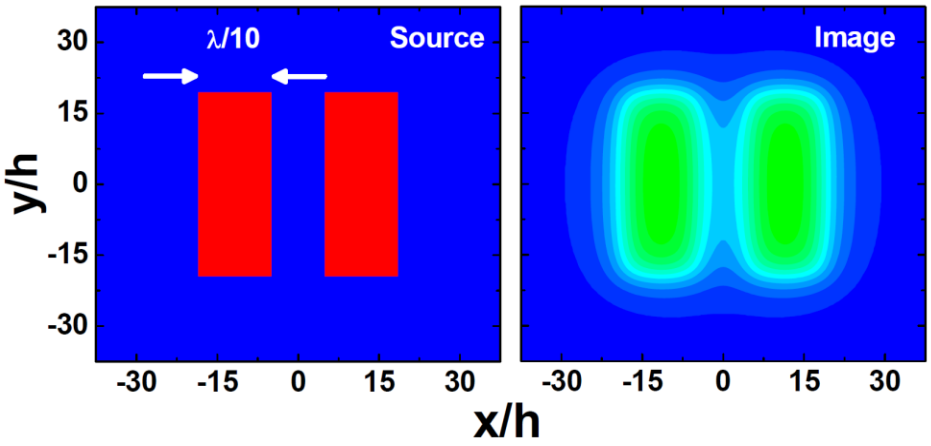

Fig. 1

Financial support from the following sources is acknowledged: NMP4-2006-016881- SPANS, NMP4-SL-2008-213669-ENSEMBLE, FP7-ICT-2009-4-248855, MICINN (MAT2010-14885, Consolider NanoLight.es, Carlsberg Foundation under contract QUANTONICS 2009-01-0167 and The Danish Council for Independent Research (Natural Sciences - 10-093234 - Metacoustics2011).

References

[1] T. W. Ebbesen, H. J. Lezec, H. F. Ghaemi, T. Thio, and P. A. Wolf, Nature 391 , 667 (1998).
[2] J. B. Pendry, Phys. Rev. Lett. 85, 3966 (2000), R. A. Schelby, D. R. Smith and S. Schulz, Science 292, 77 (2001), N. I. Landy et al., Phys. Rev. Lett. 100, 207402 (2008).
[3] Z. Liu, X. Zhang, Y. Mao, Y. Y. Zhu, Z. Yang. C. T. Chang and P. Sheng, Science 289, 1734 (2000).
[4] N. Fang, D. Xi, J. Xu, M. Ambai, W. Srituravanish, C. Sun and X. Zhang, Nature Material 5, 452 (2006).
[5] B. Hou et al. Phys. Rev. B 76, 054303 (2007), J. Christensen et al. Nature Physics 3, 851 (2007), J. Christensen, L. Martin-Moreno and F. J. Garcia-Vidal, Phys. Rev. Lett. 101, 014301 (2008)
[6] J. Zhu et al. Nature Physics 7, 52 (2011), J. Christensen et al. Appl. Phys. Lett. 97, 164103 (2010)
[7] J. Christensen and F. J. Garcia de Abajo, under preparation (2011).
[8] J. Christensen, L. Martin-Moreno and F. J. Garcia-Vidal, Appl. Phys. Lett. 97, 134106 (2010)

Phononics 2011: First International Conference on Phononic Crystals, Metamaterials and Optomechanics

Santa Fe, New Mexico, USA, May 29-June 2, 2011

PHONONICS-2011-0144

Phononics 2011: First International Conference on Phononic Crystals, Metamaterials and Optomechanics
Santa Fe, New Mexico, USA, May 29-June 2, 2011
PHONONICS-2011-0150

Phononic Band Structure of a Silicon Plate with Periodic Array of Cylindrical Metallic Pillars

R. Pourabolghasem[1], A. Khelif[2], A. A. Eftekhar[1], S. Mohammadi[1], A. Adibi[1]

[1] *School of Electrical and Computer Engineering, Georgia Institute of Technology, Atlanta, GA 30324, USA*
pourabolghasem@gatech.edu, eftekhar@gatech.edu, saeedm@gatech.edu, adibi@ece.gatech.edu
[2] *Institut FEMTO-ST, CNRS UMR 6174, Université de Franche-Comté, 32 Avenue de l'Observatoire, 25044, Besançon Cedex, France*
akhelif3@mail.gatech.edu

Abstract: We investigate theoretically the phononic band structure in a 2D array of cylindrical pillars on the surface of a slab. Simulations are based on the finite element method (FEM) using tungsten pillars on silicon as the structure of interest. We show that the phononic structure supports band gaps and study the behavior of band structure with respect to lattice symmetry and geometrical parameters.

During the past decade, synthetic periodic acoustic structures (i.e., phononic crystals) have attracted significant attention as they enable designers to control the elastic properties of the material. Specific focus of researchers in this field has been on the search for phononic crystal structures that support phononic band gaps (PnBGs). In particular, it has been shown that a honeycomb array of circular holes in a silicon (Si) slab can support sizable PnBGs[1]. However, this requires relatively large aspect ratios that make their fabrication challenging for high frequencies. Recently, 2D structures consisting of an array of cylindrical pillars on a plate have been introduced that display large PnBGs with more relaxed fabrication requirements[2,3].

In this paper we investigate different phononic crystal structures composed of 2D array of tungsten (W) pillars on a silicon plate with different lattice structures, namely, triangular and honeycomb lattices. We show that triangular lattice structures support multiple wider PnBGs for a wide range of geometrical parameters compared to square lattice structures. On the other hand, honeycomb array of pillars do not support any wide PnBGs with similar dimensions.

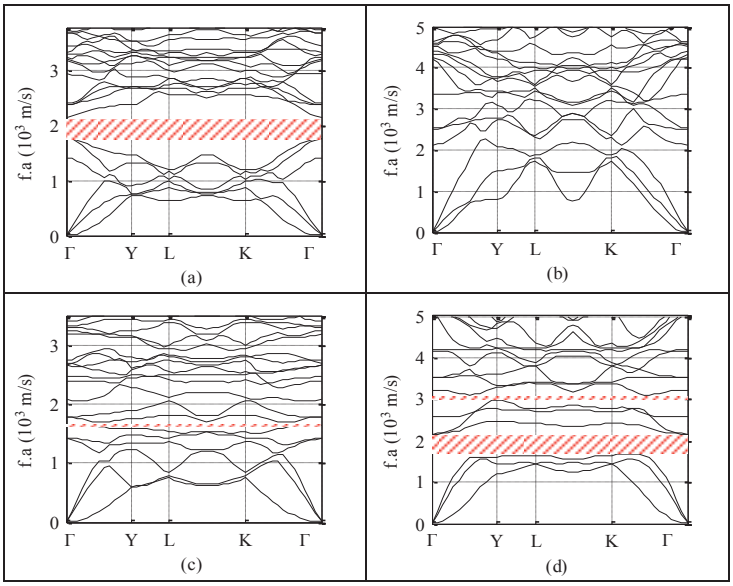

Figure 1 Band diagrams of (a,b) a honeycomb and a triangular array of holes in Si, respectively, with r/a = 0.4, d/a = 0.87; band diagrams of (c,d) a honeycomb and triangular array of W pillars on Si with r/a = 0.25, h/a = 0.15, d/a = 0.5. Here r, a, and d represent the hole (or pillar) radius, the lattice constant, and the slab thickness, respectively. In the case of pillars, h represents the height of the pillar.

Figure 1a shows the band diagram for a sample design of a honeycomb array of holes in Si. The existence of a wide band gap is evident from Fig. 1a. On the other hand, as shown in Fig. 1b, a triangular array of holes with similar dimensions does not support PnBG. On the contrary, Figs. 1c and 1d show that a honeycomb array of W pillars on Si does not support any significant PnBG while its triangular counterpart provides a wide PnBG. In order to investigate this phenomenon, we have studied the effects of the normalized slab thickness (d/a), and the normalized radius (r/a) and height (h/a) of the pillars on the PnBG.

Phononics 2011: First International Conference on Phononic Crystals, Metamaterials and Optomechanics
Santa Fe, New Mexico, USA, May 29-June 2, 2011
PHONONICS-2011-0150

Figures 2a and 2b show the gap maps (the extent of the PnBG as a function of design parameters) for a honeycomb and a triangular phononic crystal of W pillars on a Si slab, respectively, for a fixed pillar radius and slab thickness. Fig. 2 suggests that a triangular phononic crystal has a wider PnBG with band openings (PnBG frequency extent divided by the PnBG center frequency) of up to 25%. It is also seen that the triangular lattice structure displays band opening at *h*/a of as low as 0.1. Further assessment of dispersion diagram of this PnBG proves that this band opening is due to the lattice periodicity, which results in the folding of the first order mode of the structure in the dispersion diagram. Also, in this example, we can see the honeycomb lattice starts to open a PnBG at $h/a \sim 0.15$ around $f.a \sim 2700$m/s. This behavior is also seen in the triangular lattice only resulting in wider gaps. In addition, other gaps at similar frequencies (with different widths) can be observed for both lattices. Considering the fact that the same band gaps are supported in two structures with similar pillars and completely different lattice constants (the lattice period of the honeycomb lattice is 70% larger than that of the triangular lattice with the same *a*) we believe that the formation of these band gaps are mainly caused by the strong coupling between locally resonant pillar structures through the silicon slab rather than the periodic perturbation of the slab modes by the pillars.

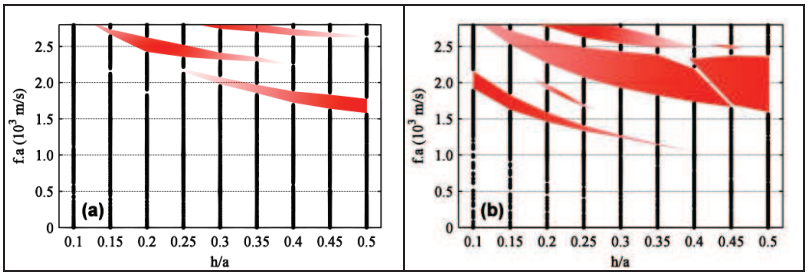

Figure 2 Existence of PnBG openings in (a) honeycomb and (b) triangular array of W pillars ($r/a = 0.40$) on a Si slab ($d/a = 0.5$) for different values of h/a.

Lattice type	α (lower edge)	α (upper edge)
Honeycomb ($h/a = 0.45$)	1.1	0.85
Triangular ($h/a = 0.45$)	0.82	11.1
Triangular ($h/a = 0.1$)	0.23	0.34

Table 1 Ratio of average elastic energy density in W pillars and Si slab (α) ($r/a = 0.40$ and $d/a = 0.5$)

In order to verify this claim, we calculate the ratio of average total elastic energy density in W pillars and Si slab (denoted as α). α's much lower than one indicate weak effect of the pillar resonances on the PnBG. As shown in Table 1, α for similar behaving band edges in the two lattices are close to one or higher; whereas, this parameter is much lower for band edges formed exclusively in the triangular lattice at lower frequency.

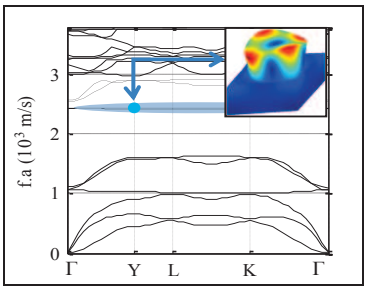

Figure 3 Band diagram of triangular array of W pillars ($r/a = 0.40$, $h/a = 0.45$) on Si slab ($d/a = 0.50$). Shown in the box: mode shape of the lattice unit cell at high symmetry point Y for upper edge of first band gap.

Another way to confirm that wide gaps appearing in the triangular lattice structure at higher pillar heights are due to the strong coupling of the local resonance modes of the W pillars is by visually investigating the mode shape at the band edges for such gaps. Figure 3 shows the band diagram of a triangular lattice with $r/a = 0.40$, $d/a = 0.5$, and $h/a = 0.45$. We can see that first band gap is bound to almost a flat upper branch. Based on our discussion, we expect this branch to correspond to the resonance mode of a W pillar. As shown in this figure, a significant amount of the mode energy for this branch at the high symmetry point Y is concentrated in the pillar.

To summarize, theoretical evidence was provided that a triangular lattice of pillars on a Si slab is more likely to provide wide PnBGs in comparison to honeycomb lattice. Further details on the properties of the PnBGs, the modes of the structure, and the potential applications will also be presented.

This work has been supported by the National Science Foundation.

References

[1] S. Mohammdi, A. A. Eftekhar, A. Khelif, W. D. Hunt, and A. Adibi, *Appl. Phys. Lett.* **92**, 221905 (2008),
[2] Y. Pennec, B. Djafari-Rouhani, H. Larabi, A. Akjouj, J. N. Gillet, J. O. Vasseur, and G. Thabet, *Phys. Rev. B* **80**, 144302 (2009),
[3] T. C. Wu, T. T. Wu, and J. C. Hsu, *Phys. Rev. B* **79**, 104306 (2009)

Phononics 2011: First International Conference on Phononic Crystals, Metamaterials and Optomechanics
Santa Fe, New Mexico, USA, May 29-June 2, 2011
PHONONICS-2011-0172

Dissipative Effects in Acoustic Metamaterials

Michael J. Frazier, Mahmoud I. Hussein

Department of Aerospace Engineering Sciences, University of Colorado - Boulder, Boulder, Colorado 80309, USA
michael.frazier@colorado.edu, mih@colorado.edu

Abstract: We demonstrate the consequences of energy dissipation in acoustic metamaterials. A nested mass-spring-dashpot system serves as our model. In the context of Bloch theory, we utilize the familiar structural dynamics techniques of modal analysis and state-space transformation to investigate the damped frequency band structure and its impact on effective properties.

In the context of acoustic wave propagation, a class of acoustic metamaterials (AMs) has the feature of spatial periodicity whereby the repeating unit cell can be orders of magnitude smaller than the travelling wavelength. This "acoustical atom" construction gives rise to effective, frequency-dependent properties including negative mass and negative elastic modulus. Ingenuity may exploit these unnatural properties in such novel applications as superlensing[1] and acoustic cloaking.[2] To date, however, theoretical studies of AMs have not adequately incorporated the effects of energy dissipation (i.e., damping) on the band structure and subsequently on the negative properties. The study of the effects of dissipation in AMs and its potential impact on the expression of negative effective properties is therefore the main objective of our present study.

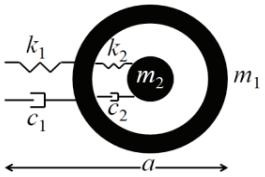

Figure 1. Acoustic meta-material unit cell

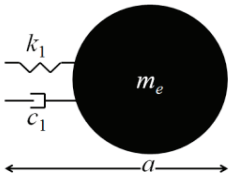

Figure 2. Equivalent model unit cell

To demonstrate the consequences of dissipative wave propagation in AMs, we consider a nested 1D lumped parameter mass-spring-dashpot model similar to that found in the literature.[3,4] Infinite in extent, our metamaterial model is constructed by appending copies of the unit cell of Fig. 1 ad infinitum along the line of motion. Likewise, this construction applies to the equivalent lattice architecture of Fig. 2, which we require to exhibit the same dynamic behaviour as our original model. In both models, the constant a defines the lattice spatial periodicity. For the equivalent model, m_e is the effective mass.

At present, we focus on the acoustic metamaterial model. To establish the damped frequency band structure we reformulate a quadratic eigenvalue problem representation[5] and incorporate the Bloch modal analysis technique.[6,7] Consequently, for this extended abstract, we consider only Rayleigh-type damping, in particular, stiffness-proportional damping. In addition, we consider constant damping parameters; however, the viscous dissipation force is frequency-dependent.

For the AM model, we derive the governing equations of motion, and assume a time-harmonic solution of the following form for the time-dependent displacement u_l of mass l:[6,7]

$$u_l(t) = \widetilde{U}_l e^{\lambda t}. \tag{1}$$

In Eq. 1, $\widetilde{U}_l$ denotes the complex wave amplitude. Naturally, for the undamped scenario, $\lambda = i\omega$. For our study, per the results of Ref. 7, $\lambda = -\omega\left(q\omega - \sqrt{q^2\omega^2 - 4}\right)/2$ where q is the damping intensity.

For the specific set of material properties provided in Table 1, the dispersion curves following our formulation is shown in Fig. 3. The wavenumber $\kappa = \kappa_R + i\kappa_I$ consists of a real component, κ_R (right side of figure), and an imaginary component, κ_I (left side of figure). The damped natural frequency is $\omega_d = \mathrm{Im}[\lambda(\omega; q)]$. In contrast to the

$r_m = m_2/m_1 = 1/100$
$r_k = k_2/k_1 = 3/100$
$\bar{\omega} = \sqrt{m_2/k_2} = 149.07\ \mathrm{rad/s}$

Table 1. Material properties

Phononics 2011: First International Conference on Phononic Crystals, Metamaterials and Optomechanics
Santa Fe, New Mexico, USA, May 29-June 2, 2011
PHONONICS-2011-0172

dramatic change seen in the optical branch in response to the changing damping intensity, the change in the acoustical branch is relatively modest.

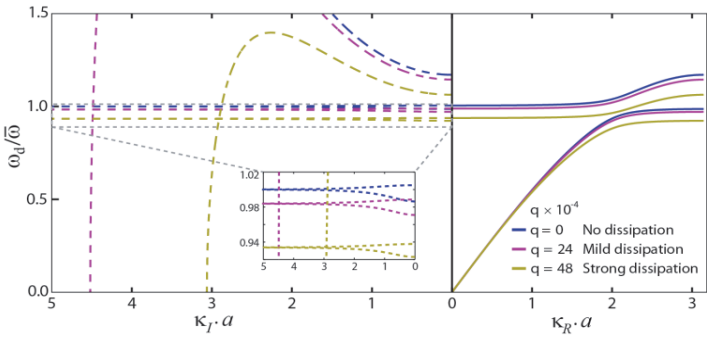

Figure 3. Dissipative frequency band structure

We now turn our attention to the dynamics of the equivalent model in Fig. 2. In order to exhibit the same dynamic behaviour as the lattice in Fig. 1, the value m_e must become frequency-dependent. The equations of motion are derived anew following the approach in Ref. 7 where the Bloch wave solution is assumed. For the nested-mass lattice model, this avenue yields a homogeneous system of equations with mass matrix $\mathbf{M}$, stiffness matrix $\mathbf{K}(\kappa)$, and damping matrix $\mathbf{C}(\kappa)$ (recall, $\mathbf{C}(\kappa) = q\mathbf{K}(\kappa)$ is our present interest). Specifically,

$$\mathbf{M} = m_2 \begin{bmatrix} 1/r_m & 0 \\ 0 & 1 \end{bmatrix}, \mathbf{K}(\kappa) = k_2 \begin{bmatrix} 2(1-\cos\kappa a)/r_k + 1 & -1 \\ -1 & 1 \end{bmatrix}. \quad (2)$$

For the equivalent lattice, the characteristic equation is algebraically manipulated to the following form:

$$-\lambda^2 \frac{m_r(1+r_m)}{\bar{\omega}^2 r_m(1+\lambda q)} = \frac{2}{r_k}(1-\cos\kappa a), \quad (3)$$

where, for convenience, we have defined the effective mass ratio $m_r = m_e/(m_1+m_2)$.

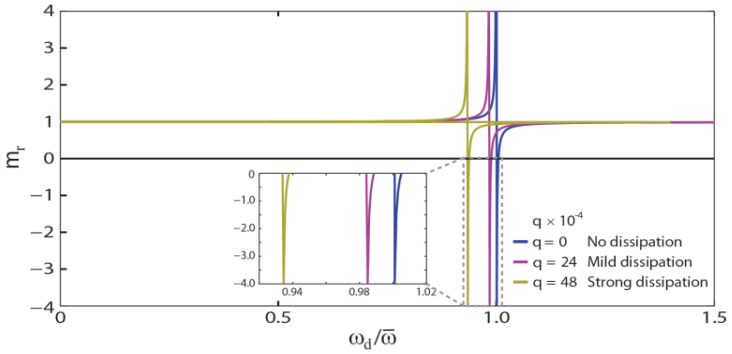

Figure 4. Effective mass ratio for dissipative acoustic metamaterial

By substituting Eq. 3 into $\mathbf{K}(\kappa)$ in Eq. 2, we tie the dynamic behaviour of the equivalent model to that of the nested-mass model. Using the redefined $\mathbf{K}(\kappa)$and Bloch modal analysis yields two characteristic equations in $\lambda(m_r; q)$. We proceed to solve one of these equations (the choice is inconsequential) for m_r and make the substitution $-\omega\left(q\omega - \sqrt{q^2\omega^2 - 4}\right)/2$ so that we have $m_r(\omega; q)$. Thus, we are able to produce Fig. 4. Upon closer inspection of Fig. 4, for each value of q, it is evident that the effective mass of the dissipative system is negative over the a region approximating the band gap of Fig. 3.

References

1. Zhu, J., Christensen, J., Jung, J., Martin-Moreno, L., Yin, X., Fok, L., et al. (2010). A holey-structured metamaterial for acoustic deep-subwavelength imaging. *Nature Physics*, *18* (4), 1-4.
2. Cummer, S.A., Popa, B., Schurig, D., Smith, D., Pendry, J., Rahm, M., et al. (2008). Scattering Theory Derivation of a 3D Acoustic Cloaking Shell. *Phys. Rev. Lett.*, *100* (2).
3. Huang, H., Sun, C., & Huang, G. (2009). On the negative effective mass density in acoustic metamaterials. *International Journal of Engineering Science*, *47* (4), 610-617.
4. Liu, Z., Chan, C. T., & Sheng, P. (2005). Analytic model of phononic crystals with local resonances. *Phys. Rev. B*, *71* (1).
5. Farzbod, F., & Leamy, M.J. (2010). Analysis of Bloch's method in structures with energy dissipation. *ASME International Mechanical Engineering Conference & Exposition.* Vancouver, British Columbia, Canada.
6. Hussein, M.I. (2009). Theory of damped Bloch waves in elastic media," *Phys. Rev. B*, 80, 212301.
7. Hussein, M.I. & Frazier, M.J. (2010). Band structures of phononic crystals with general damping. *J. Appl. Physics, 108* (9).

Phononics 2011: First International Conference on Phononic Crystals, Metamaterials and Optomechanics

Santa Fe, New Mexico, USA, May 29-June 2, 2011

PHONONICS-2011-0184

Multi-field Internally Resonating Metamaterials

Luca Airoldi[1], Matteo Senesi[1] and Massimo Ruzzene[1]

[1] *Daniel Guggenheim School of Aerospace Engineering, Georgia Institute of Technology, 270 Ferst Drive N.W. Atlanta, GA 30332, USA, luca.airoldi@gatech.edu, matteo.senesi@gatech.edu, massimo.ruzzene@aerospace.gatech.edu*

Abstract: Two examples of internally resonating metamaterials with multi-field coupling are presented. A one-dimensional waveguide with a periodic array of shunted piezoelectric patches features resonant characteristics associated with the shunting electrical impedance. The second part presents the study of piezoelectric superlattices as an additional example of an internally resonant metamaterial.

In this work wave propagation in periodic systems which comprise multi-field elements is analyzed. The study is based on the general observation that the presence of elements capable of energy conversion between two fields offers extensive opportunities for the achievement of unusual and novel wave propagation characteristics. In this regard, multi-field coupling in periodic materials is an excellent candidate for the design of novel metamaterials. One of the concepts illustrated involves the use of piezoelectric materials for the conversion of elastic into electrical energy, and the use of shunting circuits to generate an equivalent resonant system in parallel to the mechanical waveguide. The resonant characteristics of the shunts can be tuned by modifying the circuit electrical impedance, which suggests the possibility for the system to achieve unusual mechanical properties at selected frequencies. The second concept investigates acousto-electromagnetic coupling resulting from the periodic polarization of a piezoelectric waveguide. In this case, the resonant behavior is associated with the generation and excitation of polaritons, which resonate at frequencies defined by the periodicity and physical properties of the lattice. At these frequencies, wave motion is characterized by strong attenuation, and maximum energy transfer between the acoustic and electromagnetic fields.

The analysis of the dispersion properties of the two waveguides underlines the common characteristics associated with internally resonating properties, and suggests potential applications such as vibration attenuation and isolation, and the development of novel acousto-optical devices. Homogenized theories for both types of waveguides are developed to derive expressions for their equivalent properties, which effectively illustrate their resonant characteristics, and show how they affect the propagation of waves.

The two types of multi-field waveguides presented in this work provide examples of systems where wave attenuation occurs through an internal resonance mechanism. The resonant condition is characterized by maximum coupling between the waveguide, acting as a primary system, and a resonating secondary system. The condition of maximum coupling is identified by the matching of the dispersion properties of the primary and secondary system. The dispersion relation for a secondary system comprising a set of periodically placed resonators generally appears as a flat curve, which corresponds to spatially localized modes in the resonators themselves, as defined by a null group velocity. The intersection of this flat mode with the dispersion branch of the primary structure defines the condition of maximum coupling between the two systems. When the primary and secondary systems belong to a multi-field domain, their coupling requires a mechanism through which energy transfer occurs. The presence of such mechanism leads to a new dispersion branch for the coupled system, which essentially coincides with the branches for the primary system away from the intersection condition, and undergoes a resonance at the coupling frequency. This behavior is illustrated in Figure 1 where the dispersion branches of the uncoupled primary and secondary system are respectively represented as dashed black and red dashed lines. The frequency of intersection of the two branches is the frequency of internal resonance for the uncoupled resonating primary system. Coupling leads to the new dispersion branch (solid blue line) which mostly follows the dispersion branch of the primary system, and is distorted by the resonant behavior at the frequency of internal resonance.

Phononics 2011: First International Conference on Phononic Crystals, Metamaterials and Optomechanics

Santa Fe, New Mexico, USA, May 29-June 2, 2011

PHONONICS-2011-0184

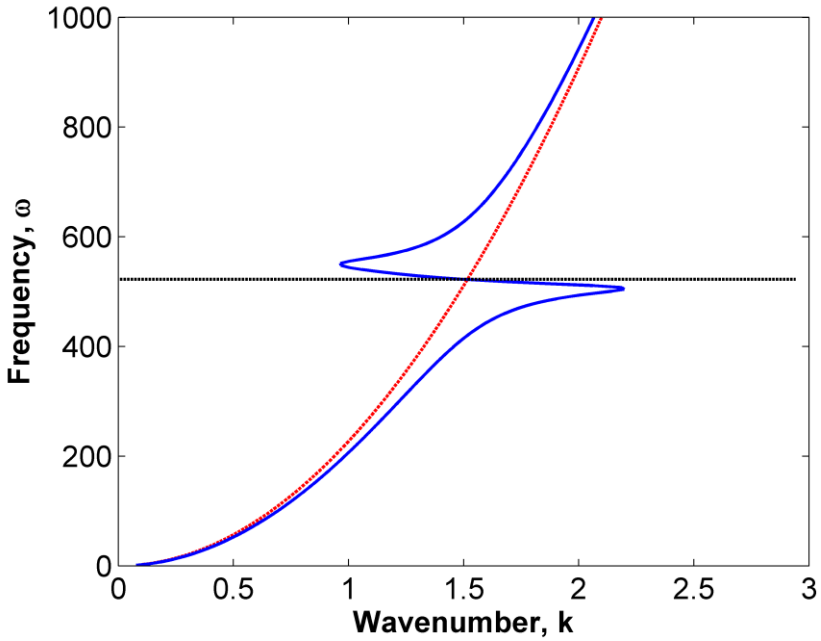

Figure 1. Typical dispersion relations for a waveguide with internal resonators: uncoupled systems (dashed lines), coupled system (solid blue line).

In the considered waveguides, the coupling mechanisms is provided by the piezoelectric effect. In the case of the periodic piezoelectric shunted network, the secondary system is effectively characterized by a flat dispersion mode corresponding to the resonant behavior of the shunting circuits, while for the case of piezoelectric superlattices, the flat dispersion modes corresponds to an elastic mode at very low wavelength. In this case, coupling is made possible by the folding of the branch caused by the periodicity of the waveguide.

The work is organized in two parts covering the two concepts. Part 1 presents the study of one-dimensional waveguides with periodic shunted piezo arrays. Numerical and experimental results illustrate their attenuation characteristics, and their tunable properties. Numerical investigations are performed through the application of the Transfer Matrix method, which is briefly reviewed. Experimental investigations performed on a beam structure, confirm the numerical predictions and show the attenuation characteristics of the waveguide. Part 2 is devoted to the study of piezoelectric superlattices. Numerical studies of one-dimensional and two-dimensional configurations are performed through the application of the Plane Wave Expansion method, which is presented in some detail. Multifield coupling and internal resonant behavior of piezoelectric superlattices are illustrated through a series of numerical examples, and the evaluation of equivalent dielectric properties using a long wavelength approximation approach.

1ST INTERNATIONAL CONFERENCE ON PHONONIC CRYSTALS, METAMATERIALS & OPTOMECHANICS

Extended Abstracts

Track 3: Periodic Structures

Phononics 2011: First International Conference on Phononic Crystals, Metamaterials and Optomechanics
Santa Fe, New Mexico, USA, May 29-June 2, 2011
PHONONICS-2011-0009

Elastic waves in a three-dimensional hexagonal close-packed granular crystal: observation of rotational modes and nonlinear effects

A. Merkel[1], V. Tournat[1*], V. Gusev[2]
[1]LAUM, [2]LPEC, CNRS, Université du Maine, Le Mans, France.
aurelien.merkel.etu@univ-lemans.fr, vincent.tournat@univ-lemans.fr,
vitali.goussev@univ-lemans.fr

Abstract: Noncohesive granular phononic crystals show peculiar features related to the elastic nonlinearities at the contacts and the rotational degrees of freedom of the grains. Evidence of rotational mode propagation and non reciprocity for nonlinear acoustic effects is found in a hexagonal close-packed crystal layer with a gravity-induced elasticity gradient.

Noncohesive granular crystals are periodic arrangements of elastic spheres with noncohesive contacts [1,2]. Due to the intrinsic elastic nonlinearity of the interaction between the beads, these media are found to exhibit an overall high nonlinearity[3]. Moreover, the fact that the grains are spherical and weakly frustrated for rotation due to the non cohesive character of the arrangement, provides appropriate conditions for the observation of rotational modes of propagation and coupled rotational-transverse modes[2,4,5].

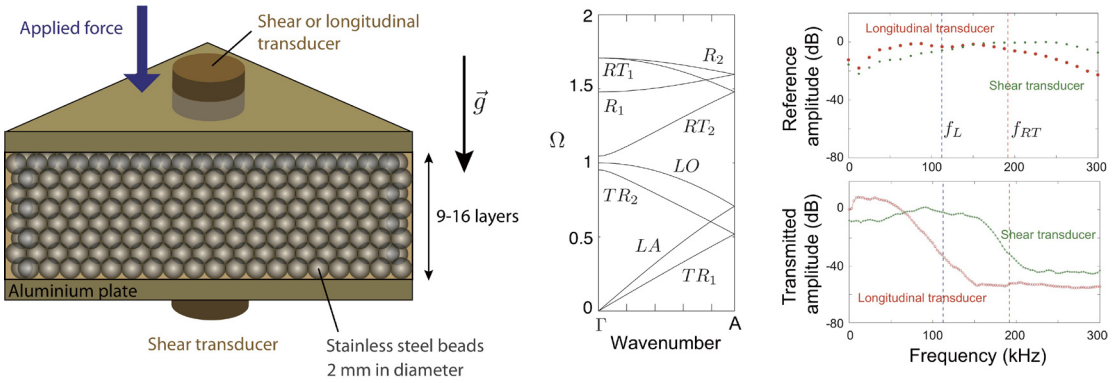

Figure 1: (left) Schematics of the experimental setup. (center) Normalized dispersion curves in the z direction. (right) Reference and transmitted amplitude through the granular layer for shear and longitudinal detection.

The theory developed in Ref. 2, taking into account friction and the rotational degrees of freedom, shows that there should exist in the z direction, longitudinal modes (LA and LO), transverse-rotational modes (TR_1 and TR_2), rotational-transverse (RT_1 and RT_2) and pure rotational modes (R_1 and R_2), see Fig. 1 (center). When shear and longitudinal waves are excited from one side of the granular crystal layer, a pass-band up to f_L (predicted here for an applied static force of 780 N) is observed for

Phononics 2011: First International Conference on Phononic Crystals, Metamaterials and Optomechanics
Santa Fe, New Mexico, USA, May 29-June 2, 2011
PHONONICS-2011-0009

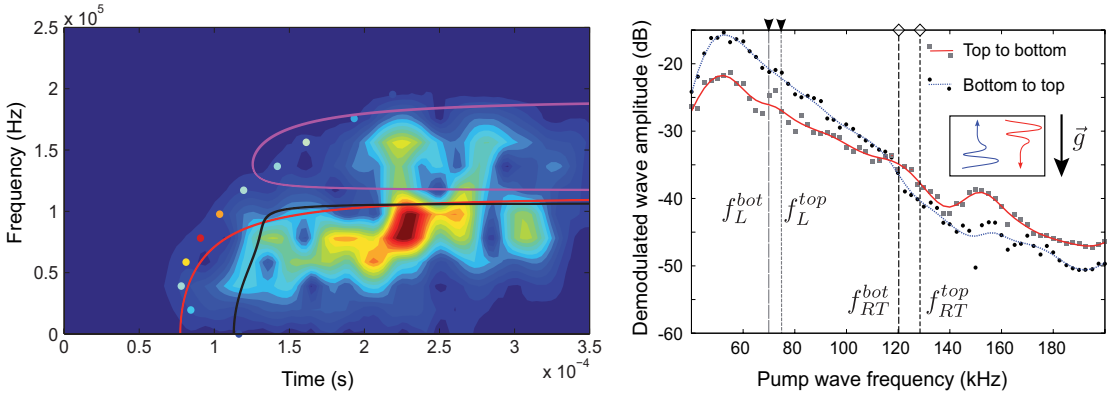

Figure 2: (left) Spectrogram of a wide-frequency-band pulse transmitted through the layer. (right) Demodulated wave amplitude for bottom-to-top and top-to-bottom paths of propagation.

longitudinal waves (detection with the longitudinal transducer, Fig. 1 (right)). With shear detection, a pass-band up to f_{RT} (cut-off frequency for rotational-transverse modes) is observed, showing that the higher frequency modes associated to rotation of the beads propagate. Complementary experimental results will be discussed, such as the static pressure dependence of the cut-off frequencies.

In Fig. 2 (left), the theoretical group delays for the detectable modes (L, TR, RT, shown as lines) are compared to the energy front arrival time of the transmitted energy and are in qualitative agreement for both longitudinal and rotational-transverse modes, confirming the role of the rotational degree of freedom. Non reciprocity for nonlinear effects is finally reported in Fig. 2 (right). Wave packets are generated by a transducer and then are nonlinearly self-demodulated in the medium[6]. This frequency-down conversion does not exhibit the same efficiency for propagative or evanescent pump waves and is direction dependent. This phenomenon is explained by the existence of a vertical gradient of medium properties, induced by gravity, both for the wave attenuation and the nonlinearity of the medium. We believe that our experiments provide the first experimental evidence of the dependence of nonlinear acoustic phenomena on propagation direction in spatially inhomogeneous granular media.

This work is supported by ANR grant STABINGRAM.

References

[1] A. Merkel, V. Tournat, V.E. Gusev, Ultrasonics 50, 133-138 (2009).
[2] A. Merkel, V. Tournat, V.E. Gusev, Phys. Rev. E 82, 031305 (2010).
[3] V. Tournat, V.E. Gusev, Acta-Acustica united with Acustica 96, 208-224 (2010).
[4] E. Cosserat, F. Cosserat, Théorie des Corps déformables (Herman et fils, Paris, 1909).
[5] A. C. Eringen, Microcontinuum Field Theories.1 : Foundations and Solids (Springer Verlag Inc., New York, 1999).
[6] V. Tournat, B. Castagnède and V.E. Gusev, Phys. Rev. E 70, 056603 (2004).

Phononics 2011: First International Conference on Phononic Crystals, Metamaterials and Optomechanics
Santa Fe, New Mexico, USA, May 29-June 2, 2011
PHONONICS-2011-0011

Out-of-plane acoustic modes in monolayer phononic granular membranes

I. Perez-Arjona[1], A. Merkel[2], V. Tournat[2*], V. Gusev[3], V. Sanchez-Morcillo[1]
[1]IGIC, Universidad Politècnica de Valencia, 46730 Grau de Gandia, Spain.
[2]LAUM, [3]LPEC, CNRS, Université du Maine, Le Mans, France.
[*]vincent.tournat@univ-lemans.fr

Abstract: Waves in hexagonal monolayer granular membranes are studied theoretically. The predicted propagation modes involve an out-of-plane displacement and two rotations with axes in the membrane plane. Shear and bending rigidities at the contact are considered, as well as coupling with a substrate. Dispersion relations and band gaps are presented and discussed for various contact properties.

Recently, ordered monolayer nanoparticle arrays have been successfully produced by self-assemblage during a drying process[1], and can be stretched across micrometer size holes to provide freely suspended monolayer membranes[2,3]. Such granular membranes, with peculiar elastic and optical properties could lead to a wide range of sensor applications. Here, we report a theoretical work on the vibrational properties of such granular membranes. The specificities of these granular systems compared to classical membranes come from the particle finite dimensions and their finite rotational inertia (rotational degree of freedom) which lead to elastic interactions through non-central forces. In particular, it provides in addition to shear and longitudinal acoustic modes, the existence of rotational (or so-called micro-rotational) modes[4–6].

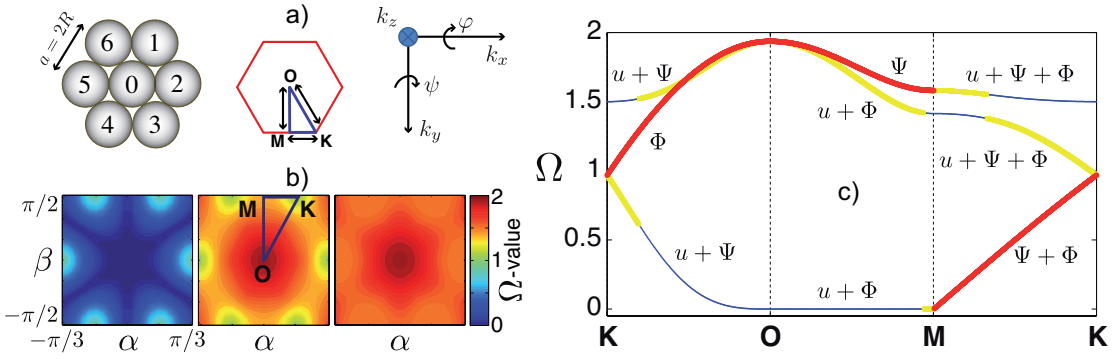

Figure 1: a) Geometrical arrangement of the beads in the elementary cell of the hexagonal membrane crystal and definition of the Brillouin zone and coordinate axes. b) Iso-surface plots of the lowest eigenvalue $\Omega = \omega^2/(4\xi/m)$ of the dynamical matrix (left), the middle eigenvalue (center) and the largest eigenvalue (right) ($\alpha = k_x/4$ and $\beta = \sqrt{3}k_y/4$). c) Dispersion relations and associated symmetries of the modes.

In order to model out-of-plane mode propagation in monolayer granular membranes, the equations of motion for the displacement u_0 of the center of the central particle 0, and

Phononics 2011: First International Conference on Phononic Crystals, Metamaterials and Optomechanics
Santa Fe, New Mexico, USA, May 29-June 2, 2011
PHONONICS-2011-0011

the equations for the rotations φ_0 and ψ_0 (defined in Fig. 1(a)) are written in the form

$$m\ddot{u}_0 = -\xi\left[(\delta u_1 + \delta u_4) + (\delta u_3 + \delta u_6) + (\delta u_2 + \delta u_5)\right], \quad (1)$$

$$I\ddot{\varphi}_0 = \frac{\sqrt{3}}{2}\xi R\left[(\delta u_1 - \delta u_4) - (\delta u_3 - \delta u_6)\right], \quad (2)$$

$$I\ddot{\psi}_0 = \frac{R}{2}\xi\left[(\delta u_1 - \delta u_4) + (\delta u_3 - \delta u_6)\right] + R\xi\left[\delta u_2 - \delta u_5\right], \quad (3)$$

where m is the mass of the particle, ξ is the contact shear rigidity and, for the particular case of homogeneous spheres, the momentum of inertia is $I = \frac{2}{5}mR^2$. The terms δu_i denote elongations of the spring at the contact between the central and $i-$particle, that is, the relative displacement between 0 and $i-$particle at the contact point.

After plane wave substitution, the dynamic matrix is obtained whose eigenvalues provide the dispersion relations plotted in Fig. 1(c) in the case where only shear rigidity between spheres is taken into account. Pure rotational modes are predicted in both x and y propagation directions, as well as a zero frequency mode along the path OM.

Fig. 2 shows an example of the modified dispersion relations when bending rigidity at the contacts is introduced.

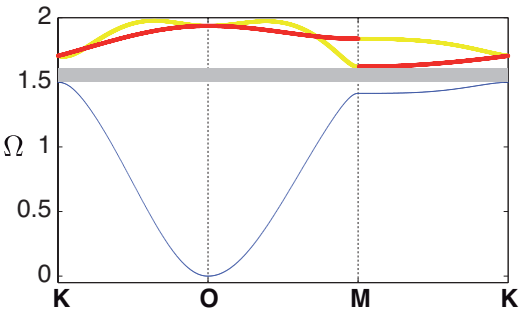

Figure 2: Dispersion relations obtained when shear and bending rigidities at the contacts are taken into account. Here a bending rigidity of 0.7 times the shear rigidity is used. An absolute band gap appears starting from a bending to shear rigidity ratio of 8/15. The zero frequency mode of Fig. 1 when bending is neglected is not predicted anymore.

Furthermore, the influence of the interaction with a rigid substrate has been taken into account. It is expected that these results will be useful for describing the phonon transport in two-dimensional nano-crystals, and vibration properties of micrometer scale granular membranes potentially used as sensors in the near future.

This work is supported by ANR grant STABINGRAM.

References

[1] T. P. Bigioni et al., Nature Materials 5, 265-270 (2006).
[2] K. E. Mueggenberg et al., Nature Materials 6, 656-660 (2007).
[3] W. Cheng et al., Nature Materials 8, 519-525 (2009).
[3] E. Cosserat, F. Cosserat, Théorie des Corps déformables (Herman et fils, Paris, 1909).
[4] A. C. Eringen, Microcontinuum Field Theories.1 : Foundations and Solids (Springer Verlag Inc., New York, 1999).
[5] A. Merkel, V. Tournat, V.E. Gusev, Ultrasonics 50, 133-138 (2009).

Phononics 2011: First International Conference on Phononic Crystals, Metamaterials and Optomechanics
Santa Fe, New Mexico, USA, May 29-June 2, 2011
PHONONICS-2011-0018

2D Wave Propagation in Periodically Layered Composite Structures with Damages

Mikhail V. Golub[1] , **Chuanzeng Zhang**[2]

[1] *Institute for Mathematics, Mechanics and Informatics, Kuban State University, Stavropolskaya Str. 149, 350040 Krasnodar, Russian Federation*
m_golub@inbox.ru
[2] *Department of Civil Engineering, University of Siegen, D-57068 Siegen, Germany*
c.zhang@uni-siegen.de

Abstract: Plane SH-wave propagation in periodically layered elastic composites with a single strip-like crack and an array of cracks (periodic or stochastic) is investigated using the transfer matrix method and the boundary integral equation method. The focus of this analysis is on the wave transmission and reflection, band gaps, localization and resonance phenomena due to crack-like damages.

Wave propagation in periodic composite structures is usually accompanied by localization phenomena and band-gaps, which are observed in photonic and phononic crystals[1]. Elastic waveguides are susceptible to damages like cracks during the manufacturing or in service. In particular, the delamination at imperfect interfaces between the constituents, interior cracks in the individual layers can occur. Such interface or interior damages could change the dynamic properties of the periodic composites and correspondingly cause noticeable alterations in band gaps and wave transmission spectra etc. To simplify the analysis, imperfect interfaces are usually simulated by a periodic/stochastic distribution of interface cracks or by spring boundary conditions[2;3], where the latter in a limiting case corresponds to a crack. Several analytical and numerical approaches have been developed so far for wave propagation analysis in periodic structures[4] including the transfer matrix method employed in the present work. Wave propagation and diffraction by a crack in multilayered composite structures can be efficiently investigated by using integral representations and Green's functions in conjunction with the integral-transform technique[5].

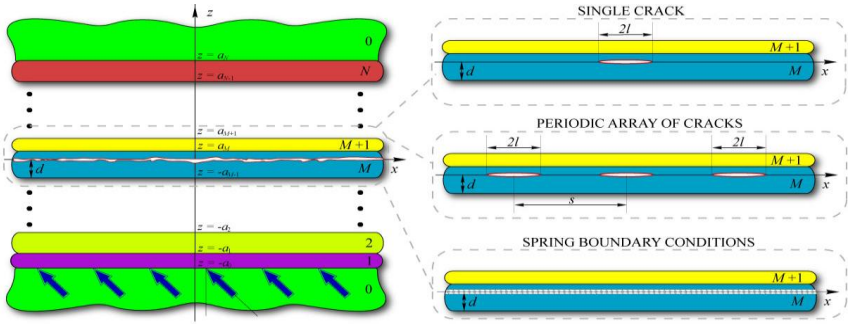

Figure 1 Geometry of the problem and mathematical model of a multi-layered composite between two identical half-planes with a damaged zone (a single crack, a periodic array of cracks, and a spring model).

In this paper, we consider time-harmonic plane wave propagation with circular frequency ω in a layered waveguide composed of two half-planes with a set of N elastic layers and one damaged layer in the stack. The Cartesian coordinate system $\boldsymbol{x}=(x,z)$ associated with the damaged zone is introduced: the Ox axis and the damaged interface are assumed to be parallel to the interfaces between the layers. The i-th layer occupying the domain $|x|<\infty$, $a_{i-1}<z<a_i$ of the thickness $d_i=a_i-a_{i-1}$ has the shear modulus μ_i and the mass density ρ_i. The damage is situated in the M-th layer at a distance d from the interface $z=a_{M-1}$. The following three damage types are considered here: a single strip-like crack of length $2l$, a periodic array of cracks of length $2l$ with a crack-distance s, and distributed damages modeled by spring boundary conditions[3] (see Figure 1). The problem for a single crack and for an array of cracks is solved by using a boundary integral equation method for the unknown crack-opening-displacement (COD), while the application of the spring boundary conditions allows us to use the T-matrix method with an approximate estimation of the spring stiffness[3].

Numerical examples will be presented to show the resonant and non-resonant regimes of the wave motion in the periodically layered composites weakened by a single strip-like crack or a periodic array of cracks and wave localization in the vicinity of the damages. Wave motion with large amplitudes for

Phononics 2011: First International Conference on Phononic Crystals, Metamaterials and Optomechanics
Santa Fe, New Mexico, USA, May 29-June 2, 2011
PHONONICS-2011-0018

some parameter combinations is found through the analysis of the COD, and it is shown that such resonant regimes are quite different within band gaps and pass bands. Dynamic stress intensity factors (SIFs), average energy density flow, energy transmission coefficient κ^+ and average COD normalized by the amplitude of the incident wave field v_u are also investigated to gain a better understanding of the wave propagation processes. If cracks are present in the layered composites, then the local maxima and minima of the COD and the SIFs are related to the maxima of the energy amount transferred through the layered composites, to be more precise, the extremal values of these quantities occur at the same frequencies in the pass bands. On the other hand, the amplitude of the wave motion at frequencies within the band gaps decreases rapidly in the direction of wave propagation, whereas the presence of cracks may cause noticeably larger amplitudes of the wave motion in their vicinity, i.e., wave localization. Stress and displacement fields of largest amplitudes are observed at resonance frequencies.

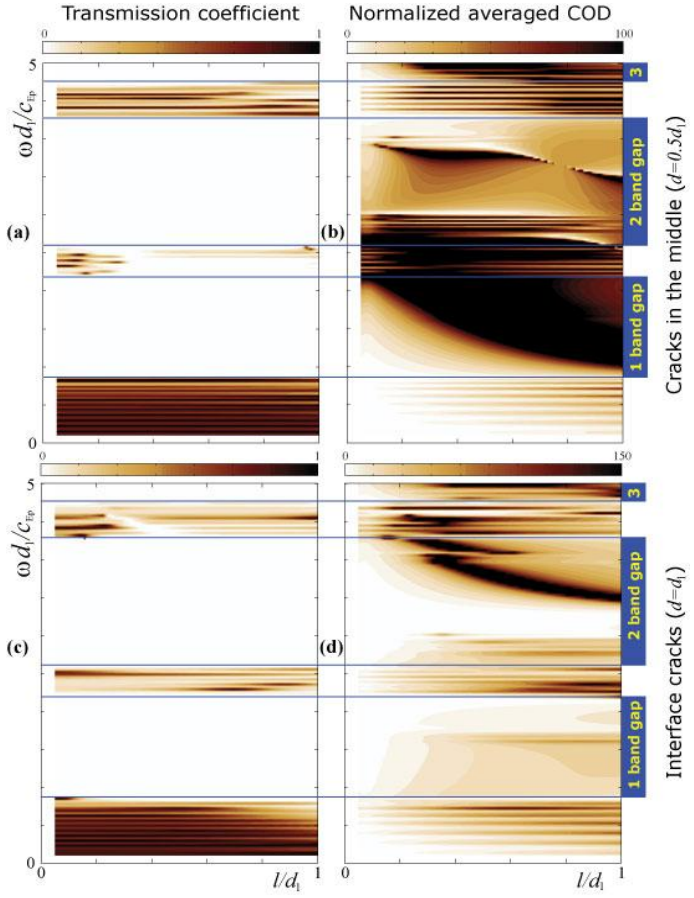

Figure 2 The transmission coefficient $\kappa^+(\omega,l)$ **(a,c)** and the normalized average COD $v_u(\omega,l)$ **(b,d)** for a periodic array of cracks with $s=3$ and situated in the middle of the 15-th layer**(a,b)** and at the interface between the 15-th and 16-th layer **(c,d)**. Band gaps are marked.

Without loss of generality we assume 32 layers in a waveguide and a unit-cell composed of 2 layers (Plumbum/Epoxy), and the damaged layer is in the middle of the stack of layers $M=15$. A single crack does not influence the band gaps due to the attenuation of the scattered wave field, while it changes, of course, wave pattern in the vicinity of the crack. Within the pass bands two kinds of resonances with intensified wave motion in the vicinity of the crack are observed.

An illustration example is given in Figure 2, where the transmission coefficient $\kappa^+(\omega,l)$ and the normalized average of COD $v_u(\omega,l)$ for a normally incident SH-wave are presented. Obviously, the presence of a damaged zone can only extend the band gaps, while for a periodic array of cracks two types of resonances are also observed. A "weak" resonance is observed in the pass bands, and it corresponds to relatively high amplitudes. A "strong" resonance is noted within the bang gaps, which is characterized by dark zones in Figs. 2**(b)** and 2**(d).** The "strong" resonances are induced by the localization of the wave motion near the damages.

The work is supported by the Ministry of Education and Science of Russian Federation, the German Research Foundation (DFG, Project No. ZH 15/11-1) and the German Academic Exchange Service DAAD, which are gratefully acknowledged.

References

[1] P. G. Martinsson, A. B. Movchan, *Quarterly Journal of Mechanics and Applied Mathematics*. **56**, 45-64 (2003).
[2] J. Baik, R. Thompson, *Journal of Nondestructive Evaluation*, **4**, 177-196 (1984).
[3] A. Boström, M.V. Golub, *Quarterly Journal of Mechanics and Applied Mathematics*, **62**, 39-52 (2009).
[4] M. Sigalas et. al., *Zeitschrift fur Kristallographie,* **220**, 765-809 (2005).
[5] E.V. Glushkov, N.V. Glushkova, *Journal of Computational Acoustics*, **9(3)**, 889-898 (2001).

Phononics 2011: First International Conference on Phononic Crystals, Metamaterials and Optomechanics
Santa Fe, New Mexico, USA, May 29-June 2, 2011
PHONONICS-2011-0030

Tailoring Stress Waves in 2-D Highly Nonlinear Granular Crystals: Simulations and Experiments

Andrea Leonard[1], Amnaya Awasthi[2], Philippe Geubelle[2], Chiara Daraio[1]

[1] Division of Engineering and Applied Sciences
California Institute of Technology, Pasadena CA, USA
andreal@caltech.edu, daraio@caltech.edu
[2] Dept. of Aerospace Engineering and Dept. of Computational Sciences and Engineering
University of Illinois Urbana Champaign, IL, USA
amnaya@illinois.edu, geubelle@illinois.edu

Abstract: We study the propagation of elastic stress waves in two-dimensional highly nonlinear granular crystals composed of square packings of spheres with and without cylindrical intruders, via experiments and numerical simulations. By varying the intruder material, we show the ability to alter the propagating wave front characteristics. Experiments agree well with discrete particle simulations.

Granular crystals are materials composed of ordered arrangements of particles in contact with each other, characterized by a highly nonlinear dynamic response. The transient dynamic response of one-dimensional highly nonlinear (uncompressed) granular crystals has been studied extensively[1,2], however few reports have explored wave propagation in two-dimensional systems[3]. The present work investigates the propagation of stress waves, or acoustic waves, in highly nonlinear two-dimensional granular crystals composed of a squared array of steel spheres and interstitial cylindrical intruders (Figure 1). Specifically, we analyze the influence of underlying particle composition on the wave front shape. We report that it is possible to substantially alter the shape of the wave front traveling through the system after impulsive loading by methodically varying the intruder material. These findings could lead to the development of new shock protecting materials and acoustic filters.

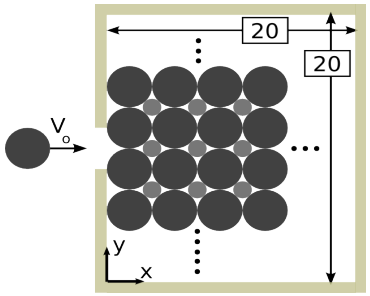

Figure 1 Schematic diagram of the experimental setup.

Numerical simulations were performed using a discrete particle model, in which each sphere or cylinder is modeled as a point mass connected by nonlinear springs. Hertzian potential[4] is used to model the sphere-sphere and sphere-wall interactions and a similar potential[5] is used to model the sphere-cylinder force displacement relation. Dissipative terms, such as friction, were not included in the simulations. Material properties chosen for the simulations are given in Table 1.

Experiments were performed on self-standing crystals assembled within a confining box made of delrin-lined walls (Figure 1). The array of particles included a 20 by 20 array of large steel spheres (19.05 mm diameter) with small interstitial intruders (7.89 mm diameter and 19.05 mm height). A striker-sphere identical to the particles composing the array was used to generate stress waves between two central particles in the array. The striker velocity was recorded with an optical velocimeter just before impact, and the recorded value was used as input in the numerical simulations. Several custom-fabricated sensor particles, instrumented with calibrated miniature tri-axial accelerometers, were positioned in selected locations in the array. The recorded accelerations were then compared with the acceleration of the center of mass of each particle obtained from the numerical simulations.

Material	Mass density (kg/m^3)	Young's Modulus (GPa)	Poisson's Ratio
Stainless Steel (type 316)	8000	193	0.30
Aluminium	2740	69	0.33
Teflon (PTFE)	1200	0.5	0.46

Table 1 Material properties used in numerical simulations.

Experiments were performed on the square packing of spheres with and without the presence of the cylindrical intruders, and were shown to be in good agreement with the numerical simulations (see Figure 2, comparing experimental and simulation results for an array without intrud-

Phononics 2011: First International Conference on Phononic Crystals, Metamaterials and Optomechanics
Santa Fe, New Mexico, USA, May 29-June 2, 2011
PHONONICS-2011-0030

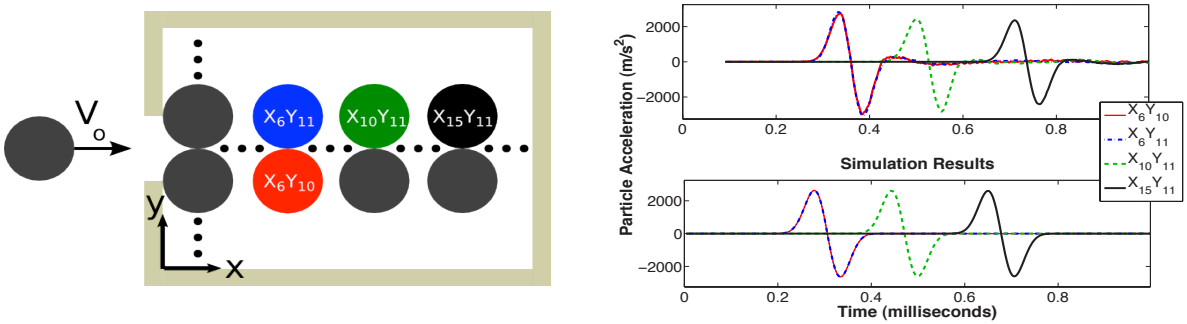

Figure 2 The left figure shows locations of sensor particles in the experimental setup (V_o = 0.29 m/s). The right figure compares experimental results (top right) with the simulation results (bottom right) for each of the sensor locations.

ers). In the absence of cylindrical intruders, the crystal was shown to support the propagation of solitary waves with comparable properties to the solitary waves previously observed in one-dimensional systems[1,2].

Numerical simulations showed the ability to significantly alter the stress wave front by introducing indruder particles of variable materials. A crystal composed of a squared array of particles without intruders supports the formation and propagation of highly nonlinear solitary waves along the two central chains (in line with the impact direction) and along the side of the crystal (following a quasi one-dimensional behavior, see Figure 3a). However, when cylindrical intruders were included the shape of the wavefront was observed to vary. When Teflon cylinders were used as intruders (Figure 3b) the wave front remained highly directional, similar to the case where intruders are absent, but the initial pulse begins to spread and shed energy in trailing pulses. The use of aluminium intruders allowed spreading of the wavefront into a triangular pattern (Figure 3c). Finally, when stainless steel intruders were used, we observed a nearly circular wavefront (Figure 3d) with particle velocities distributed over a larger area of the crystal. The ability to control the stress wave properties in these granular cystals may allow for the development of new wave-tailoring materials which could be used, for example, as protective layers capable of redirecting and trapping impact energy.

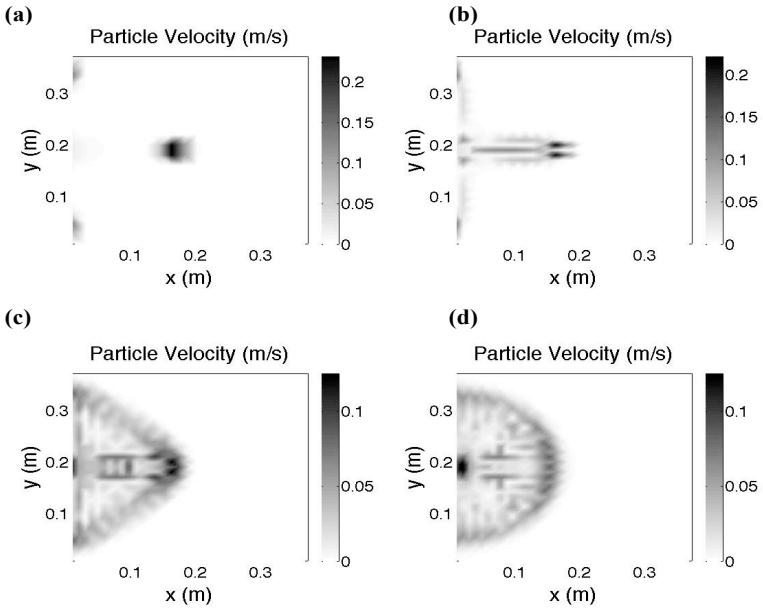

Figure 3 Numerical results showing the wave front shape in terms of particle velocity magnitude at simulation time 0.35 ms after the striker impact (V_o = 0.6 m/s) for test configurations composed of steel spheres in a square packing with **(a)** no intruders **(b)** PTFE intruders **(c)** aluminium intruders and **(d)** steel intruders.

This work was supported by the DOE SCGF and the Army Research Office MURI (Dr. David Stepp).

References

[1] V.F. Nesterenko, *Dynamics of Heterogeneous Materials*, Springer, USA (2001).
[2] C. Coste, E. Falcon, and S. Fauve, *Phys. Rev. E* **56,** (1997).
[3] A. Shukla, C.Y. Zhu, and M. Sadd, *Journal of Strain Analysis* **23**, (1988).
[4] K.L. Johnson, *Contact Mechanics*, Cambridge University Press, USA (1985).
[5] M. J. Puttock and E. G. Thwaite, *National Standard Laboratory Technical Paper No.25*, CSIRO, Australia (1969).

Phononics 2011: First International Conference on Phononic Crystals, Metamaterials and Optomechanics
Santa Fe, New Mexico, USA, May 29-June 2, 2011
PHONONICS-2011-0031

Active Control of Band Gaps by Periodically Distributed Piezo-shunts

S. B. Chen , J. H. Wen, G. Wang, D. L. Yu, X. S. Wen

Institute of Mechatronical Engineering, National University of Defense Technology, Changsha 410073, China, csbuniversity.student@sina.com, wenxs@vip.sina.com

Abstract: Periodic arrays of inductive or negative capacitive shunted piezoelectric patches are employed to control the band gaps of phononic beams. An epoxy beam with periodically surface-bonded piezoelectric patches is designed. The band gaps, when each piezo-patch is connected to a single inductive or negative capacitive circuit, are investigated in detail.

In the last decades, extensive efforts have been exerted to analyse the propagation of elastic or acoustic waves in periodic composite materials called phononic crystals[1-3]. A lot of work is particularly focused on the characteristics of so-called phononic band gaps, in which elastic wave propagation is completely blocked. These are referred to as stop bands or band gaps. The development of smart materials used to design intelligent phononic crystals whose spectral width and band gap location can be actively tuned has received considerable attention[4-10].

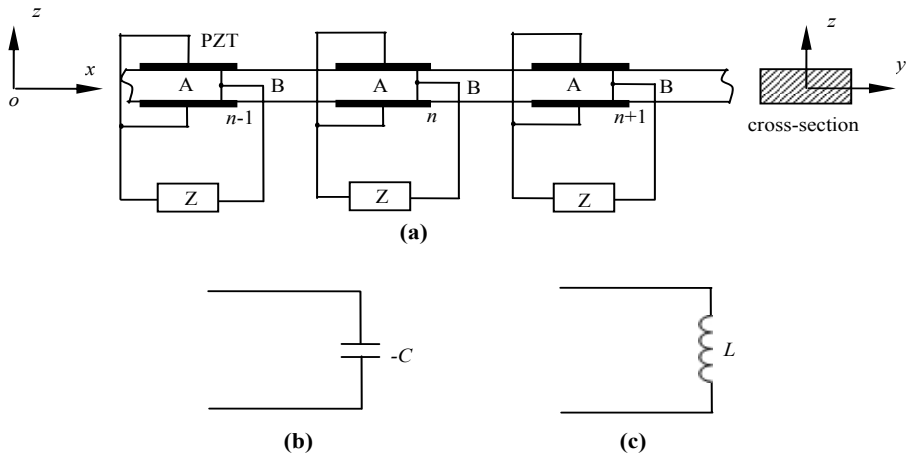

Figure 1 Phononic beam with negative capacitive or inductive piezo-shunts; **(a)** Schematic diagram of the configuration; **(b)** Negative capacitive shunting circuit. **(c)** Inductive shunting circuit.

Periodic arrays of inductive or negative capacitive shunted piezoelectric patches are employed to control the band gaps of phononic beams. An epoxy beam with periodically surface-bonded piezoelectric patches is designed, as shown in Figure 1. Each piezoelectric patch is connected to a single, independent inductive or negative capacitive circuit.

The location and the extent of induced band gaps depend on the mismatch in impedance genera-ted by each patch. The total impedance mismatch is deter-mined by the added mass and stiffness of each patch as well as the shunting electrical impedance. Therefore, the band gaps of the shunted phononic beam can be actively tuned by properly selecting the parameters of shunting circuits.

The shunting inductance combining with the intrinsic capacitance of piezoelectric patch constitutes an oscillator, which interacts with the matrix beam through electromechanical coupling effect. In analogy to locally resonant structures with mechanical vibrators, the beam with periodic inductive-shunts can form a locally resonant gap in it as well, which is closely related to the eigenfrequency of the resonant shunts. The eigenfrequency of the inductive shunting circuit can be expressed as

$$f = \frac{1}{2\pi\sqrt{LC_p}} \tag{1}$$

Phononics 2011: First International Conference on Phononic Crystals, Metamaterials and Optomechanics
Santa Fe, New Mexico, USA, May 29-June 2, 2011
PHONONICS-2011-0031

where C_p is the inherent capacitance of piezoelectric patches. However, the locally resonant gap induced by inductive shunts is not completely identical with the conventional locally resonant gap induced by mechanical vibrators in that the eigenfrequency of former type is out of the band gap, while the latter is in.

Different from the inductive shunts, the negative capacitive shunts are used to tune the Bragg gaps of the beam, because there is no local resonance in the shunting circuits. Nevertheless, the negative capacitive shunts can effectively increase the electromechanical coupling factor of the piezo-patches and modify the equivalent modulus of the elements bonded with piezo-patches in the beam, which can be given by

$$E_{\mathrm{p}} = \frac{h_p\left(C_p - C\right)}{h_p s_{11}^E\left(C_p - C\right) - {d_{31}}^2 A_s} \tag{2}$$

where s_{11}^E is the piezoelectric material's compliance coefficient at constant electric field intensity. d_{31} is the piezoelectric constant that couples the mechanical and electrical properties of the piezoelectric material. A_s is the area of electrodes. h_p is the thickness of piezoelectric patch. Contrary to inductive shunts which are passive circuits, the negative capacitive shunts are active circuits that have external energy input, so the proposed approach will be afflicted by instability problems[11,12]. To avert the system being destabilized by negative capacitive shunts, the stable conditions of the shunting system are investigated in detail.

Control of the band gaps of phononic beam with piezo-shunts is demonstrated numerically, employing transfer matrix method with periodic boundary conditions and the Bolch theorem. The variations of band gaps with different shunting parameters are discussed in the paper, subsequently. The result reveals that inductive shunts can induce local resonances in the beam and form locally resonant gaps around the eigenfrequency, but negative capacitive shunts can tune the Bragg gaps readily and effectively. The theoretical results are verified with commercial finite element software by calculating transmission properties of finite periods. Because negative capacitive shunted phononic beam are a non-conservative system with external energy input, the stability conditions are investigated in this paper. The result reveals that the stability can be judged readily by the value of equivalent modulus of the elements bonded with piezo-patches. Though negative modulus will occur in both inductive and negative capacitive shunting systems, the inductive shunting system is a conservative system which is stable, because its negative modulus is a dynamic value and frequency dependent, while the negative capacitive shunting system will become unstable, if the equivalent modulus becomes negative, which is a static value and frequency independent.

References

[1] D. J. Mead, *J. Sound Vib.* **11**, 181-197 (1970)
[2] D. J. Mead and S. Markus, *J. Sound Vib.* **90**, 1-24 (1983)
[3] M. S. Kushwaha, P. Halevi and L. Dobrzynski, *Phys. Lett. A* **71**,2022-2025 (1993)
[4] M. Ruzzene and A. Baz, *Proc. SPIE* **3991**, 389-407 (2000)
[5] A. Baz *J. Vibration and Acoustics*. **123**, 472-479 (2001)
[6] O. Thorp, M. Ruzzene and A. Baz, *Proc. of SPIE* **4331,** 218-238 (2001)
[7] O. Thorp, M. Ruzzene and A. Baz, *Smart Mater. Struct.* **14,** 594-604 (2005)
[8] A. Spadoni, M. Ruzzene and K. A. Cunefare, *J. Intell. Mater. Syst. Struct.* **20,** 979-90 (2009)
[9] F. Casadei, M. Ruzzene, L. Dozio and K. A. Cunefare, *Smart Mater. Struct.* **19,** 015002 (2010)
[10] S. B. Chen, X. Y. Han, D. L. Yu and J. H. Wen, *Acta Phys. Sin.* **59,** 387-392 (2010)
[11] S. Behrens, A. J. Fleming and S. O. R. Moheimani, *Smart Mater. Struct.* **12**, 18-28 (2003)
[12] B. de Marneffe and A. Preumont, *Smart Mater. Struct.* **17**, 035015 (2008)

Phononics 2011: First International Conference on Phononic Crystals, Metamaterials and Optomechanics
Santa Fe, New Mexico, USA, May 29-June 2, 2011
PHONONICS-2011-0041

The Role of Array Symmetry in the Transmission of Ultrasound through Periodically Perforated Plates

H. Estrada[1,2], P. Candelas[1], F. Belmar[1], A. Uris[1], V. Gómez[1], F. J. García de Abajo[3], F. Meseguer[1,2]

[1]Centro de Tecnologías Físicas, Unidad Asociada ICMM–CSIC/UPV, Universidad Politécnica de Valencia, Av. de los Naranjos s/n. 46022 Valencia, Spain
hector.estrada@icmm.csic.es, pcandelas@fis.upv.es, fbelmar@fis.upv.es, auris@fis.upv.es, vgomez@fis.upv.es, fmese@fis.upv.es
[2]Instituto de Ciencia de Materiales de Madrid (CSIC), Cantoblanco, 28049 Madrid, Spain
[3]Instituto de Óptica - CSIC, Serrano 121, 28006 Madrid, Spain
J.G.deAbajo@csic.es

Abstract: We present angle-resolved experimental results on the role of array symmetry in the transmission features of periodically perforated plates. A very rich interplay between Fabry-Perot single-hole resonances, coherent scattering and plate vibration is found. By comparing several spatial hole arrangements, the effects of the geometry are disentangled from the contribution of plate vibrations.

The study of periodic structures interacting with sound can be tracked back to the end of the 19th century with the work of Rayleigh[1], who studied the reflection coefficient of a one dimensional grating. Later, in 1953, Brillouin[2] attempted a unification of the concepts involved in the behavior of electromagnetic and mechanical waves in periodic media. More recently, the propagation of electromagnetic waves through metallic membranes perforated with subwavelength periodic hole arrays has received considerable attention. Experiments[3] have showed that at certain frequencies strongly correlated with the array period, light transmission per hole is higher than predicted for non-interacting holes theory[4]. These ideas, originally developed in the context of electromagnetic waves, have been transferred to acoustic waves[5-8] and this phenomenon is now known as Extraordinary Acoustic Transmission (EAT), although it has been recently demonstrated[9] that for the acoustic case there is not as extraordinary as in optics. Fabry-Perot resonances in the holes produce the main contribution to the full transmission peaks.

Our experimental setup is based on the well-known ultrasonic immersion technique. The plate is placed between the ultrasonic transducers (around 250 kHz) in a water tank. Measurements of transient signal are averaged over 100 runs. The plate is then rotated to obtain the dependence on the parallel-to-the-plate wave-vector (see Fig. 1). The transmission spectrum is normalized with the spectrum measured without the plate. The plate thickness is 2 mm and more than 1500 holes of 3 mm in diameter were drilled in aluminum and brass plates having different array geometries such as square, rectangular, triangular, and pseudo random. Transmission dispersion for these different array arrangements are shown in Fig. 2. The sound line does not correspond to the line where the data ends because our experimental setup cannot be used to measure plate rotation angles above 60º. In agreement with previous results[8,10] , a very rich interplay between hole resonances, coherent interference, and plate modes is observed in Fig. 2 **(a)**, **(b)**, and **(d)**. However, when the translational symmetry is broken by drilling the holes in a pseudo-random manner (Fig. 2**(c)**), the transmission dispersion becomes smoother. This allow us to identify the contribution of the perforated plate vibration, which can be seen as a minimum corresponding to a leaky surface mode.

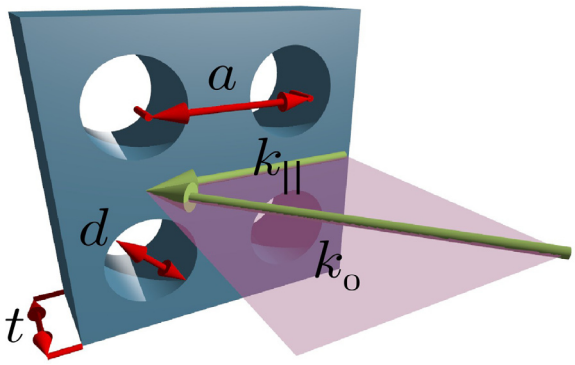

Figure 1 Scheme of the geometry for the transmission of ultrasound through perforated plates. An incident wave having wave-vector k_0 arrives at the plate of thickness t, which is perforated with holes of diameter d and period a. The parallel to the plate component of the incident wave-vector $k||$ is varied by rotating the plate with respect to the source.

Phononics 2011: First International Conference on Phononic Crystals, Metamaterials and Optomechanics
Santa Fe, New Mexico, USA, May 29-June 2, 2011
PHONONICS-2011-0041

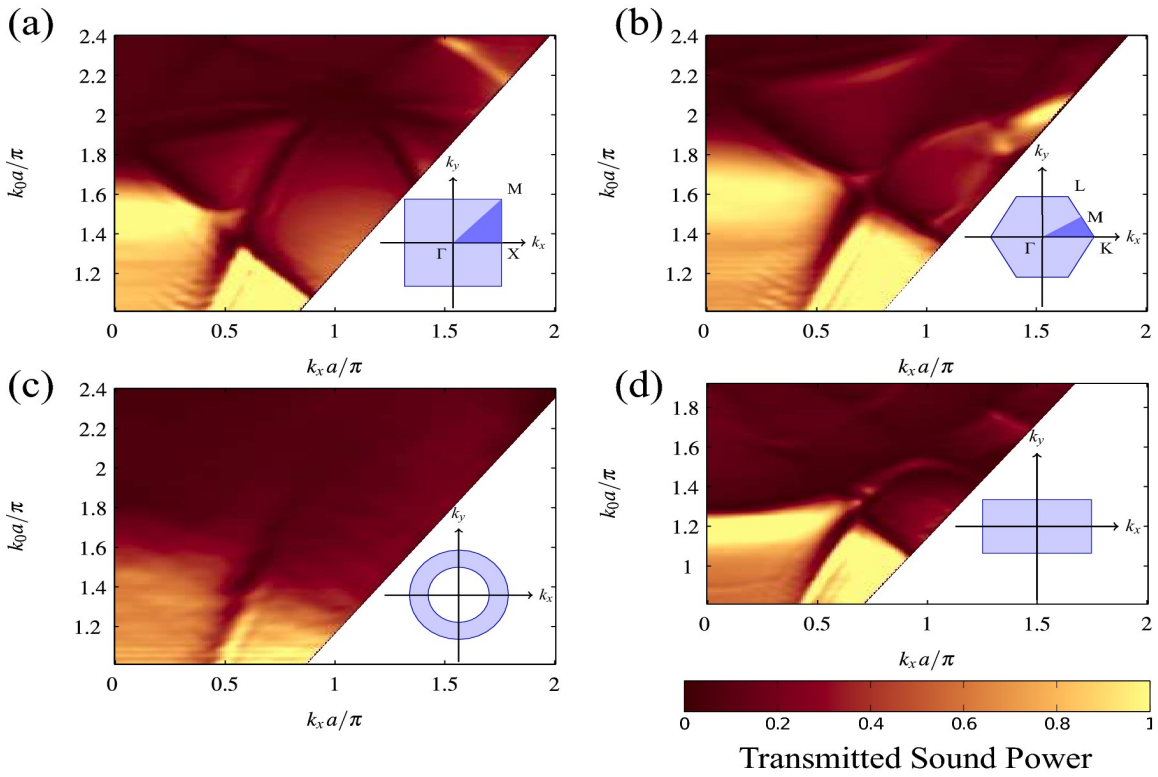

Figure 2 Transmitted sound power measured at ultrasonic frequencies for perforated plates of thickness t=2 mm immersed in water and different array geometries. The insets show the reciprocal space of the hole arrays and their corresponding orientation relative to the first Brillouin zone. **(a)** Square array of period a=5 mm drilled in an Al plate. **(b)** Triangular array of period a=5 mm drilled in an Al plate. **(c)** Pseudo-random array having an average period a=5 mm, also drilled in an Al plate. **(d)** Rectangular array of periods a_x=4 mm, a_y=6 mm drilled in a brass plate.

Additionally, full transmission is quenched to 1/2 in the absence of coherent interference. Translational symmetry is also the key factor for the appearance of the observed dips which vary depending on the geometry. These minima arise from the hybridization of Wood anomalies[11] (i.e. lattice modes) with plate modes. Pure Wood anomaly minima can be observed if the impedance mismatch between the holey plate and the surrounding fluid is large enough to assume that the plate is perfectly rigid and the sound cannot penetrate it. The crossing between the Wood anomaly and the surface mode can be clearly seen for the three symmetric arrays. This crossing is particularly interesting because it involves the surface mode, the Wood anomaly minimum, and the transmission peak, all of them hybridized. Thus, the array symmetry plays a key role in the transmission features of perforated plates. The existence of full transmission peaks and Wood anomaly minima, both depending on coherent interference among holes, can be only guaranteed by the translational symmetry of the array.

References

[1] Lord Rayleigh. *The Theory of Sound*, Vol. II. 2nd edition, Macmillan London (1896).
[2] L. Brillouin. *Wave Propagation in Periodic Structures*. Dover New York (1953).
[3] T. W. Ebbesen, H. J. Lezec, H. F. Ghaemi, T. Thio, and P. A. Wolff, *Nature*, **391**,667–669 (1998).
[4] H. A. Bethe. *Phys. Rev.*, **66**, 163–182 (1944).
[5] Bo Hou, Jun Mei, Manzhu Ke, Weijia Wen, Zhengyou Liu, Jing Shi, and Ping Sheng, *Phys. Rev. B*, **76**, 054303 (2007).
[6] J. Christensen, L. Martin-Moreno, and F. J. Garcia-Vidal, *Phys. Rev. Lett.*, **101**, 014301 (2008).
[7] H. Estrada, P. Candelas, A. Uris, F. Belmar, F. J. García de Abajo, and F. Meseguer, *Phys. Rev. Lett.*, **101**, 084302 (2008).
[8] H. Estrada, F. J. García de Abajo, P. Candelas, A. Uris, F. Belmar, and F. Meseguer, *Phys. Rev. Lett.*, **102**, 144301 (2009).
[9] F. J. García de Abajo, H. Estrada, and F. J. Meseguer, *New J. Phys.*, **11**, 093013 (2009).
[10] H. Estrada, P. Candelas, A. Uris, F. Belmar, F. J. García de Abajo, and F. Meseguer, *Appl. Phys. Lett.*, **95**, 051906 (2009).
[11] R. W. Wood, *Phil. Mag.*, **4**, 396 (1902).

Phononics 2011: First International Conference on Phononic Crystals, Metamaterials and Optomechanics
Santa Fe, New Mexico, USA, May 29-June 2, 2011
PHONONICS-2011-0044

Phonons on Complex Networks

Guimei Zhu[1,2] and Baowen Li[1,2]

[1] *NUS Graduate School for Integrative Sciences and Engineering, Singapore 117456, Singapore,*
[2] *Department of Physics, National University of Singapore, Singapore 117542, Singapore,*
g0801859@nus.edu.sg, phylibw@nus.edu.sg

Abstract: We map the nodes and edges of complex network to oscillators and couplings between them. We thus can study the multi-scale structures of networks through the properties of eigenmodes of laplacian matrix – *the phonons on complex networks*. The phonons from low to high frequencies are used as probes of the structural characteristics from macro- to micro-scales. This characteristic can be used as a structural measure of complex networks. These findings may have potential applications in real networks, such as heat conduction on nanotube/nanowire networks and biological networks.

Introduction

Vibrational dynamics has been widely used to study thermodynamic properties of various structures in solid-state physics and/or other disciplines. Since the structure is considered as a primary factor responsible for physical properties, reaching a reliable comparison of the structure patterns at different scales in a quantitative way is of primary importance for us to know the underlying structure how the dynamic transport processes of mass, energy, signal and/or information from micro- to macro-structural scales. The effect of network structures on electronic and thermal properties has been one of the most active topics in recent years[1, 2].

Methods

In this paper, we map the nodes and the edges to oscillators and couplings between them. The *vibration modes (phonons)* are used as probes of the structural patterns. One phonon with a specific frequency is sensitive only to the structural patterns matching in size with its frequency. By using all the vibration phonons from low to high frequencies we can detect the pattern properties from macro- to micro- scales.

The topological structure of a network can be described by an adjacency matrix A. The elements A_{ij} are 1 and 0 if the nodes i and j are connected and disconnected, respectively. We map the nodes to oscillators and the edges to harmonic couplings between the connected nodes. Denoting the displacements of the oscillators with $(y_1, y_2, \ldots y_N)$ the equations governing the dynamical process of the network reads, $\mu \ddot{y}_i = k\sum_{s=1}^{N} A_{is}\left(y_s - y_i\right)$, N is the network size, μ the mass of each oscillator and k the coupling strength. For simplicity, let $k/\mu = 1$. Assuming $Y \equiv Xe^{i\omega t}$, $Y^T \equiv [y_1, y_2, \ldots y_N]$, $X^T \equiv [x_1, x_2, \ldots x_N]$, the equations can be rewritten as, $\omega^2 X = GX$, G the coupling matrix, also named Laplacian Matrix, which reads,

$$G_{ij} = \begin{cases} \sum_{i=1}^{N} A_{ij} = k_i, & (i = j) \\ -A_{ij}, & (i \neq j) \end{cases} = k_i \delta_{ij} - A_{ij}. \qquad (1)$$

The eigenvalues of G are nonnegative and can be ranked as, $0 = \lambda_1 \leq \lambda_2 \cdots \leq \lambda_N$. Assuming the network is in a thermal bath with a definite temperature, a simple computation leads to the cross-correlations between the fluctuations of the phonons,

$$\left\langle y_i \cdot y_j \right\rangle \propto \left(G^{-1}\right)_{ij} = \sum_{m=2}^{N} \left(\lambda_m^{-1} \cdot X_m X_m^T\right)_{ij}. \qquad (2)$$

Phononics 2011: First International Conference on Phononic Crystals, Metamaterials and Optomechanics
Santa Fe, New Mexico, USA, May 29-June 2, 2011
PHONONICS-2011-0044

It follows that the contribution of an individual phonon is, $G_{ij}(m) \propto \left(\lambda_m^{-1} \cdot X_m X_m^T\right)_{ij}$. The phonons with small values of λ_i , the corresponding motions are collective and global, and can measure the characteristics of macro-scale patterns. The phonons with large values of λ_i, on the other hand, describe uncorrelated motions occurring in different micro-scale regions, which are sensitive to micro-scale patterns. Hence, the phonons can detect the structural patterns from macro- to micro-scales.

Results:

Figure 1 demonstrates that a phonon with a specific frequency is sensitive only to the structural patterns matching in size with its frequency.

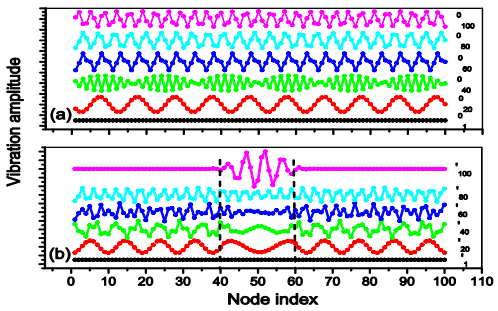

Figure 1 phonons on networks can be used as probes of structural patterns at different scales. (a) A circular network is constructed by connecting each nodes with its nearest four neighbors. The sizes is N=100. On this regular network, the phonons are periodic waves. The wavelength is measured in unite of the lattice size. (b) A densely connected deformation is constructed in the segment 40-60 by connecting each node in this region with its six nearest neighbors (instead of the originally four nearest neighbors). Phonons with comparatively large wavelenghths keep unchanged or deform slightly, while phonons matching with the deformation(e.g., λ'_{100}) become localized in the deformation region

We have applied the method to the Santa Fe Institute collaboration network[3]. We first normalize the components of the phonons, namely, $X_i^s = | X_i / \max(X_i) |,\ i = 1, 2, \cdots, N.$ Then a threshold τ^s can be used to identify the nodes involved in the phonons, respectively. The nodes with large values of component X_i^s ($\geq \tau^s$) are regarded as the nodes involved in the corresponding phonons. For each phonon, the components of the nodes involved in it are distinguishably large compared with that of the others. Hence, the τ^s -based results are robustness. In the present work, we choose the $\tau^s = 0.1$. The detail results are shown in Fig 2 (details can be seen from Ref [4]).

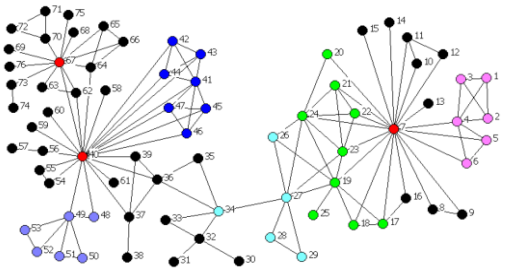

Figure 2 A part of largest component of the Santa Fe Institute collaboration network. There are totally 76 nodes. The phonons $\lambda_{76}, \lambda_{75}$ *and* λ_{74} can detect the three hubs 40, 7 and 67, marked with red color. The phonon. λ_{73} involves nodes 17 ~ 25 (green nodes), while the phonon λ_{72} covers the nodes 26 ~29 and 34 also (green and cyan). The three clusters 41 ~47 (blue), 1 ~ 6 (magenta), and 48 ~ 53 (violet), correspond to the phonons $\lambda_{70}, \lambda_{69}$ and λ_{68}, respectively.

Conclusions

To summarize, we have used the *phonon* to detect the structural patterns at different scales in model network and Santa Fe institute collaboration network. Because the phonons are sensitive only to the structural patterns matching in size with their wavelengths, the phonon from high to low frequencies can capture the pattern characteristics in a coarse-grain way.

References:

1 G. Zhu, H. Yang, C. Yin, B. Li, *Physical Review E* **77**, 066113 (2008).
2 H. J. Yang, C. Y. Yin, G. M. Zhu, B. Li, *Physical Review E* **77**, 045101 (2008).
3 M. Girvan and M. E. J. Newman, *Proceedings of the National Academy of Sciences of the United States of America* **99**, 7821 (2002).
4 G. Zhu, H. Yang, J. Ren, B. Li, *to be published.*

Phononics 2011: First International Conference on Phononic Crystals, Metamaterials and Optomechanics
Santa Fe, New Mexico, USA, May 29-June 2, 2011
PHONONICS-2011-0055

Optimal Design of Nonlinear Wave Devices

Jakob S. Jensen

Department of Mechanical Engineering, Technical University of Denmark
Nils Koppels Allé, Building 404, DK-2800 Kgs. Lyngby, Denmark
jsj@mek.dtu.dk

Abstract: The method of topology optimization is applied to wave propagation problems with nonlinearities. In the general case the iterative design procedure should be based on transient simulation of the wave propagation, but in the special case of non-instantaneous nonlinearities a steady-state optimization formulation can be applied. The latter case is exemplified by the design of a 1D optical diode.

Topology optimization has within the last decade been used successfully to design bandgap materials and devices. A gradient-based material distribution method is used to design photonic crystals with maximized bandgaps[1] and later a similar method was applied to design phononic crystals[2] and finite structures and devices with bandgap properties[2-4].

In this work we aim to extend the use of gradient-based material distribution methods to deal with wave devices that display nonlinear behavior. As is well known, the presence of nonlinearities can significantly alter the behavior of bandgap materials and structures, but can also be used to create devices with novel functionality that cannot be accomplished with a pure linear behavior.

In the general case the presence of nonlinearities generates higher order harmonics in the response and transient simulations are thus needed for the analysis of the device performance.

Steady-state model with a non-instantaneous nonlinearity
However, in certain cases it may be relevant to study a steady-state model of the nonlinear wave propagation problem. Such a model may arise if we consider a non-instantaneous nonlinearity such as e.g. in nonlinear optics with a dielectric permittivity that depends on the time-averaged intensity of the electric field.

By treating the nonlinear wave propagation problem in a steady-state framework we can reduce the computational requirements considerably. The general nonlinear model is written as follows

$$\nabla \cdot (A(u)\nabla u) + B(u)k^2 u = 0 \tag{1}$$

in which A and B are two material coefficients that depend on the local field intensity and k is the wavenumber.

Equation (1) can conveniently be solved using a standard finite element method combined with a complex incremental Newton-Raphson procedure[4]. In addition design sensitivity analysis can be performed for the finite element model using the adjoint method[4].

Example: one-dimensional optical diode
As an application example we demonstrate the design of an optical diode[5]. Ideally, the diode allows for undisturbed transmission in one direction whereas the propagation in the opposite direction is hindered. As objective for the optimization we choose to maximize the difference in transmission in the two opposing directions and thereby create a diode-like performance of the device. The optimization problem is illustrated in Figure 1(**a**).

In the device we aim to distribute two materials, a linear dielectric material with the relative permittivity $\varepsilon_r=1$ and a nonlinear material with relative permittivity $\varepsilon_r=\varepsilon(1+\gamma|e|^2)$, in which ε is the linear permittivity of the material, $|e|^2$ is the intensity of the electric field and γ is a nonlinear parameter. The permittivity in each finite element in the discretized model is governed by a single continuous design variable. The optimized set of design variables is found with an iterative gradient-based procedure using the method of

Phononics 2011: First International Conference on Phononic Crystals, Metamaterials and Optomechanics
Santa Fe, New Mexico, USA, May 29-June 2, 2011
PHONONICS-2011-0055

moving asymptotes[6].

Figure 1(**b**) shows a specific optimized design obtained for ε=1.1 and γ=0.1. Plotted in the figure are the values of the continuous design variable for each finite element with the value 0 corresponding to the linear material and the value 1 corresponding to the nonlinear material. It is seen that the optimized design consists of alternating sections of nonlinear and linear dielectric material. Figure 1(**c**) shows the magnitude of the effective permittivity for waves propagating in opposing directions, indicating the large difference in material properties which is obtained.

As a result of the material distribution a difference in transmission in the two opposing propagation direction of about 10 percent is noted. However, larger differences can be obtained if the structure is longer compared to the wavelength.

The results for the 1D diode was supplemented with an optimization study for a 2D waveguide that displays a transmission that is a highly nonlinear function of the input intensity[5]. Currently, the diode example is being re-investigated using a transient formulation including an investigation of design of an optical switch. Additionally, the transient problem is being implemented for mechanics problems as well.

References

[1] S. J. Cox and D. C. Dobson, *SIAM J. Appl. Math.* **59**, 2108-2120 (1999).
[2] O. Sigmund and J. S. Jensen, *Phil. Trans. R. Soc. Lond. A* **92**, 1001-1019 (2003).
[3] M. I. Hussein, K. Hamza, G. M. Hulbert, and K. Saitou, *Waves in Random and Complex Media* **17**, 491–510 (2007).
[4] C. J. Rupp, A. Evgrafov, K. Maute, and M. L. Dunn, *Structural and Multidisciplinary Optimization* **34**, 111–121 (2007).
[5] J. S. Jensen, submitted (2011).
[6] K. Svanberg, *Int. J. Numer. Methods Eng.* **24**, 359–373 (1987).

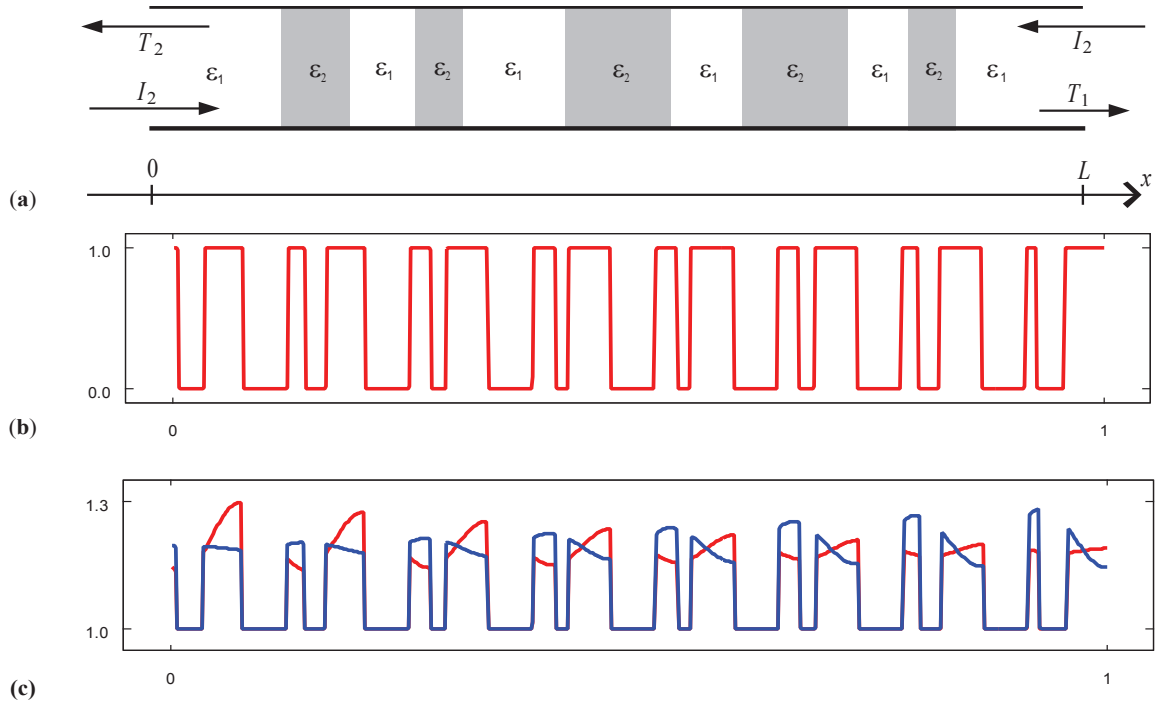

Figure 1 Example of an optimized 1D nonlinear wave device. (**a**) Design problem: the difference in transmission of incoming waves from opposing directions is maximized by distribution a linear dielectric material ε_1 and a nonlinear dielectric material ε_2, (**b**) the resulting design illustrated by the elementwise optimized values of the design variable (0 is linear and 1 is nonlinear), (**c**) the effective material permittivity in the structure when the wave propgates towards right (red line) and towards left (blue line).

Phononics 2011: First International Conference on Phononic Crystals, Metamaterials and Optomechanics
Santa Fe, New Mexico, USA, May 29-June 2, 2011
PHONONICS-2011-0057

EFIT Simulation of Ultrasonic Wave Propagation in Complex Microfluidic Structures

M. Zubtsov[1], R. Grundman[1], R. Lucklum[1]

[1] *Institute of Micro and Sensor Systems, Otto-von-Guericke-University, Magdeburg, Germany*
mikhail.zubtsov@ovgu.de, ralf.lucklum@ovgu.de

Abstract: The Elastodynamic Finite Integration Technique (EFIT) is used to simulate ultrasonic wave propagation in complex microfluidic structures comprising fluidic channels, phononic crystal structures and piezoelectric transducers. An EFIT computational math is combined with MATLAB coding. The viability of the approach is demonstrated.

The precise spatial and temporal control afforded by microfluidic devices make them uniquely suited to solve many challenging problems in sample treatment and analysis at micro and nano scales. Dealing with the dynamics and engineering of fluids confined on the micrometer scale microfluidics involves the large number of different basic phenomena and a combination of a broad variety of effects and means including ultrasound, which has shown to be a viable technique for some microfluidic tasks like microparticles manipulation, stirring, mixing and streaming of microvolumes [1] as well as characterization. Phononic crystal devices may significantly expand the use of ultrasound in microfluidic systems, since they offer a wide range of functionalities [2, 3], which can be beneficially utilized to improve microfluidic system operation and enable new applications.

However, in order to integrate this new class of acoustically active and reactive devices into existing liquid manipulation units, an analysis of the total acoustic field is required. There is an apparent need for a better understanding of interactions between ultrasonic waves and complex structures comprising both active and reactive components. We consider an EFIT, which relies on the direct discretization of the Newton-Cauchy's equation of motion and the equation of deformation rate, and where all field quantities are function of position and time, as a proper math ground for an efficient simulation tools which can solve this problem.

The EFIT starts with the elastodynamic governing equations in integral form and simulates the ultrasonic wave field without any approximations. Using unique discretization of the basic field equations on a staggered grid the method permits to implement a pertinent code for widely arbitrary inhomogeneous composites [4]. In general, the FIT also permits a unified treatment of the acoustic, electromagnetic, elastodynamic and piezoelectric cases [5]. In all these instances, the underlying governing equations in integral form are discretized on the same a dual grid complex in space and time, which yields the so-called discrete grid equations. Another advantage of the FIT approach is that the resulting discrete matrix equations represent a consistent one-to-one translation of the underlying field equations. The use of discrete topological operators ensures important vector analytical properties in the discrete grid space.

The FIT implicitly insures that the numerical results are free of late-time instabilities and artificial sources. On account of the complexity of multiple acoustically active and reactive units including PZT devices integrated into a single structure we consider this unified approach as the most appropriate to the problem, in particular, taking into account simplicity of the FIT, which allows an easy and efficient implementation on various computer architectures.

Phononics 2011: First International Conference on Phononic Crystals, Metamaterials and Optomechanics
Santa Fe, New Mexico, USA, May 29-June 2, 2011
PHONONICS-2011-0057

A regularly perforated wall between two parallel and adjacent fluidic channels has been used as the first test sample to evaluate applicability of the method. This model represents one of possible setups of phononic crystal sensor integrated into a microfluidic system. The EFIT-code and other relevant routines are implemented with MATLAB which provides a user interface and different output opportunities that help to analyze and visualize the simulation results. The possibility of parallel computing to afford bigger and/or more detailed models has also been realized.

A good agreement between the first EFIT results and similar simulations using COMSOL Multiphysics™ and FTDT has been demonstrated. Basic simulations we have performed show all the kind of interactions between propagating wave and the structure, which are typical for an acoustic-structure interaction,

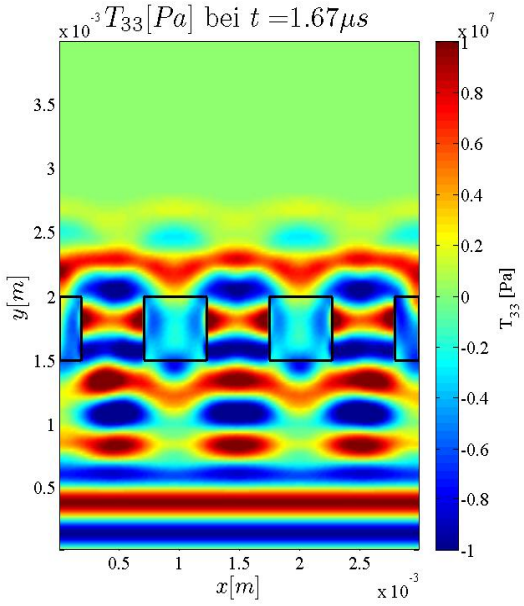

Figure 1 Spatial distribution of T_{33} field in the diffraction of plane wave at subwavelength regime. Perforation periodicity **a**=1 mm, the wavelength **λ**=**a**, and the size of the perforation **b**=**a**/2.

including those which are not available in semi-analytic methods. Some are illustrated on the Fig.1. This presents a time-domain snapshot of a time-harmonic acoustic plane wave impinging on an infinite and regularly perforated quasi-1D plate. This particular setup, specifically, diffraction of emanating from the wall of fluidic channel plane wave and impinging on regularly perforated intermediate wall at the subwavelength regime, relates to one of possible sensing applications. Namely, we consider presented here effects of mode conversion as well as effects which are coupled with the resonant propagation through the plate as good candidates that may afford a distinctive measurand feature.

References

[1] T. Torii, *Advances in Biochemical Engineering-Biotechnology*, **119**, 165-177 (2010).
[2] R. H. Olsson III and I. El-Kady, *Meas. Sci. Technol*., **20** (2008).
[3] Sz-Chin Steven Lin et al., *Phys. Rev*. B **79**, 094302 (2009).
[4] R. Marklein, *Numerical Methods for the Modeling of Acoustic, Electromagnetic, Elastic and Piezoelectric Wave Propagation Problems in the Time Domain Based on the Finite Integration Technique*, Shaker Verlag, Aachen, (1997).
[5] R. Marklein, *The Finite Integration Technique as a General Tool to Compute Acoustic, Electromagnetic, Elastodynamic, and Coupled Wave Fields*, in W. R. Stone (ed.), Review of Radio Science, 1999-2002 URSI, IEEE Press and John Wiley and Sons, pp. 201-244 (2002).

Phononics 2011: First International Conference on Phononic Crystals, Metamaterials and Optomechanics
Santa Fe, New Mexico, USA, May 29-June 2, 2011
PHONONICS-2011-0058

Acoustic Beams in Finite Sonic Crystals

V. Romero-García[1,4], R. Picó[2], V. Sánchez-Morcillo[2], L.M. Garcia-Raffi[3], J.V. Sánchez-Pérez[4], K. Staliunas[5]

[1] *Instituto de Ciencia de Materiales de Madrid, Consejo Superior de Investigaciones Científicas, Spain*
virogar1@gmail.com,
[2] *Instituto de Investigación para la Gestión Integrada de zonas Costeras, Universidad Politécnica de Valencia, Spain*
rpico@fis.upv.es, victorsm@upv.es,
[3] *Instituto Universitario de Matemática Pura y Aplicada, Universidad Politécnica de Valencia, Spain*
lmgarcia@mat.upv.es
[4] *Centro de Tecnologías Físicas: A.M.A, Universidad Politécnica de Valencia, Spain,*
virogar1@gmail.com, jusanc@fis.upv.es
[5] *Departament de Fisica i Enginyeria Nuclear, Universitat Politecnica de Catalunya (UPC), Spain*
kestutis.staliunas@icrea.es

Abstract: The physical properties of 2D finite periodic arrays are explored using acoustic beams with finite spatial width. Multiple Scattering Theory and the Plane Wave Expansion Method are used to study the differences between the approximation of infinite periodic medium and the finite case. In the most experimental cases the physical properties of the system are constrained by both the size of the sample and the width of the acoustic beam.

A Sonic Crystal is a periodic arrangement of cylindrical inclusions embedded in a homogeneous host material. The host material may be solid, the term Phononic Crystal is used in this case. For many applications usually these scatterers can be considered as infinitely rigid and the propagation inside them is not possible. Sonic Crystals can be designed in order to guide the acoustic energy in an appropriate way to present particular effects like focalization, auto-collimation or filtering.

The propagation of acoustic waves in a 2D periodic media can be described from its dispersion relation and the iso-frequency contours. Band gaps and propagation curves describe the propagation features for a specific direction in an infinite crystal. However, the sonic crystal is composed by a finite number of scatterers and thus, its finite size must be taken into account. The theoretical approach for a 2D finite period array is more complicated. If the beam is wide enough to be comparable to the size of the crystal at the front interface, the edge effects may become important and they cannot be neglected. It is the same case at opposite case: extremely narrow beams (comparable to the period of the crystal) do not propagate though the crystal as plane waves in a periodic medium. In the field acoustics, little attention has been paid to investigate how the finitude of the beam and the size of the sample may affect wave propagation through and outside the crystal.

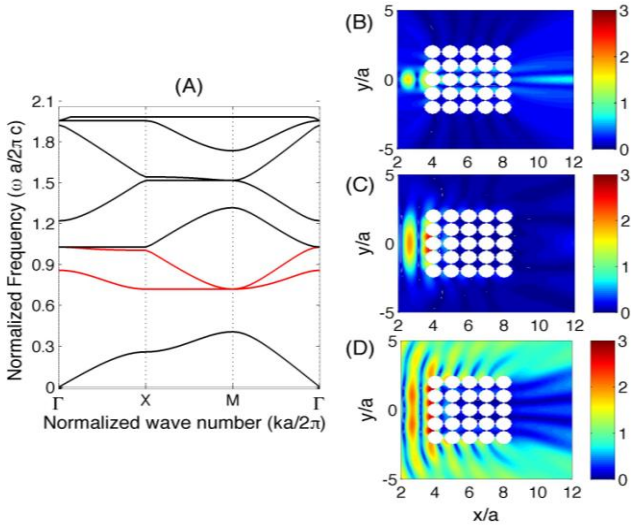

Figure 1 (A) Acoustic Band Structure of a Sonic Crystal with square periodicity (r=1m, a=0.4545). Beam propagation trhough the crystal for different beam widths (B) s=0.5, (C) s=2, and (D) s=1000 (plane wave) at f=170Hz

Multiple Scattering Theory[1] (MST) is used to solve the scattering problem of a **finite** width beam produced by the array of scatterers. A distribution of 5x5 infinite straight cylinders with radius a=0.4545 and separated r=1 (normalized units), parallel to the *z*-axis are located at (R_i, θ_i) of diameters D_i with

Phononics 2011: First International Conference on Phononic Crystals, Metamaterials and Optomechanics
Santa Fe, New Mexico, USA, May 29-June 2, 2011
PHONONICS-2011-0058

i=1, *2*, …, *N.* to form a regular square array perpendicular to the *x*-*y* plane. The total pressure in the point (*x*,*y*) is

$$P(x,y) = e^{ikx} e^{\frac{-y}{\sigma}} + \sum_{l=1}^{N} \sum_{s=-\infty}^{\infty} A_{ls} H_s(kr_l) e^{is\theta_l} \qquad (1)$$

where A_{ls} are determined by the solution of the system of equations obtained by MST, r_l and θ_l are the polar coordinates of the measuring point respect to the *l*–th scatterer and σ determines the width of the beam.

The transmission properties of the crystal are evaluated using MST. Figure 1A shows the band structure of the SC obtained using the plane wave expansion[2]. For a frequency lying in the Band Gap Figures 1B,1C and 1D show the transmission of beams with different sizes impinging at the left side of the crystal. The attenuation is optimized if the width of the beam is similar to the size of the sample.

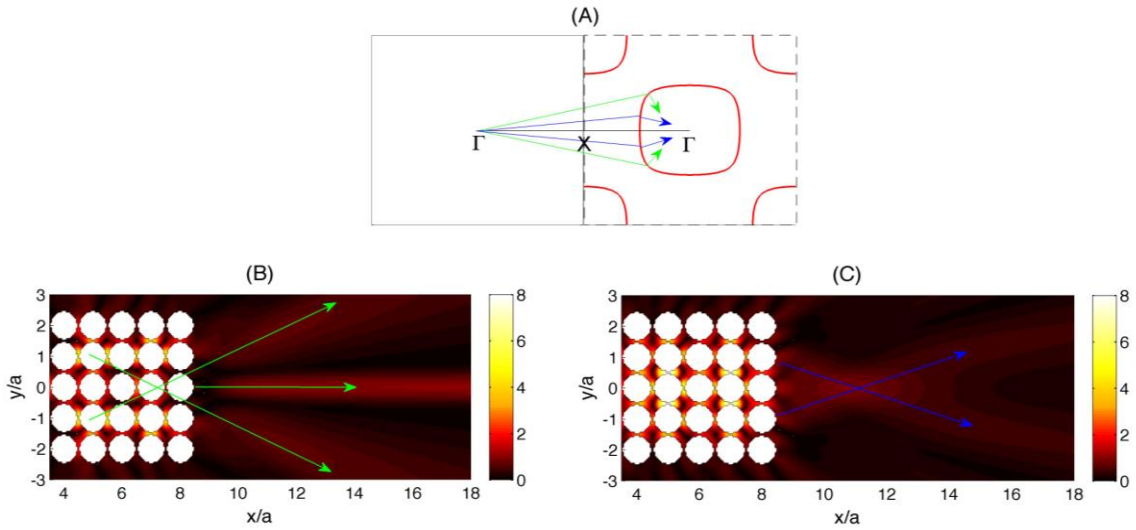

Figure 2. (A) Iso-frequency contours of the Bloch modes for the same SC as in Figure 1. The curves correspond to f=270Hz (second and third bands, in red in Figure 1A). Blue and green lines represent the projection on the curves of the spatial components of a wide and narrow beam respectively. Beam propagation behind the crystal for (B) a narrow beam (s=0.5) and (C) a plane wave (s =1000).

For wider beams (Figure 1D), the diffraction effect at the edges becomes important. The propagation of waves around the sample increases the total sound field behind the crystal. In the case of very narrow beams (Figure 1B), the propagation through the crystal is like in a homogeneous medium. In this case, the beam is not impinging the scatterers, and despite the frequency corresponds to the bandgap, it propagates through the crystal with a very low attenuation.

Special phenomena like focalization induced by propagation in a periodic medium may be significantly altered if the size of the beam is considered. For very narrow beams (Figure 2B) the Sonic Crystal in the second and third bands splits into three beams. Besides, for a beam as wide as the sample (Figure 2C) the focalization is produced some periods behind the crystal.

References

[1] P.A. Martin, *Multiple Scattering: Interaction of Time-Harmonic Waves with N Obstacles*, Cambridge University Press, UK (2006).
[2] M.S. Kushwaha, P. Halevi, G Martínez, L dobrynski and Djafari-Rouhani. *Phys. Rev. B* **49**, (4) 2313 (1994).

Phononics 2011: First International Conference on Phononic Crystals, Metamaterials and Optomechanics
Santa Fe, New Mexico, USA, May 29-June 2, 2011
PHONONICS-2011-0067

Broadband Vibration Attenuation Induced by Periodic Arrays of Feedback Shunted Piezoelectric Patches on Beams

Gang Wang, Shengbing Chen, Jihong Wen

Institute of Mechatronical Engineering, National University of Defense Technology, Changsha, China
and the Key Laboratory of Photonic and Phononic Crystal, Ministry of Education, China
wg.nudt@gmail.com

Abstract: The effect of periodic arrays of feedback shunted piezoelectric patches in vibration attenuation of flexible beams is analyzed theoretically and experimentally. Broadband vibration attenuations are observed no mater in or out of the band gaps. The proposed concept is validated experimentally on a suspended epoxy beam.

The present work involves a feedback shunting strategy in the phononic crystals (PCs) composed of periodic array of shunted PZT patches and a flexible beam for the broadband attenuation of vibration. The effect of periodic arrays of feedback shunted piezoelectric (PZT) patches in vibration attenuation of flexible beams is analyzed theoretically and experimentally. Each pair of surface-bonded piezoelectric patches is linked with a uniform and isolated feedback circuit. The voltage generated by one piezoelectric patch of the pair is amplified and applied to the other. Numerical model based on the transfer matrix methodology are developed to predict the transmission of vibration and the frequency ranges of band gaps in the proposed periodic smart structure. Broadband vibration attenuations are observed no mater in or out of the band gaps. The proposed concept is validated on a suspended epoxy beam driven by a shaker. Experimental results are presented in terms of vibration transmissions recorded using two accelerometers placed on both sides of the beam.

As illustrated in Fig. 1, pairs of PZT patches are periodically stuck to the surface of a beam to construct a 1D PC. Each pair of PZT patches are placed with opposite polarizing directions along the *z*-axis and linked with a uniform shunting circuit. The beam's segments with the PZT patch are denoted as I, while the others are denoted as II. Each shunting circuit is composed a operational amplifier (opamp) and two resistors R_1 and R_2. The voltage signal from one PZT patch is amplified and adds on the other. We call it the feedback shunts.

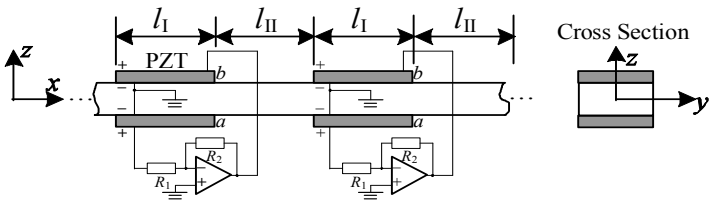

Figure 1 Beam with arrays of PZT patches and feedback shunting circuits.

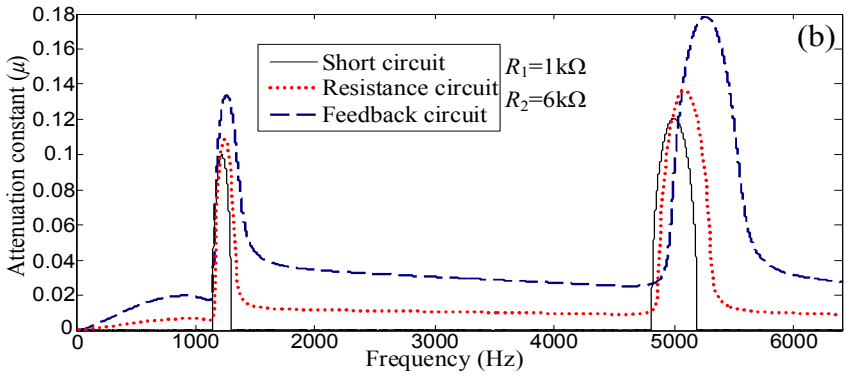

Figure 2 Calculated attenuation constants of the one-dimensional phononic crystals composed of an epoxy beam and shunted PZT patches. The solid, dotted and dashed lines represent the results for short, resistance, and feedback shunting circuits respectively.

Figure 2 illustrates the calculated attenuation constants of 1D PCs containing different shunting circuits. The dashed lines in Fig. 3 represent the results corresponding to the feedback shunting circuit

Phononics 2011: First International Conference on Phononic Crystals, Metamaterials and Optomechanics
Santa Fe, New Mexico, USA, May 29-June 2, 2011
PHONONICS-2011-0067

in this paper. For comparison, results corresponding to the resistance (R_1) shunting circuit and short circuit are also calculated and illustrated as solid and dotted lines in Fig. 2, respectively. Compared with other shunting circuits, the feedback one can evidently increase the attenuations at almost all frequencies no matter in or out of band gaps. In detail, original band gaps are widened and the corresponding attenuations are strengthened. Moreover, the attenuations out of band gaps that caused by damping are also enlarged dramatically by the feedback shunting circuits.

To validate the theoretical results, vibration experiments were performed on a 1D PC composed of an epoxy beam and periodic arrays of PZT-5H patches. The total length of the beam was 0.64 meters, where a periodic structure with 8 periods is constructed.

Figure 3 illustrated the measured transmission of the 1D PC. The overall view of the experimental results is shown in Fig. 3(a), while other subfigures (b)-(d) are zoomed in view of Fig. 3(a) within different frequency ranges. For comparison, the transmission of the 1D PC with short cut circuits, i.e., all electrodes of the PZT patches are shorted, is plotted as thin solid line in Fig. 3. All the experimental results illustrate in Fig. 3 basically match with the theoretical predictions. Moreover, the dashed and dotted lines in Fig. 3 represent the results corresponding to that only 5 or 2 PZT patches near the exciting point that are connected to the feedback shunting circuits. Coinciding with a basic characteristic of PCs, the attenuations are always weakened proportionally when the number of periodicity decreases.

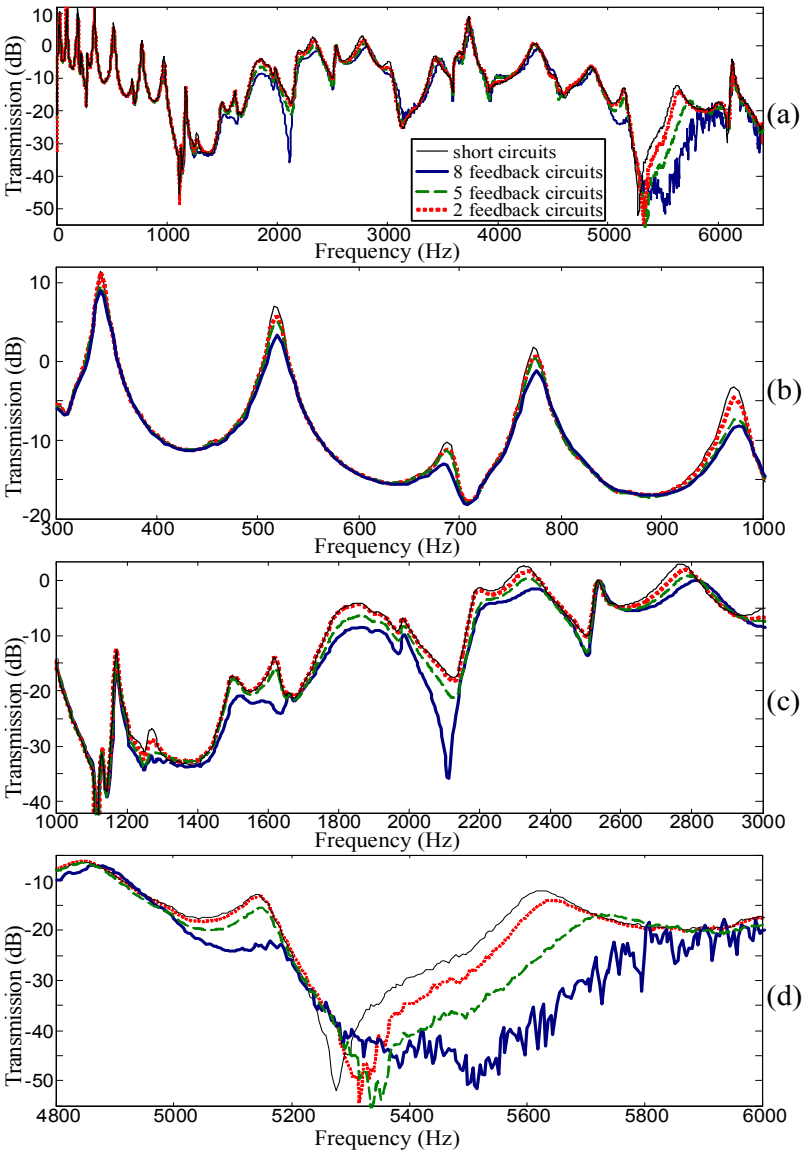

Figure 3 Measured transmission of the 1D phononic crystal with feedback shunting circuits. The thick solid lines, dashed line and dotted line represent the results corresponding to the cases when 8, 5 and 2 PZT patches near the exciting point are connected with the feedback shunting circuits, respectively. The thin solid lines represent the result when all electrodes of the PZT patches are shorted and are used for comparison.

Phononics 2011: First International Conference on Phononic Crystals, Metamaterials and Optomechanics
Santa Fe, New Mexico, USA, May 29-June 2, 2011
PHONONICS-2011-0069

Phase-controlling properties in phononic crystals

N. Swinteck [1], S. Bringuier [1], J.-F. Robillard [2], J.O. Vasseur [2], A.C. Hladky [2] and P.A. Deymier [1]

[1]*Department of Materials Science and Engineering, University of Arizona, Tucson, Az 85721, USA*

[2]*Institut d'Electronique, de Micro-électroniqueet de Nanotechnologie, UMR CNRS 8520, CitéScientifique, 59652 Villeneuve d'AscqCedex, France*

swinteck@email.arizona.edu

Abstract: We deliver a complete phase-space analysis of two well-studied PC systems to reveal the mechanisms behind phase-manipulation of propagating elastic waves in these composite structures. A triangular-array of steel cylinders embedded in a host matrix of methanol and a square-array of Polyvinylchloride cylinders embedded in a host matrix of air show band structures and equi-frequency contours (EFCs) with very different features, yet phase-control is possible in both systems. We find that phase-control depends on (1) whether or not the wave and group velocity vectors in the PC are collinear and (2) whether or not the excited Bloch waves in the PC have the same phase velocity. The results gathered in this study can be used to draw general conclusions about the reality of phase-control in many other types of PCs.

Phononic crystals (PCs) are composite materials comprised of periodic arrays of elastic inclusions embedded in an elastic matrix. The majority of research in the field of phononics has been aimed at understanding how the scattering of elastic waves impacts the spectral and wave-vector properties of the crystal. Past efforts have shown PCs with numerous, useful properties including transmission band gaps, local wave-guiding modes, filtering and multiplexing capabilities, and unique refractive behavior [1-4]. Several functional acoustic devices have resulted from exploitation of these exceptional properties. Progress in the field of phononics is directly coupled to the development of new acoustic based technologies, and for this, it is important for researchers to adventure beyond the contemporary functionalities of today's PCs.

An avenue that has been overlooked in the field of phononics is the impact PCs have on the relative phase of propagating elastic waves. The concept of phase-control between incident waves in any PC can be realized through thorough analysis of its band structure and equifrequency contours (EFCs). One condition must firstly be satisfied for the possibility of phase-control: all incident elastic waves that are transmitted through the PC must have an associated Bloch wave with a non-zero degree of refraction. If the degree of refraction for all incident waves is zero, then the projection of each wave vector in the PC onto the direction consistent with the group velocity vector is the same and a phase-shift cannot possibly result. The EFC corresponding to this very unique scenario is a perfect square either centered on or off the gamma point. With the knowledge that positive or negative refraction must occur, there are two general schemes amongst PC EFCs that outline the possibility for phase-control. One scheme is where the phase velocity of all excited Bloch modes is identical—a circular EFC centered on the Gamma point has such a property because the magnitude of all wave vectors in the PC is the same. A relative phase-shift between propagating waves in this type of PC comes from waves of the same phase velocity traveling different distances through the crystal. The second scheme applies to most PC EFC structures. In the case where wave vectors in the PC are non-collinear with group velocity vectors (phase velocities of Bloch waves are different) and each excited Bloch wave has a unique degree of refraction, a relative phase shift occurs

Phononics 2011: First International Conference on Phononic Crystals, Metamaterials and Optomechanics
Santa Fe, New Mexico, USA, May 29-June 2, 2011
PHONONICS-2011-0069

between propagating waves. Each wave vector in the PC projects differently onto its associated path of propagation (group velocity vector) and the phase velocity of the excited mode is different along this path, giving a slightly different quantification for phase shift as compared to scheme one. Interestingly, since these two scenarios apply to most types of PC EFCs, phase-control can be realized with a large number of different PCs. Changing the incident angles of the elastic waves entering the PC, varying the PC length, and altering the initial relative phase between input signals, are some means of controlling the output signal of the PC device. Such knowledge can possibly enhance the performance of current acoustic based technologies utilizing PCs and lead to completely novel concepts of future phononic devices.

We investigate the phase-properties of two PCs to link EFC features with the phase-relationship between propagating elastic waves. Our first PC is a triangular lattice of steel cylinders embedded in a host matrix of methanol, all in water. The diameter of the inclusions is 1.02 mm and the lattice spacing is 1.27 mm. Our second PC is a square lattice of Polyvinylchloride (PVC) cylinders embedded in a host matrix of air, all in a surrounding environment of air. The diameter of the inclusions is 25.8 mm and the lattice spacing is 27 mm. The first PC, at an operating frequency of 530 – 570 kHz, has a circular EFC centered on the Gamma point whereby the wave and group velocity vector are collinear and the phase-velocity of all excited Bloch modes is identical. The second PC, at an operating frequency of 13.5 kHz, has a square-like EFC centered off the Gamma point. Here, the wave and group velocity vectors are non-collinear and each excited Bloch mode has a unique phase velocity associated with it. Figure 1 shows the relative phase-shift between several pairs of incident acoustic waves for the PC consisting of a triangular lattice of steel cylinders embedded in a host matrix of methanol (550 kHz). Figure 2 shows the relative phase-shift between several pairs of incident acoustic waves for the PC consisting of a square lattice of PVC cylinders embedded in a host matrix of air (13.5 kHz). By utilizing the phase-information contained in Figure 2 and including an additional assessment for the phase-shift incurred on the exit side of the PVC-Air PC, we demonstrate complete control over the relative phase of two acoustic inputs by modulating their initial relative phase by π and 2π radians. Figures 3a and 3c show finite-difference-time-domain simulations (plots of instantaneous pressure) of two acoustic beams entering the PVC-Air PC. Figure 3a shows a crystal of length 621mm and Figure 3c shows a crystal of length 1242 mm. The time average of instantaneous pressure taken over one cycle (reported as average pressure) is shown in Figures 3b and 3d. Average pressure readings are taken along cuts where the acoustic beams intersect (black lines in Figures 3a and 3c). If the beams are in-phase, the average pressure reading will yield a maximum. If the beams are out of phase, the average pressure cut will show a minimum. Figure 3b shows that with a crystal of length 621mm, we observe a change in relative phase of π—the input average pressure cut shows a minimum, while the output average pressure cut shows a maximum. Figure 3d shows that with a crystal of length 1242mm, we observe a change in relative phase of 2π— the input average pressure cut shows a minimum and the output average pressure cut shows a minimum. This demonstrates a phase modulation of π and 2π radians based solely on changing the PC length. Similar control can be achieved by altering the angles and keeping the PC length constant. This is one example, of many, where precise phase-control exists between acoustic beam pairs.

Phononics 2011: First International Conference on Phononic Crystals, Metamaterials and Optomechanics
Santa Fe, New Mexico, USA, May 29-June 2, 2011
PHONONICS-2011-0071

New Directions in the Analysis of Nano-Scale Phononic and Nonlinear Metamaterial Systems

Michael J. Leamy[1]

[1] *George W. Woodruff School of Mechanical Engineering, Georgia Institute of Technology,771 Ferst Drive N.W., Atlanta, GA, USA*
michael.leamy@me.gatech.edu

Abstract: This talk will focus on two directions being pursued by the author and his co-workers in the areas of (i) multi-scale modeling of phonon spectra and dispersion in reduced dimensional nano-scale systems (e.g., carbon nanotubes), and (ii) analysis of phononic wave propagation in nonlinear metamaterials using asymptotic techniques.

The first part of this talk will address a multi-scale modelling approach being pursued by the author for predicting phonon spectra and dispersion in reduced dimensional materials, such as graphene sheets, nanotubes, and nanotoroids. For reduced-dimension nanophononic systems with large unit cells (e.g., 'supercells' housing defects or unit cells capturing non-ideal geometries such as embodied by 'wavy' nanotubes), manifold-based finite element modelling is advantageous for several reasons, to include large reduction in degrees of freedom, applicability to complex geometries, and the presence of a natural curvilinear basis for describing wave vector components. Reduced-dimension materials are quite unlike full-dimensional materials in that they are neither space-filling nor simply-connected, and thus require manifolds for representation. For example, a carbon nanotube unit cell must fully wrap around the circumference in order to truly repeat, which results in two ends of the unit cell sharing the same atoms. This complex geometry can be described efficiently using an intrinsic set of basis vectors whose (reduced) dimension equals the dimension of the manifolds describing the system. Continuum modeling on manifolds generates the necessary basis vectors, while significantly reducing the degrees of freedom.

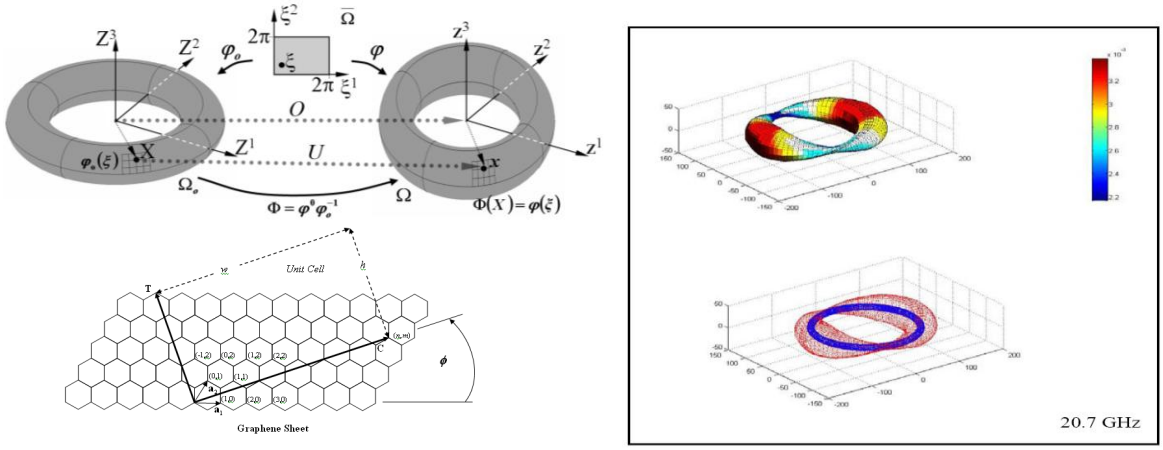

Figure 1 (a) Continuum computation approach used to study reduced-dimension materials. Intrinsic basis vectors $\boldsymbol{G}^i$ and the use of representative area elements to sample interatomic potential energy allow the phonon spectra to be accurately predicted. **(b)** Typical acoustic mode of vibration predicted using the continuum approach.

A recently-developed multi-scale continuum approach[1] forms the basis for reduced-order modeling of the reduced-dimension nanophononic systems (see Fig. 1a for an example nanotoroid) discussed during the talk. This approach employs intrinsic basis vectors defined on a reduced-dimension surface (manifold) of the nanostructured material. Changes in interatomic potential energy arising from lattice vibrations are equated to changes in continuum strain energy, allowing non-quantum atomistic beha-

Phononics 2011: First International Conference on Phononic Crystals, Metamaterials and Optomechanics
Santa Fe, New Mexico, USA, May 29-June 2, 2011
PHONONICS-2011-0071

vior to be captured using continuum techniques. The energy change is sampled using representative area elements. A subsequent finite element discretization results in a significant decrease in the deformation degrees of freedom present, while at the same time accurately capturing the acoustic range of the phonon spectra. Figure 1b displays a typical acoustic mode of vibration predicted using this procedure. Applying Bloch analysis, dispersion relationships have also been obtained and will be discussed during the talk. In particular, the author will discuss the accuracy of the obtained acoustic and optic branches, and will discuss in general what can be expected from any multi-scale approach.

The second part of this talk will address asymptotic techniques being developed by the author and his co-workers for analyzing wave propagation in nonlinear periodic metamaterials. Gigahertz communication devices, such as mobile phones, use phononic-based systems for their low-power filtering characteristics. Many sensing devices based on resonators, acoustic logic ports, and surface acoustic wave-based filters rely on the unique band gap characteristics of phononic crystals, an important class of periodic metamaterials. The majority of recent research on wave propagation in periodic metamaterials has been devoted to linear media, with little attention paid to characterize, analyze and exploit the effects of nonlinearities for wave propagation management and control. As devices miniaturize further, nonlinear behavior becomes the norm and not the exception, as witnessed in part by the complex potentials used to describe small-scale interactions. The effects nonlinearities exert on dispersion characteristics, band-gaps, and directionality have not been the focus of a concerted research effort, and as a result are not well-understood. Most importantly, nonlinearities should be explored as means to achieve novel functionalities which potentially enrich the design space of periodic media.

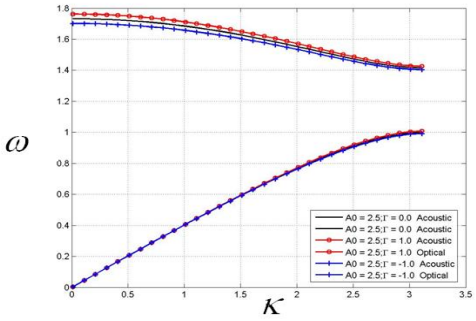

Figure 2 Amplitude-dependence of diatomic chain's dispersion behavior.

The considerations above have led us to investigate discrete (and continuous systems following discretization) of the following form,

$$\mathrm{M}\ddot{\underline{u}}_j + \mathrm{K}\underline{u}_j + \underline{F}^L(u_{j-1,N}, u_{j+1,1}) + \varepsilon \underline{F}^{NL}(\underline{u}_j, u_{j-1,N}, u_{j+1,1}) = 0\,, \tag{1}$$

where the displacement vector $\underline{u}_j = [u_{j,1}\ u_{j,2}\ u_{j,3}\ldots..\ u_{j,N}]^T$ contains the displacements of the masses of the j^{th} unit cell, the unit cell mass and stiffness matrices are denoted by $\mathrm{M} \in R^{N\times N}$ and $K \in R^{N\times N}$, and $\underline{F}^L \in R^{N\times 1}$ contains linear restoring forces associated with masses *neighboring* the unit cell while $\underline{F}^{NL} \in R^{N\times 1}$ contains all nonlinear restoring forces. As such, (1) governs an open set of nonlinear difference equations and therefore requires a solution procedure unlike that traditionally used in weakly nonlinear systems. However, ideas similar in spirit to the Lindstedt-Poincaré and multiple scales perturbation techniques have been developed by the author and co-workers to solve for amplitude-dependent dispersion relations corrected up to second order[2,3].

Figure 2 plots the dispersion trend for the two wave modes predicted by the perturbation analysis of a cubically-hardening chain. The trends pictured have been verified via comparison with numerically simulated diatomic chains[2]. The figure demonstrates that an increase in wave amplitude shifts both dispersion branches upwards, effectively moving (or tuning) the band gap location. We have also predicted similar dispersion shifts when multiple waves interact[3]. Possible devices exploiting this amplitude-dependent dispersion behavior will be discussed during the talk.

References

[1] Leamy, M.J., and DiCarlo, A., *Comput. Method. Appl. M.* **198**, 1572-1584 (2009).
[2] Narisetti, R.K., Leamy, M.J., and Ruzzene, M., *J. Vib. Acoust.* **132**(3): 031001 (2010).
[3] Manktelow, K., Leamy, M.J., and Ruzzene, M., 2010, *Nonlinear Dyn.* **63**, 193-203.

Phononics 2011: First International Conference on Phononic Crystals, Metamaterials and Optomechanics
Santa Fe, New Mexico, USA, May 29-June 2, 2011
PHONONICS-2011-0076

An Effective Medium Model for Sonic Crystals with Composite Resonant Elements

Olga Umnova[1] , Anton Krynkin[1], Alvin Y.B.Chong[2], Shahram Taherzadeh[2], Keith Attenborough[2]

[1] Acoustics Research Centre, The University of Salford, Salford, Greater Manchester, UK, o.umnova@salford.ac.uk, a.krynkin@salford.ac.uk
[2] Department of Design Development, Environment and Materials, The Open University, Milton Keynes, UK y.b.a.chong@open.ac.uk, s.taherzadeh@open.ac.uk, k.attenborough@open.ac.uk

Abstract: Using a self-consistent method, analytical expressions are derived for the parameters of an effective medium of composite scattering elements in air. The scatterers consist of concentrically arranged thin elastic shells and 4-slit cylinders. Predictions and data confirm that the use of coupled resonators results in a substantial insertion loss peak related to the modified resonance of the shell.

Periodic arrays of resonant scatterers such as thin elastic shells [1] or split ring resonators [2-3]can support low frequency band gaps in addition to those associated with array periodicity [1]. With finite periodic arrays they correspond to frequency intervals of low transmission and lead to an improved attenuation below the first of the Bragg's band gaps. To describe low frequency behaviour, an effective medium model has been developed for an array of c concentrically arranged hollow rigid cylinderswith multiple slits (N-slit rigid cylinder) and thin elastic shells (Fig.1).

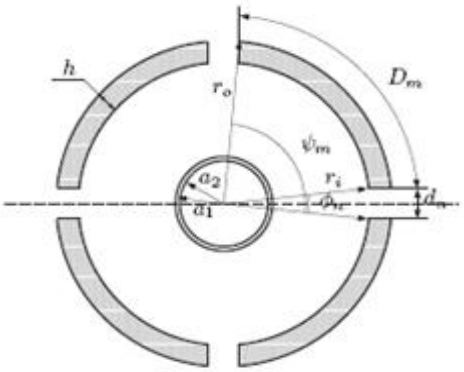

Figure 1. Cross-section of composite element consisting of a concentric arrangement of an outer 4-slit rigid cylinder and an inner elastic cylindrical shell.

The composite scatterer is a system of coupled resonators and gives rise to multiple resonances. The corresponding analytical model employs polar angle dependent boundary conditions on the surface of N-slit cylinder. The solution inside the slits assumes plane waves. The simplified low frequency description of the composite scatterer relies on the replacement of the N-slit cylinder by an equivalent fluid layer. The concentric arrangement results in resonances associated with both circular and annular cavities. An axisymmetric resonance of the shell is preserved but shifted to the lower frequency range by the presence of the cavity. This is similar to the effect observed in mass-spring system with multiple degrees of freedom.

Using a self-consistent approach [4], e analytical expressions are derived for the characteristic impedance and the wavenumber of an effective medium comprised of composite scatterers in air. The approximation is applicable when wavelengths in both air and effective medium exceed the size of a single scatterer. The model takes into account viscoelastic losses in the shells. The effective medium model predictions are compared with the solutions for infinite doubly periodic arrays and insertion loss data for finite arrays of composite scatterers. In laboratory experiments 2m long and 0.25mm thick Latex cylinders with outer diameter of 43mm and 55mm outer diameter slitted PVC pipes were used. Concentric arrangements of pairs of Latex and 4-slit PVC cylinders were formed as shown in Figure 1.The cylinders were arranged in a periodic (square) array with lattice constant of 8cm. The Bragg frequency for the array is around 2kHz. It is demonstrated that the model predicts negative real part of the effective compressibility around the modified axisymmetric shell resonance (Fig.2) at 1.1kHz.

Phononics 2011: First International Conference on Phononic Crystals, Metamaterials and Optomechanics
Santa Fe, New Mexico, USA, May 29-June 2, 2011
PHONONICS-2011-0076

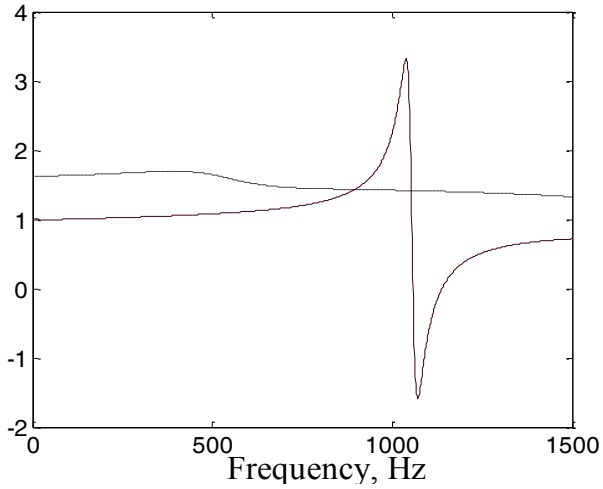

Figure 2. Real part of normalised effective density (– –) and effective compressibility (——) as a function of frequency.

As shown in Fig. 3, for an array of 21 composite scatterers the effective medium model correctly predicts the frequency of the corresponding insertion loss peak, but overestimates its value.

Plane waves were assumed and the array was modelled as infinitely wide slab. One of the reasons for disagreement is the limited validity of the plane wave approximation; the second is the inapplicability of the long wave approximation around the resonant frequency. A better agreement is obtained between the effective medium model and multiple scattering theory predictions for larger arrays with receiver placed further away from the array. Characteristic impedance and wavenumber are deduced from laboratory data and predictions of the multiple scattering theory using methods developed in paper [5] and compared with those predicted by the effective medium model.

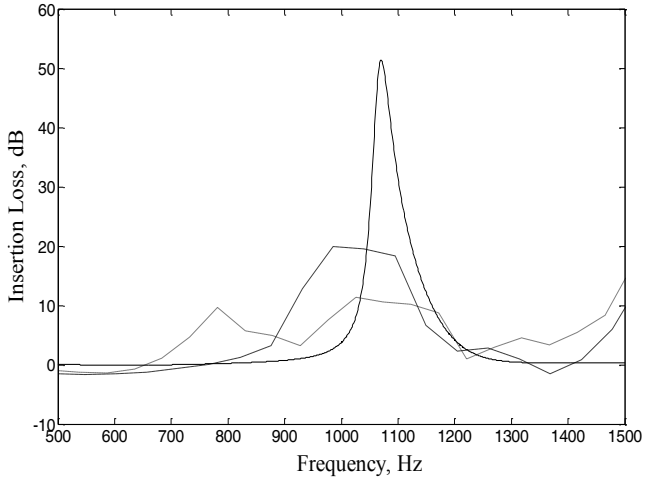

Figure 3. Multiple scattering (– –) and effective medium (——) predictions compared with data (– - –) for 7X3 array of composite scatterers. Distances to the source and receiver are 1.5m and 0.05m, respectively.

References

[1] A.Krynkin, O.Umnova, A.Y.B.Chong, S.Taherzadeh and K.Attenborough,, *J.Acoust.Soc.Am*, **128,** 3496-3506 (2010).
[2] A.B.Movchan, S.Guenneau, *Phys.Rev.B*, **70**, 125116 (2004)
[3] S.G.L.Smith, A.M.J.Davis, *Proc.R.Soc.A*, **466**, 3117-3134 (2010)
[4] J.G Berryman, *J.Acoust.Soc.Am*, **68,** 1809-1819 (1980).
[5] V.Fokin, M.Ambati, C.Sun, X.Zhang, *Phys.Rev.B* **76**, 144302 (2007)

Phononics 2011: First International Conference on Phononic Crystals, Metamaterials and Optomechanics
Santa Fe, New Mexico, USA, May 29-June 2, 2011
PHONONICS-2011-0079

Control of Vibrational Energy in Nonlinear Granular Crystals

Georgios Theocharis[1], **Nicholas Boechler**[1], **Chiara Daraio**[1]

[1] *Graduate Aerospace Laboratories (GALCIT) California Institute of Technology, Pasadena, CA 91125, USA*
georgiostheocharis@gmail.com boechler@caltech.edu daraio@gmail.com

Abstract: We describe recent work on nonlinear granular crystals. We explore phenomena related to vibrational energy localization, re-distribution, and rectification enabled by the spatial discreteness, disorder, and nonlinearity of granular crystals. In addition, we note how an understanding of dynamic phenomena in granular crystals can enable the design of novel engineering devices.

The ability of periodic structures to affect wave propagation – through the existence of phenomena such as band gaps – has been studied across a wide array of fields. This includes the propagation of light in photonic crystals and elastic/acoustic waves in phononic crystals[1]. The scalability of such concepts has been shown, at the intersection of these two fields, in the development of optomechanical crystals[2], which produce phononic waves as a result of photonic excitation. However, the majority of these studies have focused on the linear dynamical behaviour of these systems. Although studying the linear response is an important first step, it is more often the exception than the rule in naturally occurring systems. Nonlinear systems, albeit more difficult to study, are more general, and offer the possibility of new phenomena and functionality.

Granular crystals are systems composed of a tightly packed array of elastically interacting particles. With the Hertzian contact that governs the interaction between the particles, granular crystals are both spatially discrete (dispersive) and nonlinear systems. Granular crystals have drawn recent interest due to the tunability of their dynamic vibrational response (with the application of a static load) to encompass linear, weakly nonlinear, and strongly nonlinear regimes; the simplicity of their construction; and their applicability to engineering devices[3]. The study of granular crystals has seen the emergence of coherent structures such as solitary waves[3], intrinsic and extrinsic nonlinear localized modes[4,5], and other nonlinear phenomena such as tunable frequency band gaps[4], bifurcations[6], and chaos[7].

Here we show a specific example of a nonlinear coherent structure, a discrete breather (DB), which can be found in granular crystals. DBs have been a central theme for numerous theoretical studies while the past several years they have been observed in a myriad of physical systems ranging from biological to microengineered and condensed matter systems covering all the length scales [8]. In Fig. 1, we show an experimental observation of a DB, generated in an 80 particle diatomic granular crystal. This example shows how the interplay of nonlinearity and discreteness/periodicity leads to the localization of vibrational energy to a narrow spatial regime, at a specific frequency. The underlying physical mechanism, as described in[4], that leads to the development of an intrinsically localized mode, is the modulational instability of the lower optical cutoff mode of the diatomic granular crystal. A systematic study of the existence and stability of these nonlinear localized vibrations in a diatomic granular crystal can be found in[5].

In contrast with traditional types of localization in disordered media, the discrete breathers are "intrinsic" as they do not require the presence of any defects, and can occur in perfectly periodic chains. However, the inclusion of an extrinsic disorder in granular crystals, in combination with their nonlinear response, leads to other interesting phenomena such as nonlinear defect modes and symmetry breaking bifurations[6]. Such modes allow the response of the system to be tunable, not only with the application of static load, but with a change in the amplitude of the propagating wave; another example of increased functionality resulting from nonlinearity. Furthermore, in the presence of a defect and a driver at one end of the chain, hopf bifurcations can lead to the appearance of quasiperiodic and chaotic vibrations in granular crystal systems[7]. Such instabilities and bifurcations, resulting from, and in combination with nonlinearity, enables the re-distribution of energy amongst other frequencies of

Phononics 2011: First International Conference on Phononic Crystals, Metamaterials and Optomechanics
Santa Fe, New Mexico, USA, May 29-June 2, 2011
PHONONICS-2011-0079

the system – a characteristic previously unavailable to linear systems. Taking advantage of such phenomena, we have proposed a tunable rectifier of vibrational energy[7]. Such a system could have importance in a wide array of applications, including: biomedical imaging technologies, vibrational and thermal energy logic systems, and energy harvesting devices.

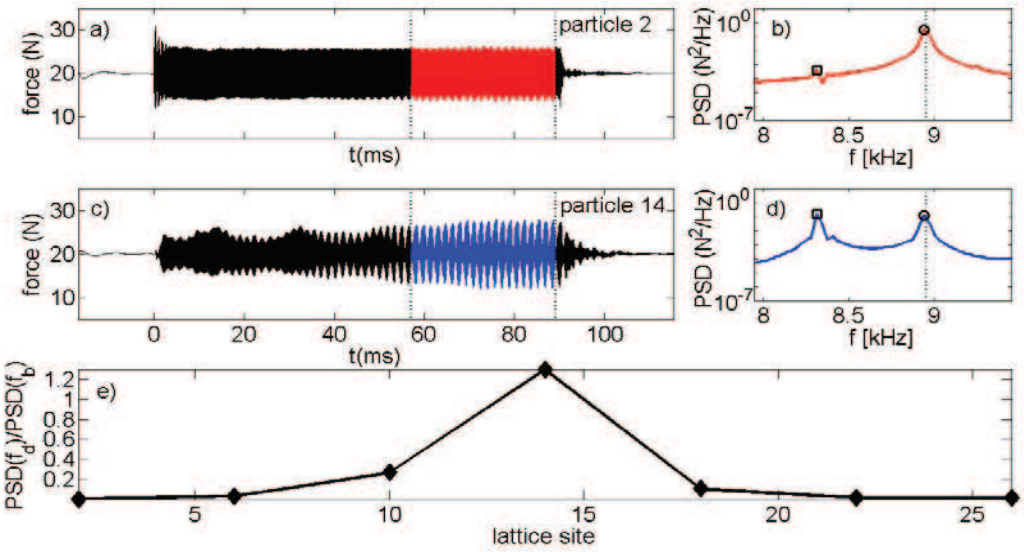

Figure 1: Experimental observation of a DB, in an 80 particle granular crystal, at f_b=8.31 kHz. **(a),(b)** Force at particle 2 and 14, respectively. **(c),(d)** Power spectral density (PSD) for the highlighted time regions in **(a),(c)** of the same color. Square [circular] markers denote the DB [driving] frequency and PSD amplitude. **(e)** The ratio of the PSD amplitude at the discrete breather frequency divided by the PSD amplitude of the driving frequency as a function of sensor location. The vertical dashed line in **(b)** and **(d)** denotes the lower cutoff frequency of the optical band, and the vertical dashed lines in **(a)** and **(c)** denote the time region for the PSD calculation.

Mirroring the evolution of the study of photonic crystals, we aim to extend the study of the emerging field of phononics into the realm of nonlinearity. Nonlinearity has the potential to break the restrictions imposed by linearity, and enable the design of new devices. This includes mechanisms for controlling the spatial distribution of vibrational energy, and for the conversion of energy to other frequency waveforms. In granular crystals, we have found a useful test-bed and model for such an investigation. Accordingly, we have also developed the theoretical, numerical, and experimental tools for furthering the understanding of nonlinear phononic phenomena, and developing novel applications.

References

[1] T. Gorshnvyy, M. Maldovan, C. Ullal, E. Thomas, *Phys. World*, **18**, 24 (2005).
[2] M. Eichenfield, J. Chan, R. Camacho, K. J. Vahala, O. Painter, *Nature*, **462**, 78 (2009).
[3] V. F. Nesterenko, *Dynamics of Heterogeneous Materials,* Springer-Verlag, New York, USA (2001).
[4] N. Boechler, G. Theocharis, S. Job, P. G. Kevrekidis, M. A. Porter, and C. Daraio, *Phys. Rev. Lett.* **104**, 244302 (2010).
[5] G. Theocharis, N. Boechler, P. G. Kevrekidis, S. Job, M. A. Porter, and C. Daraio, *Phys. Rev. E* **82**, 056604 (2010).
[6] G. Theocharis, G.; Kavousanakis, M.; Kevrekidis, P. G.; Daraio, C.; Porter, M. A. and Kevrekidis, Y., *Phys. Rev. E* **80**, 066601 (2009).
[7] N. Boechler, G. Theocharis, and C. Daraio, *in preparation* (2011).
[8] S. Flach and A. V. Gorbach, *Phys. Rep.* **467**, 1 (2008).

Phononics 2011: First International Conference on Phononic Crystals, Metamaterials and Optomechanics
Santa Fe, New Mexico, USA, May 29-June 2, 2011
PHONONICS-2011-0098

Second harmonics, instabilities and hole solitons in 1D phononic granular chains

Víctor J. Sánchez-Morcillo[1*], I. Pérez-Arjona[1], V. Gusev[2], V. Tournat[3]

[1] IGIC, Universidad Politécnica de Valencia, Paranimf 1, 46730 Grau de Gandia, Spain,
[2] LPEC, [3] LAUM, CNRS, Université du Maine, Av. Olivier Messiaen 72085, Le Mans, France
**victorsm@upv.es*

Abstract: The propagation of nonlinear compressional waves in a 1D compressed granular chain driven at one end by a harmonic excitation is theoretically studied. The chain is described by a FPU lattice model with quadratic nonlinearity. We predict and describe different nonlinear phenomena, as the generation of second harmonics, modulational instabilities and the existence of hole (or dark) solitons.

We consider the propagation of a harmonic signal applied to one end of a homogeneous 1D chain of spherical beads in contact, each with a mass *m* and a radius *R*, as shown in Fig. 1. Under the effect of an external constant force F_0 [Fig.1] the chain is compressed, and the distance between centers is reduced by an amount δ_0 resulting in $a = 2R-\delta_0$. Denoting by u_n the displacement of the *n*-th bead from its equilibrium position, and assuming that the beads repel upon Hertz-type potential $V(\delta) \propto \delta^{5/2}$, with $\delta = \delta_0 - (u_n - u_{n-1})$ being the bead-bead overlap, the dynamics of the chain is described by a system of coupled ordinary differential equations for the displacements, which for $\delta_0 >> | u_n - u_{n-1} |$ can be written as a quadratic FPU equation, as [1]

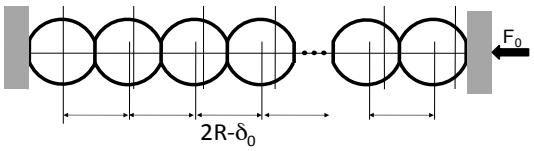

Figure 1 1D chain of spherical beads in contact compressed by an external constant force.

$$\frac{\mathrm{d}^2 u_n}{\mathrm{d}t^2} = \frac{1}{4}\left(u_{n+1} - 2u_n + u_{n-1}\right) - \frac{\varepsilon}{8}\left(u_{n+1} - 2u_n + u_{n-1}\right)\left(u_{n+1} - u_{n-1}\right) \qquad (1)$$

where $\varepsilon = u_0 / 2\delta_0$ is the nonlinearity parameter. We consider a driven lattice, subjected to the boundary condition $u_0(t) = \sin(\Omega t)$, being Ω the driving frequency. Neglecting nonlinearity, we obtain the dispersion relation of the chain, $\Omega = \left|\sin\left(k/2\right)\right|$ defining the cutoff frequency Ω=1.

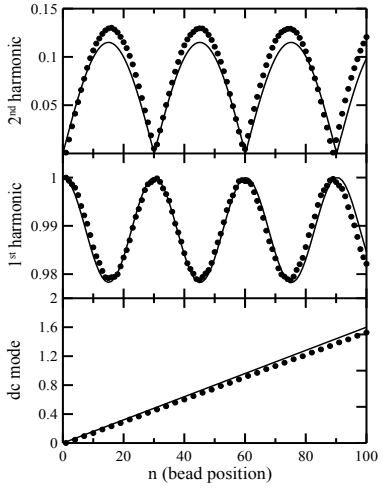

A successive approximations method is used to find the analytical expressions for the amplitudes of the static displacement field, and of the fundamental and second harmonics propagating through the lattice. We distinguish two regimes, depending on whether the second harmonic is a propagating (0<Ω<1/2) or evanescent (1/2<Ω<1) mode. The results for the propagative case are shown in Fig. 2, where we depict the amplitude of the different modes. Note the mode beating induced by the lattice dispersion. In both cases, it is found that second harmonic is present, and influences the propagation characteristics of the fundamental mode. The comparison of the analytical results (full lines) and numerical results (dots) is shown in Fig. 2.

Figure 2. Amplitudes of the different modes (static, fundamental and second harmonic) in the case ε=0.1 and Ω=0.4 (propagative case) along the chain, for the first 100 beads. Note the linear growth of the static mode, and the beatings of fundamental and second harmonics.

Phononics 2011: First International Conference on Phononic Crystals, Metamaterials and Optomechanics
Santa Fe, New Mexico, USA, May 29-June 2, 2011
PHONONICS-2011-0098

The successive approximations method allows predicting the amplitudes of the different modes propagating in the chain, but is not appropriate to study other dynamical effects induced by the nonlinearity, like instabilities or envelope solitons. In other to study these phenomena, a technique based in a multiple scales expansion method together with the so-called quasi-discreteness approximation [2] is used instead. Considering both slow temporal and spatial scales, the following equation for the envelope A of the fundamental wave can be obtained:

$$\frac{\partial A}{\partial \tau} = iP\frac{\partial^2 A}{\partial x_n^2} + iQ|A|^2 A, \tag{2}$$

where $P = \frac{1}{2}\frac{\partial^2 \Omega}{\partial k^2}$ is the dispersion coefficient, $Q = \frac{1}{4}\Omega\left(1-3\Omega^2\right)\varepsilon^2$ the nonlinearity coefficient and we have defined the retarded time $\tau = t - x_n / v_g$ where x_n identifies the bead position and v_g the group velocity. Equation (2) is the well-known Nonlinear Schrödinger (NLS) equation. The NLS equation provides a canonical description for the envelope dynamics of a quasi-monochromatic plane wave (the carrying wave) propagating in a weakly nonlinear dispersive medium when dissipative processes are negligible [3]. From Eq. (2) it follows that the uniform solution is always modulationally unstable when $PQ > 0$, provided some threshold amplitude is reached. This is known as the Benjamin-Feir instability and results in a long-wavelength modulation of the propagating signal, which eventually breaks into a sequence of pulses or bright solitons. Since in Eq. (2) P is always positive, the analysis predicts that constant amplitude solutions (plane waves) can be unstable when $\Omega < \Omega_{mi} = 1/\sqrt{3} \approx 0.577$. On the contrary, when $\Omega > \Omega_{mi}$ and solutions are stable, the chain supports propagative localized solutions known as dark (or grey) hole solitons. They have the analytical expression

$$A = A_0\sqrt{1 - d^2 \sec h^2\left(\frac{x - vt}{L}\right)}e^{i\Theta} \tag{3}$$

which is an exact solution of Eq. (2). The existence and stability of such solutions has been demonstrated numerically, and the results are shown in Fig. 3 for ε=0.3 and Ω=0.8. The temporal behaviour of bead labelled as N=50 is shown at the right. The left picture compares the numerical solution with the analytical profile given by Eq. (3), shown in continuous line. The agreement is excellent, demonstrating the existence of the predicted hole solitons. While bright solitons in granular chains have been deeply studied, this is the first prediction of hole solitons in such discrete systems.

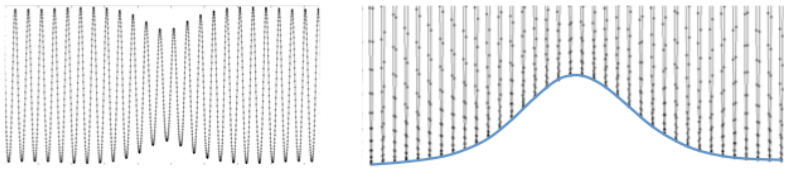

Figure 3. Hole soliton obtained for the case ε=0.3 and Ω=0.8. The temporal behaviour of bead labelled as N=50 is shown.

The work was financially supported by the MICINN of the Spanish Government, under FIS2008-06024-C03-03, and by ANR projects “grANuLar”, NT05-3_41989, and “Stabingram”.

References

[1] V. Tournat, V.E. Gusev and B. Castagnède, Phy. Rev. E 70, 056603 (2004).
[2] T. Taniuti and N. Nayima, J. Math. Phys. 10, 1369 (1969)
[3] C. Sulem and P.L. Sulem, *The Nonlinear Schroedinger Equation*, Springer-Verlag, New York (1999).

Phononics 2011: First International Conference on Phononic Crystals, Metamaterials and Optomechanics
Santa Fe, New Mexico, USA, May 29-June 2, 2011
PHONONICS-2011-0101

Theoretical and Experimental Evidence of Evanescent Modes in Finite Sonic Crystals

V. Romero-García[1,3], L.M. Garcia-Raffi[2], J.V. Sánchez-Pérez[3]

[1] *Instituto de Ciencia de Materiales de Madrid, Consejo Superior de Investigaciones Científicas, Spain*
virogar1@gmail.com,
[2] *Instituto Universitario de Matemática Pura y Aplicada, Universidad Politécnica de Valencia, Spain*
lmgarcia@mat.upv.es
[3] *Centro de Tecnologías Físicas: A.M.A, Universidad Politécnica de Valencia, Spain,*
virogar1@gmail.com, jusanc@fis.upv.es

Abstract: Evanescent modes in complete sonic crystals (SC) and SC with point defects are both theoretically and experimentally reported in this paper. Finite element method and an extension of the plane wave expansion with supercell approximation to solve the invers problem $k(\omega)$ is used to predict the evanescent modes. Experimental data and numerical results are in good agreement with the predictions.

Propagating waves inside a periodic medium represent a set of solutions to the wave equation that satisfy the translational symmetry and they are characterized by the transmission bands obtained using the Bloch's theorem and Fourier expansion of the periodic physical properties. Then the acoustic wave equation can be transformed in an eigenvalue problem and solved using for example the plane wave expanssion (PWE) method. The eigenfrequencies $\omega(k)$ for each Bloch's vector k, inside the irreducible part of the first Brillouin zone constitute the bands structure. One of the most important properties revealed by these bands is the so-called band gaps (BGs): frequency ranges where waves do not propagate through the periodic system. The existence of these BGs leads to the emergence of several interesting physical properties, such as the localized modes within the BG when a point defect is introduced in the structure.

When the translational symmetry is broken, evanescent modes characterized by a complex wave number k, can emerge in these systems. In contrast to infinite periodic media, in the case of the finite ones, the modes inside the BG present evanescent behaviour, growing the decay rate of the mode as the frequency reaches the center of the BG. In Figure 1 we can analyze the evanescent behaviour of a mode inside the BG of a finite Sonic Crystal (SC) made of rigid cylinders with radius $r=0.1$ *m* arranged in square periodicity $a=0.22$ m, at the frequency *920* Hz. The absolute value of the pressure in the points between two rows of the SC has been numerically calculated, using finite elements method (FEM). The numerical predictions and experimental results are plotted in Figure 1 with black continuous line and connected open red circles respectively. It is possible to observe the decay of the mode with the distance all along the SC. With these experimental results, the decay of the evanescent mode inside the BG can be fitted. In order to fit an exponential decay ae^{bx} the points with maximum values have been chosen. The values of the parameters in the fit are $a=0.05597\pm0.0103$ Pa, and $b=Im(k)=-5.60\pm1.45$ m^{-1}, and

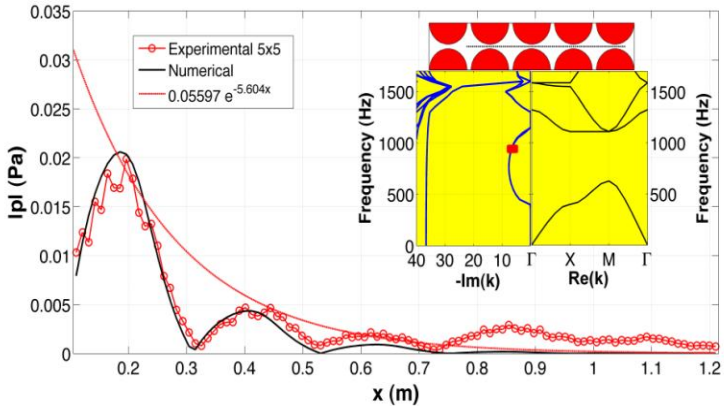

Figure 1 Acoustic pressure inside a 5x5 SC with square array with lattice constant a=22 cm for a frequency inside the BG of 920 Hz. Black continuous line (connected red open circles) represents the absolute values of the numerical (experimental) pressure inside the SC between two rows of scatterers. Red dashed line represents the fitting of the exponential like decay of the measured acoustic field inside the SC. The inset represents the measurement points inside the SC and both the complex and real band structures.

Phononics 2011: First International Conference on Phononic Crystals, Metamaterials and Optomechanics
Santa Fe, New Mexico, USA, May 29-June 2, 2011
PHONONICS-2011-0101

the result is plotted in Figure 1 in red dashed line. In the inset of Figure 1, we show the complex band structure calculated using the extended plane wave expansion (EPWE) in order to solve the inverse problem $k(\omega)$ being k possibly complex. The value of the imaginary part of the first harmonic of the wave vector is marked in the complex band structure with a red square. One can see that $Im(k)=-5.6$ m^{-1} at frequency 920 Hz in a complete SC.

One particularly interesting aspect of SC is the possibility to create point defects that confine acoustic waves in localized modes. Because of the locally breaking periodicity of the structure, defect modes can be created within the BG. These defect modes are strongly localized around the point defect[3]: once the wave is inside the defect, it is trapped because the borders of the defect act as perfect mirrors for waves with frequencies in the BG. To analyze the propagation of waves inside periodic structures with defects, authors have traditionally used PWE with supercell approximation. In this work, we develop the supercell approximation to the EPWE. This methodology enables us to obtain the relation $k(\omega)$ for N defect modes in a periodic medium.

Figure 2A shows the complex band structures for the ΓX direction and real band structures for an SC with a point defect. In our case, we use only one direction of incidence to analyze the complex band structure because the localized mode appears at the same frequency for all the incidence directions. The supercell used for the calculations is shown in the inset of Figure 2A.

Analyzing the real band structures (propagating properties) we can observe that the localized mode appears at 920 Hz (green dashed line). For frequencies in the BG, the borders of the point defect act as perfect mirrors and produce the localized mode in this cavity. Figure 2B presents the numerical results of the acoustic field inside a point defect in a SC in complete good agreement with the experimental data. Figure 2C represents the measurements of the localized mode in a cavity obtained for the first time.

In Figure 2A, the complex bands give information about the evanescent behaviour of the localized mode. We observe that a complex band obtained by EPWE becomes a purely real for the localized mode (green dashed line). The value exactly coincides with the one obtained by PWE with supercell approximation. The border of the cavity is located at approximately $x=0.6$ m as it can be observed in Figure 2B. Figure 2D presents both numerical (blue line) and experimental (blue open squares) values of the acoustic field from the end of the cavity to the end of a SC, showing the evanescent behaviour of the localized mode outside the cavity.

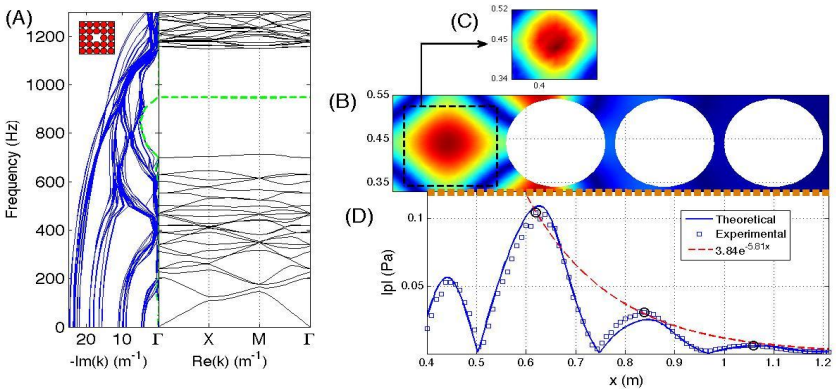

Figure 2 Evanescent behaviour of a localized mode in a point defect. (A) Complex (Blue lines) and Real (black lines) bands structures for a SC made of rigid scatterers with a point defect. Square periodicity $a=0.22$ m and radius $r=0.1$ m. (B) Numerical prediction of the acoustic field inside the point defect at the localization frequency, 920 Hz. (C) Experimental measurement of the localized field inside the point defect. (D) Analysis of the evanescent behaviour of the localized mode. Blue continuous line (Open blue squares) represents the numerical predictions (experimental data) of the acoustic field in the path between two rows of cylinders containing the point defect marked with a broad orange dashed line. Red dashed line shows the fitting of the exponential like decay of the localized mode.

The propagation of waves inside periodic structures consists on both propagating and evanescent modes. This work could well become fundamental for the correct understanding of the design of narrow filters and waveguides based on periodic media with point defects.

References

[1] Y.C. Hsue, A.J. Freeman and B.Y. Gu. *Phys. Rev. B*, **72**, 195118, (2005).
[2] V. Laude, Y. Achaoui, S. Benchabane and A. Khelif. *Phys. Rev. B*, **80**, 092301, (2009).
[3] J.D. Joannopoulos, R. D. Meade, and J.N. Winn, *Molding the Flow of Light*, Princeton University Press, USA (1995).

Phononics 2011: First International Conference on Phononic Crystals, Metamaterials and Optomechanics
Santa Fe, New Mexico, USA, May 29-June 2, 2011
PHONONICS-2011-0102

Interaction between Periodic Arrays and Finite Impedance Surface: Analytical Results and Experimental Data

V. Romero-García[1,2], J.V. Sánchez-Pérez[2]; K. Attenborough[3], S. Taherzadeh[3]; A. Chong[3], A. Krynkin[4]; O. Umnova[4];

[1] *Instituto de Ciencia de Materiales de Madrid, Consejo Superior de Investigaciones Científicas, Spain*
virogar1@gmail.com
[2] *Centro de Tecnologías Físicas: Acústica, Materiales y Astrofísica. Universidad Politécnica de Valencia, Cno de Vera s/n 46020 Valencia, Spain*
virogar1@upvnet.upv.es, jusanc@fis.upv.es
[3] *Department of Design, Development, Environment and Materials. The Open University Walton Hall Milton Keynes MK7 6AA United Kingdom*
k.attenborough@open.ac.uk, s.taherzadeh@open.ac.uk, y.b.a.chong@open.ac.uk
[4] *School of Computing, Science & Engineering The University of Salford, Salford,Great Manchester, M5 4WT. United Kingdom*
a.krynkin@salford.ac.uk, O.Umnova@salford.ac.uk

Abstract: The design of devices based on phononic crystals seems a hot topic nowadays. However, there are some effects that have to be into account for the development of their technology, as for instance the existence of a close surface that could interfere with their acoustic properties. We present here an analytical model to analyze this interaction based on the Multiple Scattering Theory in good agreement with experimental data.

The acoustic interaction between both the scattered field produced by a phononic crystal (PC) and the reflected field from a line source in a finite impedance surface is reported in this work. This interference pattern is analyzed using an analytical model, based on the multiple scattering theory[1,2], called by us Image Multiple Scattering Theory (IMST). The analytical predictions have been compared with experimental data showing good agreement. We have considered throughout this work a line source and the case of cylindrical scatterers in air. Although the most interesting situation is likely to involve periodic arrays of cylinders with their axes perpendicular to the surface, this would require solution of a 3D problem. Therefore we have considered the tractable 2D problem involving a periodic array of cylinders with their axes parallel to the surface.

This analytical method developed in this work modifies the classical Multiple Scattering Theory using the method of images in order to add the reflected field on the finite impedance surface. According to this methodology, two sources have been considered: the real source located in the real space and an image source located in the image space. Moreover, the image of the real array is also considered to solve the problem. In Figure 1 (left panel), we represent the real case for a square array of cylinders with lattice constant *a,* and radius *r*. In Figure 1 (right panel) we show the scheme of images: one can observe the real space XY with the real array of scatterers and the real source O, and the image space (XY´) with the image array of scatterers and the image source O´.

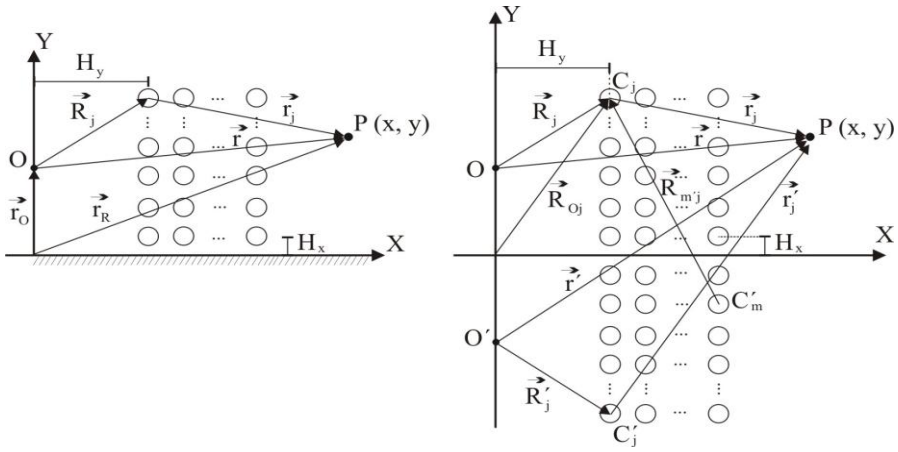

Figure 1 Left panel: Array of scatterers in the real case. Right panel: scheme of the method of images for the array of the left panel.

To add the effect of the surface in our analytical scattering model, we have characterized

Phononics 2011: First International Conference on Phononic Crystals, Metamaterials and Optomechanics
Santa Fe, New Mexico, USA, May 29-June 2, 2011
PHONONICS-2011-0102

it by means of the reflection coefficient $R(r_O,r_C;\ v)$ of the surface. If $R(r_O,r_C;\ v)=1$ we are in the case of acoustically hard ground but, generally speaking, $R(r_O,r_C;\ v)$ will be a function that will depend on the positions of both the source and the receiver and on the frequency. Specifically $R(r_O,r_C;\ v)$ can be characterized by the finite impedance of the surface. In this work, the finite impedance surface is represented by a two parameter impedance model[3]:

$$Z_{ground} = \rho c_0 (0.434 \sqrt{\frac{\sigma_e}{f}} (1+i) + 9.75 i \frac{\sigma_e}{f}) \tag{1}$$

Taking into account these considerations, the total acoustic field obtained using the IMST is:

$$P(\vec{r}) = H_0(kr) + R(\vec{r}_O, \vec{r}_C; f) H_0(kr') + \sum_{m=1}^{M} \sum_{l=-L}^{L} A_l^m (H_l^{(1)}(kr_m) e^{il\theta_m} + R(\vec{r}_O, \vec{r}_C; f) H_l^{(1)}(kr_{m'}) e^{-il\theta_{m'}}) \tag{2}$$

Where M is the total number of the scatterers in the real space. The analytical Insertion Loss (IL) spectra for an array of cylinders placed over a soft plane are studied. The characteristics of the considered system are: *21* rigid cylinders with $r=0.055$ m arranged in a square array with $a=0.069$ m and with the bottom row placed near to a finite impedance surface with σ_e = *4000* Pa s/m^2 and α_ε = *105* m^3. The line source is placed at point O = *(0, 0.235)* m. The distance between the source and the array is $d=0.755$ m. In Figure 2 we can observe the comparison between measured and calculated the IL in three points, with coordinates at (A) *(1.203, 0.117)* m, (B) *(1.203, 0.235)* m and (C) *(1.203, 0.352)* m. The agreement between analytical predictions and experimental data are fairly good.

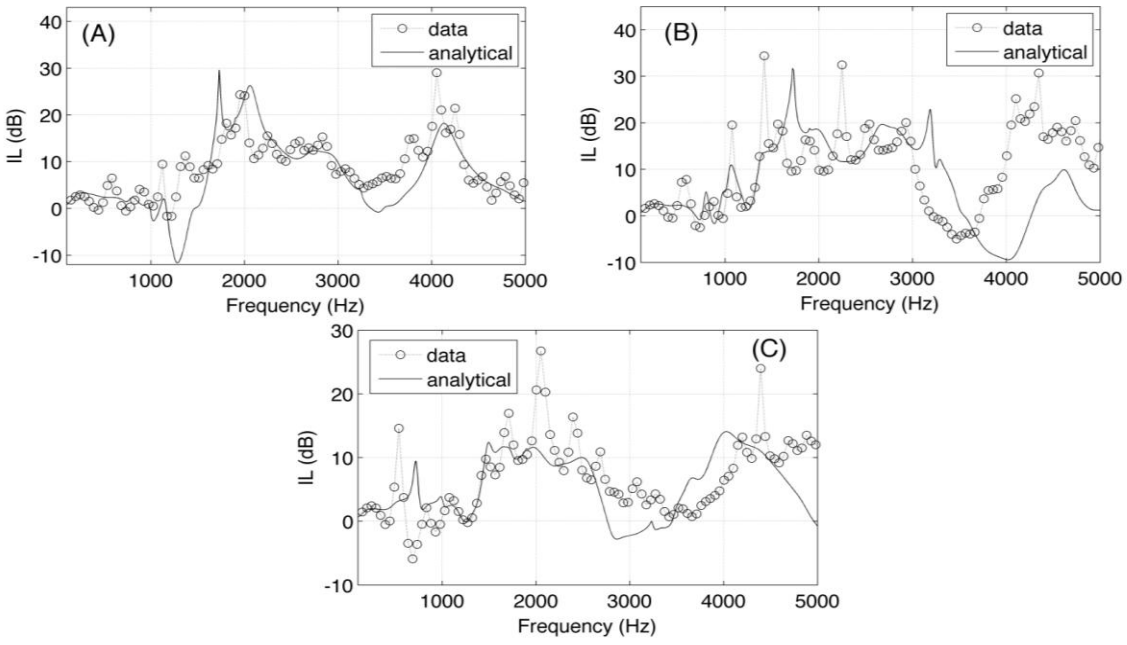

Figure 2 Measured and predicted Insertion Loss spectra for the three points indicated in the text.

This model can be applied in several technological applications of PC as for instance in the case of the design of acoustic barriers based on arrays of scatterers, where the effect of the excess attenuation produced by the reflected wave by the ground has a great influence on the acoustical properties of the PC.

References

[1] P.A. Martin, *Multiple Scattering: Interaction of Time-Harmonic Waves with N Obstacles*, Cambridge University Press, UK (2006).
[2] Y. Y. Chen and Z. Ye, *Phys. Rev. E* **64**, 036616 (2001).
[3] S. Taherzadeh and K. Attenborough, *J. Acous. Soc. Am.* **105**, 2039 (1999).

Phononics 2011: First International Conference on Phononic Crystals, Metamaterials and Optomechanics
Santa Fe, New Mexico, USA, May 29-June 2, 2011
PHONONICS-2011-0107

Lattice Materials: A Unified Structural Mechanics Perspective

A. Srikantha Phani

Department of Mechanical Engineering, 6250 Applied Science Lane, The University of British Columbia, Vancouver, BC, V6T 1PZ, CANADA,
srikanth@mech.ubc.ca

Abstract: Lattice materials with a periodic microstructure are suitable for multifunctional structures with high specific stiffness, favourable acoustic and thermal properties. Their mechanical response under static and dynamic loads is considered from a unified structural mechanics perspective combining Bloch wave theory with Finite Element Method.

Lattice materials possess a spatially repetitive unit cell geometry on the length scales of a few millimetres [1–5]. Typical applications include sandwich beams, panels and space trusses [6]. It has been observed that the unit cell geometry has a profound influence upon their macroscopic mechanical response [2] under static and dynamic loading conditions [7]. Optimal design of lattice microstructures for wave bearing properties such as bandgaps have been studied [8]. Ideas from solid state physics [9] have been combined with structural mechanics principles [10,11] and applied to periodic *structural* systems for aerospace applications. This interdisciplinary approach has lead to significant insights, most notably the exposition of Anderson localisation phenomena in macro scale periodic structures [12]. More recent studies [7,13,14] approach lattice and phononic materials in the spirit of earlier pioneering works in periodic structure theory [10,11].

Response/Phenomenon	Loading Type	Deformation Type	Remarks
Passband [7]	Dynamic	Spatially extended	Linear, infinite, perfect lattice material
Stopband (Bandgap) [7]	Dynamic	Spatially localised	Linear, infinite, perfect lattice material
Saint Venant effects [15]	Static	Spatially localised	Linear, finite, perfect lattice material with a boundary or interface
Rayleigh waves [15]	Dynamic	Spatially localised	Linear, finite, perfect lattice material with a boundary or interface
Anderson Localisation [12]	Dynamic	Spatially localised	Linear, imperfect lattice material
Discrete Breathers [16,17]	Dynamic	Spatially localised	Nonlinear, perfect lattice material in the weak coupling limit

Table **1** A classification of mechanical response of lattice materials. Here a perfect lattice material contains no defects such as cracks, whereas an imperfect lattice material does. Symmetries present in the perfect lattice are perturbed or destroyed in the imperfect lattice.

A unified structural mechanics perspective on mechanical response of lattice materials viewed as a periodic network of beams will be presented. Two distinct regimes of mechanical response are identified: in spatially extended response regime the entire lattice can sustain deformation; deformation can be confined to a spatially localised region due to defects, interfaces, and nonlinearity. A wide range of phenomena can be incorporated within this perspective as shown in Table 1.
Eigenvalue problems using Bloch theory will serve to unify the spatially localised and spatially extended deformation phenomena in Table 1 for linear systems. A quadratic eigenvalue problem proposed in an earlier work [15] to study elastic boundary layers will be revisited and generalised to include surface waves of Rayleigh type. Numerical results will be provided for one-dimensional linear nonlinear systems. Interaction between the defects and nonlinearity will be highlghted.

Phononics 2011: First International Conference on Phononic Crystals, Metamaterials and Optomechanics
Santa Fe, New Mexico, USA, May 29-June 2, 2011
PHONONICS-2011-0107

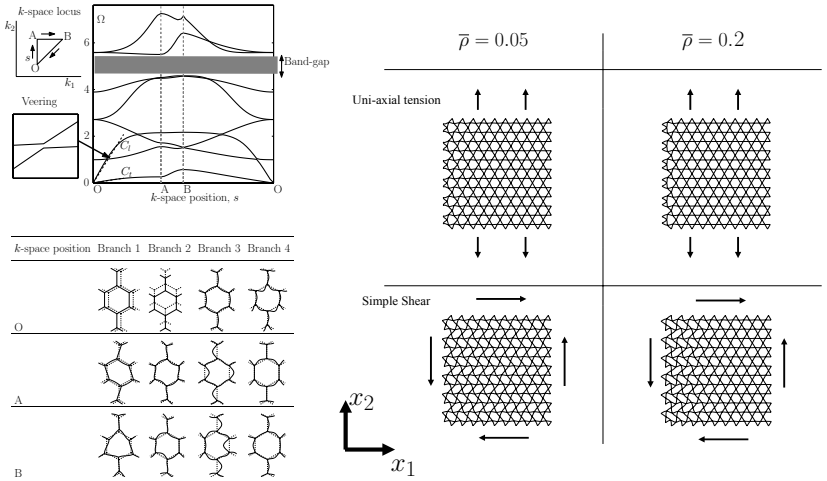

Figure **1** Dispersion curves for a hexagonal lattice exhibiting bandgaps and curve veering (left)[7]; Elastic boundary layers of Saint Venant type in a Kagome lattice subjected to stretching and shear deformations (right)[15]: $\overline{\rho}$ denotes relative density.

Acknowledgement: Financial support from Natural Sciences and Engineering Research Council (NSERC) of Canada through the award of Discovery Grant and support from Canada Research Chairs (CRC) program and Canada Foundation for Innovation (CFI) are thankfully acknowledged.

References

1 M.F. Ashby and L.J. Gibson, *Cellular solids: structure and properties*, Cambridge University Press, UK, (1997).

2 N.A. Fleck, V.S. Deshpande, and M.F. Ashby, Micro-architectured materials: past, present and future, *Proceedings of the Royal Society of London, Series A*, **466**, 2495–2516, (2010).

3 W.E. Warren and A.M. Kraynik, Foam mechanics: the linear elastic response of two-dimensional spatially periodic cellular materials, *Mechanics of Materials*, **6**, 27–37, (1987).

4 R.M. Christensen, Mechanics of cellular and other low density materials, *International Journal of Solids and Structures*, **37**(1), 93–104, (2000).

5 R.S. Lakes, Foam structures with a negative Poisson's ratio, *Science*, **235**, 1038–1040, (1987).

6 N. Wicks, and J.W. Hutchinson, Optimal truss plates, *International Journal of Solids and Structures*, **38**, 5165–5183, (2001).

7 A.S. Phani, J. Woodhouse, N.A. Fleck, Wave propagation in two-dimensional periodic lattices, *Journal of the Acoustical Society of America*, **119**(4), 1995–2005, (2006).

8 O. Sigmund and J.S., Jensen, Systematic design of photonic band-gap materials and structures by topology optimization, *Proceedings of the Royal Society of London, Series A*, **361**, 1001–1019, (2003).

9 C. Kittel, *Elementary solid state physics: a short course*, John Wiley & Sons, inc., USA, (1962).

10 D.J. Mead, Wave propagation in continuous periodic structures: research contributions from Southampton 1964-1995, *Journal of Sound and Vibration*, **190**(3), 495–524, (1996).

11 R.S. Langley, N.S. Bardell, and H.M. Ruivo, The response of two-dimensional periodic structures to harmonic point loading: a theoretical and experimental study of a beam grillage, *Journal of Sound and Vibration*, **207**(4), 521–535, (1997).

12 C.H. Hodges, and J. Woodhouse, Vibration isolation from irregularity in a nearly periodic structure: theory and measurements, *Journal of the Acoustical Society of America*, **74**, 894–905, (1983).

13 M. Ruzzene, F. Scarpa, F. Soranna, Wave beaming effects in two-dimensional cellular structures, *Smart Materials and Structures*, **12**, 363–372, (2003).

14 M. I. Hussein, Reduced Bloch mode expansion for periodic media band structure calculations, *Proceedings of the Royal Society of London, Series A*, **465**, 2825–2848, (2009).

15 A.S. Phani, and, N.A. Fleck, Elastic Boundary Layers in Isotropic Periodic Lattices, *ASME: Journal of Applied Mechanics*, **75**(2), 021020–021027, (2008).

16 R.S. Mackay, and, S. Aubry, Proof of existence of breathers for time-reversible or Hamiltonian networks of weakly coupled oscillators, *Nonlinearity*, **7**, 1623–1643, (1994).

17 S. Aubry, Discrete Breathers: Localization and transfer of energy in discrete Hamiltonian nonlinear systems, *Physica D*, **216**, 1–30, (2006).

Phononics 2011: First International Conference on Phononic Crystals, Metamaterials and Optomechanics
Santa Fe, New Mexico, USA, May 29-June 2, 2011
PHONONICS-2011-0117

Phononic Crystals with Applications to Sound and Vibration Control

Jihong Wen

Key Laboratory of Photonic and Phononic Crystals of Ministry of Education, and Institute of Mechatronical Engineering, National University of Defense Technology, Changsha, Hunan 410073, P.R. China
wenjihong@vip.sina.com

Abstract: A two dimensional binary locally resonant phononic crystal (PCs) has been fabricated and thoroughly analyzed. A lumped-mass method has been proposed as an efficient tool to calculate the band structure of PCs. The concept of PCs is introduced into the design of beam and plate structures, and the acoustic materials to improve their vibration and sound performance.

The propagation of acoustic/elastic waves in periodic composite materials known as phononic crystals (PCs) has received considerable attention in recent years. The emphasis is placed on the existence of band gaps within which acoustic/elastic waves are all forbidden. Moreover, when point defects or linear/planar defects are introduced into perfect PCs, acoustic/elastic waves within band gaps will be restricted to the point defects or can only propagate along the linear/planar defects. Such unique properties of PCs are of great interest in the field of confinement, waveguiding and filtering, as well as the area of noise and vibration isolation.

Since the year 2001, funded by the State Key Development Program for Basic Research of China and the National Science Foundation of China, we started research work on PCs and their applications in the area of sound and vibration control. Our research interests focused on the band gap formation mechanisms, band gap calculation methods and potential applications in vibration and noise reduction.

1. Band gap formation mechanism

A crucial foundational problem involved in the investigations of PCs is to gain a clear understanding of the band gap formation mechanisms. Two kinds of mechanisms have been developed: Bragg reflection mechanism and locally resonant (LR) mechanism. Resonance gaps formed by the LR mechanism can be tuned to a very low frequency range with a far smaller lattice constant than that governed by the Bragg condition.

A thorough study has been carried out on the Bragg reflection mechanism and we have revealed the resonance modes near the edges of the first absolute band gap in a two-dimensional (2D) PC with a matrix of epoxy, which lead to a wide band gap. The resonance of the upper band edge is induced by Bragg scattering, and the resonance is mainly concentrated in the matrix. The lower edge resonance is induced by the joint effects of the Bragg and Mie scattering and presents a rotary resonance mode. The gap induced by the rigid-body resonance coalesces with the Bragg gap, so a wider gap comes into being.

The previous LR PCs are all ternary systems, which consist of a cubic array of coated spheres immersed in epoxy or of a lattice of coated cylinders in epoxy (the coatings are thin films of soft rubber). In contrast, we fabricate a 2D binary LR PC composed of periodic soft rubber cylinders immersed in epoxy host. A comprehensive study has been performed. Numerical simulations predict that subfrequency gaps also appear because of the high contrast of mass density and elastic constant of the soft rubber. The LR mechanism in forming the subfrequency gaps is thoroughly analyzed.

Generally, the Bragg reflection mechanism and the locally resonant mechanism focus on the effects of the periodic structure and the single unit cell respectively. We have developed a model including these two factors simultaneously. Through analysing the elastic wave modes in 2D PCs by MST, the uncoupling effects between the differently ordered cylindrical wave components have been identified at the edge of the band gaps. For the uncoupled modes of the lowest gap, a simple analytic expression is presented, which comprises the Mie scattering of a single unit cell and the effects of the periodic structure simultaneously. A comprehensive physical insight into the formation mechanism of the band

Phononics 2011: First International Conference on Phononic Crystals, Metamaterials and Optomechanics
Santa Fe, New Mexico, USA, May 29-June 2, 2011
PHONONICS-2011-0117

gaps is provided, no matter the band is derived of Bragg reflection or local resonance. In addition, a clear physical understanding of the formation of full band gaps is also proposed.

2. Band gap calculation methods

Several theoretical methods have already been developed for the calculation of band structures of PCs. Mostly, the calculations are based on the plane-wave expansion (PWE) method, in which the wave equations are solved in Fourier space. Nevertheless, PCs involving media with a large contrast in their elastic/density properties are not easy to treat with PWE because a large number of plane waves are required to obtain reliable band structures. Other methods such as the variational method and the finite difference time domain algorithms overcome the convergence problem in a certain extent. The multiple scattering theory (MST) has advantages in convergence. However, it can only handle specific arrays of spheres (3D) or cylinders (2D) up to now and complicated mathematical deductions are always required.

A lumped-mass method that works in the direct space based on the discretization of continuous systems has been proposed by us as a new way to compute the band structure of PCs. We conclude that the lumped-mass method converges faster and its convergence is insensitive to the sharp variation of elastic constants on the interfaces inside the PCs. Especially, the latter advantage is unique in comparison with other studies on the improvement of plane-wave expansion methods. Another unique feature of the new method is that it needs not deduce the structure factors for every inerratic shape thus it can be used to deal with PCs with any unit shapes directly.

3. Applications in vibration and noise reduction

The investigations on PC materials/structures are driven partly by their potential applications such as wave filters, vibrationless environments for high-precision systems, transducer design, etc. By introducing the idea of PCs into the design of engineering structures, such as beams and plates, band gaps can be achieved to control the transmission of vibrations. Vibration band gaps in these structures, based on either the Bragg reflection mechanism or the locally resonant mechanism, have been found theoretically and experimentally. Furthermore, the characteristics of directional propagation of elastic waves in 2D PCs within specific pass band frequencies has be studied and utilized to control the direction of the vibration transmission. These studies provide new ideas for the application of PCs in the field of structural vibration control.

The idea of localized resonance in PCs is introduced to improve the low-frequency acoustic absorption of viscoelasitc materials. Both the theoretical results and the experimental measurements show the phenomenon of low-frequency absorption. The outputs of our work may be useful for tailoring the acoustic absorption properties and are expected to have applications in underwater acoustic absorption materials.

Phononics 2011: First International Conference on Phononic Crystals, Metamaterials and Optomechanics
Santa Fe, New Mexico, USA, May 29-June 2, 2011
PHONONICS-2011-0121

Using classical FEM to predict the dynamical response of periodic devices in acoustic and vibration applications

Miguel M. Neves[1], Olavo M. J. Silva[2], Hugo Policarpo[3], António G. Cartaxo[3]

[1] IDMEC-IST, DEM, TULisbon, Av. Rovisco Pais, 1049-001Lisboa, Portugal., maneves@dem.ist.utl.pt,
[2] Laboratory of Acoustics and Vibration, Federal University of Santa Catarina, Brazil olavo@lva.ufsc.br,
[3] DEM, TULisbon, Av. Rovisco Pais, 1049-001Lisboa, Portugal., hugo.policarpo@ist.utl.pt, antonio.cartaxo@sapo.pt

Abstract: The task of predicting the dynamical response and tailoring wave propagation filters for practical frequency ranges is here presented. Finite element steady-state analysis is performed on periodic devices of finite length considering periodic distribution of materials, addition of masses to a tube and periodic curvatures. Validation obtained with prototypes, one for attenuation of axial vibration and other for sound propagation, is also mentioned.

Four periodic devices were studied for passive control of elastic wave propagation. Analytical, numerical and experimental results were obtained to verify and validate the models used. In the first example, it is considered the case of the dynamical characterization of the axial harmonic response (U) at one end of a multi-laminated periodic bar. The bar is excited by an axial harmonic force (F) at the other end (see Fig. 1). Design of such devices can be found in literature, see for e.g. in Hussein et al.[1]. In order to have the device working within a frequency range of interest, it was recommended to use a periodic sequence of cells built from steel and cork agglomerate. The main purpose of this material choice was to play with the high contrast in the wave propagation speeds. This is done to maximize vibration attenuation regions present where predictable stop-bands regions are known to exist for the case of infinite periodic structures. Experimental results confirmed the predicted attenuation regions (for details see, Policarpo et al.[1]).

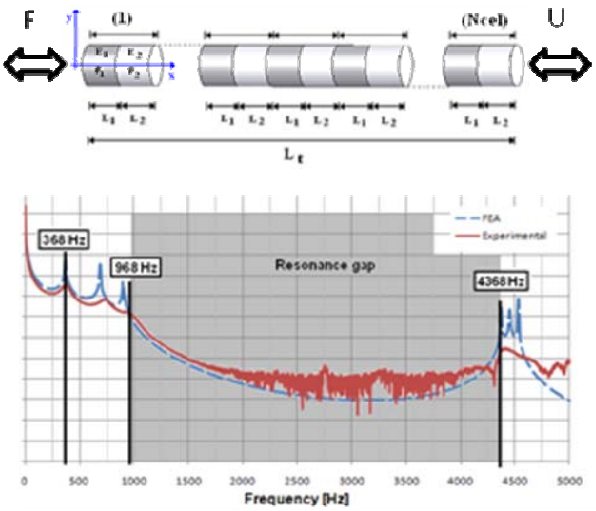

Figure 1 At the top, distribution of two material components along the rod. At the bottom, predicted (FEA) and experimental responses.

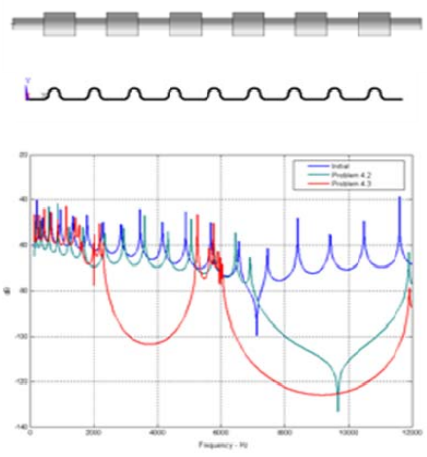

Figure 2 At the top, straight hollow tubes with periodically repeated diameter or curvature. At the bottom: harmonic responses from the periodic tubes and from a straight hollow tube of constant diameter (for the same weight, length and internal diameter).

The second and third examples are from a similar attenuation problem for the flexural vibrations at one end of a hollow shaft excited by a transversal force at the other end. A straight tube with periodically repeated piecewise constant diameter (also seen as added masses) is presented in the second problem. For the third case, the tube is defined as a sequence of periodically-repeated

Phononics 2011: First International Conference on Phononic Crystals, Metamaterials and Optomechanics
Santa Fe, New Mexico, USA, May 29-June 2, 2011
PHONONICS-2011-0121

curvatures (see Fig. 2). Although authors found this parametrization interesting for some pratical applications, it was not found in scientific literature. The corresponding frequency response graphics illustrate practical improvements of their response in comparison to the equivalent straight hollow tube of the same length, weight and internal diameter. For the sake of simplicity, the FE models were limited to the elastic bar (i.e., link or rod elements) and to Euler-Bernoulli beams, but in principle the algorithms used can be applied to shells and solids as well.

As a last example, sound transmission through a periodically spaced array of steel cylinders (Fig. 3) was also studied for comparison between analytical, numerical and experimental results (obtained in an anechoic chamber). It required the building of two classical FE models and a prototype. First, a Fluid-Structure Interaction (FSI) modeled by a finite element technique is used to analyze the case of a wave propagating in the air through a periodic distribution of cylinders perpendicular to the direction of the wave propagation. Second, the FSI is deactivated, resulting in a model with only an acoustic fluid with fixed holes instead of the cylinders. The experiments confirmed that the prototype exhibits strong sound attenuation bands at the frequencies predicted in literature (Sánchez-Pérez et al. [2]). The effect is considerably well reproduced by means of numerical simulations (in this case, for the frequency range of 1250 up to 1750 kHz). Experimental results with the prototype in an anechoic chamber confirmed the predicted attenuation.

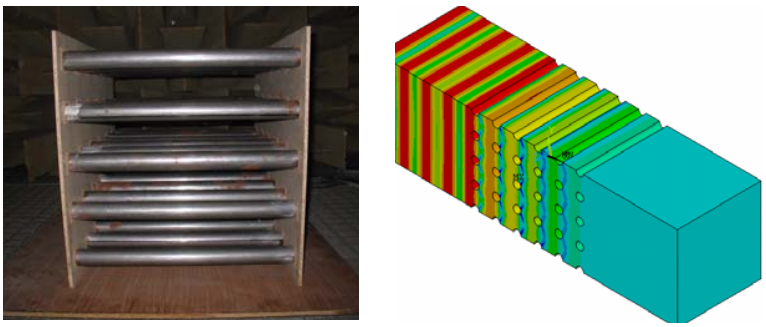

Figure 3 Left: A photo of the experimental device built from a periodically spaced array of metallic cylinder elements in air. Right: A plot of the air pressure distribution predicted from the harmonic FE analysis considering a plane wave at the entry and anechoic boundary condition at the exit.

In conclusion, the use of classical finite elements with harmonic (steady-state) analysis allowed to correctly predict the behavior of these simple devices. Although frequencies were not very low, the frequency ranges were considered of interest for engineering applications. The results showed a good correlation with the predictions of the corresponding Bloch wave analysis, as long as the number of finite elements used per wavelength is adequate. Simple finite element meshes were used. Experimental tests performed at axial vibration devices and at the set of parallel cylinders shown good correlation with the numerical predictions. It is expected that these contributions can make it easier for engineers to understand and to use the advantages of the actual phononics knowledge.

Acknowledgements
This study received financial support from FCT (Portuguese Science Foundation) through the project PTDC/EME-PME/71488/2006 (NM) and IDMEC-IST (Portugal).

References
[1] M. I. Hussein, G. M. Hulbert, and R. A. Scott, Dispersive elastodynamics of 1D banded materials and structures: design. *J Sound Vib* **307**:865-893 (2007).
[2] H. Policarpo, M.M. Neves, A.M.R. Ribeiro, Dynamical response of a multi-laminated periodic bar: Analytical, numerical and experimental study, *SHOCK AND VIBRATION*, **17** (4-5), 521-535 (2010).
[3] J. V. Sánchez-Pérez, D. Caballero, R. Mártinez-Sala; C. Rubio; J. Sánchez-Dehesa; F. Meseguer; J. Llinares; F. Gálvez; Sound Attenuation by a Two-Dimensional Array of Rigid Cylinders, *Physical Review Letters*, **80** (24), 5325-5328 (1998).

Phononics 2011: First International Conference on Phononic Crystals, Metamaterials and Optomechanics
Santa Fe, New Mexico, USA, May 29-June 2, 2011
PHONONICS-2011-0123

Dynamical effective properties of elastic multilayers

O. Poncelet[1], A. N. Norris[1,2], A. L. Shuvalov[1], A. A. Kutsenko[1]

[1] Université de Bordeaux, CNRS UMR 5295, I2M, Talence, France
olivier.poncelet@u-bordeaux1.fr, alexander.shuvalov@u-bordeaux1.fr, kucenkoa@rambler.ru
[2] Mechanical & Aerospace Engineering, Rutgers University, Piscataway NJ, USA
norris@rutgers.edu

Abstract: Based on the state-vector formalism, a material with the Willis type of constitutive relations is recovered as the model of an homogeneous dispersive effective medium that emulates periodic multilayered or graded materials. The effective material constants are defined through the actual physical parameters in the form, which is not, in principle, restricted to low frequency and which can reveal both the dispersion and the stopbands. Some examples for the out-of-plane case are provided.

The state-vector formalism and the wave number matrix K

The state-vector formalism is well-suited for describing elastic waves in anisotropic 1D-heterogeneous media with density $\rho(y)$ and stiffness tensor $c_{ijkl}(y)$. Consider quasi-plane modes with the phase factor $\exp \mathrm{i}(k_x x - \omega t)$, where ω is the frequency and k_x the wavenumber in an arbitrarily chosen direction X orthogonal to Y. Taking the Fourier transforms of the equilibrium ($\sigma_{ij,i} = \rho \ddot{u}_j$) and stress–strain ($\sigma_{ij} = c_{ijkl} e_{kl}$) equations in all variables except y leads to an ordinary differential system for the state vector $\boldsymbol{\eta}(y) = \left(\mathbf{u}(y) \quad \mathrm{i}\mathbf{n}\boldsymbol{\sigma}(y)\right)^{\mathrm{T}}$:

$$\frac{\mathrm{d}}{\mathrm{d}y}\boldsymbol{\eta}(y) = \mathbf{Q}(y)\boldsymbol{\eta}(y), \quad \mathbf{Q}(y) = \mathrm{i}\begin{pmatrix} k_x \mathbf{N}_1 & \mathbf{N}_2 \\ k_x^2 \mathbf{N}_3 - \rho\omega^2 \mathbf{I} & k_x \mathbf{N}_1^{\mathrm{T}} \end{pmatrix}, \quad \begin{array}{l} \mathbf{N}_1 = \mathbf{N}_4^{\mathrm{T}} = -(nn)^{-1}(nm) \\ \mathbf{N}_2 = -(nn)^{-1} \\ \mathbf{N}_3 = (mm) - (mn)(nn)^{-1}(nm) \end{array} \tag{1}$$

where $\mathbf{m}$ and $\mathbf{n}$ denote the unit vectors parallel to X and Y, and $(nn)_{jk} = n_i c_{ijkl} n_l$, $(nm)_{jk} = n_i c_{ijkl} m_l = (mn)_{kj}$, $(mm)_{jk} = m_i c_{ijkl} m_l$. Given the initial condition at some $y_0 (\equiv 0)$, the solution to system (1) is $\boldsymbol{\eta}(y) = \mathbf{M}(y,0)\boldsymbol{\eta}(0)$, where $\mathbf{M}(y,0)$ is the 6×6 matricant evaluated by the product of the matrix exponentials of the homogeneous layers or more generally by the Peano series in case of a graded material[1].

Now let ρ, c_{ijkl} and hence $\mathbf{Q}$ depend on y periodically with a period T. In this case the central role is played by the matricant $\mathbf{M}(T,0)$ over the unit cell $[0,T]$ which is called the monodromy matrix. For instance, $\mathbf{M}(T,0) = \prod_n^{j=1} \mathrm{e}^{\mathbf{Q}_j d_j}$ for a piecewise homogeneous (layered) medium. The wavenumber matrix $\mathbf{K}$ is introduced by denoting $\mathbf{M}(T,0) = \exp(\mathrm{i}\mathbf{K}T)$ whence $\mathrm{i}\mathbf{K} = \frac{1}{T}\ln \mathbf{M}(T,0)$. For relatively low frequency, it can be evaluated as $\mathrm{i}\mathbf{K} = \langle \mathbf{Q} \rangle + \Sigma_{m=1}^{\infty} \mathrm{i}\mathbf{K}^{(m)}$ where $\langle\cdot\rangle$ denotes the average over a period and $\mathbf{K}^{(m)}$ are the matrix coefficients of the Magnus expansion of matrix logarithm ($\mathbf{K}$ is thereby defined in the first Brillouin zone that corresponds to the zeroth Riemann sheet of $\ln z$ with a cut $\arg z = \pm\pi$).

Dynamic homogenization and constitutive equations

Formally, $\exp(\mathrm{i}\mathbf{K}y)$ is a solution to equation (1) with the actual matrix of coefficients $\mathbf{Q}(y)$ replaced by the constant matrix $\mathrm{i}\mathbf{K}$. This motivates the concept of an effective homogeneous medium, whose material model admits the wave equation in the form (1) with a constant system matrix $\mathbf{Q}_{eff} \equiv \mathrm{i}\mathbf{K}$. Dynamic properties are realized by taking $\mathbf{Q}_{eff} = \mathrm{i}\mathbf{K}$ beyond the zero-order term $\langle \mathbf{Q} \rangle$ that describes the quasi-static limit only. It turns out[2] that the dispersive density matrix $\boldsymbol{\rho}^{(eff)}$ and elastic tensor $c_{ijkl}^{(eff)}$ of the effective medium must be complemented by a stress-impulse coupling that leads to the motion and constitutive equations in the Willis form:

$$\sigma_{ij,i} = \dot{p}_j, \qquad \sigma_{ij} = c_{ijkl}^{(eff)} e_{kl} + S_{ijr}\dot{u}_r, \qquad p_q = S_{klq} e_{kl} + \rho_{qr}^{(eff)} \dot{u}_r, \tag{2}$$

where $\mathbf{p}$ is the vector of momentum density, and $S_{ijk} = S_{jik}$ is the Willis coupling tensor[4]. The effective material constants $c_{ijkl}^{(eff)}(\omega)$, $S_{ijr}(\omega)$ and $\rho_{qr}^{(eff)}(\omega)$ can be expressed via the actual material properties $c_{ijkl}(y)$ and $\rho(y)$.

Phononics 2011: First International Conference on Phononic Crystals, Metamaterials and Optomechanics
Santa Fe, New Mexico, USA, May 29-June 2, 2011
PHONONICS-2011-0123

Examples for the case of SH waves in a periodically bilayered medium

We illustrate the general formulation by considering SH waves propagating in a periodic structure of isotropic unit cells. In this case, the out-of-plane effective constitutive relations are as follows:

$$\sigma_{13} = c_{55}^{(eff)} u_{,1} + c_{54}^{(eff)} u_{,2}\,, \qquad \sigma_{23} = c_{45}^{(eff)} u_{,1} + c_{44}^{(eff)} u_{,2} + S_{43}\dot{u}\,, \qquad p_3 = S_{43} u_{,2} + \rho^{(eff)}\dot{u}\,. \tag{3}$$

If the unit cell consists of two homogeneous isotropic layers, then the effective material parameters involved in (3) can be found beyond the low-frequency range in an exact form of transcendental functions of unrestricted ω and k_x, see Ref. 2. Figure 1 shows these effective parameters computed for the normal propagation ($k_x = 0$) through the periodic stack of layers $j = 1,2$ of equal thickness ($d_j = \frac{1}{2}$) with $\rho_1 = 1$, $c_1 = 1$ and $\rho_2 = 2$, $c_2 = 2$, where $c_i = \sqrt{\mu_i / \rho_i}$ is the shear wave speed. The vanishing of both $c_{44}^{(eff)}$ and $\rho^{(eff)}$ at the band edge at $\omega = \omega_1 \approx 2.6$ is expected on the basis of the fact that $\mathbf{Q}_{eff}$ is singular at the band edge and scales as $(\omega - \omega_1)^{-1/2}$ near it[3]. The square root decay of both $c_{44}^{(eff)}$ and $\rho^{(eff)}$ is apparent in figure 1.

As an example of the type of boundary problem that can be solved using the effective medium equations, consider reflection–transmission of SH waves at a bonded interface $y = 0$ between the half-space of the periodically stratified medium ($y > 0$) and a uniform half-space ($y < 0$) of isotropic material with ρ_0 and $c_0 = \sqrt{\mu_0 / \rho_0}$. An SH wave is incident from the uniform half-space with propagation direction at angle θ from the interface normal. The total solution is taken as $u(x,y) = e^{\mathrm{i}k_x x}\left(e^{\mathrm{i}k_y y} + Re^{-\mathrm{i}k_y y}\right)$ for $y \le 0$ and $u(x,y) = Te^{\mathrm{i}k_x x}e^{\mathrm{i}K(\omega,k_x)y}$ for $y \ge 0$, with $(k_x, k_y) = \omega / c_0\,(\sin\theta, \cos\theta)$. Taking into account the continuity conditions for displacement and traction at $y = 0$ yields the reflection and transmission coefficients R and T in the standard form $R = (Z_- - Z_+)/(Z_- + Z_+)$ and $T = 2Z_-/(Z_- + Z_+)$, where $Z_- = \rho_0 c_0 \cos\theta$ is the impedance in the uniform half-space and $Z_+ = \omega^{-1}\left(Kc_{44}^{(eff)} + k_x c_{45}^{(eff)} - \omega S_{43}\right)$ is the impedance for the effective medium equivalent to the periodic half-space. It is noteworthy that the effective impedance Z_+ is identical to the impedance of the actual periodic material because they both imply a ratio of components of the outgoing eigenvector that is common for $\mathbf{M}(T,0)$ and $\mathbf{K}$. Thus the above solution for the reflection and transmission coefficients, which is expressed via the effective material parameters, is an exact result. Figure 2 shows its calculation for the case of normal incidence.

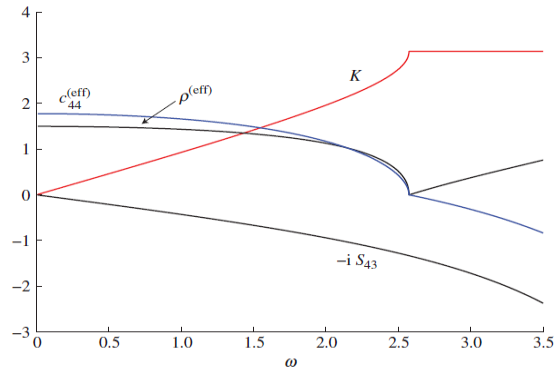

Figure 1 The effective material constants of Eq. (2) at $k_x = 0$ (elastic in blue, inertial in black) for the periodically bilayered medium (see its parameters in the text). The vertical wavenumber is added (in red). The frequency range includes the first band edge which is at the frequency where $\mathrm{Re}\,K = \pi$ first occurs. Only the real parts of the quantities indicated are plotted (for ω in the stopband the imaginary parts of $c_{44}^{(eff)}$, $\rho^{(eff)}$ and K are non-zero but not shown).

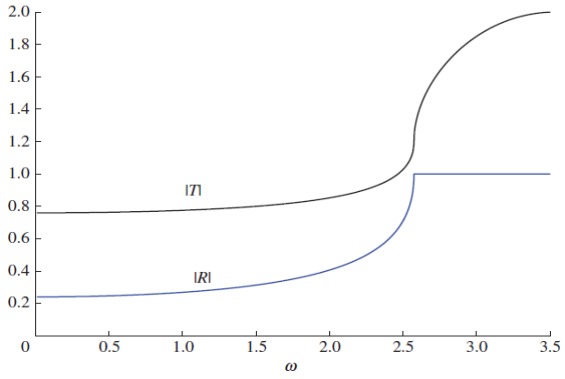

Figure 2 The magnitude of the reflection and transmission coefficients $|R(\omega)|$ and $|T(\omega)|$ for normal incidence ($\theta = 0$ or $k_x = 0$) from a uniform half-space with $\rho_0 = 1$, $c_0 = 1$ on a periodically bilayered structure which was used in figure 1. As expected, $|R| \le 1$ with total reflection in the stopband.

References

[1] M. C. Pease-III, *Methods of matrix algebra*, Academic Press, New-York, NY (1965).
[2] A. L. Shuvalov, A. A. Kutsenko, A. N. Norris, and O. Poncelet, *Proc. R. Soc. A,* doi:10.1098/rspa.2010.0389 (2011).
[3] A. L. Shuvalov, A. A. Kutsenko, and A. N. Norris, *Wave Motion* **47**, 370–382 (2010).
[4] G. W. Milton, and J. R. Willis, *Proc. R. Soc. A* 463, 855–880 (2007).

Phononics 2011: First International Conference on Phononic Crystals, Metamaterials and Optomechanics

Santa Fe, New Mexico, USA, May 29-June 2, 2011

PHONONICS-2011-0137

Structurally-Inspired Phononic Metamaterials

Gregory M. Hulbert[1] , Julien Meaud[1], Zheng-Dong Ma[1]

[1] Department of Mechanical Engineering, University of Michigan, Ann Arbor, MI 48109-2125, USA, hulbert@umich.edu, jmeaud@umich.edu, mazd@umich.edu

Abstract: The distinction between materials and structures has blurred. The development of phononic metamaterials based upon novel structural systems is considered in this work. In particular, a Negative-Poisson Ratio (NPR) structure is used as the foundation for developing phononic metamaterials comprising a 'structural' framework of stiff material and a more compliant material that can dissipate energy.

The distinction between materials and structures, has, in the past decade, become blurry. In a recent publication[1] that received some publicity, the discovery of ice crystals on the moons of Saturn and Neptune exhibit negative linear compressibility, also known as Negative-Poisson Ratio (NPR) response and negative thermal expansion. The underlying molecular structure shown resembles mechanism-like topologies. In the context of phononics, dispersive behavior exhibited by materials[2-4] motivated the development of structurally-based systems with the ability to mitigate energy propagation through structures[5-7].

Inspired by the progess in phononic metamaterials and the applications of NPR materials[8], we recently began investigating the development of phononic metamaterials based upon novel structural systems. In particular, a Negative-Poisson Ratio (NPR) structure is used as the foundation for developing phononic metamaterials comprising a 'structural' framework of stiff material and a more compliant material that can dissipate energy. The goal of this work is to model, analyze and design NPR structures at different length scales with an aim towards creating structurally-based materials, which can be manufactured practically at the sub-millimeter scale.

Figures 1 and 2 depict two baseline structural topologies that exhibit significantly different effective Poisson ratios. The configuration of Figure 1 has an effective Poisson ratio of -0.8 while that of Figure 2 is -7.5. The loading direction is considered as vertical with the effective response measured laterally. Figure 3 shows one of the baseline topologies, including the void space filled with a soft, polymer fill.

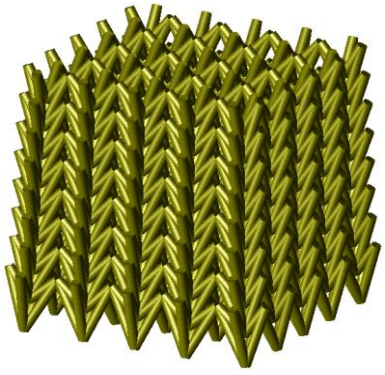

Figure 1 NPR structural configuration with $\nu = -0.8$

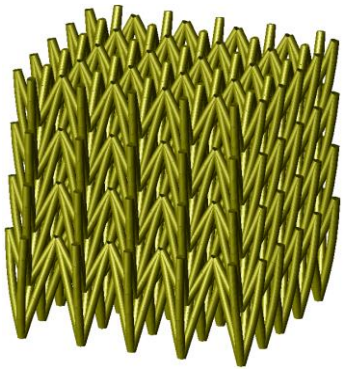

Figure 2 NPR structural configuration with $\nu = -7.5$

Phononics 2011: First International Conference on Phononic Crystals, Metamaterials and Optomechanics
Santa Fe, New Mexico, USA, May 29-June 2, 2011
PHONONICS-2011-0137

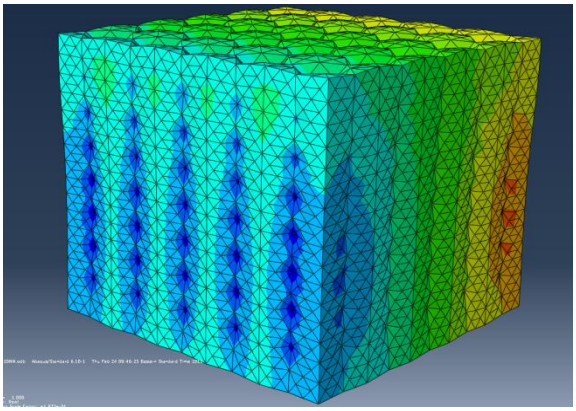

Figure 3 NPR structural configuration with polymer fill

The dynamic response of the NPR-based material/structural concepts is computed using a unit cell analysis for both the void and polymer filled architectures. The effective performance of these concepts is assessed for energy attenuation across frequency bases, with consideration of different cell sizes associated with a structural-sized unit cell and with a unit cell size on the millimeter or smaller scale.

References

[1] A.D. Fortes, E. Suard, and K.S. Knight, *Science*, **331**, 742-746 (2011).
[2] M.I. Hussein, G.M. Hulbert, and R.S. Scott, *JSV,* **289**, 779-806 (2006).
[3] M.I. Hussein, G.M. Hulbert, and R.S. Scott, *JSV,* **307**, 865-893 (2007).
[4] M.I. Hussein, K. Hamza, G.M. Hulbert, and K. Saitou, *Waves in Random and Complex Media,* **17**, 491-510 (2007).
[5] E. Dede, and G.M. Hulbert, *IJNME,* **73**, 470-492 (2008).
[6] E. Dede, and G.M. Hulbert, *JSV,* **313**, 493-509 (2008).
[7] E. Dede, and G.M. Hulbert, *FEAD,* **44**, 819-830 (2008).
[8] Y. Liu, and Z.-D. Ma, IMECE 2007, **10B**, 965-973 (2008).

Phononics 2011: First International Conference on Phononic Crystals, Metamaterials and Optomechanics
Santa Fe, New Mexico, USA, May 29-June 2, 2011
PHONONICS-2011-0148

Longitudinal Vibration Band Gaps in Rods with Periodically Attached Multi-Degree-of-Freedom Vibration Absorbers

Yong Xiao, Jihong Wen, Xisen Wen

Institute of Mechatronical Engineering, and Key Laboratory of Photonic and Phononic Crystals of Ministry of Education, National University of Defense Technology, Changsha 410073, China
xiaoyong.nudt@gmail.com

Abstract: Band gap behavior in rods with periodically mounted multi-degree-of-freedom resonators (vibration absorbers) is concerned. Explicit expressions are derived for the calculation of complex band structures. The effects of absorber parameters on the band gap properties are studied. The band gap formation mechanisms of the system are explained by analytical models with explicit formulations.

Band gap characteristics of uniform rods with periodically attached multi-degree-of-freedom (MDOF) resonators (or call "vibration absorbers" in the context of mechanical engineering) are investigated. The system considered is sketched in Figure 1.

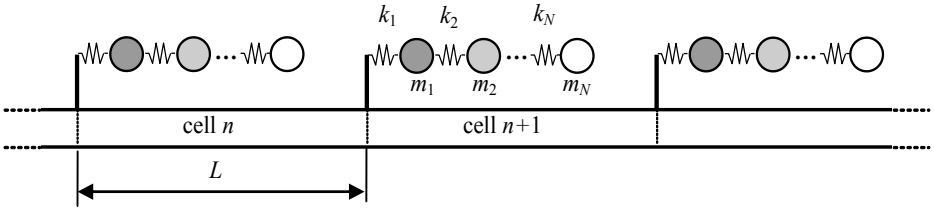

Figure 1 An infinite uniform rod with periodically attached MDOF vibration absorbers.

Using the well-known transfer matrix method, explicit formulation is derived for the calculation of complex band structures of the system

$$\cosh(\pm\mu) = \cos(\beta L) + (\bar{D}/2)\sin(\beta L) \tag{1}$$

where μ is the so-called propagation constant [1, 2], β is the wavenumber for the longitudinal waves in the rods, $\bar{D}$ is the non-dimensional dynamic stiffness of the absorber. Generally, the band gap behaviour can be well represented by the attenuation constant, $\mathrm{Re}(\mu)$, which can be mathematically described by a multivariable function as

$$\mathrm{Re}(\mu) = f(E, A, \rho, L, \omega, m_0, k_1, m_1, k_2, m_2, ...) = \mathrm{Re}\left\{\mathrm{acosh}[\cos(\beta L) + (\bar{D}/2)\sin(\beta L)]\right\} \tag{2}$$

It is demonstrated that both Bragg-type and resonance-type band gaps co-exist in the system. Multiple desired resonance gaps can be achieved due to the multiple natural frequencies of the MDOF absorbers. This is different from the case of single-degree-of-freedom (SDOF) absorber attachments, which produces only one tunable resonance band gap.

The effects of absorber parameters on the band gap behaviour are studied by employing the so-called "attenuation constant surface (ACF)", as first introduced in Ref.[3]. For example, the parametric influence analysis for locally resonant rods with 2DOF absorbers can be performed by employing the following bivariable function

Phononics 2011: First International Conference on Phononic Crystals, Metamaterials and Optomechanics
Santa Fe, New Mexico, USA, May 29-June 2, 2011
PHONONICS-2011-0148

$$\mathrm{Re}(\mu) = f(\omega, k_1)\big|_{k_1 \in (k_{1,\min}, k_{1,\max})} \tag{3}$$

For convenience, the spring stiffness can be nondimensionalized as $\mathrm{K}_1 = k_1/(EA/L)$, and a nondimensional frequency can be defined as $\Omega = \beta L/\pi$. Two numerical examples of ACF defined by Equation (3) are shown in Figure 2. In the first example, the resonance frequencies of the absorber, i.e. Ω_1 and Ω_2, are both tuned to well below the first Bragg condition, thus two low frequency resonance gaps around these frequencies can be achieved. In the second example, the first absorber frequency is set below the first Bragg condition, while the second one it tuned to be equal to the Bragg condition (i.e., $\Omega_2 = 1$). It can be

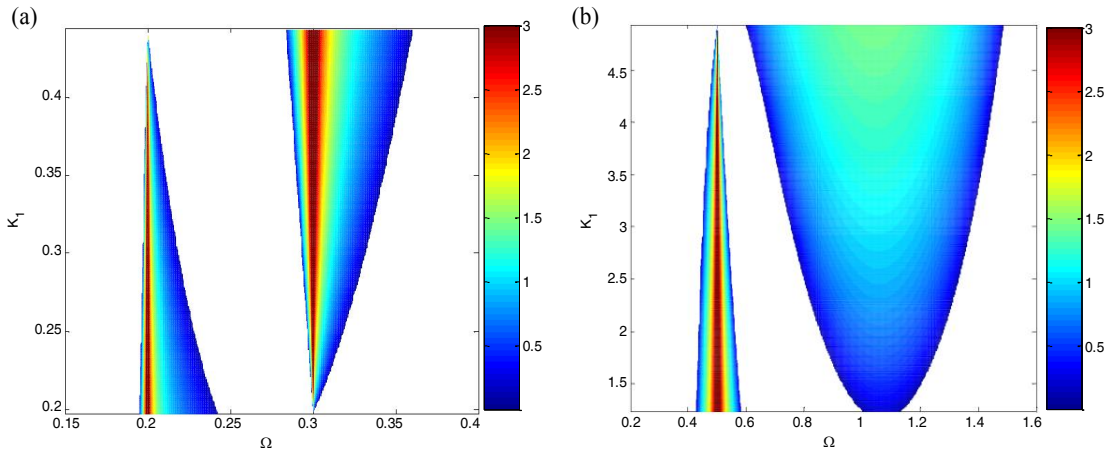

Figure 2 Attenuation constant surfaces of locally resonant rods with 2DOF absorb**ers**. **(a)** $\Omega_1 = 0.2$, $\Omega_2 = 0.4$; **(b)** $\Omega_1 = 0.5$, $\Omega_2 = 1$. The mass ratio of the absorbers is fixed to be $\gamma = 0.5$.

seen band gap coupling phenomenon occurs in this case, giving rise to a super-wide coupled band gap. Such a unique property can be utilized in the broadband control of wave propagation in rods. According to the ACS plots depicted in Figure 2, the width of the band gaps can be adjusted by varying the designing parameter k_1.

Finally, in order to explain the band gap behaviour of the system, both rigorous derivations and physical models are provided to understand the band gap formation mechanisms. Exact expressions are obtained to predict all the band edge frequencies as well as the band gap coupling conditions directly, without the calculation of band gaps.

References

[1] D.J. Mead, *J. Sound Vib*, **27**. 236-260 (1973).
[2] D.J. Mead, *J. Sound Vib*, **319**. 282-304 (2009).
[3] Y. Xiao, B.R. Mace, J. Wen, and X. Wen, *Phys. Lett. A*, **375**, 1485-1491 (2011).

Phononics 2011: First International Conference on Phononic Crystals, Metamaterials and Optomechanics

Santa Fe, New Mexico, USA, May 29-June 2, 2011

PHONONICS-2011-0166

Intensity-Dependent Dispersion in Nonlinear Phononic and Photonic Layered Systems

Kevin L. Manktelow[1] , Michael Leamy[1], Massimo Ruzzene[1]

[1] George W. Woodruff School of Mechanical Engineering, Georgia Institute of Technology, 771 Ferst Drive N.W. Atlanta, GA 30332, USA,

kevin.manktelow@gatech.edu, michael.leamy@me.gatech.edu, massimo.ruzzene@ aerospace.gatech.edu

Abstract: Intensity-dependent dispersion relationships of nonlinear phononic and photonic layered systems are produced. Analysis techniques common in optics are applied to phononic systems, and a recently introduced perturbation approach for discrete phononic systems is applied to optical systems after a finite element discretization. The results are validated with numerical simulation and show that both approaches may be beneficial for system analysis.

Structures with periodically varying geometry and material properties are known to exhibit advantageous wave propagation properties such as negative refractive indices, frequency band gaps and spatial beaming. Periodic layering of materials with differing mass and stiffness properties produces phononic crystals, which tailor elastic and acoustic wave propagation. The optical analogue of phononic crystals is the photonic crystal which is typically formed by periodic layering of materials with alternating permittivity.

Phononic and photonic crystals are typically considered to operate in regimes where a linear constitutive relationship (e.g., stress-strain) provides an adequate representation. For high intensity wave propagation, however, weak nonlinearities can affect performance. For example, a cubic nonlinearity gives rise to frequency shifting and thus a shift in band gap location. In the study of nonlinear optics, a cubic term has been treated using a quasi-linear constitutive relationship with intensity dependent properties. This nonlinearity is known as the Kerr nonlinearity and gives rise to a refractive index proportional to intensity. This technique is explored herein for generating nonlinear dispersion relationships for the elastic case. In addition, a perturbation method developed previously for discrete elastic systems, used in conjunction with a finite element discretization, is proposed as an alternative dispersion analysis tool in both photonic and phononic systems.

One of the simplest phononic or photonic crystals is a one-dimensional bilayered material, consisting of alternating material layers with contrasting properties. This type of structure exhibits many of the interesting properties of more complex photonic or phononic crystals such as non-trivial dispersion and band gaps. Phononic and photonic systems with linear constitutive relationships are governed by the same one-dimensional wave equation. The nonlinear constitutive laws typically employed for phononic and photonic systems result in different nonlinear terms in the fully nonlinear wave equations.

When nonlinearities are excluded from the analysis, an analytical dispersion relation may be obtained succinctly using the transfer matrix method. The transfer matrix method is also applicable to the nonlinear bilayered rod when quasi-linear intensity-dependent material properties replace the full nonlinear model. In this work, the bilayered material system is first discretized using a Galerkin weighted-residuals approach. The discretized system is then analyzed with (1) a linear stress-strain relationship, (2) a quasi-linear stress-strain relationship and the transfer matrix approach, and (3) a perturbation analysis of the fully nonlinear governing equations. The perturbation approach results in fundamentally different band gap structure in some cases and predicts a frequency shift which is less than that estimated by the quasi-linear transfer matrix approach.

Phononics 2011: First International Conference on Phononic Crystals, Metamaterials and Optomechanics

Santa Fe, New Mexico, USA, May 29-June 2, 2011

PHONONICS-2011-0166

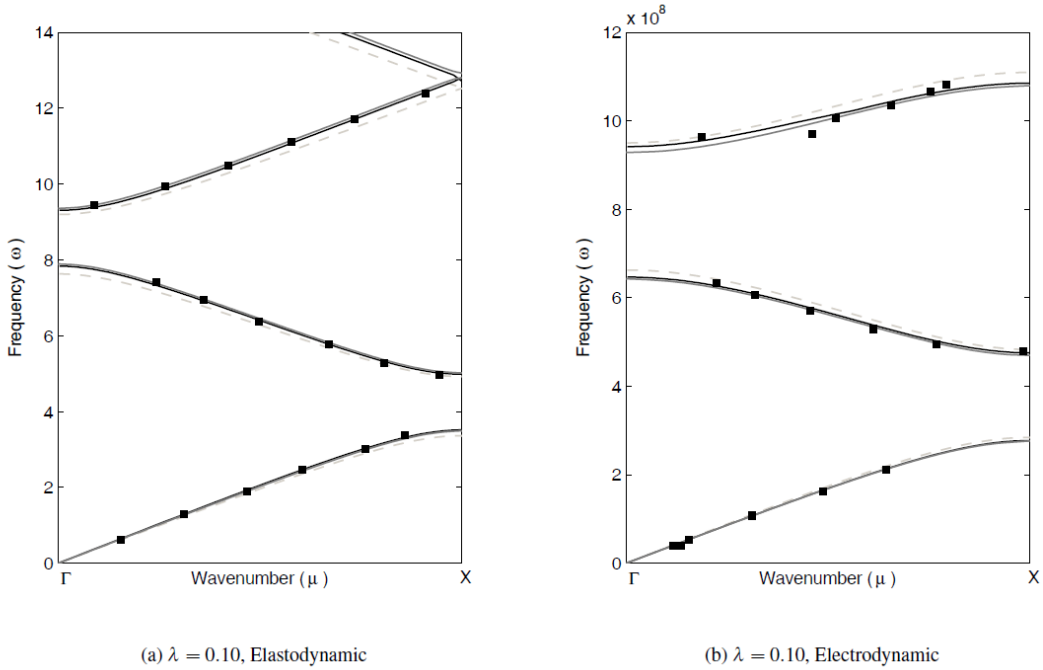

Figure 1. Dispersion band structure for (a) Phononic layered material, and (b) Photonic layered material at relatively large nonlinearities. Dispersion curves are drawn for systems with linear material properties (light-gray dashed), quasi-linear material properties applied using the transfer matrix method (solid dark gray), and fully nonlinear material properties analyzed using finite element discretization and perturbation analysis (solid black). Black markers indicate the results of transient finite element simulations.

Numerical simulations using the fully nonlinear finite element equations are included for validation of the predicted dispersion curves. Numerical simulations are performed using the discretized model over a domain large enough to be considered infinite. The resulting space-time data is analyzed using a two-dimensional discrete Fourier transform to obtain wavenumber/frequency data points. The results show good agreement with the perturbation approach, and indicate that it may provide a simple and accurate framework for the design and optimization of nonlinear phononic and photonic band gaps.

Phononics 2011: First International Conference on Phononic Crystals, Metamaterials and Optomechanics
Santa Fe, New Mexico, USA, May 29-June 2, 2011
PHONONICS-2011-0177

Characterization of Band Gap Resonances in Finite Periodic Structures

Andrew S. Tomchek, Edgar A. Flores, Liao Liu, Bruce L. Davis, Mahmoud I. Hussein

Department of Aerospace Engineering Sciences, University of Colorado at Boulder, CO 80309, USA
andrew.tomchek@colorado.edu, edgar.flores@colorado.edu, liao.liu@colorado.edu, bruce.davis@colorado.edu, mih@colorado.edu

Abstract: While resonant propagation modes are non-existent within band gaps in infinite periodic structures, it is possible for anomalous band-gap resonances to appear in finite periodic structures as a result of the periodicity truncation. We establish two criteria for the characterization of band-gap resonances and propose an approach for their elimination. By considering flexural periodic beams, we show that as the number of unit-cells is increased the vibration response corresponding to band-gap resonances (1) does not shift in frequency, and (2) drops in amplitude. Both these outcomes are not exhibited by regular pass-band resonances, nor by resonances in finite homogenous beams when the length is changed. Our conclusions stem from predictions based on Timoshenko beam theory coupled with matching experimental observations.

We consider a periodic beam structure composed of alternating layers of Aluminum (Al) and the polymer ABS. First we utilize Bloch theory, and following a Bloch FE formulation[1,2] we compute the band structure of an infinite periodic structure. This calculation shows that three relatively large band gaps exist between 0 and 9 kHz, as shown in Fig. 1 (top). In order to study the finite-size effects, we seek an FRF for the same periodic structure with a finite number of unit-cells. Fig. 1 (bottom) shows this result obtained theoretically (solid line) and experimentally (dashed line) for a 5-unit-cell beam in which the "input" force excitation and the "output" displacement evaluation are at the extreme ends of the structure. We observe that a clear anomalous resonance peak exists well inside the second band gap. We refer to this as a band-gap resonance. To distinguish between this type of resonance and regular pass-band resonances, we increase the number of unit-cells in the finite structure and note the effects on all the resonances within our covered frequency range of 0-9 KHz. The results are shown in Fig. 2, from both theory and experiment. First we observe in Fig, 2 (top) that the frequency of the band-gap resonance does not shift as the number of unit-cells is incremented from 5 to 6, while in contrast the frequencies of all the regular pass-band resonances experience clear shifts. Second we observe in Fig. 2 (bottom) that the amplitude of the band gap resonance drops significantly as the number of unit-cells in increased from 5 to 15, while the amplitudes of all the regular pass-band resonances do not experience any noticeable drops. These two traits can be used as criteria for the characterization of band-gap resonances.

We next examine the sensitivity of the frequency values corresponding to band-gap resonances to smooth variations in the unit-cell geometric configuration. In the baseline configuration considered above, the length-fraction of ABS in the unit-cell is $a_{ABS}/a = 0.2$, where a_{ABS} denotes the length of the ABS polymer layer. This length-fraction is now varied over that full range $0 \le a_{ABS}/a \le 1$, which at one extreme ($a_{ABS}/a = 0$) represents a homogenous Al beam, and at the other extreme ($a_{ABS}/a = 1$) represents a beam composed of only ABS polymer. Fig. 3 shows the resonances (solid thin lines) of a 5 unit-cell structure as a function of a_{ABS}/a. Experimental results corresponding to an ABS length-fraction of 0.1, 0.15, 0.2, 0.25 and 0.3 are shown as discrete data points (dots). Superimposed in the figure, are the boundaries of all band gaps (solid thick lines) as determined from the application of Bloch theory to corresponding infinite periodic structures. The band-gap resonances, characterized by the two criteria mentioned above, appear inside the band-gap boundaries. It can be seen that the band-gap resonances are noticeably more sensitive to varying the unit-cell layer dimensions than the regular pass-band resonances. Once they exit the band gaps however, these unique resonances become less sensitive to varying a_{ABS}/a, and their sensitivity becomes similar to that of the regular resonances. Furthermore, once outside the band gaps these resonances no longer appear to satisfy the first criterion outlined above, thus losing their uniqueness and transforming to regular pass-band resonances them-

Phononics 2011: First International Conference on Phononic Crystals, Metamaterials and Optomechanics
Santa Fe, New Mexico, USA, May 29-June 2, 2011
PHONONICS-2011-0177

selves. To investigate the effect of unit-cell length (and hence total length of a finite periodic structure) on band-gap resonances, we varied a while keeping $a_{ABS}/a = 0.2$. The results, which are shown in the inset of Fig. 3, indicate that the relative location of a band-gap resonance within a band gap is independent of the unit-cell (or full structure) size. We conclude that varying the topology of the unit cell can be used as an approach for eliminating band gap resonances that arise due to periodicity truncation.

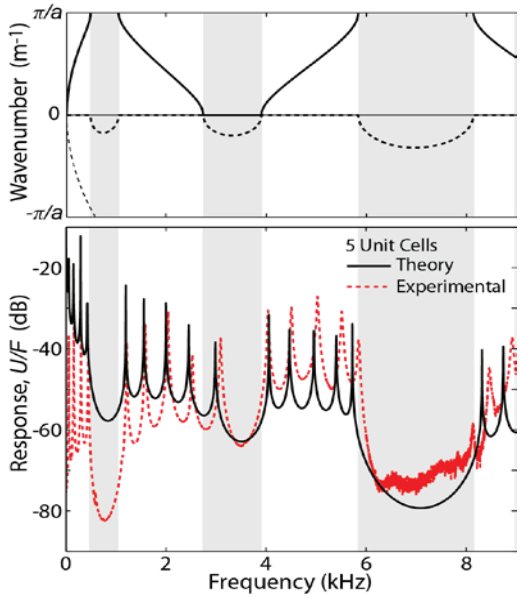

Figure 1. Frequency band diagram of the infinite version of the periodic beam structure (top), and FRF results for the finite periodic beam structure (bottom). In the top sub-figure, the solid line represents propagation modes, and the dashed line represents attenuation modes. The band gaps corresponding to the frequency band structure are shaded in grey in both sub-figures.

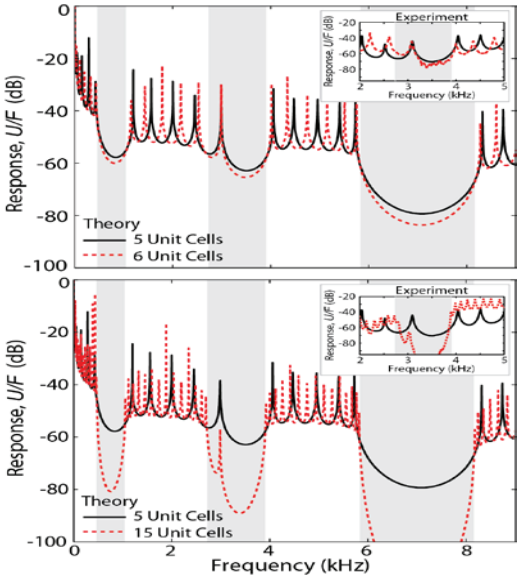

Figure 2. FRF comparison for finite periodic beam structure with different number of unit-cells. The results show that band-gap resonances do not shift in frequency (top) and drop in amplitude (bottom) as the number of unit cells is increased.

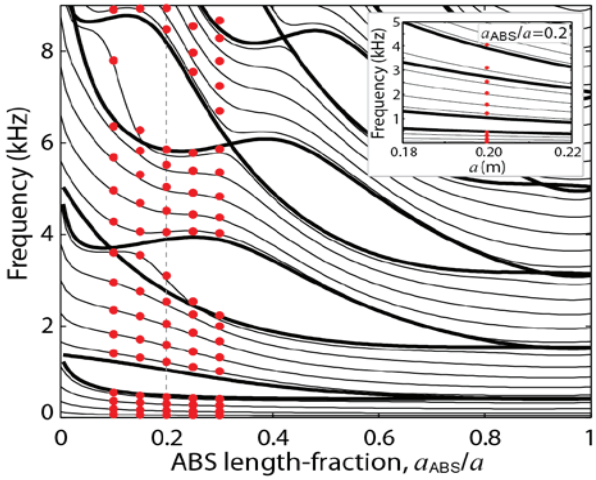

Figure 3. Resonance frequency (thin solid lines, theory; dots, experiment) versus ABS length-fraction for 5-unit-cell finite periodic beam structures. Inset: Resonance frequency (thin solid lines, theory; dots, experiment) versus unit-cell length, a, for a 5-unit-cell periodic beam structure. The thick solid lines in both the main figure and the inset represent the boundaries of the band gaps for corresponding infinite periodic structures.

References

[1] Hussein, M. I., *Proc. R. Soc. A*, **465**, pp. 2825-2848 (2009).
[2] L. Liu and M. I. Hussein, *Seventeenth International Conference on Sound and Vibration,* pp. 1- 7 (2010).

1ST INTERNATIONAL CONFERENCE ON PHONONIC CRYSTALS, METAMATERIALS & OPTOMECHANICS

Extended Abstracts

Track 4: Phonon Transport

Phononics 2011: First International Conference on Phononic Crystals, Metamaterials and Optomechanics
Santa Fe, New Mexico, USA, May 29-June 2, 2011
PHONONICS-2011-0022

Band-gap Acoustic States in 1D and 2D Single Layer Graphene Sheet Systems

Fabrizio Scarpa[1] , **Massimo Ruzzene**[2]

[1] *ACCIS, University of Bristol, BS8 1TR Bristol, UK, f.scarpa@bris.ac.uk,*
[2] *D. Guggenheim School of Aerospace Engineering, Georgia Institute of Technology, Atlanta, GA 30332. massimo.ruzzene@ae.gatech.edu*

Abstract: We evaluate the pass-stop band characteristics of mechanical wave propagating in periodic nanostructures made with nanoribbons or graphene sheets with non-reconstructed defects..

In this work we study the acoustic wave propagation and band-gap characteristics in 1D and 2D single layer graphene sheets with periodic boundary conditions. The 1D graphene systems are represented by graphene nanoribbons with periodic clamped conditions (bridges). The calculation of the wave dispersion characteristics is performed using an atomistic-FE method where the equivalent properties of the C-C bonds [1,2], considered as structural beams, are computed through the minimisation of the Hamiltonian of the system for a specific set of wave propagation constants [3]. The graphene sheets are assembled using the classical FE techniques relative to truss structures, while the pass-stop band characteristics calculated using methods developed by the Authors for periodic 1D and 2D beam assemblies. The periodic graphene nanoribbons show specific wave dispersion properties depending on the edges (zigzag or armchair) along which the acoustic waves are propagating. From a mechanical perspective, the edges of the finite graphene nanoribbons induce a global mechanical special orthotropy of the nanostructures, justifying the assumption that any beam-like wave dispersions could be represented using different Young's moduli along the various directions. We explore also the possibility of nanophononics patterns [4] using periodic non-reconstructed vacancies (NRVs), or assemble graphene sheets with cross-rectangular geometry. The periodic nanostructures provide phase constant surface characteristics, which can used to design novel generation of photonics devices with high GHz bands.

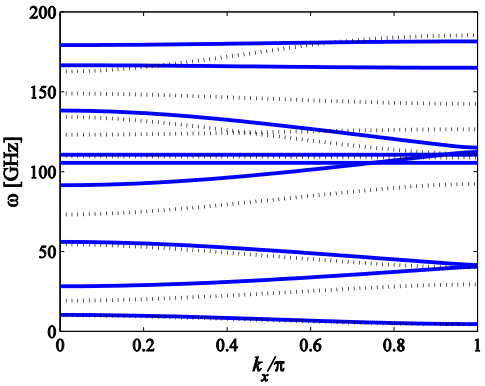

Figure 1. Wave dispersion characteristics for a zigzag (8,0) nanoribbon in minimised (continuous) and non-minimised configuration.

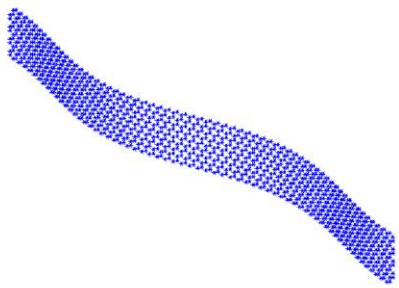

Figure 2 2nd modeshape for the propagation constant kx (0,π) in 1D wave propagation of a nanoribbon.

Phononics 2011: First International Conference on Phononic Crystals, Metamaterials and Optomechanics
Santa Fe, New Mexico, USA, May 29-June 2, 2011
PHONONICS-2011-0022

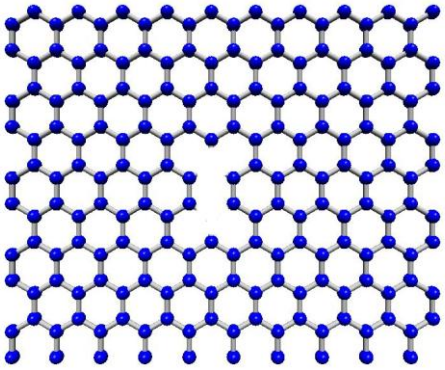

Figure 4. Unit element with double NRV for a 2D periodic array of graphene sheets

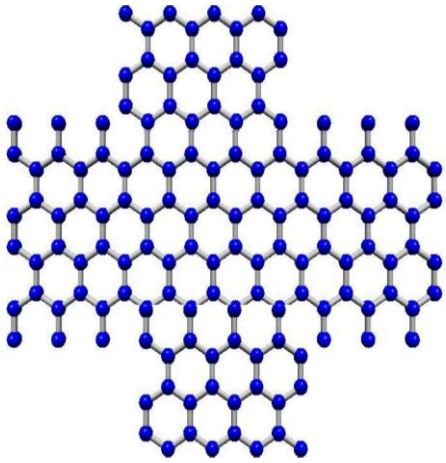

Figure. 5. Periodic unit of assembled (10,0) and (4,0) graphene sheets.

References

[1] Scarpa F, Adhikari S, Srikantha Phani A, 2009. *Nanotechnology*, 20, 065709 (11pp)
[2] Scarpa F, Boldrin L, Peng H X, Remillat C D L, Adhikari S, 2010. *App. Phys. Lett*. 97, 0345012.
[3] Scarpa F, Ruzzene M, Adhikari S, Kam K, 2010. Proceedings of SPIE, San Diego, CA, 6-10 March
[4.] Spadoni A, Ruzzene M, Gonella S and Scarpa F., 2009. *Wave Motion*, 46(7), 435

Phononics 2011: First International Conference on Phononic Crystals, Metamaterials and Optomechanics
Santa Fe, New Mexico, USA, May 29-June 2, 2011
PHONONICS-2011-0042

Phononics: a new science and technology in processing information and controlling heat flow by phonons

Baowen Li[1,2]

[1] *NUS Graduate School for Integrative Sciences and Engineering, Singapore 117456, Singapore*
[2] *Department of Physics, National University of Singapore, Singapore 117542, Singapore*
phylibw@nus.edu.sg

Abstract: Heat due to lattice vibration – *phonons*- is usually regarded as harmful for information processing. However, studies in recent years have changed this mindset. In this paper, I will demonstrate via numerical simulation, theoretical analysis and experiments that, phonons, can be manipulated like electrons. They can be used to carry and process information. Basic phononic devices such as thermal diode, thermal transistor, thermal logic gate and thermal memory can be worked via nonlinear lattice and/or low dimensional nanostructures such as nanowire, nanotube, graphen nanoribbon etc. .

Heat conduction and electric conduction are two fundamental energy transport phenomena in nature, however, they have never been treated equally. The micro electronics, which is based on the inventions of electronic transistor and other relevant devices that control electric flow, has led to an impressive technological development that has changed many aspects of our life. Unfortunately, similar technology in direct controlling heat flow has still not been mastered by human being even though many-attempts have been made. Since in nature, original signals presented by heat are much more prevalent than those by electricity, the application of the latter one can be even more extensive. Thus one would like to know: *is "phononics", the counterpart of the electronics, that provides useful functions by controlling and managing heat current, only a dream?*

It is indeed much more difficult to artificially control the flow of heat in a solid, than to control the flow of electrons. The main reason is, unlike electrons, the carriers of heat -- *phonons* -- are not real particles with definite properties, but rather bundles of energy that have no mass and charge and are therefore unaffected by electromagnetic field. However, compared with the short, several-decade long history of our control over electronic flow, nature has been managing the flow of heat for billions of years, especially inside living bodies, just look at how exact the body temperature is controlled?

This fact not only raises an interesting question to us: how is it possible, but also provides us much confidence that it must be possible even if with completely different mechanism. Thanks to the rapid developments that have taken place in the recent years, we may finally be about to turn *phononics* from a dream into reality. In particular, researchers have recently built varies of heat flow control devices, e.g., thermal diodes and transistors etc, opening the door to functional thermal materials that control the flow of heat at the microscopic level. Moreover, by combining thermal transistors, all thermal logic gates and thermal memory are proposed which allow us to process information with phonons. Here we will demonstrate several basic phononic elements: thermal diode, thermal transistor, thermal logic gate and thermal memory.

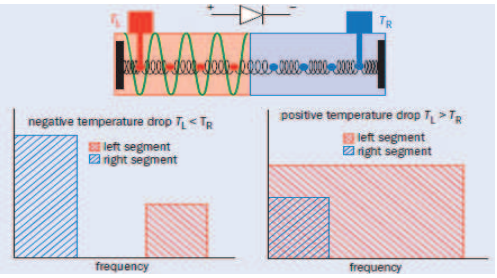

Figure 1. Thermal diode. By coupling two materials or "segments" with different resonant frequencies together, a thermal current can be stopped at or let through the interface depending on the temperatures of the segments (top). The right segment is an array of coupled nonlinear oscillators. The vibration frequency (red in bottom panel) depends on the vibrational amplitude – thus depends on the temperature. The right segment is an array of harmonic oscillator, thus its frequency does not change with temperature (blue in bottom panel). Therefore, in the case of $T_L > T_R$, there is current, whereas when $T_L < T_R$, there is no current. (Picture taken from Wang and Li [1])

Thermal diode: Thermal diode can rectify thermal current. In this device, when we apply temperature gradient in one direction, there is heat current flow through the system, however, when the temperature gradient is reversed the heat low is blocked. The physical principle of the diode is

Phononics 2011: First International Conference on Phononic Crystals, Metamaterials and Optomechanics
Santa Fe, New Mexico, USA, May 29-June 2, 2011
PHONONICS-2011-0042

illustrated in Fig 1. More details can be found in Ref.[1]. This basic phononic device has been demonstrated experimentally by using asymmetric nanotubes [2]

Thermal transistor: Like an electronic transistor, a thermal transistor consists of two segments, the source and the drain, as well as a third segment -the gate- through which the input signal is transferred (top). Crucially, negative differential thermal resistance (NDTR) is possible between the source and drain segments, which allows a heat current to be amplified. The transistor has two functions: switch and amplifier. The schematic picture is given in Fig. 2. More details can be found in Ref.[3]

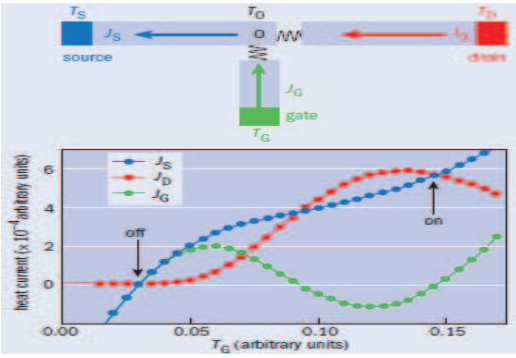

Figure 2: Thermal transistor

Calculations reveal that when the gate temperature (T_G) rises, both the drain current (J_D) and the source current (J_S) increase by a factor of almost 100. In particular, the gate current $J_G = J_S - J_D$ is zero when $T_G \approx 0.03$ and $T_G \approx 0.14$. Because the source current is so very different at the two temperatures, we can turn the transistor "off" by making $T_G = 0.03$ and switch it "on" by making $T_G = 0.14$. By making the thermal resistance between the output (O) and the gate very small, the temperature of the output (T_O) is always close to T_G. This switch function means that a thermal transistor can also be used to carry out thermal logic operations such as NOT, AND and OR. (Picture taken from Wang and Li [1].)

Thermal Logic gate: Thermal transistor provides not only the functions of thermal switch and thermal modulator which will greatly improve our ability to control heat flow, but also the essential functions of signal repeater and NOT gate: digitization and reversion. Based on the successful theoretical realization of thermal transistor, models of all thermal logic gates that can perform all logic operations have thus been presented recently [4]. We show the signal repeater (left panel), NOT gate (middle panel) and AND/OR Gate (right panel) in Figure 3. Details are given in [4].

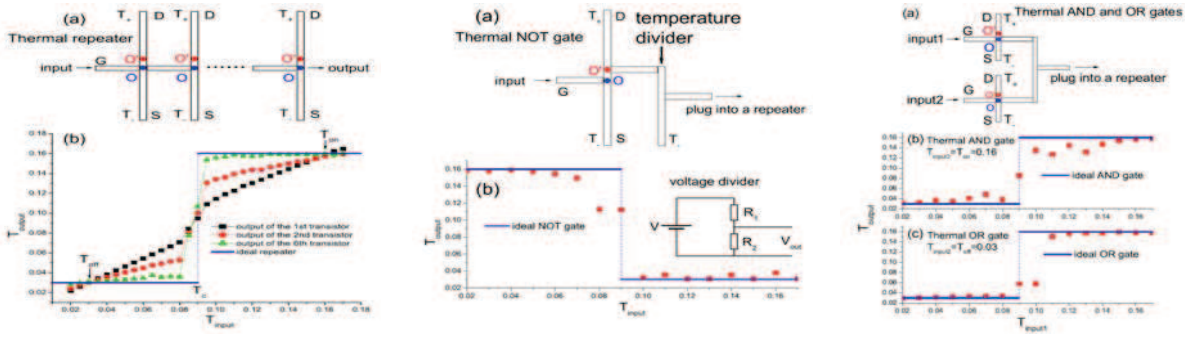

Figure 3. Thermal logic gates. Thermal **Repeater** (left panel), **NOT** gate (middle panel), **AND/OR** Gate (right panel)

Thermal Memory. Memory is an indispensable element for computer besides logic gates. Based on our thermal transistor model, we have demonstrated numerically the principle of thermal memory. Details can be found in Ref.[5]. Most recently, we have demonstrated it experimentally [6].

In summary, we have briefly shown phononic devices such as thermal diode, thermal transistor, thermal logic gate and thermal memory. Some of them have already been demonstrated experimentally. Phononics opens door for controlling and managing thermal current.

References

[1] B. Li, L Wang and G Casati, *Phys Rev. Lett* **93**, 184301 (2004); L Wang and B Li *Physics World* **21** (3), 27 (2008).
[2] C. W Chang, D. Okawa, A. Majumdar, and A. Zettl, *Science* **314**, 1121 (2006).
[3] B. Li, L Wang, and G Casati, *Appl. Phys. Lett.* **92**, 233504 (2006).
[4] L Wang and B Li, *Phys. Rev. Lett* **99,** 177208 (2007).
[5] L Wang and B Li, *Phys. Rev. Lett* **101**, 267203 (2008).
[6] R.-G Xie et al, *Adv. Funct Mat*. (2011) (in press).

Phononics 2011: First International Conference on Phononic Crystals, Metamaterials and Optomechanics
Santa Fe, New Mexico, USA, May 29-June 2, 2011
PHONONICS-2011-0046

Divide and Conquer Quantum Mechanical Methods for Phononic Applications

Rudolph C. Magyar[1]

[1] *Sandia National Laboratories, USA,*
rjmagya@sandia.gov

Abstract: Density functional theory is a highly efficient computational framework that describes structural properties of materials such as phonon frequencies and densities of states. In this talk, we suggest how the divide and conquer scheme may be well suited to determine phononic response in materials with supermolecular scale features.

Density functional theory is a highly efficient computational framework that describes structural properties of materials such as phonon frequencies and densities of states. Applications of DFT demonstrate the theory's reliability for calculating bond lengths and phonon frequencies. One of the greatest challenges to applying DFT to general problems is the increasing computational cost required when treating larger systems. Ideally, the cost would increase linearly with the number of atoms involved, but current workhorse implementations typically increase greater than quadratically. The divide and conquer scheme that was first proposed many years ago has seen a recent resurgence in the study of energetic materials and provides route towards linear scaling calculations of atomic forces and phonon frequencies. In this talk, we suggest how the divide and conquer scheme may be well suited to determine phononic response in materials with supermolecular scale features. We illustrate this with some examples using a computational tool newly developed at Sandia. Sandia National Laboratories is a multi-program laboratory operated by Sandia Corporation, a wholly owned subsidiary of the Lockheed Martin company, for the U.S. Department of Energy's National Nuclear Security Administration under contract DEAC04-94AL85000.

Phononics 2011: First International Conference on Phononic Crystals, Metamaterials and Optomechanics

Santa Fe, New Mexico, USA, May 29-June 2, 2011

PHONONICS-2011-0046

Phononics 2011: First International Conference on Phononic Crystals, Metamaterials and Optomechanics
Santa Fe, New Mexico, USA, May 29-June 2, 2011
PHONONICS-2011-0047

Predicting Phonon Properties Using the Spectral Energy Density

Alan J. H. McGaughey[1], Joseph E. Turney[1], John A. Thomas[1], Haibin Chen[1], Ryan M. Iutzi[1], Alexandre D. Massicotte[1], Cristina H. Amon[1,2]

[1] *Department of Mechanical Engineering, Carnegie Mellon University, Pittsburgh, PA, USA*
[2] *Department of Mechanical & Industrial Engineering, University of Toronto, Toronto ON, Canada*
mcgaughey@cmu.edu

Abstract: The spectral energy density technique for predicting phonon dispersion relations and relaxation times is presented. This technique, which uses atomic velocities obtained from a molecular dynamics simulation, incorporates the full anharmonicity of the atomic interactions. Results for a Lennard-Jones face centered cubic crystal are provided.

The usefulness of analytical models of thermal transport has been hampered by the necessary approximations and assumptions (e.g., a Debye solid, ignoring optical phonons), permitting only qualitative or semi-quantitative predictions.[1] When used with the Green-Kubo or direct methods, molecular dynamics (MD) simulations can predict thermal conductivity.[2-4] Because the analysis in these two methods is performed at the system level, however, no information about the phonons is obtained. The phonon properties needed to calculate thermal conductivity (group velocities, relaxation times) can be predicted using MD simulation and normal mode analysis, but this method requires *a priori* knowledge of the phonon frequencies and polarization vectors and is time-intensive.[2,5] Phonon frequencies and relaxation times can be obtained from harmonic and anharmonic lattice dynamics (LD) calculations, but these are theoretically and computationally complex and only valid at low temperatures.[5-8]

The spectral energy density (SED) presents a straightforward alternative by which phonon frequencies and relaxation times can be obtained using only atomic velocities from an MD simulation as input.[9-11] Here, we present the SED and describe how it can be used to obtain phonon frequencies and relaxation times, which can then be used to predict thermal conductivity. We calculate the SED using results from MD simulations of a test system of Lennard-Jones argon and compare the predicted phonon properties to predictions made using (i) anharmonic LD calculations and (ii) normal mode analysis performed on the results of the MD simulations.

The spectral energy density, Φ, is derived by projecting the velocities of the atoms in a crystal onto the normal modes of vibration. It is given by[11]

$$\Phi(\boldsymbol{\kappa},\omega)=\frac{1}{4\pi\tau_o N_T}\sum_\alpha\sum_b^B m_b\left|\int_0^{\tau_o}\sum_{n_{x,y,z}}^{N_T} v_\alpha\left(n_{x,y,z},b;t\right)\,\exp\left[i\boldsymbol{\kappa}\cdot\mathbf{r}\left(n_{x,y,z},0\right)-i\omega t\right]dt\right|^2, \quad (1)$$

where $v_\alpha(n_{x,y,z},b;t)$ is the α-direction velocity of atom b (with mass m_b) in unit cell $n_{x,y,z}$, $\mathbf{r}(n_{x,y,z},0)$ is the equilibrium position of unit cell $n_{x,y,z}$, B is the number of atoms in the unit cell, N_T is the total number of unit cells, t is time, τ_o is the length of the simulation, $\boldsymbol{\kappa}$ is wave vector, and ω is frequency.

The frequency dependence of the SED for a face-centered cubic Lennard-Jones argon crystal at a temperature of 20 K at selected wave vectors along the [100] direction is shown in Figs. 1(b), 1(c), and 1(d). There is a clear correlation between the locations of the frequency peaks and frequencies calculated using harmonic lattice dynamics calculations, which are shown in the [100] dispersion curves plotted in Fig. 1(a). For each phonon mode, the range of frequencies accessed by the atoms is related to the anharmonicity of the interatomic potential and the corresponding rate of multi-phonon scattering processes. For fixed wave vector, the frequency spread is the Lorentzian function[11]

$$\Phi(\boldsymbol{\kappa},\omega)=\frac{I}{1+[2\tau(\omega-\omega_c)]^2}, \quad (2)$$

Phononics 2011: First International Conference on Phononic Crystals, Metamaterials and Optomechanics
Santa Fe, New Mexico, USA, May 29-June 2, 2011
PHONONICS-2011-0047

where I is the peak height, ω_c is the peak location (i.e., the phonon frequency), and τ is the relaxation time. Thus, by fitting Eq. (2) to each peak in the SED, it is possible to obtain the phonon frequencies and relaxation times. The frequencies plotted versus wave vector give the phonon dispersion curves. The phonon group velocity is the slope of the dispersion curve.

A selection of the relaxation times extracted from the SED plots shown in Fig. 1 are provided in Table 1. The table also includes predictions made using the normal-mode decomposition MD method and anharmonic LD calculations. The normal-mode decomposition predictions are made using the same simulations as those used for the SED. The agreement between the SED method and the normal-mode decomposition method is generally good, as in both methods, the system energy is being mapped from direct space and time to reciprocal space and frequency. The agreement with the anharmonic LD predictions is not as good. This result may be due to the low temperature approximations inherent in LD techniques. The normal-mode decomposition method will lose accuracy at higher temperatures because quasi-harmonic phonon frequencies and polarization vectors are used to perform the energy mapping. The SED method, however, does not suffer from this limitation and should be applicable at higher temperatures as long as the weakly-interacting phonon interpretation is valid.

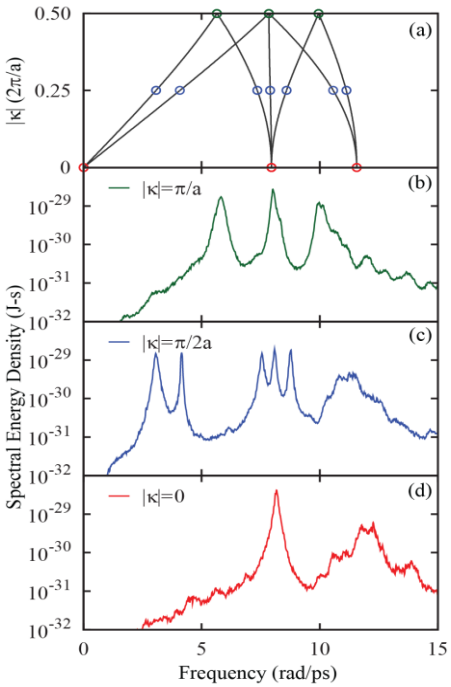

Figure 1 (a) LJ argon [100] dispersion based on a four-atom conventional unit cell representation. (b), (c) and (d): Spectral energy density at select points in the [100] direction at a temperature of 20 K. The modes indicated with open circles on the dispersion curves can be seen as peaks in the SED.

$\|\kappa\|$	Frequency (1/ps)	Spectral Energy Density	Normal Mode Decomposition	Anharmonic Lattice Dynamics
0	8.17	6.02	5.15	12.7
0	12.0	1.10	1.36	1.45
π/a	3.07	5.45	7.43	6.74
π/a	11.4	1.19	1.29	1.57
$2\pi/a$	5.81	3.32	4.28	6.68
$2\pi/a$	10.0	2.47	2.58	4.19

Table 1 Lennard Jones argon [100] relaxation times at 20 K in ps predicted by three different methods.

References

[1]M. G. Holland, *Phys. Rev.* **132**, 2461-2471 (1963).
[2]A. J. H. McGaughey and M. Kaviany, *Phys. Rev. B* **69**, 094303 (2004).
[3]P. K. Schelling, S. R. Phillpot, and P. Keblinski, *Phys. Rev. B* **65**, 144306 (2002).
[4]D. P. Sellan, E. S. Landry, J. E. Turney, A. J. H. McGaughey, and C. H. Amon, *Phys. Rev. B* **81**, 214305 (2010)
[5]A. J. C. Ladd, B. Moran, and W. G. Hoover, *Phys. Rev. B* **34**, 5058-5064 (1986).
[6]A. A. Maradudin and A. E. Fein, *Phys. Rev.* **128**, 2589-2608 (1962).
[7]D. C. Wallace, *Thermodynamics of Crystals*, Cambridge University Press, UK (1972).
[8]J. E. Turney, E. S. Landry, A. J. H. McGaughey, and C. H. Amon, *Phys. Rev. B* **79**, 064301 (2009).
[9]S. Maruyama, *Nano. Micro. Therm. Eng.* **7**, 41-50 (2003).
[10]N. de Koker, *Phys. Rev. Lett.* **103**, 125902 (2009).
[11]J. A. Thomas, J. E. Turney, R. M. Iutzi, C. H. Amon, and A. J. H. McGaughey, *Phys. Rev. B* **81**, 081411(R) (2010).

Phononics 2011: First International Conference on Phononic Crystals, Metamaterials and Optomechanics

Santa Fe, New Mexico, USA, May 29-June 2, 2011

PHONONICS-2011-0049

Heat dissipation in silicon and quartz nanoridges

Pierre-Olivier Chapuis[1,a,*], Mika Prunnila[2], Andrey Shchepetov[2,a], Lars Schneider[1], Emigdio Chavez[1,3], Sampo Laakso[2], Jouni Ahopelto[2], and Clivia M. Sotomayor Torres [1,3,4]

[1] Institut Català de Nanotecnologia (ICN), Centre d'Investigacio en Nanociencia e Nanotecnologia (CIN2), Campus UAB, 08193 Bellaterra (Barcelona), Spain

[2] VTT Microelectronics, PO Box 1000, 02044 VTT, Espoo, Finland

[3] Department of physics, Universitat Autonoma de Barcelona, 08193 Bellaterra (Barcelona), Spain

[4] Institució Catalana de Recerca i Estudis Avançats (ICREA), 08010 Barcelona, Spain

[1] These authors contributed equally.

[*] E-mail: olivier.chapuis@cin2.es

Abstract: We have investigated experimentally the effect of confinement of thermal acoustic phonons in 100 nm large ridges of silicon and quartz. We quantify the deviation to Fourier and ballistic predictions as a function of two characteristic numbers, the constriction Knudsen number describing the transmission of the phonons and a dimensionless number based on the nanoridges volume/surface ratio.

We have investigated experimentally the effect of lateral confinement of thermal acoustic phonons in nanoridges of silicon and of quartz as a function of the temperature. Electrical methods are used to generate phonons in 100nm large nanostructures and to probe the nanostructure temperature in the same time, what allows tracking the heat flux generated and its possible deviation to Fourier diffusive heat conduction. It is now well-established that Fourier's law of heat diffusion in solids breaks down when device sizes reaches the nanometer-scale[1]. Detailed studies of the characteristic lengths where the law has to be replaced or modified are required as these lengths might depend on the considered device geometries. We have fabricated special devices made of nanostructured ridges on top of planar substrate as represented on Figure 1. The top of a ridge is a wire made either of metal or of doped silicon that acts as a heater and as a thermometer in the same time. The lower part that supports the wire is made of an etched part of the wafer substrate of silicon or quartz. This type of structure enables to generate phonons in the ridge and to measure the heat flux flowing to the substrate.

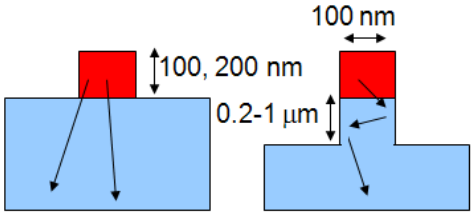

Figure 1 *Schematic of the nanostructures*

Different electrical methods such as the 3ω method[2] are used to heat the wire. The goal is then to measure a wire-voltage component (dc or ac) proportional to the wire temperature. A model enables then to link the wire temperature to the heat flux transmitted to the substrate. In addition to the localized heat source effect due to the sub-mean free path size of the source[3], we have investigated experimentally the consequences of the fact that the source cannot be considered as a proper heat bath at equilibrium.

Phononics 2011: First International Conference on Phononic Crystals, Metamaterials and Optomechanics

Santa Fe, New Mexico, USA, May 29-June 2, 2011

PHONONICS-2011-0049

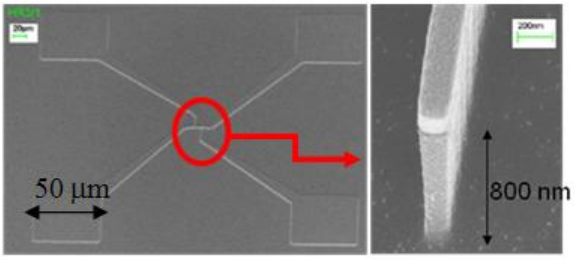

Figure 2 *Electrical accesses and ridge before mask removal*

We have quantified the effect as a function of the two characteristic numbers that can be associated with the problem, namely the constriction Knudsen number describing the transmission of the phonons and the nano-structure Knudsen number characterizing the nonequilibrium of the source. We compare our results with those of a recent theoretical paper[4] based on the ballistic-diffusive equations. The determination of the mean free paths of phonons as a function of the frequency remains a key point due to the consequences for heat transport and thermal management[1].

We observe a strong decrease of the thermal conductance through the ridge in comparison to a prediction based on the Fourier diffusive as expected. But, more strikingly, we also observe a decrease in comparison to the ballistic prediction. We aim at ascribing part of this decrease to an effect of phonon confinement in the ridge.

Acknowledgements

We acknowledge the support of EU FP7 projects NANOPACK and NANOPOWER. We also acknowledge the support of Spanish MICINN project ACPHIN.

References

[1] D. G. Cahill, W. K. Ford, K. E. Goodson, G. D. Mahan, A. Majumdar, H. J. Maris, R. Merlin, S. R. Phillpot, J. Applied Physics 93, 793-818 (2003).
[2] D. Cahill, Rev. Scient. Instr. 61, 802 (1990)
[3] M.E. Siemens, Q. Li, R. Yang, K.A. Nelson, E.H. Anderson, M.M. Murnane, and H.C. Kapteyn, Nature Materials 9, 26 (2010)
[4] S. Volz and P.O. Chapuis, J. Applied Physics 103, 34306 (2008)

Phononics 2011: First International Conference on Phononic Crystals, Metamaterials and Optomechanics
Santa Fe, New Mexico, USA, May 29-June 2, 2011
PHONONICS-2011-0050

Temperature and Size Dependence of Thermal Conductivity in Single Crystal ZnO Nanowires

Cong-Tinh Bui[1], Rongguo Xie[2], Baowen Li[1, 2, 3], John T. L. Thong[1, 4]

[1] *NUS Graduate School for Integrative Sciences and Engineering, National University of Singapore, Singapore 117456, Republic of Singapore, tinhbc@nus.edu.sg*
[2] *Department of Physics, National University of Singapore, Singapore 117542, Republic of Singapore, xierg2001@nus.edu.sg*
[3] *Centre for Computational Science and Engineering (CCSE), National University of Singapore, Singapore 117456, Republic of Singapore, phylibw@nus.edu.sg*
[4] *Department of Electrical and Computer Engineering, National University of Singapore, Singapore 117576, Republic of Singapore, john_thong@nus.edu.sg*

Abstract: We report on measurements of thermal conductivity (κ) of single crystal zinc oxide (ZnO) nanowires. The thermal conductivity firstly increases and then decreases with temperature as $T^{-\alpha}$ (α in the range of 1.42 – 1.49). Thermal conductivity is also found to be increased linearly with the cross-section area (~d^2) of nanowires in studied diameter range.

Introduction

Zinc oxide (ZnO) is a wide and direct band gap (3.5 eV at room temperature) oxide semiconductor. It has attracted a lot of research interest because of its optoelectronic and electronic properties[1, 2]. ZnO nanowires owning unique physical properties have been demonstrated to be promising for various applications such as piezoelectronic power generators, field effect transistors, piezoelectric sensors, etc. Since most applications are related to high-power electronic and optoelectronic device, it is necessary to understand the thermal behaviour of ZnO nanowires. In this work, we have studied temperature and size dependence of thermal conductivity of single crystal ZnO nanowires in order to understand phonon transport mechanism behind thermal behaviour in 1-dimensional lattice structures.

Measurement method

Single crystal ZnO nanowires used in this study were synthesized via vapor transport process in a sealed horizontal tube. The micro-thermal measurement (MTM) devices was fabricated and measurement method was described similarly with those of others previously[3, 4]. MTM devices consist of two suspended SiN_x membranes with Pt loops. One membrane serves as a heater to create temperature gradient and the other serves as a sensor to measure the temperature change. A nano-manipulator in SEM chamber was then used to pick up and place single ZnO nanowire onto the MTM device. The Pt/C composite pads were then deposited on two ends of nanowires using focus electron beam to reduce thermal contact resistance as well as to stick nanowires to the membranes. Fig. 1 shows scanning electron microscope (SEM) image of the MTM device with single ZnO nanowire. In this study, we have prepared and measured thermal conductivity of five ZnO nanowire samples with diameter of 70; 84; 120; 166; and 209 nm. For each sample, the measurement was performed in vacuum chamber with temperature varies from 77K to 400K which is controlled by cryostat.

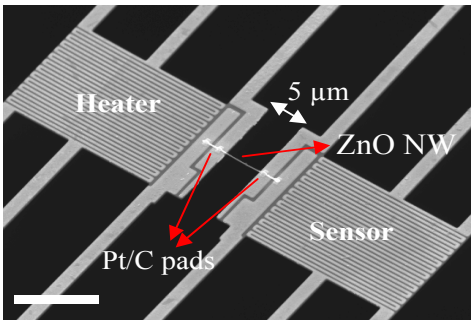

Figure 1 SEM image of ZnO nanowire sample on micro-thermal measurement device. Scale bar: 10μm

Results and Discussion

Fig.2 shows the measured thermal conductivity (κ) as a function of temperature for ZnO nanowires. For all samples, when the temperature increases κ increases to maximum value (at turnover temperature between 120 and 150K) and then decreases. κ at room temperature for 70; 84; 120; 166; and 209 nm diameter nanowires is 7.04; 7.52; 9.06 11.78 and 14.41 W/m.K, respectively, which is one order of magnitude lower than that of bulk ZnO. To understand thermal transport in ZnO nanowires, we

Phononics 2011: First International Conference on Phononic Crystals, Metamaterials and Optomechanics
Santa Fe, New Mexico, USA, May 29-June 2, 2011
PHONONICS-2011-0050

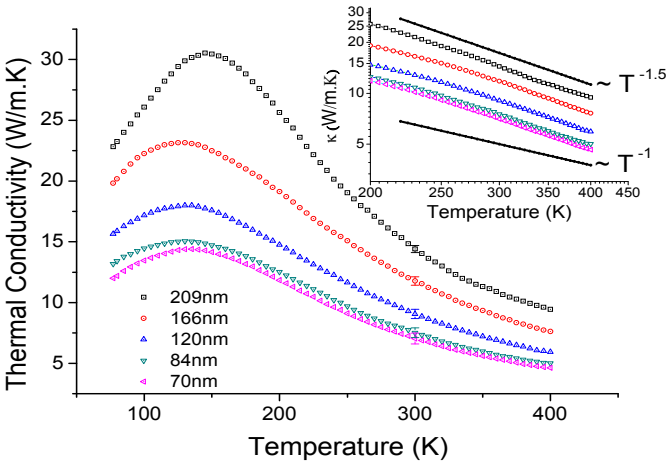

Figure 2 Temperature dependence of thermal conductivity of ZnO nanowires with different diameters. Inset: log-log scale in temperature range 200K – 400K.

consider all phonon scattering processes which induce thermal resistance in single crystal nanowires. The phonon relaxation time corresponding to various scattering mechanisms is employed to describe thermal transport. The total inverse phonon relaxation time, which is followed Matheissen's rule, equals to the sum of the inverse relaxation time corresponding to boundary scattering, phonon – phonon scattering (including normal three-phonon processes and Umklapp processes), and impurity/isotope scattering[5]

$$\tau^{-1} = \tau_b^{-1} + \tau_p^{-1} + \tau_i^{-1} \quad (1)$$

The behaviour of the observed thermal conductivity with temperature can be explained qualitatively as follows: at low temperature phonon mean free path is larger. Phonon will be scattered with the boundary before colliding with other phonons. The boundary scattering predominates and the thermal conductivity increases with temperature. When the temperature increases, it is easier to create higher frequency phonons which are scattered efficiently by impurities, hence the isotope scattering rapidly becomes dominant. Consequently, the thermal conductivity reaches a maximum and then declines. As the temperature further increases, normal three-phonon scattering and umklapp scattering become important and dominate over the isotope scattering. As the result, thermal conductivity of nanowires further decreases with increasing temperature. The temperature dependence of thermal conductivity of ZnO nanowires between 200 and 400K is plotted logarithmically in the inset of Fig.2. We observed that, after the maximum at low temperature, thermal conductivity decreases following the power law $T^{-\alpha}$. For all five ZnO nanowires, the measurement results give a factor α in the range of 1.42 to 1.49 which is close to that of Callaway's model for lattice thermal conductivity taking into account the boundary scattering[6] (α = 1.5).

The size dependence of thermal conductivity of ZnO nanowires were show in Fig. 3, in which κ is plotted as function of d^2. In the measured diameter range, thermal conductivity increases with increasing of cross-section area. This effect is obviously understood because of less phonon boundary scattering for larger nanowires and hence will reach to saturation when diameter of nanowire goes to certain value (bulk limit). Interestingly, κ increases almost linearly with cross-section area in studied diameter range, especially at room temperature (300K).

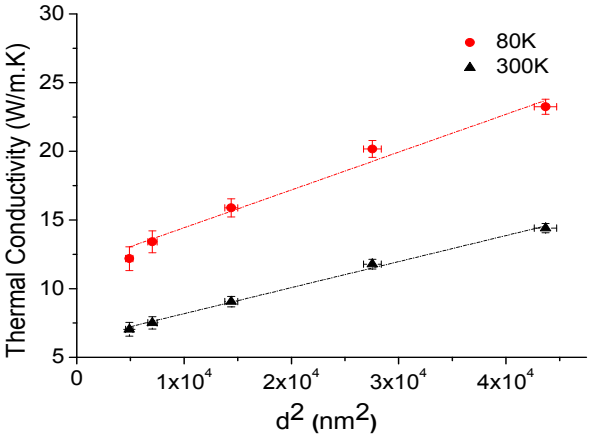

Figure 3 Diameter dependence of thermal conductivity of ZnO nanowires at 80K and 300K. Dash-dot lines are to guide eyes.

References

[1] Z. K. Tang, G. K. L. Wong, and P. Yu, *Appl. Phys. Lett.* **72**, 3270-3272 (1998).
[2] A. Tsukazaki, A. Ohtomo, T. Onuma, M. Ohtani, T. Makino, M. Sumiya, K. Ohtani, S. F. Chichibu, S. Fuke, Y. Segawa, H. Ohno, H. Koinuma, and M. Kawasaki, *Nat. Mater.* **4**, 42-46 (2005).
[3] L. Shi, D. Li, C. Yu, W. Jang, D. Kim, Z. Yao, P. Kim, and A. Majumdar, *J. Heat Transf.* **125**, 881-888 (2003).
[4] Z. Wang, R. Xie, C. T. Bui, D. Liu, X. Ni, B. Li, and J. T. L. Thong, *Nano Lett.*, Article ASAP (2010).
[5] M. A.Palmer, K. Bartkowski, E. Gmelin, M. Cardona, A. P. Zhenov, A. V. Inyushkin, A. Taldenkov, V. I. Ozhogin, K. M. Itoh, and E. E. Haller, *Phys. Rev. B* **56**, 9431-9447 (1997).
[6] J. Calaway, *Phys. Rev.* **113**, 1046-1051 (1959).

Phononics 2011: First International Conference on Phononic Crystals, Metamaterials and Optomechanics
Santa Fe, New Mexico, USA, May 29-June 2, 2011
PHONONICS-2011-0051

Phononic Thermal Transport in Thin Nanoscale Membranes

Ilari J. Maasilta[1], Jenni T. Karvonen[1], Thomas Kühn[1]

[1] *Nanoscience Center,Department of Physics, P. O. Box 35, FI-40014 University of Jyväskylä, Finland*
maasilta@jyu.fi

Abstract: We have studied experimentally the thermal conductance of thin free-standing silicon nitride membranes at sub-Kelvin temperatures as a function of membrane thickness between 40 nm and 750 nm, using normal metal-insulator-superconductor (NIS) thermometry. Effects of dimensionality cross-over from 3D to 2D phonons are seen, however not all observations follow the simplest theory.

Introduction

It is essential to understand the thermal transport properties of thin insulating membranes from the point of view of applications. Often devices, such as bolometric low-temperature radiation detectors[1], are placed on top free standing silicon nitride membranes (SiN) so that the thermal isolation from the environment can be engineered. Although heavily used in applications, the fundamental understanding of the physics of phonon transport in thin membranes is still not deeply understood, however. Only a few previous experiments have been performed at sub-Kelvin temperature range [2-4], with very little emphasis on the interpretation of the results.

On the other hand, theoretical advances in recent years have discussed some interesting results, especially in the limit where the membrane becomes so thin that only the lowest two-dimensional (2D) phonon modes are occupied at low temperatures[5-7]. In this case, the usual 3D plane wave phonon modes are not eigenmodes anymore: instead more complex displacement field distributions occur in the direction perpendicular to the membrane plane. These phonon modes (Lamb-modes) have been known in acoustics since the work of Rayleigh and Lamb in late 1800's. However, only recently has their importance in low-temperature thermal transport been investigated further [5-7]. Theoretical results predict that for the Lamb-modes, the temperature dependence of thermal conductance G should change from the 3D case, from the usual $G \sim T^3$ to a weaker $G \sim T^{1.5}$ at the lowest temperatures, if the phonon transport is ballistic [6] or if it is diffusive but limited by a constant (non temperature dependent) mean free path [5]. Even more interestingly, at a constant temperature, the thermal conductance depends inversely on the membrane thickness d as $G \sim 1/\sqrt{d}$: in other words, thinner membranes have higher thermal conductance [6,7].

The experiment

Here, we present the first experiments on phonon thermal transport in thin silicon nitride (SiN) membranes that clearly span the expected 3D-2D crossover for SiN: The theoretical crossover temperature is given[6,7] by $T_{cr} = \hbar c_t/(2k_B d)$, where c_t is the transverse speed of sound. This predicts $T_{cr} \sim 0.6$ K for the thinnest membranes in this study with d= 40 nm, and means that our experiment, reaching a temperature of 0.1 K, is well within the 2D limit. Two other membrane thicknesses were studied for comparison: d= 200 nm and d= 750 nm. Both of these samples are expected to be in the 3D limit. Our recent experiments on electron-phonon interaction in metal wires fabricated on similar suspended SiN membranes have in fact confirmed that the thinnest membrane is in the 2D limit[8].

The membranes were fabricated using standard bulk micromachining techniques[8] by chemically etching the Si substrate in KOH. A circular shaped Cu wire heater (radius 7 μm, width ~ 300 nm, thickness 30 nm) was fabricated at the center of the membrane, which was typically of a size 500 μm x 500 μm. The Cu heater was connected by superconducting Nb leads to the external voltage source used for heating. This ensured that all the Joule heat was dissipated in the Cu wire. A superconductor-insulator-normal metal-insulator-superconductor (SINIS) tunnel junction pair was placed some specified distance away from the heater, and used for thermometry. More details on the sample fabrication and SINIS thermometry can be found in Refs. 9,10.

Phononics 2011: First International Conference on Phononic Crystals, Metamaterials and Optomechanics
Santa Fe, New Mexico, USA, May 29-June 2, 2011
PHONONICS-2011-0051

By sweeping the heater voltage and measuring the current and voltage across the wire, one can measure the dissipated phonon power P emitted from the heater, in addition to the temperature T at the SINIS thermometer, and study how the temperature rises with given power input. Differential thermal conductance could then be computed as $G = \partial P/\partial T$. Representative results for P vs. T curves for all membrane thicknesses are shown in Fig. 1 for a thermometer that was located ~40 μm away from the center of the heater.

The first main conclusion from the data is: The temperature exponent is a bit surprisingly approximately the same for all membrane thicknesses. In terms of G, the observed dependence is $G \sim T^{2.5}$ ($P \sim T^{3.5}$). This does not agree with the simplest theories either for 3D or for the 2D limit. The only possible explanation is that some scattering mechanism for phonons exists in the membranes with a temperature dependent mean free path. One likely mechanism could be two-level systems[11], as the membranes are amorphous and are known contain lots of them.

On the other hand, the absolute values of the conductance do change with thickness. For 3D phonon transport, the emitted power at a given T should simply scale linearly with d. Looking at Fig.1 this is clearly not the case: in fact the 40 nm membrane power is higher than the 200 nm one at temperatures below 0.4 K. This observation qualitatively agrees with the theoretical results on thickness dependence of the Lamb modes in the 2D limit[6,7].

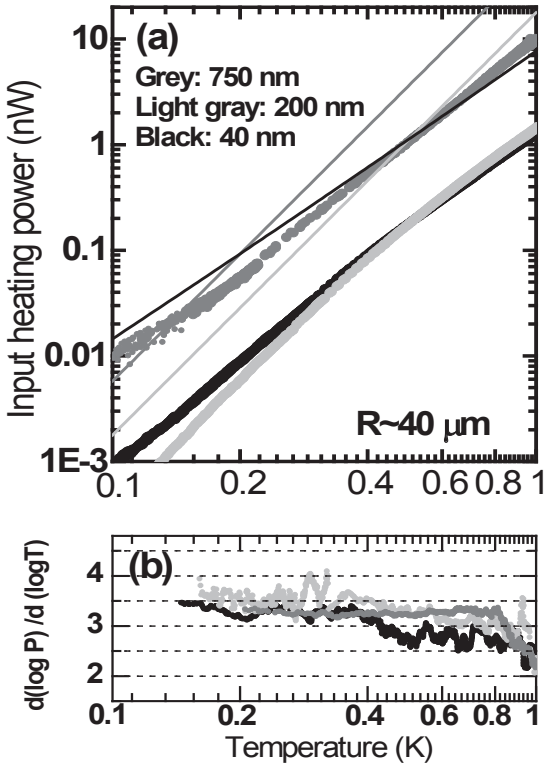

Figure 1 (a) Measured input heating power vs. phonon temperature. SINIS thermometer was 40 μm away from the center of the heater. Lines show the expected theoretical curves in the ballistic limit for each membrane thickness. (b) The logarithmic derivative of the data, giving the temperature exponent.

Lastly, we have plotted the theoretical upper limits for the power vs. temperature in Fig. 1 based on the ballistic limit theory (3D theory for 750 and 200 nm, 2D theory for 40 nm). It is clear that the 750 nm membrane is essentially at the ballistic limit at 0.1 K, in agreement with earlier data[2]. However, the thinner membranes start to deviate more and more, with the 40 nm results being furthest from the ballistic limit. More detailed modeling including diffusive surface scattering is in progress to understand the experiments more deeply.

References

[1] Ch. Enss, ed., *Cryogenic Particle Detection*, Springer, Heidelberg (2005).
[2] W. Holmes, J. M. Gildemeister, P. L. Richards, and V. Kotsubo, *Appl. Phys. Lett.* **38**, 2250 (1998).
[3] M. M. Leivo and J. P. Pekola, *Appl. Phys. Lett.* **70**, 1305 (1998).
[4] H. F. C. Hoevers, M. L. Ridder, A. Germeau, M. P. Bruijn, and P. A. J. Korte, *Appl. Phys. Lett.* **86**, 251903 (2005).
[5] T. Kühn, D. Anghel, J. Pekola, M. Manninen, and Y. Galperin, *Phys. Rev. B.* **70**, 125425 (2004).
[6] T. Kühn and I. J. Maasilta, *Nucl. Instr. and Meth. A* **559**, 724 (2006).
[7] T. Kühn and I. J. Maasilta, *J. Phys. Conf. Series* **92**, 012082 (2007).
[8] J.T. Karvonen and I.J. Maasilta, *Phys. Rev. Lett.* **99**, 145503 (2007).
[9] P.J. Koppinen and I.J. Maasilta, *Phys. Rev. Lett.* **102**,165502 (2009).
[10] J. T. Karvonen, Ph. D. Thesis, University of Jyväskylä (2009).
[11] T. Kühn, D. V. Anghel, Y. M. Galperin, and M. Manninen, *Phys. Rev. B* **76**, 165425 (2007).

Phononics 2011: First International Conference on Phononic Crystals, Metamaterials and Optomechanics
Santa Fe, New Mexico, USA, May 29-June 2, 2011
PHONONICS-2011-0078

Coherent phonons in polycrystalline bismuth film monitored by ultrafast electron diffraction

A. Bugayev and H. E. Elsayed-Ali

Applied Research Center, Old Dominion University, Norfolk, VA 23529,USA,

abugayev@odu.edu, helsayed@odu.edu

Abstract: The generation of coherent phonons in polycrystalline bismuth film is observed by ultrafast time-resolved electron diffraction. The dynamics of the diffracted intensities from the (110), (202), and (024) lattice planes show pronounced oscillations at 130–150 GHz. The anisotropy in the energy transfer rate of coherent optical phonons is discussed.

The interaction of femtosecond laser pulses with semimetals and semiconductors produces electronic excitations coupled with lattice vibrations through the deformation potential and stimulated Raman scattering . If the frequencies of Raman active phonons in the laser-excited material are smaller than the inverse duration of the laser pulse, then the laser-induced change in the equilibrium positions of the nuclei (displacive excitation) results in generation of coherent optical and acoustical phonons. Numerous studies were performed on the dynamics of coherent phonons in bismuth (Bi) by monitoring of the optical reflectivity modulation with femtosecond pump-probe techniques, and by femtosecond time-resolved X-ray diffraction of lattice dynamics [1-4].

We report on the characteristics of coherent phonons as observed in modulation of temporal behavior of the electron-diffracted intensities from three (110), (202), and (024) lattice planes of polycrystalline free-standing 22±2 nm thick Bi film. An electron gun, described in our previous publication [5], was used to produce electron pulses of ~1.5 ps duration by photoemission from silver thin film photocathode excited by frequency-tripled femtosecond (110 fs duration, 800 nm wavelength, at 1 kHz repetition rate) laser pulses. The Bi film was exposed to the fundamental 800 nm wavelength at a pulse energy density ~2 mJ/cm^2 that corresponds to excited carrier's density ~10^{21} cm^{-3}. The intensity changes of the diffraction rings are given in terms of contrast value $V(r) = (I(r) - I_{bg}(r))/(I(r) + I_{bg}(r))$ ($I_{bg}(r)$ is the background intensity distribution), which takes into account both the changes in diffraction peak and background intensities after the laser exposure. Each time-resolved electron diffraction scan was acquired twice and the average value was used for analysis. To analyze the data, the Boltzmann (sigmoidal) fit was used such that $V(\tau) = V_{min} + (V_{max} - V_{min})/(1 + \exp(\frac{\tau - \tau_{infl}}{\tau_{rate}}))$ where τ_{infl} is the inflection point of the dependence of $V(\tau)$ on the delay time τ, and τ_{rate} is the rate (slope) of the process at this point. The dynamics of the intensity change $V(\tau)$ were characterized by the coordinate of the inflection point τ_{infl} and by the drop-off intensity time τ_{hkl}, which is determined as the full width at e^{-1} level of the maximum of the first derivative of the Boltzmann fit. The Fourier transform was used for frequency analysis.

The temporal development of the contrast values $V(r)$ of the diffraction orders as a function of delay time is shown in Figure. It is seen that all three diffraction orders $I_{hkl}(\tau)$ follow the same temporal behavior, namely, the intensity decrease, which is accompanied with high frequency oscillations in a frequency band centered at 130–150 GHz (see insets in Figure). Since an optical phonon can emit two acoustic phonons, different combinations of two or more phonons can give rise to a generation of new phonon frequencies like $A_{1g}(\Gamma) \rightarrow 2\mathrm{LA}(\Lambda)$, $A_{1g}(\Gamma) \rightarrow \mathrm{LA}(T) + \mathrm{LA}(X)$, $2\mathrm{LA}(X) - \mathrm{LA}(\Lambda) \rightarrow \mathrm{TA}(X)$, and so on. Therefore, one can find that the combination $A_{1g}(\Gamma) - E_g(\Gamma) - 2\mathrm{LA}(X)$ yields the phonon frequency 134 GHz, which is in good agreement with our results. An interesting feature is the different drop time in the diffraction orders τ_{hkl} extracted from the Boltzmann fit, which are τ_{110} ~ 8.6 ps, τ_{202} ~ 18 ps, and τ_{024} ~ 7.8 ps. In general, two mechanisms could contribute to the energy transfer $\tau_{e\text{-}ph}$ from electrons to the phonon subsystem resulting in lattice heating. The first one is direct-energy transfer from electrons to phonons through optical phonon decay. This can be evaluated from the following $\tau_{e-ph} \approx (\hbar\omega_D^2 T_L^2 / T_D^2 \varepsilon_F)$ ratio (here ω_D, T_D, T_L is the Debye frequency, the Debye temperature, and lattice temperature, respectively, ε_F is the Fermi level). At our experimental conditions, the energy transfer rate $\tau_{e\text{-}ph}$ is 5–20 ps. The second mechanism affecting $\tau_{e\text{-}ph}$ is the electron-hole pair recombination

Phononics 2011: First International Conference on Phononic Crystals, Metamaterials and Optomechanics
Santa Fe, New Mexico, USA, May 29-June 2, 2011
PHONONICS-2011-0078

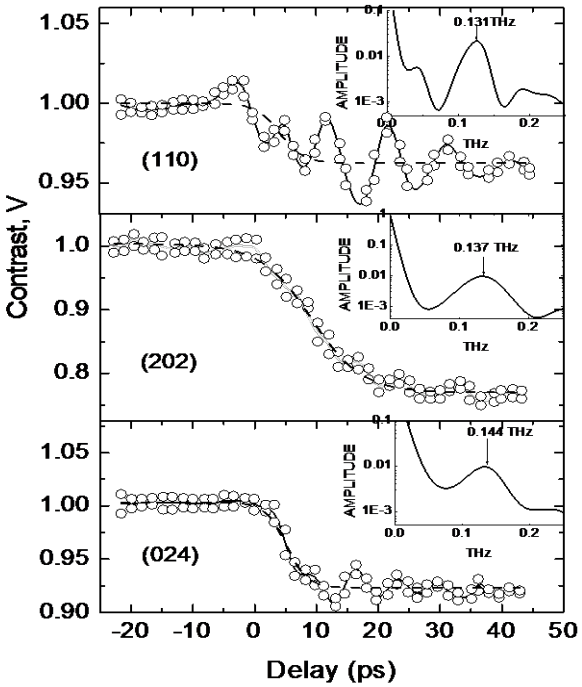

Figure 1 Normalized contrast $V(r)$ of diffraction orders as a function of the delay time. Dashed line is Boltzmann fit. Solid line is to guide the eyes only. Insets show the the Fourier transform.

accompanied by phonon emission. For Bi at room temperature this process can be as fast as a 2–3 ps [6].

The energy transfer depends on the lattice plane {*hkl*} of Bi. The anisotropy manifests itself not only in different drop time τ_{hkl} but also in different time of the inflection points: the maximum slope of the intensity change is achieved at ~ 5 ps for (110), at ~ 9 ps for (202), and at ~ 4 ps for (024) lattice planes. Hence, the drop-off amplitude of the intensity of the diffraction orders does not follow a single Debye-Waller factor written for the harmonic approximation as $V_g = V_g^0 \exp(-Bs^2) = V_g^0 exp\left[-B(T)\left(\frac{\sin\theta}{\lambda}\right)^2\right]$ (here V_g^0 denotes the structure factor of a perfect crystal, θ is the Bragg scattering angle, λ is the electron wavelength, and $B(T)$ is the Debye-Waller factor). According to this expression, the decrease in the intensity of the diffracted beam is expected to be more pronounced for high-order diffraction, but this is not supported by our measurements shown in Figure 1. Two mechanisms can possibly affect the expected dynamics of the intensity decay. The first one is the anisotropy of $B(T)$ for bismuth caused by the different means-square displacements of the atoms parallel $B_\parallel(T)$ and perpendicular $B_\perp(T)$ to the hexagonal *c* axis [7]. For Bi, $B_\perp(T) = 2B_\parallel(T)$ at $T = 293$ K and $B_\perp(T) = 8B_\parallel(T)$ at $T = 516$ K, therefore, the influence of anisotropy is very considerable. The second mechanism is the atomic motion of coherent optical phonons A_{1g} that takes place along the elongated body diagonal, whereas the atomic motion of E_g phonons occurs in the plane perpendicular to this diagonal [8]. The combined action of these two mechanisms on the differently oriented planes (110), (202), and (024) can result in significant change of the energy transfer rate of coherent optical phonons as well as of the amplitude of the diffraction intensity response.

This work was supported by Department of Energy and National Science Foundation. We acknowledge the contribution of A. Esmail and M. Abdel-Fattah in construction of the diffraction system.

References

[1] A. Q. Wu and X. Hu, "Coupling of ultrafast laser energy to coherent phonons in bismuth", Appl. Phys. Lett. 90, 251111/1-251111/3 (2007)
[2] M. F. DeCamp, D. A. Reis, P. H. Bucksbaum, and R. Merlin, "Dynamics and coherent control of high-amplitude optical phonons in bismuth", Phys. Rev B 64, 092301/1-092301/3 (2001).
[3] D. Boschetto, E. G. Gamaly, A. V. Rode, B. Luther-Davies, D. Glijer, T. Garl, O. Albert, A. Rousse, and J. Etchepare, "Small Atomic Displacements Recorded in Bismuth by the Optical Reflectivity of Femtosecond Laser-Pulse Excitations" Phys. Rev. Lett. **100**, 027404/1-027404/4 (2008).
[4] K. Sokolowski-Tinten, C. Blome, J. Blums, A. Cavalleri, C. Dietrich, A. Tarasevitch, I. Uschmann, E. Förster, M. Kammler, M. Horn-von-Hoegen, and D. von der Linde, "Femtosecond X-ray measurement of coherent lattice vibrations near the Lindeman stability limit", Nature, **422**, 287-289 (2003).
[5] B.-L. Qian and H. E. Elsayed-Ali, "Electron pulse broadening due to space charge effects in a photoelectron gun for electron diffraction and streak camera systems", J. Appl. Phys. **91**, 462-469 (2002).
[6] A. A. Lopez, "Electron-hole rcombination in bismuth", Phys. Rev. **175**, 823-840 (1968).
[7] P. Fisher, I. Sosnowska, and M. Szymanski, "Debye-Waller factor and thermal expansion of arsenic, antimony and bismuth", J. Phys. C: Solid State Phys. **11**, 1043-1051 (1978).
[8] E. S. Zijlstra, L. L. Tatarinova, and M. E. Garcia, "Laser-induced phonon-phonon interactions in bismuth", Phys. Rev. B74, 220301/1-220301/4 (2006)

Phononics 2011: First International Conference on Phononic Crystals, Metamaterials and Optomechanics
Santa Fe, New Mexico, USA, May 29-June 2, 2011
PHONONICS-2011-0080

Phonon scattering at structurally variant boundaries

Patrick E. Hopkins

[1] *Engineering Sciences Center, Sandia National Laboratories, 1515 Eubank SE, Albuquerque, NM, USA 87185*
[2] *Department of Mechanical and Aerospace Engineering, University of Virginia, 122 Engineer's Way, Charlottesville, VA, USA 22904*
pehopki@sandia.gov

Abstract: Phonon scattering at boundaries drives the thermal transport in nanosystems. In this work, I will discuss various projects in which solid boundaries and interfaces are used to reduce the thermal conductance in nanosystems. These studies include cross plane thermal conductivity in periodic, porous silicon films and thermal boundary conductance across random and quantum dot roughened Si interfaces.

Successful reduction of the thermal conductivity in nanosystems has been achieved through the alteration of structure and interface density in different types of nanoparticle films and periodic composites.[1] These material systems have attracted significant attention due to their unique phonon-scattering mechanisms, where the increase in the density of inclusions increases the number and frequency of boundary scattering events, in turn resulting in lower realized values of effective thermal conductivity. Thus, through varying the frequency and strength of phonon scattering at interfaces, one is able to obtain a unique method for controlling the effective thermal conductivity of a given nanosystem.

In this work, I will review various projects in which we have studied thermal transport in nanosystems with periodic and structurally variant boundaries to reduce and control thermal transport. First, I will discuss recent measurements of the cross plane transport in periodically patterned porous silicon membranes; these silicon membranes are low frequency phononic crystals and we study the effects of coherent and incoherent mechanisms contributing to the cross plane thermal conductivity.[2] Secondly, I will review various projects in which structurally variant solid interfaces are used to decrease the thermal boundary conductance.[3,4] We show that roughening is an effective tool to systematically decrease the thermal boundary conductance. Finally, I will discuss recent measurement of thermal boundary conductance across silicon interfaces with quantum dot patterning. We show that quantum dot synthesis is an effective tool to control the thermal conductance in nanosystems due to phonon scattering and attenuation effects around the quantum dots.

We measure the thermal processes in the various nanosystems presented in this work with time domain thermoreflectance (TDTR).[5,6] TDTR is a non-contact, pump-probe technique in which a modulated train of short laser pulses (in our case ~ 100 fs) is used to create a heating event (pump) on the surface of a sample. This pump-heating event is then monitored with a time-delayed probe pulse. The change in the reflectivity of the probe pulses at the modulation frequency of the pump train is detected through a lock-in amplifier; this change in reflectivity is related to the temperature change on the surface of the sample. Details of the specific experimental setup at Sandia National Laboratories and the thermal analysis used to determine thermal conductivity and thermal boundary conductance is discussed elsewhere.[7]

Figure 1 shows the the thermal conductivity of periodically porous Si structures at room temperature as a function of the characteristic limiting distance, L, for the phononic crystal patterns (unfilled squares – numbers represent hole diameters/pitch in hundreds of nanometers), microporous solids (filled pentagons),[8] and nanomesh (filled diamond).[9] The measured thermal conductivities are multiplied by a factor of $\left[\left(1+2\phi/3\right)/\left(1-\phi\right)\right]$ to account for the porosity of the structures, and thereby directly compare the thermal conductivity of the solid matrix in the porous structures to a model accounting for phonon boundary scattering and thermal conductivity in porous solids.[10] The solid line represents predictions of this model at room temperature as a function of L. This model predicts the thermal conductivity of the microporous solids well. This model, however, overpredicts the porous silicon measurements. The dashed line represents predictions of the porous silicon thermal conductivity, which accounts for a change in mode density using a plane wave expansion method.[11]

Phononics 2011: First International Conference on Phononic Crystals, Metamaterials and Optomechanics
Santa Fe, New Mexico, USA, May 29-June 2, 2011
PHONONICS-2011-0080

Figure 2 shows the measured thermal boundary conductance, h, as a function of surface roughness, δ, for a series of Al/Si samples. We roughen the Si interfaces via tetramethyl ammonium hydroxide (TMAH) solution at 80°C for various times to induce different degrees of Si surface roughness. We also treat a series of the Si surfaces with buffered oxide etch immediately before Al deposition to minimize the oxide layer at the interface. The thermal boundary conductances show a dependency on δ, which is not predicted by the traditional diffuse mismatch model.[12] We develop a new model that accounts for thermal conductance at rough interfaces and oxide formations, as shown by the solid lines in Fig. 2. Based on these results at the roughened Al/Si interfaces, we patterned a series of samples with Ge_xSi_{1-x} quantum dots on a Si surface and studied the thermal transport across Al/Si interfaces with quantum dot roughened surfaces. The measured thermal boundary conductance decreases with increased RMS roughness induced from the quantum dots, and our model for thermal boundary conductance across rough interfaces predicts the measured values well. The precise quantum dot patterning yields a method to control the thermal transport.

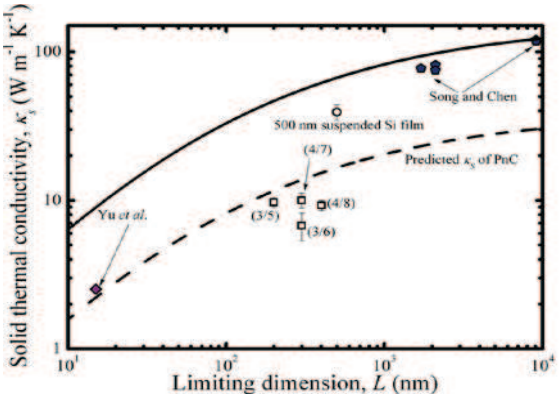

Figure 1. (see Ref. 2)

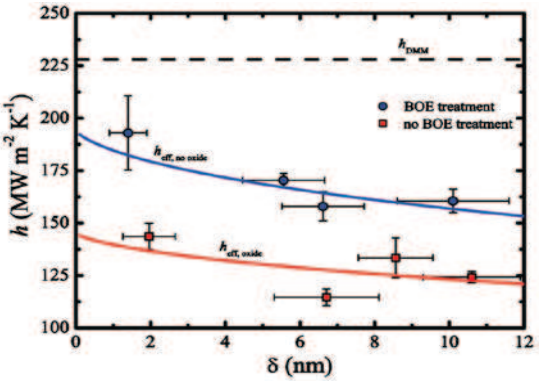

Figure 2. (See Ref. 4)

Acknowledgements
I would like to thank my collaborators on these various projects. I am greatly appreciative for funding from the LDRD Program Office through the Harry S. Truman Fellowship Program. This work was performed, in part, at the Center for Integrated Nanotechnologies, a U.S. Department of Energy, Office of Basic Energy Sciences user facility; the authors would like to thank John Sullivan for assistance regarding work at the Center for Integrated Nanotechnologies. Sandia National Laboratories is a multi-program laboratory operated by Sandia Corporation, a wholly owned subsidiary of Lockheed Martin Corporation, for the United States Department of Energy's National Nuclear Security Administration under Contract DE-AC04-94AL85000.

References
[1]D. G. Cahill, W. K. Ford, K. E. Goodson, G. D. Mahan, A. Majumdar, H. J. Maris, R. Merlin and S. R. Phillpot, J. Appl. Phys. **93**, 793 (2003).
[2]P. E. Hopkins, C. M. Reinke, M. F. Su, R. H. Olsson I I I, e. A. Shaner, Z. C. Leseman, J. R. Serrano, L. M. Phinney and I. El-Kady, Nano Letters **ASAP**, 10.1021/nl102918q (2010).
[3]P. E. Hopkins, P. M. Norris, R. J. Stevens, T. Beechem and S. Graham, J. Heat Transfer **130**, 062402 (2008).
[4]P. E. Hopkins, L. M. Phinney, J. R. Serrano and T. E. Beechem, Phys. Rev. B **82**, 085307 (2010).
[5]D. G. Cahill, K. E. Goodson and A. Majumdar, J. Heat Transfer **124**, 223 (2002).
[6]D. G. Cahill, Review of Scientific Instruments **75**, 5119 (2004).
[7]P. E. Hopkins, J. R. Serrano, L. M. Phinney, S. P. Kearney, T. W. Grasser and C. T. Harris, J. Heat Transfer **132**, 081302 (2010).
[8]D. Song and G. Chen, Appl. Phys. Lett. **84**, 687 (2004).
[9]J.-K. Yu, S. Mitrovic, D. Tham, J. Varghese and J. R. Heath, Nature Nanotechnology **5**, 718 (2010).
[10]P. E. Hopkins, P. T. Rakich, R. H. Olsson I I I, I. El-Kady and L. M. Phinney, Appl. Phys. Lett. **95**, 161902 (2009).
[11]M. S. Kushwaha, P. Helevi, G. Martinez, L. Dobrzynski and B. Djafari-Rouhani, Phys. Rev. B **49**, 2313 (1994).
[12]E. T. Swartz and R. O. Pohl, Reviews of Modern Physics **61**, 605 (1989).

Phononics 2011: First International Conference on Phononic Crystals, Metamaterials and Optomechanics
Santa Fe, New Mexico, USA, May 29-June 2, 2011
PHONONICS-2011-0081

Thermal conductance behavior of self-assembled lamellar block copolymer thin films

Matthew C. George, Patrick E. Hopkins, Mark A. Rodriguez

Sandia National Laboratories, PO Box 5800 Albuquerque, NM 87185, USA
mcgeorg@sandia.gov, pehopki@sandia.gov, marodri@sandia.gov

Abstract: We measure the thermal conductance of both disordered and self-assembled lamellar polystyrene-block-poly(methyl methacrylate) copolymer films and compare the results to literature reports on thin homopolymer films and polymer brushes. We see a 150% increase in thermal conductivity for a single self-assembled PS-b-PMMA layer.

The control of nano-scale phonon/thermal transport properties is a growing technical challenge in the fields of thermoelectrics, integrated circuits, and high power density lasers. Of particular importance in microelectronics packaging and integrated circuit thermal management are polymer and polymer composite films in the form of encapsulants and coupling compounds. Chain alignment has been shown to affect thermal transport in drawn polymers, polymer brushes, and self-assembled monolayers. In this work we examine the thermal conductance behavior of thin self-assembled block copolymer films. In particular we examine both ordered and disordered copolymer films of polystyrene-block-poly(methyl methacrylate) (PS-b-PMMA) and compare the results to literature reports on thin homopolymer films, polymer brushes, and bulk drawn homopolymers. Figure 1 depicts the sample configuration in which *n* is the number of lamellar periods in the ordered films. Previous reports typically show a modest increase in axial thermal conductivity (10-50%) for elongated PMMA polymer chains compared to random coil chain configurations. We see up to a 150% increase in thermal conductivity for a single self-assembled layer of PS-b-PMMA. Increasing the film thickness in a stepwise fashion to incorporate additional self-assembled layers of block copolymer decreased the thermal conductivity towards that of the amorphous state, which is close to reported values for the individual homopolymers (0.17 and 0.20 $Wm^{-1}K^{-1}$ for PS and PMMA respectively)[1].

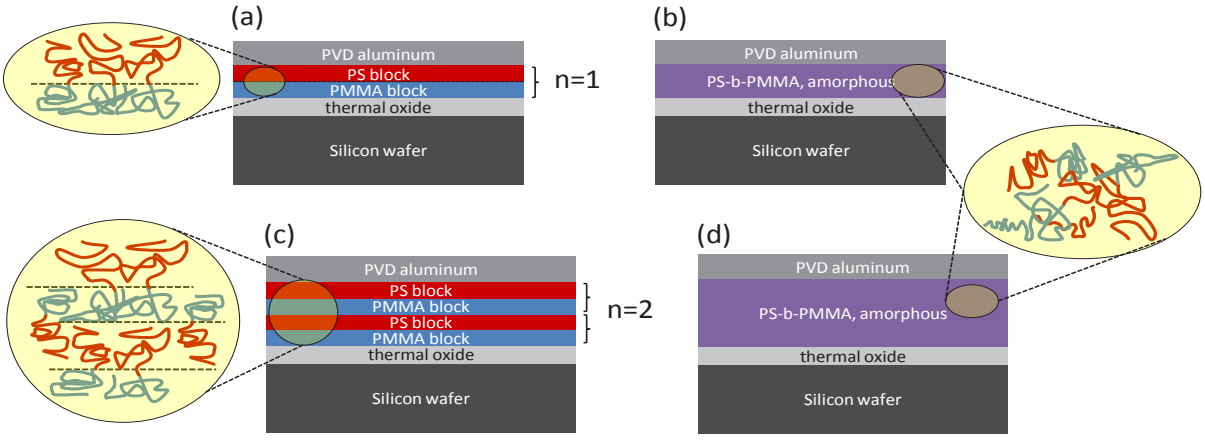

Figure 1 Schematic of ordered **(a)**, **(c)** and disordered **(b)**, **(d)** block copolymer thin films of PS-b-PMMA coated with aluminum via physical vapor deposition (PVD) on a thermal oxide silicon substrate. The number of lamellar periods is denoted by *n*. Exploded insets depict expected polymer chain conformation.

The PS-b-PMMA films were spun-cast from toluene solutions to thickness values commensurate with the natural lamellar period of the block copolymer. Film thickness was verified with ellipsometry. The spun-cast films are initially amorphous, but one set is annealed in a vacuum oven below the order-disorder transition temperature to promote self-assembly into the lamellar phase, which is aligned to the film substrate due to preferential segregation of PMMA to the polar thermal oxide surface, and PS to the vacuum interface[2-4]. The assembly of the annealed films into the stacked lamellar form as depicted in figure 1a and 1c was verified with X-ray reflectivity measurements. Rocking curves were

Phononics 2011: First International Conference on Phononic Crystals, Metamaterials and Optomechanics
Santa Fe, New Mexico, USA, May 29-June 2, 2011
PHONONICS-2011-0081

also collected to detect off-specular (diffuse) scattering in order to compare the in-plane film homogeneity. We measured the thermal conductivity of the lamellar and amorphous copolymer films with TDTR[5,6]. TDTR is a non-contact, pump-probe technique in which a modulated train of short laser pulses (in our case ~ 100 fs) is used to create a heating event (pump) on the surface of a sample. This pump-heating event is then monitored with a time-delayed probe pulse. The change in the reflectivity of the probe pulses at the modulation frequency of the pump train is detected through a lock-in amplifier; this change in reflectivity is related to the temperature change on the surface of the sample. This temporal temperature data is related to the thermophysical properties of the sample of interest. We monitor the thermoreflectance signal over 4.0 ns of probe delay time. We deposit a 90 nm Al film on the samples as a transducer that relates the measured reflectivity to the temperature change on the surface. The deposited energy takes approximately 100 ps to propagate through the Al layer, and the remaining delay time is related to the heat flow across the copolymer films and the thermal diffusivity in the underlying substrate. Our specific experimental setup is described in detail elsewhere[7]. The thermoreflectance signal we monitor is the ratio of the in-phase to the out-of-phase voltage recorded by the lock-in amplifier, which is related to the temperature change on the surface of the sample. The thermal model and analysis used to predict the temperature change and subsequent lock-in ratio is described in detail in the references[7]. We assume bulk values for the thermophysical properties of the Al, SiO_2, and Si,[8] and we verify the Al film thickness via picosecond ultrasonics[9,10].

The measured thermal conductivity of our copolymer films is depicted in Fig. 2 along with the thermal conductivity of spun cast polymer films and brushes[11]. The ordered films exhibit a higher thermal conductivity than the disordered films, with the thermal conductivity decreasing as the number of block copolymer layers was increased. For the single period, ordered PS-b-PMMA film, we believe preferential polymer chain alignment parallel to the film normal is the main factor accounting for the increased out of plane thermal conductivity. This is likely due to the increased anisotropy and effectiveness of intra-chain thermal transport, whereby vibrations are transmitted along the covalent bonds of the polymer backbone. Increasing the number of periods *n*, or reducing the film order, results in more inter-chain thermal transport, in which vibrations must be transferred through weaker van der Waals and dipole interactions[12]. In addition to partial chain alignment, we suspect that boundary scattering and phonon-phonon scattering are also contributing factors to the observed behavior.

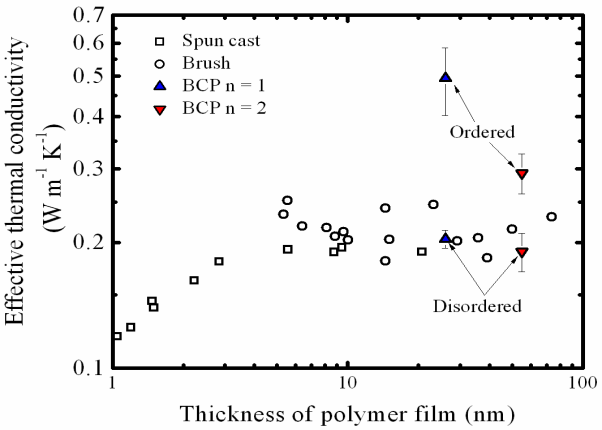

Figure 1 Thermal conductivity of our block copolymer (bcp) films compared to that of spun-cast PMMA films and polymer brushes[11]. The ordered films exhibit a higher thermal conductivity than the disordered films, spun-cast films, and brushes.

References

[1] H. Lee, *Rev. Sci. Instrum.* **53**, 884 (1982).
[2] G.H. Fredrickson, *Macromolecules* 20, 2535 (1987)
[3] A. Menelle, T.P. Russell, S.H. Anastasiadis, S.K. Satija, C.F. Majkrzak, *Phys. Rev. Lett.* **68**, 67 (1992)
[4] H. Hasegawa, T. Hashimoto, *Macromolecules* **18**, 589 (1985)
[5] D.G. Cahill, K.E. Goodson and A. Majumdar, *J. Heat Transfer* **124**, 223 (2002).
[6] D.G. Cahill, *Rev. Sci. Instrum.* **75**, 5119 (2004).
[7] P.E. Hopkins, J. R. Serrano, L.M. Phinney, S.P. Kearney, T.W. Grasser, C.T. Harris, *J. Heat Transfer* **132**, 81302 (2010).
[8] F. Incropera and D.P. DeWitt, *Fundamentals of Heat and Mass Transfer*, Wiley and Sons, Inc., New York, (1996).
[9] C. Thomsen, H.T. Grahn, H.J. Maris and J. Tauc, *Phys. Rev. B* **34**, 4129 (1986).
[10] C. Thomsen, J. Strait, z. Vardeny, H.J. Maris, J. Tauc and J.J. Hauser, *Phys. Rev. Lett.* **53**, 989 (1984).
[11] M.D. Losego, L. Moh, K.A. Arpin, D.G. Cahill and P.V. Braun, *Appl. Phys. Lett.* **97**, 011908 (2010).
[12] D. Yorifuji, S. Ando, *Macromolecules* **43**, 7583 (2010)

* A portion of this work was supported by the Laboratory Directed Research and Development program at Sandia National Laboratories. Sandia is a multiprogram laboratory operated by Sandia Corporation, a Lockheed Martin Company, for the United States Department of Energy's National Nuclear Security Administration under Contract DE-AC04-94AL85000.

Phononics 2011: First International Conference on Phononic Crystals, Metamaterials and Optomechanics
Santa Fe, New Mexico, USA, May 29-June 2, 2011
PHONONICS-2011-0088

Low-Temperature Thermal Conductance of Periodically Perforated Silicon Nitride Membranes

N. Zen[1], T. J. Isotalo[1], I. J. Maasilta[1]

[1] *Nanoscience Center, University of Jyväskylä, Finland*
nobuyuki.zen@jyu.fi, ilari.j.maasilta@jyu.fi

Abstract: In order to enhance the thermally insulating propertiy of a silicon nitride (Si_3N_4) membrane, we have micromachined periodic holes through it with the intent of producing a complete phononic bandgap. The observation of the thermal transport in the phononic crystal is carried out by using a well-established Normal metal-Insulator-Superconductor (NIS) tunnel junction thermometer at sub-Kelvin temperatures. In addition, numerical calculations of the thermal conductance of the structure are in progress.

Periodically Perforated Si_3N_4 Membrane as a Phononic Crystal

Phononic crystals are promising devices[1] for ultrasonic sensors, acoustic filters or waveguides, as well as high efficient thermoelectric transducers, and the next-generation ultra high sensitive superconducting radiation detectors, whose performance strongly depend on the phonon thermal conductance. Because the superconducting detectors convert the energy of the photons[2] or proteins[3] from the Time-Of-Flight Mass Spectrometer (TOF MS) into phonons, it is important to mount the detector on the infrastructure which can enclose phonons and prevent them from dissipating to surroundings too quickly. A silicon nitride (Si_3N_4) membrane is frequently used material for this purpose because of its low thermal conductivity and the ease of controlling its dimension and structure[2]. In order to enhance the sensitivity of the superconducting detectors, we have started developing periodically perforated Si_3N_4 membranes which are expected to perform as phononic crystals. Using finite element method based calculations (COMSOL Multiphysics), we have successfully found the proper geometry which has a complete phononic bandgap extended from 17.7 GHz to 22.0 GHz, as shown in Figure 1 (a). For the 3-D Debye model, the dominant thermal phonon frequency at a temperature T is expressed as $\omega = 2.8k_BT/\hbar$. In our case, however, the perforated-membrane structure has only in-plane periodicity, therefore we should compare the bandgap with the 2-D Debye model, whose dominant thermal frequency is expressed as $\omega = 1.5k_BT/\hbar$. At the temperature of 100 mK, it corresponds to $\omega = 20$ GHz, just in the middle of the complete bandgap of Figure 1. Hence, we can expect the suppression of the thermal conductance in our modeled geometry. Moreover, the simulation of the constant energy surface in Figure 1 (b) shows that the perforated membrane exhibits a strong directionality in the thermal transport, which is isotropic in the case of the unperforated membrane in Figure 1 (c). This effect, known as phonon focusing in regular crystals[4] will also contribute to the thermal properties of the membrane.

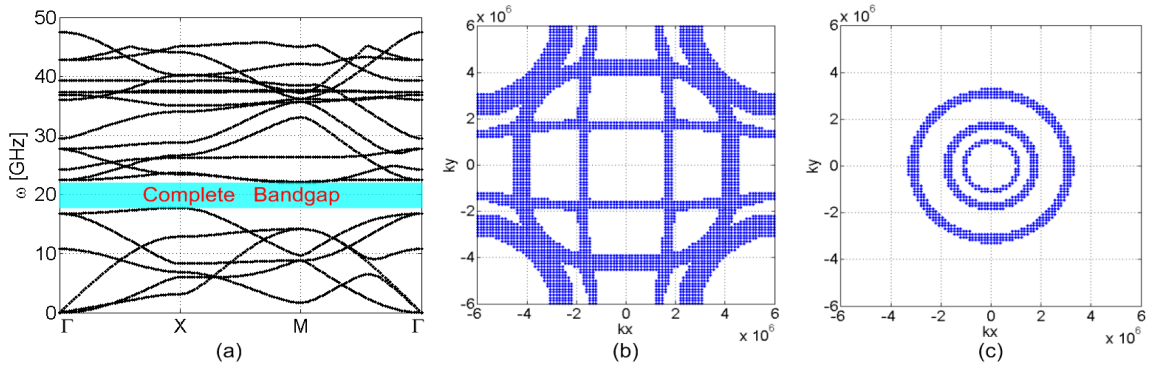

Figure 1 (a) A dispersion relation of the perforated Si_3N_4 membrane, calculated by COMSOL Multiphysics with the Matlab environment. The complete bandgap extends from 17.7 GHz to 22.0 GHz. **(b)** Constant energy surface of the perforated Si_3N_4 membrane and **(c)** unperforated membrane at the frequency of 10 GHz in k_x, k_y space.

Phononics 2011: First International Conference on Phononic Crystals, Metamaterials and Optomechanics
Santa Fe, New Mexico, USA, May 29-June 2, 2011
PHONONICS-2011-0088

NIS Tunnel Junction Thermometry for Phonons

In order to investigate phononic thermal conduction, we have been using the Normal metal-Insulator-Superconductor (NIS) tunnel junctions as thermometers[5,6]. A SEM image of a NIS thermometer and its operating circuit is shown in Figure 2 (a). NIS junctions are fabricated using an electron-beam lithography and an ultra-high-vacuum e-beam evaporation. A typical size of the junction is a several hundreds of nm each as in the inset of Figure 2 (a). The red part in the figure (online) is a normal metal (Cu) island which can absorb phonons from the environment. The thermometer works with a constant-current bias, with the voltage being inversely proportional to the normal metal electron temperature[5,6]. As the superconducting leads (Al) of the NIS junctions do not carry any heat electronically, all the absorbed and emitted power is carried by phonons. In this dynamic equilibrium case, the electron temperature follows the phonon temperature. The sensitivity of the NIS thermometer is extremely high as much as 0.9 μV/mK below 200 mK. The small length of the island of the order of μm is also suitable for measuring the local phonon temperature.

Figure 2 (c) is a dark-field micrograph of a perforated Si_3N_4 membrane of the thickness of 300 nm with a hole diameter of 5 μm and a lattice constant of 10 μm. Two SINIS junctions located at the center act as a thermometer and a heater, respectively. Holes are uniformly formed across the whole membrane size of 360 × 360 μm^2.

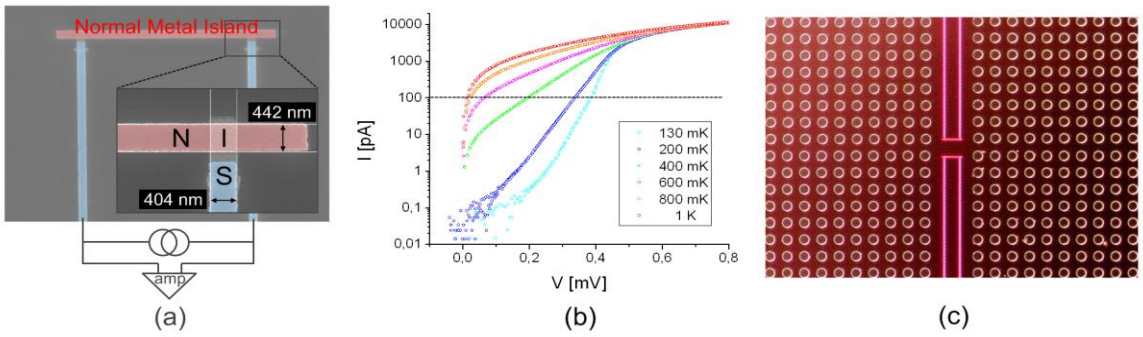

Figure 2 (a) A SEM image of the NIS thermometer and its operating circuit. NIS thermometers are operated by a constant-current biasing. **(b)** *I-V* characteristics of the NIS thermometer at various temperatures. **(c)** A dark-field micrograph of the perforated Si_3N_4 membrane with a SINIS thermometer and a heater.

References

[1] Y. Pennec, J. O. Vasseur, B. Djafari-Rouhani, L. Dobrzynski, and P. A. Deymier, *Surface Sci. Reports* **65**, 229-291 (2010).
[2] C. Enss, *Cryogenic Particle Detection*, Springer, Germany (2005).
[3] A. Casaburi, M. Ejrnaes, N. Zen, M. Ohkubo, S. Pagano, and R. Cristiano, *Appl. Phys. Lett.* **98**, 023702 (2011).
[4] J. P. Wolfe, *IMAGING PHONONS*, Cambridge University Press, UK (1998).
[5] J. T. Karvonen, and I. J. Maasilta, *Phys. Rev. Lett.* **99**, 145503 (2007).
[6] P. J. Koppinen, and I. J. Maasilta, *Phys. Rev. Lett.* **102**, 165502 (2009).

Phononics 2011: First International Conference on Phononic Crystals, Metamaterials and Optomechanics
Santa Fe, New Mexico, USA, May 29-June 2, 2011
PHONONICS-2011-0094

Dispersion of Confined Acoustic Phonons in Ultra-Thin Si Membranes

J. Cuffe[1,2], E. Chavez[2,3], P-O. Chapuis[4], E. H. El Boudouti[4,5], F. Alzina[2], D. Dudek[2], Y. Pennec[5], B. Djafari-Rouhani[5], A. Shchepetov[6], M. Prunnila[6], J. Ahopelto[6], C. M. Sotomayor Torres[2,7]

[1] Dept. of Physics., University College Cork, Tyndall National Institute, Prospect Row, Cork, Ireland
[2] Catalan Institute of Nanotechnology (ICN-CIN2), Campus UAB, 08193 Bellaterra (Barcelona), Spain
[3] Dept. of Physics, UAB, 08193 Bellaterra (Barcelona), Spain
jcuffe@icn.cat,echavez@icn.cat,olivier.chapuis@cin2.es,francesc.alsina.icn@uab.es,clivia.sotomayor@icn.cat
[4] Institut d'Electronique, de Microélectronique et de Nanotechnologie (IEMN), Université de Lille 1, France
yan.pennec@univ-lille1.fr, bahram.djafari-rouhani@univ-lille1.fr
[5] LDOM, Faculté des Sciences, Université Mohamed 1, Oujda, Morocco
[6] VTT Technical Research Centre of Finland, PO Box 1000, 02044 VTT, Espoo, Finland
Jouni.Ahopelto@vtt.fi, Andrey.Shchepetov@vtt.fi,Mika.Prunnila@vtt.fi,
[7] Institució Catalana de Recerca i Estudis Avançats (ICREA), 08010 Barcelona, Spain

The dispersion curves of confined acoustic phonons in ~10 and ~30 nm Si membranes were measured using Brillouin Light Scattering (BLS) spectroscopy. The dispersion relations of the confined phonons were calculated from a semi-analytical model based on continuum elasticity theory. Green's function simulations were used to simulate the Brillouin spectra.

The acoustic properties of ultra-thin Si layers are important for many areas of nanofabrication, impacting on both structural integrity and thermal transport. The effect of phonon confinement is particularly important, affecting both heat dissipation and charge carrier mobility[1,2]. The goal of this work is to obtain a deeper understanding of phonon confinement and propagation in materials with dimensions comparable to thermal phonon wavelengths. Previous studies have investigated out-of-plane confined acoustic phonons in 30 nm Si membranes by inelastic light scattering at normal incidence, with use of a triple grating Raman spectrometer[3,4]. In this work the in-plane propagation of these modes is investigated as a function of the parallel component of the wavevector, using a high-resolution Tandem Fabry-Perot Interferometer. The effect of the ~1 nm native oxide layer in such thin systems was also calculated using a three-layer model.

Methods

Brillouin Light Scattering (BLS) spectroscopy is an inelastic light scattering technique, which can directly measure acoustic phonon dispersion in a non-destructive manner. Using an angle-resolved approach, out-of-plane confined phonons as well as flexural, dilatational, and shear modes propagating in the plane of the membrane were investigated. The dispersion curves were calculated from numerical solutions to the analytic equations for the acoustic modes in a membrane, based on a continuum elasticity model[5]. Green's function simulations were also used to calculate the density of states of the phonon modes and to simulate the Brillouin spectra[6]. The membranes of area 500 x 500 μm^2 were fabricated on nominally undoped 150 mm thin SOI wafers using Si MEMS processing techniques. The thin SOI wafers were produced by bonding the standard SOI wafers from SOITEC company[7] with a Si oxidized wafers.

Results

The BLS spectra of the membranes corresponded to calculated thicknesses of 12 and 28 nm. Calculations for the 12 nm membrane showed that mode frequencies exhibit a detectable shift of 8% with changes in the thickness of the membrane of 1 nm, which is of the order of the uncertainty in the thickness measurement. The ultra-thin nature of the membranes resulted in a slow phase and group velocity for the first order flexural (A0) modes, with a phase velocity down to 320 m s^{-1} recorded for the 12 nm membrane. This is 15 times smaller than the comparable bulk value (Rayleigh Wave)

v_{RSAW} = 4921 m s^{-1}. This resulted in a large phonon density of states, as evidenced by an enhanced acousto-optic interaction and therefore a strong scattered signal. It was observed that the experimental

Phononics 2011: First International Conference on Phononic Crystals, Metamaterials and Optomechanics
Santa Fe, New Mexico, USA, May 29-June 2, 2011
PHONONICS-2011-0094

data agree with the dispersion curves calculated from continuum elasticity theory to within experimental error, apart from the dilatational mode of the 12 nm membrane (Figure1a), which is under further investigation.

Calculations for a three layer system were also performed to take account of the native oxide layer, which was found to cause a detectable change in the dispersion of the higher order (n>0) acoustic modes. (Figure 1b)

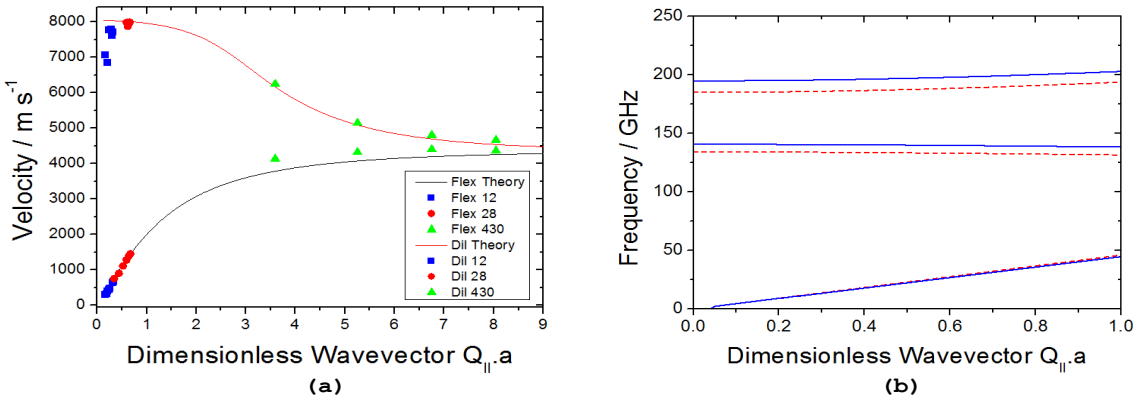

Fig. 1: (a) Phase velocity vs. dimensionless parallel wavevector for 12 nm (blue squares), 28 nm (red circles) and 430 nm (green triangles) membranes, with theoretical calculations for the first order flexural (black line) and dilatational (red line) modes of a Si membrane. (b) : Dispersion curves of the dilatational modes of a 30 nm Si membrane, (blue solid line) and 28.4nm Si with 1.6 nm SiO2 on the top and bottom surfaces (red dashed line).

Conclusions

The acoustic dispersion relations of confined phonons in ultra-thin Si membranes, with thicknesses of 12 and 28 nm, were measured. The experimental results were compared with semi-analytic and Green's function calculations with satisfactory agreement, confirming a small phase and group velocity for the first order flexural mode. Calculations show that the spectra are sensitive to changes in thickness of the membrane on the order of 1 nm. The higher order acoustic modes were also shown to be sensitive to the presence of the thin native oxide layer. This work provides a basis to investigate the effect of acoustic phonon confinement on thermal transport in systems with sub- 50 nm dimensions.

Acknowledgements

The authors are grateful for financial support from the FP7 projects ICT FET TAILPHOX (grant nr. 233883), ICT IP NANOPACK (grant 216176) and the MICINN project ACPHIN (FIS2009-10150). J.C. gratefully acknowledges financial support under an Irish Research Council for Science, Engineering, and Technology (ICRSET) scholarship.

References

[1] L. Donetti, F. Gamiz, J. B. Roldan and A. Godoy, *J. App. Phys.*,**100**, 013701 -013701-7 (2006)
[2] Huang, M.-J.; Chang, T.-M.; Chong, W.-Y.; Liu, C.-K. & Yu, C.-K.*Int. J. of Heat and Mass Transfer,* **2007**, *50*, 67 - 74
[3] C. M. Sotomayor-Torres, A. Z. F. Poinsotte, J. Groenen, M. Prunnila, J. Ahopelto, A. Mlayah and V. Paillard, *Physica Status Solidi (C), **1**(11)*, 2609-2612 (2004)
[4] J. Groenen, F. Poinsotte, A. Zwick, C. M. Sotomayor-Torres, M. Prunnila and J. Ahopelto, *Phys. Rev. B*, **77**, 045420 (2008)
[5] Lamb, H. *Proc. Lond. Math. Soc*. **93** 114 (1917)
[6] E. H. El Boudouti, B. Djafari-Rouhani, A. Akjouj, and L. Dobrzynski, *Surface Science Reports*, **64**, 471 – 594 (2009)
[7] M. Bruel, B. Aspar, and A. J. Auberton-Herve, *Jpn. J. Appl. Phys., Part 1 **36***, 1636 (1997)

Phononics 2011: First International Conference on Phononic Crystals, Metamaterials and Optomechanics
Santa Fe, New Mexico, USA, May 29-June 2, 2011
PHONONICS-2011-0103

Acoustic Phonon Transmission and Heat Conduction Through Vacuum

Mika Prunnila, Johanna Meltaus

VTT Technical Research Centre of Finland, P.O.Box 1208, FIN-02044 VTT, Espoo,Finland
mika.prunnila@vtt.fi, johanna.meltaus@vtt.fi

Abstract: We describe theoretically how acoustic phonons can directly transmit energy and conduct heat between bodies that are separated by a vacuum gap. This effect is enabled by introducing a coupling mechanism, such as piezoelectricity, that strongly couples electric field and lattice deformation.

Advances in experimental techniques have enabled near-field heat transfer measurements from μm down to 10 nm body distances[1]. We have recently proposed that at such distances a new type of evanescent field heat transfer mechanism due to acoustic phonons can exist[2]. Significant energy transmission and heat flux across a vacuum gap is possible if the acoustic phonons can induce a quasi-static electric field, which then can leak into the vacuum [see Figs. 1(a) and 1(b)]. Such a mechanism is provided, for example, by the piezoelectric (PE) effect.

Our approach involves the determination of the scattering matrix of the system and the resulting energy transmission coefficients T_γ.[2] The thermal boundary conductance G_γ arising from transmission of mode γ is calculated by phonon Landauer formula, which we write in the form

$$G_\gamma = \frac{2\pi^2}{30} v_\gamma k_B q_T^3 \left(1 + \frac{q_T}{4}\frac{\partial}{\partial q_T}\right) T_\gamma^{eff} \tag{1}$$

$$T_\gamma^{eff} = \frac{15}{\pi^4}\left\langle \int_0^{q_c/q_T} dx \frac{x^3}{e^x - 1} T_\gamma(q_T d, \theta, \phi) \right\rangle, \tag{2}$$

where T_γ^{eff} is the effective transmission coefficient, v_γ is phonon velocity and $q_T = 2\pi k_B T/\hbar v_\gamma$ is the thermal wave number (T being the temperature). Mode indices $\gamma=L$ and $\gamma=S$ stand for longitudinal and transversal, respectively (the two transversal modes are not written explicitly). Here q_c is the Brillouin/Debye cut-off and <…> stands for solid angle average.

Coupling of lattice deformation and (quasistatic) evanescent electric field leads to certain type of scattering matrix and energy transmission without specifying the details of the (linear) coupling mechanism. This general analysis anticipates exponentially low "tunneling" regimes and also strong resonances in solid-vacuum-solid phonon transmission[2]. Here the numerical transmission calculation examples rely on piezoelectric coupling and, therefore, show some similarities with Refs. 3.

Figure 2(a) shows numerically calculated energy transmission T_γ from a PE material to another across a vacuum gap following the S-matrix approach of Ref. 2. We have adopted material parameters that are close to that of ZnO with the simplifying approximation of only one nonzero element of the piezo tensor (e_{33} = 1.3 C/m^2). Note that for this approximation the acoustic and electric fields are decoupled for the transversal mode whose polarization is parallel to the interfaces. Therefore, in Figure 2 the S mode refers to the mode whose polarization is in the plane of incidence and we need to consider only single angular variable θ, the angle of incidence. We can observe that the transmission probability of both modes exhibit strong resonances in the (qd,θ)-plane. Most striking feature is that at/around the resonances the phonons can go through the gap with (or close to) unity transmission.

Figure 2(b) shows T_γ^{eff} and G_γ obtained from Eqs. (1) and (2) and T_γ of Fig. 2(a). At low temperatures the S-mode thermal conductance G_S is ~15 % of the unity transmission thermal conductance. At high temperatures G_S saturates, because only long wavelength transversal phonons can go across the gap.

Phononics 2011: First International Conference on Phononic Crystals, Metamaterials and Optomechanics
Santa Fe, New Mexico, USA, May 29-June 2, 2011
PHONONICS-2011-0103

The L-mode shows no saturation, because of the strong resonances at large q. These resonances enable some of the small wavelength longitudinal phonons to be transmitted across the vacuum gap even with unity transmission. It should be noted that if we introduce a finite cutoff q_c then G_L also saturates at the limit $q_T / q_c >> 1$.

We conclude that, essentially, this work describes how acoustic phonons can directly transmit energy and heat between bodies without any mechanical inter-body contact. We believe that this novel effect is of interest in phononics and nanoscale heat transport.

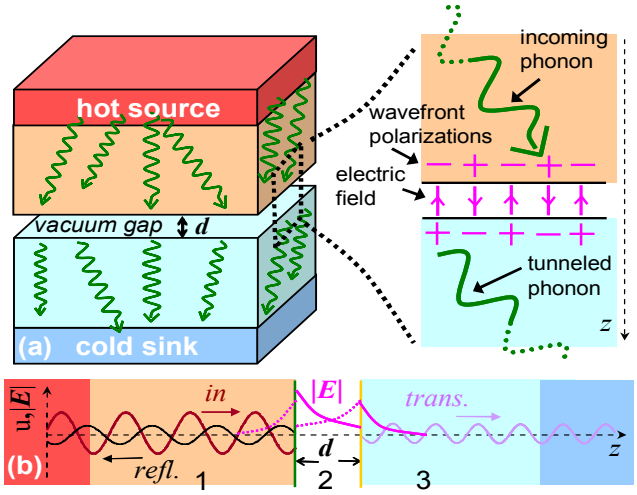

Figure 1 Illustration of the phonon transmission/tunneling effect through a vacuum gap. (a) Hot source radiates phonons towards cold sink. Single phonon carries an electric field, illustrated by + or - signs of wavefront polarization. The polarization induces an electric field into the vacuum gap. The field enables finite transmission over the gap. (b) A projection showing the spatial behaviour of the phonon waves (***u***) and of the evanescent electric ***E***. The dashed curves depict the "reflected" evanescent field.

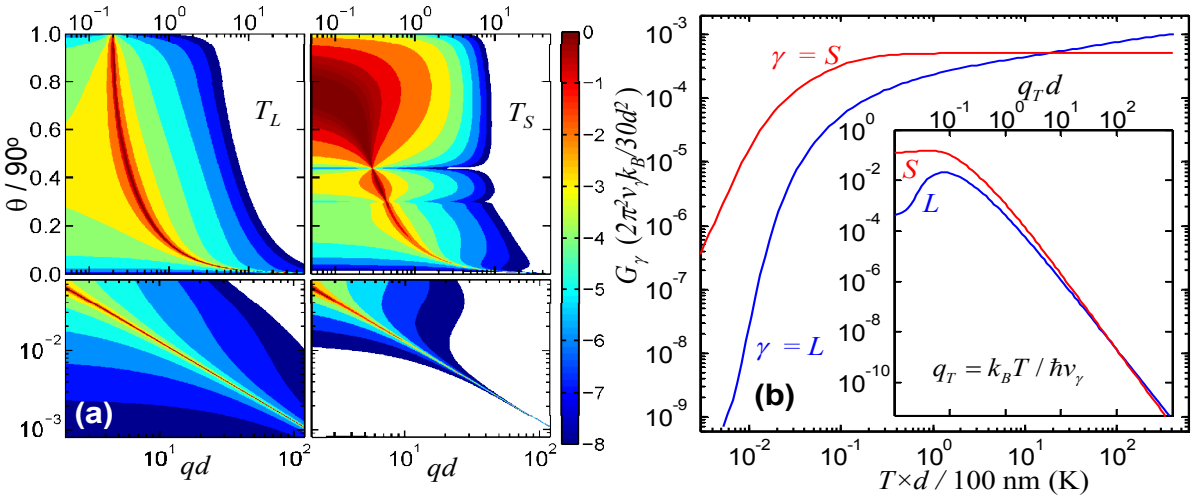

Figure 2 (a) Logarithmic contour plot of energy transmission coefficients T_γ between two PE bodies as a function of normalized wave vector qd (d is the gap width) and the angle of incidence θ. The lower panels show log-log blow-up of the small-θ large-qd region. **(b)** Effective transmission T_g^{eff} (the inset) as a function of $q_T d$ and the interface thermal conductance G_γ (the main part) as a function of temperature (we have set $q_c \to \infty$). The curves are obtained from the T_γ of (b) by using Eqs. (1) and (2). For the y-axis units of the main figure we have $2\pi^2 v_\gamma k_B / 30d^3 = Y_g \times (100\ \text{nm}/d)^3$ W/Km^2, where $Y_{L(S)}$ = 55.6 (24.9).

References

[1] See, for example, E. Rousseau *et al.*, Nature Photonics **3**, 514 (2009).
[2] M. Prunnila and J. Meltaus, Phys. Rev. Lett. **105**, 125501 (2010).
[3] M. K. Balakirev and A. V. Gorchakov, Sov. Phys. Solid State **19**, 355 (1977); M.K. Balakirev, S.V. Bogdanov, and A.V. Gorchakov, Sov. Phys. Solid State **20**, 338 (1978); Y. V. Gulyaev and V. P. Plesskii, Sov. Phys. Solid State **20**, 71 (1978).

Phononics 2011: First International Conference on Phononic Crystals, Metamaterials and Optomechanics
Santa Fe, New Mexico, USA, May 29-June 2, 2011
PHONONICS-2011-0104

Nanostructured two-dimensional phononic materials

K. Muralidharan[1], P.A. Deymier[1], N. Swinteck[1], K. Runge[1], and J-F. Robillard[2]

[1] *Department of Materials Science and Engineering, University of Arizona, Tucson, Arizona 85721, USA,*
krishna@email.arizona.edu, deymier@email.arizona.edu, swinteck@email.arizona.edu,
[2] *Institut d'Électronique, de Microélectronique et de Nanotechnologie, UMR CNRS 8520, Cité Scientifique, 59652 Villeneuve d'Ascq Cedex, France,*
jean-francois.robillard@isen.fr

Abstract: Phononic properties of nanostructured two-dimensional materials such as graphene and boron nitride (BN) sheets are calculated using the method of molecular dynamics. Nanophononic crystals composed of periodic array of holes in graphene exhibit Bragg scattering at non-cryogenic temperatures leading to reduction in thermal conductivity. The transport of phonons across non-periodic arrays of asymmetric holes in BN sheets is discussed in the context of scattering and non-linear effects that may lead to thermal rectification.

Phonons contributing to thermal conductivity have wavelengths ranging from nanometers to several hundreds of nanometers. Nanofabrication techniques have the potential of structuring materials in a way that may affect the propagation of thermal phonons. This possibility opens perspectives in the fields of thermal management and thermoelectrics. Modulating the thermal properties by creating a nanoscale composite material is an approach that has been extensively studied in the case of superlattices [1-3]. These stacks of nanoscale layers have been shown theoretically and experimentally to impact thermal transport due to scattering effects of phonons. In contrast to the 1-D superlattice structures, not much is known of the effect of 2D nanophononic structures on thermal conductivity and phonon transport. In this work we report on the phononic properties of nanostructured two-dimensional materials such as graphene and boron nitride (BN) sheets. Specifically we examine periodically patterned anti-dot graphene structures and defected BN sheets. Thermal properties and phonon transport behavior are modeled using the method of molecular dynamics (MD). The forces between atoms are determined from Tersoff-Brenner family of interatomic potentials . Both equilibrium as well as non-equilibrium MD formulations are used in this work to examine thermal properties of the systems under study.

MD simulations are carried out in conjunction with phononic band structure calculations in order to characterize the thermal transport properties of graphene-based nanophononic crystals composed of periodic arrays of hole inclusions (Fig. 1). In particular, the heat current autocorrelation function is calculated using the Green-Kubo equilibrium method, enabling the estimation of the lifetimes of acoustical and optical phonons as well as the thermal conductivity as functions of the filling fraction of the phononic crystals and temperature (Figs. 2a and 2b). We observe that Bragg scattering of thermal phonons leads to dramatic changes in the phonon lifetimes for filling fractions as low as 2.5% over a significant range of temperature. This change of lifetimes is followed by a corresponding change in the thermal conductivity. We discuss the results on the phonon lifetime in the context of competition between elastic Bragg scattering and inelastic phonon-phonon scattering. Our results suggest that in addition to impacting elastic scattering, band effects due to the phononic structure may also impact inelastic scattering.

Boron nitride (BN) sheets and thin films can contain non-periodic distributions of triangular holes as shown in Ref [4]. Using non-equilibrium molecular dynamics methods, the thermal transport perpendicular to an array of triangular holes in a BN sheet (Fig. 2) is studied as a function of thermal gradient of variable magnitude and sign. Results indicate that there is asymmetry in the magnitude of thermal flux when the thermal gradient changes sign, due to the interplay between geometrical effects (phonon scattering by asymmetric holes) and non-linear effects such as temperature dependent phonon density of states. Further, asymmetry in thermal transport is observed over a broad range of temperatures. These effects suggest

Phononics 2011: First International Conference on Phononic Crystals, Metamaterials and Optomechanics
Santa Fe, New Mexico, USA, May 29-June 2, 2011
PHONONICS-2011-0104

that BN sheets containing oriented non-periodic triangular holes may serve as a platform for designing a thermal rectifier or thermal diode.

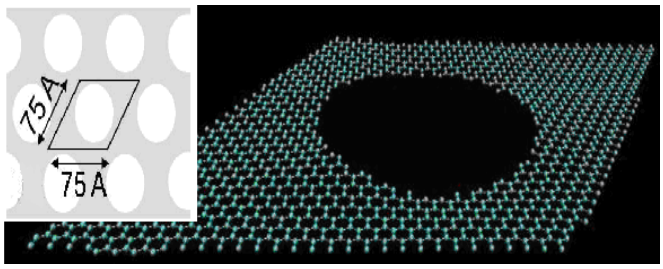

Figure 1: Illustration of the patterned graphene structure.

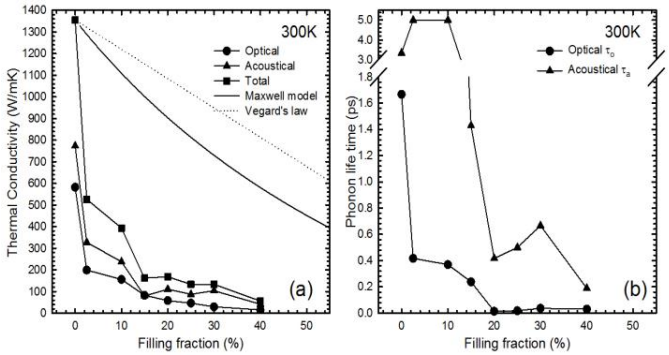

Figure 2: (a) Thermal conductivity deduced from the Green-Kubo method as a function of the filling fraction at 300 K (Squares). The contribution of the optical (Circles) and acoustical phonons (Triangles) are distinguished. These data are compared to a parallel (dotted line) and Maxwell (solid line) mixing model. (b) Mean acoustical and optical phonons lifetimes as a function of the filling fraction at 300K. These lifetimes are estimated from the fit of the heat current correlation functions. Error bars on calculated lifetime and thermal conductivity due to the exponential fit of the heat current autocorrelation functions are the size of the data points.

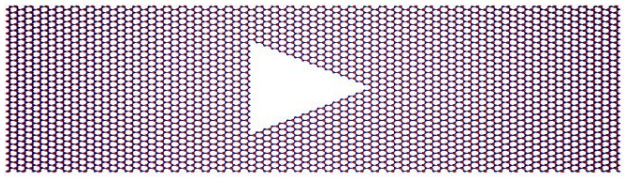

Figure 3: An illustration of the 2-D BN sheet with the triangular defect. The X-Y dimensions of the sheet are 175 Å x 70 Å, and periodic boundary conditions are employed in the Y direction, and the temperature gradients are applied in the X direction.

References

[1] P. Hyldgaard and G. D. Mahan, in *Thermal Conductivity*, Vol. 23, (Technomic, Lancaster, PA, 1996)
[2] G. Chen, C. L. Tien, X. Wu, and J. S. Smith, J. Heat Transfer **116**, 325 (1994)
[3] W. S. Capinski and H. J. Maris, Physica B **219**, 699 (1996)
[4] C. Jin, F. Lin, K. Suenaga, and S. Iijima, Phys. Rev. Lett. 102, 195505 (2009).

Phononics 2011: First International Conference on Phononic Crystals, Metamaterials and Optomechanics
Santa Fe, New Mexico, USA, May 29-June 2, 2011
PHONONICS-2011-0108

Effect of Interface Roughness on Phonon Transport in Superlattices

Kevin P. Pipe[1,2] and Huarui Sun[1]

[1]Department of Mechanical Engineering
[2]Department of Electrical Engineering and Computer Science
University of Michigan, Ann Arbor, MI, USA
pipe@umich.edu, hrsun@umich.edu

Abstract: We present a boundary perturbation method to analyze phonon reflection, transmission, and mode conversion at a rough interface, and extend these calculations using a transfer matrix approach to examine the effects of interface roughness on phonon transport in multilayer thin films.

Superlattices have been used to control the transport of acoustic phonons for coherent phonon[1,2] and heat transfer applications. In phonon "lasers" and terahertz phonon devices, superlattices are used as Bragg reflectors for acoustic cavities[3-5]. In thermoelectric devices, superlattices are used to increase phonon scattering and hence reduce thermal conductivity, leading to higher thermoelectric energy conversion efficiency[6-8].

Coherent effects that rely on interface periodicity, such as Bragg reflection, are sensitive to fluctuations in interface position caused by roughness. Interface roughness can disrupt specular interference effects, increase parasitic coupling into other phonon modes (e.g., longitudinal acoustic into transverse acoustic), and increase diffusive scattering. Since the acoustic phonons relevant for terahertz devices and most heat transfer applications have wavelengths less than 10 nm, atomic-scale interface roughness is expected to play a much more significant role than it does at optical wavelengths.

Previous work has examined the interaction of acoustic phonons with interface roughness by implementing an empirical specularity parameter[9-11] or by summing a collection of specular reflections off of a defined roughness geometry[12]. Such approaches are limited in their ability to account for phonon mode conversion at the interface. Lattice dynamics and Green's function formulations[13,14] have also been utilized for this purpose but are often computationally expensive and restricted to unrealistic roughness profiles (such as short in-plane correlation lengths).

We have developed a boundary perturbation method to model phonon transport at rough solid-solid interfaces, building off of previous work that has applied such methods to rough interfaces between liquid helium and copper[15,16] as well as ice and water[17]. This approach allows interface roughness to be characterized by statistical parameters such as the standard deviation of interface height (RMS roughness) and the in-plane correlation length, making calculations of mode conversion and separation into specular and diffuse components straightforward.

Using the boundary perturbation method, we predict the frequency (wavelength) and angle of transverse (TA) and longitudinal (LA) acoustic phonons emitted when an LA phonon is incident on a single rough interface at a particular angle. We then utilize these parameters within a transfer matrix approach to calculate the phonon transmission and reflection characteristics of a superlattice with a specified roughness profile. Metrics of interest for phonon Bragg reflectors (e.g., coherent reflectivity, full with at half maximum of the stop band) are calculated for superlattices in relevant material systems such as $SrTiO_3/BaTiO_3$ with various roughness profiles and numbers of superlattice periods. A quantitative analysis is performed to assess the relative contributions of acoustic impedance contrast and interface flatness to superlattice reflectivity. Implications for heat transfer applications (e.g., thermal boundary resistance) at low temperature are discussed.

This work was supported by the United States Air Force Office of Scientific Research (AFOSR) through the Multidisciplinary University Research Initiative (MURI) program under grant number FA9550-08-1-0340.

Phononics 2011: First International Conference on Phononic Crystals, Metamaterials and Optomechanics

Santa Fe, New Mexico, USA, May 29-June 2, 2011

PHONONICS-2011-0108

References

[1] N. M. Stanton, R. N. Kini, A. J. Kent, M. Henini, and D. Lehmann, *Phys. Rev. B* **68**, 113302 (2003).
[2] A. Bartels, T. Dekorsy, H. Kurz, and K. Köhler, *Phys. Rev. Lett.* **82**, 1044 (1999).
[3] M. Trigo, A. Bruchhausen, A. Fainstein, B. Jusserand, and V. Thierry-Mieg, *Phys. Rev. Lett.* **89**, 227402 (2002).
[4] A. J. Kent et al., *Phys. Rev. Lett.* **96**, 215504 (2006).
[5] P. A. Fokker, J. I. Dijkhuis, and H. W. de Wijn, *Phys. Rev. B* **55**, 2925 (1997).
[6] R. Venkatasubramanian, *Phys. Rev. B* **61**, 3091 (2000).
[7] M. N. Touzelbaev, P. Zhou, R. Venkatasubramanian and K. E. Goodson, *J. Appl. Phys.* **90**, 763 (2001).
[8] S.-M. Lee, David G. Cahill and R. Venkatasubramanian, *Appl. Phys. Lett.* **70**, 2957 (1997).
[9] J. M. Ziman, *Electrons and Phonons* (Oxford, 1960).
[10] G. Chen, *Phys. Rev. B* **57**, 14958 (1998)
[11] P. M. Norris and P. E. Hopkins, *J. Heat Transfer* **131**, 043207 (2009)
[12] A. Majumdar, *J. Heat Transfer* **113**, 797 (1991)
[13] B. C. Daly, H. J. Maris, K. Imamura and S. Tamura, *Phys. Rev. B* **66**, 024301 (2002)
[14] H. Zhao and J. B. Freund, *J. Appl. Phys.* **105**, 013515 (2009)
[15] A. D. Lapin, *Sov. Phys. Acoust.* **15**, 635 (1970).
[16] N. S. Shiren, *Phys. Rev. Lett.* **47**, 1466 (1981).
[17] W. A. Kuperman, *J. Acoust. Soc. Am.* **86**, 1511 (1989).

Phononics 2011: First International Conference on Phononic Crystals, Metamaterials and Optomechanics
Santa Fe, New Mexico, USA, May 29-June 2, 2011
PHONONICS-2011-0111

Acoustic phonon relaxation rates in nanometer-scale membranes

E. Chavez[1], P.O. Chapuis[2], J. Cuffe[2], F. Alzina[2], C.M. Sotomayor-Torres[2,3]
[1] *Dept. of Physics, Universitat Autònoma de Barcelona and Catalan Institute of Nanotechnology CIN2(ICN-CSIC), Campus de la UAB, 08193 Bellaterra (Barcelona), Spain, emigdio.chavez@icn.cat*
[2] *Catalan Institute of Nanotechnology CIN2(ICN-CSIC), Campus de la UAB 08193 Bellaterra (Barcelona), Spain, p2n@icn.cat*
[3] *Catalan Institute for Research and Advanced Studies (ICREA) 08010 Barcelona, Spain*

Abstract: The elastic continuum model is applied to analyse the acoustic phonon modes for single and three-layer membranes. The dispersion relations are computed using a numerical approach and are compared with experimental and theoretical results. These values are used to compute the rate of relaxation, considering a three-phonon Umklapp process.

The electronic properties of free-standing membranes, nanowires and ultrathin films, which are the buildings block of the components for the future electronics devices and nano-electrical mechanical nanostructures, have been the subject of the extensive studies. On the contrary, their thermal properties have received comparatively less attention. The phonon dispersion relation and the phonon interaction in such nanostructures are expected to be significantly different from due to bulk due to the confinement effects.

Our approach to investigate the phonon dispersion in free-standing layers is based in the elastic continuum model in isotropic media. Within this model, the equation of the phonon displacement vector, "***u***", may be written as[1]:

$$\partial^2 u / \partial t^2 = c_t^2 \nabla^2 u + (c_l^2 - c_t^2)\nabla(\nabla u) \tag{1}$$

where c_t and c_l are transversal and longitudinal sound speeds, respectively. The movement was solved for two different systems: (i) one layer of medium ***A*** of thickness ***a*** embedded in air, (ii) a stacking of three layers of alternating A and B media (see figure **1**).

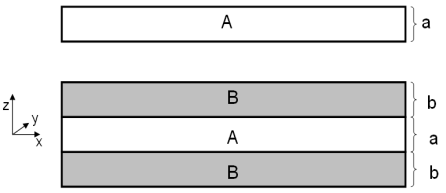

Figure 1 Structures considered for the present study

The general solution for the 1-layer system are: shear waves, dilatational (symmetric) and flexural (antisymmetric) waves[2]. The solutions for the 3-layer structures are: shear waves (only nonzero *y* components), symmetric *x* component and antisymmetric z component (SA waves), and antisymmetric x component and symmetric z component. The SA (AS) waves consists of dilatational (flexural) waves in the "***A***" layer and a linear combination of all waves in the two "***B***" layers. The calculated dispersion relations for flexural and SA waves are shown in the fig. **2** for a monolayer of silicon and the 3-layers structure SiO_2-Si- SiO_2. Note that the native oxide layers are in principle always present. Once obtained the dispersion relation we can derivate the group and phase velocity as well as the density of states.

From the first-order perturbation theory, the single-mode relaxation rate of Umklapp process (U) for a thermal mode $\boldsymbol{q}$ can written be as[3]:

$$\tau_U^{-1} = \sum_q \frac{8\gamma^2\hbar}{3\rho v^2}\omega_i\omega_j(\omega_i+\omega_j)\pi\delta[\Delta\omega][n(\omega_i)-n(\omega_i+\omega_j)] \tag{2}$$

where $\boldsymbol{\gamma}$ is the Grüneisen parameter, $\boldsymbol{v}$ is the sound velocity, $\boldsymbol{n(\omega_i)}$, $\boldsymbol{n(\omega_i+\omega_j)}$ are the equilibrium occupation of the states of $\boldsymbol{q_i}$, $\boldsymbol{q_i+q_j}$ and $\boldsymbol{\rho}$ is the density.

Phononics 2011: First International Conference on Phononic Crystals, Metamaterials and Optomechanics
Santa Fe, New Mexico, USA, May 29-June 2, 2011
PHONONICS-2011-0111

We calculate the different relaxation rates without approximation and compare our results with ref. **4**. We find a significant modification of the U-process in comparison to the case of bulk medium. Our aim is in particular to identify the implications of the presence of native oxide on the dispersion curves and the relaxation rates.

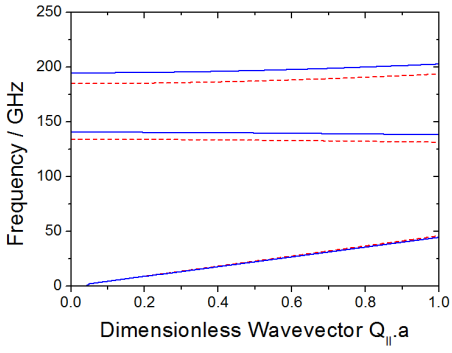

Figure 2: Dispersion curves of the flexural modes of a 30 nm Si membrane, (blue solid line) and 28.4nm Si with 1.6 nm SiO_2 on the top and bottom surfaces (red dashed line).

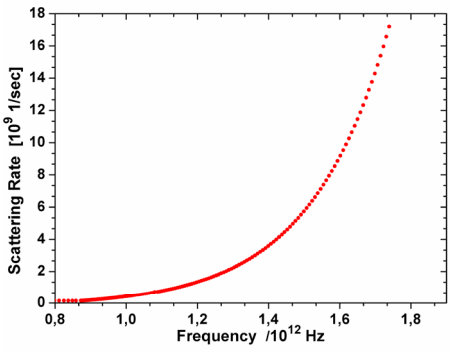

Figure 3: Phonon relaxation rates due to Umklapp process at T=300 K

References

[1] N. Bannov, V. Aristov, V. Mitin and M.A. Stroscio, *Phys. Rev. B*, **51**, 9930(1995).
[2] L. Donetti, F. Gámiz, J.B. Roldán and A. Godoy, *J. Appl. Phys.*, **100**, 013701 (2006).
[3] Y. Chen, D. Li, J.R. Lukes and A. Majumdar, *J. Heat Transf.*, **127**, 1129 (2005)
[4] A. Balandin and K.L. Wang, *Phys. Rev. B*, **58**, 1544(1998)

Phononics 2011: First International Conference on Phononic Crystals, Metamaterials and Optomechanics
Santa Fe, New Mexico, USA, May 29-June 2, 2011
PHONONICS-2011-0133

Nanoscale Phonon Engineering: From Quantum Dots and Nanowires to Graphene and Topological Insulators

Alexander A. Balandin

Department of Electrical Engineering and Materials Science and Engineering Program, Bourns College of Engineering, University of California – Riverside, Riverside, California 92521 U.S.A.
E-mail address: balandin@ee.ucr.edu

Abstract: I describe the nanoscale phonon engineering concept and its possible applications. Nanostructures offer new ways for controlling phonon transport via tuning phonon dispersion. Engineering the phonon spectrum can become as powerful a technique as the electron band-gap engineering, which revolutionized electronics. I outline recent examples of phonon engineering in quantum dot superlattices, nanowires, graphene ribbons and topological insulators. Particular attention is given to the phonon thermal transport in graphene and graphene's applications in thermal management.

The *nanoscale phonon engineering* is defined as controlled modification of the phonon spectrum and phonon transport in nanostructures with the goal of achieving higher electron mobility or changed thermal conductivity or other property, allowing for performance enhancement of electronic, thermoelectric or optoelectronic devices. The phonon engineering concept was initially introduced for nanostructures and nanodevices made of conventional semiconductors [1]. Tuning of the acoustic phonon spectrum in nanostructures with the acoustic impedance mismatch can help in achieving enhanced functionality such as decreased phonon thermal conductivity, beneficial for thermoelectric applications [2], or increased electron mobility [3]. The nanometer length scale, which is comparable to the thermal phonon wavelength in semiconductors, is essential for the phonon confinement effects and phonon engineering near room temperature (RT).

The change in the thermal conductivity of semiconductors due to the phonon – boundary scattering and phonon confinement effects bares important consequences for electronic industry in a view of continuous miniaturization. Heat in technologically important semiconductors is mostly carried by acoustic phonons. The feature size of the state-of-the-art transistor is already well below the RT phonon mean-free path (MFP) in Si, which is ~50 nm according to Debye model. In nanostructures with feature size W much smaller than the phonon MFP, the acoustic phonon spectrum undergoes modification and appears quantized provided that the structures are free standing or embedded within material with different elastic properties (acoustic impedance). This modification is particularly strong when W approaches the scale of the dominant phonon wavelength $\lambda \approx 1.48 \upsilon_S \hbar / k_B T$. Here k_B is the Boltzmann constant, T is the absolute temperature, $\hbar$ is the Plank's constant, and υ_S is the sound velocity. For many crystalline solids, λ is on the order of ~1.5 – 2 nm at RT, which is comparable to the thickness of the transistor gate dielectric or period of superlattices used in optoelectronic or thermoelectric devices.

The newly developed synthesis techniques have expanded the list of nanostructures and materials suitable for engineering the phonon spectrum. The "graphene revolution" started by the mechanical exfoliation of the single atomic layer graphene (SLG) made possible investigation of phonons in strictly two-dimensional (2D) systems. The knowledge about optical phonons in graphene led to the development of Raman spectroscopy as nanometrology tool for graphene identification on variable substrates and at different temperatures [4]. We have discovered experimentally that suspended graphene reveals an unusually high intrinsic thermal conductivity exceeding that of carbon nanotubes [5]. In order to measure the thermal conductivity of "free" graphene we developed on original optical non-contact technique (see Figure 1). The fact that the phonon thermal conductivity of large enough graphene flakes should be higher than that of the basal planes of bulk graphite was predicted theoretically by Klemens a decade ago. He pointed out at the fundamental differences in the long-wavelength phonon transport in 2D graphene and 3D graphite. Unlike in bulk graphite, in SLG the phonon transport remains 2D down to zero phonon energy, which results in larger contributions of long-wavelength

Phononics 2011: First International Conference on Phononic Crystals, Metamaterials and Optomechanics
Santa Fe, New Mexico, USA, May 29-June 2, 2011
PHONONICS-2011-0133

phonons to heat conduction [6]. It is also related to the fact that the intrinsic thermal conductivity in 2-D anharmonic crystals manifests divergence with the size of the system [7]. We were able to study the dimensional crossover of phonon transport both theoretically and experimentally using suspended few-layer graphene (FLG) flakes [7]. It was found that the "intrinsic" thermal conductivity of FLG reveals completely opposite dependence (see Figure 1) on the number of atomic planes (thickness) than the extrinsic thermal conductivity in conventional thin films, which is dominated by the phonon – boundary scattering. The extremely high thermal conductivity of graphene coupled with its flat geometry and demonstrated ability for functioning in Si-based devices make graphene promising material for engineering heat fluxes and thermal management of nanoelectronic circuits [8]. We extended the "graphene-like" mechanical exfoliation and phonon engineering techniques to other materials such as bismuth telluride, which are used for thermoelectric and topological insulator applications [9]. The knowledge of optical phonons allowed us to use Raman spectroscopy as nanometrology tool for topological insulators [10]. A detail review of the nanoscale phonon engineering in quantum dot superlattices, heterostructures and nanowires with acoustically mismatched barriers can be found in Ref. [11].

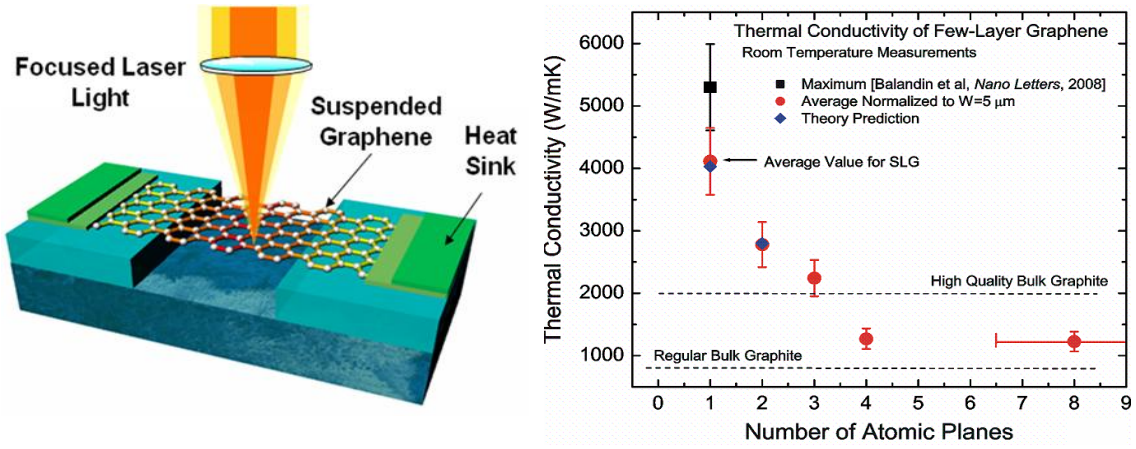

Figure 1 (Left panel) Schematic of the experimental set up, which was used for the first measurement of the thermal conductivity of graphene. In this experiment the excitation laser light focused on graphene suspended across a trench in Si wafer. Laser power absorbed in graphene induces a local hot spot and generates heat wave propagating toward the heat sinks. The local temperature rise was determined from the G peak shift in graphene Raman spectrum. (Right panel) The evolution of the phonon transport as system dimensionality changes from 2-D graphene to 3-D graphite revealed using suspended few-layer graphene samples. The figure is after Ref. [7].

This work was supported, in part, by AFOSR grant on Phonon Engineering, ONR grant on Graphene Quilts and SRC – DARPA Focus Center Research Program (FCRP) through its Functional Engineered Nano Architectonics (FENA) center.

References

[1] A. Balandin and K.L. Wang, *Phys. Rev. B*, **58**, 1544 (1998).
[2] J. Zou and A. Balandin, *J. Appl. Phys*., **89**, 2932 (2001).
[3] V.A. Fonoberov and A.A. Balandin, *Nano Letters*, **6**, 2442 (2006); D.L. Nika, et al., *Appl. Phys. Lett.*, **93**, 173111 (2008).
[4] I. Calizo, et al., *Nano Letters*, **7**, 2645 (2007); I. Calizo, et al., *Appl. Phys. Lett*., **91**, 201904 (2007).
[5] A.A. Balandin, et al., *Nano Letters*, **8**, 902 (2008); S. Ghosh, et al., *Appl. Phys. Lett*., **92**, 151911 (2008).
[6] D.L. Nika, et al., *Appl. Phys. Lett*., **94**, 203103 (2009); D.L. Nika, et al., *Phys. Rev. B*, **79**, 155413 (2009).
[7] S. Ghosh, D.L. Nika, W. Bao, S. Subrina, E.P. Pokatilov, C.N. Lau and A.A. Balandin, *Nature Materials,* **9**, 555 (2010).
[8] A.A. Balandin, *IEEE Spectrum*, 29, October (2009); S. Subrina, et al., *IEEE Electron Device Lett*., **30**, 1281(2009).
[9] D. Teweldebrhan, et al., *Nano Letters* (2010); D. Teweldebrhan, et al., *Appl. Phys. Lett*., **96**, 053107 (2010).
[10] K.M.F. Shahil, M.Z. Hossain, D. Teweldebrhan and A.A. Balandin, *Appl. Phys. Lett*., **96**, 153103 (2010).
[11] A.A. Balandin, *J. Nanoscience Nanotech*., **5**, 7 (2005); A.A. Balandin, E.P. Pokatilov and D.L. Nika, *J. Nanoelectron. Optoelectron*, **2**, 140 (2007).

Phononics 2011: First International Conference on Phononic Crystals, Metamaterials and Optomechanics
Santa Fe, New Mexico, USA, May 29-June 2, 2011
PHONONICS-2011-0145

Improved Lattice-Bath Phonon Relaxation in Nanoscale Oxides

Michael W. Blair[1], Bryan L. Bennett[1], Stephanie C. Tornga[1], Nickolaus A. Smith[1], Ross E. Muenchausen[1]

[1] *Materials Science and Technology, Los Alamos National Laboratory, P. O. Box 1663, MS E546, Los Alamos, NM, 87545, USA*
mblair@lanl.gov, blbennett@lanl.gov, sitarz@lanl.gov, nsmith@lanl.gov, rossm@lanl.gov

Abstract: Electron paramagnetic resonance (EPR) spectroscopy has been used to study energy transport properties of bulk and nanophosphor oxyorthosilicate samples. The bulk samples displayed a slight phonon bottleneck while energy relaxation in the nanophosphor samples was not influenced by the lattice-bath relaxation time and was more rapid.

Introduction

The scintillation properties of oxyorthosilicate materials doped with Ce such as Lu_2SiO_5 (LSO), Y_2SiO_5 (YSO), and Gd_2SiO_5 (GSO) have been studied extensively[1]. These materials are of particular interest for gamma ray detection as they have a high effective atomic number, high light output, fast decay times, and emit in the blue region which is advantageous for most detection systems.

LSO[2] and YSO[3] have also been studied by Electron Paramagnetic Resonance (EPR) spectroscopy in order to study the coordination environment of the Ce^{3+} sites. These studies determined that Ce replaces Lu or Y in the phosphors and occupies two different crystallographic sites corresponding to the two sites for Lu or Y. In previous papers[4] we have reported on EPR spectra of Ce^{3+} in both bulk and nanophosphor LSO and YSO and noted evidence of an increased disorder in the nanophosphor samples. However, the previous analysis used the simplified model of Pidol *et al.*[2], but, as will be shown, the EPR linewidths and relaxation mechanisms are more complicated than previously assumed. The goal of this paper is to further explore the temperature-dependent relaxation lifetimes and mechanisms of LSO:Ce and YSO:Ce for both Czochralski grown (bulk) samples and SCS nanophosphors.

Results and Discussion

Due to lifetime broadening the Ce^{3+} resonances can only be detected below approximately 50 K[4], and only the lowest doublet is occupied at this temperature. Figure 1 shows the Ce g_z resonance for nanophosphor YSO doped with 1% Ce for various temperatures where an increase in linewidth with increasing temperatures is evident. Nanophosphor LSO doped with 1 % Ce shows a similar behavior.

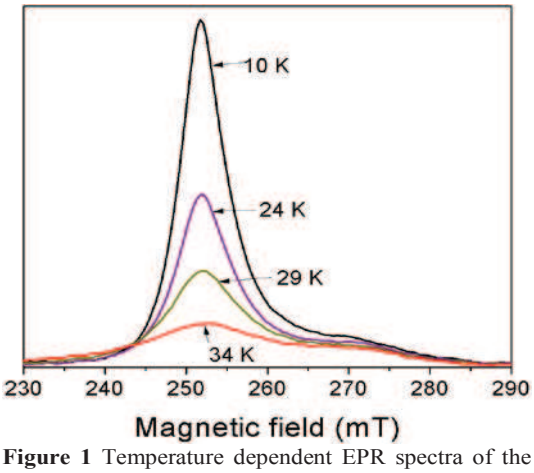

Figure 1 Temperature dependent EPR spectra of the Ce g_z resonance for SCS YSO with 1% Ce.

Although the increased linewidth with increasing temperature in Figure 1 is typical of an Orbach relaxation process, the analysis is complicated by the temperature-dependent lineshape of the samples. Pidol *et al.*[2] has previously noted that the EPR resonances of Ce-doped LSO were Gaussian at low temperatures and became progressively more Lorentzian with increasing temperatures, and our measurements follow the same pattern. In an attempt to separate these contributions to the overall lineshape, we fit the temperature-dependent EPR linewidths of Ce-doped YSO and LSO with a Voigt lineshape[5]. The results for the pure Lorentzian (w_L), pure Gaussian (w_g), and total (w_L+w_G) linewidths are shown in Figure 2 (a), (b), and (c), respectively.

The Lorentzian linewidths of Figure 2 (a) are related to the EPR relaxation lifetime τ by $\tau^{-1}=(2\pi g\beta L/h)$, and the lifetimes can be fit by a combination of a direct phonon relaxation process and the two phonon Orbach relaxation[6]:

Phononics 2011: First International Conference on Phononic Crystals, Metamaterials and Optomechanics
Santa Fe, New Mexico, USA, May 29-June 2, 2011
PHONONICS-2011-0145

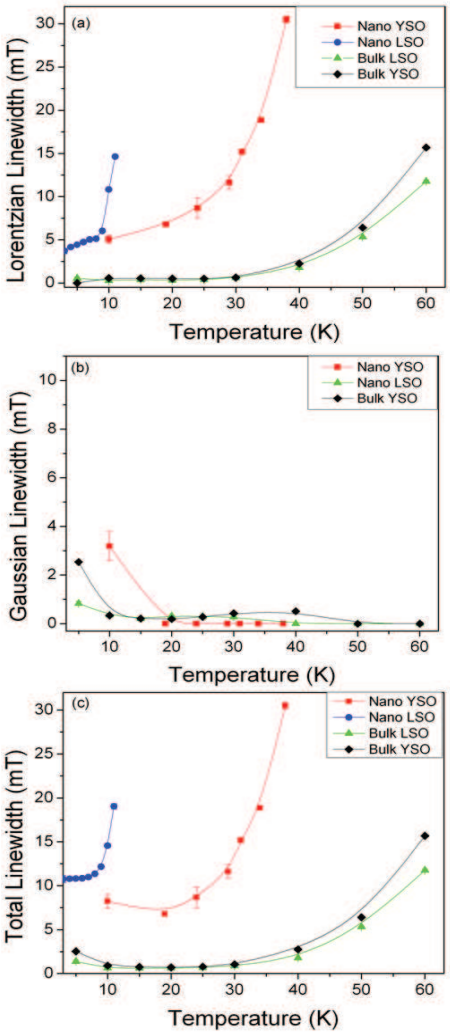

Figure 2 (a) Pure Lorentzian (wL), (b) pure Gaussian (wG), and (c) total (wL+wG) linewidths for bulk LSO, bulk YSO, nanophospor LSO, and nanophosphor YSO derived from fitting the Ce gZ resonance with a Voigt lineshape. The solid lines are guides for the eye only.

$$\frac{1}{\tau} = A*T^{n} + \frac{C*\Delta*^{3}}{\exp(\Delta E/k_B T) - 1)} \qquad (1)$$

where A is the direct phonon relaxation constant, k_B is Boltzmann's constant, T is the absolute temperature, C is the Orbach constant, and ΔE is the energy gap between the ground state of the Kramers doublet and the first excited state. In most cases n=1, but n=2 in the case of a phonon bottleneck where the heat transferred to the lattice cannot be effectively dissipated and the likelihood of phonon heating or energy transfer back to the spins is increased.

For bulk specimens, the temperature-dependent relaxation lifetimes could be fit with n=2 in Equation 1 and show a slight phonon bottleneck where the lifetime due to lattice-bath relaxation is comparable to the lifetime due to spin-lattice relaxation. The relaxation lifetime for the nanophosphors, though, do not show a dependence on the lattice bath relaxation process.

Conclusions and Future Work

The temperature dependence of the Ce g_z resonances was studied for both bulk and 1 % Ce-doped nanophosphor samples. By separating the homogeneous and inhomogeneous parts of the linewidths through Voigt lineshape analaysis, we were able to fit the Lorentzian linewidths to phonon relaxation processes that involve direct phonon relaxation and the two-phonon Orbach process[6]. The bulk samples displayed a weak phonon bottleneck where the lifetime of the lattice-bath relaxation process is comparable to the spin-lattice relaxation lifetime. The nanophosphor oxyorthosilicates, on the other hand, did not show any evidence of a phonon bottleneck. Unfortunately, due to the large uncertainties involved in this study, the analysis cannot be more quantitative but can identify significant and interesting trends.

The current study suggests the possibility of studying the complicated phonon relaxation process and energy transport in more detail. Future work will involve identifying a system or systems to address the various aspects of the phonon relaxation process. The ideal systems would allow for crystallite size and paramagnetic species concentration control at both the bulk (> 1 μm) and nanoscale. In addition, a symmetric crystal structure (e.g., cubic or hexagonal) that is invariant with reduced dimensionality, has well characterized sites for paramagnetic ions, and yields Lorentzian lineshapes would be preferred. Rare earth doped oxide crystals such as YAG:Ce or Y_2O_3:Tb may be suitable systems and are readily obtainable.

References

[1] R. Lecomte, C. Pepin, D. Rouleau, A. Saoudi, M.S. Andreaco, M. Casey, R. Nutt, H. Dautet, and P.P. Webb, *IEE Nucl. Sci. Symp.* **1,** 212 (1997).
[2] L. Pidol, O. Guillot-Noël, A. Kahn-Harari, B. Viana, D. Pelenc, and D. Gourier, *J. Phys. Chem. Solids* **67,** 643 (2006).
[3] I.N. Kurkin, K.P. Chernov, *Physica B & C* **101B+C,** 233 (1980).
[4] D.W. Cooke, M.W. Blair, J.F. Smith, B.L. Bennett, L.G. Jacobsohn, E.A. McKigney, and R.E. Muenchausen, *ITNS* **55,** 1118 (2008).
[5] A. Cabral-Prieto, H. Jiménez-Domínguez, L. González-Tovany, S. Galindo, H. Flores-Llamas, and M. Torres-Valderrama, *JMagR* **89,** 568 (1990).
[6] A. Abragam, B. Bleaney, *Electron Paramagnetic Resonance of Transition Ions*. Oxford University Press, London (1970).

Phononics 2011: First International Conference on Phononic Crystals, Metamaterials and Optomechanics

Santa Fe, New Mexico, USA, May 29-June 2, 2011

PHONONICS-2011-0156

Understanding and Controlling High-Frequency Phonon Thermal Energy Transport in Nanostructures

M. Maldovan[1]

[1] *Department of Materials Science and Engineering, Massachusetts Institute of Technology, 77 Massachusetts Av., Cambridge, MA 02139USA*
maldovan@mit.edu

Abstract: We present a novel theoretical approach based on the kinetic theory of transport processes to understand and accurately describe the transport of high-frequency phonon thermal energy in nanostructures over a broad range of temperatures and across multiple length scales, i.e. from nano to micro. Good agreement with experiments is obtained.

Modern experimental technologies enable the fabrication of complex nanostructures such as nanofilms, multilayers, superlattices, nanowires and nanotubes, nanoparticle composites, quantum dots, micro and nanoelectronic devices and MEMS. In many of the applications for which these nanomaterials are designed, the control of phonon heat transport is critical for the resultant energy efficiency of the device.[1-8] For example, materials with high thermal conductivities are necessary to rapidly dissipate heat in increasingly dense electronic devices such as computer microprocessors or semiconductor lasers. On the other hand, materials with low thermal conductivities are needed to increase the efficiency of energy conversion materials such as thermoelectrics (which can convert waste heat into electricity) or to create highly efficient thermal insulators (which can increase building energy efficiency for heating and cooling). The understanding and controlling of high-frequency phonon energy transport in nanostructured materials is thus crucial for the development of the new generation of energy efficient nanoscale devices in science and technology.

Thermal transport in solids is not necessarily a fixed material property but it can be controlled by modifying the thermal properties of phonons through different methods (e.g. impurities, lattice defects, geometry, etc.). Although the physical mechanisms governing the thermal conductivity of solids have been understood for years, a comprehensive theoretical method to accurately calculate the transfer of thermal energy, particularly at small scales, has not been available. This is due to the physical and mathematical complexity of three-phonon anharmonic processes and the effects of phonon scattering at the boundaries. At normal temperatures, phonon mean free paths are much smaller than the dimensions of macroscopic materials and the thermal conductivity is independent of material size and shape. As the material size is decreased, however, the thermal conductivity is reduced below that of the bulk material. This effect is mainly assigned to the shortening of the phonon mean free paths by collisions with the boundaries. One of the main difficulties of current theoretical models is to accurately calculate and predict this surface related reduction of the phonon mean free paths.

In this talk, we present a novel theoretical approach to understand and accurately describe the transport of phonon thermal energy in nanostructures over a broad range of temperatures and across multiple length scales, i.e. from nano to micro. The theoretical model is based on the kinetic theory of transport processes and includes the directional and spatial dependence for the reduction of the phonon mean free paths due to surface scattering. The model also considers general expressions for *all* physical variables involved in the transport of thermal energy such as dispersion relations $\omega_j(\mathbf{k})$, bulk phonon mean free paths $\ell_0(\mathbf{k})$, and surface specularity parameters $p(\mathbf{k})$. The thermal conductivity is calculated by using the formula

$$\kappa = \frac{1}{(2\pi)^3}\sum_j \int k_B(\hbar\omega_j/k_BT)^2 \frac{\exp(\hbar\omega_j/k_BT)}{[\exp(\hbar\omega_j/k_BT)-1]^2}\ \nu_j(\mathbf{k})\cos\theta\ \ell_j(\mathbf{k})\cos\theta\ d\mathbf{k} \qquad (1)$$

Phononics 2011: First International Conference on Phononic Crystals, Metamaterials and Optomechanics

Santa Fe, New Mexico, USA, May 29-June 2, 2011

PHONONICS-2011-0156

where $\hbar$ and k_B are the Planck and Boltzmann constants respectively, T is the temperature, $\omega_j = \omega_j(\mathbf{k})$ is the phonon frequency, $v_j(\mathbf{k}) = \nabla_{\mathbf{k}} \omega_j(\mathbf{k})$ is the group velocity, j refers to the different polarizations, and θ is the angle between the wavevector $\mathbf{k}$ and the thermal gradient ∇T.

We successfully applied the proposed theoretical model describing nanoscale heat transport to calculate the thermal conductivity of nanostructures (e.g. thin films, layered materials, nanowires, etc.). We obtained good agreement between our theoretical calculations and experimental measurements across different nanostructures, length scales, and temperatures. The final goal of this project is to be able to design, develop, and fabricate novel materials with specific (low or high) thermal conductivities and to create energy efficient microelectronic and optoelectronic devices and to increase the efficiency of many energy saving devices such as thermoelectrics and thermal insulators.

References

[1] D. G. Cahill *et al.* J. Appl. Phys. **93**, 793 (2003).
[2] A. I. Hochbaum *et al*., Nature **451**, 163 (2008).
[3] A. Boukai *et al*., Nature **451**, 168 (2008).
[4] R.M. Costescu *et al*., Science **303**, 989 (2004).
[5] C. Chiritescu *et al.*, Science **315**, 351 (2007).
[6] K. F. Hsu, *et al*., Science **303**, 818 (2004).
[7] B. Poudel, *et al*. Science **320**, 634 (2008).
[8] R. Venkatasubranian, E. Siivola, T. Colpitts, and B. O'Quinn. *Nature,* **413**, 597 (2001).

Phononics 2011: First International Conference on Phononic Crystals, Metamaterials and Optomechanics
Santa Fe, New Mexico, USA, May 29-June 2, 2011
PHONONICS-2011-0158

Nanophononics using Acoustic and Optical Cavities

N. D. Lanzillotti-Kimura[1,2], A. Fainstein[1], B. Jusserand[3], B. Perrin[3], A. Lemaitre[4], D. G. Schlom[5], A. Soukiassian[5]

[1] Centro Atómico Bariloche & Instituto Balseiro, C.N.E.A., R8402 AGP S. C. De Bariloche, Río Negro, Argentina
kimura@cab.cnea.gov.ar, afains@cab.cnea.gov.ar
[2] University of California – Berkeley, CA 94720, USA
[3] Institut des NanoSciences de Paris, CNRS – Université Pierre et Marie Curie, 75004 Paris, France
bernard.jusserand@insp.jussieu.fr, bernard.perrin@insp.jussieu.fr
[4] Laboratoire de Photonique et des Nanostructures, C.N.R.S., Route de Nozay, 91460 Marcoussis, France aristide.lemaitre@lpn.cnrs.fr
[5]Department of Materials Science and Engineering, Cornell University, Ithaca, New York, 14853-1501, USA
ds636@cornell.edu, soukiassian@gmail.com

Abstract: We report pump-probe time experiments in acoustic and optical cavities. We demonstrate that the generated coherent acoustic phonon spectra can be inhibited or enhanced in the cavity. Simulations highlight the role of the phonon density of states in the coherent phonon generation, extending concepts at the base of the Purcell effect to the field of phononics.

Changing the spontaneous light emission rate and spectra of atoms or excitons through the modification of the photon density of states has been the subject of significant efforts following Purcell's proposal and demonstration in the microwave domain.[1] This has been accomplished either by changing the dielectric boundaries close to the emitting species, or more fundamentally by embedding the emitter in an optical microcavity.[2] Depending on the tuning of the emitter spectra with maxima or minima of the modified photonic density of states, the emission can be either enhanced or inhibited. Similar ideas have been applied to modify other light-matter interactions processes. The search for large Purcell effects is at the heart of the quest for thresholdless lasing. In the field of phononics, and specifically the search of phonon lasing for efficient monochromatic THz sources, and for the control of heat at the nanoscale, these ideas have not been pursued to date. Here we demonstrate that the coherent acoustic phonon emission spectra of an impulsively excited thin metallic film can be either inhibited or enhanced by embedding the metal layer in an acoustic nanocavity.[3-6] This has been accomplished by using for the first time a hybrid metal cavity with $BaTiO_3/SrTiO_3$ epitaxial oxide phonon mirrors.

Acoustic nanocavities are the hypersound analog of the extensively studied optical microcavities.[3-6] We use a femtosecond laser light impulsion to generate a pulse of coherent sub-THz phonons in a metallic layer, and then we study how the latter is modified by changing the structure around the metal film. We compared two samples, in the first one we deposited the Ni film directly on a $SrTiO_3$ substrate, while in the second one the film is embedded in an acoustic nanocavity. In the latter, we chose as bottom broadband acoustic mirror $BaTiO_3/SrTiO_3$ superlattice (SL) grown by molecular beam epitaxy on a $SrTiO_3$ substrate. $BaTiO_3$ and $SrTiO_3$ have optical energy gaps in the 350 nm range and are consequently completely transparent at the laser energy of 750 nm. In this way, the acoustic mirrors only affect the acoustic boundary conditions of the metallic film, and thus its local acoustic density of states. The sample-air interface responds to a free surface boundary condition. This surface performs as the top mirror to complete the phonon cavity. Both the coherent phonon generation and detection are performed only at the metallic films. In the case of the acoustic nanocavity the measured spectrum presents an enhanced peak at the confined mode energy, while in the case of the naked Ni film the spectrum is broad and featureless. Moreover, we observed the inhibition of the coherent phonon emission in the region of the acoustic stop-band. In other words, within the phononic stop-band modes are expelled and they concentrate at the cavity resonance and at the stop-band edges. It is this modification of the mode density landscape that determines at which energies acoustic phonons can be emitted by the metallic layer (enhancement at the cavity mode), and at which they cannot (inhibition within the phonon gap). In addition, outside the phononic stop-band oscillations develop in the generated spectrum which, when compared with the bare Ni-film, also express weaker but clear inhibition and enhancement regions. The experiments are compared with calculations of the impulsive

Phononics 2011: First International Conference on Phononic Crystals, Metamaterials and Optomechanics
Santa Fe, New Mexico, USA, May 29-June 2, 2011
PHONONICS-2011-0158

generation and detection of coherent phonons that highlight the role of the phonon density of states on the acoustic emission rate, extending the concept of the optical Purcell effect to the field of phononics.

In addition, we report experiments performed on structures based in semiconductor optical microcavities, where acoustic phonons and photons can be confined simultaneously. Thus, both the optical and acoustic densities of states result modified.[7-8] An optical microcavity confines the electromagnetic field both spectrally and spatially, inducing strong changes in the light-matter interaction and giving rise to novel physical phenomena and devices. In the case of planar semiconductor optical microcavities, two distributed Bragg reflectors (DBRs) enclose an optical spacer. The confinement characteristics and the amplification of the electric field are determined by the selection of materials, thickness, and number of periods that constitute each DBR and the optical spacer. Optical microcavities have been the subject of very active research during the last 15 years, and have been used to study the modification of the photonic lifetimes, parametric oscillations, cavity polariton Bose-Einstein condensates, the polariton laser, and amplification of Raman scattering signals, among others.[9-11]

Particularly, the photonic confinement and amplification have been used in these high-Q resonators to amplify the optical generation of incoherent phonons through Raman processes and to evidence new effects in the phonon physics and dynamics in semiconductor nanostructures. This scheme was used to study confined phonons in acoustic nanocavities. The optical resonances can be complemented with electronic resonances giving rise to amplified Raman cross-sections of up to 10^7. On the contrary, the use of optical confinement for the enhanced coherent generation of acoustic phonons (in contrast with incoherent generation by spontaneous Raman scattering) is a concept that has been little treated up to now. The realization of a monochromatic, coherent, and intense source of ultrahigh frequency acoustic phonons based on semiconductor optical microcavities and the obtained coherent phonon enhancements will be also discussed.

References

[1] E. Purcell, in Proceedings of the American Physical Society, 1946 [Phys. Rev. **69**, 681 (1946)].
[2] E. Yablonovitch, Phys. Rev. Lett. **58**, 2059 (1987).
[3] M. Trigo, A. Fainstein, B. Jusserand, and V. Thierry-Mieg, *Phys. Rev. Lett.* **89**, 227402 (2002).
[4] A. Huynh, N. D. Lanzillotti-Kimura, B. Jusserand, B. Perrin, A. Fainstein, M. F. Pascual-Winter, E. Peronne, and A. Lemaître, Phys. Rev. Lett. **97**, 115502 (2006)
[5] N. D. Lanzillotti-Kimura, A. Fainstein, A. Huynh, B. Perrin, B. Jusserand, A. Miard, and A. Lemaître, *Phys. Rev. Lett.* **99**, 217405 (2007).
[6] A. Huynh, B. Perrin, N. D. Lanzillotti-Kimura, B. Jusserand, A. Fainstein, and A. Lemaître, Phys. Rev. B **78**, 233302 (2008)
[7] N. D. Lanzillotti-Kimura, A. Fainstein, B. Jusserand, and A. Lemaître, Phys. Rev. B **79**, 035404 (2009)
[8] N. D. Lanzillotti-Kimura, A. Fainstein, B. Perrin, B. Jusserand, A. Soukiassian, X. X. Xi, and D. G. Schlom, *Phys. Rev. Lett.* **104**, 187402 (2010).
[9] D. Sanvitto, F. M. Marchetti, M. H. Szymanska, G. Tosi, M. Baudisch, F. P. Laussy, D. N. Krizhanovskii, M. S. Skolnick, L. Marrucci, A. Lemaître, J. Bloch, C. Tejedor, and L. Vina, Nature Physics **6**, 527 (2010)
[10] E. Wertz, L. Ferrier, D. D. Solnyshkov, R. Johne, D. Sanvitto, A. Lemaître, I. Sagnes, R. Grousson, A. V. Kavokin, P. Senellart, G. Malpuech and J. Bloch, Nature Physics **6**, 860 (2010)
[11] A. Fainstein and B. Jusserand, Light scattering in Solids IX: Novel Materials and Techniques 108, 17, (Springer, Heidelberg, (2007)

Phononics 2011: First International Conference on Phononic Crystals, Metamaterials and Optomechanics
Santa Fe, New Mexico, USA, May 29-June 2, 2011
PHONONICS-2011-0174

Reduction of Thermal Conductivity in Silicon Slabs by Unit Cell Nanostructuring

Bruce L. Davis, Mahmoud I. Hussein

Department of Aerospace Engineering Sciences, University of Colorado at Boulder, Boulder, CO 80309, USA
bruce.davis@colorado.edu, mih@colorado.edu

Abstract: The emerging field of *phononics* is enabling a cross-flow of ideas pertaining to wave propagation in periodic media to be transferred from one scale to another. Just like unit cell structuring has seen much interest in phononic crystals for the control of sound and vibration, the same can be done at the nanoscale for the control of thermal properties. Here we present ideas for *unit cell nanostructuring* within thin silicon slabs for the purpose of reducing the thermal conductivity. To assess our models we use a Callaway-Holland-type scheme for the thermal conductivity prediction, and employ full-fledged lattice dynamics calculations to accurately capture the dispersion of the nanostructured silicon slabs.

The phonon band structure of a crystalline solid has a direct influence on its thermal conductivity, especially at conditions where coherent transport is dominant. Key features of the band structure are frequency band gaps and the values of the group velocity at each dispersion branch. Beyond linear dispersion, other important quantities are the nature of the different types of nonlinear wave interactions (expressed in terms of scattering/relaxation times), the heat capacity, the presence of defects, and the ambient temperature. A strong understanding of the effects of these parameters will enable a new material design paradigm towards potentially dramatic reductions in the thermal conductivity. Many applications stand to benefit from such an advance, chief among them is the development of thermoelectric energy conversion materials with very high values of the figure-of-merit (a metric for quantifying the performance of the energy conversion).

The concept of phonon engineering of nanoscale structures has been a topic of intense research in recent years, e.g., Ref. 1. Among the various phonon engineering strategies considered is the idea of utilizing phononic crystals at the nanoscale to provide a means for a controlled influence on the phonon transport properties, e.g., Refs. 2-8. Among the configurations considered is the insertion of periodic holes in silicon slabs[6,7]. By selecting appropriately large dimensions for the lattice spacing and the holes diameter, phonons will destructively interfere and will nonlinearly scatter while minimal electron scattering will be incurred. In this manner the thermal conductivity can be reduced without altering the electronic properties (a favorable outcome for thermoelectric materials). A recent study based on a continuum model for the phononic crystal band structure has demonstrated this advantage[7]. A continuum model however over-simplifies the phonon band structure and does not capture the subtle characteristics of the higher-order optical modes. In this paper we carry out full-fledged lattice dynamics calculations on the silicon slab supercells with and without holes, and proceed to investigate the effects of the periodic holes on the thermal conductivity.

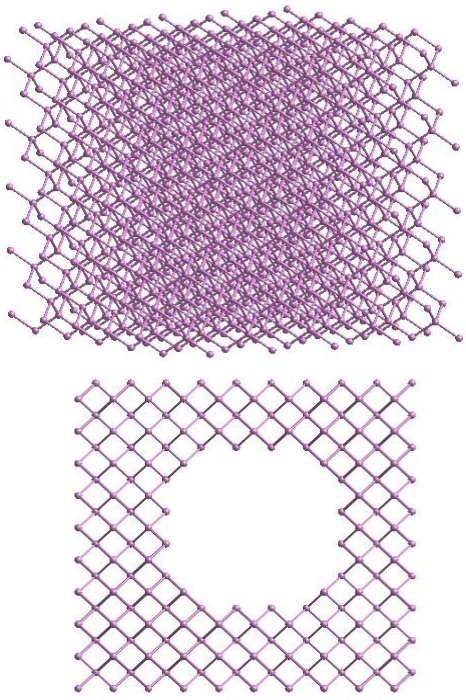

Figure 1: 5x5x5 Silicon slab (top) containing 1000 atoms. Silicon slab with periodic holes (bottom).

We consider silicon slabs formed by extending the diamond cubic 8-atom unit cell along the Cartesian directions. For the interatomic potential we utilize the Tersoff potential with second nearest neighbor interactions considered. The slab size analyzed is a 5x5x5 supercell measuring 2.7 nm along each Cartesian direction and contains 1000 atoms.

Phononics 2011: First International Conference on Phononic Crystals, Metamaterials and Optomechanics
Santa Fe, New Mexico, USA, May 29-June 2, 2011
PHONONICS-2011-0174

The hole diameter is set to be 0.6 of the lattice constant (Fig. 1). Given that the lattice dynamics formulation models the motion of each individual atom, limited computational resources prevent us from considering larger dimensions; however, this initial study provides a proof-of-concept. Prior to computing the band structure, surface relaxation along the top and bottom boundaries of the slab and around the holes is implemented. Fig. 2 (left) shows the band structure of this relaxed slab configuration compared to that of a bulk silicon supercell of the same size. Clearly, the acoustic branches exhibit slab-like properties with a reduced group velocity at low wave numbers. Upon introducing the periodic holes (Fig. 2, right), a flattening of the branches is observed within both the acoustical and optical modes in addition to a general reduction in frequencies. These band structure alterations have a significant effect on the thermal conductivity; using a Callaway-Holland-type scheme for thermal conductivity prediction, a minimum of 5% reduction is noted for the slab with periodic holes compared to the slab without the holes. This calculation was conducted for room temperature and only considered Umklapp scattering. We have neglected boundary scattering which is a conservative approximation because our interest is thermal conductivity reduction. Upon further refinement of our modeling parameters a higher reduction in thermal conductivity is expected as reported in Refs. 6,7. In future studies, we will consider nanostructuring the configuration of the supercell (see Ref. 4 for one-dimensional nanoscale phononic crystals) in order to obtain more profound changes to the band structure and consequently stronger reductions in the thermal conductivity.

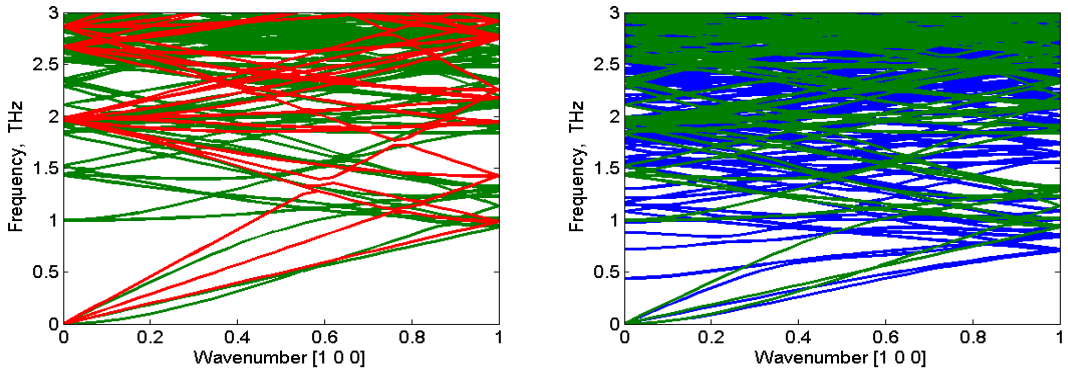

Figure 2: Silicon slab based on a 5x5x5 supercell (1000 atoms) with surface relaxation (green) compared with 5x5x5 bulk silicon (red) and a 5x5x5 slab with periodic holes (blue).

References

[1] A. A. Balandin, *J. Nanosci. Nanotechnol.* **5**, 1015 (2005).
[2] T. Gorishnyy, C. K. Ullal, M. Maldovan, G. Fytas, E. L. Thomas, *Physical Review Letters*, **94**, 115501 (2005).
[3] A. J. H. McGaughey, M. I. Hussein, E. S. Landry, M. Kaviany and G. M. Hulbert, *Physical Review B*, **74**, 104304 (2006).
[4] E. S. Landry, M. I. Hussein and A. J. H. McGaughey, *Physical Review B*, **77**, 184302 (2008).
[5] J.-N. Gillet, Y. Chalopin, and S. Volz, *Journal of Heat Transfer*, **131**, 043206 (2009).
[6] J. K. Yu, S. Mitrovic, D. Tham, J. Varghese and J. R. Heath, *Nature Nanotechnology*, **5**, pp. 718-721 (2010)
[7] P. E. Hopkins, C. M. Reinke, F. S. Mehmet, R. H. Olsson, E. A. Shaner, Z. C. Leseman, J. R. Serrano, L. M. Phinney, I. El-Kady, *Nano Letters* **11**, pp. 107–112 (2011).
[8] J. F. Robillard, K. Muralidharan, J. Bucay, P. A. Deymier, W. Beck and D. Barker, *Chinese Journal of Physics*, 49, pp. 448-461 (2011).
[9] J. Callaway, *Physical Review*, **113**,1046-1051 (1959).

Phononics 2011: First International Conference on Phononic Crystals, Metamaterials and Optomechanics
Santa Fe, New Mexico, USA, May 29-June 2, 2011
PHONONICS-2011-0176

Convergence of the Reduced Bloch Mode Expansion Method for Electronic Band Structure Calculations

Qiong. Guo, Osama. R. Bilal, Mahmoud. I. Hussein

Department of Aerospace Engineering Sciences, University of Colorado at Boulder, Boulder, USA
Qiong.Guo@colorado.edu, Osama.Bilal@colorado.edu, mih@colorado.edu

Abstract: Reduced Bloch mode expansion is a Bloch modal analysis method that enables exceptionally fast, yet accurate, periodic media band structure calculations. In this paper, the method is tested on electronic band structure calculations for a high-symmetry cubic model and a low-symmetry triclinic model, both based on the Kronig-Penney fixed potential. For both cases, the energy (eigenvalues) and wave functions (eigenvectors) demonstrate very good convergence performance.

Band structure calculations provide a basis for the study of thermal, optical and magnetic properties of crystals. Numerous techniques are available for band structure calculations. All techniques however suffer from the common problem that the computational load for solving the underlying complex eigenvalue problem over many **k**-points in the Brillouin zone is prohibitive. To expedite this process, there are several methods that aim to approximate the band structure between **k**-points[1]. We recently proposed a new method that enables such an approximation at an extremely low cost with negligible loss in accuracy. This method is referred to as the Reduced Bloch Mode Expansion (RBME) method[2]; it applies to both classical and *ab initio* band structure calculations of periodic media. Furthermore, the method is applicable to any type of wave propagation problem: phononic, photonic, electronic etc.

The RBME employs a natural basis composed of a selected reduced set of Bloch eigenfunctions. The displacement Bloch function $\tilde{u}$ is expressed as a superposition of an extremely small truncated set of m Bloch mode eigenfunctions $\tilde{v}$, thus enabling a linear transformation from the full-size problem to a set of reduced modal coordinates,

$$\tilde{u}(x) \cong \sum_{j=1}^{m} \beta_j \tilde{v}_j(x), \qquad m \in \text{integer}. \tag{1}$$

As RBME is practically a secondary expansion, we can use any of the common expansion methods to undergo a primary expansion of the periodic unit cell and solution field. In our work we use the finite element (FE) method. After discretization and application of Bloch theory to the governing equation of motion for the wave propagation problem we are considering, an eigenvalue problem emerges:

$$(A(k) - \lambda I)\tilde{U} = 0. \tag{2}$$

Solution of Eq. (2) at selected **k**-points provides the eigenvectors from which a reduced *Bloch modal matrix*, Ψ, is formed. This matrix is then used to linearly transform the problem:

$$\tilde{U}_{(n\times 1)} = \Psi_{(n\times m)} \tilde{V}_{(m\times 1)}, \quad m << n \tag{3}$$

Substituting Eq. (3) into Eq. (2), and pre-multiplying by the complex conjugate of Ψ yields a reduced eigenvalue problem of size $m \times m$:

$$(\overline{A}(\mathbf{k}) - \lambda I)\tilde{V} = 0, \quad \overline{A}(\mathbf{k}) = \Psi^* A(\mathbf{k}) \Psi. \tag{4}$$

Only if the reduced basis is suitably chosen can the proposed RBME approach produce accurate results. First, an appropriate choice of eigenfunctions in certain reference points in the **k**-space needs to be made. A "2-point expansion scheme" involves choosing eigenfunctions corresponding to the high symmetry points determined by the medium's crystal structure and group theory along the border of the IBZ. By augmenting with additional intermediate **k**-points centerally intersecting the straight lines joining the points chosen in the 2-point expansion scheme, a higher order expansion scheme is realized (Figure 1). Second, in order for the band structure calculations to be accurate up to the frequency (energy) range of interest, the number of eigenfunctions retained at each of the **k**-points selected should be slightly higher than the number of dispersion branches that are to be computed. Further resourceful utilization of the Bloch eigenfunctions is made by only using those eigenfunctions that correspond to a selection of **k**-points belonging to the current IBZ circuit line that is being evaluated; in this case the line is divided into "windows" for which only two sets of eigenfunctions are employed.

Phononics 2011: First International Conference on Phononic Crystals, Metamaterials and Optomechanics
Santa Fe, New Mexico, USA, May 29-June 2, 2011
PHONONICS-2011-0176

In this work we apply the RBME method to electronic band structure calculations for both cubic and triclinic lattices. Starting from the time-independent single electron Schrödinger equation, the three-dimensional generalized Kronig-Penney model is chosen for the electronic potential[3].

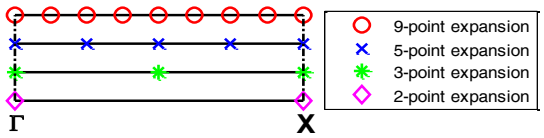

Figure 1 Illustration of four k-point selection schemes.

$$V(x)=\sum_{i=1}^{3}\bar{V}(x_i)\text{, where }\bar{V}(x_i)=\begin{cases}0, 0\le x_i<2a.u.,\\ 6.5Ry, 2a.u.\le x_i<3a.u.\end{cases} \quad (5)$$

The unit cell is discretized into 9×9×9 uniformly sized 8-node trilinear hexahedral finite elements, i.e. n_{el} =729. The **k**-space is discretized such that a total of 65 **k**-points are evaluated to generate the band structure. Figure 2 shows the electronic band structure containing the first 8 branches following the **k**-space paths $\Gamma\rightarrow$X$\rightarrow$M$\rightarrow$R$\rightarrow\Gamma$ for the cubic case (Figure 2.1), and B$\rightarrow\Gamma\rightarrow$F$\rightarrow\Gamma\rightarrow$G for the triclinic case[4] (Figure 2.4). The RBME results (based here on a 3-point expansion and use of eight Bloch modes for every selected **k**-point) provide an excellent approximation to the results of the full model, noting the reduction in the size of the matrix problem is from 729×729 to 24×24. The absolute error of eigenvalues $e_{eval}=E_{Full}-E_{RBME}$ for the cubic and triclinic cases (Figure 2.2 and 2.5) for the first three branches converges rapidly with the number of expansion points $n_{\exp}$. The rapid convergence of the maximum L^2 norm of the absolute error of eigenvectors for first 10 branches $e_{vect}=\sum_{i=1}^{10}\left|\tilde{U}_{Full,i}\right|^2-\sum_{i=1}^{10}\left|\tilde{U}_{RBME,i}\right|^2$ has also been computed (Figures 2.3 and 2.6); the order of maximum error is 1x10^{-3}.

$$V(x)=\sum_{i=1}^{3}\bar{V}(x_i)\text{,}\quad\text{where }\bar{V}(x_i)=\begin{cases}0, 0\le x_i<2a.u.,\\ 6.5Ry, 2a.u.\le x_i<3a.u.\end{cases} \quad (5)$$

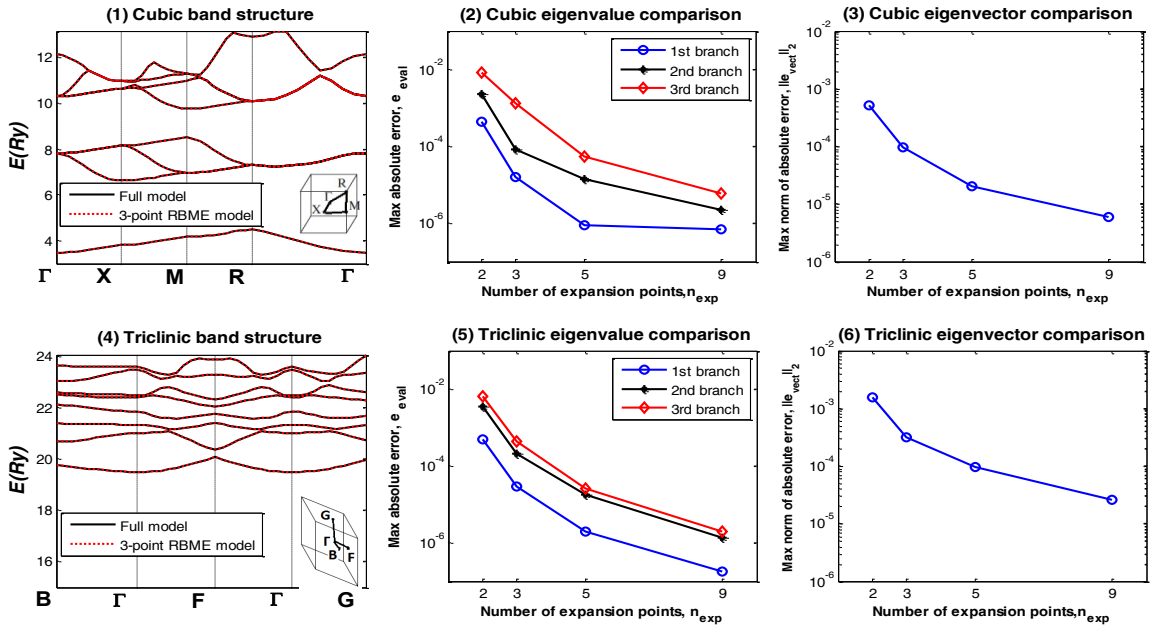

Figure 2 Performance of the RBME method in electronic band structure calculations. Band structure for the cubic (1) and triclinic (4) cases. Error of eigenvalues and eigenvectors for the cubic (2,3) and triclinic (5,6) cases.

References

[1] H. J. Monkhorst and J. D. Pack, *Phys. Rev. B* **13**, 5188-5192 (1976)
[2] M. I. Hussein, *Proc. R. Soc. A.* **465**, 2825-2848 (2009)
[3] J. E. Pask, B. M. Klein, P.A. Sterne, and C.Y. Fong, *Comp. Phys. Commun.* **135**, 1-34 (2001)
[4] T. Hahn, *International Tables for Crystallography*, *Vol. A*: Space Group Symmetry, Holland (1983)

Phononics 2011: First International Conference on Phononic Crystals, Metamaterials and Optomechanics
Santa Fe, New Mexico, USA, May 29-June 2, 2011
PHONONICS-2011-0183

Thermal Conductivity Reduction in Phononic Crystals: Interplay of Coherent versus Incoherent Scattering

Thomas E. Beechem[1], Patrick E. Hopkins[1], Charles M. Reinke[1], Mehmet F. Su[2], Bongsang Kim[1], Charles. T. Harris[1], Drew Goettler[2], Maryam Ziaei-Moayyed[1], Eric A. Shaner[1], Zayd C. Leseman[2], R. H. Olsson III[1], Alan McGaughey[3], I. El-Kady[1,2]

[1]Sandia National Laboratories, Albuquerque, NM, USA,
tebeech@sandia.gov, pehopki@sandia.gov, cmreink@sandia.gov, bonkim@sandia.gov, ctharri@sandia.gov, mziaeim@sandia.gov, eashane@sandia.gov, rholsso@sandia.gov, ielkady@sandia.gov
[2]University of New Mexico, Albuquerque, NM, USA
mfatihsu@.unm.edu, goettled@unm.edu, zleseman@unm.edu
[3]Carnegie Mellon University, Pittsburgh, PA, USA
mcgaughey@cmu.edu

Abstract: In this talk we pose the question: Can the coherent scattering events brought by the periodicity of the Phononic Crystal (PnC) lattice affect the high frequency THz phonons that dominate heat transfer process? In other words, can PnC patterning be used to manipulate the thermal conductivity of a material? We report both theoretically and experimentally on the role of coherent versus incoherent scattering of phonons by a 2D PnC structure and the efficacy of each process in both the cross-plane and in-plane directions of the PnC lattice.

Phonons propagating in a Phononic Crystal (PnC) lattice undergo two distinct types of scattering mechanisms: Coherent and incoherent scattering. Coherent scattering is brought about by Bragg scattering events which result primarily in the creation of phononic gaps where the propagation of phonons are prohibited, anomalous and flat, dispersionless bands, and negative phonon group velocities. The combination of these phenomena results in a rich complicated band structure (dispersion) compared to that of the bulk solid in absence of PnC structuring, accompanied by a redistribution of the phononic density of states (DOS). Incoherent boundary scattering, on the other hand, arises as a consequence of scattering due to the mechanical impedance mismatch between the host background matrix and the scattering centers, though the interference is not coherent. While coherent scattering phenomena have been readily validated to affect the low frequency (RF) phonons, in this communication we question the possibility of extending these effects to the high frequency THz phonons that dominate heat transfer process.

To answer this question we start by calculating the dispersion of a square PnC lattice of air holes in a Si matrix using the plane wave expansion technique. Here we draw on the fact that the longitudinal acoustic mode in silicon is linear up to ~10THz, while the transverse modes are linear up to ~3THz, thus allowing us to assume a homogenous "Ether" of Si where the average elastic properties are assumed up to 3THz. To predict the amount of thermal conductivity we expect resulting from phonon scattering by the Si/Air-PnC, we take a Callaway-Holland-type model[1]:

$$\kappa = \frac{1}{6\pi^2}\sum_j \int_q \frac{\hbar^2 \omega_j^2(q)}{k_B T^2} \frac{\exp\left[\frac{\hbar\omega_j(q)}{k_B T}\right]}{\left(\exp\left[\frac{\hbar\omega_j(q)}{k_B T}\right]-1\right)^2} v_j^2(q)\tau_j(q)q^2 dq \qquad (1)$$

where $\hbar$ is Planck's constant, $\omega(q)$ is the phonon dispersion, k_B is the Boltzmann constant, T is the phonon temperature, $v(q)=\partial\omega(q)/\partial q$ is the phonon group velocity, $\tau(q)$ is the scattering time of the phonons, q is the wavevector, and the thermal conductivity, κ is summed over all modes.

On the other hand, to investigate the effect of pure incoherent scattering by the PnC pores, lattice dynamics based calculations were performed using the Stillinger-Weber (SW) interatomic potential. Here our approach consists of combining bulk phonon properties with a boundary scattering model to predict the thermal conductivity of a nanostructure. Harmonic and anharmonic lattice dynamics calcu-

Phononics 2011: First International Conference on Phononic Crystals, Metamaterials and Optomechanics
Santa Fe, New Mexico, USA, May 29-June 2, 2011
PHONONICS-2011-0183

lations were performed to obtain the group velocity vectors ($\boldsymbol{v}_g$), and mean free paths (Λ_{bulk}) for 27,786 phonon modes (denoted by subscript i) uniformly distributed through the first Brillouin zone of bulk SW silicon. A geometric model of the PnC unit cell was created and a random point (denoted by subscript j) was randomly chosen within it. From this point, a line in the direction of the group velocity vector (the direction of energy transport) for each phonon mode is extended. The distance, d_{ij}, to the first intersection with a solid surface (the top or bottom of the film or the side of a hole) is calculated based purely on the geometry. This distance is combined with the bulk mean free path of that mode using the Matthiessen rule to obtain an effective mean free path for each mode from that starting point: $\frac{1}{\Lambda_{ij}} = \frac{1}{\Lambda_{i,bulk}} + \frac{1}{d_{ij}}$ The values of Λ_{ij} for each phonon mode are then averaged over 10,000 random points in the unit cell to give the effective mean free path of each phonon mode, Λ_i. Using the effecting mean free paths, the cross-plane thermal conductivities of the solid material in the PnC are calculated from a summation over all phonon modes as

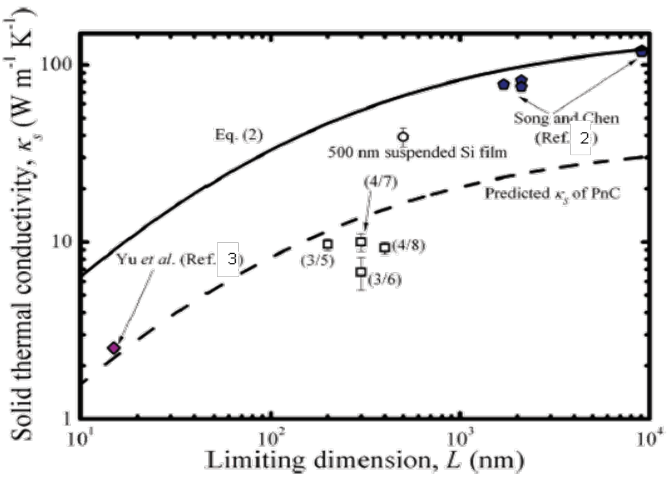

Figure 1.The measured thermal conductivity of Si structures at room temperature as a function of the minimum feature size L for the PnCs (unfilled squares)[1], microporous solids (filled pentagons),[2] nanomesh (filled diamond),[3] and a suspended 500 nm thick Si film – that is, an unpatterned Si slab (unfilled circle). The dashed line is the predictions of Eq. (1) using the PnC dispersion while the solid line corresponds to the predictions of Eq. (2) assuming only incoherent scattering.

$$\kappa_{PnC-Inconerent} = \sum_i c_{v,i} v^2{}_{g,i} \frac{\Lambda_i}{|v_{g,i}|} \tag{2}$$

where $c_{v,i}$ is the volumetric specific heat and $v_{g,i,}$ is the component of the group velocity vector in the cross-plane direction. To convert these solid thermal conductivities to values that can be compared to the experimental measurements, the porosity of the PnC is then factored in by multiplying with the factor $[(1+2\phi/3)/(1-\phi)]$, where φ is the porosity of the lattice.

The results of Eq. 1 and 2 are shown in Figure 1 as a function of the minimum feature size and is compared to measured the thermal conductivity of Si PnC plates using the time-domain thermoreflectance technique (TDTR)[1]. The results show a massive thermal conductivity reduction from 148W/mK for bulk silicon to 6.1W/mK for the Si-PnC; approximately 96% reduction. They further show that incoherent scattering over predicts the thermal conductivity of the PnC-lattice by more than a factor of 2, leading us to suspect that coherent scattering brought through by the PnC dispersion may be playing a significant role in this reduction. Similar calculations and measurements were also carried out in the in-plane direction and a discrepancy between the thermal conductivity reduction purely based on incoherent scattering effects, while not as pronounced, was also seen to be evident. In this talk we present a possible explanation for the difference between the in-plane and cross-plane results, as well as a possible theorization of the role of optical phonons in this process.

References

[1] P. E. Hopkins, C. M. Reinke, M. F. Su, R. H. O. III, E. A. Shaner, Z. C. Leseman, J. R. Serrano, L. M. Phinney, and I. El-Kady, *Nanoletters* **11**, 107-112, (2011).
[2] A. I. Hochbaum, R. Chen, R. D. Delgado, L. Wenjie, E. C. Garnett, M. Najarian, A. Majumdar, and Y. Peidong, , *Nature* **451**, 163-167, (2008).
[3] L. M. Ivanova, P. A. Aleksandrov, and K. D. Demakov, *Inorganic Materials* **42**,1205-1209, (2006).

Phononics 2011: First International Conference on Phononic Crystals, Metamaterials and Optomechanics
Santa Fe, New Mexico, USA, May 29-June 2, 2011
PHONONICS-2011-0185

Isotopically Enriched Semiconductor Superlattices for Thermoelectric Applications

A. Vogelsang[1], S. M. Ullah[1], G. Bastian[1], A. Plech[2], N. Wehmeier[3], H. Bracht[3], P.C. Howell[4]

[1] *Faculty Technology and Bionics, Rhein-Waal University for Applied Sciences, 46446 Emmerich, Germany,* Georg.bastian@hochschule-rhein-waal.de

[2] *Institute for Synchrotron Radiation, Karlsruher Institute of Technology, D-76344 Eggenstein-Leopoldshafen, Germany*

[3] *Institut für Materialphysik, Westfälische Wilhelms-Universität Münster, D-48149 Münster, Germany*

[4] *Corporate Research and Technologies, Siemens AG, 81730 München*

Abstract: A new class of phononic metamaterials based on isotopically enriched semiconductor superlattices is presented, which allows tailoring of phononic properties while leaving the electronic properties unaltered. We discuss possible fields of application in thermoelectrics, based on different complementary experimental and theoretical results.

During the last years different techniques have been established to create materials with novel phononic properties. Patterning a material in the nanoscale in one or more dimensions by growth of superlattices or etching techniques are the most common approaches. These structures enable a manipulation of phononic states and a reduced thermal conductivity. However, electronic and photonic transport properties are also negatively affected with this approach. Thermoelectric materials are good examples in which the thermal (phononic) conductivity κ has to be minimized along with a maximized electronic conductivity σ. The figure of merit Z in thermoelectric materials is given by ratio of the conductivities and the Seebeck-coefficient S:

$$Z=\sigma S^2/\kappa \quad (1)$$

Superlattice structures can exhibit an increased ratio although both conductivities are lower than the bulk values[1]. To circumvent this constraint we have investigated isotopically enriched semiconductor superlattices. A single layer consisting of silicon-28 isotope offers an increased phononic mean free path[2]. The slope of the acoustic phonon dispersion relation, i.e. the sound velocity, scales with the square-root of the atom's mass. At an interface between two layers of different isotopes a mismatch of the sound velocities occurs resulting in a small probability of back-reflection, as shown in fig. 1. Multiple interfaces of a superlattice therefore work like a Bragg-grating with an accumulated strong back-reflection, i.e. phononic bandgap.

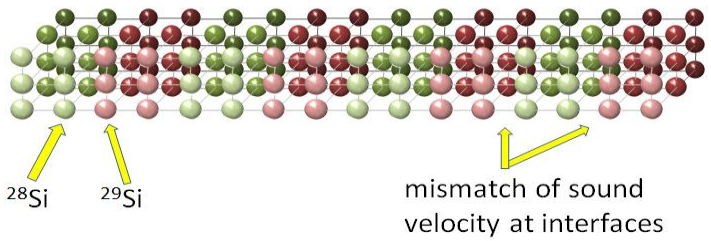

Figure 1 Alternating layers of isotopically enriched semiconductors (Si-28 and Si-29) form a heterostructure for the phonons and a homostructure for the electrons.

In order to verify the concept, different sets of isotopic superlattices made of silicon-28 and silicon-29 have been fabricated. Detailed information of the composition of each layer was gained by depth profiling, as shown in fig. 2. Various methods were applied to determine the thermal conductivity of the multilayer structures. This includes time-domain thermoreflectance, time-resolved X-ray scattering, laser-flash-method, comparative thermal conductivity measurements, and the 3ω–method. Limitations of the classical measurement techniques for thin-film anisotropic materials are discussed. The mea-

Phononics 2011: First International Conference on Phononic Crystals, Metamaterials and Optomechanics
Santa Fe, New Mexico, USA, May 29-June 2, 2011
PHONONICS-2011-0185

surements are compared with results from simulation, including a macroscopic FDTD approach, multiple-interface scattering approximation, and extensive molecular dynamics calculations.

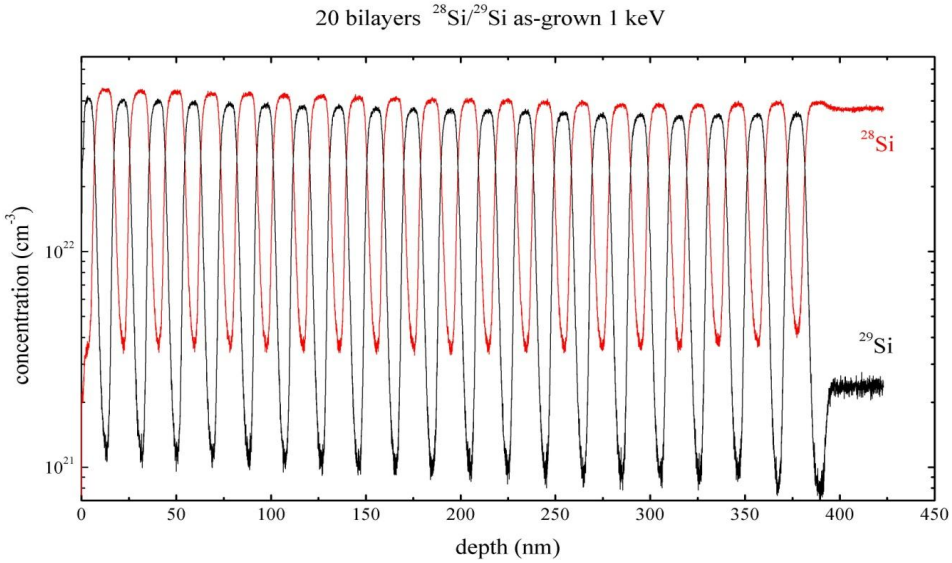

Figure 2 SIMS profiling with a high spatial resolution proves the isotopic composition of the structure: 20 bilayers with a total thickness of 380nm.

Within the uncertainties of the simulations and the uncertainties of the measurements the concept of isotopically enriched superlattices has been demonstrated: A reduction of the thermal conductivity of about 20% for 20 periods of superlattices has been shown. However, there is a limited knowledge about phononic states, anisotropy, coherence lengths, phonon-phonon-scattering and the impact of interface roughness. Therefore, further investigations are required to determine the whole potential of the concept.

References

[1] J. O. Sofo, and G. D. Mahan, *Appl. Phys. Lett.* **65**, 2690 (1994).
[2] T. Ruf, R.W. Henn, M. Asen-Palmer, E. Gmelin, M. Cardona, H.-J. Pohl, G.G. Devyatych, and P.G. Sennikov, Sol. Stat. Comm. **129**, 257 (2003)
[3] A. Plech, V. Kotaidis, S. Grésillon, C. Dahmen and G. von Plessen, Phys. Rev. B **70**, 195423 (2004)

1ST INTERNATIONAL CONFERENCE ON PHONONIC CRYSTALS, METAMATERIALS & OPTOMECHANICS

Extended Abstracts

Track 5: Optomechanics

Phononics 2011: First International Conference on Phononic Crystals, Metamaterials and Optomechanics
Santa Fe, New Mexico, USA, May 29-June 2, 2011
PHONONICS-2011-0086

Phoxonic Crystals: a Review

Sarah Benchabane[1], Said Sadat-Saleh[1], Maria-Pilar Bernal[1], Jean-Charles Beugnot[1], Vincent Laude[1], Yan Pennec[2], Bahram Djafari-Rouhani[2], Nikos Papanikolaou[3] and Alejandro Martinez[4]

[1] Institut FEMTO-ST, Université de Franche-Comté, CNRS, 32 avenue de l'Observatoire, F-25044 Besançon Cedex, France
sarah.benchabane@femto-st.fr
[2]Institut d'Électronique, de Microélectronique et de Nanotechnologie, Université de Lille 1, 59655 Villeneuve d'Ascq, France
[3]Institute of Microelectronics, NCSR, Athena, Greece
[4]Nanophotonics Technology Center, Universidad Politécnica de Valencia, Valencia, Spain

Abstract: Periodically structured materials exhibiting simultaneous photonic and phononic band gaps offer unprecedented ways to tailor photon–phonon interactions. A review of the works reported on these materials, sometimes termed "phoxonic crystals", is presented before highlighting theoretical and experimental results demonstrating phoxonic band gaps in structures relying on guided elastic waves.

The last two decades have witnessed a considerable breakthrough in the field of management of wave propagation through the fabrication and use of materials exhibiting periodical micro- or nano-structures. If it remains clear that photonic crystals have been at the forefront of this research effort, their elastic counterparts, phononic crystals, have also arisen significant interest. From an exploratory point of view, phononic crystals open the possibility to manage elastic waves but also high frequency phonon propagation and dispersion. The two types of structures rest upon the same underlying physical principle: taking advantage of the scattering phenomena occurring in a periodical composite material to give rise to frequency bands in which wave propagation is completely forbidden.

Still, photonic and phononic crystals have been studied in a quite independent fashion for the greatest part of their young existence. It is only a few years ago, with the pioneering experience of Trigo *et al*. in 2002[1], that the community started to realize that the strong velocity mismatch between electromagnetic and elastic waves actually implied that optical and elastic waves could exhibit the same wavelength and hence coexist in a same volume. Trigo and his co-workers reported on a one-dimensional doubly-resonant cavity ensuring the confinement of photons and Raman-generated high frequency phonons. The subsequent works of P. Santos' group in the Paul Drude Institut, Berlin, introduced still greater latitude in the management of the interaction by using surface acoustic waves to modulate the properties of light propagating in 1D semiconductor superlattices[2]. If these last two works obviously deserve to be mentioned, their limitations to 1D structures do not allow to make the most out of the photonic or phononic crystal concepts, as these latter do not offer the possibility to tune light or sound dispersion relations and hence, for instance, do not permit to toy with slow wave effects. P. Russell *et al*. proposed sensibly at the same period the idea to extend these highly confined acousto-optical interactions to a bi-dimensional configuration by showing experimentally that elastic waves could be confined in defect modes of a photonic fibre preform with a lattice parameter of some tens of microns[3]. Theoretical works by V. Laude *et al.* proposed an actual microstructured optical fiber geometry that would allow for simultaneous optical and elastic waveguiding[4]. None of these groups did however proceed at the time to any experimental demonstration of genuine elastic waveguiding in an on-scale "phoxonic" crystal fibre (the "x" referring indifferently to "t" or "n"), and hence did not report on the corresponding acousto-optical interactions, although control of guided acoustic waves or of acoustic resonances generated *via* nonlinear optical effects (e.g. Brillouin scattering or electrostriction) was reported[5,6,7]. It is only in 2006 that E. L. Thomas' group at the Massachusetts Institute of Technology theoretically designed a crystal blind to electromagnetic waves with wavelengths of several hundreds of nanometers and deaf to sound at similar wavelengths[8]. They also reported on the simultaneous localisation of photons and phonons in a cavity managed in the designed 2D phoXonic crystal without, however, considering interactions between sound and light. All these pioneering works now stand as amongst the starting points of a growing field dedicated to photon-

Phononics 2011: First International Conference on Phononic Crystals, Metamaterials and Optomechanics
Santa Fe, New Mexico, USA, May 29-June 2, 2011
PHONONICS-2011-0086

phonon interactions in periodically structured materials, that encompasses traditional photonic and phononic band gaps as well as the more recently introduced "opto-mechanical" structures[9].

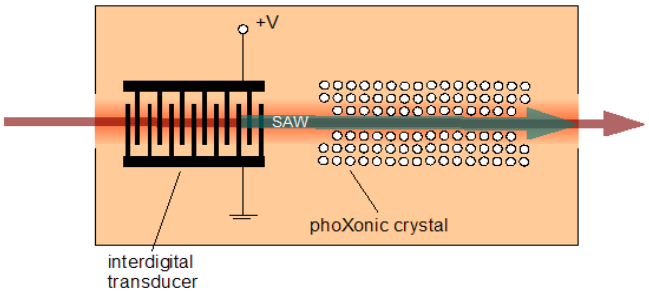

Figure 1 Schematic of a phoxonic waveguide, allowing for a joint confinement of sound and light. An integrated optics waveguide is used to channel the optical wave in the crystal while the elastic waves consists of surface-guided waves, generated by an interdigital transducer. The periodical structure should exhibit a simultaneous photonic and phononic band gap that would allow for a joint guidance of both types of waves, possibly involving slow-light and slow-sound effects.

This paper will mostly focus on phoxonic crystals: a significant series of works has indeed been dedicated to mostly theoretical, sometimes experimental, investigations of simultaneous photonic and phononic band gap materials and on the acousto-optical interaction phenomena likely to occur in such artificial media.

We will hence present a brief review of the relevant literature, including the works reported on planar structures but also on acousto-optical interactions in microstructured optical fibers. We will then more specifically highlight some results obtained in the case of potential phoxonic crystals involving guided optical and elastic waves in materials particularly relevant in integrated optics and acoustics, namely silicon[10,11,12] and lithium niobate[13]. In addition to band diagram calculations in the usual bi-dimensional case, we will present some theoretical and (possibly) experimental works showing that phoxonic band gaps can be observed in periodically structured materials in which elastic waveguiding is preliminary ensured by propagation in a slab or through the use of surface acoustic waves, in the case of a semi-infinite medium. Throwing evidence of a phoxonic band gap obviously goes through the experimental demonstration of phononic band gaps in the hypersonic frequency regime, which is an essential, but non trivial step towards a joint confinement of sound and light, and we will hence provide with additional details regarding the fabrication and characterization of phononic crystals exhibiting pitches at the micro-scale.

This work has been supported by the French National Agency (Agence Nationale de la Recherche – ANR) in the frame of the phoXcry project (n°ANR-09-NANO-004) and by the European Commission Seventh Framework Programme (FP7) under grant agreement n°233883 (TAILPHOX).

References

[1] M. Trigo, A. Bruchhausen, A. Fainstein, B. Jusserand, and V. Thierry-Mieg, *Phys. Rev. Lett*. **89**, p. 227402 (2002).
[2] M. M. de Lima, Jr., R. Hey, and P. V. Santos, *Appl. Phys. Lett.* **83**, 2997 (2003).
[3] P. S. J. Russell, E. Marin, A. Diez, S. Guenneau, and A. B. Movchan, *Opt. Exp.* **11**, 2555 (2003).
[4] V. Laude, A. Khelif, S. Benchabane, M. Wilm, T. Sylvestre, B. Kibler, A. Mussot, J. M. Dudley, and H. Maillotte, *Phys. Rev. B* **71**, 045107 (2005).
[5] P. Dainese, P. S. J. Russell, G. S. Wiederhecker, N. Joly, H. L. Fragnito, V. Laude, and A. Khelif, *Opt. Exp.* **14**, 4141 (2006).
[6] P. Dainese, P. S. J. Russell, N. Joly, J. C. Knight, G. S.Wiederhecker, H. L. Fragnito, V. Laude, and A. Khelif, *Nature Phys.* **2**, 388 (2006).
[7] J.-C. Beugnot, T. Sylvestre, H. Maillotte, G. Mélin, and V. Laude, *Opt. Lett.* **32**, 17 (2007).
[8] M. Maldovan and E. L. Thomas, *Appl. Phys. Lett.* **88**, 251907 (2006).
[9] M. Eichenfield, J. Chan, R. M. Camacho, K. J. Vahala, and O. Painter, *Nature* **462**, 78 (2009).
[10] Y. Pennec, B. Djafari-Rouhani, E.-H. El-Boudouti, C. Li, Y. El-Hassouani, J. Vasseur, N. Papanikolaou, S. Benchabane, V. Laude, and A. Martinez, Opt. Express **18**, 14301 (2010).
[11] Y. El Hassouani, C. Li, Y. Pennec, E.H. El Boudouti, H. Larabi, A. Akjouj, O. Bou Matar, V. Laude, N. Papanikolaou, A. Martinez, and B. Djafari Rouhani, *Phys.Rev.B* **82**, 155405 (2010).
[12] I. E. Psarobas, N. Papanikolaou, N. Stefanou, B. Djafari-Rouhani, B. Bonello, and V. Laude, *Phys. Rev. B* **82**, 174303 (2010).
[13] S. Sadat-Saleh, S. Benchabane, F. I. Baida, M.-P. Bernal, and V. Laude, *J. Appl. Phys.* **106**, 074912 (2009).

Phononics 2011: First International Conference on Phononic Crystals, Metamaterials and Optomechanics
Santa Fe, New Mexico, USA, May 29-June 2, 2011
PHONONICS-2011-0093

Forward Stimulated Light Scattering by Acoustic Resonances in Photonic Crystal Fiber

Myeong Soo Kang, Alexander Nazarkin, André Brenn, and Philip St.J. Russell

Max Planck Institute for the Science of Light, Guenther-Scharowsky-Str. 1/Bau 24, 91058 Erlangen, Germany
www.pcfiber.com

Abstract: Forward stimulated light scattering by transverse acoustic resonances tightly trapped in a photonic crystal fiber core is a recently reported nonlinear-optical optoacoustic phenomenon. The principles and characteristics of the scattering are described. Some potential applications are also discussed.

Photonic crystal fibers (PCFs) with a micron-sized glass core and a high air-filling fraction allow tight confinement of both acoustic phonons and light in the tiny core. Thanks to resulting strong optoacoustic interactions, forward stimulated light scattering by GHz acoustic resonances (ARs) tightly trapped in a PCF core has been recently demonstrated at modest optical powers [1,2]. When pump (frequency f_P) and Stokes (frequency f_S) waves are co-launched together into the fiber, their frequency difference being tuned to the AR frequency ($f_{AR} = f_P - f_S$), a coherent AR is efficiently generated via electrostriction, which in turn transfers power from pump to Stokes. In the dispersion diagram, the phase matching point corresponding to the driven AR is close to cut-off of the higher-order acoustic mode (where the acoustic displacement is purely in the transverse plane). Since the acoustic dispersion around the phase matching point is almost flat, forward stimulated scattering is strongly Raman-like, i.e., the frequency shift is independent of the pump laser frequency [Figure 1(a)], in strong contrast to conventional (backward) stimulated Brillouin scattering (SBS) [Figure 1(b)] [3,4].

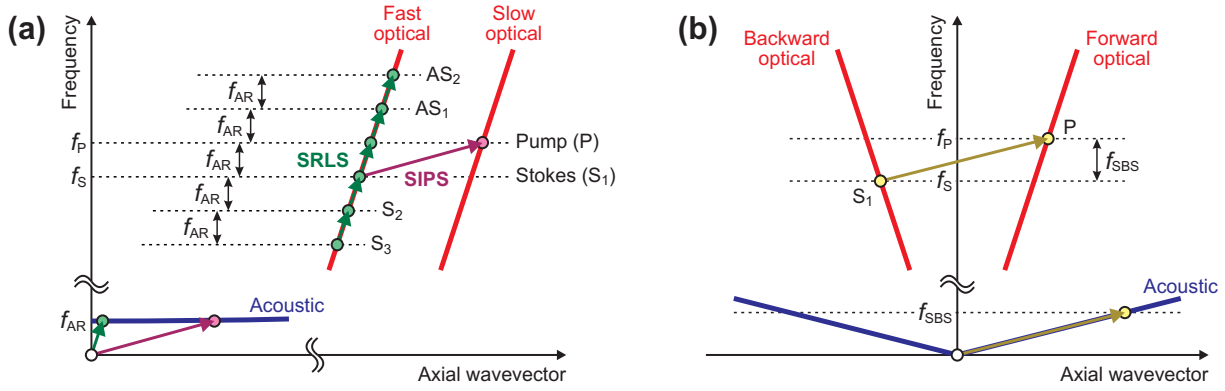

Figure 1 Dispersion diagrams (not to scale) for the optical and acoustic modes guided in a fiber, comparing forward stimulated Raman-like scattering (SRLS) and stimulated inter-polarization scattering (SIPS) (a) to conventional (backward) stimulated Brillouin scattering (SBS) (b). Circles and arrows represent phase-matched optical and acoustic waves. P: pump, S: Stokes, AS: anti-Stokes.

Two types of forward stimulated scattering have been investigated: forward stimulated Raman-like scattering (SRLS) between pump and Stokes waves in the same optical mode [1], and forward stimulated inter-polarization scattering (SIPS) between orthogonally polarized pump and Stokes waves [2]. In forward SRLS, the driven AR is automatically phase-matched with successive Stokes and anti-Stokes orders, the frequency spacing between them being constant. As a result, an equidistant comb of higher-order Stokes and anti-Stokes waves can be generated via cascaded coherent Stokes and anti-Stokes scattering at high optical powers [Figure 2(b)]. This simultaneous generation of many sidebands can be useful in applications such as frequency comb generation, pulse synthesis and laser mode-locking. On the other

Phononics 2011: First International Conference on Phononic Crystals, Metamaterials and Optomechanics
Santa Fe, New Mexico, USA, May 29-June 2, 2011
PHONONICS-2011-0093

hand, in forward SIPS, the driven AR does not have the correct axial wavevector to cause scattering into higher-order Stokes and anti-Stokes waves. Therefore, the SIPS process transfers pump power only to the Stokes wave, generation of higher-order sidebands being highly suppressed [Figure 2(c)], which is similar to the case of conventional SBS. Since the orthogonally polarized pump and Stokes waves can be easily combined and separated out by using simple polarization optics, forward SIPS can be useful in applications such as variable optical attenuation/amplification, optical signal processing and optical sensing.

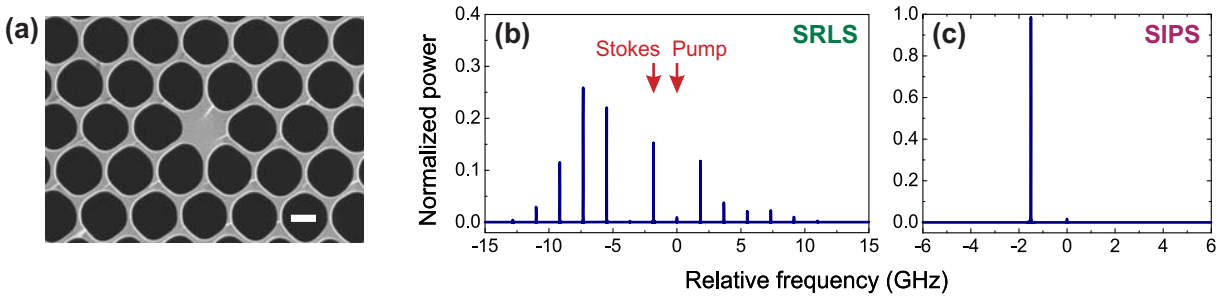

Figure 2 (a) Scanning electron micrograph of a PCF with the core diameter of 1.8 μm. The white horizontal bar corresponds to 1 μm. (b) Typical output spectrum as co-polarized pump and Stokes waves with the same optical power are launched into the PCF. The red downward-pointing arrows indicate the two incident optical waves. (c) Typical output spectrum as orthogonally-polarized pump and Stokes waves with the same optical power are coupled into the different polarization eigenmodes of the PCF.

References

[1] M. S. Kang, A. Nazarkin, A. Brenn, and P. St.J. Russell, *Nature Phys.* **5**, 276-280 (2009).
[2] M. S. Kang, A. Brenn, and P. St.J. Russell, *Phys. Rev. Lett.* **105**, 153901 (2010).
[3] G. P. Agrawal, *Nonlinear Fiber Optics*, Academic Press, San Diego (2007).
[4] R. W. Boyd, *Nonlinear Optics*, Academic Press, San Diego (2008).

Phononics 2011: First International Conference on Phononic Crystals, Metamaterials and Optomechanics
Santa Fe, New Mexico, USA, May 29-June 2, 2011
PHONONICS-2011-0128

Fundamental Limits of Transduction Efficiency and Bandwidth in Nano-Optomechanics

Peter T. Rakich[1], Zheng Wang[2], Charles E. Reinke[1], Ryan Camacho[1], Paul Davids[1]

[1] *Applied Photonic Microsystems, Sandia National Laboratories, Albuquerque NM, 87123, USA*
[2] *Physics, Massachusetts Institute of Technology, 77 Massachusetts Ave, Cambridge, MA 02139, USA*
rakich@alum.mit.edu

Abstract: Through systematic examination of material and topological degrees of freedom in nano-optomechanical systems, we identify the fundamental barriers and opportunities for the creation of large photon-phonon coupling.

Coherent phonon generation in dielectric waveguides and media was demonstrated some four decades ago via laser induced electrostrictive forces [1,2]. With the advent of nanophotonics, nano-enhanced radiation pressure from highly confined modes has been shown to produce efficient phonon generation at low powers with chip scale-devices [3]. Optomechanical photon-phonon coupling of this form has caught the attention of many since nanoscale light confinement produced remarkably large forces within miniscule volumes [3-5], and it is known to produce high frequency phonon transduction [3-5]. Furthermore, the unique range of length-scales and time-scales accessible with such nano-scale systems show the potential for benefit to numerous RF and signal processing applications, fuelling the investigation of such physical mechanism for use in high frequency signal transduction. However, without a unified framework through which optical forces and optomechanical parametric processes can be understood, it is difficult to determine whether technologically relevant data rates can be achieved through use of such phenomena.

In this paper, we develop a unified framework through which optomechanical transduction can be understood in virtually all optomechanical systems, elucidating the bandwidth and efficiency limitations of such technologies. Through examination of material and geometric degrees of freedom, we develop scaling laws which describe the magnitude of optical forces produced by electrostriction and radiation pressure in any optomechanical system [4,5]. Using these scaling laws, we explore the practical upper-bounds of light-induced forces, and identify materials systems with favourable characteristics for optomechanical transduction. Through generalized treatment of photon-phonon coupling, a fundamental scaling law that governs the efficiency and bandwidth limitations *of all radiation pressure driven optomechanical devices* can be derived, enabling the comparison of all optomechanical systems in a unified framework. With this theory, we show that the maximum transduction bandwidth and phononic power output (i.e. photon-phonon coupling) of any optomechanical device is determined by: (1) the maximum possible magnitude of radiation pressure, (2) the device dimension, and (3) the effective mechanical impedance of the system.

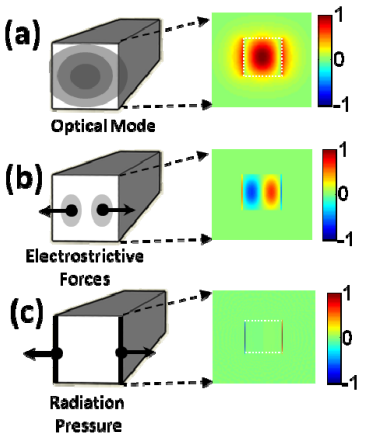

Figure 1. (a) E_y field component of TE-like mode of silicon nanowire. (b) and (c) are the x -directed force densities produced by electrostriction and radiation pressure respectively.

Simply stated, the challenges associated with broadband stimulated phonon emission in optomechanical systems arise from: (1) *limited optical forces,* and (2) the high *mechanical impedance of naturally occurring media*. One can show the maximum driving force produced by light within any optomechanical system is fundamentally limited by the optical power and energy density limitations of optical materials. However, the maximum obtainable force is highly dependent on the physical mechanism which produces the optical forces. Within dielectric media, optical forces generally arise from either (1) radiation pressure and (2) electrostrictively induced forces, both of which have historically played a very important role in the understanding of transduction with light [1-3]. In contrast to radia-

Phononics 2011: First International Conference on Phononic Crystals, Metamaterials and Optomechanics
Santa Fe, New Mexico, USA, May 29-June 2, 2011
PHONONICS-2011-0128

tion pressure, which originates from the momentum transfer from scattered photons at dielectric boundaries, electrostriction is derived from the strain-dependence of dielectric permittivity and such forces are present in all dielectric media [4,5]. For example force distributions see Fig. 1.

The fundamental connection between the maximum optical driving force and the energy density handling of materials becomes apparent once it is understood that the *exact form of the radiation pressure induced optical force density within any dielectric medium* can be expressed as [5]:

$$F_j^{rp} = \partial_i T_{ij} = \tfrac{1}{2}\varepsilon_o \,|\,\mathbf{E}(\mathbf{r})\,|^2\, \partial_j \varepsilon(\mathbf{r}). \qquad (1)$$

Here, T_{ij} is the Maxwell stress, ε_o is the free space permeability, $\mathbf{E}(\mathbf{r})$ is the electric field distribution, and $\partial_j \varepsilon(\mathbf{r})$ is the gradient of the dielectric distribution. Clearly, large dielectric gradients (i.e. high index-contrast) benefit the production of large optical forces, and optical forces occur only at dielectric surfaces in step-index structures. More importantly, optical force density is fundamentally limited by the achievable electromagnetic energy density $\frac{1}{2}\varepsilon\,|\,\mathbf{E}\,|^2$. Energy density is typically bound to 10^4 J/m^3 in high-index materials, such as silicon, before the onset of appreciable two-photon absorption and the associated heating which limit practically achievable powers. Consequently radiation pressure is fundamentally restricted to a maximum value of $\sim 10^4$ N/m^2, which we term the "Radiation Pressure Limit". Bear in mind that the "Radiation Pressure Limit " is only attainable by *optimally confined modes* which interact *very* strongly with the boundaries of the system [4,5].

Stimulated phonon emission, of the type recently reported utilizes such forces to produce stimulated phonon emission. In its most basic form, optomechanically mediated stimulated phonon emission is a third-order nonlinear process through which the interference between optical waves of two different frequencies (ω_p, ω_s) produces a time-harmonically modulated optical driving force of frequency, $\Omega = (\omega_p - \omega_s)$. In describing stimulated phonon generation, the optical powers (particle fluxes) P_p (Φ_p), P_s (Φ_s), corresponding to an optical pump (ω_p) and a Stokes waves (ω_s) are coupled by way of acoustic phonons of frequency $\Omega = (\omega_p - \omega_s)$ and power (particle flux) P_Ω (Φ_Ω). From the time-varying optical force distributions, the generated elastic wave power can be computed the parametric conversion for both photons and phonons.

Through generalized treatment, we show that a fundamental scaling law that governs the efficiency and bandwidth limitations *of all radiation pressure driven optomechanical devices* can be derived, enabling the comparison of all optomechanical systems in a unified framework. Within the constraints posed by the Radiation Pressure Limit, our scaling law reveals that the maximum quantum efficiency obtained via a radiation pressure mediated process within a unit length (Δz) of guided wave optomechanical interaction is of the form,

$$\eta^{\max} = \frac{d\Phi_\Omega}{dz}\frac{\Delta z}{\Phi_p} \cong \alpha \cdot \frac{u_{em}^{\max}}{c}\frac{\omega_s}{\Omega} \cdot \frac{(n_g - n_g)^2}{n_g \cdot Z(\Omega)}\Delta z \qquad (2)$$

Here Φ_p (Φ_Ω) is the incident (generated) photon (phonon) flux, $Z(\Omega)$ is the frequency dependent mechanical impedance of the body into which the phonon is being transduced, and α is a factor that depends weakly on geometry. Within nanoscale waveguides and cavities, u_{em}^{max} can be easily obtained at miliwatt laser powers. Thus, for energy densities corresponding to u_{em}^{max}, or the "Radiation Pressure Limit," the only means by which transduction efficiency can be increased is through: (1) an increase in modal dispersion $(n_g - n_p)$, (2) a decrease in mechanical impedance $Z(\Omega)$, or (3) an increase in interaction length, Δz. The role of dispersion $(n_g - n_p)$, is derived from its fundamental connection to radiation pressure [5]. While Eq. 2 describes a fundamental limit associated with radiation pressure induced parametric processes.

Through this talk, we describe the energy density limitations posed by various materials for the generation of both electrostrictive forces and radiation pressure. Within this framework, and by use of the above scaling law, we analyze several concrete optomechanical systems to illustrate the interplay between transduction efficiency, bandwidth, and size.

References

[1] R. Chiao, C. Townes, and B. Stoicheff, Phys. Rev. Lett., vol. 12, no. 21, pp. 592–595, 1964.
[2] E. Ippen and R. Stolen, Appl. Phys. Lett., vol. 21, no. 11, pp. 539–541, 1972.
[3] M. Eichenfield, R. Camacho, J. Chan, K. J. Vahala, and O. Painter, Nature, vol. 459, pp. 550–U79, MAY 28 2009.
[4] P. Rakich, P. Davids, and Z. Wang, Opt. Express, vol. 18, no. 14, pp. 14439–14453, 2010.
[5] P. Rakich, Z. Wang, and P. Davids, Opt. Lett., vol. 36, no. 2, pp. 217–219, 2011.

Phononics 2011: First International Conference on Phononic Crystals, Metamaterials and Optomechanics
Santa Fe, New Mexico, USA, May 29-June 2, 2011
PHONONICS-2011-0130

Mechanical Transduction in Periodic Media

Ryan M. Camacho[1] and Peter T. Rakich[1]

[1] *Sandia National Laboratories, 1515 Eubank Blvd SE, MS 1082, Albuquerque, NM 87123 USA*
rcamach@sandia.gov

Abstract: The possibility of increasing mechanical transduction efficiencies via periodic patterning of the material density is investigated. A 2D simulation suggesting low mechanical impedance over a relatively large bandwidths is presented.

Recently there has been a surge in interest in acoustic meta-materials. In analogy to optical meta-materials, much of the interest is centered on the possibility of periodically patterning materials to create negative effective densities and moduli, with possible applications in superlensing, cloaking and liquid crystal sensing[1-4]. Here, we examine a different possibility: that periodically patterned materials may also allow for dramatic increases in the mechanical transduction efficiency of signals into and out of the mechanical domain.

Mechanical transduction is of primary importance in the fields of acousto-optics, electro-mechanics, opto-mechanics and others. In general, one would like to transfer energy efficiently from one domain to another over a given bandwidth. The usual method to increase transduction efficiency is by using resonant phenomena, which limits the usable band-width of the transducer. An example is the use of electrical tank circuits in many commercially available acousto-optic modulators. Here we examine a technique to increase the mechanical transduction efficiency by modifying the mechanical impedance of the material via periodic patterning, offering the potential for broadband, coherent mechanical transduction.

When a time-harmonic force F is applied uniformly to the boundary of a uniform elastic medium of area A, the resulting time-averaged harmonic power P_m within the medium is inversely proportional to a quantity defined as the specific mechanical impedance Z:

$$P_m = \frac{F^2}{2AZ} \tag{1}$$

In media with uniform density ρ, Z is simply the ratio of the restoring pressure K (the effective bulk modulus) to the phase velocity v_p of the mechanical waves: $Z_0 = K/v_p$. Identifying the phase velocity v_p of the mechanical waves as $\sqrt{K/\rho}$, we may write the mechanical impedance as

$$Z_0 = \rho_{eff} v_p \tag{2}$$

When the material density is not uniform, however, this definition requires modification. Frequency-dependent mechanical reflection and refraction occur, giving rise to frequency-dependent phase velocities (i.e mechanical dispersion). For normal, linear mechanical dispersion, the mechanical energy propagates at the *group* velocity v_g, which can be much lower than v_p. As a result, the mechanical energy density within the material can be very high, leading to large harmonic displacements. Hence, even though the average power flux through the material may not change appreciably, the time-averaged harmonic power $P_m$can be dramatically increased. A more general expression for the mechanical impedance is

$$Z = \rho_{eff} v_g \tag{3}$$

where ρ_{eff} is the effective density of the material (i.e. spatially weighted according to the amplitude of the mechanical waves, analogous to an effective index). In the context of mechanical transduction, this simple result leads to an important conclusion: transduction mechanisms that scale with displacement amplitude can be made dramatically more efficient by lowering the group velocity and matching the forcing function to the resulting displacement field.

Phononics 2011: First International Conference on Phononic Crystals, Metamaterials and Optomechanics
Santa Fe, New Mexico, USA, May 29-June 2, 2011
PHONONICS-2011-0130

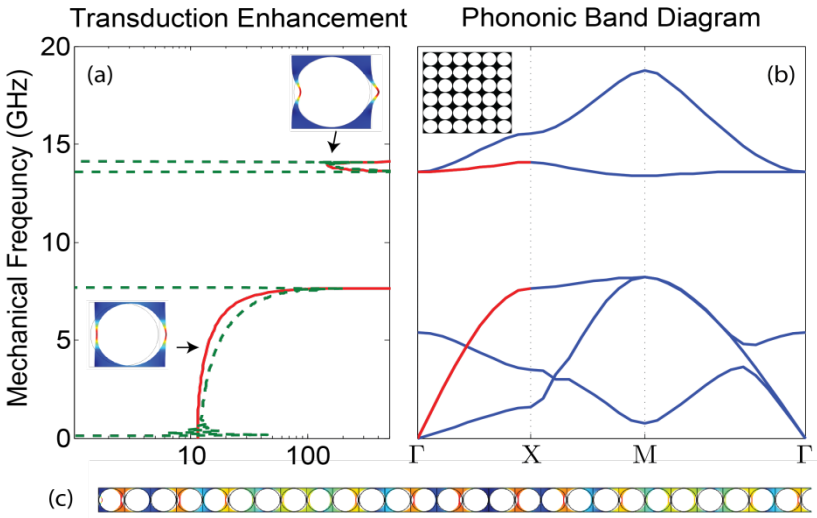

Figure 1 Mechanical transduction enhancement in 2D phononic crystals. (a) Transduction enhancement Z/Z_0 calculated from dispersion diagram (solid red) and time-harmonic 1-D forcing (dashed green). Insets show displacement profile for a single unit cell with momentum $\vec{k} = \hat{x}a/2$ (b) Mechanical dispersion in a 2d rectangular lattice of holes with a lattice constant $a = 250$ nm and hole radius $r/a = 0.48$. Longitudinal modes along the $\hat{x}$ direction are highlighted in red, as those are the modes preferentially excited in the time-harmonic forcing model. The inset shows the geometry of a 6x6 array of unit cells simulated. (c) Displacement field profile for time-harmonic forcing simulation in which a uniform harmonic force is applied to the leftmost boundary. After 20 lattice periods, isotropic loss is phenomenologically added, and increases quadratically along the $\hat{x}$ direction. The material density $\rho = 3100\ \mathrm{kg/m^3}$, Young's modulus $E = 250$ GPa, and Poisson ratio $\eta = 0.23$ are chosen to be similar to that of stoichiometric silicon nitride for all simulations.

As an illustrative numerical example, consider a two-dimensional phononic crystal consisting of a square lattice of circular holes, as shown in Fig. 1. Figure 1(a) shows the transduction enhancement Z/Z_0 calculated in two ways. The dashed green line is calculated by simulating a uniform time-harmonic forcing function applied to an array of unit cells with appropriate boundary conditions to excite longitudinal (compression) modes. The resulting mechanical power within the medium is then calculated and divided by the same quantity for the case with no patterning (i.e. $r = 0$) The low frequency oscillations result from the inability to simulate an infinitely long structure (i.e. the simulation behaves badly for wavelengths longer than the structure). The solid red line is calculated from the mechanical dispersion using a mechanical eigenmode solver for a unit cell, and then inserting the derived effective density and group velocity into Eq. (3). The small discrepancy between the two curves may be attributed to the fact that the forcing function was not perfectly matched to the resonant displacement field. Only the bands corresponding to longitudinal motion are used to generate the curves. Figure 1(b) shows the mechanical band diagram calculated from a single unit cell of the structure. The derivative of the longitudinal modes (highlighted in red) is used to calculate the mechanical impedance via Eq. (3). Figure 1(c) shows are representative displacement amplitude in a longitudinal array of cells used in the time-harmonic simulation. Periodic boundary conditions are used in the $\hat{y}$ direction (i.e. $k_y = 0$) to ensure elastic wave propagation along the $\hat{x}$ direction, and isotropic phenomenological loss is quadratically added beginning after 20 unit cells to ensure the absence of reflections and accurately simulate the power flow.

While these simulations are two-dimensional, they point to the possibility using effective phononic media as a means to enhance transduction efficiencies over relatively broad bandwidths. The result may find applications in electro-optic and acousto-optic devices, and optomechanical devices. Acousto-optic modulators, for example, rely on resonant electro-mechanical actuation and therefore operate over very limited bandwidths. Similarly, cavity based optomechanical transduction[5,6] relies on resonant mechanical and optical confinement, and faces bandwidth limitations.

References

[1] S. H. Lee, C. M. Park, Y. M. Seo, Z. G. Wang, and C. K. Kim, Physical Review Letters **104,** 054301 (2010).
[2] N. Gomopoulos, D. Maschke, C. Y. Koh, E. L. Thomas, W. Tremel, H. Butt, and G. Fytas, Nano Letters **10**, 980 (2010).
[3] R. Lucklum, J. Li, and M. Zubtsov, Procedia Engineering **5**, 436 (2010).
[4] F. Bongard, H. Lissek, and J. R. Mosig, Physical Review B **82**, 094306 (2010).
[5] M. Eichenfield, R. Camacho, J. Chan, K. J. Vahala, and O. Painter, Nature **459**, 550 (2009).
[6] R. M. Camacho, J. Chan, M. Eichenfield, and O. Painter, Optics Express **17**, 15726 (2009).

Phononics 2011: First International Conference on Phononic Crystals, Metamaterials and Optomechanics
Santa Fe, New Mexico, USA, May 29-June 2, 2011
PHONONICS-2011-0138

Integrated Transduction and Active Manipulation Methods for Nanoelectromechanical Systems

Hong Tang[1]

[1] *Department of Electrical Engineering*
Becton Center 525, Yale University
15 Prospect St, New Haven, CT 06520
hong.tang@yale.edu

Abstract: This talk will discuss integrated NEMS transduction schemes that have been developed by my research group. Methods for achieving active control and manipulation of nanomechanical motion will be also presented.

In its acronym NEMS inherited an "S" (systems) from MEMS. However, so far the impacts of nanosystems technology remain on the device or component level. Complex nanosystems consisting of integrated sensors, actuators and signal processing circuitry are still beyond our reach. Major obstacles remain in the development of suitable actuation and transduction methods that perform efficiently at nanoscale and under non-laboratory setting. From system control point of view, it is also highly desirable nanomechanical motion can be coherently manipulated, ideally not only in frequency domain but also in real time so that the large bandwidth of nanomechanical systems can be fully utilized.

This presentation first provides an overview of NEMS transduction schemes that have been developed by my research group, and then aims at establishing essential transduction criteria for building fully integrated nanoelectromechanical systems. On the component level, emphasis for NEMS transduction is focused on attaining high actuation efficiency, high sensitivity, and wide bandwidth. On the system level, I will address the more stringent requirements of NEMS integration in transduction and actuation, such as low power consumption, high dynamic range, low insertion loss, device level isolation, the ability to fan out, cascade, and fan in, as well as transduction robustness against environmental change.

In this abstract we use silicon optomechanics as a specific example platform to illustrated integrated actuation and sensing. In this platform, the actuation is based upon gradient optical force – which is generated through evanescent coupling of light in a waveguide to an adjacent structure. [1-4] Microscopically, it results from interactions between dynamic dipoles induced by the propagating light field. This optomechanical interaction not only provide efficient actuation, but also enable very sensitive detection of mechanical motion of the devices are embedded in an interferometer configuration or cavity configuration; in the latter case the transduction efficiencies (both actuation and detection) are enhanced by the cavity finesse.

Nanophotonic waveguides can manipulate light in multiple paths with very low loss and low crosstalk. Therefore our scheme is capable of parallel and serial integration of a multitude of NEMS devices in a single photonic circuit. Figure 1 illustrates the concept of parallel multiplexed cantilever arrays (The same principle is also applicable to beams). The input and output structures are designed to be 1×N and N×1 splitter and combiners, diverting the light to N independent cantilever pairs. Fig. 2a shows the FDTD simulation result of such a design. The length of the ten cantilevers varies from 2.5 to 3.5 μm. Ten resonance peaks, corresponding to the thermomechanical resonance of each cantilever, can be clearly observed as shown in Fig. 1c. The center resonance frequencies of the cantilevers

Phononics 2011: First International Conference on Phononic Crystals, Metamaterials and Optomechanics
Santa Fe, New Mexico, USA, May 29-June 2, 2011
PHONONICS-2011-0138

vary from 11 MHz to 21 MHz, showing the linear dependence with the inverse square of the cantilever lengths, as expected from the simple beam theory. Given the high signal to noise ratio and the minimum background cross talk (Fig. 1c), hundreds of mechanical resonators can be multiplexed on the photonic bus with resonance frequencies designed at fixed intervals. Therefore individual cantilever sensors can be addressed by their resonant frequencies.

This presentation will further explore examples of achieving real-time control of nanomechanical motion, in both electromechanical devices and optomechanical devices.

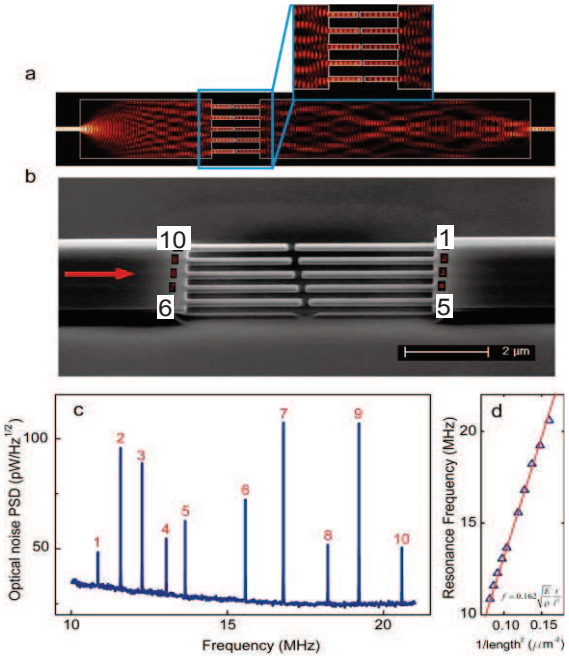

FIG. 1. Multiplexed integration of a ten-cantilever array in a photonic circuit. All the resonances are simultaneously detected at expected frequencies.

References

1. Li, M., W.H.P. Pernice, and H.X. Tang, *Broadband all-photonic transduction of nanocantilevers.* Nature Nanotechnology, 2009. **4**(6): p. 377-382.
2. Li, M., W.H.P. Pernice, and H.X. Tang, *Tunable bipolar optical interactions between guided lightwaves.* Nature Photonics, 2009. **3**: p. 464.
3. Li, M., et al., *Harnessing optical forces in integrated photonic circuits.* Nature, 2008. **456**(7221): p. 480-484.
4. Tang, H.X., *May The Force of Light Be With You.* Spectrum, IEEE, 2009. **46**(10): p. 46-51.

Phononics 2011: First International Conference on Phononic Crystals, Metamaterials and Optomechanics
Santa Fe, New Mexico, USA, May 29-June 2, 2011
PHONONICS-2011-0146

Strong Optomechanical Coupling in Slot-type Photonic Crystal Cavities

J. Zheng[1], Y. Li[1], H.-B. Tan[1], M. Aras[1], A. Stein[2], J. Gao[1], J. Shu[1], and C. W. Wong[1]

[1]Optical Nanostructures Laboratory, Columbia University, New York, NY 10027 USA
jz2356@columbia.edu, yl2584@columbia.edu; cww2104@columbia.edu
[2] Brookhaven National Laboratory, Upton, NY 11973
stein@bnl.gov

Abstract: Strong dispersive optomechanical coupling of an air-slot mode-gap photonic crystal cavity is demonstrated. The zero-point motion coupling rate can be as high as 2.56MHz. Optical and 10s of MHz mechanical frequency spectra are shown experimentally, supported by theory and numerical models.

The effects of optical forces in various mechanical and optical structures and systems have attracted intense and increasing interest for investigation. Recent studies covering a vast span of fundamental physics and derived applications. Photonic crystals nanocavity is a good candidate to realize the coupling since it exhibits an extremely high Q with a very small cavity volume[1]. Here we illustrate the properties of strong coupling of an air-slot photonic crystal cavity. Both numerical analysis and experimentally observation are illustrated.

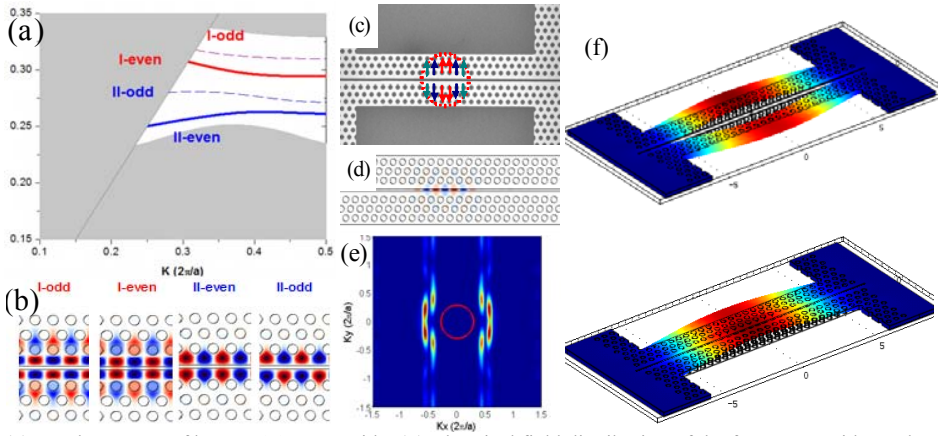

Figure 1 (**a**) Band structure of base W1.2 waveguide. (**b**) Electrical field distribution of the four waveguide mode at the mode edge in the band gap. (**c**) SEM image of the fabricated sample. The cavity region is indicated by the dashed circle and the directions of the hole shifting in the cavity are indicated by the arrows. (**d**) Optical cavity field distribution. (**e**) The spatial Fourier-transform of the cavity field. (**f**) the mechanical field distribution of the first in-plane differential and common mode pair.

The photonic crystal (PhC) cavity considered here has a similar design with that in Ref. 2-4. W1.2 waveguide is used. The PhC lattice geometrical parameters are a=450nm and r=0.29a. The slot-width is 80 nm which is narrow to achieve large optical intensity in the air slot[2-4]. The cavities are fabricated using a Silicon-On-Insulator wafer with thickness t=250 nm. There are only three layers of holes on each side of the waveguide. The band structure of this W1.2 waveguide is shown in Figure 1 (a). The electrical fields of the waveguide modes are shown in Figure 1 (b). The I-even mode is engineered to form a cavity indicated by the red dashed circle in Figure 1 (c) which is the SEM of a fabricated sample. The central holes are shifted by 10 nm, 20/3 nm, 10/3 nm respectively in the same way as in Ref. 2-4. Three-dimensional FDTD simulations show that the optical quality factor Q can be $>1.3\times10^6$. The modal volume is $\sim0.05(\lambda/n_{air})^3$ with the maximum square electrical field in the center of the cavity as is shown in Figure 1(d). The two-dimensional spatial Fourier-transform of the electrical field is shown in Figure 1 (e) with red circle indicating the light corn. It shows that almost all the spatial components of the cavity field are well confined in the cavity. To study the mechanical properties, the finite-element-method is used. Figure 1 (f) shows the mechanical displacement field of the first in-plane differential mode and common mode. According to the symmetry selection rule, only the differential mechanical mode can have a strong optomechanical coupling. The corresponding mechanical

Phononics 2011: First International Conference on Phononic Crystals, Metamaterials and Optomechanics
Santa Fe, New Mexico, USA, May 29-June 2, 2011
PHONONICS-2011-0146

frequency is 65.4 MHz. The effective volume and the effective mass for this mode are 3.14 μm^3 and 7.31 pg respectively. Mechanical quality factors are estimated to be ~10^4 based on the theory of thermoelasticity damping in a vibrating beam. The length of this cavity is larger than the one in Ref.4. The optical Q is higher. The mechanical frequency is much lower.

The optomechanical coupling rate gom is defined as $g_{om}=d\omega/d\alpha$, which represents the differential frequency shift of the cavity resonance with the mechanical displacement[5]. Using perturbation theory[6], we can calculate the coupling rate. The calculated $g_{om}/2\pi$=574 GHz/nm, the corresponding zero-point motion optomechanical coupling rate ($g_{om,zm}/2\pi$) is 2.56MHz.

Optomechanical coupling provides an optical contribution to the stiffness of the spring-mass system. The corresponding change in spring constant leads to a frequency shift relative to the unperturbed mechanical oscillator eigenfrequency. The non-adiabatic contribution in coupled equations is proportional to the velocity of the spring-mass system. The optical gradient force induced damping rate modifies the intrinsic mechanical resonator loss rate Γ_m, yielding an effective damping rate. With this classical model, the laser introduces a damping without introducing a modified Langevin force. This is a key feature and allows the enhanced damping to reduce the mechanical oscillator temperature, yielding as a final effective temperature T_{eff} for the mechanical mode under consideration: $T_{eff} \cong (\Gamma_m/\Gamma_{eff})T_R$. To characterize the mechanical properties of the oscillator, the power spectrum density of the optical transmission is usually needed.

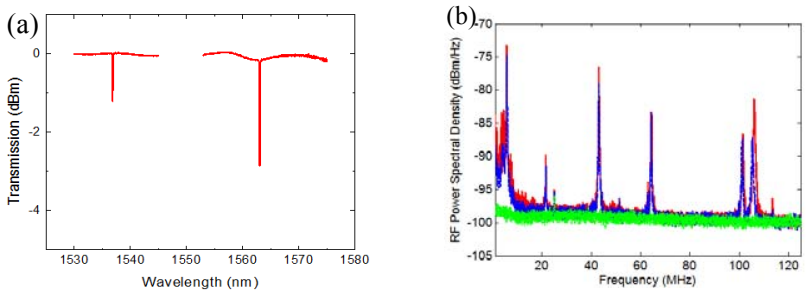

Figure 2 (**a**) Normalized optical transmission showing the intrinsic Qs for the device with resonance at 1536.65nm and 1562.75nm are 1.54×10^5 and 1.68×10^5 respectively. (**b**) RF PSD of the fiber-taper transmission for the device resonance at 1562.75nm. The detuning is set to maximize the PSD amplitude for the red line. The blue line is for a slight different detuning, while the green line indicates the noise floor of our measurements.

The devices we fabricated are characterized using a fiber-taper probe. A tunable external cavity diode laser is employed. The transmission spectrums for two adjacent devices are shown in Figure 2 (a). The two devices have different hole radius. The resonance shifts ~30nm. The intrinsic optical Qs of these two cavities are all higher than 1.5×10^5 with loaded Qs about 9×10^4. The radio frequency (RF) power spectral densities (PSD) of the optical transmission are measured by using a low-noise fast detector and a RF spectrometer. The detuning is tuned (close to the half-line width detuning) to get the maximum PSD signal as shown by the red curve in Figure 2 (b). At another detuning, we found that there are slight shift of resonances with smaller PSD peaks. The noise floor is shown by the green curve. The peaks at ~65MHz indicate the expected mechanical modes. The other peaks indicate either flexural modes or higher order in-plane and out-of-plan mechanical modes.

References

[1] H. Taniyama M. Notomi, E. Kuramochi, T. Yamamoto, Y. Yoshikawa, Y. Torii, and T. Kuga, *Phys. Rev. B* **78**, 165129 (2008).
[2] J. Gao, J. F. McMillan, M.-C. Wu, S. Assefa, and C. W. Wong, *Appl. Phy. Lett.* **96**, 051123 (2010).
[3] T. Yamamot, M. Notomi, H. Taniyama, E. Kuramochi, Y. Yoshikawa, Y. Torii, and T. Kuga, *Opt. Express* **16**, 13809 (2008).
[4] Y. Li, J. Zheng, J. Gao, J. Shu, M. Aras, and C. W. Wong, *Opt. Express* **18**, 23844 (2010).
[5] M. Eichenfield, J. Chan, A.H. Safavi-Naeini, K.J. Vahala, and O. Painter, *Opt. Express* **17**, 20078 (2009).
[6] S. G. Johnson, M. Ibanescu, M.A. Skorobogatiy, O. Weisberg, J.D. Joannopoulos, and Y. Fink, *Phys. Rev. E* **65**, 066611 (2002).

Phononics 2011: First International Conference on Phononic Crystals, Metamaterials and Optomechanics
Santa Fe, New Mexico, USA, May 29-June 2, 2011
PHONONICS-2011-0157

Cavity Quantum Optomechanics

Garrett D. Cole[1]

[1] *Vienna Center for Quantum Science and Technology (VCQ), Faculty of Physics, University of Vienna, Boltzmanngasse 5, Vienna A-1090, Austria*
garrett.cole@univie.ac.at

Abstract: The overarching research objective of cavity quantum optomechanics is to investigate quantum effects of micro- and nanoscale systems and their implications for the foundations and applications of quantum physics. Our ultimate goal is to gain access to a completely new parameter regime for experimental physics with respect to both size and complexity.

Cavity optomechanics has recently emerged as one of the most dynamic fields in experimental physics. In this presentation I will outline the fascinating perspectives of this area of research and present proof-of-concept experiments performed using high-reflectivity low-loss mechanical resonators coupled to high-finesse cryogenic optical cavities. Along the path towards the ultimate goal of macroscopic quantum state preparation, our research has led to a number of interesting technological applications including the development of a numerical solver for support-mediated losses in mechanical resonators [1] as well as new strategies for the development of low-noise multilayer mirrors for high performance optical reference cavities.

The idea that the properties of a mechanical object can be modified by radiation pressure forces in an optical cavity goes back to the pioneering work of Braginsky [2]. In essence, the response of an optical cavity to the motion of a mechanical object leads to forces that both depend on the position of the mechanics and are retarded in time (due to the finite cavity lifetime). For sufficiently strong forces, this results in a modification of the mechanical susceptibility and is the underlying mechanism for optical control over mechanical degrees of freedom and vice versa. In combination with quantum optics, such interactions allow for the realization of *quantum* control of mechanical resonators. The consequences of this realization are wide ranging, impacting such diverse fields as mechanical sensing, by enabling resolution at or even beyond the quantum limit [3], and quantum information, where optomechanical devices may act as transducers for otherwise incompatible quantum systems [4]. From a fundamental point of view, preparing superposition states of massive objects (containing $\sim 10^{20}$ atoms) provides a new avenue for novel tests of macroscopic quantum physics [5], where spatially distinct states of mechanical quantum systems could serve as a paradigm example of Schrödinger's cat.

Approaching and eventually entering the quantum regime of mechanical resonators through optomechanical interactions essentially requires the following three conditions to be fulfilled: (1) sideband-resolved operation [6] in which the cavity amplitude decay rate is small with respect to the mechanical frequency (note that recent schemes have been proposed alleviating this requirement), (2) both an ultra-low noise cooling laser and low absorption of the optical cavity field (phase noise at the mechanical frequency can act as a finite-temperature thermal reservoir while absorption may increase the mode temperature and even diminish the overall cavity performance), and (3) sufficiently small coupling of the mechanical resonator to the thermal environment entailing a low environmental temperature T and large mechanical quality factor Q. The thermal coupling rate is given by $k_B T/\hbar Q$, where k_B is the Boltzmann constant and $\hbar$ is the reduced Planck constant. Ultimately, the individual dissipation rates of the mechanical and optical systems should be exceeded by the optomechanical coupling. Currently, the major experimental hurdle in reaching the quantum ground state is the limitation in Q, thus "phononic engineering" of optimized mechanical resonators is paramount to the success of the field.

In 2006 a milestone was achieved with the first demonstration of laser-cooling of micromechanical resonators via passive radiation-pressure interactions in a high-finesse optical cavity [7]. The experimental realization in Vienna employed an optical cavity incorporating a high reflectivity microresonator as one of the end mirrors and achieved a final mode temperature of 8 K with 2 mW of detuned extra-cavity laser power. These initial results prompted a rapid expansion of the nascent field of cavity optomechanics with a proliferation of international groups working towards the ultimate goal of observing quantum effects in macroscopic mechanical resonators. In order to further reduce the

Phononics 2011: First International Conference on Phononic Crystals, Metamaterials and Optomechanics
Santa Fe, New Mexico, USA, May 29-June 2, 2011
PHONONICS-2011-0157

minimum phonon occupation, a second generation of devices was developed shortly thereafter. These structures utilized an ultra-low absorption SiO_2/Ta_2O_5 Bragg mirror in order to significantly improve the optical performance of the resonators. Furthermore, to minimize the mechanical damping from the optical coating, a specifically engineered mechanical resonator was devised, employing a mechanical resonator based on low-stress silicon nitride. Utilizing this separately-optimized design, a reflectivity >99.99% was realized (along with the complete elimination of photothermal effects), while maintaining a cryogenic Q of ~3×10^4. Operating the optical cavity in a continuous flow ^{4}He cryostat, the fundamental mode of the resonator (eigenfrequency near 1 MHz) was cooled from an initial temperature of 5 K to a final phonon occupation of ~30 [8]. Owing to their excellent optomechanical properties, these devices were additionally employed for the first demonstration of strong coupling between an optical field and a mechanical resonance [9].

In order to further reduce the mechanical damping in these structures, two generations of monocrystalline resonators have additionally been realized. These devices are etched directly from a single-crystal Bragg reflector composed of an alternating stack of ternary $Al_xGa_{1-x}As$ alloys with varying aluminum content, grown via MBE. Resonators fabricated from this material system utilized an identical geometry to the early dielectric devices (employing simple singly- and doubly-clamped beams) and exhibited nearly an order of magnitude improvement in the mechanical dissipation as compared with Ta_2O_5-based devices of similar geometry, reaching Q-values greater than 2×10^4 at eigenfrequencies up to 2 MHz at 4 K [10]. Further investigation indicated that Q was ultimately limited by support-induced losses for the geometries studied. Moving to a novel free-free resonator design has led to the demonstration of cryogenic quality factors approaching 10^5 (9.5×10^4 at 2.4 MHz) [11]. The simultaneous achievement of high reflectivity and low mechanical loss in these crystalline mirrors makes this materials system promising for application in high-performance optical reference cavities, where coating thermal noise currently represents a significant roadblock to the overall stability [12].

In order to gauge the design-limited Q in our devices we have recently completed a theoretical and experimental effort aimed at quantifying the effects of support-induced damping, a key dissipation mechanism in high-quality-factor micro- and nanomechanical resonators [1]. Such studies are vitally important not only for advancing optomechanical experiments, but additionally for pushing the limits of general micro- and nanomechanical resonators, which have emerged as ubiquitous devices for use in advanced technological applications. To numerically predict the design limited Q in mechanical resonators we have developed an efficient FEM-enabled numerical solver, which employs the recently introduced "phonon-tunneling" approach [13]. This solver represents a substantial simplification over previous methods, allowing for the investigation of complex geometries, as well as taking proper account of interference effects between the radiated waves. To experimentally verify the results generated from the solver we characterize sets of custom resonators which exhibit a significant variation in geometry, while approximately preserving the frequencies and effective surface-to-volume ratios of the resonators. As these characteristics are kept constant, one can rule out the influence of additional damping mechanisms on the variation in Q and hence isolate support-induced losses. The results from these devices show excellent agreement with the theoretical predictions, thus, in combination with existing models for other damping channels, our phonon-tunneling solver makes further strides towards *a priori* prediction of Q in micro- and nanoscale mechanical resonators.

References

[1] G. D. Cole, I. Wilson-Rae, K. Werbach, M. R. Vanner, and M. Aspelmeyer, *Nature Communications*, **2**, 231 (2011).
[2] V. B. Braginsky, S. E. Strigin, and S. P. Vyatchanin, *Physics Letters A*, **287**, 331 (2001).
[3] A. Mari and J. Eisert, *Phys. Rev. Lett.*, **103**, 213603 (2009) and K. Jähne, et al., *Phys. Rev. A*, **79**, 063819 (2009).
[4] A. N. Cleland and M. R. Geller, *Phys. Rev. Lett.*, **93**, 070501 (2004) and P. Rabl, et al., *Nature Physics*, **6**, 602 (2010).
[5] A. J. Leggett, *J. Phys.: Condens. Matter*, **14**, R415 (2002) and M. Arndt, et al., *Fortschr. Phys.*, **57**, 1153 (2009).
[6] A. Schliesser, R. Rivière, G. Anetsberger, O. Arcizet, and T. J. Kippenberg, *Nature Physics* **4**, 415 (2008).
[7] S. Gigan, et al., *Nature* **444**, 67 (2006) and O. Arcizet, et al. *Nature*, **444**, 71 (2006).
[8] S. Gröblacher, et al., *Nature Physics*, **5**, 485 (2009).
[9] S. Gröblacher, K. Hammerer, M. R. Vanner, and M. Aspelmeyer, *Nature*, **460**, 724 (2009).
[10] G. D. Cole, S. Gröblacher, K. Gugler, S. Gigan, and M. Aspelmeyer, *Appl. Phys. Lett.*, **92**, 261108 (2008).
[11] G. D. Cole, et al., IEEE MEMS, Hong Kong SAR, China, TP133 (2010).
[12] Y. Y. Jiang, et al.," *Nature Photonics*, **5**, 158 (2011).
[13] I. Wilson-Rae, *Phys. Rev. B*, **77**, 245418 (2008).

Phononics 2011: First International Conference on Phononic Crystals, Metamaterials and Optomechanics
Santa Fe, New Mexico, USA, May 29-June 2, 2011
PHONONICS-2011-0168

Strain Based Tuning of Ring Resonators via Hydrostatic Pressure Actuation of Membranes

Andrew Ian Young[1] , Peter T. Rakich[2], Zayd Leseman[1]

[1] *Mechanical Engineering, University of New Mexico, Address, Country,*
zleseman@unm.edu
[2] *Sandia National Laboratories*
ptrakic@sandia.gov

Abstract: In this poster, we propose a strain based tuning method of ring resonators based via pressure gradients based on a device composed of a ring resonator structure cantered on a membrane. By applying a pressure to the membrane, one can tune the resonator to a specific desired resonance that is otherwise difficult to obtain due to manufacturing defects and temperature variation in the environment.

In this poster, we discuss the development of a novel type of micromechanically tunable ring resonator, whose frequency can be swept over ultra-large fractional bandwidths by varying the hydrostatic gas pressure applied to a membrane suspended microring resonator. Variation of the hydrostatic pressure exerted on the membrane causes the membrane to deform, straining the waveguides and resulting in significant resonance frequency tuning due to both waveguide boundary deformation and photoelastically induced refractive index changes. Such tuning mechanisms are unique as they enable frequency tuning to compensate for manufacturing defects and temperature variation in the environment, enabling the resonator to be tuned to a specific wavelength that would otherwise be difficult to obtain due to aforementioned effects, and do not inherently require temperature tuning or steady-state power dissipation.

Phononics 2011: First International Conference on Phononic Crystals, Metamaterials and Optomechanics

Santa Fe, New Mexico, USA, May 29-June 2, 2011

PHONONICS-2011-0168

Phononics 2011: First International Conference on Phononic Crystals, Metamaterials and Optomechanics
Santa Fe, New Mexico, USA, May 29-June 2, 2011
PHONONICS-2011-0170

Analysis of Optomechanical Forces in Nano-Photonic Waveguides

Charles M. Reinke[1], Rohan Kekatpure[1], Ryan Camacho[1], Ihab El-Kady[1], Peter T. Rakich[1]

[1] *Photonic Microsystems Technologies, Sandia National Laboratories, Albuquerque, NM 87123, USA*
cmreink@sandia.gov

Abstract: We present a theoretical analysis of optomechanical forces in nano-scale photonic waveguides. In particular, we show that significant forces due to radiation pressure can be generated in dielectric slab and photonic crystal waveguides having sub-micron dimensions. We also investigate how such forces can be optimized for optomechanical transduction.

Optomechanical forces created by radiation pressure have been studied extensively in the context of optical traps and tweezers. The interaction of photons and phonons has also been observed in nano-scale devices, where high-Q cavities are used to enhance the forces generated by the optical fields [1]. However, the optomechanical forces generated in nano-photonic travelling-wave systems have largely been neglected in literature. In addition, the common technique for calculating optical forces in such structures involves a numerical Maxwell stress tensor (MST) computation, which requires knowledge of the full electromagnetic field distribution in the computational domain surrounding the structure.

In this work, we calculate the expected optically induced forces in an ordinary dielectric slab waveguide due to radiation pressure analytically using the response theory of optical forces (RTOF) [2]. The prediction that the resulting forces are confined to the boundaries of the waveguide where there is a discontinuity in refractive index is confirmed, and values of the force density agree well between the analytical approach using RTOF and using the brute-force method (i.e., MST). It is shown through a scaling-law argument that the optical forces are directly related to the group index of the waveguide. Thus, the optomechanical forces in a photonic crystal (PhC) waveguide, which can exhibit anomalous dispersion and hence large group index values in the "slow-light" regime, were calculated using the same formalisms. We show that the distribution of forces due to radiation pressure is again isolated to the regions of discontinuous refractive index, in this case at the boundaries of the air holes, as shown in Figure 1.

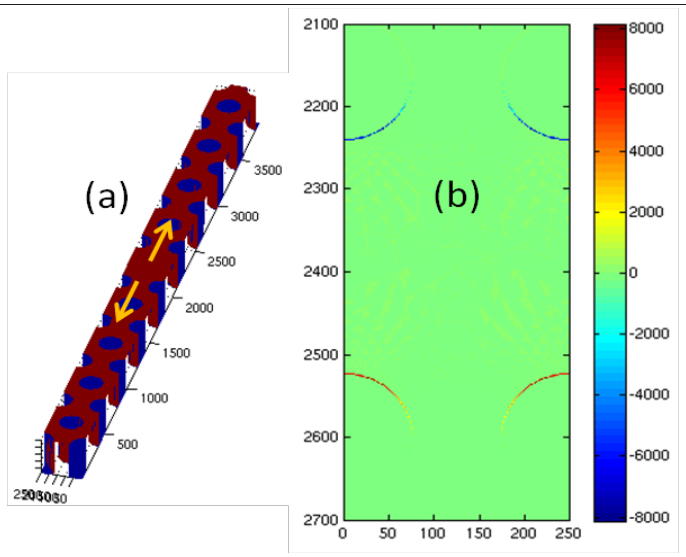

Figure 1 (a) Schematic showing the unit cell of a PhC waveguide; yellow arrows indicate the mean direction of the optical forces due to radiation pressure. **(b)** Plot of the optical forces in the region of the air holes closest to the guiding region of the PhC waveguide.

To extend the generality of these results, scaling-law theory is used to examine the dependence of optical forces from radiation pressure on the topological parameters of the PhC waveguide. Using this theory, we can relate the dispersion of the waveguide to its dimensions as

$$n_g - n_{eff} = \frac{\partial n_{eff}}{\partial w} w + \frac{\partial n_{eff}}{\partial a} a + \frac{\partial n_{eff}}{\partial r} r \qquad (1)$$

where n_g is the group index of the waveguide, n_{eff} is the effective index, w is the hole edge to hole edge width, a is the lattice constant of the PhC, and r is the radius of the air holes. In particular, a trend for the ideal thickness of the PhC waveguide for optimal optomechanical forces can be found and related to the dispersion of the waveguide.

Phononics 2011: First International Conference on Phononic Crystals, Metamaterials and Optomechanics
Santa Fe, New Mexico, USA, May 29-June 2, 2011
PHONONICS-2011-0170

Our technique outlines a generalized method for optimizing optomechanical forces due to radiation pressure in nano-photonic waveguides using analytical expressions that avoid full-wave electromagnetic calculations. We demonstrate that optical forces in such systems are optimized in highly dispersive waveguides that exhibit large values of group refractive index. Finally, we show how the geometrical parameters of a PhC waveguide can be related to the optical forces due to radiation pressure in a straightforward analytical manner, enabling an intuitive approach to engineering larget optical forces in nano-photonic systems.

Sandia National Laboratories is a multi-program laboratory managed and operated by Sandia Corporation, a wholly owned subsidiary of Lockheed Martin Corporation, for the U.S. Department of Energy's National Nuclear Security Administration under contract DE-AC04-94AL85000.

References

[1] M. Eichenfield, R. Camacho, J. Chan, K. J. Vahala, and O. Painter, *Nature* **459**, 550 (2009).
[2] P. T. Rakich, M. A. Popovic, and Z. Wang, *Opt. Express* **17**, 18116 (2009).

Phononics 2011: First International Conference on Phononic Crystals, Metamaterials and Optomechanics
Santa Fe, New Mexico, USA, May 29-June 2, 2011
PHONONICS-2011-0178

Cooling of a Micromechanical Oscillator into the Quantum Regime

R. Riviere[2], S. Deleglise[1,2] S. Weis[1,2], E. Verhagen[1] 1 E. Gavartin[1], A. Schliesser[1,2], T. J. Kippenberg[1,2]
[1]*Swiss Federal Institute of Technology (EPFL), CH1015 Lausanne, Switzerland*
[2]*Max-Planck-Instiut für Quantenoptik, 85748 Garching, Germany*

Abstract: Using optical sideband cooling, a micromechanical oscillator is cooled to a phonon occupancy below 10 phonons, corresponding to a probability of finding it in its quantum ground state more than 10% of the time.

The control of low-entropy quantum states of a micro-oscillator could not only allow researchers to probe quantum mechanical phenomena—such as entanglement and decoherence—at an unprecedentedly large scale, but also enable their use as interfaces in hybrid quantum systems. Preparing and probing an oscillator in the conceptually simplest low-entropy state, its quantum ground state, has now become a major goal in Cavity Optomechanics[1]. However, to experimentally achieve this goal, two challenges have to be met: its effective temperature T has to be reduced sufficiently so that $\hbar\Omega_m > k_B T$ ($\hbar$ is the reduced Planck constant, k_B the Boltzman constant, and Ω_m the mechanical resonance frequency). Second, quantum-limited measurements of the oscillator's displacement must be performed at the level of the zero-point displacement fluctuations $x_{zpf} = \sqrt{\hbar/2m\Omega_m}$. Using conventional cryogenic refrigeration, a nanomechanical oscillator has recently been cooled to the quantum regime and probed by a superconducting qubit to which it was coupled through its specific piezoelectric properties[2].

Here, we demonstrate a different technique, applying optical sideband cooling[3] to a cryogenically precooled silica toroidal optomechanical micoresonator (Fig. 1). This versatile technique, conceptually similar to laser cooling techniques known in atomic physics, can be applied to a wide range of opto- and electromechanical systems which exhibit parametric coupling of high-quality electromagnetic and mechanical modes.

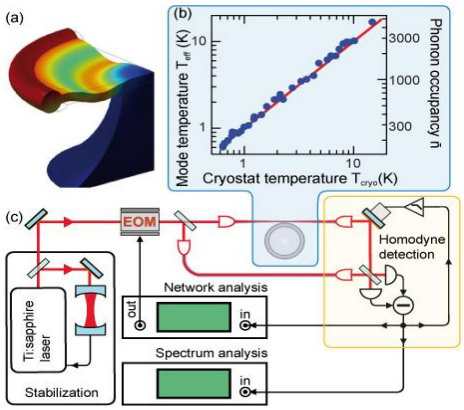

Figure 1 Cooling a micromechanical oscillator. (a) High-Q mechanical and optical modes are co-located in a silica mi- crotoroid, and are mutually coupled by radiation pressure exerted by the mechanical mode. (b) Thermalization of the mechanical mode to the temperature of the 3He gas in the cryostat down to an occupancy of 200 quanta. (c) Optical setup used for displacement monitoring of the mechanical mode, based on homodyne analysis of the light re-emerging from the optical resonance.

With a resonance frequency of $\Omega_m/2\pi$=72 MHz of the mechanical radial breathing mode (RBM), and an optical linewidth of $\kappa/2\pi$=6 MHz, the used toroidal resonator resides deeply in the resolved sideband regime, as required for ground-state cooling[4]. Thermalizing the resonator to a 850-mK cold ^{3}He buffer gas, the RBM is already cooled to an occupation of 190 quanta as determined by noise thermometry (Fig. 1). A low-noise cooling laser (λ~780 nm) is

Phononics 2011: First International Conference on Phononic Crystals, Metamaterials and Optomechanics
Santa Fe, New Mexico, USA, May 29-June 2, 2011
PHONONICS-2011-0178

subsequently coupled to a whispering gallery mode (WGM) using a tapered fiber. Figure 2 shows the optically measured mechanical resonance frequency and damping when the detuning Δ of the cooling laser is tuned through the lower mechanical sideband of the (split) optical WGM at a power of 2 mW[5]. The strong modification of the oscillator's properties can be modeled with the well-understood radiation pressure-induced dynamical backaction. This allows extracting the additional mechanical damping due to defects in the glass described as an ensemble of two-level systems (TLS)[6]. Its strong temperature dependence enables an independent determination of the toroids' temperature, which can be compared to the noise temperature of the mechanical mode (Fig. 2c). We find excellent agreement between the two methods. At a higher cooling laser power (4 mW) both methods congruently yield a minimum occupation below 10 quanta, corresponding to a >10% probability to find the oscillator in its quantum ground state.

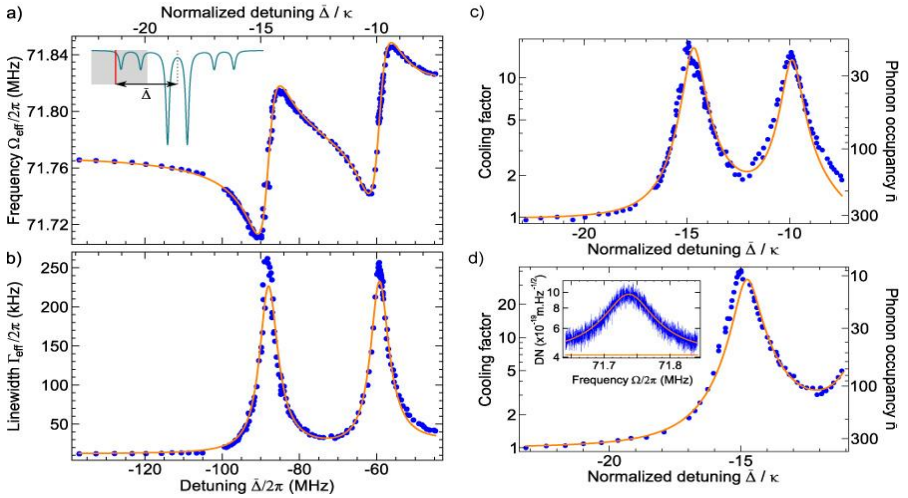

Figure 2 Cooling results. Resonance frequency (a) and linewidth (b) of the RBM when a 2 mW-power cooling laser is tuned through the lower mechanical sideband of the split optical mode (inset). Blue points are measured data extracted from the recorded spectra of thermally induced mechanical displacement fluctuations, solid lines are a coupled fit based on dynamical backaction and TLS-induced effects. c) Cooling factor (temperature reduction induced by sideband cooling) and phonon occupation of the RBM as a function of normalized detuning as determined by noise thermometry (points) and from a dynamical backaction model, taking into account possible optical heating of the structure and TLS-induced effects.

Further optimization of the silica toroids for stronger optomechanical coupling and lower dissipation can enable cooling the resonator deeper into quantum regime. It furthermore appears realistic to achieve the regime of strong coupling[7] while the resonator is in a low-entropy state. This constitutes an important step towards the coherent manipulation of the quantum state of the mechanical oscillator.

References

[1] T. J. Kippenberg, K. J. Vahala, *Science*, **321**, 1172-1176 (2008)
[2] A. D. O'Connell *et al., Nature*, **464**, 697-703 (2010)
[3] A. Schliesser, R. Rivièrere, G. Anetsberger, O. Arcizet, T. J. Kippenberg, *Nature Physics,* **4**, 417-419 (2008)
[4] I. Wilson-Rae, N. Nooshi, W. Zwerger, T. J. Kippenberg, *Phys. Rev. Lett*. **99**, 093901 (2007)
[5] R. Rivière, S. Deléglise, S.Weis, E. Gavartin, O. Arcizet, A. Schliesser, T. J. Kippenberg, "Optomechanical sideband cooling of a micromechanical oscillator close to the quantum ground state," *submitted*. Preprint at arXiv:1011.0290
[6] O. Arcizet, R. and Rivière, A. Schliesser, G. Anetsberger, T. J. Kippenberg, *Phys. Rev. A*, **80,** 021803(R) (2009)
[7] S. Gröblacher, K. Hammerer, M .R. Vanner, M. Aspelmeyer, *Nature*, **460**, 724-727 (2009)

Phononics 2011: First International Conference on Phononic Crystals, Metamaterials and Optomechanics

Santa Fe, New Mexico, USA, May 29-June 2, 2011

PHONONICS-2011-0180

Optomechanical Crystals

Oskar Painter[1]

[1] *Thomas J. Watson, Sr., Laboratory of Applied Physics, California Institute of Technology, Pasadena CA 91125 USA*
opainter@caltech.edu

Abstract: In the last several years, rapid advances have been made in the field of cavity optomechanics, in which the usually feeble radiation pressure force of light is used to manipulate (and precisely monitor) mechanical motion. In this talk I will describe these advances, and discuss our own work to realize radiation pressure within nanoscale structures in the form of photonic and phononic crystals.

In the last several years, rapid advances have been made in the field of cavity optomechanics, in which the usually feeble radiation pressure force of light is used to manipulate (and precisely monitor) mechanical motion. These advances have moved the field from the multi-km interferometer of a gravitational wave observatory, to the optical table top, and now all the way down to a silicon microchip. In this talk I will describe these advances, and discuss our own work to realize radiation pressure within nanoscale structures in the form of photonic and phononic crystals (dubbed optomechanical crystals). Applications of these new nano-opto-mechanical systems include: all-optically tunable photonics, optically powered RF and microwave oscillators, and precision force/acceleration and mass sensing. Additionally there is the potential for these nanomechanical systems to be used in hybrid quantum networks, enabling storage or transfer of quantum information between disparate quantum systems. I will introduce several conceptual ideas regarding phonon-photon translation and slow light effects which may be used in such quantum settings, and discuss recent experiments to realize them in practice.

Phononics 2011: First International Conference on Phononic Crystals, Metamaterials and Optomechanics

Santa Fe, New Mexico, USA, May 29-June 2, 2011

PHONONICS-2011-0180

Phononics 2011: First International Conference on Phononic Crystals, Metamaterials and Optomechanics

Santa Fe, New Mexico, USA, May 29-June 2, 2011

PHONONICS-2011-0181

Mechanical Whispering-Gallery Modes

Tal Carmon, Gaurav Bahl, and Matthew Tomes

Electrical Engineering and Computer Science, University of Michigan, Ann Arbor, Michigan, 48109, USA

tcarmon@umich.edu

Abstract: We experimentally excite mechanical Whispering-Gallery resonances that are vibrating from 50 MHz to 12 GHz rates.

Just like their optical parallel, mechanical whispering-gallery modes can offer low-loss resonances in devices from mm[1] to micron[2] in scale. The fact that the modes are propagating azimuthally, orthogonal to the radial direction where they can leak through the support, suggests a nearly material limited mechanical Q.

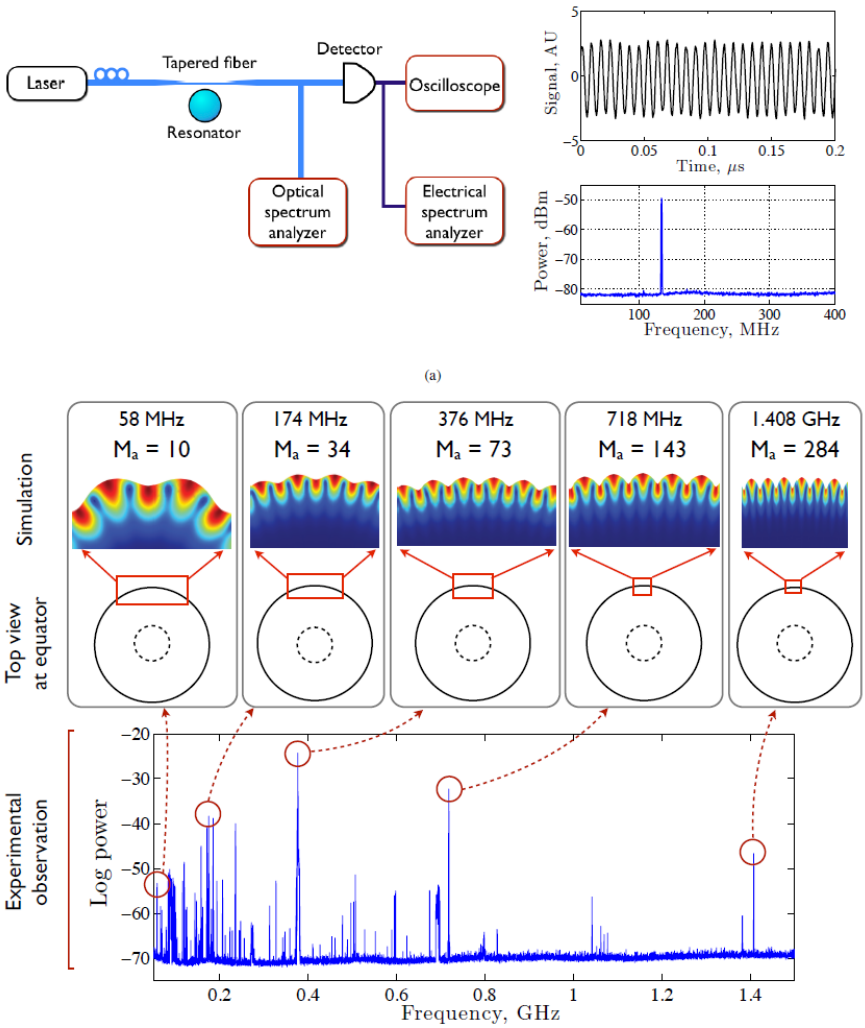

Figure 1: Experimental setup of excitation of mechanical whispering gallery modes followed by experimental observation and theoretical calculation of such modes.

Figure 1 shows the experimental setup for excitation of such modes, followed by their experimental observation and by the corresponding calculated natural vibration modes.

Phononics 2011: First International Conference on Phononic Crystals, Metamaterials and Optomechanics

Santa Fe, New Mexico, USA, May 29-June 2, 2011

PHONONICS-2011-0181

[1] Grudinin, I., Matsko, A. & Maleki, L. Brillouin Lasing with a CaF_ {2} Whispering Gallery Mode Resonator. *Physical Review Letters* **102**, 43902 (2009).

[2] Tomes, M. & Carmon, T. Photonic micro-electromechanical systems vibrating at X-band (11-GHz) rates. *Physical Review Letters* **102**, 113601 (2009).

1ST INTERNATIONAL CONFERENCE ON PHONONIC CRYSTALS, METAMATERIALS & OPTOMECHANICS

Extended Abstracts

Track 6: Fabrication and Characterization for Phononics

Phononics 2011: First International Conference on Phononic Crystals, Metamaterials and Optomechanics
Santa Fe, New Mexico, USA, May 29-June 2, 2011
PHONONICS-2011-0038

Nanoscale Tip Fabrication for Plasmon Induced Field-Enhancement

Won S. Chang[1] , Sung-H. Cho[1]

[1] *Nano Convergence and Manufacturing Systems Research Division, KIMM, 171 Jang-dong Yuseong-gu Daejeon, 305-343, South Korea,*
paul@kimm.re.kr, shcho@kimm.re.kr

Abstract: Nanoscale tip is designed for enhancement of optical resolution of near-field scanning optical microscopy (NSOM). To fabricate a tip-on-aperture NSOM probe, a tip is generated at the end of the probe. Focused ion beam (FIB) process is applied to the process to make an aperture and a tip, so the aperture and the tip are generated at the same time. With this process, possibilities tofabricate tip-on-aperture probes with various tips were shown.

The resolution of commercial optical system is limited to about the wavelength of incident light by the refraction limit. However, a resolution beyond the diffraction limit can be achieved at near-field. Near-field scanning optical microscope (NSOM) is a kind of scanning probe microscope; it can realize a sub-wavelength scale resolution. In NSOM, light is illuminated through an aperture smaller than the wavelength of incident light, and then the small aperture is used as an excitation source. The resolution of the NSOM is determined by the size of the aperture; to achieve a higher resolution, a smaller aperture is required. However, when the diameter of an aperture is smaller than the wavelength of the incident light, the transmission efficiency is proportional to the sixth power of the diameter of the aperture. Thus, a smaller aperture greatly reduces the transmission efficiency. To obtain a sufficiently strong signal from a small aperture, high-intensity light is needed[1]. However, high-intensity light can damage the metal layer of the probe. The typical resolution of aperture NSOM is about 50 nm – 100 nm. In this work, the shape of a NSOM probe was modified using the resolution of numerical analysis based on a finite-difference time-domain (FDTD) algorithm. This probe has a narrow slit or small tip on its aperture. Especially in the near-field area, the electric field intensity distribution is heavily dependent on the polarization of incident light. In the plane of polarization, the electric field intensity of the NSOM aperture probe is strongly enhanced at the edge of the aperture. Simulation results show that this enhancement can be totally or partially removed according to the size of the slit, if the slit carved on the probe is aligned with the polarization direction of the incident light. When a long slit is carved on the probe (slit-on-aperture probe), the electric field intensity of the NSOM aperture probe in the plane of polarization shows a Gaussian distribution because the points of enhanced electric field intensity are totally removed. However, when a short slit is carved on the probe, the point of enhanced electric field intensity is removed at one edge of the aperture, and consequently the electric field intensity is enhanced only at the other edge. Moreover, when a tip is put on the probe (tip-on-aperture probe), the electric field intensity is enhanced only near the tip. This means that a higher intensity electric field can be obtained on the surface to be processed in an area smaller than the aperture size.
The tip of a tip-on-aperture (TOA) probe is illuminated through an aperture at the near-field of the probe and electromagnetic interaction between the structure sharp tip at the end of the probe and the surface is used for measurements and materials processing. A novel TOA probe is described, which has a polygonal cross-sectioned tip that can make the strong and local enhancement of electromagnetic field[3,4]. A right triangular pillar was selected as optimal shape of the tip among the several polygonal pillars. The electromagnetic energy distributions at the near-field of the probe and of a typical TOA probe (with circular tip) were calculated numerically, and the results were analyzed. The results show that a TOA probe with a triangle tip confines electromagnetic energy within the smaller area than a typical tip-on-aperture probe, and has 6.7 times the maximum intensity. Moreover, the electric field distributions at the near-field of a TOA probe were calculated numerically to analyze the effects of polarization direction on the characteristics of measurement and processing. A TOA probe is asymmetric for the axis, since it has a probe at metal coated layer on the aperture. The geometrical relationship between this asymmetric shape and polarization direction is the reason for the change of the electromagnetic energy distributions. Numerical analysis shows that a TOA probe can make the best use of the tip for high resolutions when the tip is located on the parallel axis with the polarization

Phononics 2011: First International Conference on Phononic Crystals, Metamaterials and Optomechanics
Santa Fe, New Mexico, USA, May 29-June 2, 2011
PHONONICS-2011-0038

direction. After analyzing the trend in the magnitude of the electric field, it was proposed that a localized, enhanced field at the tip apex was caused by the local electric field at the aperture and surface plasmons excited and propagating on the outer surface of the probe.
An NSOM probe is a tinned, metal coated optical fiber with an aperture. To fabricate a TOA NSOM probe, a tip is generated at the end of the probe. FIB processing is applied to the process to make an aperture and a tip, so the aperture and the tip are generated at the same time. With this process, possibilities to fabricate TOA probes with various tips and were shown. And resolution enhancement for optical measurement and patterning was verified using the TOA probe fabricated in this study.

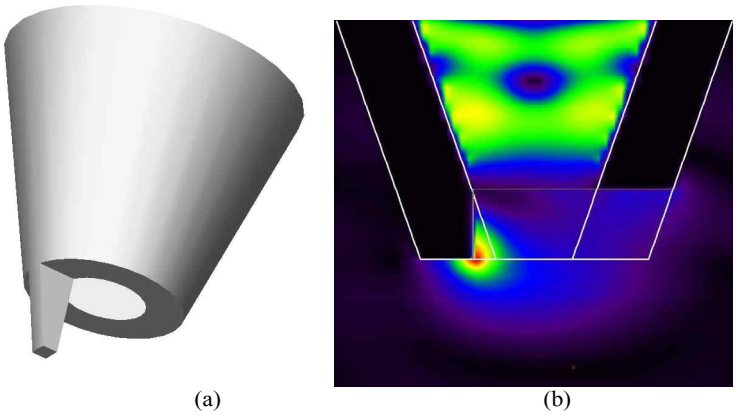

(a) (b)

Figure 1 (a) Three-dimensional modeling of nanoscale tip on NSOM probe and (b) FDTD analysis of electric field distribution on TOA probe

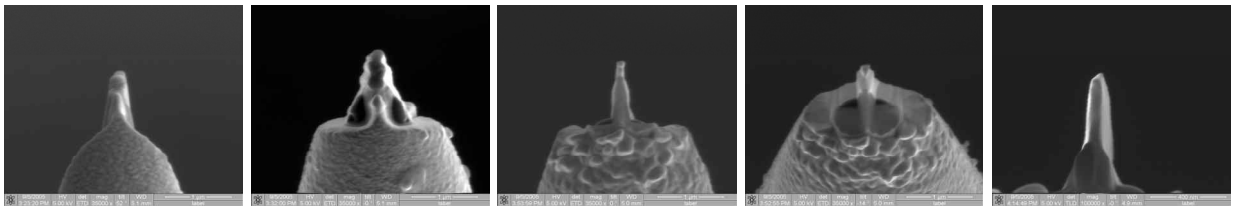

Figure 2 FIB machined TOA probe on fiber NSOM probe

References

[1] M. Stähelin, M. A. Bopp, G.. Tarrach, A. J. Meixner, and I. Zschokke-Gränacher: *Appl. Phys. Lett*. **68** 2603 (1996).
[2] T. Matsumoto, T. Ichimura, T. Yatsui, M. Kourohi, T. Saiki, and M. Ohtsu: *Opt. Rev*. **5** 369 (1998).
[3] H. G. Frey, F. Keilmann, A. Kriele, and R. Guckenberger: *Appl. Phys. Lett.* **81** 5030 (2002).

Phononics 2011: First International Conference on Phononic Crystals, Metamaterials and Optomechanics
Santa Fe, New Mexico, USA, May 29-June 2, 2011
PHONONICS-2011-0075

Larger Scale Fabrication of Nanometer to Micron Sized Periodic Structures in 2D and 3D: Approaches and Trends

Gregory R. Bogart[1]

[1] *Sandia National Laboratories, P.O. Box 5800 MS1080, Albuquerque, NM, USA*
grbogar@sandia.gov

Fabrication of periodic structures for photonic or phononic wavelength interaction and manipulation at the small scale (<100um x 100 um) in planar dimensions using a variety of materials and techniques has been documented in the literature. Often structures are conceived and built with only a single device needing to be made. Some applications require that structures be fabricated in three dimensions or with multiple layers placing additional constraints on the fabricator. If a structure proves to be useful and a demand to have it appears, the researcher is often asked, "Can you make more of it?" The challenge to manufacture larger, better structures, and more of them is not new in the history of product innovation and manufacture. However, the combination of requirements for accurate microscopic dimensional control over large spatial scale needed to make useful devices requires both out of the box thinking to manufacture them and familiarity and the ability to adapt tried and true scaling techniques.

Human ingenuity and desire for efficiency has used the "stamp" for thousands of years to impart a repeated pattern into materials that served, speed, ease of use, and functionality requirements. Signet rings or "seals" were used with waxes or inks to authenticate the earliest hand written documents and are still in use today. (1) The method of placing multiple patterns or individual stamps next to each other surfaced in China in the early 11th century (2). Combining the patterns with a proper substrate material (paper) made communication easier and faster. Researchers in photonic crystal fabrication have leveraged the established stamping technique to deliver fabrication of large area 3D photonic crystal designs. Instead of clay tablets, engineered siloxanes have allowed for durable and re-usable stamps that are able to replicate the molded features at the nanometer scale. The stamping technique can be enhanced by combining with well established optical principles to generate three dimensional periodic structures. Further leveraging sophisticated modeling, semiconductor processes and engineered materials enables fabrication of large area, three dimensional periodic structures with submicron features. Figure 1a is a photograph of a large area silicone based stamp used to imprint phase masks into the surface of photo resists. Figure 1b is a photograph showing the diffraction pattern created by the phase mask using collimated light (3).

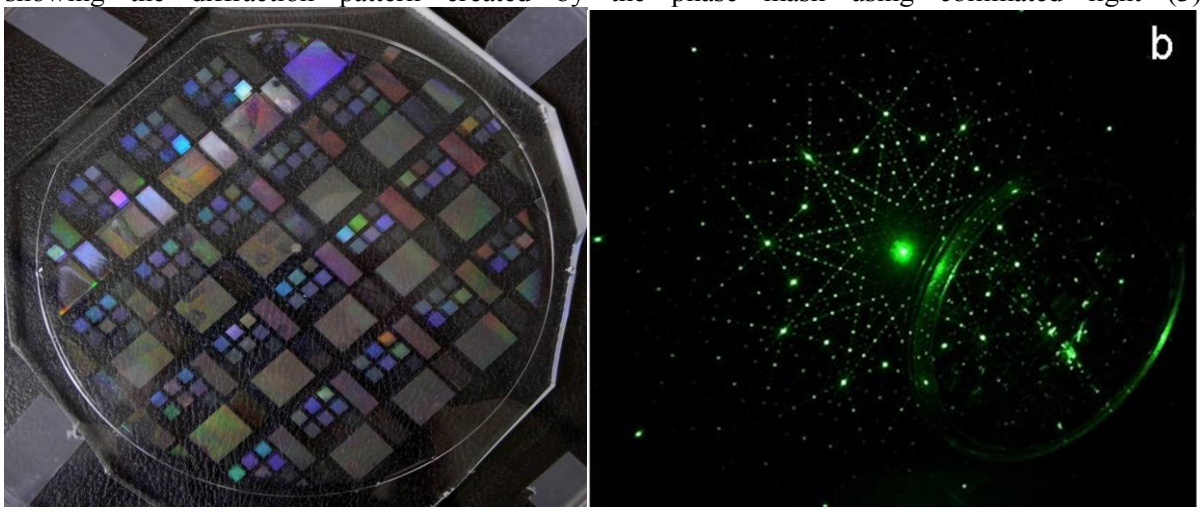

Figure 1. a.) 150mm diameter stamp master for proximity nano patterning of quasi crystal pattern. b.) diffraction pattern generated using an engineered phase mask.

Phononics 2011: First International Conference on Phononic Crystals, Metamaterials and Optomechanics
Santa Fe, New Mexico, USA, May 29-June 2, 2011
PHONONICS-2011-0075

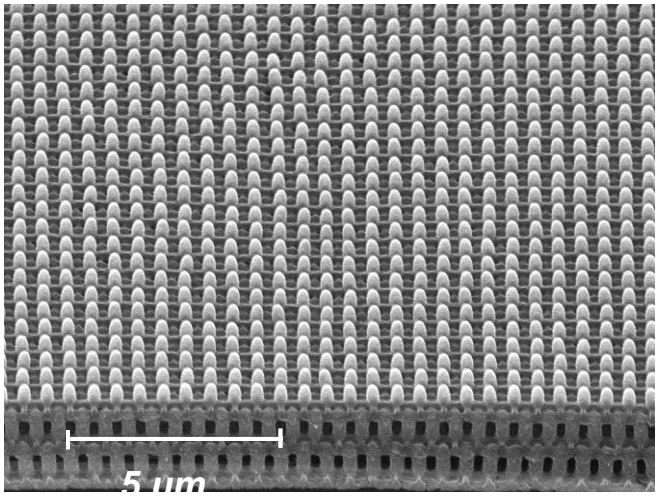

Figure 2. Cross section SEM of a resist structure generated with a stamped phase mask on the surface of the resist.

Collimated light used for exposure combined with the surface relief generated by the stamp creates constructive and destructive interference patterns in three dimensions. Figure 2 contains a cross sectional scanning electron micrograph of exposed and developed photoresist using an optical phase mask generated with a stamped surface and optical interference. Note the periodic nature in all three dimensions.

Many materials that are suitable for optoelectronics and CMOS device manufacturing are also finding uses in the phononics area. Lithium niobate has been used extensively in optoelectronic fabrication due to its desirable optical properties. It is particularly challenging to process using conventional CMOS process techniques as it is both pyroelectric and piezoelectric. Processing limitations can impact the usefulness and implementation of these materials.

Large scale fabrication of these types nanometer sized periodic structures requires an integrated approach. In this presentation I will review other scaling approaches to making large area phononic or photonic crystals in 2D and 3D such as direct write and self assembly. In addition, I will touch on the necessary infrastructure required to develop these techniques including modeling, design, and material considerations appropriate for the various methods. Lastly, I will discuss future trends of the technology.

References: 1.) Kipfer, B. A. , Encylcopedic Dictionary of Archaeology. Springer, 2000 (501)

2.) Day, L., McNeil I.; Biographical Dictionary of the History of Technology. Taylor and Francis, 1998 (123)

3.) Shir, D.J, et al. ; Tharee-Dimensiional Nanofabrication with Elastomeric Phase Masks, Journal of Physical Chemistry B 111, 12945-12958 (2007)

Sandia is a multiprogram laboratory operated by Sandia Corporation, a Lockheed Martin Company, for the United States Department of Energy under contract DE-AC04-94AL85000.

Phononics 2011: First International Conference on Phononic Crystals, Metamaterials and Optomechanics
Santa Fe, New Mexico, USA, May 29-June 2, 2011
PHONONICS-2011-0105

Microfabricated GHz Phononic Band Gap Structures

Gianluca Piazza, Nai-Kuei Kuo

Department of Electrical and Systems Engineering, University of Pennsylvania, Philadelphia, PA, 19104, USA
piazza@seas.upenn.edu, kuo1@seas.upenn.edu

Abstract: This paper reports the latest development on the synthesis of phononic band gaps (PBG) in AlN/Air and SiC/Air structures operating in the GHz range by means of inverted cylindrical geometries or fractal-based designs. Finite element methods used to design and confirm the PBG dispersion curve and amplitude-frequency response are also presented.

Microscale phononic crystals (PC) have emerged as a new class of devices that can be employed to understand and engineer the fundamental properties of low loss acoustic materials at the nanoscale, demonstrate novel acoustic functionalities such as tunneling, waveguiding and multiplexing and synthesize miniaturized and low loss radio frequency (RF) signal processors that are not attainable with state-of-the-art micro/nano mechanical (M/NEMS) resonators. Since the introduction of PCs in 1998, PC-based devices such as wave guides, filters and structures for acoustic focusing have been demonstrated, but are all limited in operating frequencies below 1 MHz due to their fabrication by means of hand-assembly. Recently, via microfabrication techniques, substantial progress has been made in extending PC structures in the very and ultra high frequency (VHF and UHF) range [1-3]. The extension of the frequency range of these PC-based devices makes them amenable to applications in RF communications.

Within PCs, Phononic Band Gaps (PBG) are the most important building blocks. PBG structures form frequency ranges in which the propagation of specific elastic waves is prohibited by the size, periodicity and arrangement of a unit cell. Most of the micromachined PC demonstrations to date have been either limited to low MHz frequencies when using air/solid configurations, or have used complex manufacturing processes relying on several refill and planarization steps when pushed close to 1 GHz.

To synthesize PBGs that can be easily microfabricated and integrated with electro-acoustic transducers, we have designed and experimentally demonstrated new classes of PCs that rely on alternating in two dimensions (2D) regions of high acoustic velocity and low loss materials such as aluminum nitride, or silicon carbide with air (low acoustic velocity material) (Fig. 1-3). Unit cell geometries in the form of a cylinder supported by four tethers (inverted configuration with respect to the conventional cylindrical air hole) (Fig. 1), an X-shape (Fig. 2) or a fractal-based square design (Fig. 3) have been introduced to reduce the manufacturing constraints associated with either the film thickness or the lithographically defined in-plane dimensions, so that operation between 500 MHz and 1 GHz could be attained. The selection of AlN or SiC as the structural layer for the definition of the PBG unit cell was made to gain access to some of the highest acoustic velocity materials with low losses that are easily integrated with electro-acoustic AlN transducers.

The experimental results (Fig. 1-3) confirm the existence of the designed PBGs, show high rejection and match the theoretical analysis performed via COMSOL Finite Element Methods (FEM). Frequency dispersion response curves predicting the presence of full or longitudinal-wave-specific band gaps (Fig. 1-3) were obtained by 3D eigenfrequency analysis of the unit cell block on which periodic boundary conditions had been applied according to the Bloch theorem. Amplitude-frequency response curves (Fig. 2) that reproduce the experimentally-obtained transmission data were simulated in COMSOL FEM by performing a frequency sweep in the acoustic module and using perfectly matched layers at the edges of the PBG in order to accurately model acoustic adsorption. A single row of unit cells was modeled and periodic conditions in the 3rd direction were assumed.

The reported experimental and modeling efforts lay the foundations for the synthesis of GHz PC devices that will find practical applications in RF communication systems.

References

1. Olsson, R.H., III and I. El-Kady, *"Microfabricated phononic crystal devices and applications"*, Measurement Science & Technology, 2009, **20**(1), p. 012002 (13 pp.).
2. Mohammadi, S., et al., *"Evidence of large high frequency complete phononic band gaps in silicon phononic crystal plates"*, Applied Physics Letters, 2008, **92**(22), p. 221905-1.

Phononics 2011: First International Conference on Phononic Crystals, Metamaterials and Optomechanics
Santa Fe, New Mexico, USA, May 29-June 2, 2011
PHONONICS-2011-0105

3. Xinya, Z., et al., "*Evidence of surface acoustic wave band gaps in the phononic crystals created on thin plates",* Applied Physics Letters, 2006, **88**(4), p. 41911-1.

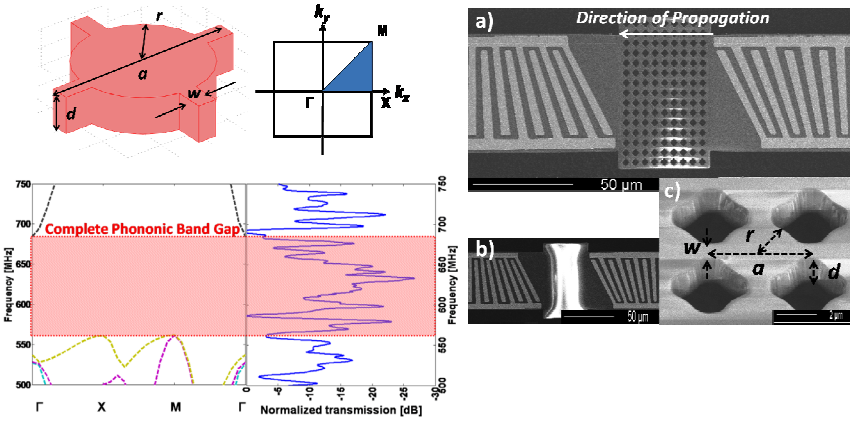

Figure 1: AlN/Air inverted cylinder PBG: (top-left) unit cell geometry and first symmetric Bruillon zone for square lattice; (right) SEM of PBG integrated with AlN electro-acoustic transducers; (bottom-left) dispersion curve and amplitude-frequency experimental response of this PBG.

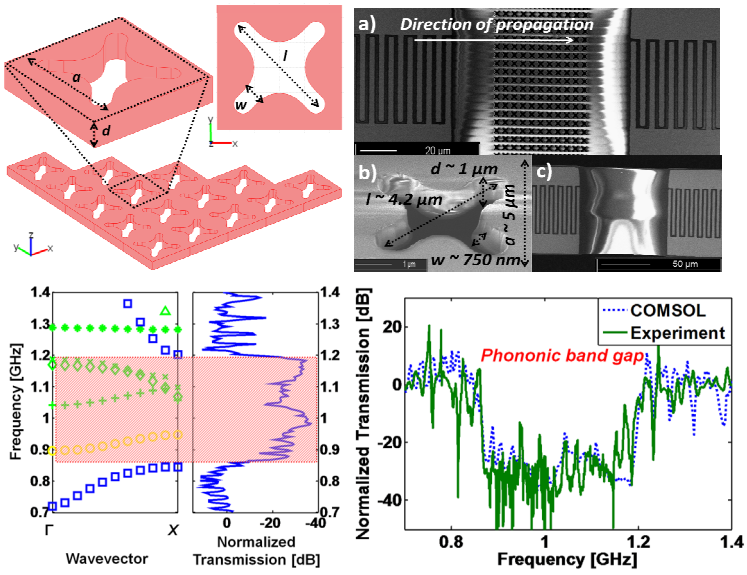

Figure 2: AlN/Air X-shaped PBG: (top-left) unit cell geometry and periodic arrangement; (top-right) SEM of PBG integrated with AlN electro-acoustic transducers; (bottom-left) dispersion curve and amplitude-frequency response obtained by COMSOL FEM for this PBG; (bottom-right) normalized experimental transmission response compared to COMSOL FEM analysis.

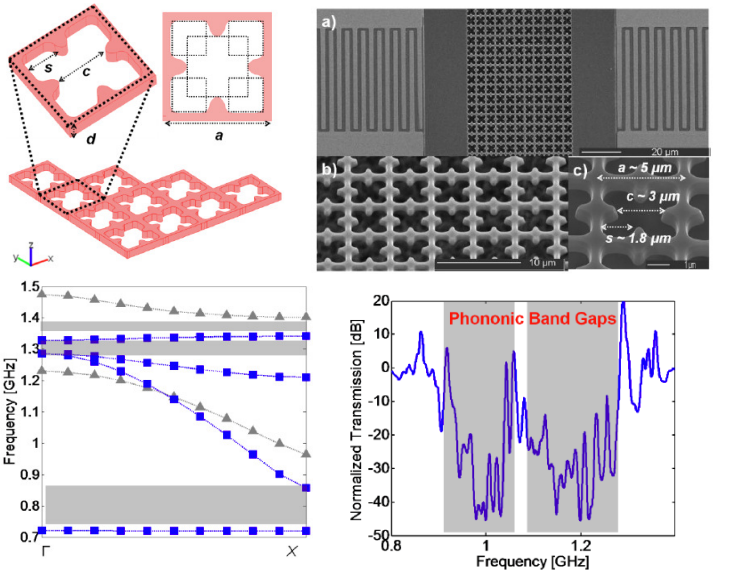

Figure 3: SiC/Air fractal-based PBG: (top-left) unit cell geometry and periodic arrangement; (top-right) SEM of PBG integrated with AlN electro-acoustic transducers; (bottom-left) dispersion curve obtained by COMSOL FEM for this PBG; (bottom-right) normalized experimental transmission response.

Phononics 2011: First International Conference on Phononic Crystals, Metamaterials and Optomechanics
Santa Fe, New Mexico, USA, May 29-June 2, 2011
PHONONICS-2011-0113

Thermal Conductivity Reduction in Lithographically Patterned Single Crystal Silicon Phononic Crystal Structures

Bongsang Kim[1], Janet Nguyen[1,2], Eric A Shaner[1], Ihab El-Kady[1], Roy H. Olsson III[1]

[1] *Department of Advanced MEMS, Sandia National Laboratories, NM, USA*
bonkim@sandia.gov, jhnguyen@sandia.gov, eashane@sandia.gov, ielkady@sandia.gov, rholsso@sandia.gov
[2] *Department of Electrical and Computer of Engineering, University of New Mexico, NM, USA*

Abstract: In-plane thermal conductivity of lithography-based phononic crystals has been investigated. Sub-micron holes were lithographically patterned in a 500nm-thick single crystal silicon thin-film and the thermal conductivity was measured as low as 30 W/mK (at and slightly above room temperature, 20~80°C), which is a 50% reduction even after accounting for the effect of volume reduction of the holes.

Thermal conductivities of many materials used in micro/nano-machining, such as silicon, have shown dramatic reduction in micro/nano-scale structures[1]. In such materials, the dominating heat transfer mechanism is through lattice vibration (phonons). Therefore, as the dimensions of thermal pathways become comparable to the phonon mean-free-path, phonon scattering increases, resulting in reduction in thermal conductivity. Recently, researchers have demonstrated successful control over thermal conductivity by patterning periodic nano-holes in a silicon membrane[2]. Despite such promising results, however, due to complexity of the fabrication processes and lack of effective integration methods, very few examples of application could be found among the demonstrated structures. Alternately, a much simpler way of phonon manipulation has been demonstrated with the recent advances in lithographic technologies. For example, phononic crystals were fabricated by lithographically defined sub-micron holes in a silicon layer to construct waveguides successfully achieving 30dB acoustic rejection at 67MHz for RF communication applications[3].

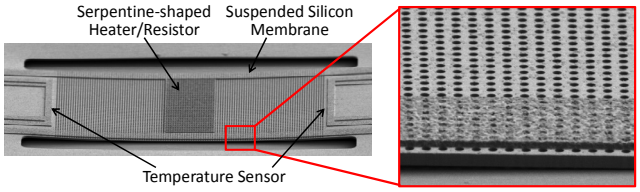

Figure 1 SEM image of a bridge-shaped test structure. Phononic crystals were formed by sub-micron diameter holes which were lithographically defined in a 500nm-thick single crystal silicon thin film.

In this work, we studied the effect of lithography-based phononic crystals on conductive heat transfer of single crystal silicon thin-film. Specifically, periodic sub-micron diameter through-holes were defined using a deep UV ASML scanner and patterned in a 500nm-thick silicon layer by plasma etching. To measure their in-plane thermal conductivity, a bridge-shaped test structure was designed as shown in Figure 1. A serpentine-shaped aluminum trace was placed in the middle and two temperature sensors were installed at the bridge edges. While heat is supplied to the aluminum trace at the center, the resistance change of each trace was measured to estimate the temperature increase. Temperature dependences of each trace resistance were separately calibrated by a heated chuck measurement. Figure 2 shows ANSYS finite element simulation and the equivalent thermal circuit model of the test structure. By using these models, the device thermal resistances and the thermal conductivity of the phononic crystal layers are calculated.

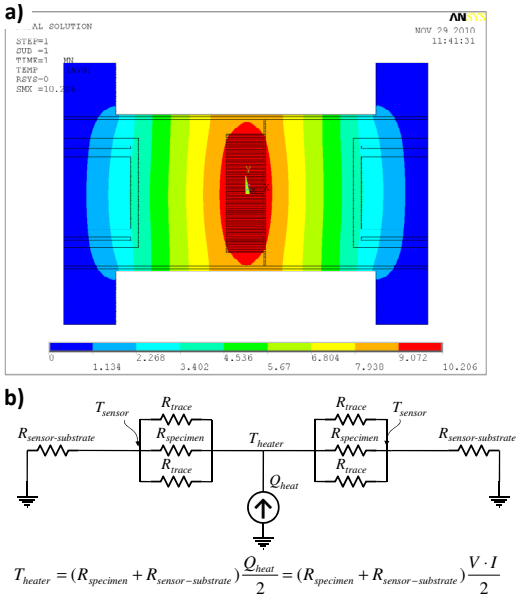

Figure 2 a) ANSYS finite element model and b) equivalent thermal circuit model of the test structure.

Phononics 2011: First International Conference on Phononic Crystals, Metamaterials and Optomechanics
Santa Fe, New Mexico, USA, May 29-June 2, 2011
PHONONICS-2011-0113

For each pitch-diameter combination a total of four samples were tested at and slightly above room temperature (20~80°C). The obtained thermal resistance, $R_{specimen}$, and thermal conductivity, $k_{measured}$, values from the measurement are summarized in Figure 3 and Table 1. The thermal conductivity of metric samples, which don't have any through holes, was measured as 97.8 W/mK, which is consistent with values from the literature[1]. In all measured samples, significant reductions in thermal conductivity could be observed. It is observed that the $k_{measured}$ values were much smaller than $k_{M\text{-}E}$, inferring the reduction in thermal conductivity is beyond the contribution from the volume reduction effect alone. ($k_{M\text{-}E}$ is the prediction of Maxwell-Eucken theory which models only the effect of volume reduction in porous materials[4].) The difference between the measured values and those predicted by the Maxwell-Eucken Model increases as the minimum feature size decreases, which is likely due to enhanced phonon scattering as the size of the thermal pathways shrink. Among tested samples, the device with 0.45um diameter holes with 0.70um pitch (limiting dimension is 0.25um) showed the highest reduction in thermal conductivity, i.e., $k_{measured}$ is 30W/mK which is only 30% of the metric sample's $k_{measured}$ and 50% of that predicted by the Maxwell-Eucken model, $k_{M\text{-}E.}$

This result indicates that material thermal conductivity can be effectively controlled via phonon-scattering enhancement from lithographically defined sub-micron features. The availability of such lithography-based phononic crystals has huge potential to open direct applications to many micromachined devices without much modification in the original fabrication process. For example, by reducing thermal conductivity with much less alteration in electrical conductivity, the use of lithographically patterned phonon manipulators will be able to significantly enhance the performance of micromachined thermoelectric coolers or energy harvesters.

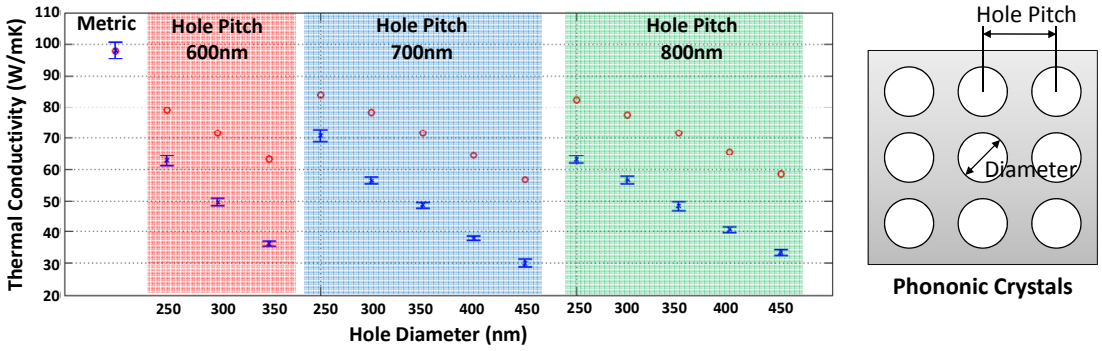

Figure 3 Measured thermal conductivities, $k_{measured}$ (blue error bars) and predicted thermal conductivities using Maxwell-Eucken Model, $k_{M\text{-}E}$ (red circles).

Pitch (nm)	1	0.6	0.6	0.6	0.7	0.7	0.7	0.7	0.7	0.8	0.8	0.8	0.8	0.8
Diameter (nm)	1	0.25	0.3	0.35	0.25	0.3	0.35	0.4	0.45	0.3	0.35	0.4	0.45	0.5
Porosity (%)	0	14	20	27	10	14	20	26	32	11	15	20	25	31
$R_{specimen}$ **(K/W)**	12247	18563	23046	30485	16640	20442	23490	29311	35862	18456	20408	23616	27519	32873
$k_{M\text{-}E}$ **(W/mK)**	97.8	79	71.5	63.2	83.8	78	71.5	64.4	56.8	82.4	77.3	71.5	65.4	58.8
$k_{measured}$ **(W/mK)**	97.8	62.7	49.5	36.2	70.6	56.5	48.5	37.8	30	63.1	56.6	48.2	40.6	33.2
$k_{measured}/k_{M\text{-}E}$ **(%)**	100	79	69	57	84	72	68	59	53	77	73	67	62	56

Table 1 Summary of measured thermal conductivities, $k_{measured}$, predicted thermal conductivities using Maxwell-Eucken Model, $k_{M\text{-}E}$, and their ratio for each sample.

References

[1] M. Asheghi, M. N. Touzelbaev, K. E. Goodson, Y. K. Leung, and S. S. Wong, *Journal of Heat Transfer* **120**, 30-36 (1998).
[2] J. Tang, H.-T. Wang, D. H. Lee, M. Fardy, Z. Huo, T. P. Russell, and P. Yang, *Nano Letters* **10**, 4279-4283 (2010).
[3] R. H. Olsson III, I. El-Kady, M. F. Su, M. R. Tuck, J. G. Fleming, *Sensors and Actuators A: Physical* **145-146**, 87-93 (2008).
[4] A. Eucken, *Forschung auf dem Gebiete des Ingenieurwesens*; VDIverlag g.m.b.h.: Dusseldorf, 1932, Ausgabe B, 3/4 VDI Forschungsheft 353.

Phononics 2011: First International Conference on Phononic Crystals, Metamaterials and Optomechanics
Santa Fe, New Mexico, USA, May 29-June 2, 2011
PHONONICS-2011-0122

Micromachined Phononic Band-Gap Crystals and Devices

Roy H. Olsson III[1], Bongsang Kim[1], Maryam Ziaei-Moayyed[1], Charles M. Reinke[1], Mehmet M. Su[2], Yasser M. Soliman[2], Zayd C. Leseman[2], Ihab El-Kady[1,2]

[1] Sandia National Laboratories, Albuquerque NM, USA
rholsso@sandia.gov, bonkim@sandia.gov, mziaeim@sandia.gov, cmreink@sandia.gov, ielkady@sandia.gov
[2] University of New Mexico, Albuquerque NM, USA
mfatihsu@ece.unm.edu, yasser.soliman@gmail.com, zleseman@unm.edu

Abstract: Micromachined phononic crystals are an emerging technology with applications in radio frequency communications, sensors and thermal energy harvesting. This paper presents work at Sandia National Laboratories in the realization of micromachined phononic crystal devices across a broad frequency range and in a number of material systems.

Phononic crystals are an emerging field poised to impact radio frequency (RF) communications[1], thermal management[2], acoustic imaging[1] and a number of other fields where phonon propagation and control leads to improved system performance. Over the past decade phononic crystals have been scaled from large hand assembled balls in acoustically lossy materials such as water and epoxy to micro and nano fabricated 2D structures realized in low loss materials operating at frequencies from 10 MHz to 10 GHz and beyond. Batch fabrication and the ability to co-integrate piezoelectric transducers with phononic crystals have lead to experimentation on a wide variety of geometries, materials and devices. The ability to suspend 2-D phononic crystals above the substrate using micromachining techniques has allowed for low loss phononic waveguides[1,3-4] and cavities[5-6] to be demonstrated. The wide range of materials available and the implications of finite membrane thickness require careful consideration when designing a phononic crystal for a specific application. Phononic crystals and devices have been studied theoretically and experimentally in numerous material systems including Si-air[2,4-5], SiC-air[6], AlN-air[7], Si-W[8] and SiO_2-W[3,9]. Phononic band gaps at GHz frequencies have been demonstrated in each of these material systems with complete phononic band-gap widths exceeding 10% of the center frequency and band gaps for longitudinal waves in excess of 50%. Solid-Solid phononic crystals based on tungsten inclusions in low impedance media have demonstrated less sensitivity to membrane thickness and lithography when compared to solid-air phononic crystals[10]. Certain devices, such as cavities, requiring very low material damping have been best realized in solid-air material systems using high-Q materials such as SiC. Recent results indicate that phononic crystals formed using both solid and air inclusions results in superior band-gap properties when compared to solid or air inclusions alone[9]. While much recent progress has been achieved in realizing micro and nano scale phononic crystals several challenges and opportunities are emerging including: the need for much wider bandwidth piezoelectric transducers for interrogating the phononic crystals, the ability to combine phononic and photonic crystals to increase phonon-photon interactions and for processing light signals in the acoustic regime and the introduction of non-linearity with phononic band-gap materials.

References

[1] R. H. Olsson III, and I. El-Kady, *Meas. Sci. Technol*. 20, 012002 (2009).
[2] P. E. Hopkins, C. M. Reinke, M. F. Su, R. H. Olsson, III, E. A. Shaner, Z. C. Leseman, J. R. Serrano, L. M. Phinney, and I. El-Kady, *Nano Lett.,* 11, (2011).
[3] R. H. Olsson-III, S. X. Griego, I. El-Kady, M. F. Su, Y. M. Soliman, D. F. Goettler, and Z. C. Leseman, IEEE Ultrasonics Symp., 1150-1153 (2009).
[4] S. Mohammadi, A. A. Eftekhar, W. D. Hunt, A. Adibi, IEEE Freq. Cntrl. Symp., 768-772 (2008).
[5] M. Ziaei-Moayyed, M. F. Su, C. M. Reinke, I. El-Kady, and R. H. Olsson III, IEEE Ultrasonics Symp., (2010).
[6] S. Mohammadi, A. A. Eftekhar, A. Khelif, H. Moubchir, W. D. Hunt, and A. Adibi, *Appl. Phys. Lett.*, **95**, 051906 (2009).
[7] N. Kuo, C. Zuo, and G. Piazza, *Appl. Phys. Lett.* **95**, 093501 (2009).
[8] Y. M. Soliman, M. F. Su, Z. C. Leseman, C. M. Reinke, I. El-Kady, and R. H. Olsson III, *Appl. Phys. Lett.* **97**, 193502 (2010).
[9] M. F. Su, R. H. Olsson III, Z. C. Leseman, and I. El-Kady, *Appl. Phys. Lett.* **96**, 053111 (2010).
[10] C. M. Reinke, M. F. Su, R. H. Olsson III, and I. El-Kady, *Appl. Phys. Lett.,* In-Press (2011).

Phononics 2011: First International Conference on Phononic Crystals, Metamaterials and Optomechanics
Santa Fe, New Mexico, USA, May 29-June 2, 2011
PHONONICS-2011-0122

Phononics 2011: First International Conference on Phononic Crystals, Metamaterials and Optomechanics
Santa Fe, New Mexico, USA, May 29-June 2, 2011
PHONONICS-2011-0125

Fabrication of 2-D Phononic Crystals via Focused Ion Beam

D. F. Goettler[1], M. F. Su[1], R. H. Olsson III[2], I. El-Kady[2], and Z. C. Leseman[1]

[1] *Mechanical Engineering, University of New Mexico, Albuquerque, NM USA 87131*
goettled@unm.edu, mfatihsu@unm.edu, and zleseman@unm.edu
[2] *Sandia National Laboratories, Albuquerque, NM USA 87105*
rholsso@sandia.gov and ielkady@sandia.gov

Abstract: A technique for the fabrication of 2-D Phononic Crystals (PnCs) is described that utilizes a focused ion beam (FIB) instrument. In particular, the details of the microfabrication procedure are discussed which creates the main structure from which the PnC is created. Following the microfabrication is the nanoFIBrication of the microstructure to create a PnC with nanoscale features. Results will be presented for the fabrication of a 33 GHz PnC.

In order to achieve PnCs that operate above 10 GHz nanofabrication techniques will need to be utlized. PnCs that manipulate phonons above even 1 GHz have shown a tremendous ability to alter the thermal conductivity of materials[1]. In order to achieve an operating frequency above 10 GHz the dimensions of the inclusions on the lattice points and their spacing need to be < 100 nm. We have recently utilized a FIB instrument to attain PnCs with these dimensions.

The following is a discussion on the method we have recently utilized to create a PnC that has a bandgap at 33 GHz. Fabrication is a two part process. First, the microstructure from which the PnC is created is fabricated by standard microfabrication procedures. Then the nanostructure of the PnC can be defined using the FIB via nanoFIBrication.

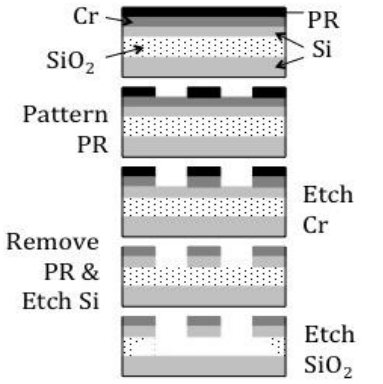

Figure 1: Fabrication process for creating a thin, freestanding membrane for 2-D PnC's

The scaffolding of the PnC is initially microfabricated using a silicon-on-insulator (SOI) wafer. Our group's studies show that thin membranes produce a bandgap that is unaltered by slab modes[2]. In particular, the thickness of the membrane from which the 2-D PnC is to be made must be less than the lattice spacing. The SOI is initially thinned down using alternating oxidations and HF etches. A protective layer of Cr is evaporated onto the SOI's device layer and then patterned. The BOX layer is then etched leaving a freestanding Si membrane on which the 2-D PnC will be defined. The full process is illustrated in Figure 1.

Using a FIB instrument we have been successful in creating a 33 GHz phononic crystal on the Si membrane. The PnC is composed of a Si matrix (the membrane) with W inclusions placed in a square array. The Si matrix was a freestanding membrane that was 100 nm thick and 10 x 10 μm area. Holes 30 nm in diameter were milled with the ion beam and subsequently backfilled with W using an e-beam deposition method.

Figure 2 shows details of the fabricated PnC. The leftmost image shows a 10 μm x 10 μm freely suspended membrane tethered on either side to the SOI device layer that is still anchored to the handle layer by the BOX layer which has not been released. In the center of the area is the patterned PnC. The upper right image is of a sample area which has had the same process performed on it as in the leftmost image. The Cr layer is still present in this image; its purpose is to protect the Si membrane from Ga ion implantation. Note that under the freestanding membrane are holes in the handle layer which correspond to the holes milled through the device layer. These holes serve as proof to full penetration of the device layer by the FIB. These thru holes are then backfilled with tungsten using a gas injection system (GIS) which introduces a precursor gas with W attached. When the precursor gas is exposed to an ion or electron beam W is deposited. An electron beam is directed in the center of the PnC inclusion holes and W is deposited to create a solid plug. Solid inclusion have been shown to create wider bandgaps in PnCs[3,4]. A cross section of the sample is shown in the lower right most image of Figure 2.

Phononics 2011: First International Conference on Phononic Crystals, Metamaterials and Optomechanics
Santa Fe, New Mexico, USA, May 29-June 2, 2011
PHONONICS-2011-0125

The operating frequency of 33 GHz was determined by simulation. Our group has developed several numerical tools for investigations of the behavior of PnCs[2,3,4]. These tools include the plane wave expansion (PWE) method, finite difference time domain (FDTD) method, and finite element analysis (FEA). Each method has its benefits and limitations. The PWE method allows us to determine bandgaps and density of states. While the FDTD and FEA methods allow us to determine bandgaps and vibrational modes. We find that using a commercial FEA software allows us to more accurately determine the behavior of devices under test by simulating the experimental conditions as well. Results from these simulations will be presented to supplement the new fabrication method introduced above and in the presentation.

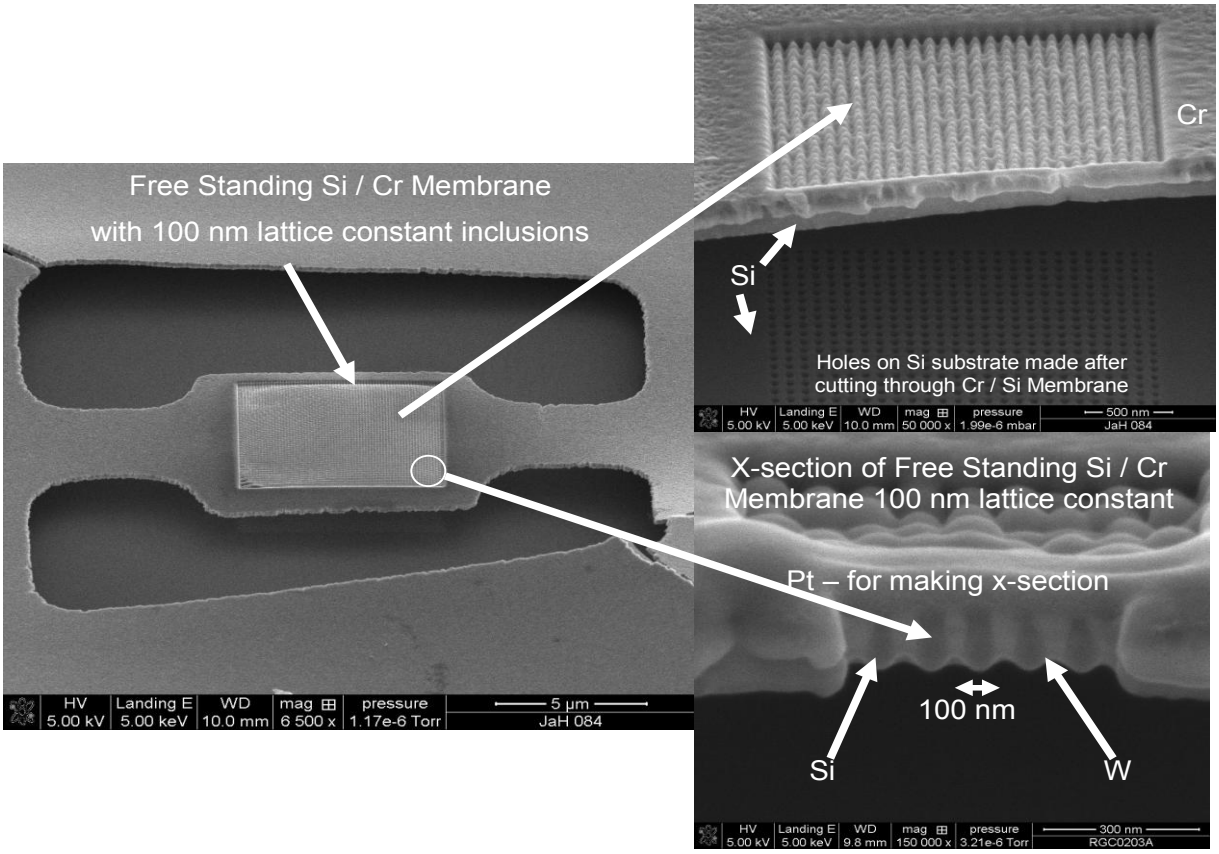

Figure 2: 33 GHz PnC fabricated with a focused ion beam with a 100 nm lattice constant and 30 nm W inclusions.

REFERENCES

[1]P. E. Hopkins, C. M. Reinke, M. F. Su, R. H. Olsson III, E. A. Shaner, Z. C. Leseman, J. R. Serrano, L. M. Phinney, and I. El-Kady, *Nano Letters*, **11**, (2011).

[2]M. F. Su, R. H. Olsson, Z. C. Leseman and I. El-Kady, *Appl. Phys. Lett.* **96** (2010).

[3]Y. M. Soliman, M. F. Su, Z. C. Leseman, I. El-Kady, R. H. Olsson III, *Appl. Phys. Lett.* **97** (2010).

[4]Y. M. Soliman, M. F. Su, Z. C. Leseman, C. M. Reinke, I. El-Kady, R. H. Olsson III, *Appl. Phys. Lett.* **97** (2010).

Phononics 2011: First International Conference on Phononic Crystals, Metamaterials and Optomechanics
Santa Fe, New Mexico, USA, May 29-June 2, 2011
PHONONICS-2011-0131

High Frequency Soft Phononics

George Fytas,[1,2,3] **Tim Still,**[1] **Dirk Schneider,**[1] **Nikos Gomopoulos,**[1] **Uli Jonas** [4]

[1] *Max Planck Institute for Polymer Research, P.O.Box 3148, 55128 Mainz, Germany*
[2] *Department of Materials Science and Technology, University of Crete, Heraklion, Greece*
[3] *FORTH, Institute of Electronic Structure & Laser (IESL), P.O. Box 1527, 71110 Heraklion, Greece*
fytas@mpip-mainz.mpg.de
[4] *FORTH, Bio-Organic Materials Laboratory (BOMBCLab), P.O. Box 1527, 71110 Heraklion, Greece*

Abstract: Propagation of hypersonic elastic/acoustic waves in polymer- and colloid-based nanostructures emerges as a powerful characterization tool of thermo- mechanical properties and reveals new structure related collective phenomena .Particle vibration spectroscopy and engineering of the phonon dispersion band diagram are highlighted in this presentation.

Phononic crystals become the acoustic equivalents of the photonic crystals controlled, however, by a larger number of material parameters. In contrast to the sonic and ultrasonic crystals, the study of hypersonic crystals (at the submicron scale), imposes substantial demand on fabrication and characterization techniques. Colloid and polymer science offer methods to create novel materials that possess periodic variations of density and elastic properties at mesoscopic length scales commensurate with the wave length of hypersonic phonons and hence photons of the visible light. Polymer-and colloid-based phononics is an emerging new field at the interface of soft materials science and condensed matter physics with rich perspectives ahead.

The key quantity for phononics is the dispersion of high frequency (GHz) acoustic excitations in mesoscopic structures which is nowadays at best measured by high resolution spontaneous Brillouin light scattering (BLS) at thermal equilibrium. Depending on the components of the nanostructured composite materials, the resolved vibration eigenmodes (the music) of the individual particles sensitively depend on the particle architecture and their thermo-mechanical properties. In periodic structures (the concert) of polymer based colloids, the dispersion relation $\omega(k)$ between the frequency and the phonon wave vector k has revealed hypersonic phononic band gaps of different nature.

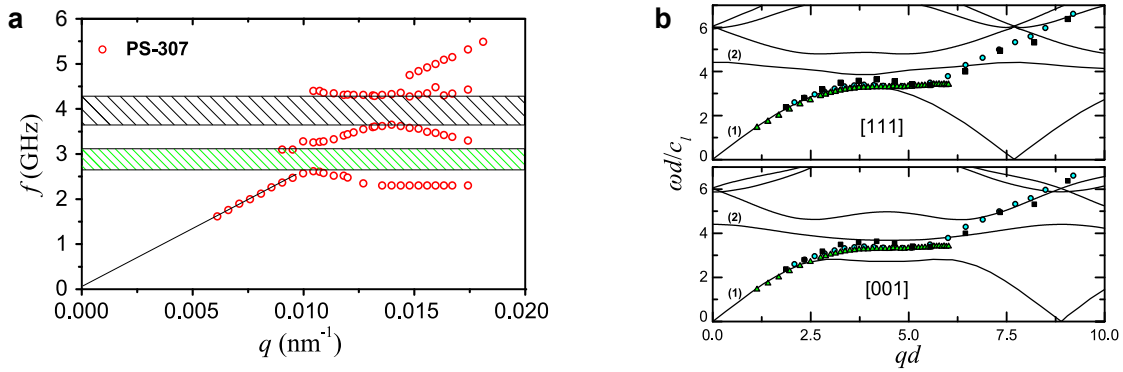

Figure 1 Phononic band diagram for an elastically soft polystyrene (PS) **(a)** and hard SiO_2 **(b)** colloidal crystal. Hybridization (green) and Bragg band gap (gray hatched area) in **(a)** and slow phonons (experimental points) due to strong coherent multiple scattering in a fcc crystal of closely packed SiO_2 spheres (three different diameters d=192nm (triangles) 354nm (circles) and 632nm (squares)) along its two symmetry directions in **(b)**.

Bragg gap for propagation near the edge of the first Brillouin zone due to destructive interference and hybridization gap due to the interaction of particle eigenmodes with the effective medium acoustic branch; the latter is therefore robust against structural. This seems to be the case for colloidal crystals based on elastically soft particles (Fig.1a). Boosting the strength of the phonon scattering by the individual spheres,

Phononics 2011: First International Conference on Phononic Crystals, Metamaterials and Optomechanics
Santa Fe, New Mexico, USA, May 29-June 2, 2011
PHONONICS-2011-0131

e.g., elastically hard SiO_2 particles can activate additional mechanisms for tunability of the phononic band structure as indicated in Fig.1b. In contrast to soft colloidal crystals, the phonon dispersion of dense SiO_2 colloids exhibits novel and unexpected features. Apart from the extended effective-medium band (1) and narrow bands stemming from localized particle resonances at relatively high frequencies, we identified additional almost dispersionless collective modes (2) at lower frequencies. These originate from strong coherent phonon multiple scattering and are localized in regions of the fluid matrix; their bending arises from strong hybridization. The elucidation of all important parameters towards the general design of optimal phononic structures remains complicated due to the vector nature of elastic wave propagation. In this regard, 1D phononic crystals (SiO_2/PMMA) multilayer films turn out to be a model system. Since hypersonic crystals can simultaneously exhibit phononic and photonic band gaps in the visible spectral region, many technological applications are feasible.

Like small molecules colloidal particles undergo vibrational motions, e.g., and shape fluctuations due to thermal energy. The acoustic vibrations of free homogeneous spheres predicted by Lamb in 1882, are classified as torsional and spheroidal ones and their frequencies $\omega(n,l)$, depend on the diameter and the elastic constants of the particle. For submicron sizes, BLS is the most sensitive technique to probe numerous eigenmodes in GHz frequencies and reveal the $\omega(n,l) \sim d^{-1}$ scaling for the spheroidal modes with order n and angular momentum "quantum number" l. The estimation of the thermo-mechanical properties (T_g, Young's and shear moduli) at nanoscale, which can deviate from the bulk values, is straightforward, provided a unique assignment of all observed eigenmodes is warranted. This requires a consensus on the existence of "selection rules" and on the contribution of torsional modes in the BLS spectra. These two important issues have very recently addressed through the full theoretical account of the experimental spectrum $I(\omega(n,l),q)$ at different probing wave vectors q. It is the dependence on qd that selects which spheroidal modes will be revealed experimentally. This emerging particle vibration spectroscopy for spherical shape has rich perspectives. Different particle morphologies, extension to non-spherical particles and the possibility to sense particle interactions are now being unexplored. Understanding of elastic energy localization in different compartments of the nanostructures is a precondition to access fundamental concepts such as engineering the flow of elastic energy and nanomechanics.

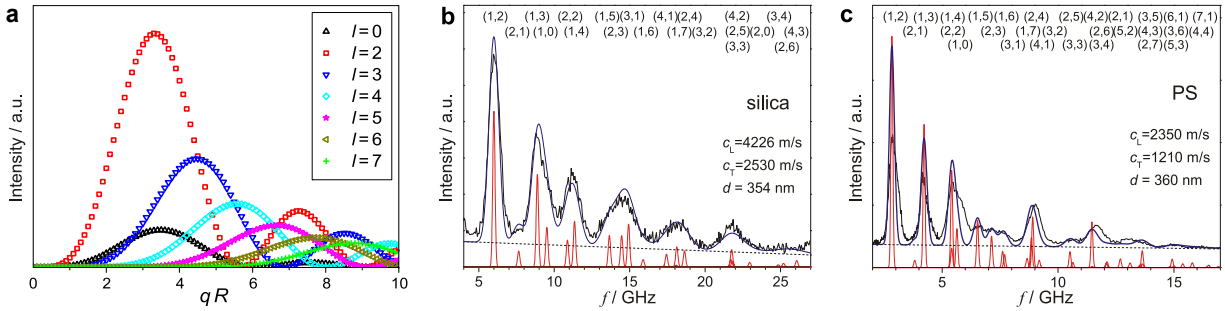

Figure 1 (a) The amplitude of the fundamental ($n = 1$) vibrational eigenmodes with $l = 0$ and $2 \le l \le 7$ for a free vibrating polystyrene (PS) latex spheres as a function of the product of the scattering wave vector q and particle radius R. **(b, c)** Comparison between experimental (black solid line) and calculated (blue) eigenmode spectra of SiO2 and PS spheres (diameter d). The sharp red lines denote the contribution of the individual $(n.l)$ modes labeled in the plots and the blue line is the sum of all modes.

References

[1] W. Cheng, M. Retsch, U. Jonas, G. Fytas, N. Stefanou, *Nature Mater.* **5**, 830 (2006).
[2] T. Still, W. Cheng, M. Retsch, R. Sainidou, J. Wang, U. Jonas, N. Stefanou, G. Fytas, *Phys. Rev. Lett.* **100**, 194301 (2008).
[3] N. Gomopoulos, D. Maschke, C. Y. Koh, E. L. Thomas, W. Tremel, H.-J. Butt, G. Fytas, Nano Lett. 10, 980 (2010).
[4] W. Cheng, J. Wang, U. Jonas. W. Steffen, G. Fytas, R. S. Penciu, E. N. Economou, J. Chem. Phys. 123, 121104 (2005).
[5] T. Still, R. Sainidou, M. Retsch, U. Jonas, P. Spahn, G. Hellmann, G. Fytas, Nano Lett. 10, 3194 (2008).
[6] T. Still, M. Mattarelli, D. Kiefer, G. Fytas, M. Montagna, *J. Phys. Chem. Lett.* **1**, 2440 (2008).

Phononics 2011: First International Conference on Phononic Crystals, Metamaterials and Optomechanics
Santa Fe, New Mexico, USA, May 29-June 2, 2011
PHONONICS-2011-0143

Techniques for Self-Assembled Phononic Crystals

T. J. Isotalo[1] , N. Zen[1], Y. Tian[1], I. J. Maasilta[1]

[1] *Nanoscience Center, Department of Physics, University of Jyväskylä, P.O. Box 35 FIN 40014, Finland,*
tero.isotalo@phys.jyu.fi, ilari.maasilta@phys.jyu.fi

Abstract: In this project, we study the assembly of periodic arrays of nanospheres and their crystalline properties. The vertical deposition technique is investigated along with the effects of substrate surface modifications for improvement of order and directed self-assembly. Dipping speed and PS sphere concentration are taken as the primary parameters affecting crystalline quality.

Arrays of monodisperse spherical particles, known as artificial opals, are commonly used to make photonic crystals for various applications. Similarly, an ordered array of spherical particles should exhibit a phononic band gap depending on the particle diameter. At temperatures around 100 mK, the thermal phonon wavelength is on the order of 100 nm. Thus, the thermal properties of phononic crystals made from 260 nm and 140 nm spheres should be strongly modified, and will be studied at sub-Kelvin temperatures using tunnel junction thermometry.

A vertical deposition technique [1], spinning and simple gravitational deposition [2] have been examined as methods for the fabrication of self-assembled arrays of nanospheres. Solutions of 10% and 2% of polystyrene (PS) nanospheres were studied on substrates of silicon, thermally grown SiO_X, PECVD SiN_X and glass, using a thin layer of Ti to provide an adhesion layer [3]. Hexagonal close packed structures have been produced with some regions exhibiting a cubic lattice. Directed self-assembly [4,5] of PS sphere arrays, 1-D chains and individual sphere placement was also investigated by using the vertical deposition method on substrates with patterned surfaces. Additionally, direct e-beam lithography of poly-methyl methacrylate (PMMA) nanospheres has been tested. Verifying the resulting lattice structures of deposited nanospheres was performed with scanning electron microscopy (SEM).

Experimental Methods

Of the three deposition methods investigated, the vertical deposition process appears to have the greatest utility and potential for reproducible monolayer and multi-layer arrays of polystyrene spheres. Spinning resulted in significantly lower order even at speeds of ~500 rpm. Gravitational deposition involved placing a droplet on the substrate surface and allowing the spheres to sediment during drying. Though noticeably greater order was observed, this method is inherently inconsistent from one sample to another as well as across individual sample surfaces. While the dipping process is time consuming, it is simple and reliable. A thin film of UHV evaporated Ti can be used to significantly improve adhesion on glass and SiN_X substrates. The samples are dipped either vertically or at an angle of 45° into the solution and withdrawn again. The angled depositions tend to give a lower quality film compared to vertical. This is likely due to dynamics of the contact angle between solution meniscus and substrate [6]. To further probe the control of crystalline quality, dipping speed and PS sphere concentration were studied as controls for domain size. Dipping speeds of 0.01 mm/min up to 0.1 mm/min were investigated with concentrations of 10, 2, 0.2 and 0.02%. Images were taken at several locations on each sample using SEM. Figure 1 shows an example of a measurement image. A rough estimate of domain area was obtained by taking length and width measurements of the domains and multiplying the two values. Measurement data from all the images were collected and used

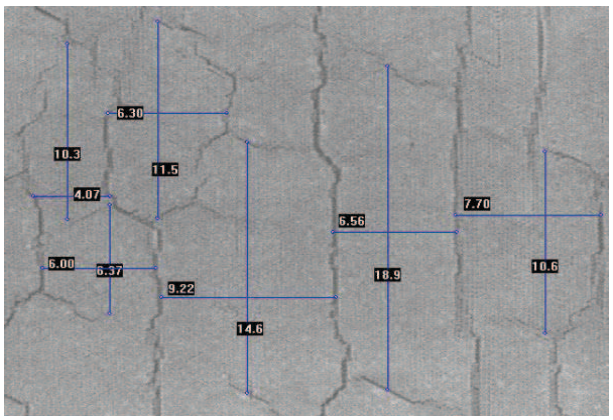

Figure 1 SEM image shows an example of domain measurements. An approximate area for domains is obtained by multiplying these length and width values.

Phononics 2011: First International Conference on Phononic Crystals, Metamaterials and Optomechanics
Santa Fe, New Mexico, USA, May 29-June 2, 2011
PHONONICS-2011-0143

to get an average value for the whole sample. From these images, one can also find indications of directionality in the domains. This effect tends to follow the dipping direction, with higher speeds displaying greater directionality.

Results

As expected, lower dipping speed results in larger domains. With slower speeds, the spheres have a longer time in contact with the substrate while in solution, allowing development of long-range order. However, there appears to be an optimum dipping speed at a given concentration, above and below which the quality declines. At higher than optimum speeds for a given concentration, there is little if any aggregation. The result is that spheres are located in small groups of three or four across most of the sample surface. Below the optimum speed, domain size varies greatly and thus results are unreliable. While a few larger domains are found, the variation is larger than the change in average domain size from one dipping speed to the next. Concentration follows a similar pattern. Higher concentrations produce larger domains and lower concentrations produce smaller domains. There is of course, a limit below which aggregation is no longer present. With lower concentrations at the same dipping speed, the size dispersion of domains is smaller indicating that consistency in long-range order suffers with increasing concentration.

An estimate of the number of layers deposited was also obtained using a profilometer. While the precise number of layers is not reliably measured in this way, a relation between dipping speed, PS sphere concentration and thickness can be discerned. Again, as expected, lower dipping speed and higher concentration result in greater thickness. The nanosphere arrays in this study ranged in thickness from 1 to approximately 20 layers. Gathering information about ordering in the thickness direction has been difficult for lack of a reliable method to image the side face without significantly changing the self-assembly conditions or altering the structure in post-processing.

Conclusions and prospects

The fabrication of thick and large area self-assembled phononic crystals requires time. The results of this study show that simply slowing down the process, however, is not sufficient to increase the domain size. PS sphere concentration plays a significant role in domain size and needs to be considered in parallel with dipping speed. We have shown initial trends for these two parameters and further development is ongoing.

Initial tests of directed self-assembly of nanosphere arrays are promising. Standard e-beam lithography techniques are used to produce channels of different shapes and sizes into which the nanospheres are selectively deposited. Arrays with dimensions in tens of microns are reproducible while chains and individual placement have shown positive results. Lithographically directed self-assembly can be used to place individual spheres on the substrate surface, allowing even more freedom to design the array patterns. Lithographic methods may also allow for imaging of the side wall to observe ordering in the thickness direction.

Direct lithography of PMMA nanospheres also shows promise. Different geometries have been patterned into pre-assembled PMMA sphere arrays. Reproducible lithography will still require some development in the alignment process. Ongoing experiments are focused on improving pattern design and further increasing the size of ordered domains.

References

[1] Z. Lü, W. Ruan, N. Ji, L. Ren, Q. Cong, B. Zhao, *J. Bionic Eng.* **3**, 059 (2006).
[2] Y. Xia, B. Gates, Y. Yin, Y. Lu, *Adv. Mater.*, **12**, 693 (2000).
[3] S. Karuppuchamy, J.M. Jeong, *Mater. Chem. Phys* **93**, 251 (2005).
[4] M. Allard, E.H. Sargent, P.C. Lewis, E. Kumacheva, *Adv. Mater.* **16**, 1360 (2004).
[5] C.A. Fustin, G. Glasser, H.W. Spiess, U. Jonas, *Langmuir* **20**, 9114 (2004).
[6] P.I. Stavroulakis, N. Christou, D. Bagnall, *Mater. Sci. Eng. B* **165**, 186 (2009).

Phononics 2011: First International Conference on Phononic Crystals, Metamaterials and Optomechanics
Santa Fe, New Mexico, USA, May 29-June 2, 2011
PHONONICS-2011-0151

The Effect of Phononic Crystal Lattice Type and Lattice Spacing on the Reduction of Bulk Thermal Conductivity in Silicon and Silicon Nitride

Drew F. Goettler[1], Bongsang Kim[2], Roy H. Olsson III[2], Zayd C. Leseman[1], Charles M. Reinke[2], Ihab I. El-Kady[2]

[1] *Mechanical Engineering, University of New Mexico, Albuquerque, NM, USA,*
goettled@unm.edu, zleseman@unm.edu
[2]*Sandia National Laboratories, Albuquerque, NM, USA*
bonkim@sandia.gov, rholsso@sandia.gov, cmreink@sandia.gov, ielkady@sandia.gov

Abstract: Phononic crystals are a promising method of reducing a material's bulk thermal conductivity. Changing a phononic crystal's lattice type or its lattice spacing are two ways of reducing a material's thermal conductivity. Results of different lattice types and lattice spacings on the reduction of bulk thermal conductivity in silicon and silicon nitride at room temperature will be presented.

Phononic crystals (PnCs) were recently shown to reduce the thermal conductivity of bulk silicon by more than an order of magnitude[1]. The PnCs were fabricated using photolithography and utilized a two-dimensional simple cubic pattern with a lattice constant ranging between 800 and 500 nm.

As an alternative to using photolithography for fabricating phononic crystal arrays, a focused ion beam (FIB) can fabricate various patterns in a short amount of time without the need for additional photolithography masks. In this report, we use two different setups to measure the thermal conductivity of PnCs fabricated in silicon and silicon nitride with a FIB. The first setup uses a heater in the middle of two identical PnCs on a freestanding Si membrane 500 nm thick. Current flowing through the resistive element provides joule heating. Due to symmetry, half of the heat flows to each side of heater. Temperature sensors, which are calibrated prior to the experiments, are located at each end of the phononic crystal and measure the temperature of the Si. By knowing the amount of heat flowing into the system, the change in temperature across the phononic crystal, and the PnC's dimensions, a thermal conductivity of the specimen can be calculated using

$$k_{PnC} = \frac{Q_{heat}}{2wt\Delta T} \tag{1}$$

where k_{PnC} is the effective thermal conductivity of the PnC, Q_{heat} is the input heat, w and t are the width and thickness of the PnC, and ΔT is the change in temperature across the PnC.

The second set up, based on a design by Li Shi[2], is used to measure the thermal conductivity of a PnC in silicon nitride. In this configuration, a thin strip of silicon nitride containing a PnC milled with the FIB separates two freestanding islands of silicon nitride. Since the islands and the PnC are made of the same material, there is no worry of contact resistance. Each island is supported by four legs 1 μm wide. One island acts as a heat source, and the other island is the sensing island. A top view of this set up is shown in Figure 1.

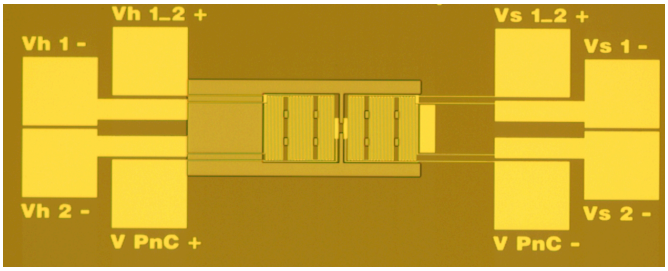

Figure 1 Set up for determining thermal conductivity of silicon nitride PnC. The two islands are separated by a 5x15 μm area of silicon nitride.

Phononics 2011: First International Conference on Phononic Crystals, Metamaterials and Optomechanics
Santa Fe, New Mexico, USA, May 29-June 2, 2011
PHONONICS-2011-0151

In the middle of the figure are the two suspended islands with platinum serpentine heaters on top of each silicon nitride membrane island. Each heater is connected to contact pads by metal lines on the support legs. Between the islands is a small area of silicon nitride where the PnC is fabricated. Isolation of the two islands forces a majority of the heat to flow across the silicon nitride PnC. Finite element analysis performed with ANSYS shows a uniform temperature distribution on the heating island and on the sensing island as well (see Figure 2). This supports the assumption that the silicon nitride PnC can be treated as a one-dimensional component.

Results from both setups will be presented.

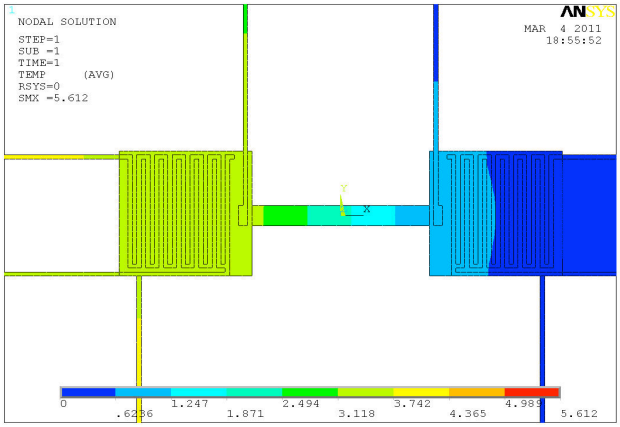

Figure 2 FEM analysis of temperature gradient across silicon nitride membrane connecting heating and sensing island. A temperature scale bar is shown at the bottom, where red indicates a higher temperature and blue corresponds to a lower temperature. Notice the uniform temperature of the heating island (yellow) and planar heat flow across the sensing island (blue). ANSYS was used to perform the FEM analysis.

References

[1] P. E Hopkins, C. M. Reinke, M. F. Su, R. H. Olsson III, E.A. Shaner, Z. C Leseman, J. R. Serrano, L. M. Phinney, I. El-Kady, *Nano Lett*, **11**, 107-112, (2011).
[2] L. Shi, Ph.D thesis, University of California, Berkley, (2001).

Phononics 2011: First International Conference on Phononic Crystals, Metamaterials and Optomechanics
Santa Fe, New Mexico, USA, May 29-June 2, 2011
PHONONICS-2011-0158

Nanophononics using Acoustic and Optical Cavities

N. D. Lanzillotti-Kimura[1,2], A. Fainstein[1], B. Jusserand[3], B. Perrin[3], A. Lemaitre[4], D. G. Schlom[5], A. Soukiassian[5]

[1] *Centro Atómico Bariloche & Instituto Balseiro, C.N.E.A., R8402 AGP S. C. De Bariloche, Río Negro, Argentina*
kimura@cab.cnea.gov.ar, afains@cab.cnea.gov.ar
[2] *University of California – Berkeley, CA 94720, USA*
[3] *Institut des NanoSciences de Paris, CNRS – Université Pierre et Marie Curie, 75004 Paris, France*
bernard.jusserand@insp.jussieu.fr, bernard.perrin@insp.jussieu.fr
[4] *Laboratoire de Photonique et des Nanostructures, C.N.R.S., Route de Nozay, 91460 Marcoussis, France aristide.lemaitre@lpn.cnrs.fr*
[5] *Department of Materials Science and Engineering, Cornell University, Ithaca, New York, 14853-1501, USA*
ds636@cornell.edu, soukiassian@gmail.com

Abstract: We report pump-probe time experiments in acoustic and optical cavities. We demonstrate that the generated coherent acoustic phonon spectra can be inhibited or enhanced in the cavity. Simulations highlight the role of the phonon density of states in the coherent phonon generation, extending concepts at the base of the Purcell effect to the field of phononics.

Changing the spontaneous light emission rate and spectra of atoms or excitons through the modification of the photon density of states has been the subject of significant efforts following Purcell's proposal and demonstration in the microwave domain.[1] This has been accomplished either by changing the dielectric boundaries close to the emitting species, or more fundamentally by embedding the emitter in an optical microcavity.[2] Depending on the tuning of the emitter spectra with maxima or minima of the modified photonic density of states, the emission can be either enhanced or inhibited. Similar ideas have been applied to modify other light-matter interactions processes. The search for large Purcell effects is at the heart of the quest for thresholdless lasing. In the field of phononics, and specifically the search of phonon lasing for efficient monochromatic THz sources, and for the control of heat at the nanoscale, these ideas have not been pursued to date. Here we demonstrate that the coherent acoustic phonon emission spectra of an impulsively excited thin metallic film can be either inhibited or enhanced by embedding the metal layer in an acoustic nanocavity.[3-6] This has been accomplished by using for the first time a hybrid metal cavity with $BaTiO_3/SrTiO_3$ epitaxial oxide phonon mirrors.

Acoustic nanocavities are the hypersound analog of the extensively studied optical microcavities.[3-6] We use a femtosecond laser light impulsion to generate a pulse of coherent sub-THz phonons in a metallic layer, and then we study how the latter is modified by changing the structure around the metal film. We compared two samples, in the first one we deposited the Ni film directly on a $SrTiO_3$ substrate, while in the second one the film is embedded in an acoustic nanocavity. In the latter, we chose as bottom broadband acoustic mirror $BaTiO_3/SrTiO_3$ superlattice (SL) grown by molecular beam epitaxy on a $SrTiO_3$ substrate. $BaTiO_3$ and $SrTiO_3$ have optical energy gaps in the 350 nm range and are consequently completely transparent at the laser energy of 750 nm. In this way, the acoustic mirrors only affect the acoustic boundary conditions of the metallic film, and thus its local acoustic density of states. The sample-air interface responds to a free surface boundary condition. This surface performs as the top mirror to complete the phonon cavity. Both the coherent phonon generation and detection are performed only at the metallic films. In the case of the acoustic nanocavity the measured spectrum presents an enhanced peak at the confined mode energy, while in the case of the naked Ni film the spectrum is broad and featureless. Moreover, we observed the inhibition of the coherent phonon emission in the region of the acoustic stop-band. In other words, within the phononic stop-band modes are expelled and they concentrate at the cavity resonance and at the stop-band edges. It is this modification of the mode density landscape that determines at which energies acoustic phonons can be emitted by the metallic layer (enhancement at the cavity mode), and at which they cannot (inhibition within the phonon gap). In addition, outside the phononic stop-band oscillations develop in the generated spectrum which, when compared with the bare Ni-film, also express weaker but clear inhibition and enhancement regions. The experiments are compared with calculations of the impulsive

Phononics 2011: First International Conference on Phononic Crystals, Metamaterials and Optomechanics
Santa Fe, New Mexico, USA, May 29-June 2, 2011
PHONONICS-2011-0158

generation and detection of coherent phonons that highlight the role of the phonon density of states on the acoustic emission rate, extending the concept of the optical Purcell effect to the field of phononics.

In addition, we report experiments performed on structures based in semiconductor optical microcavities, where acoustic phonons and photons can be confined simultaneously. Thus, both the optical and acoustic densities of states result modified.[7-8] An optical microcavity confines the electromagnetic field both spectrally and spatially, inducing strong changes in the light-matter interaction and giving rise to novel physical phenomena and devices. In the case of planar semiconductor optical microcavities, two distributed Bragg reflectors (DBRs) enclose an optical spacer. The confinement characteristics and the amplification of the electric field are determined by the selection of materials, thickness, and number of periods that constitute each DBR and the optical spacer. Optical microcavities have been the subject of very active research during the last 15 years, and have been used to study the modification of the photonic lifetimes, parametric oscillations, cavity polariton Bose-Einstein condensates, the polariton laser, and amplification of Raman scattering signals, among others.[9-11]

Particularly, the photonic confinement and amplification have been used in these high-Q resonators to amplify the optical generation of incoherent phonons through Raman processes and to evidence new effects in the phonon physics and dynamics in semiconductor nanostructures. This scheme was used to study confined phonons in acoustic nanocavities. The optical resonances can be complemented with electronic resonances giving rise to amplified Raman cross-sections of up to 10^7. On the contrary, the use of optical confinement for the enhanced coherent generation of acoustic phonons (in contrast with incoherent generation by spontaneous Raman scattering) is a concept that has been little treated up to now. The realization of a monochromatic, coherent, and intense source of ultrahigh frequency acoustic phonons based on semiconductor optical microcavities and the obtained coherent phonon enhancements will be also discussed.

References

[1] E. Purcell, in Proceedings of the American Physical Society, 1946 [Phys. Rev. **69**, 681 (1946)].
[2] E. Yablonovitch, Phys. Rev. Lett. **58**, 2059 (1987).
[3] M. Trigo, A. Fainstein, B. Jusserand, and V. Thierry-Mieg, *Phys. Rev. Lett.* **89**, 227402 (2002).
[4] A. Huynh, N. D. Lanzillotti-Kimura, B. Jusserand, B. Perrin, A. Fainstein, M. F. Pascual-Winter, E. Peronne, and A. Lemaître, Phys. Rev. Lett. **97**, 115502 (2006)
[5] N. D. Lanzillotti-Kimura, A. Fainstein, A. Huynh, B. Perrin, B. Jusserand, A. Miard, and A. Lemaître, *Phys. Rev. Lett.* **99**, 217405 (2007).
[6] A. Huynh, B. Perrin, N. D. Lanzillotti-Kimura, B. Jusserand, A. Fainstein, and A. Lemaître, Phys. Rev. B **78**, 233302 (2008)
[7] N. D. Lanzillotti-Kimura, A. Fainstein, B. Jusserand, and A. Lemaître, Phys. Rev. B **79**, 035404 (2009)
[8] N. D. Lanzillotti-Kimura, A. Fainstein, B. Perrin, B. Jusserand, A. Soukiassian, X. X. Xi, and D. G. Schlom, *Phys. Rev. Lett.* **104**, 187402 (2010).
[9] D. Sanvitto, F. M. Marchetti, M. H. Szymanska, G. Tosi, M. Baudisch, F. P. Laussy, D. N. Krizhanovskii, M. S. Skolnick, L. Marrucci, A. Lemaître, J. Bloch, C. Tejedor, and L. Vina, Nature Physics **6**, 527 (2010)
[10] E. Wertz, L. Ferrier, D. D. Solnyshkov, R. Johne, D. Sanvitto, A. Lemaître, I. Sagnes, R. Grousson, A. V. Kavokin, P. Senellart, G. Malpuech and J. Bloch, Nature Physics **6**, 860 (2010)
[11] A. Fainstein and B. Jusserand, Light scattering in Solids IX: Novel Materials and Techniques 108, 17, (Springer, Heidelberg, (2007)

Phononics 2011: First International Conference on Phononic Crystals, Metamaterials and Optomechanics

Santa Fe, New Mexico, USA, May 29-June 2, 2011

PHONONICS-2011-0164

nanoFIBrication of Phononic Crystals in Freestanding Membranes

D. F. Goettler[1], M. F. Su[1], R. H. Olsson III[2], I. El-Kady[2], and Z. C. Leseman[1*]

[1] Mechanical Engineering, University of New Mexico, Albuquerque, NM USA 87131
goettled@unm.edu, mfatihsu@unm.edu, and zleseman@unm.edu
[2] Sandia National Laboratories, Albuquerque, NM USA 87105
rholsso@sandia.gov and ielkady@sandia.gov

Abstract: For this poster, we describe a novel method for the fabrication of phononic crystals in freestanding membranes using a method dubbed 'nanoFIBrication.' The method is demonstrated by nanoFIBricating a 35 GHz phononic crystal. Post fabrication of phononic crystals shows that the vias flare out at their exit, which we call the 'trumpet effect.'

For this poster, we describe a novel method for the fabrication of phononic crystals in freestanding membranes using a method dubbed 'nanoFIBrication.' The method is demonstrated by nanoFIBricating a 35 GHz phononic crystal. Initially, a square array of vias with 150 nm spacing (center-to-center) is generated over an area of 6.75 x 6.75 μm. The vias are then backfilled with void-free tungsten. Each tungsten plug has a diameter of 48 nm – these constitute the scatterers of the phononic crystal. A protective layer of chromium is used to minimize the amount of contamination by Ga from the focused ion beam. The chromium is removed at the end of the process. Post fabrication of phononic crystals shows that the vias flare out at their exit, which we call the 'trumpet effect.' The trumpet effect is explained by modeling the lateral damage in the freestanding member via Monte Carlo simulations.

Phononics 2011: First International Conference on Phononic Crystals, Metamaterials and Optomechanics

Santa Fe, New Mexico, USA, May 29-June 2, 2011

PHONONICS-2011-0164

1ST INTERNATIONAL CONFERENCE ON PHONONIC CRYSTALS, METAMATERIALS & OPTOMECHANICS

Extended Abstracts

Track 7: Phononic MEMS and RF Applications

Phononics 2011: First International Conference on Phononic Crystals, Metamaterials and Optomechanics
Santa Fe, New Mexico, USA, May 29-June 2, 2011
PHONONICS-2011-0053

Tunable magnetoelastic phononic crystals

J.O. Vasseur[1], O. Bou-Matar[1], J-F. Robillard[1], A.-C. Hladky-Hennion[1], and P.A. Deymier[2]

[1] *Institut d'Électronique, de Microélectronique et de Nanotechnologie, UMR CNRS 8520, Cité Scientifique, 59652 Villeneuve d'Ascq Cedex, France,*
Jerome.Vasseur@univ-lille1.fr, olivier.boumatar@iemn.univ-lille1.fr, jean-francois.robillard@isen.fr, anne-christine.hladky@isen.fr

[2] Department of Materials Science and Engineering, University of Arizona, Tucson, Arizona 85721, USA
deymier@email.arizona.edu

Abstract: The feasibility of contactless tunability of the band structure of two-dimensional phononic crystals is demonstrated by employing magnetostrictive materials and applying an external magnetic field. The influence of the amplitude and of the orientation with respect to the inclusion axis of the applied magnetic field are studied in details. Applications to tunable selective frequency filters are discussed.

Phononic crystals may have potential applications in numerous technological domains [1]. Nevertheless, one of the major stumbling block to the application of phononic crystals is the lack of practical frequency tunability of their properties. Tunability could be achieved by changing the geometry of the inclusions [2] or by varying the elastic characteristics of the constitutive materials through application of external stimuli [3]. For instance, some authors have proposed the use of electrorheological materials in conjunction with application of external electric field [4]. Other authors have considered the effect of temperature on the elastic moduli [5]. In all cases, significant effect on the band structure of the phononic crystal can only be achieved by applying stimuli with very large magnitude. Recent work [6] exploits the change of the structure of the phononic crystal due to an external stress to alter the band structure. However this approach requires physical contact with the phononic crystal. We propose a contactless way to tune the properties of phononic crystals using magnetoelastic components. The elastic properties of a magnetoelastic material are very sensitive to its magnetic state and on the applied external magnetic field. For instance, in giant magnetostrictive material, such as Terfenol-D, this dependence can lead to more than 50% variation of some of the elastic constants, even at ultrasonic frequencies [7]. Moreover, for some directions of the applied external magnetic field, a spin reorientation transition (SRT) appears leading to even more variations of the elastic constants. So, if one of the components of a phononic crystal is a magneto-elastic medium, then one can expect that the elastic contrast, and subsequently the phononic crystal properties could be controlled without any contact by a magnetic field.

We studied in details the tuning of the properties of a bulk two-dimensional magnetoelastic phononic crystal when an external magnetic field is applied. We developped first a theoretical model allowing to derive for an arbitrary direction and amplitude of the applied magnetic field, an equivalent piezomagnetic material of a polarized ferromagnet, with field dependent elastic C_{ijkl}, piezomagnetic q_{lij} and magnetic permeability μ_{ij} constants. For example, Figure 1 presents the variations of these constants as functions of the applied magnetic field in the case of an infinite Terfenol square rod and for a magnetic field parallel to the direction of the rod. One observes that some of these constants strongly depend on the magnetic field amplitude. Using the equivalent constants, we computed the band structures of two-dimensional arrays of Terfenol-D square rods embedded in an epoxy matrix with the help of the well-known Plane Wave Expansion (PWE) method [8]. The band structures of Figs. 2(b) and 2(c) illustrate the effect of the external magnetic field. In absence of an external stimulus, the phononic crystal possesses two absolute band gaps ranging from approximately 0.5 to 0.8 MHz and from 0.89 to 1 MHz. Application of a magnetic field parallel to the Terfenol-D rods with a magnitude of 13 kOe enlarges the first band gap from 0.5 to 0.92 MHz and closes the second band gap. This shows that this phononic crystal behaves like a tunable filter with switching functionality for frequencies around 1 MHz.

Phononics 2011: First International Conference on Phononic Crystals, Metamaterials and Optomechanics
Santa Fe, New Mexico, USA, May 29-June 2, 2011
PHONONICS-2011-0053

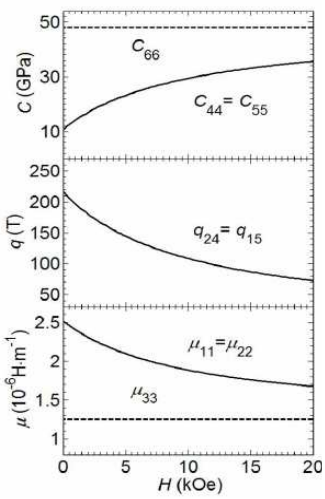

Figure 1: Evolution of the effective elastic moduli, piezomagnetic constants, and magnetic permeabilities of a Terfenol-D rod as a function of the static external magnetic field applied along the rod axis. The effective elastic and piezomagnetic constants are expressed in Voigt notation.

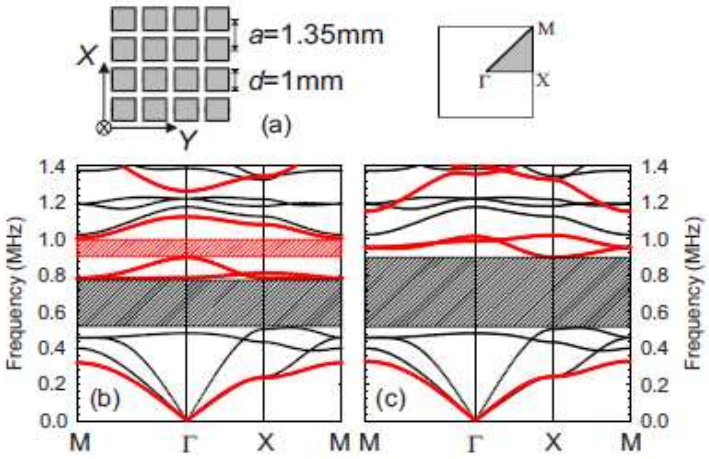

Figure 2: (a) The square-lattice 2D phononic crystal consisting of magneto-elastic square rods of infinite length along the *Z* direction made of Terfenol-D and embedded in an epoxy matrix. Band structure of a square lattice of Terfenol-D square rods with a filling factor $f=(d/a)^2=0.55$, embedded in an epoxy matrix for two applied static magnetic fields: (b) *H*ext =0 kOe and (c) *H*ext=13 kOe. The inset shows the irreducible Brillouin zone of the square array.

We will discuss the effect of the magnitude and of the orientation of the magnetic field on the band structure of the phononic crystal.

The introduction of a magnetoelastic constituent opens the possibility of easy controllability of the properties of a phononic crystal without any contact. Using this controllability, one may imagine to design devices with tunable functionalities such as frequency filters, superlens for acoustic imaging, etc... Some of these possible applications will be presented during this talk.

References

[1] Y. Pennec, J. O. Vasseur, B. Djafari-Rouhani, L. Dobrzynski, P. A. Deymier, Surf. Sci. Reports **65**, 229 (2010).
[2] C. Goffaux and J. Vigneron, Phys. Rev. B **64**, 075118 (2001).
[3] J. Baumgartl, M. Zvyagolskaya, and C. Bechinger, Phys. Rev. Lett. **99**, 205503 (2007).
[4] J.-Y. Yeh, Physica B **400**, 137 (2007).
[5] Z.-G. Huang and T.-T. Wu, IEEE Trans. Ultrason. Ferroelectr. Freq. Control **52**, 365 (2005).
[6] K. Bertoldi and M. Boyce, Phys. Rev. B **77**, 052105 (2008).
[7] Y. Wang, F. Li, Y. Wang, K. Kishimoto, and W. Huang, Acta Mecha. Sinica **25**, 65 (2009).
[8] J. Cullen, S. Rinaldi, and G. Blessing, J. Appl. Phys. **49**, 1960 (1978).
[9] J.-F. Robillard, O. Bou Matar, J. O. Vasseur, P. A. Deymier, M. Stippinger, A.-C. Hladky-Hennion, Y. Pennec and B. Djafari-Rouhani, App. Phys. Lett. **95**, 124104 (2009).

Phononics 2011: First International Conference on Phononic Crystals, Metamaterials and Optomechanics
Santa Fe, New Mexico, USA, May 29-June 2, 2011
PHONONICS-2011-0054

Band Gaps and Defect Modes in Phononic Strip Waveguides

Y. Pennec[1], C. Li[1], Y. El Hassouani[1], J. M. Escalante[2], A. Martinez[2], B. Djafari Rouhani[1]

[1] *Institut d'Electronique, de Microélectronique et de Nanotechnologies, UMR CNRS 8520, Université de Lille1, Avenue Poincaré, Cité Scientifique, 59652 Villeneuve d'Ascq, France*
yan.pennec@univ-lille1.fr
[2] *Nanophotonics Technology Center, Universidad Politécnica de Valencia, Camino de Vera s/n 46022, Spain*

Abstract: We study the elastic wave propagation in different geometries of strip waveguides obtained by extracting a row out of a phononic crystal slab made up of a square array of air holes in a silicon plate. We show that the existence of band gaps is strongly dependent on the cutting direction. We also study the existence of localized modes in cavities inserted inside the perfect strip waveguides.

We investigate the existence of band gaps in three kinds of phononic strip waveguides obtained by extracting a row in a phononic crystal slab constituted by a periodic array of air holes in a silicon plate. Figure 1 displays the three structures when the slab is cut along [1,0] and [1,1] directions. The band structures are calculated mostly by the finite element method using COMSOL Multiphysics. For each cutting direction, we discuss the existence and the behavior of band gaps as a function of the reduced geometrical parameters r/a and h/a where 'r' represents the radius of the holes, 'h' the thickness of the plate and 'a' the lattice parameter. Then, we have investigated the possibility of confined modes inside cavities inserted in the phononic strip waveguide. Figure 2 illustrates the example of a defect cavity obtained by reducing the radius of one hole from r/a=0.3 in the perfect structure to r/a=0.2. Using a super-cell to calculate the band structure of the waveguide with the defect, one can observe the existence of a flat branch in the band gap. The map of the displacement field at the frequency of the flat band shows a localization of the mode in the cavity around the defect hole.

Currently, we are investigating the design of strip waveguides that allow dual phononic and photonic band gap, simultaneous confinement of both elastic and electromagnetic waves in cavities, and the possibility of single guided mode which presents a slow light and/or sound velocity.

Acknowledgments: This work was supported in part by the European Commission Seventh Framework Programs (FP7) under the FET-Open project TAILPHOX N° 233883 and IP project NANOPACK N° 216716.

Figure 1

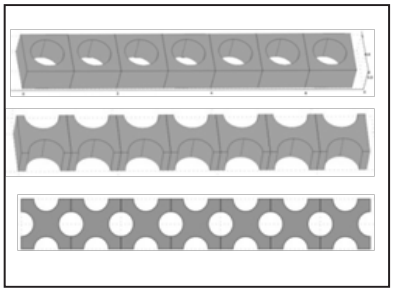

Figure 2

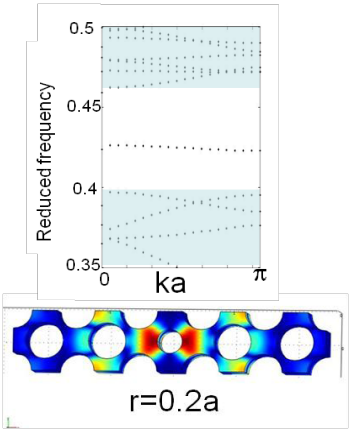

Phononics 2011: First International Conference on Phononic Crystals, Metamaterials and Optomechanics

Santa Fe, New Mexico, USA, May 29-June 2, 2011

PHONONICS-2011-0054

Phononics 2011: First International Conference on Phononic Crystals, Metamaterials and Optomechanics
Santa Fe, New Mexico, USA, May 29-June 2, 2011
PHONONICS-2011-0070

Multi-phonon Processes in PhoXonic Cavities

I.E. Psarobas[1,2], N. Papanikolaou[2], N. Stefanou[1]

[1] *Section of Solid State Physics, University of Athens, Panepistimioupolis, 15784, Athens, Greece, ipsarob@phys.uoa.gr, nstefan@phys.uoa.gr*
[2] *Institute of Microelectronics, NCSR "Demokritos", 15310, Athens, Greece N.Papanikolaou@imel.demokritos.gr*

Abstract: Long lifetime photons and phonons, confined in the same region of space, inside a phoXonic cavity, can interface with each other via strong nonlinear acousto-optic interactions. We unveil physics of distinct importance as the hypersonic modulation of light is substantially enhanced through multi-phonon exchange mechanisms.

Classical wave transport in periodic media can provide the means to control light, sound or both with the development of phoXonic crystals[1], a special class of dual spectral-gap materials which can integrate the management of sound, heat and light in a versatile manner, although the manipulation of phonon states to achieve heat management is somewhat a more complicated issue. An example of a 3D phoXonic crystal with predicted dual functionality is given in Fig.1 after Ref. 1. Such structures are an essential step towards the hypersonic modulation of light and could lead to the development of efficient acousto-optical devices.

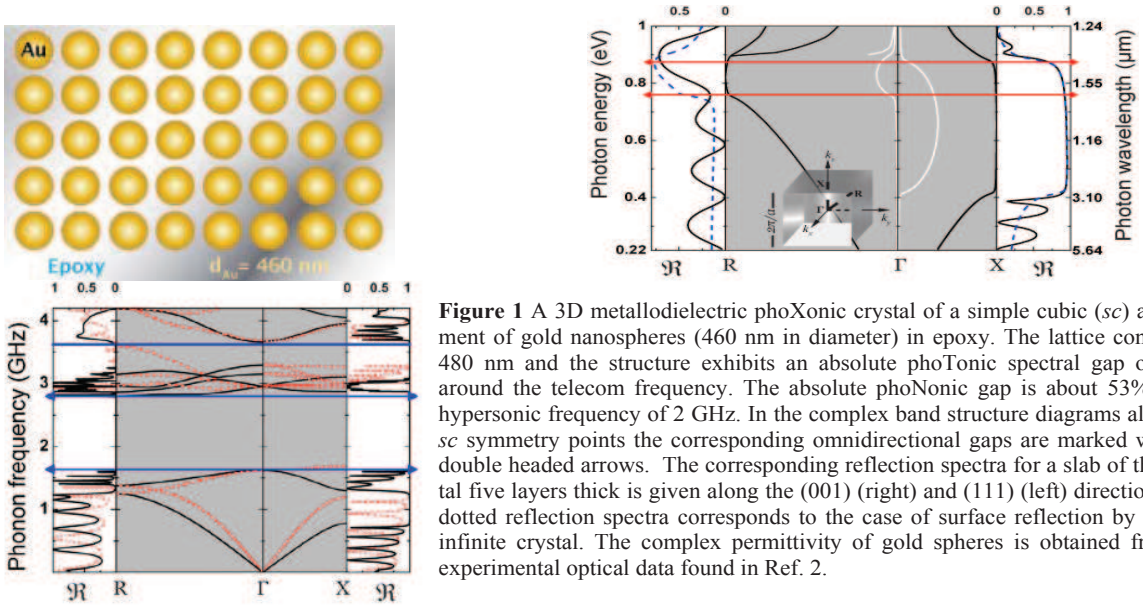

Figure 1 A 3D metallodielectric phoXonic crystal of a simple cubic (*sc*) arrangement of gold nanospheres (460 nm in diameter) in epoxy. The lattice constant is 480 nm and the structure exhibits an absolute phoTonic spectral gap of 15%, around the telecom frequency. The absolute phoNonic gap is about 53% at the hypersonic frequency of 2 GHz. In the complex band structure diagrams along the *sc* symmetry points the corresponding omnidirectional gaps are marked with the double headed arrows. The corresponding reflection spectra for a slab of the crystal five layers thick is given along the (001) (right) and (111) (left) directions. The dotted reflection spectra corresponds to the case of surface reflection by a semi-infinite crystal. The complex permittivity of gold spheres is obtained from the experimental optical data found in Ref. 2.

Nevertheless, the physics of photon-phonon interaction inside a phoXonic structure, is still under serious investigation and can be summarized in two major categories, the optomechanics[3] and the acousto-optics[4]. The acousto-optic (AO) interaction realized in the merging fields of nanophoTonics and nanophoNonics could lead to novel unprecedented control of light and sound in very small regions of space. In the regime of inelastic light scattering by sound, one can have phonon-assisted light emission, control of light speed (delay-storage) by stimulated Brillouin scattering and the realization of highly sensitive dual phoXonic sencors. In particular, phoXonic resonant cavities have the ability to enhance the acousto-optic interaction between localized photonic and phononic states in a Raman-Nath-like scattering pattern through multi-phonon exchange mechanisms. As an example, in Fig. 2 we present a model 1D resonant phoXonic cavity realized by Bragg mirrors consisting of homogeneous SiO_2 and Si multilayers. The time evolution of the

Phononics 2011: First International Conference on Phononic Crystals, Metamaterials and Optomechanics
Santa Fe, New Mexico, USA, May 29-June 2, 2011
PHONONICS-2011-0070

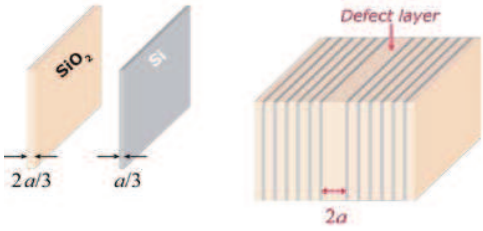

Figure 2 A 1D phoXonic cavity consisting of homogeneous SiO_2 and Si layers with a SiO_2 layer in the middle. The structure has lattice constant a = 300 nm.

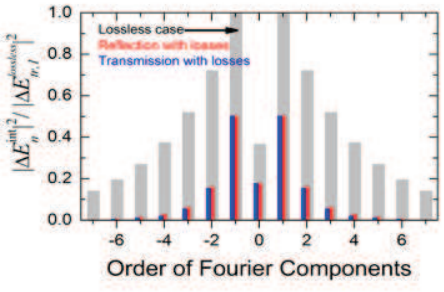

Figure 3 Optical reflection-transmission through the phoXonic structure of Fig. 2 under a continuous acoustic excitation of input level u_0 = 0.1 nm (at 10.9 GHz), for normally incident light at the resonance wavelength. The Fourier components of the AO interaction are normalized with respect to the first order component with a resonant acoustic excitation without losses.

scattered optical field of the structure, excited by an acoustic wave (injected by picosecond-ultrasonics techniques), changes dramatically when the AO interaction is considered in the case of resonant against nonresonant phoXonic modes. At acoustic resonance, we provide evidence for strong nonlinear AO effects in the phoXonic cavity which lead to efficient enhanced modulation of the optical resonant mode with sound through multi-phonon exchange mechanisms. When the structure is continuously excited by a resonant compressional acoustic wave of frequency Ω, the optical response is accordingly modulated. Off the optical resonance at a frequency ω_1, the AO interaction manifests itself in the temporal variation of the EM field as a frequency modulation consisting only by the contribution of the first order components of the Fourier spectrum, which is of the form $\omega_1 \pm \Omega$ (Stokes - anti-Stokes). At the optical resonance the temporal variation of the scattered EM field at ω_0 in addition to the strong first harmonics, has a significant contribution of higher-order terms so that the modulation is of the form $\omega_1 \pm n\Omega$ (where n=0,±1,±2,±3…). The scattering process is nonlinear, and in the particle picture, implies strong probability amplitudes for multi-phonon absorption and emission processes. Obviously the effect is somewhat diminished, as compared to the lossless acoustic case, when hypersonic attenuation is considered. Nevertheless, the assumption of a strong inelastic light scattering process is still valid[4]. Starting from the above Raman-Nath-like effect, we are going to present potential polymer phoXonic structures, as well as cases of phoXonic resonant cavities accommodating localized modes or zones of slow light and sound, in order to unveil interesting physics of distinct importance.

Finally, we note that all calculations were carried out by the layer-multiple-scattering (LMS) method[5], which is well documented for both elastodynamics[6] and electrodynamics[7]. The theory provides a framework[5] for a unified description of wave propagation in 1-3D periodic structures, finite slabs of layered structures, and systems with impurities: isolated impurities, impurity aggregates, or randomly distributed impurities. Recently, we have extended its capability to cases of any axisymmetric scatterer, besides spheres. This powerful tool describes accurately the acoustic and the optical response of composite structures made of a number of different layers having the same 2D periodicity and computes a full complex band structure and the response (transmission, reflection, absorption) of finite and semi-infinite systems.

This work was financially supported by the EU FET- Open project TAILPHOX Grant No. 233883 (http://www.tailphox.org).

References

[1] N. Papanikolaou, I. E. Psarobas, and N. Stefanou, *Appl. Phys. Lett.* **96**, 231917 (2010).
[2] P. B. Johnson and R. W. Christy, *Phys. Rev. B* **6**, 4370 (1972).
[3] M. Eichenfield, J. Chan, R. M. Camacho, K. J. Vahala, and O. Painter, *Nature* **462**, 78 (2009).
[4] I.E. Psarobas *et al.*, *Phys. Rev. B* **82**, 174303 (2010).
[5] A. Modinos, N. Stefanou, I. E. Psarobas, and V. Yannopapas, *Physica B* **296**, 167 (2001).
[6] R. Sainidou, N. Stefanou, I. E. Psarobas, and A. Modinos, *Comput. Phys. Commun.* **166**, 197 (2005).
[7] N. Stefanou, V. Yannopapas, and A. Modinos, *Comput. Phys. Commun.* **132**, 189 (2000).

Phononics 2011: First International Conference on Phononic Crystals, Metamaterials and Optomechanics

Santa Fe, New Mexico, USA, May 29-June 2, 2011

PHONONICS-2011-0090

Band-gap operating in the gigahertz frequencies for a bi-layer phononic crystal slab

A.Talbi, A. Soltani, Y. El Hassouani, Y. Pennec*, B. Djafari-Rouhani and A. Akjouj

Institut d'Electronique, de Microélectronique et de Nanotechnologie, CNRS UMR 8520, Université Lille Nord de France, Lille 1, 59655 Villeneuve d'Ascq, France

** yan.pennec@univ-lille1.fr*

Abstract: We investigate a phononic slab composed by two different layers. The phononic crystal is obtained drilling the bi-layer phononic slab by air holes. We study the existence and the behavior of absolute band gaps in such membrane both in theory and experiment.

We investigate the possibility of designing phononic crystal-based devices for telecommunication applications using materials commonly employed in microfabrication. The phononic crystal is composed by an aluminum nitride (AlN) slab of thickness 2800nm deposited on a thin metallic membrane of titanium Nitride (TiN) of thickness 250nm. This original native bi-layer membrane has been chosen to avoid the fragility of the whole structure. The purpose of this presentation is to show that such a structure presents absolute band gaps and to study its behavior as a function of the geometrical parameters. This theoretical study is completed by an experimental evidence of the band gap.

As an example of the experimental work, the figure (a) shows a SEM micrograph of the manufactured square array phononic crystal structure. The lattice parameter is a=1μm and the radius of the holes is r=450nm, corresponding to the high filling factor β=64%. The figure (b) corresponds to a measurement of the transmission spectrum through the bi-layer phononic slab which contained ten periods of the square lattice. The propagation corresponds to the principal direction ΓX of the Brillouin zone. As seen in the normalized transmission spectrum, we have obtained a band gap closed to 1 GHz. The measured results are in good agreement with the theoretical predictions (not shown here) which lead to an absolute band gap in the same frequency range.

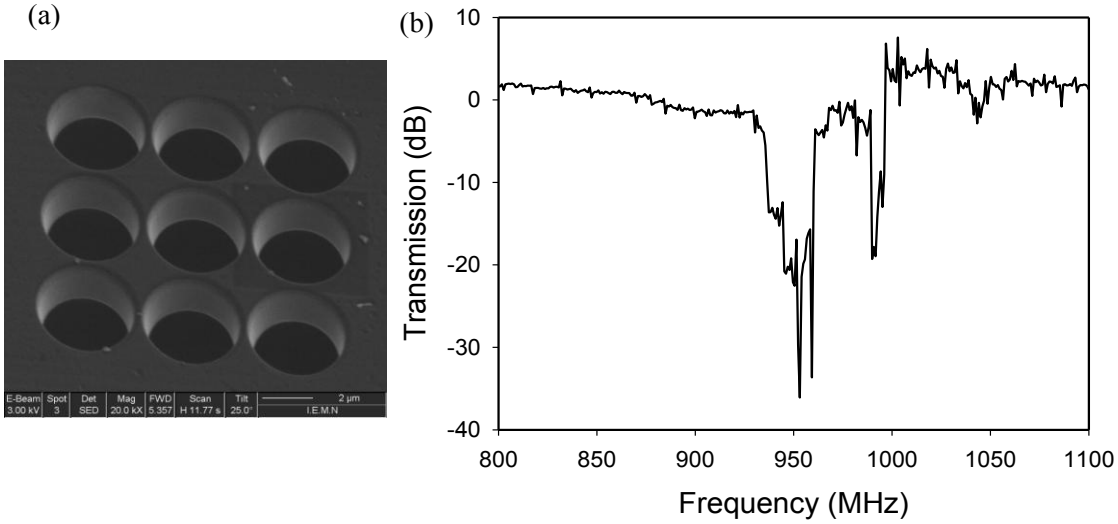

Figure: (a) Top view of one of the fabricated devices with the square lattice phononic structure. (b) Normalized average transmission measured through the phononic slab structure shown in Fig. (a) as a function of frequency. The figure presents one absolute band gaps in the GHz frequency range.

Phononics 2011: First International Conference on Phononic Crystals, Metamaterials and Optomechanics

Santa Fe, New Mexico, USA, May 29-June 2, 2011

PHONONICS-2011-0090

Phononics 2011: First International Conference on Phononic Crystals, Metamaterials and Optomechanics
Santa Fe, New Mexico, USA, May 29-June 2, 2011
PHONONICS-2011-0126

Silicon Carbide Phononic Crystals for Communication, Sensing, and Energy Management

Maryam Ziaei-Moayyed[1], Charles Reinke[1], Mehmet Su[2], Ihab El-Kady[1], and Roy H. Olsson III[1]

[1] Sandia National Laboratories, Albuquerque, NM, USA
[2] Department of Electrical and Computer of Engineering, University of New Mexico, NM, USA
mziaeim@sandia.gov, creink@sandia.gov, mfatihsu@ece.unm.edu, ielkday@sandia.gov, rholsso@sandia.gov

Abstract: We demonstrate design, fabrication, and characterization of silicon carbide phononic crystals used to confine energy in lateral overtone cavities in 2-3GHz range with high f.Q products in air. The SiC cavities are fabricated in a CMOS-compatible process with applications in communication systems, sensing, and thermal energy management.

Phononic crystals (PnC) have recently gained much attention due to their ability to precisely control and manipulate propagation of acoustic waves for applications in wireless communication, sensing, acoustic isolation, imaging, and thermal energy management. By strategically placing defects in the phononic crystal through removal or distortion of inclusions, cavities and waveguides have been demonstrated at RF frequencies [1-3]. Microfabricated phononic crystal cavity resonators provide a lower power small-footprint, CMOS-compatible alternative to discrete components in communication systems. Silicon carbide (SiC) due to its mechanical strength, high acoustic velocity, and low intrinsic material damping is a desirable structural material with applications from high temperature microelectronics to micromechanical oscillators and harsh environment sensors [4]. This paper describes the design, optimization, fabrication, and characterization of SiC PnC-based devices. Figure 1 shows a schematic of a SiC Fabry-Perot cavity suspended above the substrate with SiC/air PnCs as high reflectivity acoustic mirrors on each side of the cavity. Aluminum Nitride (AlN) transducers with interdigitated Al top electrodes are designed to excite and sense the acoustic resonances in the cavity. This device combines the benefit of piezoelectric transduction, while storing the acoustic energy in a low loss material resulting in high $f.Q$ and $k_t^2.Q$ products for oscillator and filter applications.

Opening a phononic bandgap requires proper selection of inclusion and matrix materials that yield the desired mismatch between the acoustic impedance and velocity. We will compare solid-air and solid-solid SiC phononic crystals using plane approximation method to understand the behaviour of the PnC bandgap. A typical dispersion diagram of elastic waves in a SiC/air phononic crystal with normalized inclusion radii r/a ranging from 0.35 to 0.5 and normalized slab thicknesses t/a from 0.25 to 5 is shown in Fig.2 (a), exhibiting a complete bandgap about 2.7GHz. Figure 2(b) shows simulated normalized transmission versus frequency and volume filling fraction, r/a, for a 7 period, cubic lattice of vacuum inclusions in SiC plate. As the filling fraction is increased, the bandgap width and depth increases while moving to lower frequencies.

The SiC cavities were fabricated in a six mask CMOS-compatible surface micromachining process [3]. The highly-textured cubic SiC film is deposited in a low pressure chemical vapor deposition system and optimized to have low stress and low surface roughness for high quality factor. Figure 3(a) shows a SEM of a 10^{th} overtone SiC cavity separated from the AlN transducers by 5 layers of cubic SiC/Air PnC acoustic mirrors. Figure 3(b) shows a close-up SEM of the PnC with a lattice constant of 1.8μm and a filling fraction of 0.44. Figure 3(c) shows a close up view of one of the air holes etched in SiC with a nearly vertical sidewall (sidewall angle <5°). The SiC cavity resonators with frequencies ranging from 2 to 3GHz were tested in air using direct two-port transmission measurements. Aluminum nitride piezoelectric transducers were used to excite and detect the overtone acoustic cavities with frequencies ranging from 2 to 3GHz. Figure 4(a) shows the normalized transmission response of a 10^{th} overtone cavity (cavity length=19.8μm) with 5 PnC layers at 2.24GHz with a quality factor of 2000. Figures 4(b) shows the normalized transmission response for a 50^{th} overtone cavity (cavity length=99μm) with 3 PnC layers resulting in two resonant peaks with quality factors of 500 and 1000. The quality factors are improved to ~2200 and 3500 respectively by using 5 PnC layers (Fig.5(c)). These PnC–based cavities can be used to construct highly efficient acoustic signal processing elements such as filters and waveguides. These resonators are ideal for on-chip multi-frequency multi-bandwidth filter banks, on-chip spectrum analyzers, low phase noise oscillators, and ultra sensitive chemical and biological sensors. Furthermore, phononic crystals can be used in thermal energy management by shaping thermal phonon distribution resulting in reduced thermal conductivities [5]. Silicon carbide phononic crystal thermoelectric devices have a wide range of applications such as harsh environment microelectronics, thermoelectric energy generation, and satellite communication systems.

Phononics 2011: First International Conference on Phononic Crystals, Metamaterials and Optomechanics
Santa Fe, New Mexico, USA, May 29-June 2, 2011
PHONONICS-2011-0126

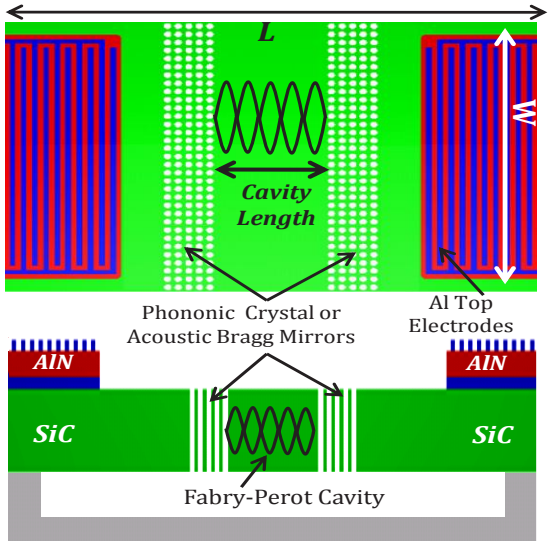

Figure 1 Schematic of a SiC overtone phononic crystal cavity with 5 layer phononic crystals on each side of the cavity. The acoustic mirrors separate the cavity from the AlN piezoelectric transducers.

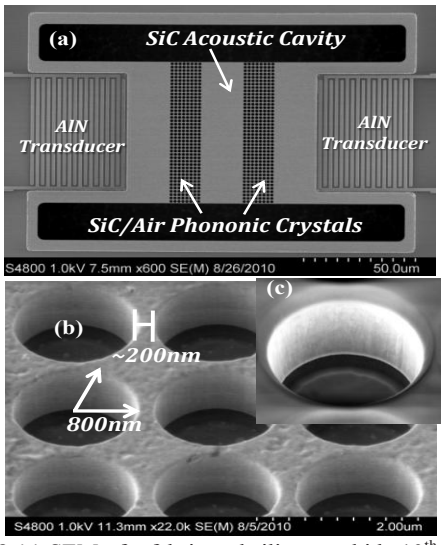

Figure 3 (a) SEM of a fabricated silicon carbide 10th overtone cavity with drive/sense AlN transducers and 5 layers of PnC (b) close-up SEM of the SiC/air PnC with a 1.83μm pitch and filling fraction of 0.44 (c) SEM of one of the holes with vertical sides walls.

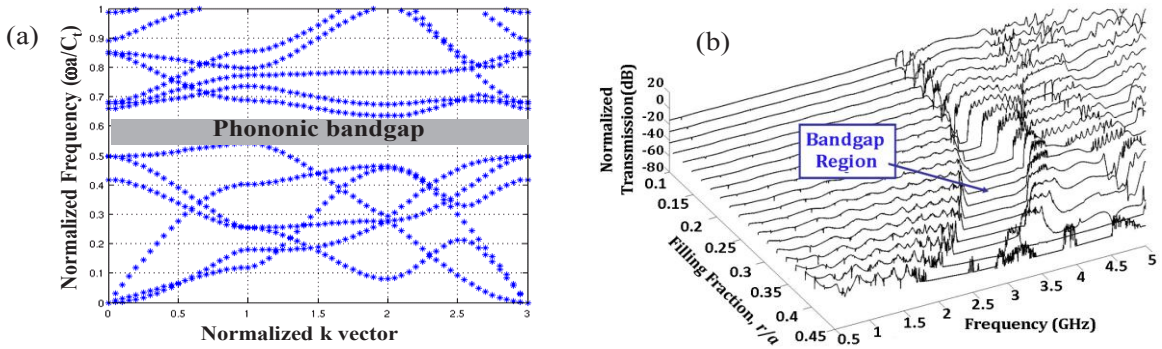

Figure 2 *(a)* Acoustic band diagram of a 2D simple cubic SiC/air phononic crystal obtained from PWE simulations with r/a=0.45 and t/a=0.5. (b) Simulated FDTD normalized transmission vs. frequency for a 7 layer cubic lattice of vacuum inclusions embedded in an infinitely thick SiC plate vs. inclusion filling fraction, r/a. The lattice constant, a, is 1.8μm.

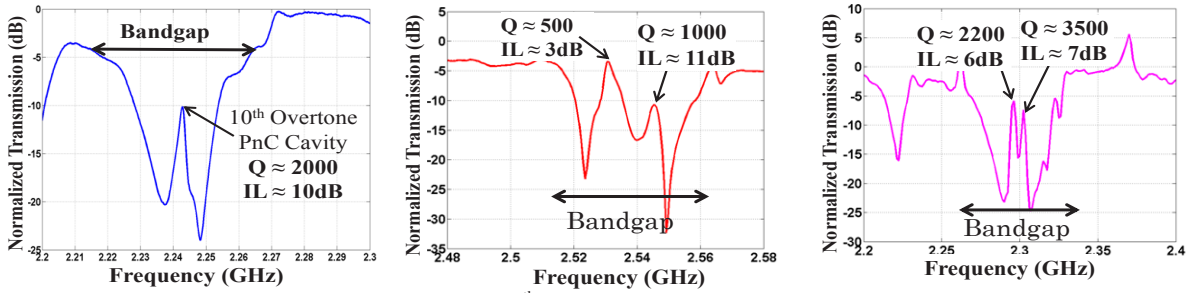

Figure 4 Normalized transmission response of (a) 10th overtone cavity with 5 PnC layers and Q of ~2000 at 2.24GHz (b) 50th overtone cavity with 3 PnC layers and Q's of 500 and 1000 at 2.53 and 2.55GHz respectively (c) 50th overtone cavity with 5 PnC layers and Q's of 2200 and 3500 at 2.295 and 2.305GHz respectively.

References

[1]R. H. Olsson III, I. F. El-Kady, M. F. Su, M. R. Tuck, and J. G. Fleming *Sensors Actuators* A , **145–146**, pp. 87–93 (2008).
[2] S. Mohammadi, A. A. Eftekhar, A. Khelif, H. Moubchir, W. D. Hunt, and A. Adibi, *Appl. Phys. Lett.*, **95**, 051906 (2009).
[3] M. Ziaei-Moayyed, , M. Su, C. Reinke, I. El-Kady, and R. Olsson III, IEEE Ultrasonics Symposium 2010, in press.
[4]Y. T. Yang, K. L. Ekinci, K.L, M. H. Huang, L. M. Schiavone, M. L. Roukes, C. A. Zorman, and M. Mehregany *App. Phys. Lett.*, **78**, 162-164 (2001).
[5] P.E. Hopkins, C. M. Reinke, M. F. Su, R. H. Olsson III, E. A. Shaner, Z. C. Lesemna, J.R. Serrano, L. M. Phinney, and I. El-kady, *Nano Lett.*, **11**, 107-112 (2010).

Phononics 2011: First International Conference on Phononic Crystals, Metamaterials and Optomechanics
Santa Fe, New Mexico, USA, May 29-June 2, 2011
PHONONICS-2011-0169

Designing High-Q Compact Phononic Crystal Resonators

Mehmet F. Su[1], Drew F. Goettler[1], Zayd C. Leseman[1], Ihab El-Kady[1,2]

[1] *Department of Mechanical Engineering, University of New Mexico, Albuquerque, NM, USA*
mfatihsu@unm.edu, goettled@unm.edu, zleseman@unm.edu
[2] *Photonics Microsystems Department, Sandia National Laboratories, Albuquerque, NM, USA*
ielkady@sandia.gov

Abstract: Phononic crystals provide a promising method of producing resonators with very high quality factors up to the theoretical limit possible in the host material. In this study we consider Silicon based solid-solid phononic crystal resonator designs with different lattices (simple cubic, hexagonal/triangular and honeycomb), number of inclusions and cavity shapes.

Compact microresonators are a versatile class of components used in both active such as oscillators and passive devices such as filters. One crucial requirement of any resonator device is a high quality factor, resulting in highly selective and tunable devices. Phononic crystals with cavity defects provide a method of producing compact resonators with quality factors reaching the maximum achievable figure for the constituent materials[1]. This talk will discuss our experiences in designing such resonators and optimizing the quality factor.

Phononic crystals consist of commonly cylinder shaped inclusions periodically placed in a host material (matrix). This study considered 2-D phononic crystals made of Tungsten inclusions in a Silicon matrix, placed in a number of lattice formations (simple cubic, hexagonal/triangular and honeycomb). The material pair was selected due to the large gap widths realizable using modest rod radius-to lattice periodicity ratios around 0.3. Low rod radius-to lattice periodicity ratios are more amenable to miniaturization, thus allowing smaller periodicities and higher operating frequencies[2] for phononic crystal resonators.

Numerical simulations were performed using the Finite Difference Time Domain (FDTD) method[3]. The FDTD numerical grid was terminated by Mur absorbing boundary conditions[4] in the designated primary propagation direction and periodic boundary conditions in the two transverse directions. This arrangement creates structures in infinite extent in the transverse while suppressing spurious reflections from the edges of the numerical grid. A wideband longitudinal displacement pulse was used to bootstrap all simulations. Postprocessing of the FDTD results for the frequency domain response was performed with Fourier Transform and Filter Diagonalization Method[5]. Resonator quality factors were calculated after obtaining the frequency domain response in each study case.

The resonator cavity was created by displacing half of the inclusions in the propagation direction, effectively forming a cavity extending infinitely along the transverse direction. This arrangement allows one to study wave penetration into the phononic crystal to develop an approximation in the form of a solid block, thus simplifying calculations for resonators and comparison to other types of reflectors. Isolated, periodically repeating cavities were also considered. Cavity frequencies and phononic crystal gaps in this study were optimized for an operating frequency of 1.315 GHz. Cavities supporting from the first up to the seventh harmonic were studied, all operating at the aforementioned frequency, to understand how the Q factor changes for various harmonic overtones and to determine the wave penetration into the phononic crystal. In this scheme, the fundamental frequency of the nth harmonic cavity is ($1.315/n$) GHz. If there was no wave penetration, the displacement for the nth harmonic cavity would be exactly n times the displacement needed for the first harmonic cavity. The presence of a constant wave penetration (Δ) into the tungsten inclusions requires accounting for both the wave penetration itself and another correction to the effective cavity length (L_{eff}) due to the wave velocity difference between silicon and tungsten materials. This second correction factor is directly proportional to the wave velocity ratio between silicon and tungsten (c_{Si}/c_W) and the wave penetration (Δ). Thus the effective cavity length for the nth harmonic cavity can be approximated as

$$L_{eff}=nL_1+2\Delta+(2n-2)(c_{Si}/c_W)\Delta \quad (1)$$

Phononics 2011: First International Conference on Phononic Crystals, Metamaterials and Optomechanics
Santa Fe, New Mexico, USA, May 29-June 2, 2011
PHONONICS-2011-0169

where L_1 is the length for the first harmonic cavity, c_{Si} is the longitudinal wave velocity in silicon and c_W is the longitudinal wave velocity in tungsten. It is possible to solve for Δ by determining L_1 and the cavity length for any other harmonic for a predetermined operating frequency. Once Δ is known, it becomes trivial to estimate the lengths of cavities supporting other harmonics.

The results indicate that the quality factors increase linearly with the cavity harmonic number and exponentially with the number of inclusions forming the phononic crystal reflectors. Clearly, the quality factor for a real resonator is limited by the fundamental material limit. For the studied cases, the limiting factor is the Akhieser effect[6] (phonon-phonon damping) loss. Incorporating the Akhieser effect into the quality factor calculation indicates phononic crystal resonators with as few as five layers of inclusions should attain the maximum quality factor possible in silicon material.

References

[1] D. Goettler, M. Su, Z. Leseman, Y. Soliman, R. H. Olsson III and I. El-Kady, *Journal of Applied Physics,* **108**, 084505 (2010).
[2] M. F. Su, R. H. Olsson III, Z. C. Leseman and I. El-Kady, *Applied Physics Letters*, **96**, 053111 (2010).
[3] M. M. Sigalas and N. Garcia, *Journal of Applied Physics*, **87**, 3122 (2000).
[4] G. Mur, *IEEE Transactions on Electromagnetic Compatibility*, **23** (4), 377-382 (1981).
[5] V. A. Mandelshtam and H. S. Taylor, *J. Chem. Phys.* **107** (17), 6756-6769 (1997).
[6] T. O. Woodruff and H. Ehrenreich, *Phys. Rev.* **123**, 1553 (1961).

Phononics 2011: First International Conference on Phononic Crystals, Metamaterials and Optomechanics
Santa Fe, New Mexico, USA, May 29-June 2, 2011
PHONONICS-2011-0179

A Waveguide-based Phononic Crystal Micro/Nano-mechanical High-Q Resonator

Saeed Mohammadi[1], Ali A. Eftekhar[1], Ali Adibi[1]

[1] *School of Electrical and Computer Engineering, Georgia Institute of Technology, Atlanta, GA 30324, USA*
saeedm@gatech.edu, eftekhar@gatech.edu, adibi@ece.gatech.edu

Abstract: In this paper, we report the design, analysis, fabrication, and characterization of a very high frequency (VHF) phononic crystal (PnC) micro/nano-mechanical resonator architecture based on silicon (Si) PnC slab waveguides. Qs as high as 13,500 in air at a frequency of ~134 MHz with a motional resistance of ~600 Ω, and 35 dB spurious-free range of ~20 MHz are obtained.

Recently, PnC slab (plate) structures[1], with large CPnBGs have been designed and implemented in platforms compatible with micro/nano-mechanical (MM) systems CMOS technologies[2,3]. The air (or vacuum) on top and bottom of a PnC slab (or membrane) decouples the vibrations in the PnC slab from leaking into the substrate. The possibility of realizing fundamental micro-mechanical (MM) devices, i.e., waveguides[4,5] and high quality factor (or high-Q) resonators[6], which are the bases of integrated mechanical signal processing systems, have recently been demonstrated. Because of their unique properties, such PnC-based devices and systems may surpass their conventional silicon (Si) MM counterparts for a variety of applications including wireless communications and sensing.

In this paper, we introduce a new type of suspended MM resonators based on PnC slab waveguides that can effectively suppress the support loss using the CPnBG of the PnC, while providing mechanical support and a path to deliver electrical signal to interrogate the resonator. To eliminate the problem of spurious modes in the PnC slab resonators[7] and to prevent spurious interferences from other modes in the PnC structures, we start with the design of a PnC waveguide with a small number of modes. The PnC waveguide is then terminated by the PnC structure on its input and output to confine forward and backward (and hence standing) waves within the waveguide region to form a resonator.

The PnC structure studied in this paper is composed of a hexagonal (honeycomb) lattice of void cylindrical holes in a free-standing Si slab[2]. To form a PnC waveguide with small number of modes, we reduce the radius of two lines of air holes in the PnC structure. A top-view schematic of such a PnC waveguide is shown in Fig. 1. The Extensional mode of the waveguide is utilized to allow for a more efficient excitation using the transducers and to obtain a high quality confinement. The radius of the immediate holes surrounding the waveguide are carefully chosen to be $r' = 0.2a$. In order to form the waveguide-based PnC resonator, the input and output ports of a waveguide are blocked by the PnC structure as shown in Fig. 1. The length of the confined waveguide is ten periods in the x direction ($L = 10\ a\ \sqrt{3}$).

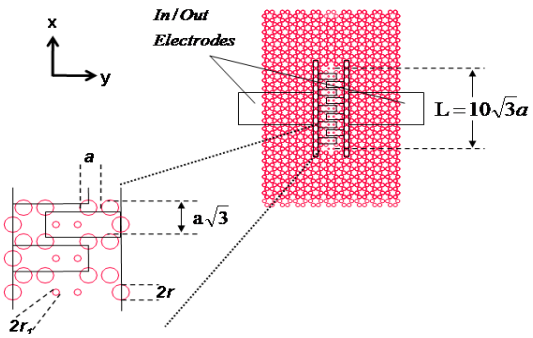

Figure 1 Schematic of the layout of a waveguide-based PnC slab resonator structure with interdigital transducers placed on top of the cavity to excite and detect the modes of the resonator. The length of the cavity is approximately 10 periods (L = 10 a).

The coupling of the resonator to/from the outside world is achieved by using piezoelectric transducers fabricated right on the PnC resonator. The number of PnC layers around the resonator in our design is 4 and 6 periods on each side of the cavity in the y and x directions, respectively, which are enough to almost completely eliminate leakage of acoustic energy from the sides of the resonator based on our previous observations[6].

The waveguide-based resonator structure is fabricated with the scaling choice of $a = d = 15$ μm for the PnC structure. The fabrication process starts with a high-resistivity (to reduce electromagnetic coupling) silicon on insulator (SOI) wafer with a 15μm device layer, a 2μm buried oxide (BOX) layer

Phononics 2011: First International Conference on Phononic Crystals, Metamaterials and Optomechanics
Santa Fe, New Mexico, USA, May 29-June 2, 2011
PHONONICS-2011-0179

and a 400μm handle layer. A 100nm/1μm/100nm stack of Mo/AlN/Mo is sputtered on top of the device layer. The top Mo layer is patterned first using optical lithography and plasma etching to form the top electrode and contact pads. PnC holes are etched using a two-step plasma etching recipe to etch the transducer stack and the Si device layer. The access to the lower Mo electrode is obtained by selective wet etching of the AlN layer to the Mo layer. Finally, the structure is etched from the back using backside-alignment lithography and deep plasma etching of the handle and the BOX layers to release the structure and form the PnC slab resonator. A top view scanning electron microscope (SEM) image of the fabricated structure is shown in Fig. 2. The approximate geometrical parameters of the fabricated PnC resonator are measured to be a = 15 μm, $2r$ = 12.5 μm ($r \sim 0.42a$), and $2r'$= 4.9 μm ($r' \sim 0.16a$) using the SEM data. The structure is characterized by using a two-port vector network analyzer with 50Ω reference impedance to obtain the scattering parameters of the device in the PnBG frequency range.

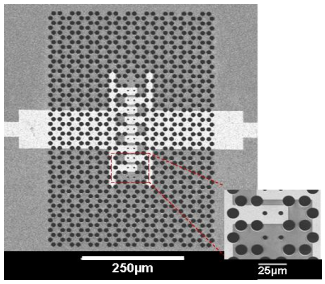

Figure 2 An SEM image of the fabricated PnC resonator and a magnified version of a subset of this image (inset).

In order to accurately evaluate the resonance properties of the main excited mode, we fitted a modified Butterworth Van Dyke (BVD) model[8] to the admittance profile of the desired mode. The fitted BVD model as well as the measured and fitted admittance and susceptance curves are shown in Figure 1, where C_p and R_p are the parallel capacitance and resistance between the upper and lower electrodes of the port, and R_r, L_r, and R_m are associated with the electrical equivalent of the resonator at its resonance frequency, where the Q can be extracted from. As can be seen in this figure, the Q of the resonance is 13,500, which is by far the highest Q reported for PnC resonators[6,9] and significantly higher (>30 %) than the results reported using the most recent techniques for resonators with a similar structure (AlN stack on 15 μm Si) measured in air[10], confirming the suppression of the support loss. The frequency of resonance of the MM resonator is 134.1418 MHz, which translates to the normalized frequency of f × a = 2012 showing a good match with the theory. The resonance is more than 10 MHz apart from any resonance within 35 dB of its power, which gives a large frequency range of operation. This result confirms that obtaining high quality support-loss free MM resonators is possible through the use of the PnC structures.

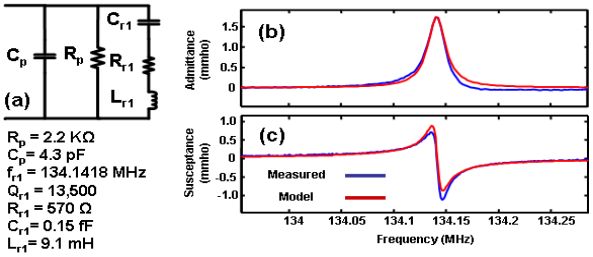

Figure 1 (Color online) (a) The modified BVD model, (b) admittance, and (c) susceptance profile of the waveguide-based PnC resonator excluding the parasitic resistor and capacitor of the device. The frequency of resonance (f_{r1}), the quality factor (Q_{r1}), the motional resistance (R_r), the resonance capacitance (C_{r1}) and inductance (L_{r1}) for the selected mode, and the values for the excluded parasitic capacitance and resistance (Cp , Rp) are given in this figure.

This work was supported by the National Science Foundation (Contract No. 2106AXJ ARRA). The authors wish to thank the staff at Georgia Tech Nanotechnology Research Center for their support in holding the fabrication equipment, Prof. Reza Abdolvand for his input in fabrication, and Prof. W. D. Hunt for providing the measurement equipment.

References

[1] A. Khelif, B. Aoubiza, S. Mohammadi, A. Adibi, and V. Laude, *Physical Review E*, **74**, 46610-46615 (2006).
[2] S. Mohammadi, A.A. Eftekhar, A. Khelif, H. Moubchir, R. Westafer, W.D. Hunt, and A. Adibi, *Electronics Letters*, **43**, 898-899 (2007).
[3] S. Mohammadi, A.A. Eftekhar, A. Khelif, W.D. Hunt, and A. Adibi, *Applied Physics Letters*, **92**, 221903-221905 (2008).
[4] S. Mohammadi, A.A. Eftekhar, W.D. Hunt, and A. Adibi, Piscataway, NJ, USA: IEEE, 768-772, (2008).
[5] R.H. Olsson, I.F. El-Kady, M.F. Su, M.R. Tuck, and J.G. Fleming, *Sensors and Actuators A-Physical,* **145**, 87-93, (2008).
[6] S. Mohammadi, A.A. Eftekhar, W.D. Hunt, and A. Adibi, *Applied Physics Letters*, **94**, 51903-51906 (2009).
[7] S. Mohammadi, A. Eftekhar, A. Khelif, and A. Adibi, Proc. of 2010 SPIE Photonics West, 76090W, (2010).
[8] K. S. Van Dyke, *Proceedings of the Institute of Radio Engineers*, **16** (6), 742-764, (1928).
[9] C.-Y. Huang, J.-H. Sun, and T.-T. Wu, *Applied Physics Letters*, **97**, 031913 (2010).
[10] B.P. Harrington and R. Abdolvand, TRANSDUCERS 2009, IEEE, 700-703 (2009).

1ST INTERNATIONAL CONFERENCE ON PHONONIC CRYSTALS, METAMATERIALS & OPTOMECHANICS

Author Index

N

O

P

Q

R

S

T

U

V

W

X

Y

Z

Discover Unmatched XHR SEM Performance in a DualBeam™

The Helios NanoLab 450S & 650 bring the most advanced SEM imaging and FIB milling capabilities to Semiconductor and Research labs.

Imaging, analysis and control of matter at the nanoscale — keys to future research and development — are routine with the Helios NanoLab™ 50 series DualBeam™. Featuring unsurpassed SEM resolution, image quality and stunning Tomahawk™ FIB performance, imaging, milling or preparing samples is fast and easy for semiconductor and data storage labs, research facilities and industrial applications.

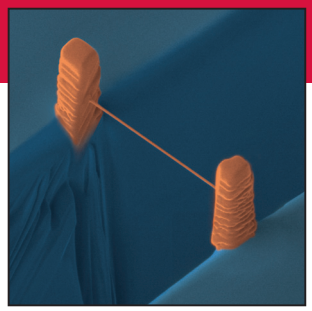

Platinum nanowire deposited and milled to about 50 nm diameter for use as a gas sensor *Courtesy of Peter Heard, Bristol University, United Kingdom*

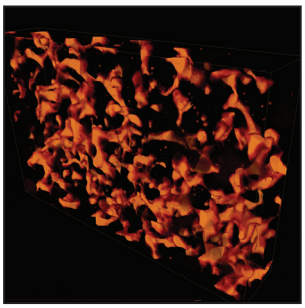

Voltex visualization of porosities in a fuel cell electrode *Courtesy of Sabanci University, Turkey*

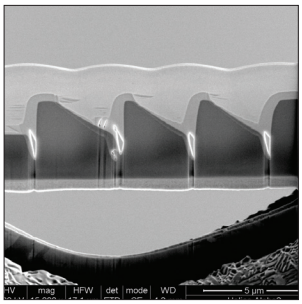

TEM lamella created to measure the amorphous damage created during FIB sample preparation *Image courtesy of D. Wall, FEI NanoPort, The Netherlands*

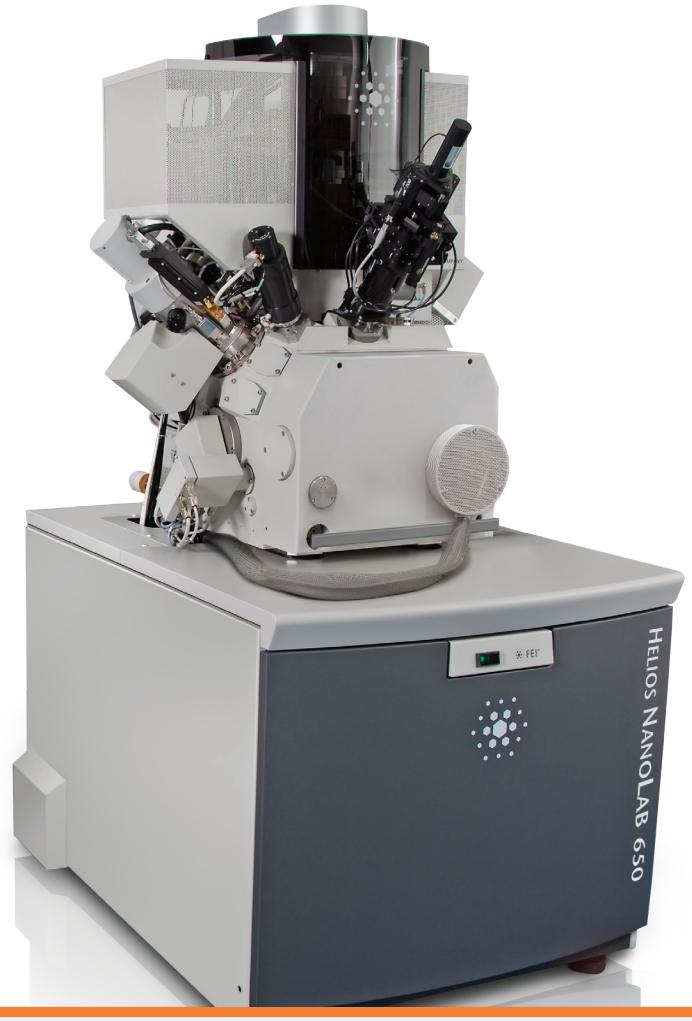

Learn more at FEI.com/helios

FEI™